Platinum Group Elements (PGE) and Platinum Group MineraIs (PGM) Distribution and petrological evolution of southern Kohistan Arc, Northern Pakistan.

Allah Bakhsh Kausar

UNIVERSITÉ JOSEPH FOURIER-GRENOBLE 1
SCIENCES ET GÉOGRAPHIE
UFR DE GÉOLOGIE

THESE

pour obtenir le grade de

DOCTEUR DE L'UNIVERSITE JOSEPH FOURIER

Discipline: Sciences de la Terre

Présentée et soutenue publiquement

par

KAUSAR Allah Bakhsh

Le 29 octobre 1998

L'ARC SUD KOHISTAN, N.PAKISTAN : ÉVOLUTION PÉTROLOGIQUE ET DISTRIBUTION DES ÉLÉMENTS ET MINÉRAUX DU GROUPE DU PLATINE.

Directeur de thèse

M.Christian PICARD, Professeur, Université de Grenoble

COMPOSITION DU JURY:

M. Arnaud PECHER	Professeur, Université de Grenoble	Président
M. Qasim JAN,	Professeur, Université de Peshawar, Pakistan	Rapporteur
M. Zdenek JOHAN,	Membre correspondant de l'Institut, Directeur Scientifique, BRGM, Orléans	Rapporteur
M. Jean AMOSSE,	Chargé de Recherche, CNRS, Grenoble	Examinateur
M. Patrick LE FORT,	Directeur de Recherche, CNRS, Grenoble	Examinateur
M. Hervé MARTIN,	Professeur, Université de Clermont-Ferrand	Examinateur

ACKNOWLEDGEMENTS

I gratefully acknowledge the French Embassy, Government of France, for sponsoring financial support for my doctoral studies in the France, LGCA for analytical support and the Geoscience Laboratory, GSP, Pakistan, for field work as well as analytical support.

Especially, I would like to thank Mr. P. Desseix, Conseiller Culturel, French Embassy, Pakistan, for his continuing enthusiasm and interest in the development of geological sciences in Pakistan.

Very special thanks to Mr. S. Hasan Gauhar, Director General, Geological Survey of Pakistan, Mr. P. Le Fort and Mr. A. Pecher for pushing me down the road of PhD and enlightening me about the structure and purpose of science.

My sincere thanks go to my thesis Director, Christian Picard, for giving me the possibility of undertaking this project and introducing me to the world of platinoids and leading me to see and understand more clearly the particular geological problems related with their distribution in an arc environment.

I also acknowledge the efforts of my examining committee towards producing an almost readable manuscript. Particularly, Mr. Qasim Jan, Vice Chancellor, University of Peshawar, a big name in Geology in Pakistan, for sparing his valuable time to participate as jury member for my doctoral defence. I wish to thank Mr. Z. Johan, Director Scientific, BRGM and Mr. H. Martin, University of Clermont-Ferrand, for accepting invitation to become the members of my doctoral defence jury.

Many people provided the author with important instruction and technical assistance. Many thanks are due to Mr. J. Amossé who helped me in all the PGE's analyses and deepened my general geological understanding about the PGE's distribution in silicate melt and for the review of the chapter on PGE's and PGM's distribution in the southern Kohistan.

A big thank to Mr. M. Piboule for helping me in solving the complexity of geochemical problems of the Jijal Complex. I also thank Madame F. Keller, Dolomieu Institute, Zafar and Naghma Haider, Geoscience Laboratory, Pakistan in helping me for analysing the major, trace and rare earth elements.

I want to thank Mr. Said Rahim who introduced me to the Jijal Complex and helped me in geological mapping and sample collection. Special thanks to Mr. Tahseenullah Khan for helping me for measuring section of Spat Complex and field excursions in the Chilas Complex and Mr. Ibrar A. Khan for providing me probe data on the Thak Gah Association and helping me in probing the minerals from the Jijal Complex.

I want to thank my office mate, Santa Man Rai who always encouraged me during the time of my depression and a big thank to all those who were helping me in the background, particularly, Mr. Gilles Brocard, who helped in translating all captions of my thesis in French language. This thesis is the result of a joint effort of all my helpers, the named and unnamed. I salute them.

Finally, I gratefully acknowledge the moral support of my wife and children through one difficult year.

L'ARC DU KOHISTAN, NORD PAKISTAN : EVOLUTION PETROLOGIQUE ET DISTRIBUTION DES ELEMENTS ET MINERAUX DU GROUPE DU PLATINE.

VERSION FRANÇAISE ABREGEE

En raison de la nationalité pakistanaise de l'impétrant et de sa langue maternelle (Urdu et Anglais), cette thèse réalisée dans le cadre d'accords bilatéraux entre la France et le Pakistan est rédigée en anglais.

Pour cette raison une version allongée du résumé est ici présentée en Français. Les légendes des figures et des tableaux sount présentées dans les deux langues.

L'ARC DU KOHISTAN, NORD PAKISTAN : EVOLUTION PETROLOGIQUE ET DISTRIBUTION DES ELEMENTS ET MINERAUX DU GROUPE DU PLATINE.

VERSION FRANÇAISE ABREGEE

Située entre les chaînes de l'Himalaya et du Korakorum, la province tectonique du Kohistan-Ladakh au nord du Pakistan relie la plaque indienne au sud à la plaque asiatique. Elle représente l'une des coupes les plus remarquables d'un complexe d'arcs. En effet du sud au nord, cette province présente une suite spatio-temporelle continue depuis un complexe d'arcs intra-téthysien d'âge Crétacé, jusqu'à un complexe de marge active de type andin d'âge Eocène - Oligocène . Au cours de la collision Himalayenne, cet ensemble d'arcs a été partiellement subducté sous la plaque asiatique, puis obducté sur la plaque indienne. Les effets conjugués de la tectonique et de l'érosion (liée à une forte remontée de la croûte), offrent l'opportunité d'observer une coupe quasi complète d'un arc intra-océanique depuis ses racines les plus profondes à l'interface manteau-croûte jusqu'à sa partie la plus superficielle où s'exprime le volcanisme. Au sud Kohistan, un tel ensemble est représenté par les complexes mafiques-ultramafiques de Spat et de Jijal, les amphibolites de Kamila et le vaste complexe gabbro-dioritique de Chilas.

Cette étude permet de préciser les processus pétrogenétiques à l'origine d'un complexe d'arc depuis la fusion du manteau, le piégeage et l'évolution des magmas dans les réservoirs profonds jusqu'à leur épanchement en surface. Les principales caractéristiques pétrographiques, minéralogiques et géochimiques des roches ignées du Sud Kohistan sont présentées et discutées dans la première partie de ce manuscrit. Elle révèle également certaines particularités métallogéniques, et permet de définir dans la seconde partie de ce manuscrit un exemple type de dépôt pour les éléments du Groupe du Platine.

Evolution Tectonique et Pétrologique du Sud Kohistan

Le complexe ultramafique à mafique de Jijal est situé au sud de l'arc du Kohistan, immédiatement au nord du chevauchement principal, le "Main Mantle Thrust" ou MMT (Fig. 3), qui sépare cette province tectonique de la plaque indienne au sud. Il constitue une intrusion litée divisée en deux ensembles d'unités. La section inférieure est composée de plusieurs horizons ultramafiques et lités de dunite, de clinopyroxénite à olivine et de webstérite, passant vers le haut à des webstérites et clinopyroxénites à grenat. La section supérieure, est principalement composée de gabbros lités à grenat et de quelques hornblendites également grenatifères.

Les données géochimiques sur roche totale et sur minéraux indiquent que le complexe de Jijal résulte de processus de cristallisation fractionnée d'un liquide tholéiitique hautement magnésien généré dans un environnement d'arc intra-océanique. Les minéraux ferro-magnésiens présentent des variations de composition chimique en accord avec le modèle d'une

seule suite de différenciation des dunites aux gabbros à grenat. En effet, le Mg# de l'olivine décroît régulièrement de Fo94 à Fo78. La formule structurale du clinopyroxène varie de $Ca_{48}Mg_{49}Fe_3$ dans les dunites à $Ca_{49}Mg_{33}Fe_{18}$ dans les gabbros à grenat, tandis que les teneurs en Al et Ti augmentent quand le Mg# diminue. L'orthopyroxène, cristallisé plus tardivement, voit son Mg# varier de 85 à 76 au cours de la cristallisation. Enfin le grenat, qui résulte de processus d'exsolution à partir du clinopyroxène, et de recristallisation subsolidus, présente une évolution de sa formule structurale depuis $Al_{37}Py_{30}Gr_{29}Sp_2Ad_2$ dans les webstérites à grenat à $Al_{43}Py_{33}Gr_{21}Sp_1Ad_2$ dans les gabbros à grenat. Les relations de phase entre les minéraux cumulus, les calculs thermobarométriques réalisés sur les couples clinopyroxène - orthopyroxène, grenat - orthopyroxène et grenat - amphibole, ainsi que les données thermométriques obtenues sur le couple olivine-spinel, montrent que les roches du complexe de Jijal ont cristallisé à partir d'un liquide magmatique sous des pressions comprises entre 10 et 12 Kbars (entre 30 et 40 Km de profondeur) et ont été équilibrées à des températures entre 800 à 1100°C. Ces données, la chimie des minéraux, les valeurs élevées du Mg# dans les équilibres minéralogiques clinopyroxène - orthopyroxène (Mg#=92-85), la composition de l'olivine (Fo 94-85), ainsi que l'absence de plagioclase dans les phases de cristallisation précoce sont autant d'arguments qui montrent que le complexe de Jijal résulte de processus de cristallisation fractionnée sous haute pression à partir de liquide magmatique hautement magnésien piégé à grande profondeur dans un réservoir à l'interface manteau-croûte.

Au sein du Complexe de Chilas, le complexe mafique-ultramafique de Thak Gah (quelques Km^2) diffère du complexe de Jijal tant par ses aspects structuraux que minéralogiques. Il est en effet caractérisé par l'intercalation de nombreux horizons de dunite, de werhlite, de pyroxénite, de troctolite et de gabbro lité qui montrent de nombreuses structures réactionnelles et de mélange à l'interface des horizons mafiques et ultramafiques indiquant qu'il résulte de la coexistence de deux magmas. Le Mg# observé dans les dunites (Mg#=69), les werhlites (Mg#=67) et les gabbros (Mg#=45), et les teneurs plus élevées en fer des pyroxènes et des spinelles, évoquent des magmas parents plus évolués qu'à Jijal. Par ailleurs, les données chimiques, thermobarométriques et thermométriques obtenues sur les couples clinopyroxène - orthopyroxène indiquent des pressions d'équilibre lors de la cristallisation des magmas plus faibles qu'à Jijal entre 5 à 6 Kbars et des températures de cristallisation entre 800° et 950°C. Ces données et les plus faibles pressions impliquent que le complexe de Thak Gah représente un réservoir magmatique formé à plus faible profondeur à partir d'un liquide magmatique déjà en partie fractionné vraisemblablement au sein du même arc intra-océanique.

La zone principale du Complexe de Chilas (plus de 300 Km d'est en ouest pour une centaine de Km de largeur) est formée en proportions à peu près égales de gabbros et

gabbros-norites et de diorites quartziques à hyperstène sous forme d'intrusions homogènes imbriquées les unes dans les autres. **Le Groupe amphibolitique de Kamila** au sud comprend trois assemblages lithologiques : i) des amphibolites à grain fin souvent très fortement déformées, interprétées comme d'anciennes métavolcanites (essentiellement des métabasaltes); ii) des amphibolites à gros grains peu déformées à l'exception de couloirs mylonitiques, nettement intrusives dans les amphibolites à grains fins et interprétées comme des intrusions de métagabbros et de métadiorites très probablement contemporaines des plutonites de la zone principale du complexe de Chilas; et enfin iii) des granites intrusifs sous forme de petits plutons au sein des deux faciès précédents.

Les amphibolites à gros grains du Groupe de Kamila et les gabbros, gabbro-norites et diorites de la zone principale du Complexe de Chilas présentent d'étroites similitudes pétrographiques et surtout géochimiques suggérant qu'ils résultent de la cristallisation fractionnée de magmas basaltiques et andésitiques dans un même environnement géodynamique d'arc au Crétacé inférieur (mêmes enrichissements en éléments lithophiles et mêmes anomalies négatives en Nb - Ta). Cependant, les amphibolites à gros grains du Groupe de Kamila présentent, comme à Jijal, davantage d'affinités avec les tholéiites d'arc insulaire, tandis que les plutonites de la zone principale du complexe de Chilas ont des signatures d'arc avec une tendance tholéiitique à calco-alcaline. Dans ces roches, les teneurs en Nb restent relativement élevées pour des tholéiites d'arc (anomalies en Nb - Ta assez peu accentuées), suggérant une mise en place à un stade immature du développement de l'arc.

Les amphibolites à grain fin du Groupe de Kamila, constituent plusieurs blocs préservés entre les filons et plutons de métagabbros, métadiorites et granites. Ces amphibolites, interprétées comme des métavolcanites, représentent les plus anciennes roches du Kohistan. Comparativement aux autres roches ignées du Kohistan, elle sont appauvries en éléments lithophiles, déprimées en terres rares légères et enrichies en éléments HFS (Ti, Ta et Nb) et en terres rares lourdes. Leur signature géochimique est analogue à celle des laves actuelles de type N-MORB. Ainsi, ces métavolcanites constituent très vraisemblablement des reliques de la croûte océanique téthysienne ainsi que le substratum du ou des arcs intra-océaniques d'âge Crétacé aujourd'hui accrétés les uns aux autres dans la partie méridionale du Kohistan. Leur rareté est la conséquence de la subduction de la croûte océanique téthysienne, puis des abondantes intrusions magmatiques qui l'ont recoupée et en grande partie résorbée.

Ainsi, il apparaît raisonnable de considérer que la partie sud de la province du Kohistan correspond à l'évolution progressive au Crétacé inférieur d'un arc construit sur la croûte océanique téthysienne, d'abord immature puis de plus en plus évolué. Au cours des premiers stades du développement de l'arc, les magmas basaltiques ont cristallisé sous forme de cumulats et se sont injectés dans l'ancienne croûte océanique téthysienne où ils ont constitué d'importants massifs de métagabbros et de métadiorites à signature géochimique d'arc. Plus

tard, les gabbros et les diorites d'affinité tholéiitique à calco-alcaline du complexe de Chilas se sont mises en place à leur tour sous forme d'un gigantesque complexe intrusif à la base de l'arc dans le substratum océanique faisant pratiquement disparaître l'ancienne croûte océanique. Le complexe de Thak Gah représente quant à lui une unité constituée dans la partie basale du réservoir magmatique, puis incorporée dans la masse principale des plutonites du complexe de Chilas. Le complexe de Jijal, représente pour sa part un réservoir magmatique dont la cristallisation fractionnée sous haute pression (10 et 12 Kbars) a produit une séquence cumulative de près de 5 000 mètres d'épaisseur. Les conditions de cristallisation et l'absence de filons le recoupant suggèrent qu'il s'est constitué entre 30 et 35 Km de profondeur sous les complexes de Kamila et de Chilas à la limite manteau-croûte. Ainsi, le complexe de Jijal semble le produit de " plaquage sous-crustal". La collision de l'arc du Kohistan avec la plaque asiatique au nord (à la fin du Crétacé), met fin au stade intra-océanique révélé par les séries du sud-Kohistan. C'est à ce stade que débute la seconde période de l'histoire du Kohistan avec la mise en place des nombreux plutons granodioritiques et granitiques du batholite du Kohistan. Au Miocène, l'ensemble du Kohistan a été obducté sur la plaque indienne, permettant ainsi la mise en exposition des différentes composantes de l'arc Crétacé.

Distribution des éléments et minéraux du Groupe du platine (PGE et PGM).

L'étude de la distribution des métaux précieux dans les complexes mafiques et ultramafiques du Sud-Kohistan révèle plusieurs caractéristiques géochimiques sur le comportement des éléments du Groupe du platine dans les environnements d'arc insulaire. Pour cela, une étude approfondie a été réalisée au sein du complexe de Jijal (où des teneurs importantes en PGE ont été antérieurement signalées par Miller et al., 1981) ainsi qu'une étude plus prospective sur les complexes de Spat et de Chilas.

A l'exception d'une valeur anomalique observée dans les péridotites à spinelle du complexe de Thak Gah, seul le complexe de Jijal révèle d'importantes anomalies en PGE. Trois types d'enrichissements en EGP sont observés dans le complexe de Jijal :

1) des concentrations en IPGE reliées à la précipitation de chromites dans les horizons de dunite.

2) des concentrations en IPGE et PPGE associées à des minéralisations disséminées en sulfures de Ni - Cu dans les horizons de webstérite et de webstérite à grenat.

3) des concentrations de PPGE (Pt et Pd) reliées à la cristallisation de chalcopyrite ± pyrite dans les gabbros à grenats de la séquence supérieure

Dans le premier type de concentration, seuls les IPGE (Ir et Ru), le chrome et le nickel sont fortement enrichis. Les concentrations en Ir et Ru sont contrôlées par les valeurs élevées de la fugacité en oxygène qui favorisent la précipitation de la chromite, du spinelle et d'éventuels alliages à Ir - Ru (non observés). L'abondance de Ni d'une part et des éléments Cr, Ir et Ru dans les dunites révèlent le comportement compatible de ces éléments vis à vis

respectivement de l'olivine et de la chromite. La précipitation de la chromite provoque une diminution de la fugacité en oxygène et en corollaire une augmentation de la fugacité en soufre dans les magmas résiduels. Ainsi les cristallisations précoces de l'olivine et de la chromite explique la diminution des teneurs en Ni et en IPGE dans les cumulats plus évolués.

Le deuxième type de concentration en IPGE, PPGE, Ni et Cu correspond à des horizons enrichis en sulfures de métaux de base (chalcopyrite, pyrrhotite, pentlandite ± pyrite) dans les deux sections analysées (vallée de Duber, et Karakoram Highway ou KKH). Les principaux Minéraux du Groupe du Platine (MGP) observés sont la témagamite, la monchéite, la mérenskyite et la spérrylite. Tous ces minéraux sont présents sous forme d'inclusions dans les assemblages silicatés ou en limites de grains dans les webstérites et les webstérites à grenat. Ces minéralisations sont interprétées comme résultant de la formation d'un liquide sulfuré immiscible au cours de la cristallisation à haute température du magma silicaté. Deux générations de MGP semblent coexister, la première contemporaine de la ségrégation des liquides sulfurés immiscibles et du clinopyroxène, la seconde formée lors de recristallisations subsolidus. La première génération de MGP est synchrone de la cristallisation du clinopyroxène et de l'orthopyroxène sous fortes pression et température (10 à 12 Kbars, 900 à 1100°C). Elles traduisent une fugacité de soufre élevée, consécutive de la précipitation des chromites dans les horizons sous-jacents. La précipitation des sulfures a drainé l'essentiel des PGE si bien que les gabbros à grenats sus-jacents apparaissent déprimés en ces éléments.

Le troisième type de concentration montre que les quelques PPGE résiduels (Pt et Pd) se sont concentrés avec la chalcopyrite sous forme de minces horizons (de type reefs) au sein des gabbros à grenat sous l'action de fluides tardi-magmatiques. Ainsi les phases fluides semblent avoir joué un rôle croissant dans les séquences supérieures. De tels fluides peuvent représenter un héritage du manteau métasomatisé dans un environnement de subduction.

Les concentrations de PGE observées dans le complexe lité de Jijal présentent d'importantes différences par rapport à celles bien connues dans d'autres complexes lités comme le Bushveld ou le Stillwater. Dans la section ultramafique, formée par au moins deux venues successives de magma, l'augmentation de la fugacité en oxygène a entraîné la précipitation de chromite et ferrochromite localement abondante dans les dunites. Ces chromites (Unité 2 du complexe) sont dépourvues de sulfure et donc pauvres en Pt et Pd. Elles peuvent s'apparenter, bien que beaucoup moins abondantes aux chromites de la "zone inférieure du complexe de Bushveld, mais en diffèrent par l'absence de concentrations en PPGE.

Les horizons enrichis en sulfures, IPGE et PPGE observés dans les webstérites et webstérites à grenat (unités 4 et 5 du complexe de Jijal), rappellent sur certains points les caractéristiques du Merensky Reef dans le complexe de Bushveld. Cependant, ce dernier résulte typiquement de l'apport d'un nouveau magma dans le réservoir sous forme d'un

"plume" turbulent et donc de processus de mélange, ces processus ayant provoqué le saturation en soufre du système et la précipitation dans un mince horizon de sulfures de nickel et de minéraux du Groupe du platine. A Jijal, aucune évidence de mélange de ce type n'a pu être observée au sein des webstérites. Par ailleurs, les concentrations en sulfures et en PGE forment plusieurs minces horizons nettement discontinus ce qui n'est pas le cas dans le Bushveld. La saturation en soufre du magma à l'origine de la précipitation des sulfures et des PGE apparaît consécutive des processus de cristallisation antérieurs (notamment la précipitation de la chromite et de l'olivine dans les horizons sous-jacents), elle n'implique pas à ce stade des mélanges de magma. Cependant les données de terrain et les observations sur la chimie des minéraux, impliquent que les processus de distributions des PGE et la précipitation des MGP dans les webstérites à grenat ont été au moins en partie contrôlée par l'action de phases fluides riches en Te et Hg tardivement exprimées lors de la cristallisation, ces fluides ayant joué un rôle déterminant dans la précipitation des dernières traces de Pt , Pd et Cu dans les gabbros à grenat.

En résumé, nos résultats démontrent que le complexe de Jijal dérive de la fusion partielle d'une source mantellique supra-subductive et de la cristallisation fractionnée sous haute pression et haute température à la limite manteau croûte de liquides tholéiitiques hautement magnésiens à signature d'arc insulaire intraocéanique ayant drainé depuis le manteau les éléments du Groupe du platine qui ont ultérieurement précipité sous le contrôle de facteurs tels la fugacité en oxygène et en soufre, elle même contrôlée par les fractionnements successifs. Les minéralisations en métaux de base et en métaux précieux du complexe de Jijal, apparaissent donc comme un exemple remarquable de distribution des éléments du Groupe du Platine dans un environnement d'arc pouvant être considéré comme l'une des références possibles de ce type de minéralisation.

ABSTRACT

The intra-oceanic arc crust in the southern Kohistan is represented by the Jijal- Spat-Complexes, Kamila Amphibolite and Chilas Complex.

The Jijal Complex is a layered intrusion having dunite, olivine-clinopyroxenite, websterite, garnet websterite and garnet gabbro. Geochemistry indicates that this formed by fractional crystallization from a high-Mg tholeiitic melt in an arc environment with pressures between 10 and 12 kbar, equilibrated at temperatures of 800° to 1100°C. The rocks of Thak Gah (Chilas complex) crystallized under lower pressure (5 to 6 kbar) and equilibrated at temperature between 800° and 950°C. They represent a shallow magma chamber in the same arc. Plutonic rocks from Kamila and Chilas–are also geochemically similar to modern intra-oceanic arc. However, fine-grained Kamila metavolcanics, are more akin to the N-type MORB, suggesting fragments of pre-existing oceanic crust.

In the Jijal Complex, BMS, PGM and PGE bearing phases are present in the form of inclusion in or on the edges of the silicate assemblages. The main PGM's are temagamite, moncheite, merenskyite and sperrylite. In dunites, Ir, Ru, Ni and Cr enrichments indicate that both Ir and Ru are partitioned with chromites and can be clearly correlated to high fO_2. Ir and Ru enrichments in chromite-rich dunite of Thak Gah and Spat Complexes have the same origin. In Jijal Garnet-websterite, Ir, Ru, Pt, Pd and Au correspond to a prominent peak of Ni and Cu which is due to the precipitation of sulphide under lower fO_2. In upper garnet gabbro, Pt-Pd-Cu enrichments correspond to late removal of PPGE by magmatic fluids.Such mineralizations present important variations with Bushveld-type. They indicates that sulphide saturation due to simple crystallization can give rise to deposits such as can be seen in the Ga-websterite. Such mineralization characterizes arc related PGE's deposits.

RÉSUMÉ

La croûte intra-océanique du sud-Kohistan comprend les complexes de Spat et Jijal, les amphibolites de Kamila et le complexe de Chilas.

Le complexe de Jijal est une intrusion litée constituée de dunite, clinopyroxénite à olivine, websterite, webstérite à grenat et de gabbro à grenat. Mis en place à l'interface manteau croûte, il résulte de la cristallisation fractionnée sous haute pression et haute température (10-12 Kbars; 800-1100°C) d'un liquide tholéiitique d'arc intra-océanique hautement magnésien. Les roches de Thak Gah (complexe de Chilas) ont cristallisé sous plus faible pression et température (5 - 6 kbars, 800 à 950°C) dans un réservoir magmatique plus superficiel. Les métaplutonites de Chilas et Kamila présentent également des signatures géochimiques analogues à des tholéiites d'arc insulaire. Au contraire, les amphibolites à grains fins du Groupe de Kamila apparaissent comme des métavolcanites de type N-MORB, elles représentent des reliques de croûte océanique et le substratum de l'arc du Kohistan.

Plusieurs horizons enrichis en PGE caractérisent le complexe de Jijal. Des enrichissements en Ir, Ru, Ni corrélés au Cr dans les dunites, indiquent que l'irridium et le ruthénium précipitent précocément avec la chromite sous haute fugacité d'oxygène. Des enrichissements en Ir et Ru du même type caractérisent les dunites chromifères des complexes de Thak Gah et de Spat. Dans les webstérites à grenat de Jijal, des sulfures disséminés (chalcopyrite, pentlandite, pyrrhotite± pyrite) et des minéraux du Groupe du platine (témagamite, monchéite, mérenskyite et sperrylite) correspondent à des enrichissments en Ir, Ru, Pt, Pd, Au, Ni et Cu. Ils résultent de la formation d'un liquide sulfuré consécutif à la baisse de fO_2. Dans les gabbros à grenats, des enrichissements en Pt, Pd et Cu traduisent l'action de fluides hydrothermaux tardi-magmatiques. Ces minéralisations diffèrent de celles du Bushveld. La saturation en soufre induite par les processus de cristallisation sous haute pression apparaît le moteur essentiel des dépôts observés dans les webstérites à grenats. De telles minéralisations représentent un exemple type de dépôts de PGE associés aux arcs insulaires.

TABLE OF CONTENT

Page no

TABLE OF CONTENT

Page no

TABLE OF CONTENT

LIST OF FIGURES

LIST OF FIGURES

LIST OF FIGURES

CHAPTER-2

LIST OF FIGURES

LIST OF FIGURES

LIST OF FIGURES

LIST OF FIGURES

LIST OF FIGURES

LIST OF FIGURES

LIST OF FIGURES

LIST OF TABLES

LIST OF TABLES

INTRODUCTION

PLATINUM GROUP ELEMENTS (PGE) AND PLATINUM GROUP MINERALS (PGM) DISTRIBUTION AND PETROLOGICAL EVOLUTION OF SOUTHERN KOHISTAN ARC, NORTHERN PAKISTAN

L'ARC SUD KOHISTAN, N. PAKISTAN: EVOLUTION PETROLOGIQUE ET DISTRIBUTION DES ELEMENTS ET MINERAUX DU GROUPE DU PLATINE.

INTRODUCTION

1-PURPOSE

1-1 Geodynamic Setting and Petrological Evolution of Kohistan Arc

Our knowledge about igneous processes, related to the magmatism primarily at divergent and convergent plate boundaries, is fundamental to an understanding of crustal growth. Although our understanding of these processes remains incomplete, it is clear that basaltic magmas play a fundamental role in transferring both heat and mass from the mantle to the crust. The most significant contribution to the volume of continental crust since the Archean has been the accretion of island arcs along convergent plate boundaries (Miller and Christensen, 1994), but an analogous cross-section of island arc crust (such as ophiolite) has not yet been widely accepted (Conrad and Kay, 1984). Exposed rocks in the arcs themselves reveal little information on the earliest stages of the crystallization of basaltic magmas because the chemical effects of low-pressure crystal fractionation may strongly modify the chemical compositions of magma and obscure the effects of earlier crystal fractionation processes. As sections of oceanic crust, ophiolites potentially contain a wealth of information on the physical and magmatic evolution of mid-ocean ridges (Coleman, 1977).

The Kohistan-Ladakh tectonic province of northern Pakistan is an intriguing place to study a system which includes deep magmatic processes and the overlying lower crustal cumulates. Also exposed, within the Kohistan-Ladakh tectonic province, are the higher-emplaced differentiates of lower crustal magma chambers, and the metamorphic equivalents of these cumulates and their differentiates. Commonly arranged in elongate, arcuate batholithic belts, these rocks are generally interpreted as the products of arc magmatism, formed during episodes of convergence between the Indian and Asian plates (Tahirkheli et al., 1979; Bard et al., 1980; Coward et al., 1982). The resulting terrane preserves an outstanding section from ultramafic underprinnings, at the crust/mantle boundary, to surface

volcanic rocks through the crust of an oceanic island arc. Investigations of how these batholithic rocks formed are fundamental to our understanding of the growth and evolution of northern Pakistan in particular and of continental crust in general.

An important objective, in the study of the Kohistan terrane, is to establish how the chemical and petrological characteristics are related to the tectonic environment in which the system formed. The inference that the batholiths formed at convergent plate boundaries is based on the overall geological setting of the batholiths, the close temporal, spatial and chemical association of their plutonic and volcanic elements, and the compositional similarities of these rocks to those in more well-defined magmatic arcs. However, the nature of the processes and materials involved, and how they have influenced the geometry, petrology and geochemistry of the arc magmas is poorly understood, even in modern arc systems. The relative structural and geochronological simplicity of the southern Kohistan terrane offers an opportunity to examine the systematic petrological and geochemical characteristics of a plutonic belt closely analogous to modern magmatic arcs. More recent investigations of these rocks have revealed some fundamental and remarkable geochemical and petrological regularities of longitudinal trends.

The extended exposure of the Southern Kohistan terrane, and its broad transverse expanse, invites a thorough investigation of how the tranverse asymmetries are related to the formation and evolution of magmatic arcs. In PART-I, using our data and other published information, **we will evaluate the relationships between the different rock units of the Southern Kohistan terrane (Chilas Complex, Kamila Amphibolite Belt and Jijal Complex). The present study will also address the contributions originating from more deeply seated magmatic processes and materials.**

3- PGE's Occurrences

Over the past several years, new quantitative data regarding the distribution of platinum-group elements in ophiolitic, stratiform (sulphide-rich and poor) complexes (Gijbels et al., 1974; Page et al., 1976; Naldrett et al., 1979; Keays et al., 1981; Picard et al., 1995), ultramafic nodules (Mitchell and Keays, 1981), and oceanic basalts (Crocket and Teruta, 1977) have been published. Surprisingly, few ultramafic-mafic rocks or their extrusive equivalents related to arc magmatism have been analyzed for their PGE concentration. The behaviour of PGE+Au during magma generation (e.g. Campbell and Barnes, 1984; Brugmann et al., 1987) and evolution (e.g. Crocket and Chyi, 1972; Hertogen et al., 1980; Crocket, 1981; Keays, 1982; Hamlyn et al., 1985) is poorly understood, complicating interpretation of basaltic PGE data in terms of magma generation at convergence zones. The only consistent picture to emerge from these studies is that PGE distributions appear to be principally controlled by partial melting, which determines the PGE concentrations in the magma and subsequent fractional crystallization (Hertogen et al., 1980) of poorly soluble PGE (Os, Ir, Ru) and more soluble PGE (Rh, Pt, Pd) in basaltic

melts (Amossé et al., 1987). Consequently Ir, Os and Ru tend to be concentrated earlier in the more refractory cumulates (chromite and olivine), whereas Rh, Pt and Pd behave apparently as incompatible elements and are progressively concentrated in the liquid.

The Kohistan terrane has extensive tracts of Late Mesozoic plutonic and volcanic rocks, which are commonly arranged in elongate, arcuate batholithic belts parallel to the Main Karakoram Thrust (MKT) in the north and Main Mantle Thrust (MMT) in the south. This terrane has a number of layered mafic-ultramafic complexes which either contain or have the potential for PGE mineralization. Miller et al. (1991) reported the occurrence of notable enrichments of gold and platinum-group elements (PGE) during the course of their petrochemical reconnaissance within the Jijal Complex. They have reported several zones of ppb to ppm-level precious metal enrichment zones in the Jijal Complex. A more thorough investigation of the PGEs+Au in Jijal, Chilas and Spat Complexes is warranted.

In PART-II of this manusript, we report on whole rock abundance data on PGE+Au concentrations in the ultramafic and mafic rocks of the southern Kohistan and to know the factors controlling PGE's distribution in these rocks.

2- GEOLOGICAL BACKGROUND

Three main tectonic terranes, the Indian plate, the Kohistan-Ladakh arc and the Asian plate, are distinguished in the geological sketch map of northern Pakistan (Fig. 1; Tahirkheli et al., 1979; Coward et al., 1982). These terrane were amalgamated as a result of collision between the Indian and Asian plates. Located between the Main Karakoram Thrust (MKT) to the north and Main Mantle Thrust (MMT) to the south, the Kohistan arc constitutes an important tectonic and lithological element that stretches 200 km E-W between Nanga Parbat and eastern Afghanistan, and N-S, along the Swat river, for about 70 km (Jan and Kempe, 1973). To the east of the Kohistan arc, the MKT and MMT merge to form the Indus-Tsangpo suture, where the Asian plate is thrust over the Indian plate. The arc was developed in the Cretaceous above the northward-subducting Tethyan oceanic plate. It was then accreted to the Asian plate along the MKT about 102-75 Ma (Petterson and Windley, 1985; Treloar et al., 1989). Subduction ceased with the collision between India and Kohistan about 50-40 Ma (Klootwijk et al., 1979; Patriat and Achache, 1984; Treloar et al., 1989). A model for the structural evolution of the Kohistan is given by Coward et al. (1987) in Figure 2. The northeast trending anticlinal syntaxis, Nanga Parbat Haramosh Massif (NPHM), nearly bifurcates the terrane where rapid uplift and deep erosion have exposed the underthrusting Indian plate. The Ladakh part of the arc lies to the east of the NPHM, and the Kohistan part lies to the west of it.

The following main lithologic units of the Kohistan terrane, listed from the MKT in the north to the MMT in the south, have been recognized by researchers from Pakistan,

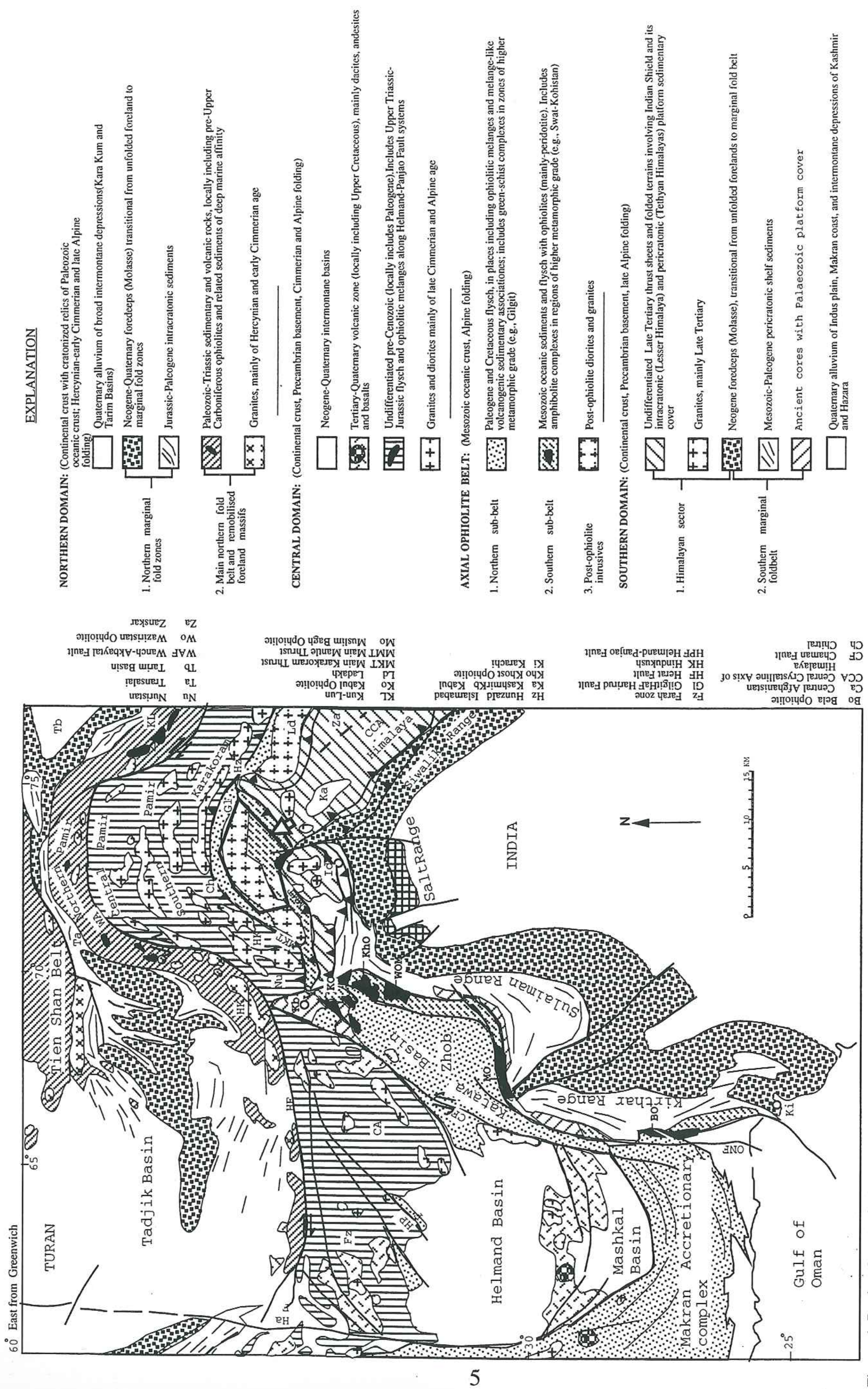

Figure. 1. Regional geological and tectonic map showing the position of Asian plate, Kohistan arc and Indian plate. (modified after Stocklin, 1977).The study area (arrow) is located in the upper right of the map.

Carte régionale géologique et tectonique montrant la position des plaques Indienne et Asiatique, et de l'arc du Kohistan (modifié d'après Stocklin, 1977). L'aire d'étude (fléche) est située dans la partie sud de l'arc du Kohistan

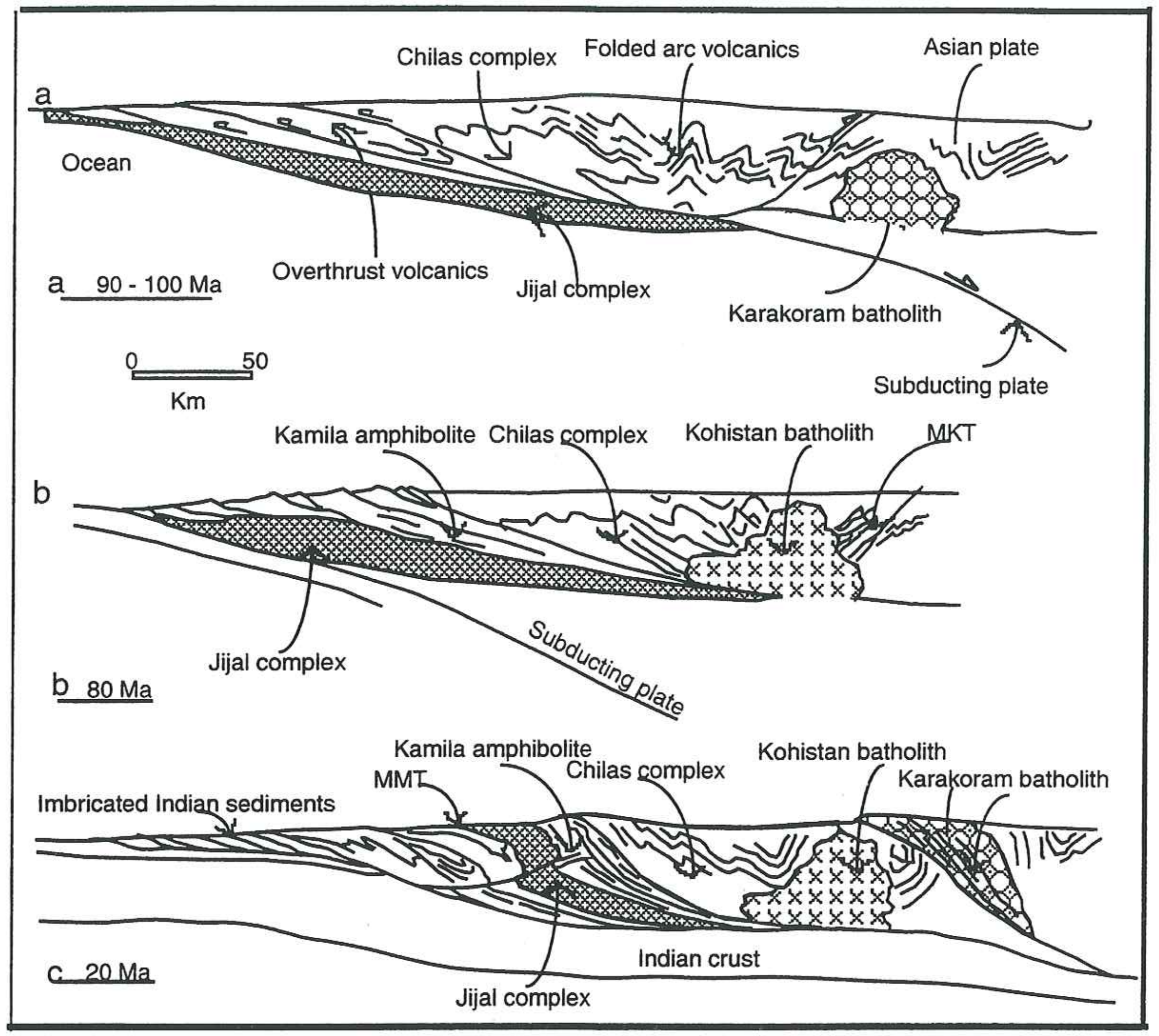

Figure 2. A model for the tectonic evolution of the Kohistan arc (based on structural data from Coward et al., 1986, 1987; Treloar et al., 1989; and radiometric age data from Petterson and Windley, 1985

Un modèle d'évolution tectonique de l'arc du Kohistan (établi d'après les données structurales de Coward et al., 1986,1987; Treloar et al., 1989; et les âges radiométriques de Petterson et Windley, 1985)

France, United States and United Kingdom (Tahirkheli et al., 1979; Bard et al., 1980; Jan and Howie 1981; Coward et al., 1982; Loucks et al., 1990; Treloar et al., 1989, 1996; Fig. 3):

1) The Yasin Group
2) The Chalt Volcanics
3)The Kohistan Batholith
4) The Chilas Complex
5) The Kamila Amphibolite Belt
6) The Jijal Ultramafic-Mafic Complex

The MKT is marked by mylonites, greenschists and ophiolitic serpentinites. South of the MKT is **the Yasin Group** which comprises volcanics, turbidites and limestones. These units are metamorphosed to slate, phyllite, schist, quartzite, semi- to medium-crystalline marble and meta-conglomerate. Pre- to post-kinematic magmatic intrusions of felsic and mafic igneous rocks are quite common (Tahirkheli, 1979). These rocks are believed to have formed in an intra-arc basin (Pudsey et al., 1986) and contain fossils of Early to Middle Cretaceous age (Ivanac, et al., 1956). In many places, the lower part of the Yasin Group contains interbedded volcanic flows of possible Chalt Group affinity.

The Chalt Volcanics lie to the south of the Yasin Group and are Cretaceous in age, possibly Late Early Cretaceous, if the Yasin Group is stratigraphically above the Chalt Volcanics (Tahirkheli, 1979). The vertically standing, Cretaceous Chalt Volcanics strike approximately east-west. The maximum thickness of this group is recorded in the Hunza Valley where it is between 3000 and 4000 m and gradually thins towards east and west (Tahirkheli, 1979). A wide range of lithologies has been found in this volcanic complex. Directly south of the Yasin Group, the Chalt Volcanics form a small upright syncline, possibly related to the Jaglot syncline and Gilgit anticline of Coward et al. (1982) and T. Khan et al. (1997), which lie further south. On the southern limb of this syncline, graywackes and shales are exposed. These rocks overlie epidote-bearing grits and hornblende-bearing tuffs which pass down into epidote-bearing tuffs, chlorite-schist and schistose amphibolite- an inceasingly volcanogenic succession. Farther to the south, lie amygdaloidal basalt, fragmental basic volcanic material, repetitions of volcanogenic sediment, mafic schist and thick piles of deformed amygdaloidal pillow lava (Coward et al., 1982). The mafic rocks are cut by thin granitic dikes and pegmatites, discordant to both cleavage and bedding. The flows are basalt, andesite, dacite and rhyolite. The deformation in the pillows shows a progressive increase towards the north.

The Yasin Group and Chalt Volcanics are intruded by numerous large to small scale gabbroic to granitic plutons called **the Kohistan Batholith**. According to Coward et al. (1982), Petterson and Windley (1985), and Treloar et al. (1989), the Kohistan Batholith is

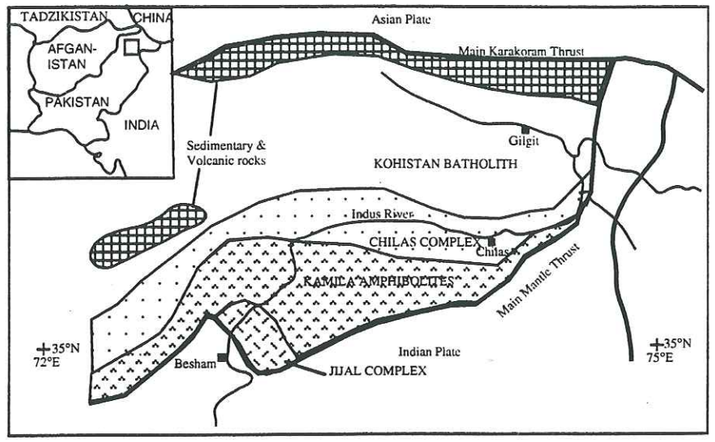

Figure 3. Simplified geologic map of the Kohistan arc. Taken from Coward et al. (1980, 1986); Yamamoto (1993).

Carte géologique simplifiée de l'arc du Kohistan. D'après Coward et al. (1980), 1986; Yamamoto (1993).

divisible into three temporal units. The oldest time unit consists of early deformed plutons, which are bimodal in composition and comprise low- to high-K phases. The plutons generally have a moderate gneissic fabric composed of alternating hornblende-biotite layers and felsic layers. Deformation is thought to have occurred before 80 Ma when the Kohistan arc collided with the Asian plate to the north. Radiometric dates (K-Ar, Ar-Ar) obtained from these deformed intrusions range from 102 to 80 Ma (Coward et al., 1982; Petterson and Windley, 1985; Debon et al., 1987; Treloar et al., 1989) and may represent ages of metamorphism rather than plutonism. The ages are consistent with the suggestion of Honegger et al. (1982) and Dietrich et al. (1983), based upon work in Ladakh, east of Nanga Parbat (Fig. 2), that the arc evolved during Late Jurassic and Cretaceous time. According to Petterson and Windley (1985), the Matum-Das pluton has a Rb-Sr isochron date of 102 ± 12 Ma and formed during the mature stage of development of the island arc. This age is close to the Aptian/Albian faunal age of the intra-arc basin sediment of the Yasin Group (Pudsey et al., 1985).

The second temporal unit consists of undeformed plutons, which cut the structures in the Rakaposhi volcanics, meta-sedimentary rocks and the deformed plutons. The main mineral phases are hornblende, plagioclase, biotite, quartz and alkali-feldspar with accessory magnetite, zircon, apatite and sphene. Radiometric dates for these undeformed plutons, at the northern margin of the batholith, range between 54 and 40 Ma (Petterson and Windley, 1985; Debon et al., 1987; Treloar et al., 1989). Honegger et al. (1982) report a Rb/Sr whole rock isochron date of 60 ± 10 Ma from similar intrusions in the Ladakh area. These plutons were emplaced after the marginal basin to the north had closed and the Kohistan arc had collided with the Eurasian plate to form the MKT. Plutonism emplacement continued until shortly after subduction ceased, following the collision between the Indian plate and the Eurasian-Kohistan plate along the MMT (Petterson and Windley, 1985).

Finally, a third stage of magmatism evolved when aplite-pegmatite dikes of leucogranitic composition were intruded. Cross-cutting relationships show that these sheets represent the last satge of magmatism of the batholith. According to Petterson and Windley (1985), radiometric dates (whole rock Rb-Sr) of this third stage range from 34 to 29 Ma. These plutonic rocks were probably the product of crustal melting, which occurred after the terminal collision between the Indian and Asian-Kohistan plates.

The Kohistan Batholith appears to grade downwards into **the Chilas Igneous Complex** which extends for more than 300 km between Nanga Parbat and western Dir and attains a maximum thickness of 50 km (Fig. 3). The Chilas Complex is a huge basic intrusion which occupies the core of the Kohistan terrane and is composed principally of gabbronorite and pyroxene diorite (**the Main Facies Zone**) with several small masses of mafic-ultramafic rocks, such as anorthosite, troctolite, layered gabbro, minor local pyroxene-bearing pegmatite (the ultramafic-mafic-anorthosite association(UMAA); Jan et al., 1984; Khan et al., 1989; Takahashi et al., 1996). There are two major ultramafic-mafic

masses exposed within the core of the complex: 1) east of Chilas, and, 2) the Thurli Complex, at the mouth of Thurli Gah. Both measure >5 km^2 in area. The ultramafic masses display excellent layering and other depositional features such as graded bedding, slump breccias and syn-depositional faults (Shams, 1975; Jan et al., 1984; Khan et al., 1985; Takahashi et al., 1996).

Khan et al. (1989) have suggested the UMA not to be ophiolitic and that the rocks have similarities with plutonic blocks from island arcs and other major mafic complexes such as the Border Ranges Complex of Alaska and those from the Ivrea Zone in the Alps. Trace and REE data suggest that the Chilas Complex either represents the root zone magma chamber of the Kohistan arc, or magma generated by diapirism in the early stages of intra-arc rifting during formation of a back-arc basin. Petrologically and geochemically, this complex resembles the Kargil complex in Ladakh (Rai and Pande, 1983). The latter is regarded, by Honegger et al. (1982) as representing the cumulates of the magma chamber of the Dras volcanics.

The rock assemblages of the Chilas Complex are moderately deformed, exhibiting foliation and ductile shear zones at places. Approximately, east-west trending antiforms and synforms are observed, indicating a folded structure in the Chilas Complex. Coward et al. (1982) have also indicated that the Chilas Complex is folded into a large asymmetric antiform with an upright to steeply north dipping cleavage parallel to the axial plane of the folds. Structural reconstructions indicate that the complex would lie near the base of the Kohistan arc sequence (Coward et al., 1987). Jan (1980), Jan and Howie (1981) and Bard (1983) indicate that the Chilas Complex was cooled and equilibrated under conditions of the pyroxene granulit facies, estimated at 750° to 850° C and 5 to 6.5 kbar.

South of the Chilas Complex is a belt of mafic to silicic intrusive rocks, metamorphosed volcanic rocks and metamorphosed sediments that have been all grouped into a single unit called **the Kamila Amphibolite Belt**, or alternatively the Kamila Shear Zone. Jan (1988) and Treloar et al. (1990) have identified two types of amphibolites within this zone: 1) fine- to medium-grained amphibolites which are either homogenous or banded, and are thought to be metamorphosed mafic to intermediate volcanics, and, 2) homogeneous, medium- to coarse-grained amphibolite that are considered to be derived from intrusive gabbros, gabbronorites and diorites. Many of the Kamila Amphibolites have been strongly sheared resulting in the obliteration of contact relations between the metavolcanic lithologies and intrusives. The metavolcanic and plutonic lithologies can, however, be identified on the basis of their relict structures. Relict structures, such as pillow lavas indicative of their submarine character, are missing in the fine-grained homogeneous amphibolites in the Indus Valley. On the basis of a traverse along the Swat Valley, Treloar et al. (1996) argued that pillow lavas are present at Chupral and at Metta Quarry, where there is a lit-par-lit intrusion of gabbro into basaltic layers. But Miller et al. (1991) argued that the

Kamila Amphibolite Belt consisted entirely of plutonic material accreted to the base of an evolving arc.

Jan (1988) suggested that the Kamila Amphibolite Belt is a highly deformed belt of arc-type plutons, metasediments, and basic volcanics of typical arc-type chemistry. Coward et al. (1986) propose that these amphibolites are a deformed arc sequence, although with possible relics of ocean floor material. Treloar et al. (1990) interpret the Kamila Shear Zone as the downfold equivalents of the Chalt supracrustal sequence, to the north, that have been overthickened by thrust faulting or as a suture formed by southward thrusting of the main island arc (Chilas Complex) over its fore arc region on the premise that the Chilas and Jijal Complexes are components of separate island arc complexes. As such, controversy still exists in the literature regarding the protolith and tectonic affinity of the Kamila Amphibolite Belt.

South of the Kamila Amphibolite Belt is the **Jijal Ultramafic-Mafic Complex**. This complex is a tectonic wedge which covers approximately 150 km^2. It is bounded to the south by the MMT (Fig. 3)that is marked in places by a melange of blueschists, greenschists, piedmontite schists and serpentinites. It has been described in detail by Jan (1979), Jan and Howie (1981), Yamamoto (1993) and Yamamoto and Nakamura (1996). The complex is composed of garnet-bearing granulites and ultramafic rocks. The garnet granulites are further classified as plagioclase-free rocks called garnet pyroxenite and plagioclase-bearing rocks called garnet gabbro. Ultramafic rocks occupy the southern part of the complex just north of the MMT, and are composed of dunite, diopsidite, harzburgite and websterite.

According to Jan and Howie (1981), the ultramafic rocks were carried tectonically, into their present position after equilibrium, under granulite-facies conditions (800-850°C, 8-12 kbar). The ultramafic rocks were metamorphosed indepently to the garnet granulite and are magmatically unrelated. It is unclear whether the ultramafic rocks represent dismembered arc cumulates, a faulted slab of oceanic crust-upper mantle, or a mantle diapir in a deep orogenic root. Jan and Windley (1990) suggest that the ultramafic rocks are cumulates, related to a primitive arc tholeiitic magma, whereas the granulites are derived from the more evolved (calc-alkaline) magma. The two suites may represent a continuous sequence of cumulates, where the granulites formed from an evolved liquid after the separation of large quantities of magnesian olivine and pyroxenes. Alternatively, the two groups may have formed from independent batches of arc-related magmas.

The Spat Complex along with Jijal Complex form a closely-spaced group of mafic-ultramafic rocks to the south of Kohistan island arc. The Spat Complex is about 30 km east of the Jijal Complex and extends NE-SW, immediately to the north of the MMT (Fig. 3). The better studied part of the complex occupies over 13 km^2 and occurs along the drainage divide between the Kaghan Valley and Kohistan. This complex may be subdivided into a lower ultramafic sequence and on overlying gabbroic sequence. The ultramafic rocks are

predominantly dunite. A NE-SW striking fault separates the gabroic rocks from the lower ultramafic sequence.

The ultramafic rocks of Spat Complex consist of two units; dunite at the base and olivine clinopyroxenite with interspersed dunite layers in the upper unit. The lower part of the dunite is strongly sheared and serpentinized and this phenomenon is also frequent in the upper part of this unit. Near the zone between dunite and olivine clinopyroxenite, very thin layers (mm to cm scale) of clinopyroxenite are present in the dunite.

The gabbroic rocks are well-layered to homogeneous and mainly composed of plagioclase, clinopyroxene, orthopyroxene and hornblende. The geology and mineral chemistry of the Spat complex has been described by Jan et al. (1993) and they interpret this complex as a basal complex related to Kohistan arc magmatism. The Jijal- and the Spat Complexes are cumulate to early arc tholeiitic magmas (Jan and Windley, 1990), implying that they cannot be equated with the Chilas Complex.

Despite the growing conviction that the southern Kohistan represents a well-documented and well-understood province, the available data are very much biased towards solving their genetic problems and their relationship to the tectonic environment in which the system formed. The range in chemical compositions throughout the southern Kohistan arc presents petrogenetic problems that have yet to be solved.

3- OBJECTIVE AND PLAN OF THIS PROJECT

One interesting aspect of the Kohistan arc is the apparent absence of oceanic basement whereupon the arc was initially built. Tahirkheli et al. (1979), Bard et al. (1980) and Bard (1983) considered the Kamila Amphibolite Belt, which envelops the Jijal and Chilas Spat Complexes, as the oceanic basement of the Kohistan arc. Recent work however shows that the Kamila Amphibolite Belt has a distinct island arc trace-element signature. Treloar et al. (1990, 1996) claim that fine- to medium-grained amphibolites are metamorphosed volcanics and represent remnants of a pre-arc oceanic crust that formed entirely within an intra-oceanic setting. In contrast, homogeneous medium- to coarse-grained amphibolites are metamorphosed gabbros and diorites and have geochemical characteristics compatible with a subduction related origin. Further, they interpret these amphibolites as the earliest, most primitive arc-related magmatic rocks within Kohistan, while Miller et al. (1991) interpret them as predominantly metaplutonics. The real bebate now centers on distinguishing between the two-types of amphibolites and their tectonic environment of formation.

The lithology of the Kamila Amphibolite Belt appears to be essentially continuous without major tectonic breaks from the Chilas Complex at least as far south as 4 km north of Kamila town. However, there is a tectonic break between the Kamila Amphibolite and the Jijal Complex (Fig. 3).

The relationship between the ultramafic and garnet granulite of Jijal Complex is unresolved. Jan and Windley (1990) suggest that either the garnet granulites constitute a continuous sequence of arc cumulates with the principal ultramafic mass, or the two are produced from a different source magma. Unsurprisingly, detailed investigations of each type is still required to elucidate with any degree of certainity their geological evolution. Understanding the origin of these complexes is pertinent to the magmatic evolution of island arcs in general and specifically in Kohistan.

With the objective of investigating, quantitatively, the geochemical variations in the Chilas Complex, Kamila Amphibolite Belt, the Jijal Complex and their source region, this project was initiated to obtain a new and more complete sample suite. Our goal is to evaluate the relationships between the different rock units and test a variety of hypotheses about the mechanism of magma generation and possible connections between plutonism and tectonic environments.

Occurrences of platinum-group elements (PGE) and sulphides with platinum-group minerals (PGM), that form an integral part of obducted oceanic island arc complexes represent a somewhat neglected target in prospecting for new PGE resources. However, during the past few years a growing body of data has shown that PGE occurrences in this tectonic environment (e.g. in the Nowegian Caledonides; the Shetland Islands, United Kingdom; Newfoundland, Canada; and Oregon, USA;) should not be entirely ignored. Todate occurrences that have been found are sub-economic, but are interesting because they concentrate a relatively large range of metals, including Pt, Pd, Cu, Ni, and, sometimes, Au.

Keeping the above observations in mind, the present study attempts to describe the distribution of platinum-group elements across the Jijal, Chilas and Spat Complexes and aims to determine the physico-chemical conditions that gave rise to local geochemical enrichments during magma crystallization.

4- MAIN AIMS OF THIS PROJECT

PART-I:

-to examine the field relationships and to present new major, trace and REE element analyses from areas in the southern Kohistan arc; to investigate, quantitatively, the petrogenetic relationships between the different complexes, in an attempt to offer an integrated model for their geochemical evolution.

-to investigate the mineral phase chemistry of the Jijal Complex as it was formed under high-temperature and pressure compared to the Chilas Complex.

PART-II:

to present new whole rock abundance data on PGE in Chilas, Spat and Jijal Complexes; to locate sulphide phase mineralogy and platinum-group minerals within the whole sequence of the Jijal Complex and to determine their textural relationship and chemical compositions; to discuss PGE's and PGM's distribution and fractionation trends and then to examine their petrogenetic and economic implications.

PART-I

PETROLOGICAL EVOLUTION OF SOUTHERN KOHISTAN ARC

INTRODUCTION

The Kohistan crustal growth can be classified into an initial immature intra-oceanic island arc stage, which developed into a mature intra-oceanic island arc and from then on to an Andean-type stage (Petterson and Windley, 1985).

The formation of the intra-oceanic stage began in Early Cretaceous time (Yasin Group carbonates of Aptian-Albian age; Pudsey, 1986, and their underlying Chalt Volcanics) and lasted sometimes between 102 and 85 Ma, when Kohistan collided with the Karakorum (Asia) across the MKT (Treloar et al., 1996). This stage is represented by lithologies such as ultramafic-mafic bulk composition, presence of pillowed lavas and marine sediments, low-K nature of associated felsic rocks, absence of continental crust or detritus (Khan et al., 1997).

The intra-oceanic arc crust is represented in the southern Kohistan terrane by the Jijal Ultramafic-Mafic Complex along with Spat Ultramafic-Mafic Complex, the Kamila Amphibolite Belt and the Chilas Complex of ultramafic-mafic to intermediate compositions (Fig. 4). It is also represented in the northern Kohistan by deformed stage-1 plutons of Kohistan Batholith (Petterson and Windley, 1985) and Gilgit Gneisses; and by the Chalt Volcanics (Khan et al., 1993). The latter magmatism in the Andean-type continental margin stage is represented by intermediate to felsic rock compositions. Much of the stage-2 plutons of the Kohistan Batholith (Petterson and Windley, 1985) and Dir Volcanic Group developed during the latter stage. This part is mainly focussed on the petrological and geodynamic evolution of the southern Kohistan arc as it is recorded in the Kamila, Chilas and Jijal suites.

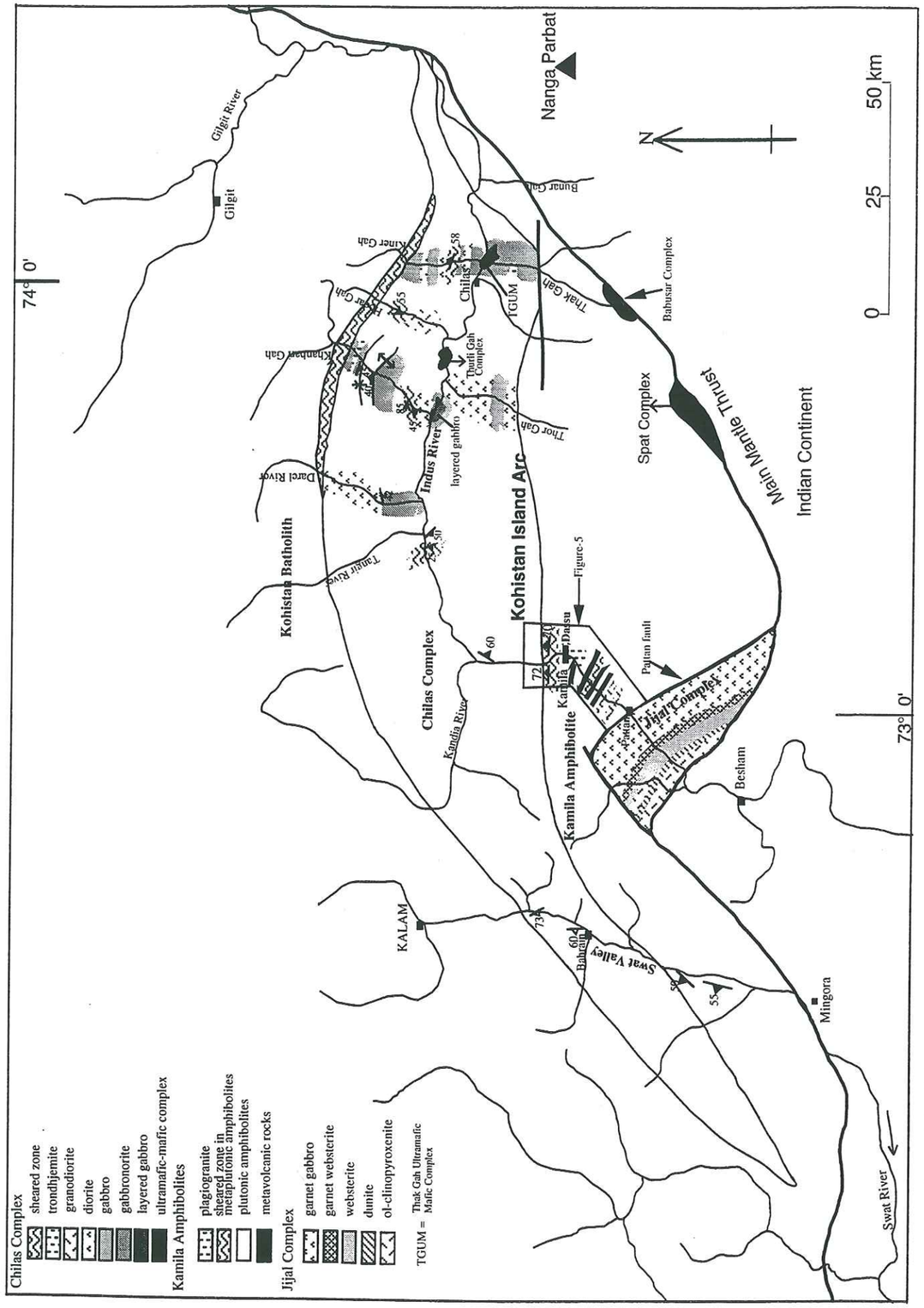

Figure 4. Map of part of the Jijal Complex, Kamila Amphibolites and Chilas Igneous Complex, Kohistan arc, northern Pakistan.
Carte géologique d'une partie du complexe Jijal de Chilas, des amphibolites de Kamila et du Complexe de Jijal, arc de Kohistan, Nord Pakistan.

CHAPTER-I

THE KAMILA AMPHIBOLITE BELT

1- GENERAL FEATURES

The main sequence of the amphibolites in the southern Kohistan is in the form of a linear belt and occupies position between the Chilas Complex in the north and Pattan fault and MMT in the south (Fig. 3). The type locality is in the Indus Valley to the south of the village Kamila in the Kohistan district (Figs. 3 & 4). Several names have been used for these amphibolites in the literature such as the Kamila Amphibolite Belt (Jan, 1979, 1988; Tahirkheli and Jan, 1979), and the Southern Amphibolites (Bard et al., 1980; Bard et al., 1983). It is generally considered that these amphibolites are continuous both to the east and west of the Indus Valley forming the southern margin of the arc, with local occurrences of ultramafic-mafic rocks such as the Jijal Complex (Jan and Howie, 1981, 1990), the Babusar Ultramafics (Ahmed and Choudhary, 1976) and the Spat Ultramafic-Mafic Complex (Jan et al., 1993; Figs. 3 &4).

The Kamila Amphibolite Belt is a composite body, predominantly consisting of amphibolites, with subordinate hornblendites, hornblende gneisses, diorites, gabbros, plagiogranites and minor metasediments (Fig. 5). Coward et al. (1987) showed the possibility that the part of the Kohistan arc to the south of the Chilas Complex may represent remanants of the earliest separate island arc which is now accreted to the northern Kohistan at the site of the Kamila Shear Zone. Geochemically, these amphibolites are interpreted as calc-alkaline in character (Jan, 1988).

Shams (1975), Ahmed and Chaudhary (1976) and Khan and Thirwall (1988) have recognized two types of amphibolites in the valleys between the MMT and eastern part of the Chilas Complex, south of Chilas (Fig. 4). The first-type of these amphibolites is situated at the southern margin of the Chilas Complex and is termed as the Jal Shear Zone (Coward et al., 1987; Khan and Thirwall, 1988). This is considered to be an equivalent of the Kamila Shear Zone of Treloar et al. (1990). The second type of amphibolite is in the Thak-Babusar valley in SE Kohistan and lies in the hanging wall of the MMT. The two amphibolite belts in this part of the Kohistan arc are intruded by small pluton of granite, a situation which is different from the Swat Valley section. In the Indus Valley near Dassu, plagiogranite also intrudes these amphibolites.

The metagabbros and metadiorites are deformed by numerous anastomosing shear zones with variable spacing and size. Such features are more frequent in the southern part of the Kamila Amphibolite Belt (Fig. 6). These shear zones are characterized by centimetre scale discontinuous to decametre anastomosing pattern of mylonitic shear zones, wrapping around lenses of less deformed gabbros and diorites and marked reduction in grain size (Fig. 6B). The anastomosing shear zones contain leucocratic, garnet-bearing veins (Fig. 6A) due to partial

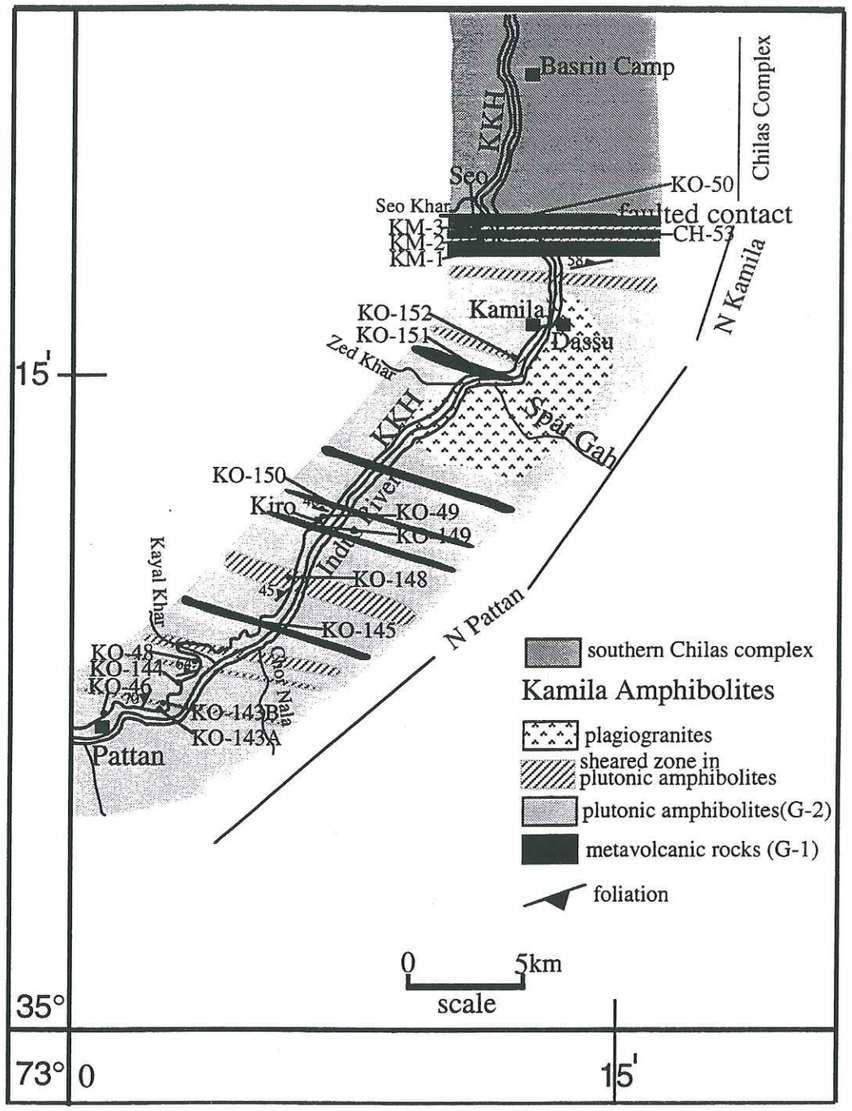

Figure 5. Geological map of part of the Kamila Amphibolite Belt, showing the spatial distribution of metaplutonic, sheared zone and metavolcanic facies rocks along the Karakoram Highway.

Carte géologique d'une partie de la ceinture amphibolitique de Kamila, montrant la distribution spatiale des faciès de zone de cisaillement, des métaplutonites et métavolcanites le long de la Karakoram Highway

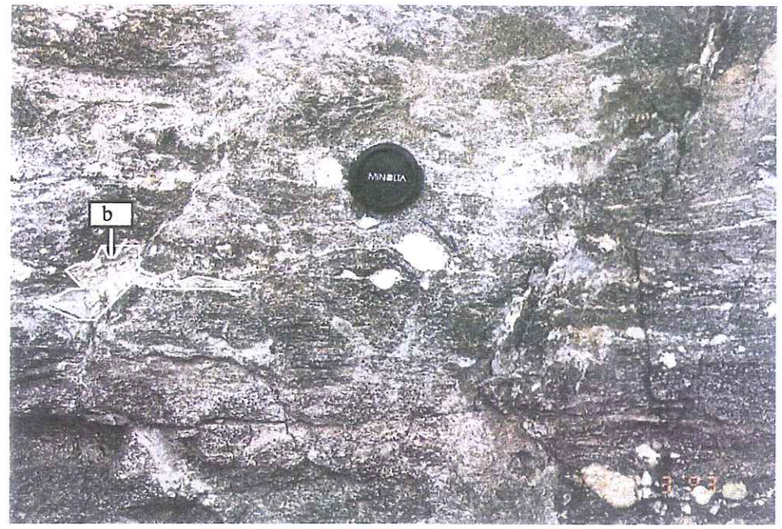

Figure 6A . Photograph showing the sheared zone, having felsic partial melt (b) with garn in the Kamila Amphibolites, 10 km north of Pattan along the KKH.

Photographie de la zone de cisaillement dans les amphibolites de Kamila, 10km a nord de Pattan, le long de la KKH, présentant .

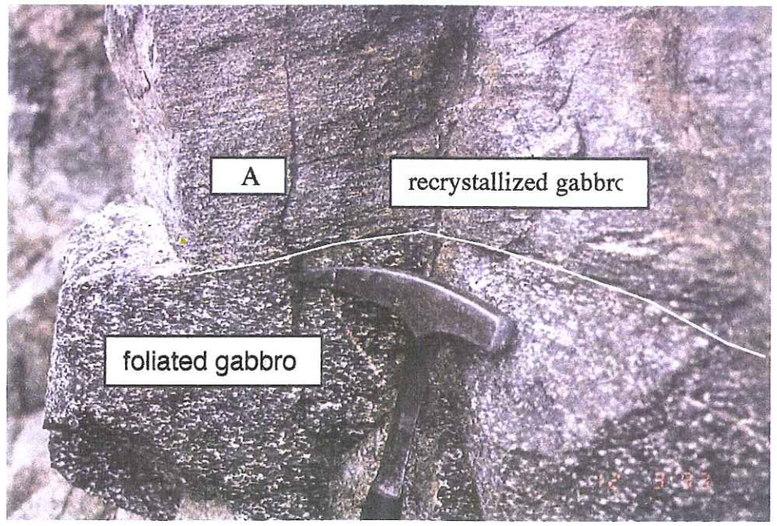

Figure 6B. Photograph of sheared zone in Kamila Amphibolites, 6 km north of Pattan along the KKH. Note that the metaplutonic rocks are recrystallized (A).

Photographie de la zone de cisaillement dans les amphibolites de Kamila, 6km au nord de Pattan, le long de la KKH. Noter que les roches métaplutoniques sont recristalisées

melting of the mylonites which, therefore, are high temperature shear zones (Arbaret et al., 1998). Such type of shear zones are also encountered in garnet gabbro, southwest of Pattan.

More in detail, two textural varieties of the Amphibolite are recognized and the relative abundance of these two varieties is variable along the strike. The part of the Kamila Amphibolite Belt exposed in the valley, to the south of Chilas, is exclusively composed of volcanogenic material (Khan, 1988), while westward in the Indus Valleys, the amphibolite belt is composed of sheared fine-grained amphibolites (with volcanic origin) which are intruded by abundant metamorphosed basic to intermediate plutonic rocks (Fig. 5). In Swat valley near Metta Quarry, Treloar et al. (1996) have also described a lit-par-lit intrusion of gabbro into basaltic layer.

In short, three facies appear to constitute the Kamila Amphibolites; 1) early fine-grained metavolcanics metamorphosed to amphibolite facies; 2) intrusive metagabbro and metadiorite; 3) plagiogranite which is intrusive into the Kamila Amphibolites.

The present study concentrates on the Kamila volcanic and mafic plutonic suites exposed in the Swat and Indus Valleys. Geochemistry of these rocks will be used to constrain their tectonic affinity for interpreting the geodynamic environment of southern Kohistan and particularly its relationship with the Chilas Complex to the north and Jijal Complex to the south.

2. PETROGRAPHIC CHARACTERISTICS

Metagabbros and metadiorites of the Kamila Amphibolites (exposed in the Swat Valley as well as along KKH between Pattan and Dassu), are mineralogically similar and are dominated by hornblende and plagioclase but at some places minor amount of relictual orthopyroxene and clinopyroxene are also preserved in the core of hornblende indicating retrograde hydration. These minerals are 0.3 mm to 1.5 mm in length and about 1.0 mm in width. The amphibole is bluish green, green or brownish green but, in some localities, it is light green or distinctly brown. Some amphiboles are sieved and contain abundant inclusions of quartz, less frequently rutile and some opaques. In some thin sections, hornblende and biotite form aggregates of fine crystals exhibiting a decussate texture. All hornblendes in the amphibolites are not of magmatic origin; probably they were formed by a reaction of Opx+Cpx+Pl+ fluid. Late biotite, quartz, epidote, rutile, chlorite, ± garnet and rare zircon are also found and these are presumably formed by the low-grade regional metamorphism or deuteric hydrothermal alteration during the later stage of their emplacement. Optical determinations suggest that plagioclase compositions range from An_{40} to An_{50}, but not so exact because these minerals have been altered more or less. Plagioclase may also be partly or totally replaced by epidote-albite-quartz (saussuritization). Opaque minerals are common in minor amounts, and interstitial quartz is also present. In some rocks, the original igneous texture is generally replaced by later deformation. All these rocks were locally affected by the generation of lowgrade metamorphic minerals such as chlorite, epidote, actinolitic hornblende,

sericite, and titanite. This low-grade overprint is never penetrative. It is always bound to joints or limited to certain minerals such as saussuritized plagioclase. In the less deformed rocks, thin sections textures are generally intergrowths of plagioclase and hornblende but poikilitic texture is also present. Pyroxene inclusions in amphibole suggest that many of the hornblende gabbros were originally two-pyroxene-bearing gabbroic rocks containing little hornblende.

Hornblendite occurs as thin and lensoid bodies in medium- to coarse-grained metagabbro, with somewhat xenolithic appearance. It is composed almost entirely of bluish green and brown hornblende, with or without a small amount of clinopyroxene and saussuritized plagioclase.

3- WHOLE ROCK GEOCHEMISTRY

3-1. Sample selection and analytical procedure

Twenty four samples from the Kamila Amphibolite Belt were selected for major and trace elements analyses. The studied rock assemblages of the Kamila Amphibolite Belt are from: "**N Pattan (NP)**"; between Pattan and Dassu, along KKH, "**N Kamila (NK)**"; from north of Kamila town to Seo, along KKH and "**Swat Valley (SV)**"; from the Swat Valley region (Fig. 4). The samples included six from north of Dassu (KM-2,KM-3, CH-50, CH-53 CH-51B-dike), thirteen samples along Karakoram Highway (KKH) in between Pattan and Dassu (KO-46, KO-48, KO-49, KO-143A, KO-143B, 143C, KO-143C, KO-145, KO-148, KO-149, KO-150, KO-151, KO-152), and four samples from Swat Valley (SW-16, SW-23B, KO-134A and 134B-dike). Sample locations for the analyzed samples are shown in Figures 5 and 7.

Selection of these samples was made on the basis of field and petrography study to maximize freshness in outcrop, as well as geographic and lithological coverage of the Kamila Amphibolite Belt. Loss on ignition (LOI) usually is between 0.20 and 2.50 wt.%. LOI was determined by heating samples to 1000°C for 1 hour. Although only dense rock chips free of weathered surfaces were analyzed, alteration is common so that alkali and alkaline earth concentrations only approximate original values.

Major and trace element contents of whole rocks were determined by XRF using RIGAKU XRF-3370E in Geoscience Laboratory, GSP, Islamabad, Pakistan. Whole rock samples for geochemical analysis were crushed in an agate swing mill. Major element compositions were determined on glass fusion disks (Fundamental Parametre Method) and trace elements were determined using powder pellet (Empirical Method). Analytical precision was controlled by standard samples and duplicate measurements. All analyses were undertaken using uniform calibration conditions and are reported in diagrammes on a 100%, volatile-free basis. Some duplicate analyses indicate precision better than two per cent for SiO_2, TiO_2,

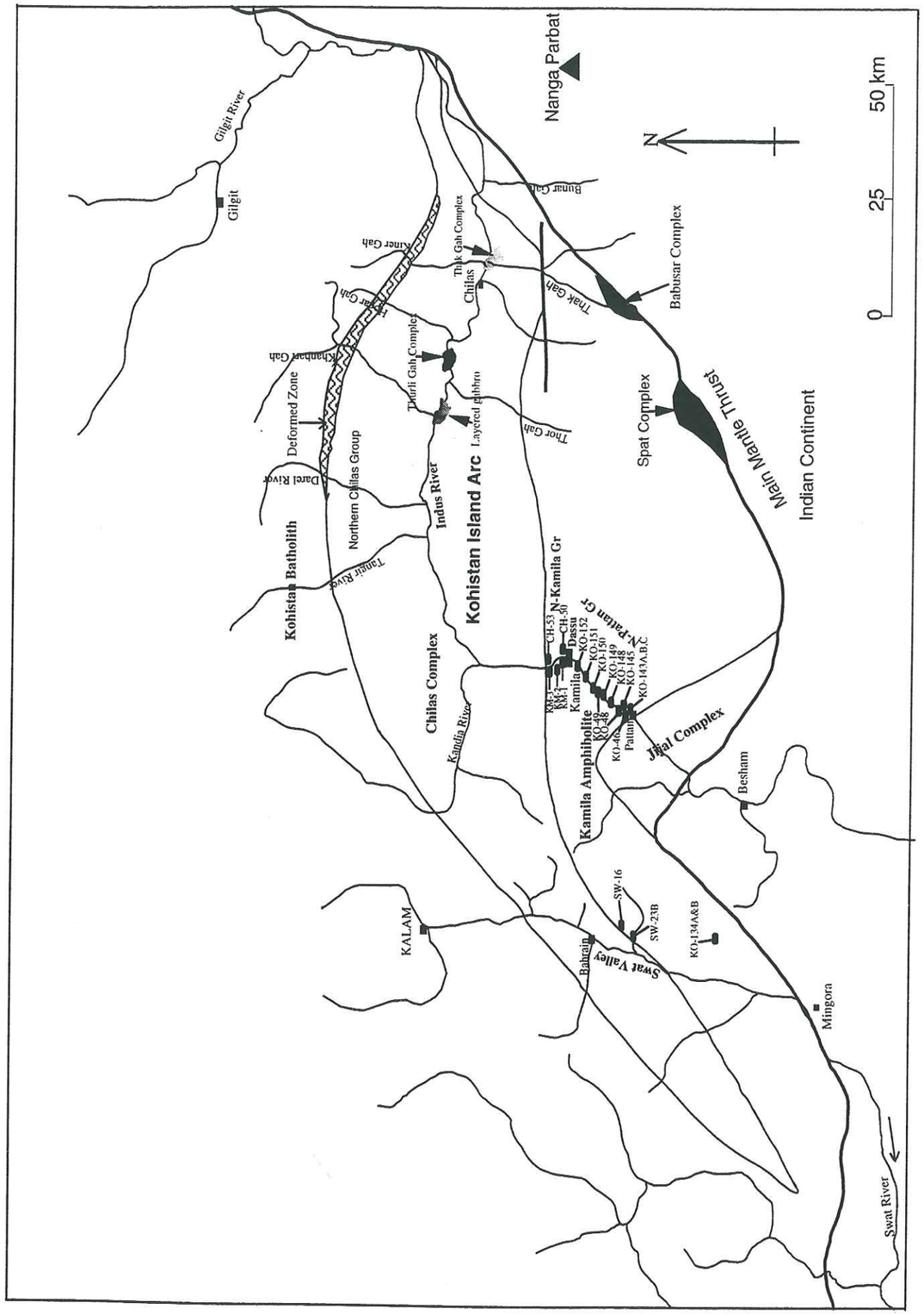

Figure 7. Sample location map of the Kamila Amphibolites , Kohistan arc, northern Pakistan.
Carte de localisation des échantillons dans les amphibolites de Kamila, arc du Kohisten, Nord Pakistan.

Fe_2O_3, MgO, CaO, Na_2O, K_2O, Rb, Sr, Zr, Sc; five per cent for Cr, Co, Ce and Nb; ten per cent for MnO, P_2O_5 and Ba. Major and trace element data are given in Table 1.

Rare earth elements (REE), Rb, Sr, Ba, Y, Zr, Nb, Cs, Ta, Th, U and Hf from selected samples were analysed by Inductively Coupled Plasma Mass Spectrometry (ICP-MS) in the " laboratoire de Geodynamique des Chaînes Alpines (LGCA-ESA5025) ", University Joseph Fourier, Grenoble, France, following procedure of Barrat et al. (1996). The precision of the technique is better than 5% for all the REE and trace elements. In some cases, some imprecisions occur on Zr and Hf elements due to formation of some chemical complexes with these elements in solutions. Systematics controls have been effected and if there is any problem, Zr values from XRF analyses have been retained but Hf values can be rejected.

3-2. Chemical mobility

The problem of chemical mobility is common to metamorphosed rocks in general, and may be especially relevant in the case of the Kamila Amphibolites particularly north of Dassu, where metamorphism to the high-amphibolite grade has taken place. The elements which are considered to be incompatible elements like Zr, Ti, P, Y, Nb and Ta are relatively immobile during alteration and metamorphism (Winchester and Floyd, 1977; Wood et al., 1981; Shervais, 1982) and should display systematic variations in a suite of cogenetic samples. Disruption of elements pair correlations may result from the preferential mobility of one element. However, Hellman and Henderson (1977) and Hellman et al. (1979) have suggested that under some metamorphic conditions, even Ti and the REEs would be mobile. They caution that Ti and REEs should not be indiscriminantly used to describe the igneous evolution of low-grade metamorphic rocks. It seems that the best approach is to show, for individual areas, that elements are indeed immobile. There is no doubt that in the rocks of the Kamila Amphibolite particularly from north of Dassu, the abundances of major elements, such as Ca, Al, K and Na, and trace elements, like Sr and Ba, have been affected by metamorphism as for lagre-ion-lithophile (LIL) we can see in Figure 8.

3-2. Major oxides behaviour

According to field and petrographic characteristics, the rock assemblages of both **N Pattan** (NP) and **N Kamila** (NK) are classified into '**fine-grained metavolcanics; referred herein as Group-1**' ; and '**coarse-grained plutonic rocks (gabbros and diorites); referred herein as Group-2**'. For example, samples KO-145, KO-149, KO-150 and KO-152 from 'N Pattan' and sample KO-50 from N-Kamila (Fig. 5) represent fine-grained metavolcanics related to Group-1.

Table 1. Major, trace and rare earth element analytical data from the Kamila Amphibolites. Major elements are recalculated to 100% without LOI.
Données analytiques pour les terres rares et les éléments majeurs et en trace des Amphibolites de Kamila.

S.No.	KO-145	KO-148	KO-149	KO-150	KO-151	KO-46 Pattan	KO-143A	KO-143B	KO-143C	KO-144	Ko-48 Pattan	Ko-49 Pattan
Name	metavolcanics	metavolcanics	metavolcanics	metavolcanics	metavolcanics	meta gabbro	meta gabbro	meta gabbro	meta gabbro	meta gabbro	meta gabbro	meta gabbro
Position	16 Km N Pattan	20 Km N Pattan	23.5 Km N Pattan	26.5 Km N Pattan	32.5 Km N Pattan	1 Km N Pattan	5.3Km N Pattan	5.3Km N Pattan	5.3Km N Pattan	6 Km N Pattan	13.4 Km N Pattan	25.2 Km N Pattan
Area	N Pattan	N Pattan	N Pattan	N Pattan	N Pattan	N Pattan	N Pattan	N Pattan	N Pattan	N Pattan	N Pattan	N Pattan
Major elements (wt%)												
SiO2	43.15	50.31	42.43	52.48	53.73	52.72	53.13	52.95	53.18	52.81	53.86	50.55
TiO2	1.77	0.77	3.53	1.95	2.42	0.70	1.16	1.11	0.64	0.68	0.96	1.05
Al2O3	16.53	16.58	13.72	15.08	15.20	18.15	17.48	17.64	18.14	18.18	17.28	19.45
Fe2O3	16.10	9.51	19.03	12.63	13.88	9.96	10.49	10.44	9.88	10.05	10.86	10.58
MnO	0.17	0.17	0.17	0.24	0.17	0.16	0.17	0.17	0.18	0.17	0.18	0.42
MgO	7.76	8.53	7.03	5.65	3.54	5.49	5.50	5.59	5.57	5.55	5.05	4.02
CaO	13.57	12.14	13.05	8.90	6.54	10.54	9.95	9.87	10.29	10.40	9.37	9.42
Na2O	0.83	1.80	1.04	2.75	3.62	1.84	1.61	1.75	1.72	1.71	1.95	4.28
K2O	0.03	0.19	0.00	0.11	0.52	0.37	0.38	0.41	0.35	0.39	0.36	0.08
P2O5	0.10	0.01	0.00	0.20	0.38	0.06	0.14	0.08	0.06	0.05	0.13	0.16
Total	100.00	100.00	100.00	100.00	100.00	100.00	100.00	100.00	100.00	100.00	100.00	100.00
LOI	1.23	1.45	0.23	0.41	1.78	0.82	0.74	0.67	0.84	0.42	0.94	1.90
Trace elements (ppm)												
Ba	11.91	37.85	24.74	9.12	108	124	142.25	160	132	117.10	147	87
Rb	0.66	6.61	2.52	0.32	16	2.17	4.05	6	4	3.41	1.72	3.47
Sr	201.86	149.40	146.21	116.93	196	272	249.52	251	262	246.91	269	284
Ta	0.19	0.07	0.49	0.05		0.06	0.17			0.12	0.14	0.14
Th	0.03	0.05	0.58	0.01	2	0.2	0.39		1	0.23	0.11	0.84
Zr	37	13	14.22	116	96	31	227	45	34	33	54	73
Nb	3.28	0.50	6.45	0.16	4	1.01	1.99	3	1	0.99	2.55	1.86
Y	27.22	15	36.93	7.10	31	17.5	17.57	14	14	14	27	26
Hf	0.84	0.51	0.73	0.30			1.33	0		0.89	0	
V	483	241	980	364	215	306	322	321	243	266	332	312
Cr	74	383	25	55	11	178	80	59	74	55	121	43
Ni	55	150	47	32	5	26	20	23	20	23.36	38	13
Co	52	59	68	42	30	35	56	53	78	63	31	23.46
U	0.01	0.02	0.14	0.01			0.14	1	1	0.09		
Sc						58					48	26
Cu	14.37	41.389	47.513	96.84	6	14	32	51	27	23.75	45	40
Zn	56	62	79	126	38	75	69	74	72	70	79	63
Pb	0.21	0.421	0.82	0.3		1.69	2.14			2.04	1.56	1.35
Cs	0.02	0.137	0.023	0.035		0.08	0.15			0.15	0.04	0.08
REE (ppm)												
La	2.24	0.95	7.28	0.27		4.29	5.67			4.24	7.63	6.34
Ce	7.87	2.94	19.32	0.89	8	10.14	13.04		13	9.40	18.90	15.68
Pr	1.46	0.55	2.90	0.19		1.43	1.75			1.25	2.67	2.24
Nd	8.43	3.40	14.53	1.23	6	6.74	8.15		11	5.81	12.32	10.39
Sm	3.19	1.45	4.63	0.66		1.98	2.34			1.75	3.25	2.87
Eu	1.21	0.81	1.65	0.37		0.81	0.76			0.72	0.99	1.00
Gd	4.02	2.05	5.51	0.98		2.59	2.70			2.13	3.80	3.74
Tb	0.77	0.40	1.03	0.20		0.44	0.47			0.38	0.67	0.67
Dy	4.86	2.58	6.45	1.32		2.90	2.97			2.42	4.35	4.41
Ho	1.10	0.59	1.45	0.30		0.64	0.67			0.56	0.95	0.98
Er	3.00	1.61	4.03	0.78		1.84	1.86			1.62	2.66	2.84
Tm						0.29					0.38	0.45
Yb	2.72	1.45	3.72	0.69		1.85	1.82			1.60	2.52	2.74
Lu	0.42	0.22	0.59	0.10		0.29	0.29			0.26	0.39	0.42
Mg-no.	29	44	24	28	18	32	31	32	33	32	29	25

Abbreviations: cr-gr = coarse-grained, f-gr = fine-grained, fol = foliated, N Pattan = area in between Pattan and Dassu, N Kamila = area in between Kamila and Seo.

Table 1. (continued)

S.No.	KO-152	93120506	93120507	KO-50	CH-53	KM-2	KM-3	CH-51B	KO-134A	SW-16	SW-23B	KO-134B
Name	meta diorite	granite	granite	metavolcanics	metavolcanics	metagabbro	meta diorite	doleritic dike	meta gabbro	meta gabbro	meta gabbro	dolerite dike
Position	42 Km N Pattan	S Dassu	S Dassu	5-6Km N Kamila	5-6Km N Kamila	10Km N Kamila	10Km N Kamila	5-6Km N Kamila	Khwazakhela	Madyan	Madyan	Khwazakhela
Area	N Pattan	S Dassu	S Dassu	N Kamila	N Kamila	N Kamila	N Kamila	N Kamila	Swat Valley	Swat Valley	Swat Valley	Swat Valley
Major elements (wt%)												
SiO2	56.69	68.57	68.85	56.65	50.77	52.63	58.90	43.69	49.48	53.81	53.79	47.94
TiO2	0.79	0.25	0.21	2.32	0.94	0.85	0.84	1.56	0.96	0.86	1.06	1.02
Al2O3	18.23	16.85	16.74	13.78	19.52	19.18	16.51	20.28	19.14	17.82	17.44	19.36
Fe2O3	8.43	2.83	2.93	12.42	9.00	8.65	8.35	13.69	12.03	8.97	9.01	12.97
MnO	0.17	0.11	0.19	0.13	0.15	0.13	0.18	0.21	0.21	0.15	0.14	0.21
MgO	3.30	0.80	0.95	4.25	5.72	5.15	3.77	6.84	5.27	5.52	5.73	5.83
CaO	8.02	5.12	4.41	7.90	9.48	9.53	8.43	11.29	10.65	9.36	9.59	11.10
Na2O	2.22	4.43	3.90	2.20	3.43	3.28	0.78	1.90	1.97	2.81	2.65	1.36
K2O	1.75	0.95	1.69	0.10	0.76	0.33	2.07	0.28	0.10	0.57	0.51	0.08
P2O5	0.38	0.10	0.11	0.24	0.23	0.28	0.16	0.26	0.18	0.13	0.08	0.13
Total	100.00	100.00	100.00	100.00	100.00	100.00	100.00	100.00	100.00	100.00	100.00	100.00
LOI	2.24	1.36	1.37	0.83		2.09	1.59	0	1.58	0.94	1.49	1.57
Trace elements (ppm)												
Ba	1091	520	820	26.79	106	59.04	289.21	37	68.78	115	99	42
Rb	50	33	66	3.25	21	2.85	100	5	0.93	6.15	12.44	3
Sr	599	370	300	166	408	465.90	290.50	354	368.91	431	402	302
Ta	0.23	1	1.5	0.7		0.18	0.47		0.10	0.2	0.19	0
Th	9.01	4	5	0.85		0.47	7.62		0.137	0.51	0.96	2
Zr	93	60	60	142	44	48	136	59	21	78	65	19
Nb	5.00	8	8	6.84	0	3.3	9.60		1.04	3.1	2.74	2
Y	19.11	12	18	50.66	16	16	35.26	23	14	18	13.34	12
Hf	0.44	2	1.5			0.62	0.56		0.37			
V	199	26	21	330	315	299	164	356	311	250	262	368
Cr	2	10	11	10	126	123	67	11	7	164	187	1
Ni	7	2	1	14	44	38	38	18	8	57	72	5
Co	40	37	22	38	43	42	53	43	45	32	35	44
U	0.89	0.6	1.4	0		0.25	0.82		0.04			1
Sc				36								
Cu	18.94			14	42	12.24	47.09	72	22.65	194	57	7
Zn	76			19	62	86	100	87	86	78	72	81
Pb	4.45			0.46		2.32	15.13		1.13	2.56	1.83	
Cs	1.23			0.11		0.17	4.88		0.11	0.19	0.44	
REE (ppm)												
La	51.23	7	13	6.89		5.38	21.98		5.18	7.44	5.83	
Ce	87.75	17	24	19.96		13.56	45.76		11.73	17.33	13.01	10
Pr	8.92	1.70	2.30	3.21		2.01	5.30		1.63	2.41	1.74	
Nd	32.01	7.00	10.00	16.77		9.91	20.75		7.85	10.92	7.38	
Sm	5.42	1.70	2.40	5.43		2.84	4.61		2.22	2.79	1.77	
Eu	1.58	0.70	1	2.24		0.96	1.23		1.06	0.95	0.74	
Gd	5.37	1.40	1.90	7.32		3.08	5.35		2.48	3.09	1.99	
Tb	0.66	0.30	0.30	1.33		0.52	0.97		0.43	0.52	0.34	
Dy	3.58	1.50	1.90	8.58		3.12	5.95		2.64	3.22	2.15	
Ho	0.77	0.30	0.50	1.85		0.69	1.30		0.59	0.67	0.46	
Er	2.08	0.70	1.20	5.24		1.88	3.58		1.62	1.88	1.27	
Tm		0.10	0.30	0.85						0.27	0.19	
Yb	1.95	0.80	1.60	4.90		1.75	3.56		1.59	1.81	1.23	
Lu	0.31	0.10	0.20	0.74		0.27	0.56		0.25	0.28	0.19	
Mg no.	25	20	22	23	35	34	28	30	27	35	35	31

Abbreviations: cr-gr = coarse-grained, f-gr = fine-grained, fol = foliated, N Pattan = area in between Pattan and Dassu, N Kamila = area in between Kamila and Seo.

Generally, rocks representing **Group-1** from **NP** have relatively low silica contents (42 to 49 wt. %), and reasonably high MgO between 7 and 8 wt %. This, combined with high total Fe (presented as Fe_2O_3 = 15 to 18 wt %), results in these samples having low Mg-number 18 to 44 but on average 25 (Table 1). Samples KO-150 and KO-151 from Group-1 have comparatively elevated silica contents (about 52 wt %) and low MgO (3 to 5 wt %) and their Mg-number is also low (28-18). The TiO_2 contents of these metavolcanis range from 1.5 to 3.5 wt%. KO-50 is a fine-grained metavolcanic rock (Group-1) from **NK** and its chemistry is similar to that observed in samples KO-150 and KO-151 of **NP** (Table 1).

Metaplutonics rocks of **Group-2** (gabbro and diorites) from **NP**, **NK** and **SV** are characterized by relatively high Al_2O_3 (13 to 19 wt %) and CaO (8 to 13 wt %), low K_2O (< 0.6 wt %, but in only two rocks < 1.7 wt %), and generally low SiO_2 (average < 58 wt %). They have a similar range in TiO_2 contents (< 1.50 wt %) and have Mg-numbers of 24 to 33.

The fine-grained metavolcanic rocks (Group-1) from **NP** as well as from **NK** show generally higher values of TiO_2 , ranging between 1.5 and 3.5 wt % than metaplutonic rocks of Group-2. Some samples like KO-148 (Group-1) have comparatively low TiO_2 (0.75 wt %). The other oxides P_2O_5, Na_2O and K_2O are slightly higher in Group-2 (metaplutonic rock assemblages) than in Group-1 (samples KO-145, KO-148 and KO-149; Table 1).

Two representative samples from **doleritic dikes**, **NK** (CH-51B) and **SV** (KO-134B) yield analyses closely comparable with each other (Table 1). Both these samples have a typical basaltic chemistry and are characterized by : 43 and 47 wt % SiO2, 19 and 20 wt % Al_2O_3, 13 wt % FeO^T, 6 and 5 wt % MgO, 11 and 10 wt % CaO, < 1 wt % K_2O and 1.55 and 1 wt % TiO_2, respectively.

Plagiogranite which are intrusive into the Kamila Amphibolites, are characterized by 67 wt % SiO_2, 16 wt % Al_2O_3, <1 wt % MgO, 4 wt % Na_2O, 1 wt % K_2O and <1 wt % P_2O_5 (Table 1). The Mg-number is between 22 to 24.

Major element contents, representing Group-1 & 2 and dikes of the Kamila Amphibolite Belt, are shown in Harker variation diagrams (Fig. 8). The Figure 8 shows the variation diagrams with nearly rectilinear trends, with a cluster of composition in the range of 45 - 55 wt % SiO_2 ; however, some major oxides such as P_2O_5 , K_2O and Na_2O against SiO_2 show scatter (Figs. 8D,B,A), which corroborates the observation that secondary processes have disturbed the primary abundances of some major elements in some of these metamorphosed samples.

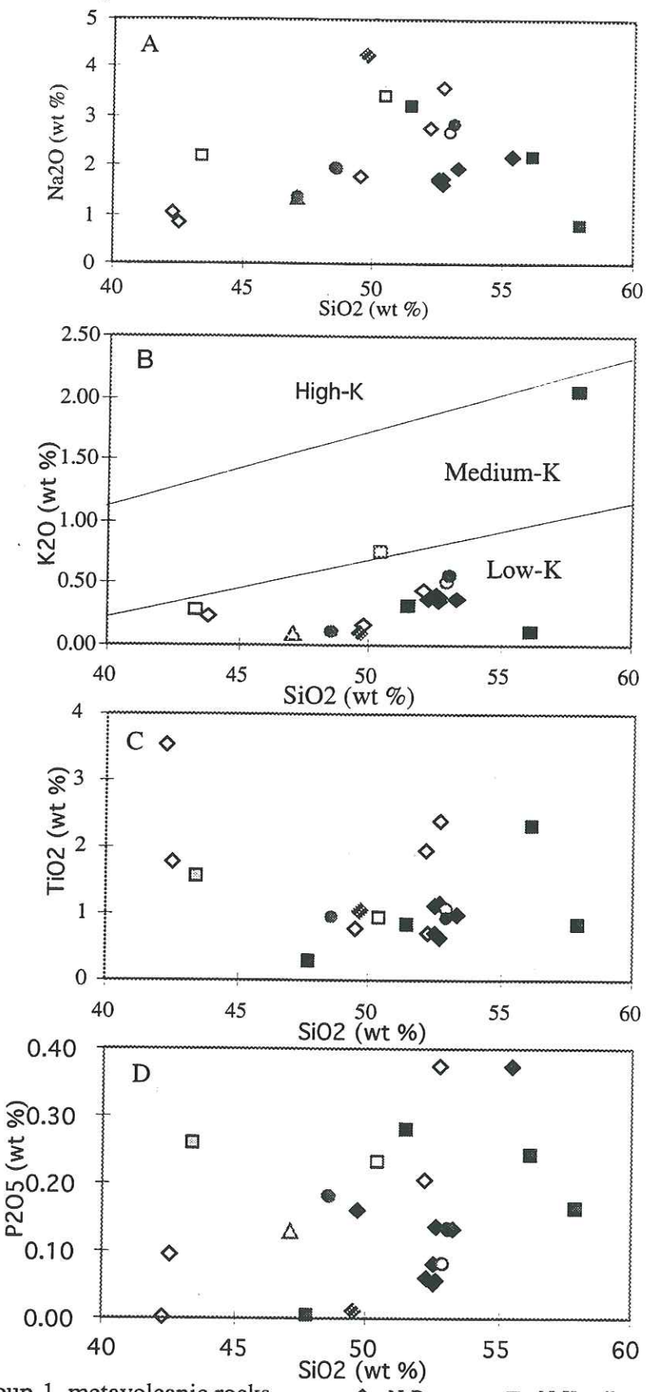

Figure 8. Harker variation diagrammes for major elements in different facies of the Kamila Amphibolites.

Diagrammes de Harker pour les différents faciès des amphibolites de Kamila.

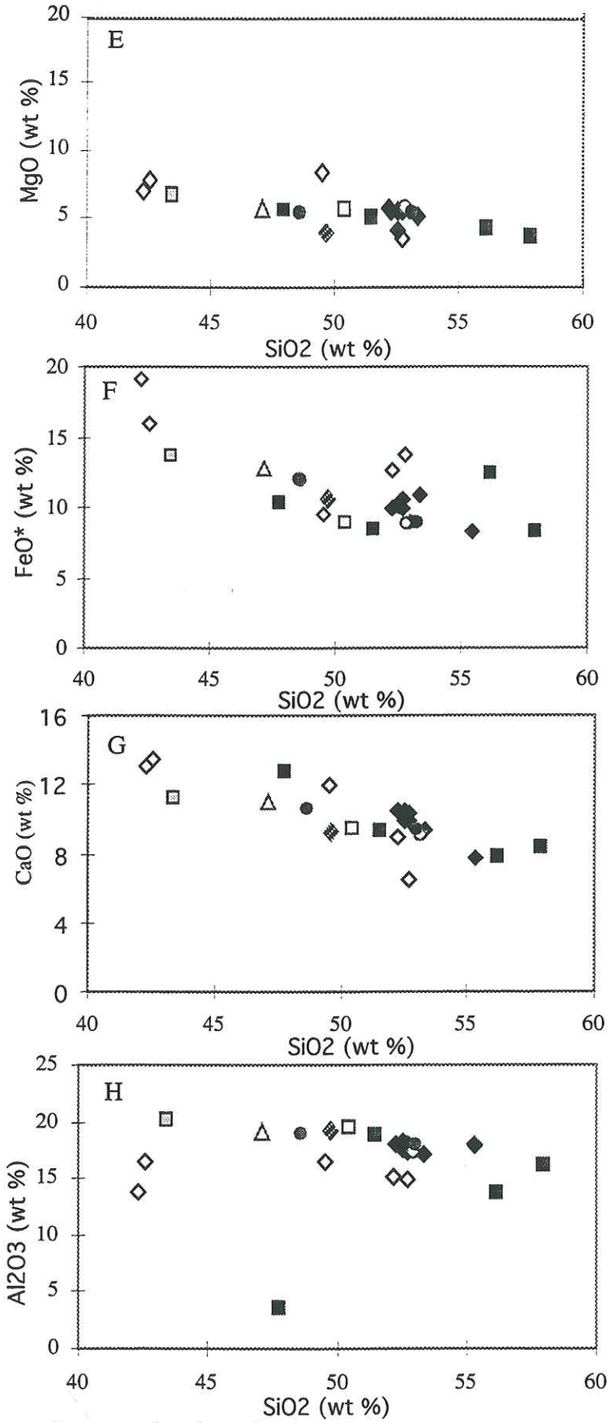

Figure 8. Harker variation diagrammes for major elements in different facies of the Kamila Amphibolites.

Diagrammes de variation de Harker pour les éléments majeurs dans différents faciès des amphibolites de Kamila.

In both, metavolcanic and metaplutonic rocks from **NP**, **NK** and **SV**; MgO, CaO, Al_2O_3 and FeO* correlate negatively with SiO_2 (Figs. 8E,G, H,F), reflecting the separation of plagioclase and pyroxene during fractionation. But metavolcanic rocks belonging to Group-1 from **NP** and **NK** show no overlap with the coarse-grained metaplutonic rocks of Group-2 on the particular plots of Al_2O_3, Fe_2O_3 and TiO_2 against SiO_2 (Figs. 8H,F,C), which in turn suggests that both the facies are geochemically distinct and may not be closely related with each others.

Sample KO-148 (Group-1) from **NP** (Fig. 5) contains high Cr (383 ppm) and Ni (150 ppm) and Mg-number 44, which suggests a relatively primitive nature. However, its low TiO_2 content could also resulted from crystal accumulation and the low value could be related to arc magmatism.

The plot of SiO_2 versus FeO* / MgO after Gill (1981) and Miyashiro (1974; Fig. 9) shows iron enrichment relative to silica and that samples from the Kamila groups plot in the field of tholeiites which is also visible in the Jensen diagramme (Fig. 10). Further evidence that these rocks are low-K tholeiites is shown on a K_2O versus SiO_2 diagramme (Fig. 8B) with field boundary from Rickwood (1989). The anomalously high alkali contents from some metavolcanic and metaplutonic samples (Table 1) cannot be attributed to an alkaline feature, and may be related to the metamorphic process. Such a finding hinders the application of alkali based classification schemes. Some samples have high TiO_2 contents suggestive of an alkaline affinity. However, using Zr/ TiO_2 versus Nb/Y classification diagram of Winchester & Floyd (1977), which involves only relatively immobile elements (Fig. 11), all the samples form a tight group within the sub-alkaline basalt to basaltic andesite and reject the alkaline nature of these samples. In diagramme (Fig. 12) of Mullen (1983), metaplutonic rocks from the Swat Valley and from the N Pattan (Group-2) plot clearly within the island-arc tholeiite field. Samples representing Group-1 (KO-150 & KO-151) from the N Pattan plot within the MORB field while one sample from N Kamila plot in the ocean-island tholeiite field in Figure 12 and are therefore clearly distinct from all other metaplutonic (Group-2) rocks of the Kamila Amphibolites.

3.4. Trace and rare earth elements

Abundances of trace elements in the samples from the Kamila Amphibolites are shown in Table 1. Most trace elements behave similarly to their related major oxides in the different rock types. All the rocks belonging to Group-2 have low concentrations of Rb (2-20 ppm) over a range of SiO_2 from 42 to 56 wt %. However, the Group-1 metavolcanic rocks from **NP** (KO-145, KO-150) and sample KO-134A from **SV** have comparatively very low abundances of Ba and Sr contents (Fig. 13; Table 1). Rb and Ba contents in many samples are the correlation mirrors of the K contents. Sr is roughly positively correlated with CaO and Al_2O_3.

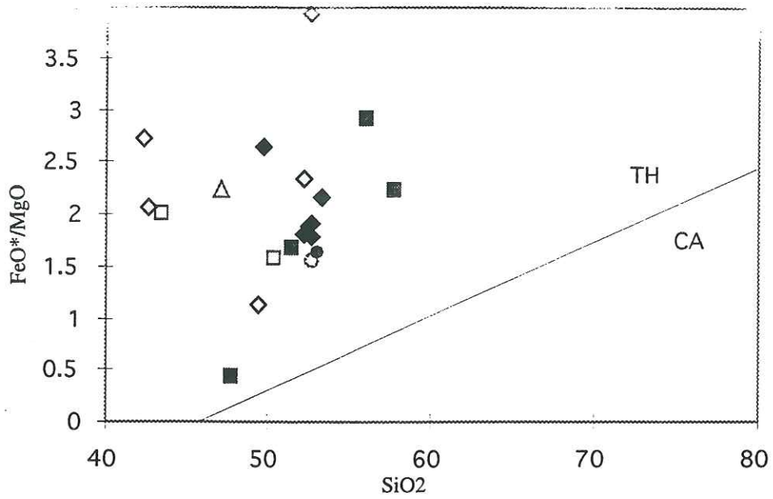

Figure 9. Classification of the Kamila Amphibolites into tholeiite and calc-alkaline magma-type based on FeO/MgO ratio versus SiO2 with discriminant line of Miyashiro (1974).

Séparation des amphibolites de Kamila en magmas de type tholéiitique et calco-alcalin sur la base du rapport Feo/MgO en fonction de la teneur en SiO_2, de part et d'autre de la ligne discriminante de Miyashiro (1974).

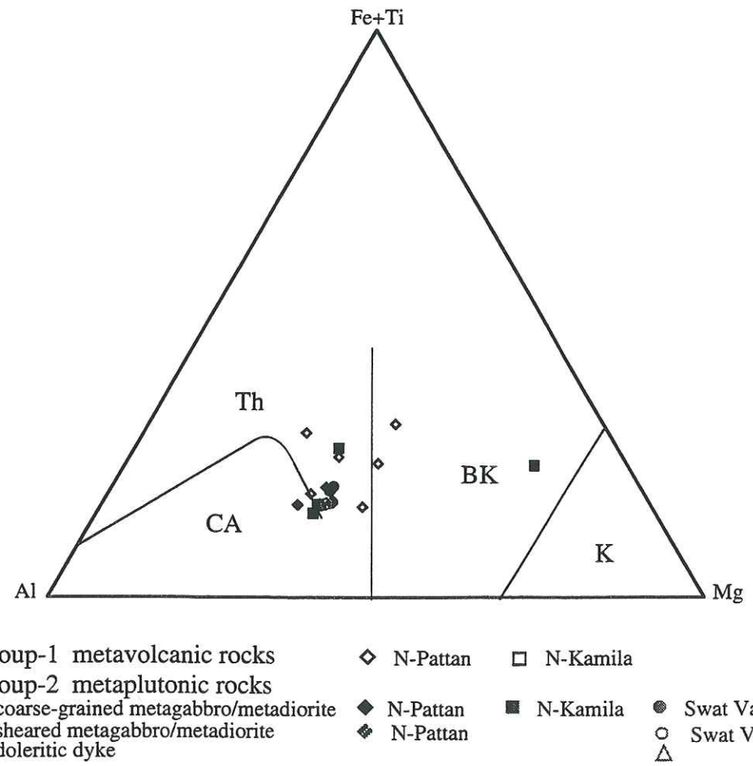

Figure 10. Classification of the rocks from the Kamila Amphibolites Belt using Jensen (1976) cation plot. K- komatiite, BK- komatiitic basalt, Th- tholeiite, CA- calc-alkaline.

Classification des roches de la ceinture amphibolitique de Kamila selon le diagramme de Jensen (1976). K: komatiite, BK: basalte komatiitique, Th: tholeiite, CA: calco-alcalin.

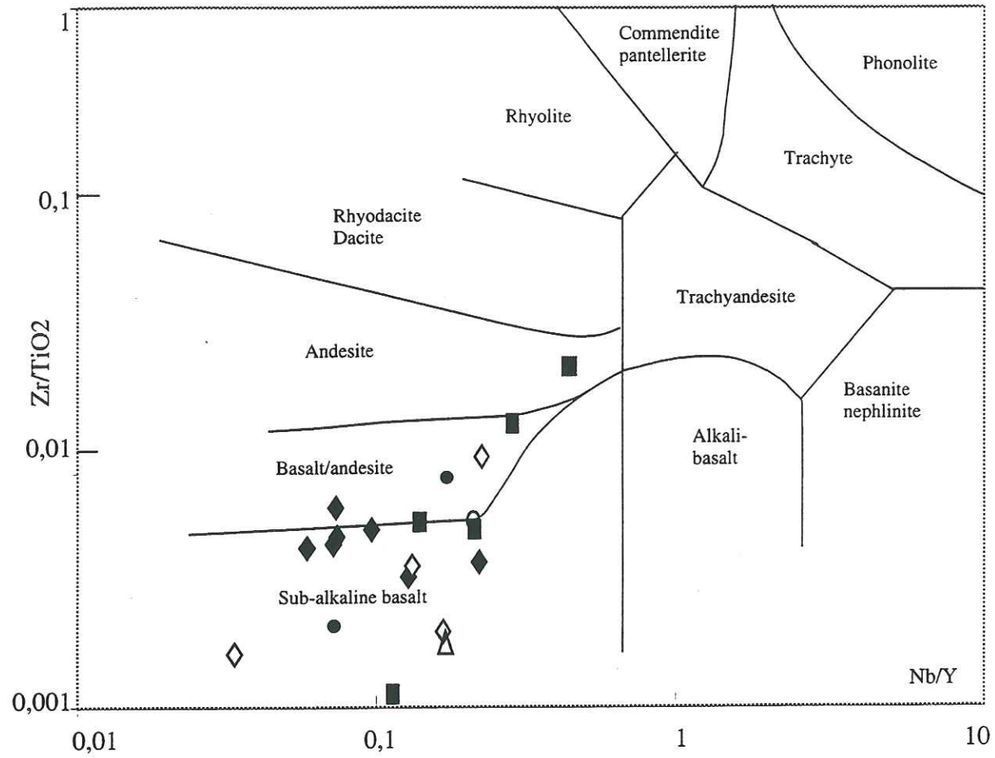

Group-1 metavolcanic rocks ◇ N-Pattan □ N-Kamila
Group-2 metaplutonic rocks
-coarse-grained metagabbro/metadiorite ◆ N-Pattan ■ N-Kamila ● Swat Valley
-sheared metagabbro/metadiorite ◈ N-Pattan ○ Swat Valley
-doleritic dyke △ doleritic dike

Figure 11. Zr/TiO2 versus Nb/Y plot (Winchester & Floyd, 1977) for the different facies of the Kamila Amphibolites.

Diagramme Zr/TiO2 fonction de Nb/Y (Winchestor & Floyd, 1977) pour les différents faciès des amphibolites de Kamila.

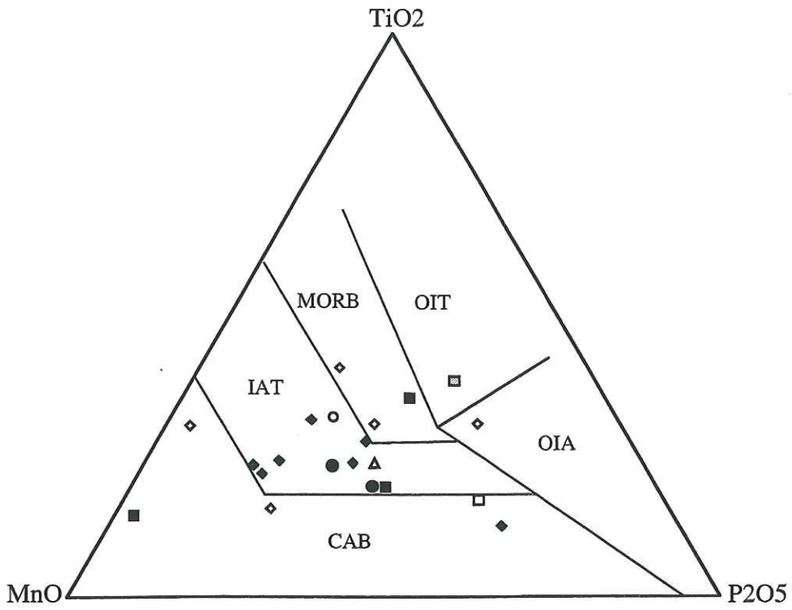

Group-1 metavolcanic rocks ◇ N-Pattan □ N-Kamila

Group-2 metaplutonic rocks

-coarse-grained metagabbro/metadiorite ◆ N-Pattan ■ N-Kamila ● Swat Valley

-sheared metagabbro/metadiorite ◈ N-Pattan ○ Swat Valley

-doleritic dyke △ doleritic dike

Figure 12. TiO2-MnO-P2O5 discrimination diagram for gabbros and diorites (after Mullen, 1983). Analyses from the Kamila Amphibolites plot in the island-arc tholeiite field but metavolcanics from N Pattan fall in the MORB field and KO-50 from N Kamila plots in the ocean-island tholeiites. The fields are MORB; OIT- ocean-island tholeiite; OIA- ocean-island alkali basalt; CAB- island-arc calc-alkaline basalt; IAT- island-arc tholeiite.

Le diagramme TiO2-MnO-P2O5 de discrimination pour les gabbros et les diorites (d'après Mullen, 1983). Les échantillons des amphibolites de Kamila sont projetés dans le champ des tholéiites d'arc, mais les métavolcanites du nord de Pattan tombent dans le champ des MORB, et KO-50 du NKamila dans celui des OIT.

Figure 13 also shows that the K-element group such as Ba, Rb and Sr (particularly Sr; Fig. 13C) display a rather erratic variation with SiO_2, reflecting redistribution of these elements by some metamorphic processes. We suggest that the K-group elements have at some stage been mobilized, and their abundance patterns should be treated with caution. However, the contents of K-group elements (Rb, Ba and Sr) in the relatively coarse-grained plutonic samples of **NP**, **NK** and **SV** are consistent with low-K orogenic basalt to andesite with some modification by metamorphic processes (e. g. amphibolites from north of Dassu). The values of Rb and Ba in these rocks are similar to those of low-K (0.2 to 0.4 wt %) of the island arc association (Jakes and Gill, 1970; Gill, 1970). In contrast, the samples from the fine-grained metavolcanics of Group-1 are more depleted in Rb, Ba and Sr relative to island arc associations and have much closer affinity with MORB. Similarly rocks from Group-1 have low Rb/Sr ratio (average 0.006) compared to rocks from Group-1 (average 0.01) and this ratio is more closer to MORB.

In Figures 14 and 15, the abundances of major as well as incompatible trace elements are plotted against Zr. Zr is considered to be a good indicator of the degree of fractionation and is apparently immobile under most metamorphic conditions (Floyd and Winchester, 1975; Pearce and Cann, 1973; Weaver and Tarney, 1981). In Figure 14A, Zr shows positive correlation with SiO_2 suggesting that zircon was not a fractionating phase in the early fractionation stage. It is clear from Figures 15D&C that elements such as Nb and Y each displays comparatively good linear covariation with Zr, and this is likely to reflect original igneous fractionation. However, the rocks from Group-1, in contrast, are distinct from the coarse-grained facies rocks (Group-2) and relatively richer in TiO_2, P_2O_5 (Figs. 14B&C).

Ni, Cr and Co have consistently low values in the rocks of the Kamila Amphibolites and are in the range of more fractionated rocks. Curvilinear correlation with differentiation exists in case of Ni, Cr and Co versus MgO (Fig. 16), as both Ni and Co partition into olivine (Frey et al., 1974; Irving, 1980). The observed trends may be explained in terms of olivine than pyroxene fractionation. Likewise Cr depletion might have been caused by precipatation of clinopyroxene. Concentrations of Ni and Cr are especially low with respect to MgO in rocks of Group-2, a frequent feature of arc tholeiites (Gill, 1981). Moreover, the Mg-number of all these samples is less than 44 and range in between 33 and 24 which suggests that these magmas are not primary and have gone olivine and pyroxene fractionation en route to the surface (Wilson, 1989).

Cr, Ni and Co abundances in Group-1 rocks are distinct and relatively high at comparable MgO contents (Fig. 16) and particularly sample KO-148 from NP has the highest abundances of Cr (383 ppm), Ni (150 ppm) and Co (50 ppm), suggesting it would be a primary liquid or close to it.

Figure 17 shows the chondrite-normalized rare earth elements (REE) pattern of the Kamila Amphibolites from the Swat and Indus Valleys. The dissimilarities between the rocks of Group-1 and Group-2 particularly in Indus Valley is further illustrated in these patterns.

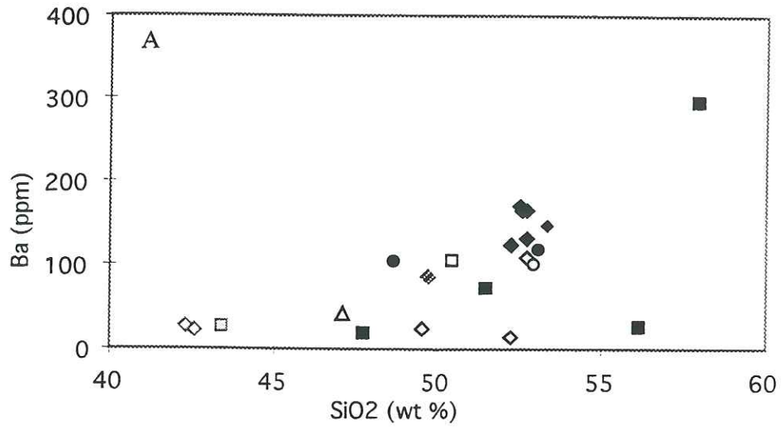

Figure 13. Plot of Ba, Rb and Sr versus SiO2 in the rocks of the Kamila Amphibolites.

Diagramme du Ba, du Rb, et du Sr en fonction du SiO_2 des amphibolites de Kamila.

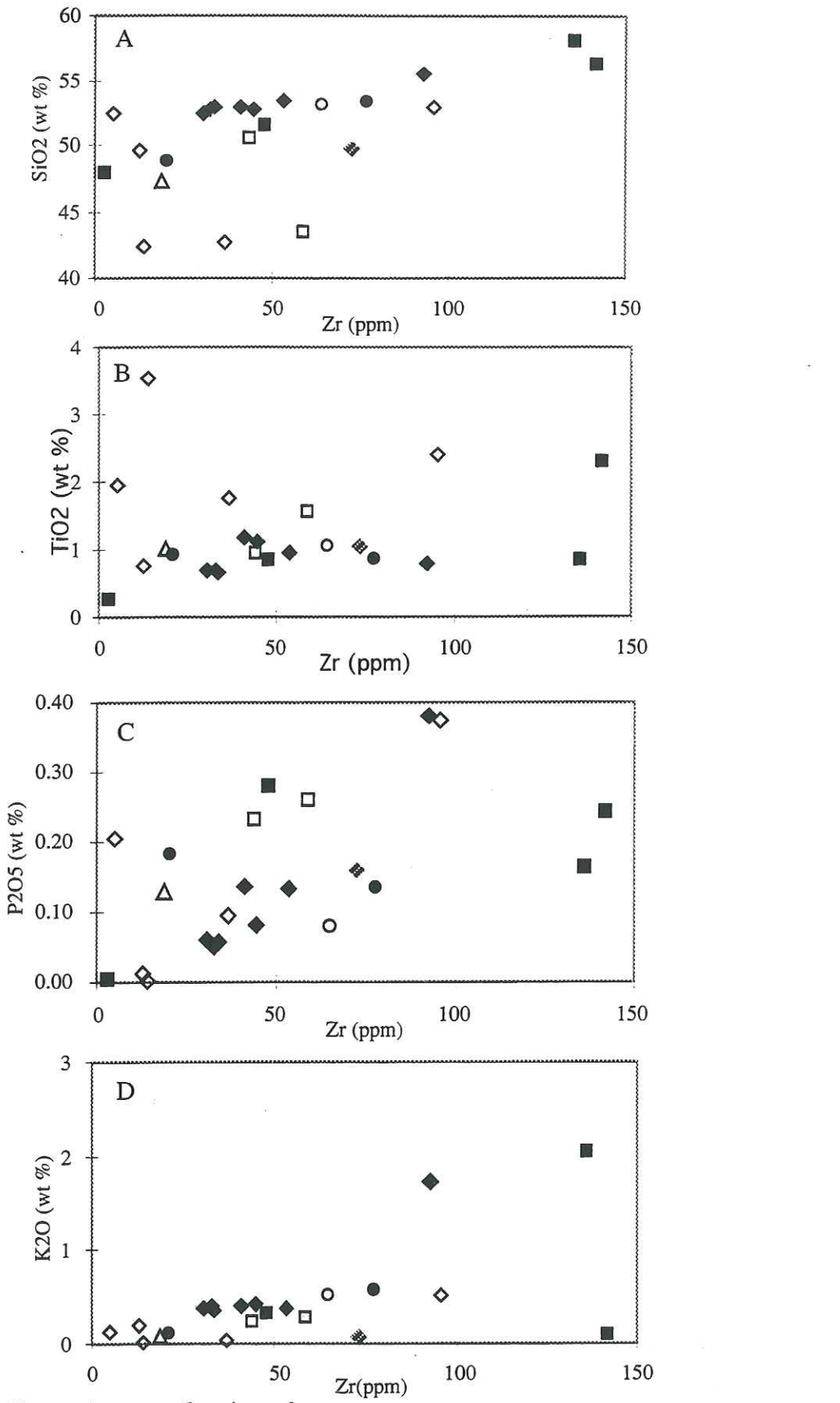

Figure 14. Major element abundances plotted against Zr abundances for the different facies of the Kamila Amphibolites.

Abondance des éléments majeurs en fonction de la teneur en Zr pour différents faciès des amphibolites de Kamila.

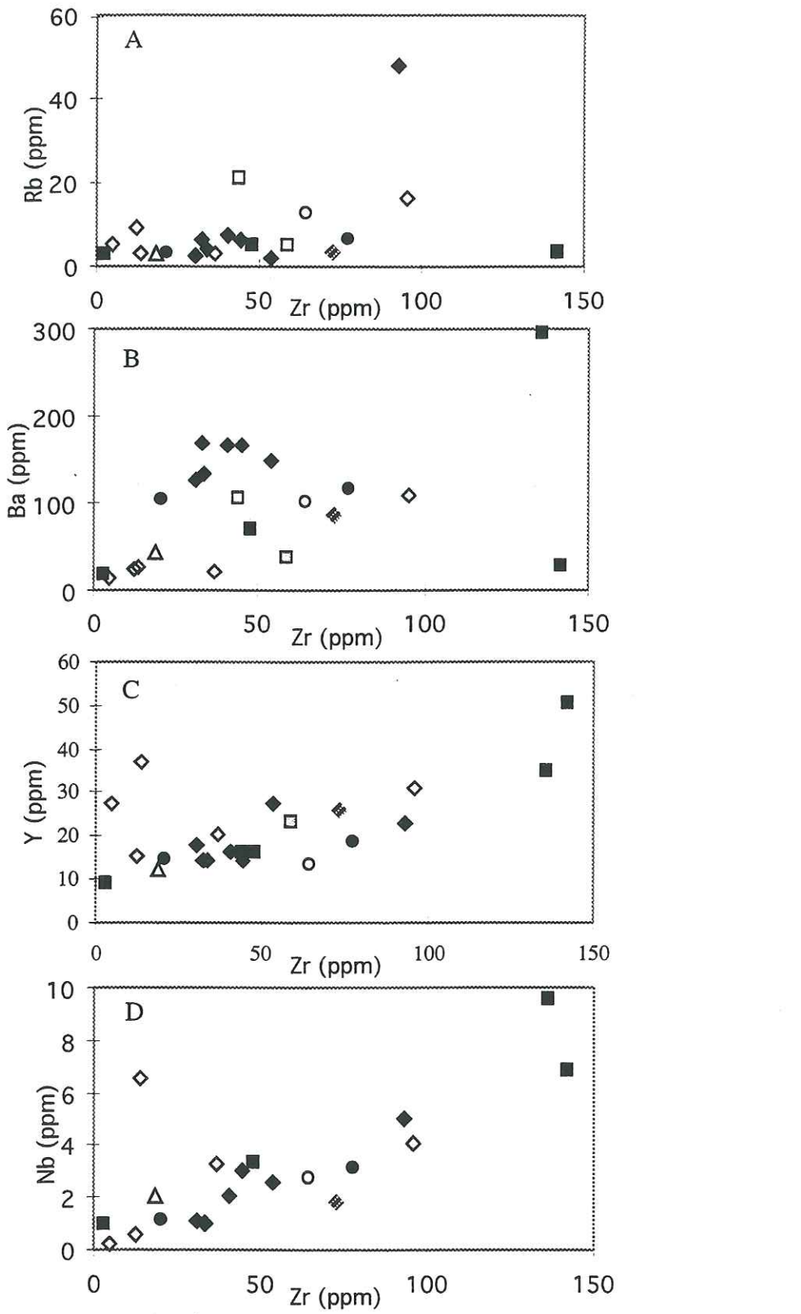

Figure 15. Incompatible trace element abundances plotted against Zr abundances for the different facies of the Kamila Amphibolites.

Teneur en éléments incompatibles en fonction de la teneur en Zr pour différents faciès des amphibolites de Kamila.

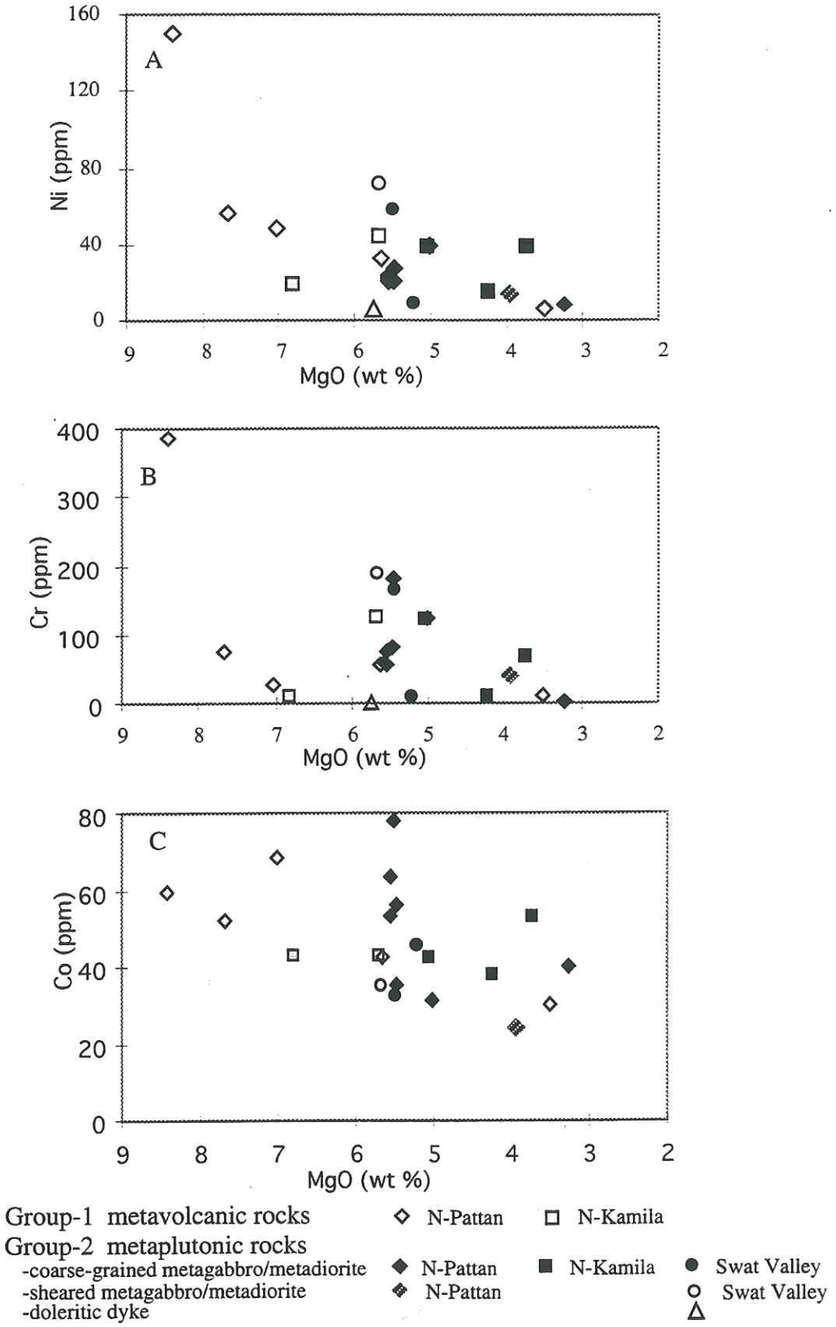

Figure 16. Variations of Ni, Cr and Co versus MgO in the different facies of the Kamila Amphibolites.

Variations du Ni, du Cr et du Co en fonction de MgO pour les différents faciès des amphibolites de Kamila.

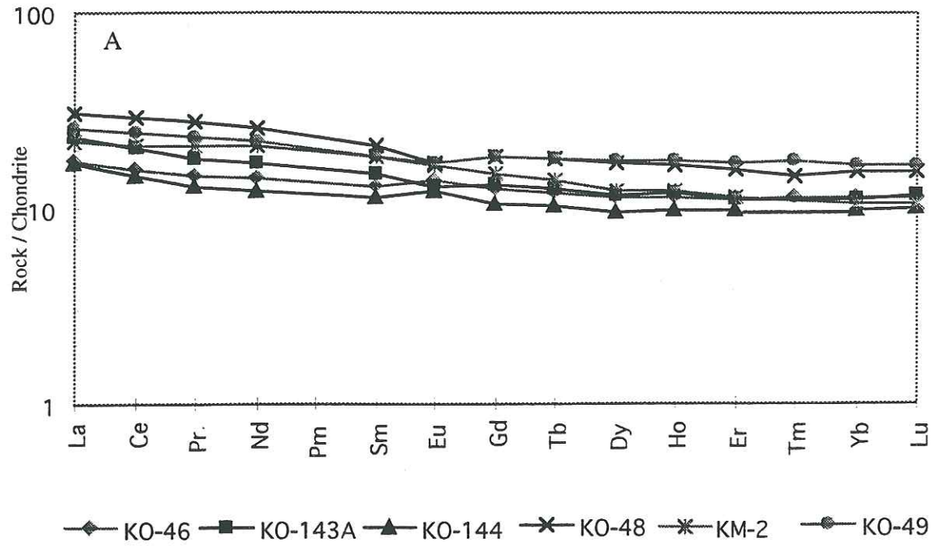

Figure 17 A. Chondrite-normalized REE plots of the N-Pattan rocks, Kamila Amphibolites. Normalizing values after Nakamura (1974).

Spectre de terres rares normalisé aux chondrites pour les roches du N-Pattan (métavolcanites), amphibolites de Kamila. Valeurs de normalisation d'après Nakamura (1974).

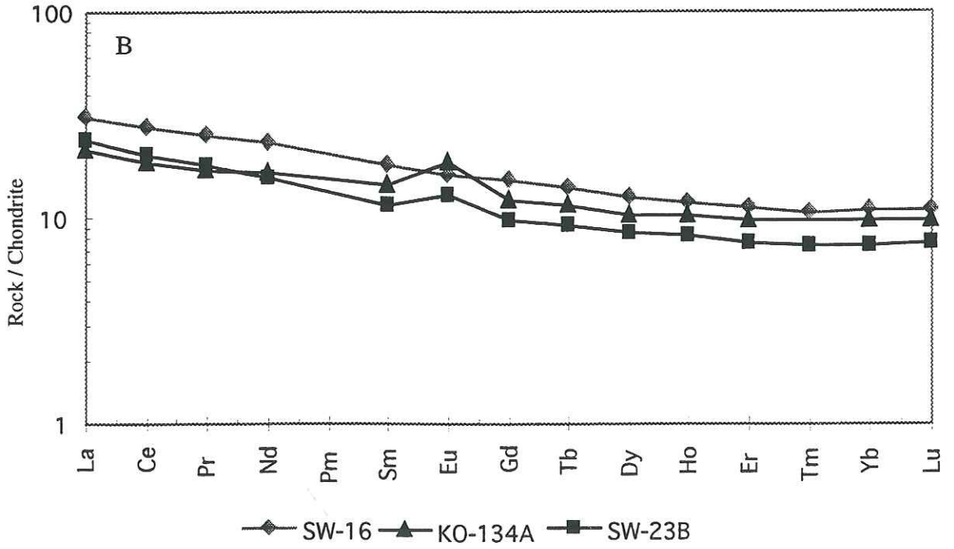

Figure 17 B. Chondrite-normalized REE plots of the Swat area, Kamila Amphibolites. Normalizing values after Nakamura (1974).

Spectre de terres rares normalisé aux chondrites pour la région de Swat, amphibolites de Kamila. Valeurs de normalisation d'après Nakamura (1974).

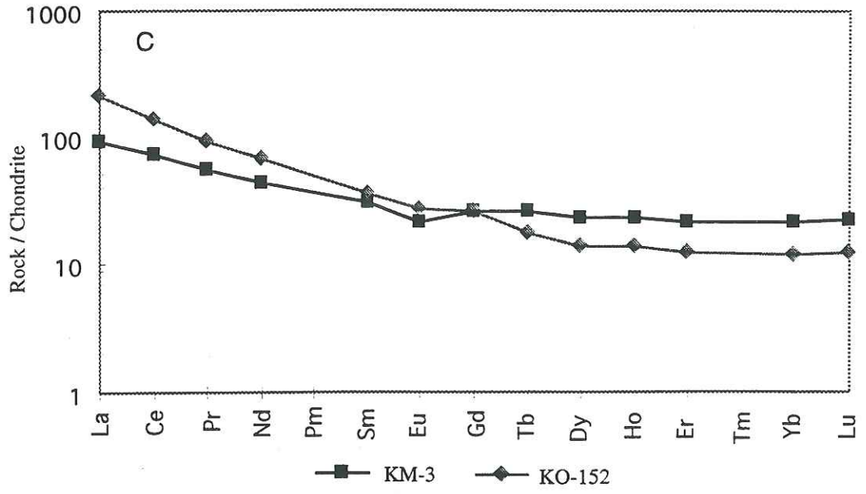

Figure 17 C. Chondrite-normalized REE plots of the N-Kamila, Kamila Amphibolites. Normalizing values after Nakamura (1974).

Spectre de terres rares normalisé aux chondrites pour le N-Kamila, amphibolites de Kamila. Valeurs de normalisation d'après Nakamura (1974).

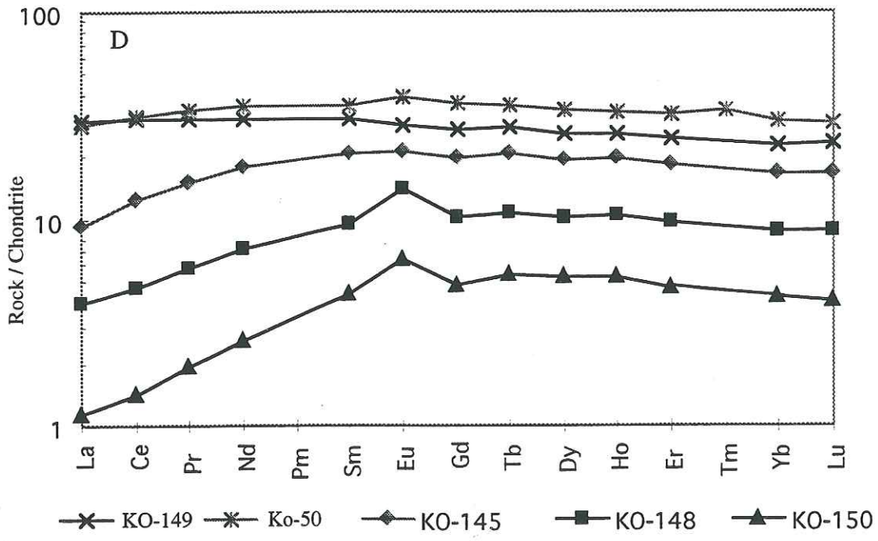

Figure 17 D. Chondrite-normalized REE plots of the N-Pattan rocks (metavolcanics), Kamila Amphibolites. Normalizing values after Nakamura (1974).

Spectre de terres rares normalisé aux chondrites pour le N-Kamila, amphibolites de Kamila. Valeurs de normalisation d'après Nakamura (1974). KM-2 et KO-50 sont des métavolcanites.

Most coarse-grained facies (Group-2) from NP, NK and SV show enrichment in LREE. Figures 17 A&B show that their patterns are rather enriched in LREE with chondrite normalized La/Yb ratios from 1.56 to 3.2. The samples show modest, positive or negative Eu anomaly due to plagioclase accumulation and fractionation. The fractionation of light and heavy REE is similar for most of the samples, and the major difference between the samples is their bulk REE content (Table 1). These patterns are closely similar and suggesting a common origin for these rock types. However, some plutonic rocks (Group-1) present some variation in the REE signature (Fig. 17C). For instance, samples KO-152 and KM-3 are very LREE enriched.

On the contrary, the chondrite-normalized patterns of rock assemblages from Group-1 (KO-145, 148, 149, 150 from **NP**, and KO-50 from **NK**) vary from highly depleted in LREE (La_N/Sm_N ratio from 0.56 in **NP** and 0.80 in **NK**) to flat REE patterns (La_N/Sm_N ratio) @ 1 in sample KO-149 (Fig. 17D). Also, there is a slight decrease in abundance from Tb to Lu giving rise to a convex-upwards pattern. The $(La/Sm)^N$ and $(La/Yb)^N$ ratio is nearly constant (≤ 1) and total REEs increase from south to north in the **NP**. Rocks with depleted LREE and TiO_2 contents between 1.7 to 1.9 typically occur in N-type MORB basalts (e.g. Wilson, 1989). Such N-type MORB have usually unfractionated HREE abundances and are strongly depleted in LREE with $(La/Sm)_N < 1$. Samples KO-150 and KO-148 from **NP** have positive Eu anomalies that may have been produced by accumulation of plagioclase. Samples KO-149 and KO-50 (from NP and NK), showing slightly depleted LREE patterns, are also the more REE's enriched (due to fractionation, and present very high enrichment in TiO_2 (2.3 and 3.5 wt %) suggesting some alkaline characters and possibly complex source origin for for Group-1 amphibolites.

The incompatible-element (REE and trace element) data from **NP**, **NK** and **SV** are plotted in order of decreasing incompatibility from left to right in Figures 18A, B, C, &D. The abundances are normalized to MORB values after Sun and McDonough (1989). A pertinent observation from these diagrams is that their multi-element variation patterns are relatively uncomplicated when normalized against MORB compositions. The trace element characteristics of rocks from **NP** again display two distinct and separate major changes in their MORB-normalized patterns. The main difference between these two facies is that plutonic rocks from Group-2 are characterizd by usually negative anomaly for Nb and Ta relative to Th and La (Figs. 18A &B), but in the fine-grained metavolcanic rocks (Group-1), negative Nb anomaly is very small to none because Th and La both are also depleted (Figs. 18C &D). However, both metaplutonic and metavolcanic rocks from Group-2 and 1 show important LIL enrichment, due possibly to effects of mantle enrichment or metasomatism.

Plagiogranite trace element data is characterized by high concentrations of LILE with 33 to 66 ppm Rb, 300 to 370 ppm Sr, 520 to 820 ppm Ba and modestly enrich 4 to 5 ppm Th. However, the heavy rare earth elements (HREE) and in particular the high field strength elements (HFSE) are relatively less abundant than the metavolcanic and metaplutonic rocks of

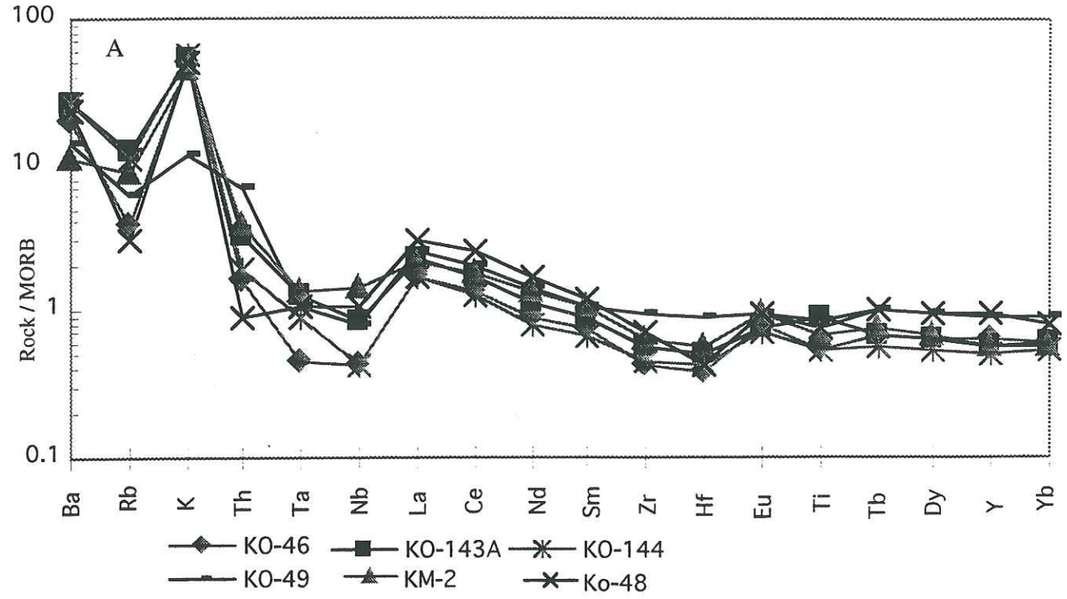

Figure 18 A. MORB-normalized multi-element diagram for the rocks of N-Pattan, Kamila Amphibolites. Normalizing values after Sun and McDonough (1989).
Spectre multi-éléments normalisé aux MORB pour les roches du N-Pattan, amphibolites de Kamila. Valeurs de normalisation d'après Sun et McDonough (1989).

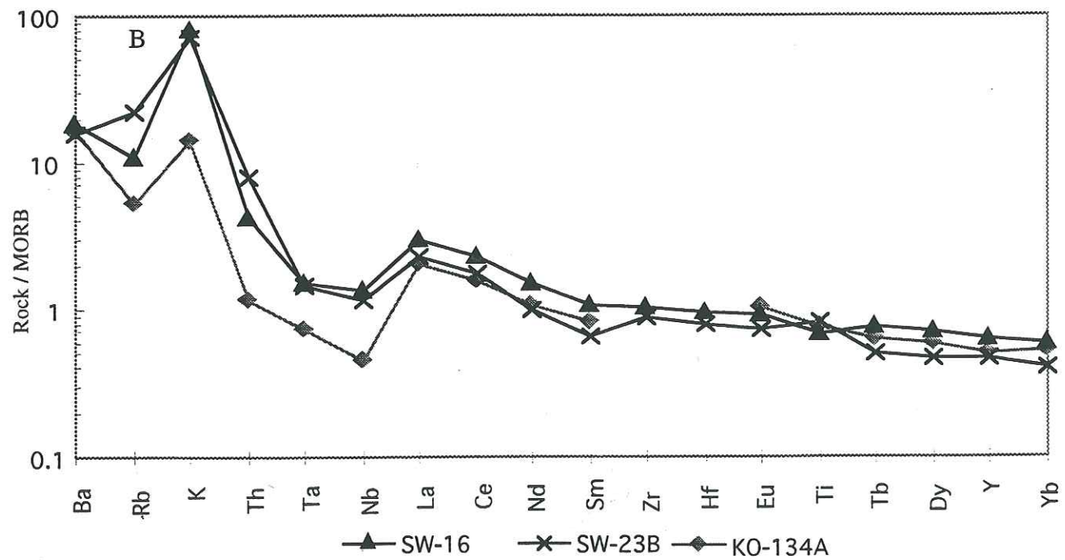

Figure 18 B. MORB-normalized multi-element diagram for the rocks of Swat area, Kamila Amphibolites. Normalizing values after Sun and McDonough (1989).
Spectre multi-éléments normalisé aux MORB pour les roches de la région de Swat, amphibolites de Kamila. Valeurs de normalisation d'après Sun et McDonough (1989).

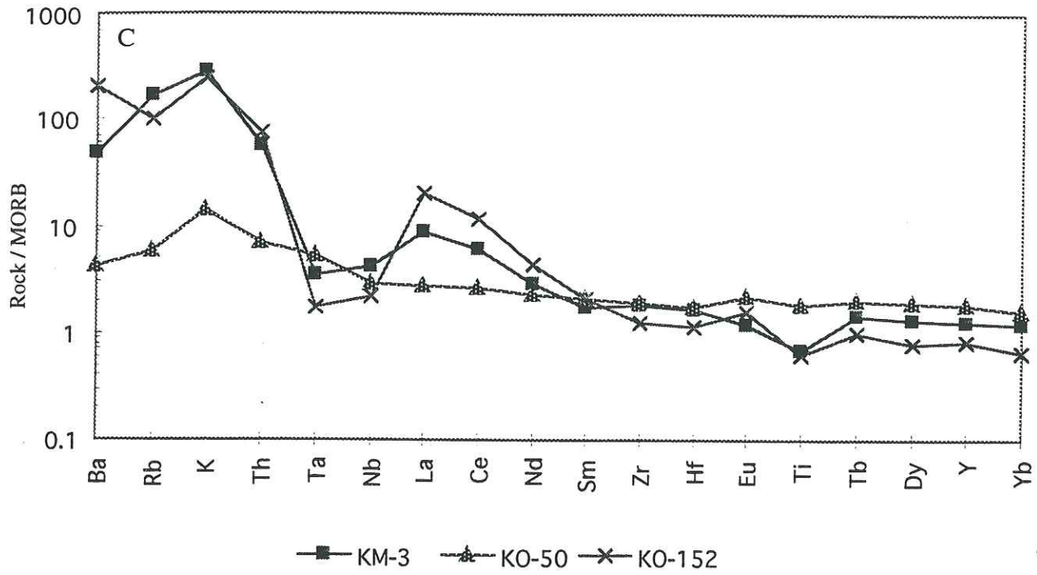

Figure 18C. MORB-normalized multi-element diagram for the rocks of N-Kamila, Kamila Amphibolites. Normalizing values after Sun and McDonough (1989).

Spectre multi-éléments normalisé aux MORB pour les roches du N-Pattan (meta-volcanites), amphibolites de Kamila. Valeurs de normalisation d'après Sun et McDonough (1989).

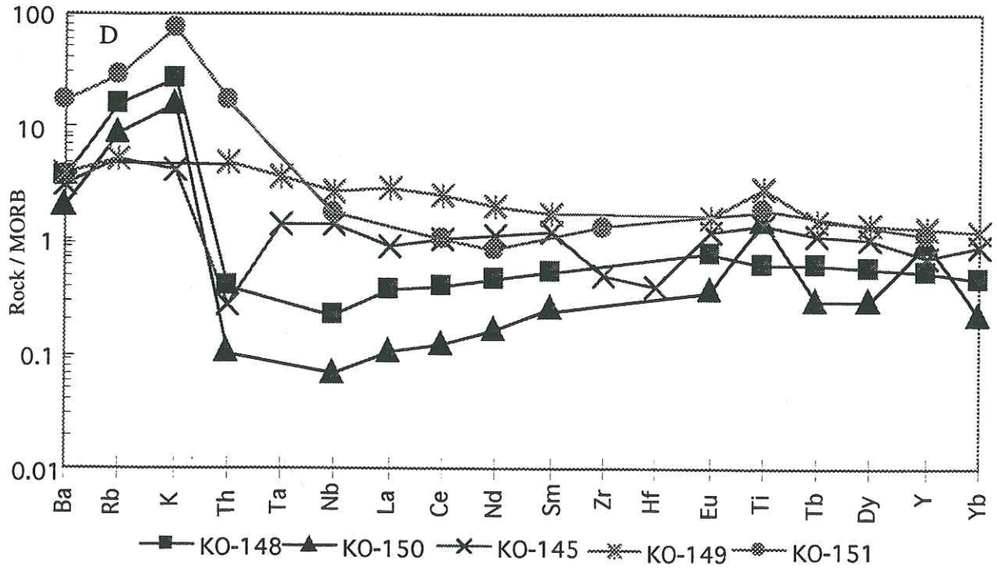

Figure 18 D. MORB-normalized multi-element diagram for the metavol. rocks of N-Pattan, Kamila Amphibolites. Normalizing values after Sun and McDonough (1989).

Spectre multi-éléments normalisé aux MORB pour les roches du N-Kamila, amphibolites de Kamila. Valeurs de normalisation d'après Sun et McDonough (1989).

Group-1 and 2. Thus these rocks have low HFSE/LREE (Nb/La) and high LILE/LREE (Ba/La) ratios as compared to the amphibolitic rocks.

Incompatible trace data for the plagiogranitic rocks are shown in MORB-normalized trace element plot (Fig. 19A). These samples are characterized by LILE and LREE enrichments relative to HFSE and HREE. Although they have relatively small positive Eu anomaly, they are enriched in Rb and Ba relative to Th. However, the general lack, or only small positive, Eu anomalies of this plagiogranite are inconsistent with fractionation of the basic melts to yield silicic magmas which would be dominated by removal of plagioclase, and thus producing pronounced negative Eu anomalies. The LREE-enriched patterns, characteristically with no negative Eu anomalies (Figs. 19A &B), would be compatible with generation by partial melting from mafic sources, in which amphibole and or/garnet is present as residual phases in the source (Hanson, 1980). Other element abundances, such as Al_2O_3 and Fe_2O_3, would be comparable with those of tonalitic melts produced by dehydration melting of amphibolites (Beard and Lofgren, 1991).

3-5. Discussion

3-5.1. Tectonic setting

There is a lot of discussion in the literature over the nature and origin of the southern Kohistan region which is considered to represent the lower to intermediate levels of an oceanic-island arc. The geochemistry and tectonic setting of this part of the Kohistan arc have been studied by several workers and different hypotheses about its origin have been presented. Tahirkheli et al. (1979), Bard et al. (1980) and Bard (1983) proposed the Kamila Amphibolite Belt as oceanic basement which was intruded by subduction-related Jijal and Chilas Complexes. However, the arguments of Jan (1988) and Treloar et al. (1990) hinge on the composite nature of the Kamila Amphibolites, consisting of metamorphosed basic volcanics and plutonics of arc magmatic affinity, while Miller et al. (1991) postulated that the Kamila Amphibolites are plutonic in nature and correlated them with the Chilas and Jijal Complexes.

More recently, Khan et al. (1993) have explained the chemical characteristics of some of the Kamila Amphibolites in more detail and classified the fine-grained metavolcanic rocks into two distinct geochemical suites: 1) Ti-rich, HFSE- and HREE-enriched suite, referred as E-type and 2) Ti-poor, HFSE- and HREE-depleted suite, alternatively called as D-type. Meta-plutonic amphibolites have chemical characteristics akin to the D-type amphibolites and their chemistry points to a subduction-related origin, while the chemical characters of the E-type amphibolitic rocks resemble those of basalts from a MORB-like source. To place further constraints on their origin, Khan et al. (1993) concluded that the MORB-like affinities of Kamila E-type metavolcanics and their intercalation with D-type, is most consistent with the interpretation that these formed in a back-arc basin (Khan et al., 1997). Whereas Treloar et al. (1996) interpreted

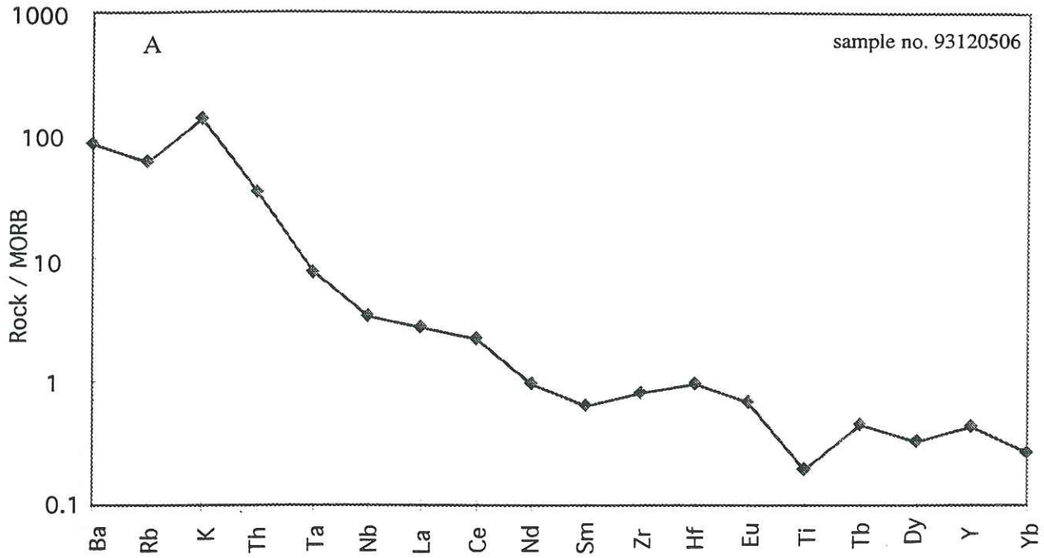

Figure 19 A. MORB-normalized multi-element diagram for the granite from N-Pattan, Kamila Amphibolites. Normalizing values after Sun and McDonough (1989).

Spectre multi-éléments normalisé aux MORB pour les plagiogranites du N-Pattan, amphibolites de Kamila. Valeurs de normalisation d'après Sun et McDonough (1989).

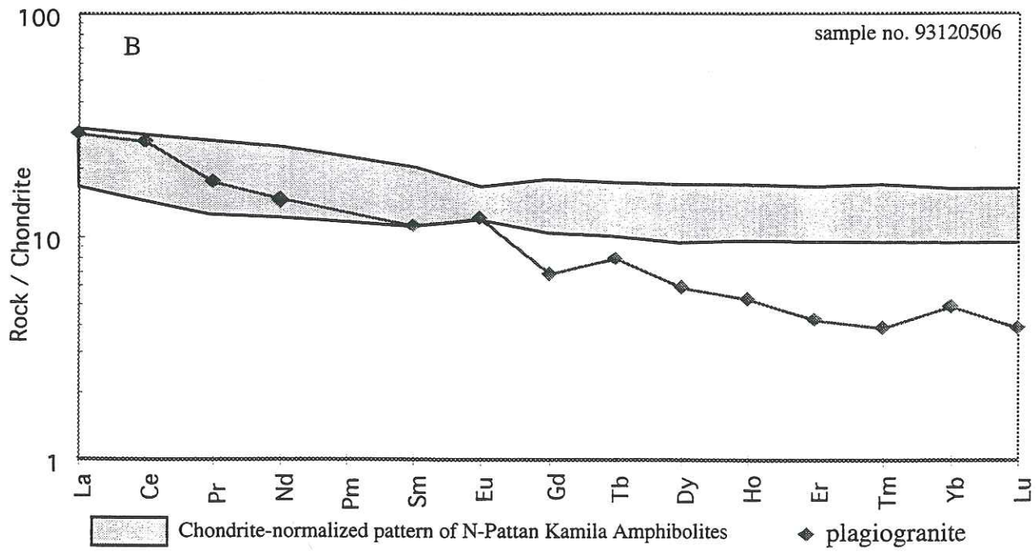

Figure 19 B. Chondrite-normalized REE plots of the Kamila Amphibolites granite. Normalizing values after Nakamura (1974).

Spectre de terres rares normalisé aux chondrites du plagiogranite des amphibolites de Kamila. Valeurs de normalisation d'après Nakamura (1974).

these E-type amphibolites as remanents of a pre-arc oceanic crust generated entirely within an intra-oceanic setting and formed the basement of the incipient Kohistan arc. Because of the slightly higher TiO_2 and HFSE values in the fine-grained amphibolites, the Kamila Amphibolites have become the centre of the controversy concerning their tectonic environment. Similarly, the nature of the processes and materials involved in their generation and how they have influenced the geometry, petrology and geochemistry of the arc magmas is incompletely understood.

The results of this study clearly show that the coarse-grained plutonic rocks from the Kamila Amphibolites from Indus Valley are chemically different from the fine-grained metavolcanics. The chemistry of the Group-1 rocks is more akin to the N-type MORB with some tendencies to OIB for some Ti-rich samples, and Group-2 have more closer affinity with arc tholeiites (with some samples showing a calc-alkaline affinity). Majority of these metaplutonic rocks have negative Ti and Zr anomalies with low Th content, typical of intra-oceanic arc lavas (Figs. 18A & B).

Texturally and geochemically, the Kamila Amphibolites are classified into three facies: 1) a coarse-grained facies representing plutonic rocks (metagabbro and metadiorite; Group-2); 2) a fine-grained facies rocks (Group-1) which are intruded by coarse-grained plutonic rocks of Group-2 and have generally volcanic protolith; and 3) plagiogranite which intruded these amphibolites. The relationship between the two main facies, which have distinctive geochemical characteristics, is not without controversy.

The dissimilarities between the two groups are illustrated by comparison of their major and trace element characteristics. In particular, the rocks belonging to Group-1 differ from the rocks of Group-2 in having relatively low SiO_2, Al_2O_3, P_2O_5 and Na_2O contents, and higher MgO, FeO, CaO and TiO_2 (Figs. 8F,E,G,C; Table 1). Trace element distinctions of Group-1 relative to Group-2 include lower abundances of most incompatiable elements (particularly Ba, Rb and Sr, LREE), lower $(La/Sm)_N$ and $(La/Yb)_N$ ratios, and higher abundances of transitional elements (Figs. 14 & 15; Table 1). The incompatible trace element chemistry of the metavolcanic rocks (Group-1) of the Kamila Amphibolites is more comparable with the basaltic rocks of N-type MORB (with some alkaline affinity) while the plutonic rocks have intra-oceanic subduction-related affinity, reflected by depletion in Nb and Ta, and relatively low Th contents.

Two chemically distinct groups can be recognized on the basis of N-MORB-normalized spidergrams, excluding alkali (K, Rb) and alkaline earth (Sr, Ba) elements. The patterns representing rocks of Group-2 (Figs. 18A & B), do not differ significantly and are remarkably parallel, with only minor crossing of these elements; and the part of the pattern from Ta to Yb (i.e. the immobile elements) lies parallel to but slightly lower than MORB, presumably reflecting the pre-subduction characteristics of the mantle wedge (Wilson, 1989). In contrast, Ba, Rb, Th and K are enriched above this level and may also be due to the subduction-zone component added to the mantle wedge. Thus the trace-element patterns of Group-2

(metagabbros and metadiorites) are bunched together with the LILE enrichment and HFSE depletion. A marked depletion at Nb and Ta is a characteristic of island arc tholeiitic magmas (e.g. Wilson, 1989; Saunders et al., 1991). Generally, all the rocks of Group-2 have high Ba/Nb and Ba/La ratios relative to chondrites and OIB, typical of island arc magmatism.

The Group-1, fine-grained metavolcanics from **NP** (such as samples KO-145, 148, 150) and north of Dassu (KO-50) are different from Group-2 in their MORB-normalized element patterns (Figs. 18C & D). The most striking difference is the relative enrichment in HFSE particularly in Ti, Ta and Nb in Group-1 relative to Group-2. By comparison with Group-2, rocks of Group-1 show no negative Ta-anomaly, and very small negative Nb-anomaly (e.g. samples KO-148, KO-150), and part of the curve from Th to Gd also discriminates these samples from the Group-2 (Fig. 18C). The melts in Group-2 are highly to moderately LREE depleted, with $(La/Yb)_N$ ranging from 0.27 to 0.54 (Table 1). Eu in this group ranges from positive to no anomalies, roughly correlating with the SiO_2 concentrations. The difference in trace element contents and patterns supports the conclusion that the rocks of Group-1 are not the deformed protolith of other plutonic rocks of the Kamila Amphibolites. On the contrary, these metavolcanic basic rocks are genetically related among themselves and the similar REE distribution in these rocks (Fig. 17C) suggests that all these rocks have a common source region and such geochemical characteristics point to an involvement of an N-type MORB source in the generation of the metavolcanics of Group-1.

Th/Yb vs Ta/Yb diagramme (Fig. 20) can also be applied in the manner proposed by Pearce (1983) to monitor the tectonic affinity of these rocks and the involvement of crustal rocks in magma (either as a recycled component or by direct contamination). Some samples from Group-2 of the Kamila Amphibolites are displaced to higher Th/Yb ratios and plot in the calc-alkaline fields of oceanic island arc, implying some influence of contribution from crustal sources during magma genesis, but this needs isotopic approach for evaluation. The metavolcanic rock assemblages belonging to Group-1 of the Kamila Amphibolites plot within the diagonal array of basalts from non-subduction settings, implying a MORB affinity and insignificant contribution from the crustal sources during basalt genesis (Fig. 20). This diagramme also illustrates that the metavolcanic amphibolites are not derived from an enriched mantle source, but show a greater influence of an N-MORB source with possible contribution of a less depleted mantle source.

The selective enrichment characteristic of the subduction component also forms the basis for a number of discrimination diagrammes. Data from the Kamila Amphibolites have been plotted in Figure 21 of Cabanis and Lecolle (1989). The data from Group-2 plots almost entirely within the tholeiitic to calc-alkaline fields of volcanic-arcs. However, the metavolcanic rocks (Group-1) plot between the Back arc and MORB fields on the diagram, consistent with the previous interpretation, despite the greater scatter.

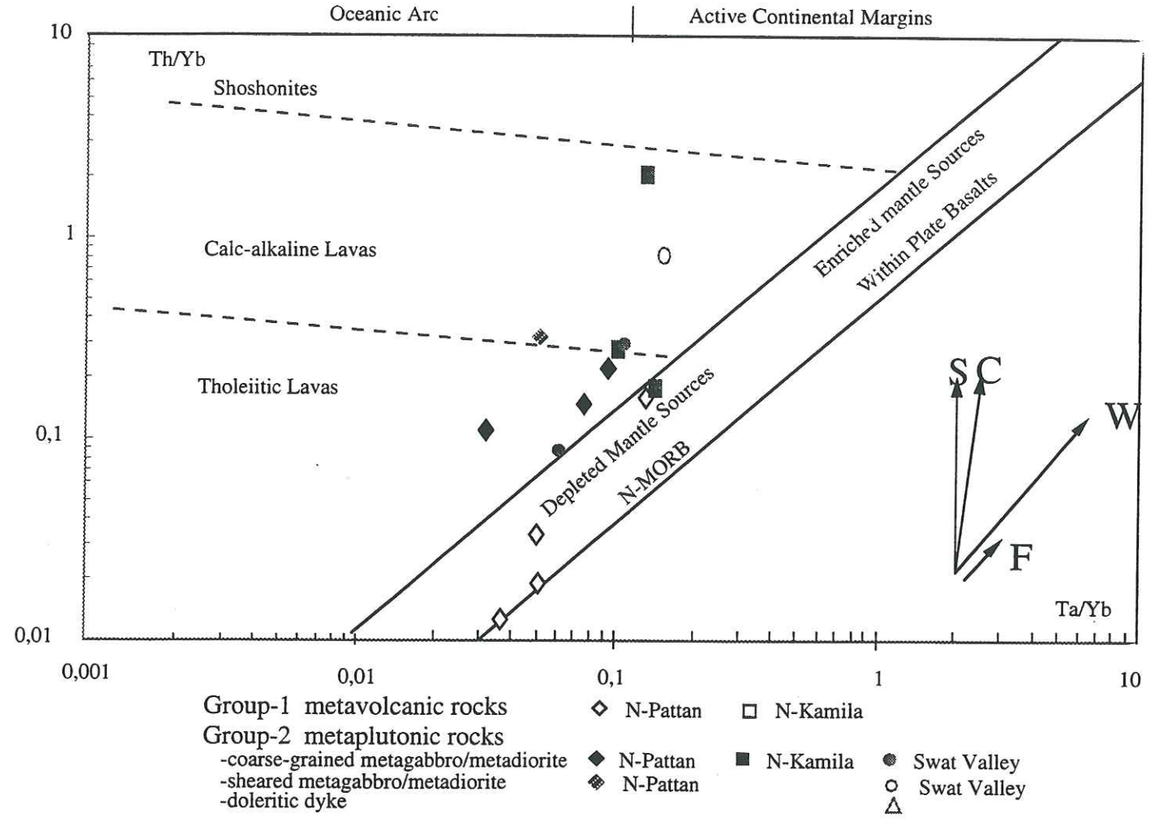

Figure 20. Th/Yb versus Ta/Yb diagramme (Pearce, 1983) indicates that metavolcanic rocks from N Pattan are plotted in the array of basalts from non-subduction settings and metaplutonic rocks are in the tholeiitic field of oceanic-island arc.
Vectors indicate contribution of : S- subduction; C- crustal contamination;
W- within-plate component; F- fractional crystallization

Le diagramme Th/Yb en fonction de Ta/Yb (Pearce, 1983) indique que les métavolcanites du N-Pattan sont localisées dans le domaine des basaltes de contexte non subductif, et les métaplutonites dans le champ tholéiitique des arcs insulaires océaniques.

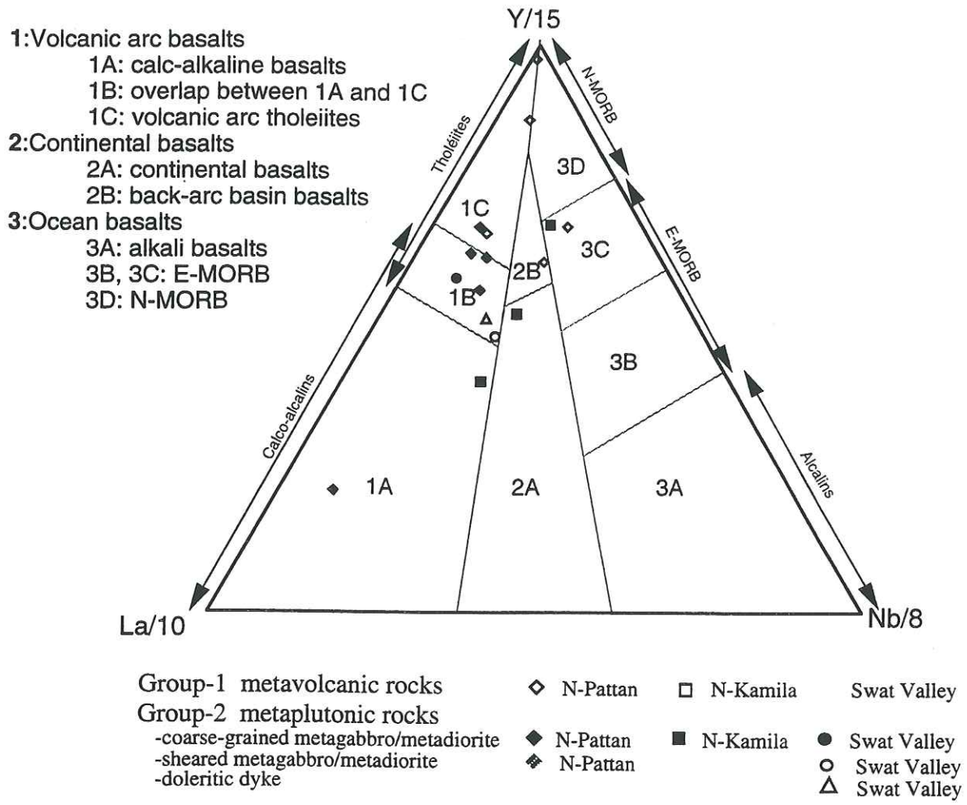

Figure 21. Y/15-La/10-Nb/8 discrimination diagram of Cabains & Lecolle (1989) showing the separation of volcanic-arc basalts, continental basalts and oceanic basalts.

Diagramme de discrimination Y/15-La/10-Nb/8 de Cabains & Lecolle (1989) faisant apparaître la distinction entre les basaltes d'arc océanique, les basalts continentaux et les basaltes océaniques.

3-5.2. Petrogenesis

In the light of abundant trace element data on basalts from various tectonic settings, it appears that differences in melting processes at ocean ridges and island arcs may also be reflected in certain key element ratios (Wood et al., 1979; Tarney et al., 1981). The production of 'tholeiitic' melts from refractory peridotite in the two environments differs largely only in terms of the P_{H2O} conditions attending melting. Partial melting under high P_{H2O} in subduction zone environments appears to stabilize phases such as phlogophite, amphibole, sphene, ilmenite or rutile which have a strong control over the abundances of the high-field strength elements (HFSE, e.g. Ti, Zr, Hf, Nb, Ta). This results in a depletion of these elements relative to the REE (i.e. La/Nb or La/Ta ratios much greater than chondritic in subduction-related basaltic and granitic magmas: Saunders et al., 1980; Wood et al., 1981). On the other hand the essentially anhydrous fusion processes at mid-ocean ridges produce little or no fractionation between the HFSE and REE, and MORB have La/Ta ratios (approximately 15) similar to chondritic value (approximately 16; Sun, 1980). Consequently, the rocks in Group-1 (metavolcanics) have low La/Ta ratio ranging from 5 to 14 and the rocks of Group-2 have La/Ta ratio of more than 30. Wood et al. (1979) note that the La/Ta ratios for N-type MORB approximate to a value of 15, while those for destructive plate margin magmas are generally greater than 30, compared with a chondritic value of approximately 16. If such chemical characteristics can with any justification be extrapolated to Group-1 of Kamila Amphibolites, the low La/Ta ratios suggest that these amphibolites have a closer affinity with ocean floor, rather than island arc affinity. While the Group-2 of the Kamila Amphibolites have high La/Ta ratio (> 30), and have a closer affinity with island arc, rather than MORB.

Similar source rocks and similar conditions of melting in the source of the parent magmas should result in consistent ratios at least of some trace elements. In the contrary, both REE and their ratios suggest different sources for the Group-1 & 2. Using Ti/V ratio, Group-1 samples KO-145, 150, 151 and KO-48 have this ratio 22, 32, 68 and 42 respectively supposed to be typical for MORB and MORB-like compositions in young settings, whereas the low values of samples in Group-2 are typical for arc tholeiites (Shervais, 1982).

Primary partial melts in equilibrium with mantle olivines should have Mg-numbers of 67 (using data of Roeder and Emslie, 1970) or larger (Nicholls, 1974; Bender et al., 1978). In contrast, the different facies of the Kamila Amphibolites have a rather wide range in, and generally low values of, Mg-number and Cr and Ni content (Table 1). Plotting the Al_2O_3/TiO_2 and CaO/TiO_2 ratios against TiO_2 (Figs. 22A & B) in the Kamila Amphibolites indicate that such trends can only be duplicated by a fractional crystallization mechanism if a very calcic plagioclase and clinopyroxene is substracted from the successive liquids. This, together with the rapid decrease in Ni and Cr with increasing Zr abundance, implies that much of the chemical variation in these metaplutonic rocks may be attributed to crystal fractionation processes.

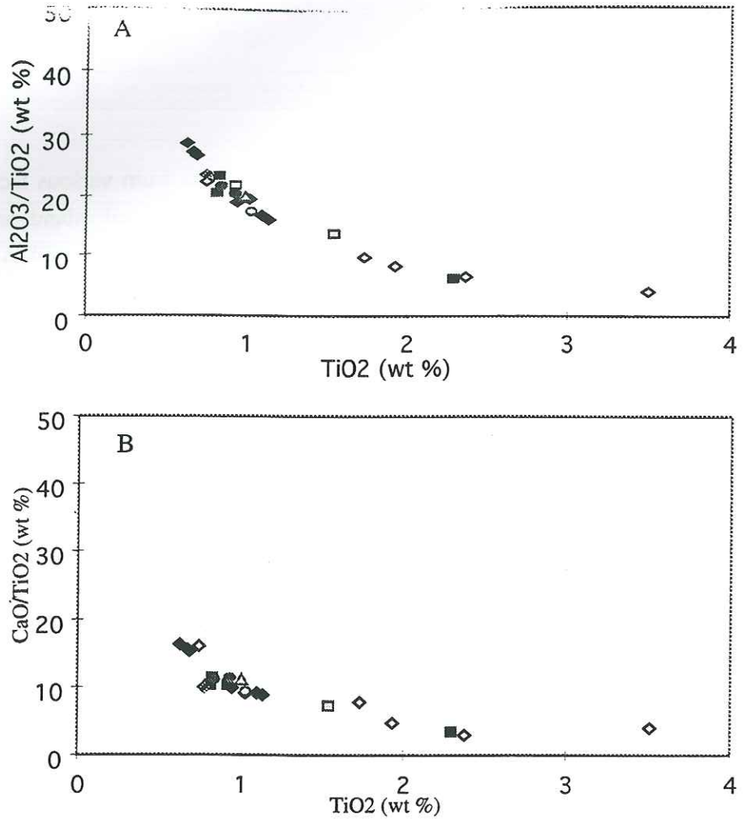

Figure 22. Plot of Al2O3 / TiO2 and CaO / TiO2 against TiO2 for the different facies of the Kamila Amphibolites.

Diagramme du rapport Al_2O_3/TiO_2 et CaO/TiO_2 en fonction de TiO_2 pour les différents faciès des amphibolites de Kamila.

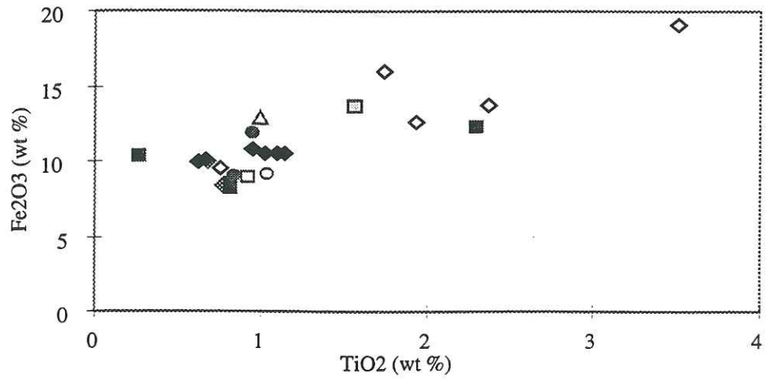

Figure 23. TiO2 versus Fe2O3 relationship during the crystallization of different facies of the Kamila Amphibolites.

Relation TiO_2-Fe_2O_3 pendant la cristallisation pour différents faciès des amphibolites de Kamila.

However, the magmas do hold clues to the origin of the within-suite variation. They are having almost invariably plagioclase, remanents of clinopyroxene and orthopyroxene in the core of hornblende, and titanomagnetite, and hence a potential for crystal fractionation clearly exists. In this instance, it is necessary to investigate the apparently anomalous behaviour shown by some samples of Group-1 (fine-grained metavolcanics) for FeO, TiO_2 and a number of trace elements (Table 1). FeO, TiO_2, V, Ta and Zr partition strongly into titanomagnetite, and hence crystallization of a relatively small proportion of this mineral could radically affect their concentrations in the magmatic system. Therefore, it would seem that crystallization of a titanomagnetite-bearing basaltic assemblage in the metavolcanic amphibolites (Group-1) can account for the anomalous values of Fe-Ti-Ta-V in these samples (Fig. 23). The result of this study suggests that most of the samples belonging to the Group-1 of the Kamila Amphibolites may be the products of cumulus enrichment processes and the anomalous values of some elements shown by these samples are due to the presence of some accessory phases like titanomagnetite (as also confirmed petrographically by Khan et al., 1993).

3-6. Conclusion

The results and the interpretations of the present study provide an important perspective on the genetic history of rock assemblages of the Kamila Amphibolites. The main conclusion that can be reached on the basis of geochemical studies is that there is a bimodality of compositions, one group having clear MORB affinities, the other having clear island-arc affinities. We would suggest that the complex-metavolcanic amphibolite association of the Kamila Amphibolites, and similar units occurring elsewhere in the Kamila Amphibolites, have N-type MORB affinity and may represent fragments of pre-existing oceanic crust (as originally suggested by Tahirkheli et al., 1979; Bard et al., 1980; Bard, 1983 and Treloar et al., 1996). But the assemblages of the metaplutonic rock of the Kamila Amphibolites from the study area differ significantly from MORB by a characteristic over-abundance of LILE over other incompatible elements such as REE or HFSE and pronounced depletion in Ta and Nb. We relate this to an original tectonic setting of southern Kohistan above the Tethyan actively subducting plate to the north. Fluids enriched in water-soluble LILE are released from the subducting slab by dehydration of OH-bearing minerals inhomogeneously impregnating the overlying mantle wedge, the actual source region of these rocks. Therefore, the mantle-derived heat and material contributed by subduction-related magmatism offer a reasonble explanation of the arc-like distribution of the rock assemblages of the metaplutonics of the Kamila Amphibolites.

CHAPTER-2

PETROGRAPHIC AND GEOCHEMICAL CHARACTERISTICS OF THE CHILAS IGNEOUS COMPLEX

CHAPTER-2

THE CHILAS IGNEOUS COMPLEX

1- GENERAL FEATURES

The Chilas Igneous Complex is a large plutonic body which extends for more than 300 km between Nanga Parbat and western Dir and attains a maximum width of 40 km in its middle part (Figs. 3&24). The geological setting of the Chilas Complex and its nature are discussed by several researchers (Jan and Mian, 1971; Jan and Kempe, 1973; Jan, 1979; Bard et al., 1980; Khan et al., 1985, 1989, 1993). Bard et al. (1980) interpreted the complex as a lopolith. The Kargil Complex in Ladakh, to the east of Nanga Parbat, resembles the Chilas Complex (Rai & Pande, 1983). Honegger et al. (1982) suggested that the Kargil Complex may represent the cumulates of the magma chamber of the Dras Volcanics.

According to Jan (1980), the Chilas Complex cooled and equilibrated under conditions of the pyroxene granulite facies, estimated at 750° to 850°C and 5 to 6.5 kbar. Partial retrogression to amphibolites and greenschists occurred extensively during uplift, especially along its southern and western margins and its central part. The complex intrudes the volcanic and sedimentary rocks, and contains xenoliths of mafic rocks, biotite schists and paragneisses. Subsequent to this pioneer works on the general geology and preliminary metamophic conditions, a detailed work on the Chilas Igneous Complex was carried out by Jan et al. (1984) and Khan et al. (1985, 1989, 1993). They described the general geology, petrography and then discussed the origin and mode of emplacement of the complex which will be discussed later on.

Basically, the Chilas Igneous Complex is composed of two distinct rock associations: 1) the **Main Facies Zone** (formely known as gabbro-norite association), and 2) the **cumulate ultramafic-mafic-anorthosite association (UMA**; Khan et al., 1989) which are distributed in the Main Facies Zone in the Indus Valley (Fig. 24).

The Main Facies Zone forms at least 85 percent of the complex and consists of various kinds of rock assemblages such as gabbronorite, massive gabbro, pyroxene-diorite, quartz-diorite, and granite. They occur as intermingled composite bodies or masses, although they may be discriminated from each other when observed in the field carefully.

There are several isolated outcrops of ultramafic-mafic-anorthosite associations (UMA), exposed in the Main Facies Zone. The largest mass of this association is **Chilas ultramafic-mafic-anorthosite association (UMA)**, located east of Chilas and described in detail by Khan et al. (1989). West of Chilas, two more bodies are exposed along KKH, 1) in the Thurli Gah valley, which is similar to Chilas UMA, and 2) a layered gabbro body, exposed south of Khanbari Gah valley (Fig. 24). In this layered body, we have not observed ultramafic rocks, but similarities of the layered gabbro with others UMA and intrusive relation with the surrounding gabbronorite of the Main Facies Zone suggest that it is also related to the others

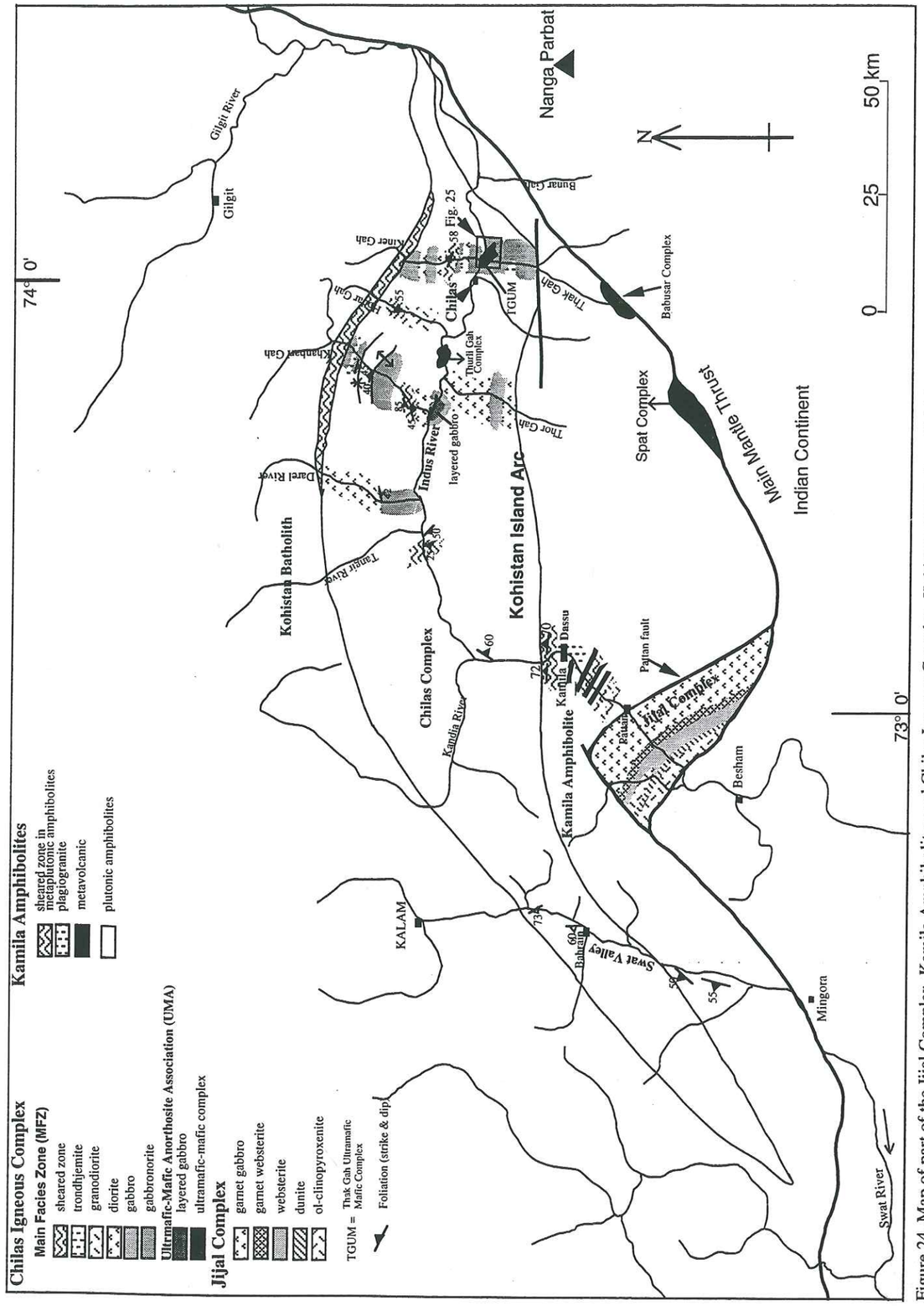

Figure 24. Map of part of the Jijal Complex, Kamila Amphibolites and Chilas Igneous Complex, Kohistan arc, northern Pakistan.
Carte géologique d'une partie du Complexe Igné de Chilas, amphibolites de Kamila et complexe de Jijal, arc du Kohistan, Pakistan Nord.

UMA. These ultramafic-mafic rocks are of cumulate origin and stratigraphically higher units are always northeast of lower units. Genetic relationship between these UMA's and host gabbronorite and the origin of their magmas are still uncertain, although many geological and petrological aspects on the Chilas Complex have been discussed by many workers (Khan et al., 1989, 1992).

In this manuscript, we will refer the Chilas ultramafic-mafic-anorthosite association of Khan et al. (1989) as **Thak Gah Ultramafic-Mafic Association (TGUM)**. The rock assemblages of the **TGUM** and as a whole **Main Facies Zone (MFZ)** do not show the effects of intense regional metamorphism but at few places ductile shear zones are exhibited. These mylonitic shear zones are similar to anastomosing shear zones such as found in the Kamila Amphibolite Belt and leucocratic, garnet-bearing veins are also associated with them locally. These shear zones in the **Main Facies Zone** are typically narrow, ranging from centimetres to tens of metres, and are heterogeneously distributed. These are often anastomosing, separating great masses of relatively undeformed gabbronorite and pyroxene diorite and are more frequently seen in the southern part of the Chilas Complex (between Seo and Shatial villages) and less frequently in the northern part of the Chilas Complex (e.g. Kinner Gah). They do not show any consistent attitude, but most of these shear zones are trending northeast-southwest, with steep northerly dip. Curvature of fabric or layering into the more intensely deformed zones and small-scale structures suggest both up dip and normal fault sense of displacements (e.g. Khan and Coward, 1982). East-west trending antiforms and synforms are observed, indicating a folded structure in the Chilas Complex. Some parts of the Chilas Complex have changed into amphibolite during uplift, but primary textures are still well preserved.

2- THAK GAH ULTRAMAFIC-MAFIC ASSOCIATION

2-1 Field Relationships

TGUM is composed mainly of ultramafic and mafic sequences and crops out in an area as large as 5 km^2. It extends 3 km along the KKH, approximately 2 km east of Chilas town and detailed schematic-section is shown in Figure 25. The body is composed of cyclic units of layered cumulate rocks. The layering suggests that northeast represents the younging of the ultramafic-mafic association. The majority of the rocks are classified into cumulates ranging from massive dunite/wehrlite, plagioclase-orthopyroxene pegmatoid, well-layered mafic gabbro and anorthosites, heterogeneous gabbro, troctolite and massive gabbro.

The ultramafic cumulate consists of olivine cumulate (dunite), associated with minor amount of olivine-clinopyroxene cumulate (wehrlite) and orthopyroxene-clinopyroxene cumulate (websterite). It occurs as 10 to 100 metres thick layers, alternating with thin layers of

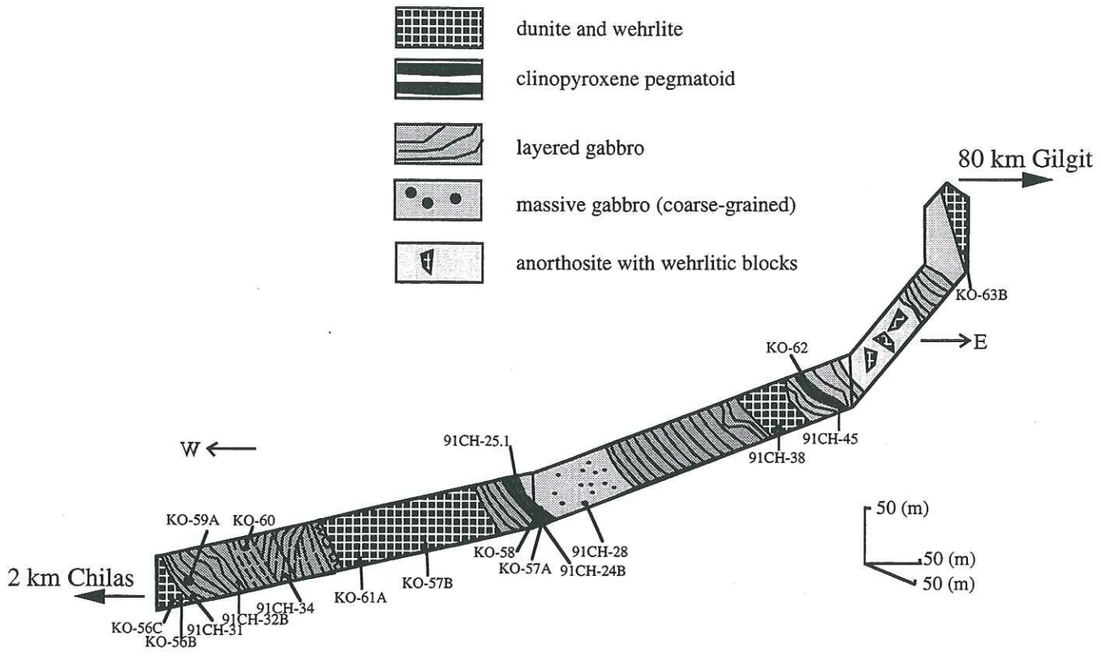

Figure 25. Detailed schematic-section of the Thak Gah Ultramafic-Mafic rocks (TGUM; modified after Takahashi et al., 1993). Locality along the Karakoram Highway, 2 km east of Chilas town. Sketch is shown as a panel diagram projected from the north.

Carte géologique d'une partie du Complexe Igné de Chilas, amphibolites de Kamila et complexe de Jijal, arc du Kohistan, Pakistan Nord.

plagioclase-dominant cumulate. Plagioclase-dominant cumulate (two pyroxene gabbro) occurs as layered, several metres thick and develops on the olivine cumulate. Sedimentary structures such as parallel-, cross-beddings, graded-beddings, convolute laminations, slumping and trough banding are prominent in the well-layered units (Fig. 26). Phase layering, resulting from the appearance or disappearance of a cumulus phase is a dominant feature of TGUM. The fine scale igneous layering is defined by sharp changes in the constituent minerals, modal proportions, or textural relations and ranges in thickness from less than a centimetre to tens of centimetres. Generally, these layers pinch out or grade laterally into other layers. Individual layers most commonly are lenticular and wedge out, commonly over a distance of only a few metres or tens of metres. Sometimes contacts with the stratigraphically younger layers are marked by abrupt mineralogical changes such as the reappearnace of olivine and pyroxene at the bottom and plagioclase at the top (Fig. 26). But sometimes contacts between these layers are gradational over several millimetres (Fig. 27). These layerings are best defined in the layered two proxene gabbro. Generally, the boundary between the top of the layered gabbro and the overlying olivine-dominant layer is generally straight, and is parallel to the rhythmic layering or lamina in the upper part of plagioclase-dominant cumulate.

The heterogeneous mafic unit comprises of troctolite, anorthosite, olivine gabbro, gabbro, gabbronorite and hornblende gabbro. This unit has a number of ultramafic xenoblocks and olivine-clinopyroxene xenocrysts (Fig. 28). The syn-sedimentary fragments and blocks of well-layered gabbroic rocks are also seen in the heterogeneous gabbros. At many places, gabbroic dykes and pockets are seen in the ultramafic cumulates, whereas in some outcrops ultramafic dykes are seen in the gabbros (Fig. 29). As seen in Figure 30, a large gabbro pocket occupies a space in the ultramafic cumulate. Similarly the contact between ultramafic cumulate (wehrlite) and heterogeneous gabbro-anorthosite is sharp and no deformational features are observed. This suggests that when wehrlite magma was intruding into the gabbro or vice versa, both the lithological units were not completely solidified. Presence of abundant wehrlitic blocks in gabbroic rocks further indicate that the hosting gabbro acted as more mobile magmas than that of the wehrlitic magma (Fig. 31). All of these rocks formed magmatic-mechanic melange and do not represent mantle tectonite. All the units from the UMA are enveloped by massive, uniform gabbronorite. Contacts between the ultramafic cumulates and the surrounding gabbroic rocks are generally sharp and without any quenching textures (Fig. 32), suggesting that the temperature difference between the two units was not significant to produce any quenching phenomenon. In contrast, the layered gabbro, exposed south of Khanbari Gah valley (Fig. 24) shows a different relationship with the surrounding gabbronorite. Its layerings are truncated by the intrusive host gabbronorite, suggesting that the gabbronorite of the Main Facies Zone is younger than the layered gabbro.

In relation to a magmatic evolution model of the Chilas Complex, Khan et al. (1989) explained that the UMA magmatism generated during intra-arc rifting. It is evident, however, that the field evidence examined here, suggests a magma/magma relationship between the

Figure 26. Photograph of isomodal layering in gabbro in Thak Gah Complex. Alternating layers result from different ratios of cumulus plagioclase and pyroxene. Note convolute lamination in plagioclase layers above the arrow.

Photographie du litage isomodal dans un gabbro dans le complexe de Thak Gah.

Figure 27. Photograph of modally-graded layering where the layers are marked by appearance and disappearance of mafic minerals and felsic minerals in Thak Gah Ultramafic-Mafic Complex, east of Chilas.

Photographie de modally-graded layering où l'alternance est gouvernée par l'apparition et la disparition des minéraux mafiques. Association mafique et ultramafique de Thak Gah , Est de Chilas.

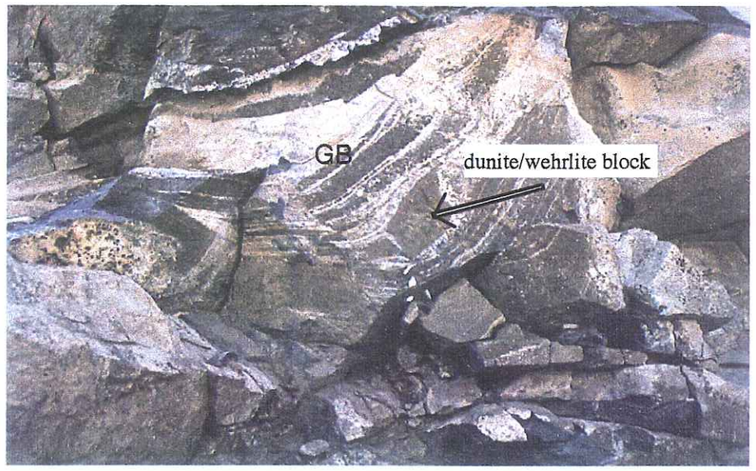

Figure 28. Photograph of rip-up clast of dunite/wehrlite in layered gabbro (GB), Thak Gah Complex, east of Chilas along the KKH.

Photographie de rip-up clastes de dunite/wehrlite dans un gabbro lité, complexe de Thak Gah, Est de Chilas, le long de la KKH.

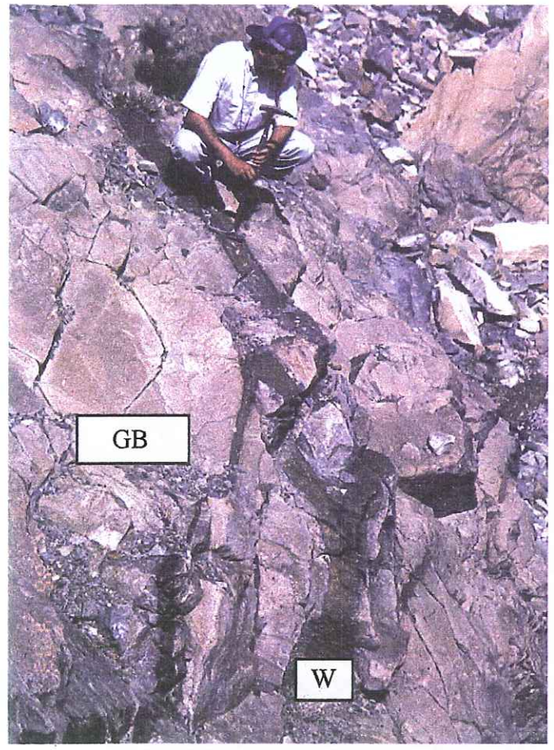

Figure 29. Photograph showing the wehrlitic dikes (W) cross-cutting the isotropic gabbroic host rocks in Thak Gah Complex, east of Chilas and along the KKH.

Photographie montrant les dykes de wehrlite (W) recoupant les gabbros isotropes dans le complexe de Thak Gah, à l'Est de Chilas et le long de la KKH.

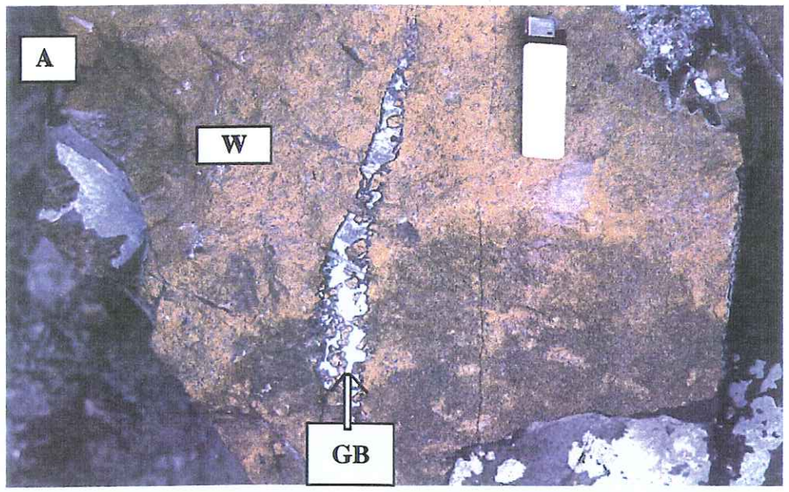

A = Anorthosite gabbro trapped in wehrlite/dunite body

Photographie d'un gabbro à anorthose (GB) piégé dans une fente ouverte dans un massif de wehrlite/dunite.

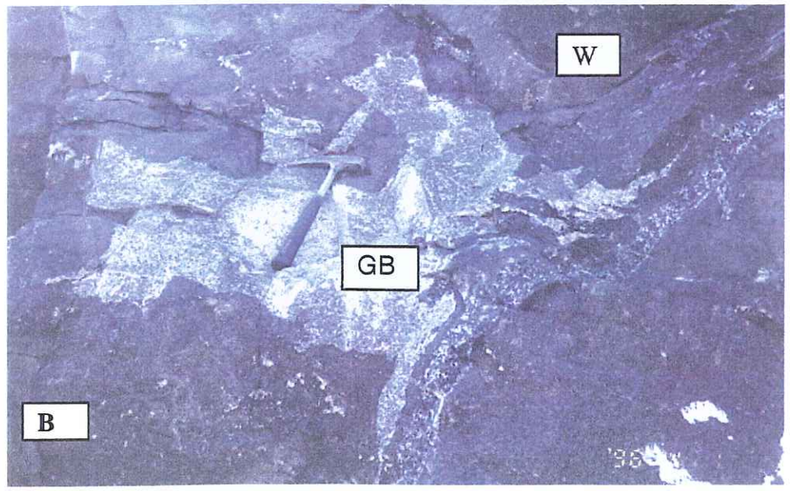

W = Wehrlite GB = Gabbro

Figure 30. Photograph of anorthositic gabbro trapped in an open crack (A) and a pocket (B) of the wehrlite body in Thak Gah Complex, east of Chilas. This shows anorthositic melt channeling from the main anorthositic body into the wehrlite body.

Photographie d'un gabbro anorthosique gabbro (GB) piégé dans une poche du massif de wehrlite body dans le complexe de Thak Gah, Est de Chilas.

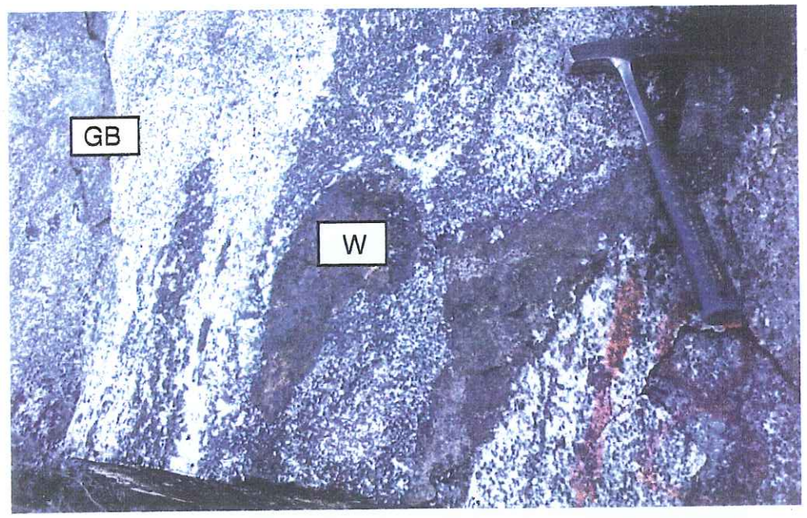

GB=gabbro W=wehrlite

Figure 31. Photograph of heterogeneous olivine gabbro and anorthosite, containing wehrlitic xenoblocks (W) and olivine xenocrysts in Thak Gah Ultramafic-Mafic Complex, east of Chilas.

Photographie d'un mélange hétérogène de gabbro à olivine et d'anorthosite, contenant des xénoblocks de wehrlite et des xénocristaux d'olivine dans le Complex Ultramafique et Mafique de Thak Gah , à l'Est de Chilas.

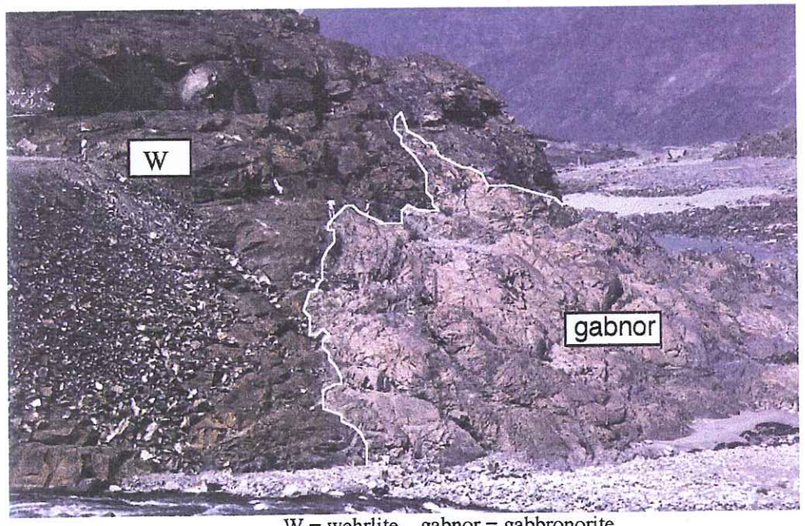

W = wehrlite gabnor = gabbronorite

Figure 32. Photograph showing sharp contact between wehrlite (W) and gabbronorite, north of Thak Gah bridge, along Indus River in Thak Gah Complex. The gabbronorite body is surrounding the Thak Gah Complex.

Photographie montrant un contact franc entre une wehrlite et une gabbronorite Nord du pont de Thak Gah bridge, le long de l'Indus dans le complexe de Thal Gah. Le massif de gabbronorite entoure le complexe de Thak Gah.

ultramafic intrusives and the gabbroic hosts. This means that both the magmatism took place at the same time.

2-2 Petrographic Characteristics

The cumulate ultramafic rocks in the TGUM are mostly dunite, wehrlite and websterite. Plagioclase is rare in some dunites. They consist mainly of olivine, with subordinate amount of clinopyroxene, orthopyroxene and ± plagioclase. The plagioclase-dominant cumulates show adcumulate textures.

Dunite occurs mainly in the lower zone but also appears several times in the upper level of TGUM (Fig. 25). It is composed predominantly of coarse (commonly 2-4 mm) olivine (91-95%). Disseminated chromite and pleonaste (about 1-2%) and trace amount of clinopyroxene, orthopyroxene and amphibole are commonly present. Amounts of clinopyroxene and plagioclase generally increase upward within the dunite unit. Grain size also increases slightly with stratigraphic height. Textures in the dunite vary from tabular equigranular to granoblastic. Evidence for both plastic deformation and static recrystallization is seen in these rocks. Some olivine displays weak undulatory extinction. Kink-banded olivine is also frequently seen. Clinopyroxene is present as cumulus phase; however, most clinopyroxene is present as intercumulus phase. Most of the orthopyroxene is fine-grained (1-2 mm), subhedral, equant, sometimes enclosing olivine and crystallized as a liquidus phase.

Wehrlite (olivine-clinopyroxenite) is composed dominantly of coarse (3 - 6 mm) cumulate crystals of clinopyroxene and olivine. Orthopyroxene, greenish spinel (pleonaste) and plagioclase are also present in varying amounts. The clinopyroxene commonly contains growth twins and, narrow exsolution lamellae of clinopyroxene (Fig. 33), orthopyroxene and green spinel (Fig. 34). Textures are generally adcumulate, with both pyroxene present as cumulate phases. Symplectitic texture between olivine and clinopyroxene is also frequent (Fig. 35). As in the dunite unit, wehrlite also show evidence for high-temperature recrystallization. Igneous olivine and pyroxene grains interfinger complexely and sometimes are surrounded by smaller, equant, recrystallized grains with polygonal textures.

Websterites are medium- to coarse-grained and are clinopyroxene-dominant. Texture ranges from adcumulate to granoblastic. Clinopyroxene has exsolution lamellae of orthopyroxene.

Gabbroic rocks comprise a heterogeneous igneous assemblage. They range from layered gabbro to massive gabbro to gabbronorite. The layered gabbro has layering and textural characteristics that indicate it originated by cumulus process (Fig. 27).

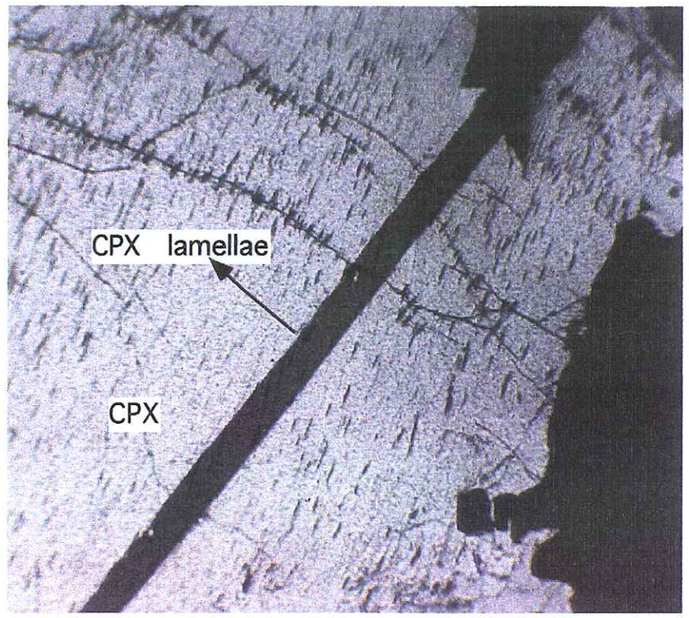

SCALE=X5

Figure 33. Photomicrograph showing the exsolution lamellae of CPX in CPX in wehrlite, Thak Gah Complex.
Microphotographie montrant les lamelles d'exsolution de clinopyroxène dans la wehrlite, complexe de Thak Gah.

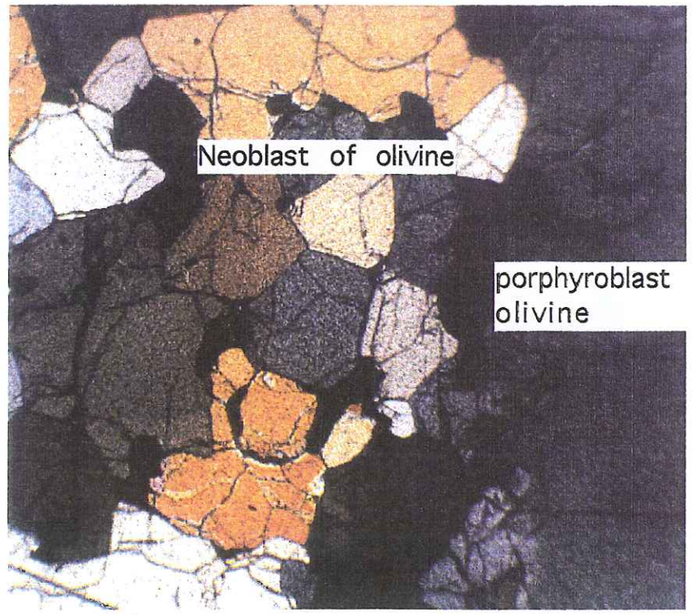

SCALE=X5

Figure 33B. Photomicrograph of recrystallized olivine in dunite, Thak Gah Complex.

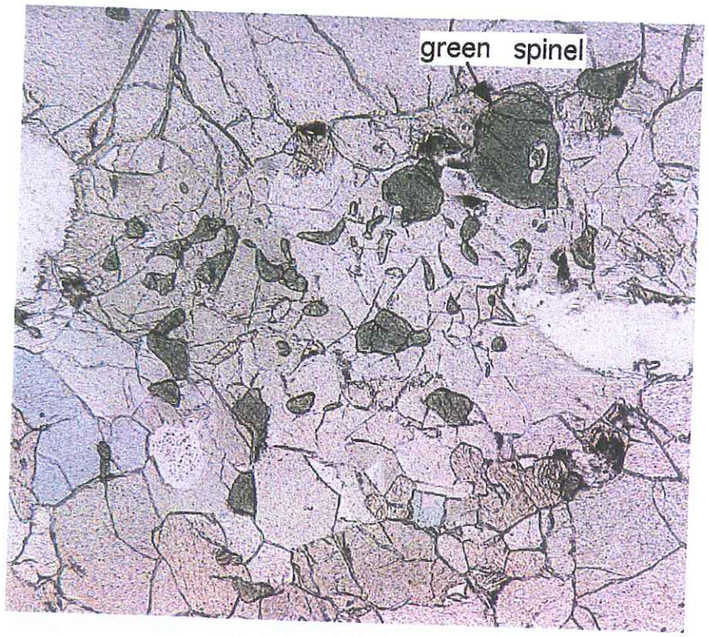

SCALE=X6,3

Figure 34. Photomicrograph showing the exsolution of green spinel in Cpx in wehrlite, Thak Gah Complex
Microphotographie illustrant l'exsolution de spinelle vert dans un clinopyroxène de la wehrlite, Complexe de Thak Gah.

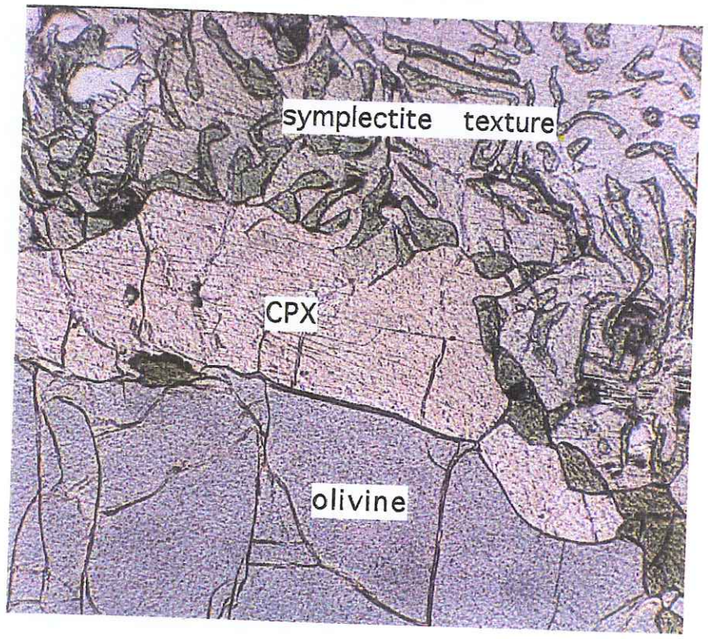

SCALE=X6,3

Figure 35. Photomicrograph showing symplectitic texture between clinopyroxene and spinel in wehrlite, Thak Gah Complex.
Microphotographie montrant la texture symplectitique entre clinopyroxène et une spinelledans la wehrlite du Complexe de Thak Gah.

They are composed of mineralogical assemblages of plagioclase-clinopyroxene-orthopyroxene-olivine in olivine-gabbronorite; plagioclase-clinopyroxene-orthopyroxene in gabbronorite; plagioclase-olivine in troctolite; plagioclase-clinopyroxene in gabbro and plagioclase cumulate in anorthosite. Optical determinations suggest that in all these cumulate assemblages, plagioclase composition ranges from anorthite to bytownite and is also confirmed by previous studies (Khan et al., 1989). Under the microscope, most of the cumulates of the layered gabbro are medium-grade and hypautomorphic and less commonly xenomorphic. Postcumulus minerals are not abundant, and poikilitic textures are seen quite often. A number of samples have a granular polygonal texture, some with 120 degree grain intersections of cumulus minerals. Although postcumulus interstitial minerals are locally preserved, the dominant polygonal fabric is believed to be due to annealing rather than cumulus processes. Coronas of clinopyroxene, orthopyroxene and amphibole around olivine are common where the olivine is in direct contact with plagioclase.

Gabbronorite which surrounds the TGUM, is part of the Main Facies Zone and its petrographic characteristics will be described under the 'Main Facies Zone' unit of this manuscript. Mineral chemistry will be described here and after getting more mineral chemistry data, this section will then be transferred in the Main Facies Zone.

2-3 Mineral Chemistry

Compositions of cumulus minerals were obtained by electron microprobe analysis at Geoscience Laboratory, Geological Survey of Pakistan, using natural and synthetic minerals of known composition as standards (ASTIMEX MIN-25.53; rutile for Ti, quartz for Si, jadeite for Na, chromite for Cr, sanidine for K, olivine for Mg, rhodonite for Mn, bustamite for Ca, YAl garnet for Al and haematite for Fe). Matrix corrections for all the minerals were made by ZAF correction procedure.

2-3.1 Olivine

Chemical composition and structural formula of olivine in the dunite, pyroxenite, layered gabbro and plagioclase-orthopyroxene pegmatoid is given in Table 2. Textures in the ultramafic rocks are characterized by coexisting phases of porphyroclastic-primary olivine and recrystallized polygonal olivine.

The composition range, is Fo_{81} in dunite, Fo_{84} in pyroxenite, Fo_{81} in plagioclase-orthopyroxene pegmatoid and Fo_{79} in layered gabbro. Olivine in layered gabbro is more Fe-rich than the olivine in the ultramafic cumulates and most Mg-rich olivine is in the pyroxenite cumulates (Fo_{84}).

Table 2. Representative olivine composition of Thak Gah Ultramafic Mafic Associations.

Composition représentative des olivines du Cortège Mafique-ultramafique de la Thak Gah.

S.No.	91CH-38	91CH-45	91CH-28	91CH-31
Mineral	olivine	olivine	olivine	olivine
Rock-type	dunite	pyroxenite	pl-opx pegmatoid	layered gabbro
n	3	2	1	2
SiO2	40.00	39.31	39.65	41.29
TiO2		0.02		0.03
Al2O3	0.01			0.01
Fe2O3	17.28	14.96	17.98	19.29
MnO	0.24	0.38	0.25	0.26
MgO	42.49	45.80	43.11	41.07
CaO	0.02	0.01	0.01	0.02
Na2O		0.03	0.01	
K2O				0.00
Cr2O3	0.06	0.07	0.06	
Total	100.09	100.59	101.06	101.97
Cation ratios(O=4)				
Si	1.012	0.984	0.998	1.031
Al-iv				
Al-vi				0.000
Ti		0.003		0.001
Fe	0.366	0.313	0.379	0.403
Mn	0.005	0.008	0.005	0.006
Mg	1.603	1.708	1.618	1.528
Ca		0.003		0.000
Na		0.002		
K				0.000
Cr	0.001	0.002	0.001	0.000
Fo	81.41	84.51	81.02	79.14
Fa	18.59	15.49	18.98	20.84

Abbreviation = pl-opx pegmatoid, plagioclase-orthopyroxene pegmatoid,
n = average of probe points.

Chemical analyses have been previously obtained for olivine from the investigated area by Khan et al. (1989). Their data demonstrate that Fo contents of olivine range from 91 to 85 in dunite, 85 to 76 in peridotite/wehrlite and 80 to 71 in troctolite and gabbro. But all these data demonstrate that the olivines are virtually pure binary Mg_2SiO_4-Fe_2SiO_4 solid solutions, containing about 19-25 percent Fa.

2-3.2 Pyroxene

Chemical composition and structural formula of pyroxenes are given in Table 3. Differences in composition from grain to grain in the same thin-section are not significant.

The Mg-number in clinopyroxene decreases from 75 in pyroxenite, 60 to 57 in layered gabbro, to 59 in massive gabbronorite. As compared to clinopyroxene, the Mg-number of orthopyroxene is low in pyroxenite and gabbronorite (Table 3). It ranges from 72 in plagioclase-orthopyroxene pegmatoid, 67 in pyroxenite, 51 in layered gabbro to 45 in massive gabbronorite.

The major chemical variations of the clinopyroxene are in the proportions of Ca-Mg-Fe, best illustrated in the conventional pyroxene quadrilateral (Fig. 36). The overall compositional range for clinopyroxene in TGUM, is $Ca_{25.5}$ $Mg_{62.6}$ $Fe_{11.8}$ to $Ca_{47.7}$ $Mg_{43.9}$ $Fe_{8.4}$ in pyroxenite, $Ca_{44.2}$ $Mg_{33.4}$ $Fe_{16.4}$ to $Ca_{46.8}$ $Mg_{46.9}$ $Fe_{6.3}$ in layered gabbro, and $Ca_{46.2}$ $Mg_{38.8}$ Fe_{15} in massive gabbronorite. Orthopyroxene is hypersthene and it has on average En_{76} in pyroxenite, En_{82} in plagioclase-orthopyroxene pegmatoid, En_{62} in layered gabbro and En_{59} in massive norite. The majority of the orthopyroxene and clinopyroxene from the TGUM plot in the island-arc gabbro field (Fig. 36). These compositions show that with increasing Fe the clinopyroxene is impoverished in Mg and the orthopyroxene is slightly enriched in the wollastonite component. In gabbro generally, the Mg content decreases while Fe and Ca contents increase, in the clinopyroxene. The diopside/augite variation trend appears more similar to that reported for plutonic rocks in island arcs. In the Border Ranges ultramafic-mafic complex of southern Alaska, orthopyroxene in the ultramafic rocks ranges from En_{87} to En_{82} and in gabbro-norites from En_{77} to En_{58} (Burns, 1985).

Clinopyroxene in the rock assemblages of the TGUM (diopside-salite) have a different composition than clinopyroxene from the gabbronorite from the MFZ, which is salite-calcic augite in composition (Fig. 36). This clearly indicates that they crystallized from a more primitive magma and predate (as suggested by field relations) the gabbronorite magma from the MFZ.

2-3.3 Plagioclase

Chemical compositions and structural formulas of plagioclase are listed in Table 4. The range in chemical compositions is shown in Figure 37. There is distinct gap in the An

Table 3. Representative clinopyroxene and orthopyroxene composition from Thak Gah Ultramafic-Mafic Association.
(Composition représentative des pyroxènes du Cortège Mafique-ultramafique de Thak Gah).

S.No.	91CH-24B	91CH-25.1	91CH-45		91CH-45	
Mineral	clinopyroxene	clinopyroxene	clinopyroxene (C)		clinopyroxene (R)	
Rock-type	pyroxenite	pyroxenite	pyroxenite		pyroxenite	
n	2	2	1		1	
SiO2 (wt%)	57.68	53.37	54.99		54.49	
TiO2	0.23	0.08	0.15		0.27	
Al2O3	2.89	2.16	1.73		2.00	
Fe2O3	6.57	5.18	2.70		3.28	
MnO	0.28	0.20	0.10		0.12	
MgO	20.01	15.23	17.29		17.07	
CaO	11.34	22.99	25.78		21.66	
Na2O	0.54	0.35	0.07		0.04	
K2O	0.05	0.03	0.01		0.02	
Cr2O3	0.27	0.39	0.08		0.27	
Total	99.86	99.99	102.89		99.21	
Cation ratios(O=6)						
Si	2.043	1.960	1.950		1.984	
Al-iv		0.040	0.050		0.016	
Al-vi	0.121	0.054	0.225		0.086	
Ti	0.006	0.002	0.004		0.007	
Fe	0.200	0.159	0.080		0.100	0.123
Mn	0.009	0.006	0.003		0.004	0.005
Mg	1.056	0.834	0.914		0.927	0.915
Ca	0.431	0.905	0.980		0.845	0.912
Na	0.037	0.025	0.005		0.003	0.029
K	0.002	0.002	0.000		0.001	
Cr	0.008	0.011	0.002		0.008	
Wo	25.53	47.66	49.64		45.15	46.78
En	62.64	43.94	46.31		49.51	46.93
Fa	11.83	8.39	4.06		5.34	6.3

S.No.	91CH-31	91CH-34	91CH-14(MFZ)	91CH-24B	91CH-25.1	91CH-28	91CH-34	91CH-14(MFZ)
Mineral	clinopyroxene	clinopyroxene	clinopyroxene	orthopyroxene	orthopyroxene	orthopyroxene	orthopyroxene	orthopyroxene
Rock-type	layered gabbro	layered gabbro	gabbro-norite	pyroxenite	pyroxenite	pl-opx pegmatoid	layered gabbro	gabbro-norite
n	3	2	2	2	1	4	2	1
SiO2 (wt%)	51.39	51.61	50.48	58.53	54.57	56.21	52.85	53.62
TiO2		0.47	0.34	0.01	0.02	1.32	0.18	0.03
Al2O3	3.76	3.11	2.36	0.86	1.44	0.02	1.62	1.30
Fe2O3	3.98	8.59	9.46	12.61	13.75	11.46	22.72	23.79
MnO	0.18	0.27	0.32	0.62	0.58	0.26	0.50	0.80
MgO	16.66	13.31	13.75	25.47	29.42	30.58	21.56	19.62
CaO	23.11	21.75	22.75	0.43	0.44	0.32	0.57	0.49
Na2O	0.41	0.51	0.42	0.15	0.01	0.00		
K2O			0.02	0.00	0.03		0.03	0.02
Cr2O3		0.04	0.02	0.07	0.03		0.05	0.02
Total	99.48	99.65	99.91	98.74	100.28	100.17	100.05	99.70
Cation ratios(O=6)								
Si	1.895	1.929	1.903	2.087	1.948	1.978	1.969	2.011
Al-iv	0.163	0.071	0.097		0.052	0.022	0.031	0.097
Al-vi		0.066	0.008	0.036	0.008	0.033	0.040	0.057
Ti		0.013	0.010	0.000	0.001	0.001	0.005	0.001
Fe	0.123	0.269	0.298	0.376	0.410	0.337	0.708	0.746
Mn	0.005	0.085	0.010	0.186	0.018	0.008	0.016	0.026
Mg	0.915	0.747	0.772	1.353	1.566	1.604	1.197	1.097
Ca	0.912	0.871	0.919	0.016	0.017	0.012	0.023	0.020
Na	0.029	0.037	0.031	0.010	0.001			0.031
K			0.001	0.000	0.001		0.001	0.001
Cr		0.001	0.001	0.002	0.001		0.001	0.001
Wo	46.78	46.17	46.19	0.94	0.84	0.6	1.18	1.07
En	46.93	39.6	38.82	77.53	78.57	82.1	62.1	58.89
Fa	6.3	14.32	14.99	21.53	20.59	17.3	36.72	40.05

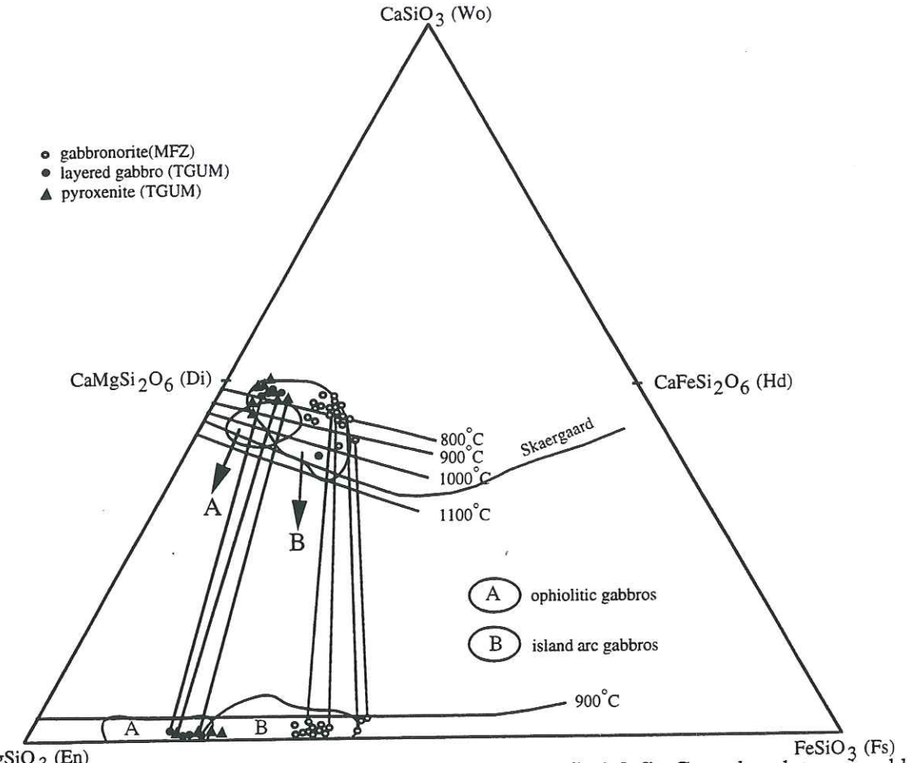

Figure 36. Pyroxene compositions from Thak Gah Ultramafic-Mafic Complex determined by electron microprobe. Compositional fields of island-arc gabbros (Arculus & Wills, 1980; Meijer & Reagan, 1981) and ophiolitic gabbros (Coleman, 1977) are also indicated. The lines connect coexisting pyroxenes. Temperature estimates from Ross and Huebner (1975).
Composition des pyroxènes du Complexe mafique-ultramafique de Thak Gah mesurée par microsonde électronique. Les lignes relient les pyroxènes coexistants

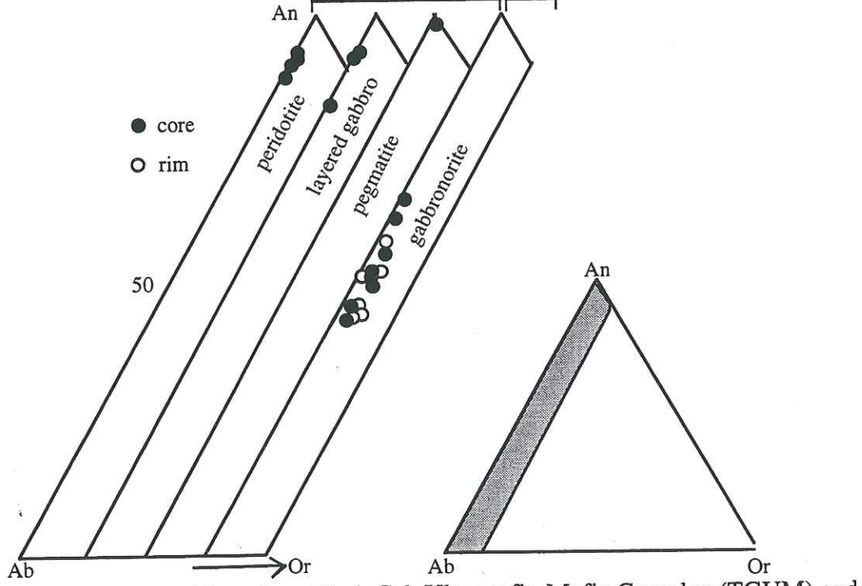

Figure 37. Plagioclase compositions from Thak Gah Ultramafic-Mafic Complex (TGUM) and gabbronorite of Main Facies zone (MFZ) determined by electron microprobe.
Composition des plagioclases du Complexe de Thak Gah (TGUM) et de la gabbronorite de la Zone du Faciès Principal (MFZ) mesurée par microsonde éléctronique.

Table 4. Representative plagioclase composition of Thak Gah Ultramafic Mafic Complex
(Composition représentative des plagioclases du Complexe de la Thak Gah).

S.No.	91CH-28	91CH-31	91CH-34	91CH-34	91CH-34
Mineral	plagioclase	plagioclase	plagioclase(C)	plagioclase(R)	plagioclase
Rock-type	plag-orthopy pegr	layered gabbro	layered gabbro	layered gabbro	gabbro-norite
SiO2 (wt %)	44.67	45.57	53.96	55.28	57.36
TiO2			0.04		
Al2O3	35.71	33.33	29.29	28.36	28.58
Fe2O3	0.03	0.04	0.10	0.01	0.15
MnO	0.004			0.08	0.08
MgO		0.04	0.04		0.02
CaO	20.19	19.14	13.84	12.64	8.58
Na2O	0.17	0.81	3.85	4.95	5.65
K2O	0.003	0.01	0.16	0.18	0.40
Total	100.77	98.89	101.27	101.49	100.83
Cation ratios	O=8	O=8	O=8	O=8	O=8
Si	2.049	2.126	2.417	2.467	2.543
Al-iv	0.951	0.874	0.584	0.572	0.457
Al-vi	0.98	0.959	0.963	1.011	1.038
Ti			0.019		
Fe	0.001	0.001	0.004	0.000	0.006
Mn				0.003	0.003
Mg		0.003	0.003		0.001
Ca	0.992	0.956	0.664	0.604	0.408
Na	0.015	0.073	0.335	0.428	0.485
K		0.000	0.009	0.010	0.023
Cr	0.002	0.002	0.001		
An	98.51	92.88	65.9	57.98	44.53
Ab	1.49	7.09	33.21	41.05	53.01
Or		0.03	0.89	0.97	2.46

content of the plagioclase from the TGUM and the host gabbronorite of the surrounding Main Facies Zone. Plagioclase from the TGUM are highly calcic and range from An98 in plagioclase-orthopyroxene pegmatoid to An93 in layered gabbros. The more calcic plagioclase is almost devoid of the Or component, and the labradorite crystals generally contain 2 to 1 mol. percent Or. Experimental work on the system albite-anorthite-water (Johannes, 1978) has shown that high water pressure causes plagioclase compositions to become anorthite rich, and Arculus and Wills (1980) note that hydrous basaltic melts characteristically crystallize more anorthitic plagioclase than anhydrous melts, even if they are otherwise similar in composition. Zonation is frequent in the plagioclase of layered gabbro and Khan et al. (1989) have noted that plagioclase is more calcic towards the margin as compared to the core.

In contrast, plagioclase from the surrounding gabbro-norite is less zoned and its composition is An_{45}. According to Khan et al. (1989), its composition ranges from An_{64} to An 40 in the gabbronorite of the Main Facies Zone.

2-4 Conditions of crystallization and temperature estimates

At low pressures, the equilibrium assemblage resulting from crystallization of a basaltic melt in a magma chamber will be olivine and plagioclase. In contrast, at high pressures typical of the base of an island arc (8 to 10 kbar), the stable assemblage for a basaltic composition is clinopyroxene+orthopyroxene+plagioclase+spinel (Kushiro and Yoder, 1966; Presnall et al., 1979). In order to describe the phase equilibrium relationships of the Thak Gah cumulates, which include pyroxenes (CPX & OPX), anorthitic plagioclase (An) and aluminous spinel (SP), the simplified system CaO-MgO-Al2O3-SiO2 (CMAS) can be used. The univariant reaction in this system is useful in defining pressure (depth) constraints.

An + 2FO = CPX + OPX + Sp (A)

Reaction (A), determined experimentally by Kushiro and Yoder (1965, 1966), Herzberg (1972) and Presnall (1976) represents the boundary between olivine gabbro and spinel gabbro. In this reaction, olivine + plagioclase assemblages are replaced at higher pressure either by aluminous pyroxenes+plagioclase+spinel (basaltic bulk composition) or aluminous pyroxenes+olivine+spinel (ultramafic bulk composition). The assemblage clinopyroxene+orthopyroxene+plagioclase+spinel in the Thak Gah cumulates can be constrained to have crystallized in the P-T region of reaction (A). Khan et al. (1989) have reported that amphibole in the Thak Gah ultramafic-mafic cumulates is pargasitic hornblende. Then, the equilibrium temperature for the assemblage is constrained to be below 1050°C, which is the maximum stability limit of pargasitic amphibole (Jenkins, 1983). The pressures for the

TGUM cumulates are constrained to be below 10 kbar. Jan (1980), Jan and Howie (1980) and Bard (1983b) tabulated temperature-pressure estimates in the Chilas Complex and based on a variety of methods, they estimated that the Chilas Complex cooled and equilibrated under conditions of the pyroxene granulite facies, at 750° to 850°C and 5 to 6 kbar.

Further constraints on the temperature region of the crystallization of the Thak Gah cumulate sequence are as follows:

According to the stable mineral assemblages observed in the different units, two geothermometers are used to constrain the crystallization history of the Thak Gah Ultramafic-Mafic Association. These crystallization temperatures were determined using geothermometers based on diopside-enstatite miscibility gap in coexisting pyroxenes (Wells, 1977). Another widely used method of evaluating the temperature of formation of orthopyroxene+clinopyroxene pairs has been presented by Wood and Banno (1973). Starting with the solvus data presented by Davis and Boyd (1966), Wood and Banno derived an empirical equation which adapts binary En-Di solvus relations to multicomponent system behaviour by assuming an ideal solid solution model, and correcting the activities of $Mg_2Si_2O_6$ in both orthorhombic and monoclinic phases for dilution by all other constituents. Nominal temperatures of formation for diopsidic pyroxenes in equilibrium with orthopyroxenes, employing the Wood and Banno (1973) equation, yielded temperatures of 933° and 927°C for troctolites of TGUM. The diopside-enstatite thermometer of Well (1977) give a good temperature estimates between 880° and 871°C in the same rock troctolite (91CH-32B). Moreover, temperature of equilibrium between coexisting orthopyroxene and clinopyroxene in the gabbro (91CH-34) is estimated at 812°C and 816°C with the calibration of Wells (1977) and Wood and Banno (1973) respectively.

In summary, we can say that pyroxenes in the mafic units of the Thak Gah cumulates must have crystallized at temperature between 927° and 880°C.

Mineralogy and crystal chemistry as well as textural relationships of the enclosing gabbronorites are quite different from these ultramafic-mafic cumulates. Textures are unmistakably igneous. Because pyroxenes are more Fe-rich (Table 3), and plagioclase is less anorthitic than in the ultramafic-mafic cumulates, the CMAS system phase relationships do not apply. Pressure of formation for these gabbronorites is minimally constrained to be above 2 kbar, owing to the presence of amphibole. Amphibole appears to be a late crystallizing phase and is not a subsolidus replacement as it is in the enclosed cumulates, indicating that temperatues were lower during crystallization than in these cumulates. In addition, the amphibole in these gabbronorite is a magnesio-hornblende (Khan et al., 1989), which has a lower stability limit than the pargasite of the Thak Gah ultramafic-mafic cumulates.

These high-level gabbronorites probably represent a contemporary, shallow magma chamber in the same Kohistan arc, and considering their mafic bulk composition probably represent crystallization of a primitive magma at shallower levels in the crust. Juxtaposition of

this shallower intrusion next to the high-pressure Thak Gah Ultramafic-Mafic cumulates could have occurred either during suturing of this arc with the Asian plate or during uplift and overthrusting over the Indian plate.

2-5 Whole rock Geochemistry

Nine samples were analysed in the present study, from the Thak Gah Ultramafic-Mafic Association. Major elements and trace elements were analysed by X-ray fluorescence techniques and REE, Ta, Nb, Th, U and Hf abundances were determined by ICP-MS. The analytical methods have already been described in Chapter-2. The major, trace and rare earth elements data are reported in Table 4A and their location is given in Figure 25.

Dunite is characterized by high MgO (43 wt %), Fe_2O_3 (15 wt %) and low Al_2O_3 (1.4 wt %), CaO (0.34 wt %) and K_2O (0.02 wt %). The Mg-number is 70.

SiO_2 concentrations in the **wehrlites** range from 40 to 47 wt % and MgO decreases continuously from 36 to 22 wt % and Mg-number from 68 to 64 (Table 4A). Al_2O_3 ranges from 1 to 4 wt % and is increasing towards higher silica concentrations. The increase of CaO from 3 to 13 wt % is in general accordance with accumulation of An-rich plagioclase and clinopyroxene as observed in the thin section study. The concentration of Fe_2O_3 decreases from 17 to 10 wt % with increase of silica contents. TiO_2 contents in wehrlite range from 0.12 to 0.29 wt %.

Layered gabbros have silica contents between 50 and 52 wt %, but with reasonably high MgO (7 to 5 wt %), Fe_2O_3 (11 to 7 wt %), Al_2O_3 (20 to 18 wt %) and CaO (11 to 7 wt %). The Mg-number varies from 49 to 45 but KO-112 from Khanberri Valley has relatively low Mg-number (29). TiO_2 and K_2O concentrations range from 0.3 to 0.4 wt % and 0.16 to 0.27 wt % respectively and P_2O_5 from 0.05 to 0.07 wt %. But sample KO-112 has notably higher TiO_2 (1.45 wt %), K_2O (0.35 wt %) and P_2O_5 (0.12 wt %).

In dunite, Ni (2100 ppm), Cr (7100 ppm) and Co (125 ppm) are high (Table 4A). Wehrlite has Ni (435 to 366 ppm) and Cr (83 to 69 ppm) but sample KO-56B has high Ni (943 ppm) and Cr (166 ppm) contents. All of the transitional elements, which are rapidly removed from magmas by mafic phases, show scatter behaviour in the layered gabbros and do not show good correlation with silica. Sample KO-59B has high contents of Ni (739 ppm) and Co (129) as compared to others gabbros where the concentrations range from 71 to 50 ppm for Ni, 161 to 65 ppm for Cr and 66 to 33 ppm for Co.

All samples are low in incompatible elements, notably Rb (>1 ppm, except sample KO-112=3.36 ppm), Ba (< 1 ppm) and Th (0.01 ppm except sample KO-112=0.23 ppm).

Table 4A. Major, trace and rare earth element data from the Thak Gah Association. Major elements are recalculated to 100% without LOI.

(Données analytiques pour les terres rares et les éléments majeurs et en trace du Cortège de la Thak Gah).

S.No.	92CH-11	KO-58	KO-62	KO-56B	KO-59B	92CH-06	KO-112	KO-59C	92CH-20
Rock name	dunite	wehrlite	wehrlite	wehrlite	gabbro	gabbro	layered-gabbro	gabbro	gab-norite
Locality	UMA	UMA	UMA	UMA	UMA	UMA	UMA(Khanberri	UMA	UMA/MFZ
Major elements (wt%)									
SiO2(wt %)	37.94	44.98	47.49	40.32	52.58	51.85	50.81	N.D.	51.70
TiO2	0.04	0.18	0.30	0.12	0.31	0.45	1.45		0.40
Al2O3	1.42	2.65	4.40	1.83	18.58	20.01	18.44		20.38
Fe2O3	15.73	11.89	11.02	17.68	8.04	7.59	11.10		7.61
MnO	0.14	0.16	0.15	0.22	0.13	0.13	0.15		0.12
MgO	44.37	29.63	22.97	36.73	7.75	6.14	5.18		5.92
CaO	0.34	10.50	13.67	3.11	9.58	10.50	10.12		10.63
Na2O					2.77	3.10	2.29		3.05
K2O	0.02				0.27	0.16	0.35		0.18
P2O5	0.01					0.07	0.11		0.01
Total	100.00	100.00	100.00	100.00	100.00	100.00	100.00		100.00
LOI		0.22	0.25						
Trace elements (ppm)									
Ba		0.76	0.91	2.18		51.51	98.38	41.98	43.20
Rb	3	0.08	0.09	0.13	0.05	0.37	3.36	0.20	0.58
Sr		21.04	25.03	20.63	202.49	424.16	413.88	400.88	391.18
Ta		0.01	0.01	0.32	0.001	0.02	0.23	0.02	0.01
Th		0.04	0.05	0.01	0.001	0.01	0.56	0.01	0.01
Zr		4.32	5.14	1.91	3	16	39	4.75	16
Nb		0.07	0.09	0.11	0.01	0.29	2.50	0.28	0.13
Y		5.91	7.03	1.85	0.58	6.73	15.56	6.29	5.52
Hf		0.25	0.29	0.09	0.02	0.24	1.06	0.22	0.23
V	97					145	392		194
Cr	7100					161	65		143
Ni	2100	366	436	944	739	72	57	73	50
Co	125	70	83	166	130	33	66	37	37
U		0.10	0.12	0.07	0.001	0.01	0.15	0.01	0.01
Sc									
Cu	2	4.46	5.30	4.47	7.65	17.10	69.27	19.16	14.07
Zn	95	24.78	29.48	48.39	38.12	34.23	67.12	29.10	38.17
Pb		0.33	0.40	0.21	0.20	1.63	4.05	1.49	1.27
REE (ppm)									
La		0.27	0.33	0.16	0.10	1.90	4.86	1.51	1.23
Ce		0.99	1.17	0.46	0.22	4.05	11.05	3.30	2.64
Pr		0.22	0.26	0.08	0.03	0.56	1.52	0.47	0.37
Nd		1.40	1.66	0.47	0.19	2.71	6.94	2.28	1.82
Sm		0.59	0.70	0.18	0.06	0.78	1.96	0.70	0.57
Eu		0.24	0.29	0.07	0.07	0.55	0.92	0.48	0.42
Gd		0.83	0.99	0.27	0.09	1.00	2.38	0.90	0.75
Tb		0.16	0.19	0.04		0.17	0.40	0.15	0.13
Dy		1.06	1.26	0.32	0.10	1.09	2.56	1.04	0.88
Ho		0.23	0.27	0.07	0.02	0.24	0.54	0.23	0.19
Er		0.63	0.75	0.20	0.07	0.69	1.53	0.64	0.58
Tm									
Yb		0.55	0.65	0.18	0.06	0.66	1.43	0.67	0.57
Lu		0.08	0.10	0.03	0.01	0.11	0.22	0.11	0.09
Mg#	71	68	64	64	45	41	29		40

REE patterns. Chondrite-normalized REE diagramme of the wehrlites and layered gabbros is shown in Figure 37A.

The **wehrlite** samples are characterized by rather consistent ratios of LREE depletion (La/Sm_N ratios all less than 1, Table 4A) and resemble the pattern of the clinopyroxene or the N-type MORB with $(Sm/Yb)_N$ =1. These patterns are very similar to the patterns of ultramafic rocks of the Jijal Complex.

The **gabbro** samples define a rather flat pattern (La_N/Sm_N ratio between 1.14 and 1.37). Eu anomalies are present in these gabbros and pointed to primary magmatic features because all these samples have abundant anorthite. Relative small Eu anomaly in sample KO-112 in spite of considerable plagioclase fractionation may be related with a high oxidation state (high Eu^{+3}/Eu^{+2}) of this magma. Sample KO-59B show low total REE contents as compared to other gabbros. All these chondrite-normalized patterns are similar and the difference is only in the overall REE abundances. Such patterns generally correspond to island-arc tholeiite basalts. These patterns show similarities to the patterns of garnet gabbros of Jijal Complex.

Spidergrammes. Figure 37B represents the MORB-normalized incompatible element abundances for gabbros from Thak Gah Association. The elements plotted from Nb to Yb vary systematically in these gabbros and show LILE enrichments and high-field strength element (HFSE) depletions (Nb and Ta) characteristic of arc magmas. To sum up the notable features, present in this diagramme are, 1) depletion in Th relative to La in all these gabbro samples except in sample KO-112 where Th is slightly enriched than La, 2) all these samples are characterized by a marked depletion in Nb and Ta relative to Th and La and, 3) there is positive Eu anomaly present in all these gabbros. The most consistent feature of these patterns is the lack of any obvious decoupling between the HFS and REE, as indicated by La/Ta ratios (between 21 and 112). The La/Ta ratio for N-type MORB approximate to value of 15, whilst those for convergence zone magmas are generally greater than 30, compared with a chondritic value of approximately 16. The high La/Ta ratios suggest that these gabbros have a closer affinity with island arc rocks. Similarly, wehrlite, layered gabbro and gabbronorite have highly variable (13-15 for wehrlite but KO-56B has 0.34; 5-13 for gabbro and 11 for gabbronorite), and generally low Nb/Ta values compared with the primitive mantle ratio (≈ 17).

The main conclusion from the study of these diagrammes is that all these gabbros indicate a clear island-arc affinity and they also show evidence of fractional crystallization.

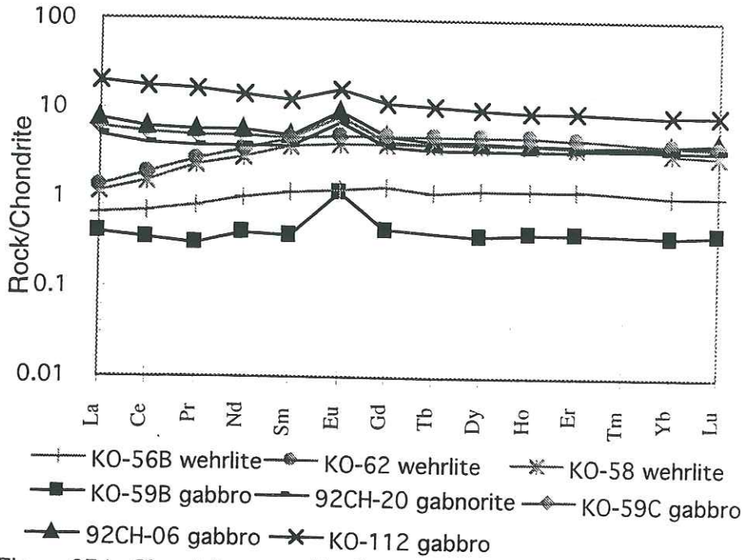

Figure 37A. Chondrite-normalized REE data for the rocks of Thak Gah Association, Chilas Igneous Complex.

Spectre de Terres rares normalisé aux chondrites des roches du Cortège de Thak Gah, Complexe Igné de Chilas.

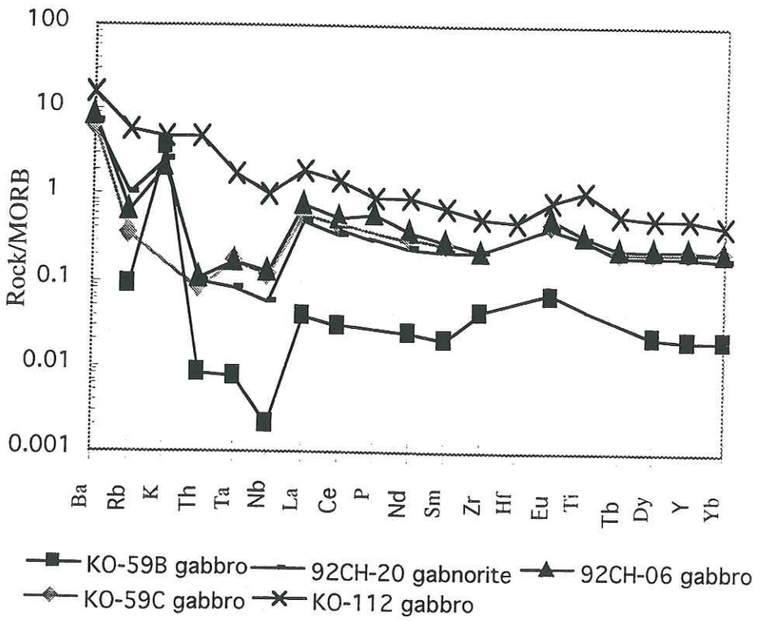

Figure 37B. MORB-normalized incompatible trace element diagramme illustrating geochemical characteristics of the Thak Gah Association in Chilas group.

Spectre des éléments traces incompatibles présentant les caractéristiques géochimiques du Cortège de Thak Gah dans le groupe de Chilas.

3- MAIN FACIES ZONE (Chilas Igneous Complex)

3-1 Field Relationships

The rock assemblages from the Main Facies Zone are distributed in the Swat as well as in the Indus Valleys and form at least 85 percent of the Chilas Igneous Complex. They range from gabbronorite, gabbro, diorite, opx-diorite, to quartz-diorite and granite. All these rock units are so complexely mixed that the contact relationship among them is difficult to decipher. Although crude lithologically continuous, but heterogeneous rock series were observed such as in the Thor Gah, Darel River and Swat Valley, real lithological zonation was not observed in the complex examined in this study. In the Thak Gah, south of Chilas, a minor body of tonalite is intruded into pegmatoidal pyroxenite and this silicic body has orthopyroxene as minor constituent. The intermediate-composition rocks (opx-diorite and diorite) constitute 40 - 45 % of the exposed rocks of the area while gabbro and gabbronorite form 50 to 55 % and other acid intrusion less than 5 %.

Rb-Sr data from the gabbro and diorite (Thor Gah Valley; Fig. 24) of the Main Facies Zone yielded an age of 111 ± 24 Ma with an average initial $^{87}Sr / ^{86}Sr$ ratio of 0.7039 ± 0.00006 (Mikoshiba et al., 1998).

3-2 Petrographic Characteristics

Rocks of the Main Facies Zone are medium- to coarse-grained and exhibit equigranular texture. Relict cumulate texture is not common, but where present, they indicate hypdiomorphic to adcumulate texture. Average grain size ranges from 1.5 mm to 4 mm. Like the Kamila Amphibolites, gabbros and diorites of this zone are mineralogically similar and major constituents are pyroxene, hornblende and plagioclase. The rocks of the Main Facies Zone are dominated by medium grained clinopyroxene and orthopyroxene, with plagioclase and minor proportion of amphibole.

Gabbronorite is prominant around the Thak Gah Ultramafic-Mafic Complex, but its relationship with the TGUM is not clear. Cumulate orthopyroxene forms 20 - 30 % of the gabbronorite and is roughly equal in abundance to clinopyroxene. Olivine is absent. Orthopyroxene is ubiquitous and forms large, equant crystals. Clinopyroxene (averaging 18-30%) is generally present as medium, subhedral crystals and generally mantled by a thin rim of hornblende. Hornblende in these rocks occurs as aggregates of subhedral to anhedral crystals and as sparse, euhedral prism. Hornblende which rims the clinopyroxene, is greenish tan to brown. Plagioclase typically forms 35 - 50 % of the gabbronorite. It is present as a cumulus or an intercumulus mineral and is zoned to unzoned. It is labradorite in composition. Magnetite

and ilmenite, presumably recrystallized titanomagnetite, commonly form 2 - 4 % of the gabbronorite.

Textures indicate that extensive recrystallization and flow banding occurred at high temperature, probably contemporaneous with crystallization from a melt.

Diorite has two main facies based on the mineral constituents: orthopyroxene diorite and hornblende diorite. At some places in the Main Facies Zone (e.g. Darel River), quartz diorite is also seen. With increasing silica content, the abundance of hornblende decreases slightly, poikilitic crystals of hornblende are less common, and inclusion of orthopyroxene are not present (in diorite having silica >57 wt%). A few quartz diorite samples contain orthopyroxene and biotite. Hornblende, orthopyroxene and plagioclase are the main constituents in orthopyroxene diorite with biotite and clinopyroxene as minor constituents. Inclusions of orthopyroxene and, less commonly, clinopyroxene are common in hornblende. Subhedral plagioclase crystals are slightly zoned and optical determination suggest that its composition ranges from oligoclase to andesine. In a few rocks, antiperthitic texture is common in plagioclase. In general, the hornblende diorites are composed dominantly of hornblende and plagioclase. The hornblende is green to greenish brown and commonly forms poikilitic or subhedral crystals. Opaque minerals are magnetite, with lesser ilmenite (0.5 - 2 %).

Tonalites display a limited range in modal and chemical composition and have several unifying characteristics. They are feldspathic, containing 40 - 55% andesine to oligoclase and 0 - 4 % alkali-feldspar. Quartz contents are typically 15 - 20 %. Hornblende and biotite (± orthopyroxene) in variable proportions are the dominant mafic constituents together yielding colour indices of 10- 25 for most. Idiomorphic sphene is common. Low-K_2O granodiorite are minor and looks gradational into tonalite (e.g. Darel River).

The order of crystallization of the primary minerals in Main Facies Zone is inferred, from reaction and inclusion relationships cited above, to be orthopyroxene and plagioclase in pyroxene diorite, clinopyroxene and plagioclase in gabbro, plagioclase, hornblende, biotite, quartz and alkali feldspar in quartz-diorite and tonalite.

3.3 Mineral Chemistry

Mineral chemistry of surrounding gabbronorite from the MFZ has been discussed in the mineral chemistry section of TGUM.

3-4 Whole Rock Geochemistry

The following discussion focusses on the whole rock geochemistry of the rocks which are exposed in the Indus Valley from Chilas to north of Dassu and in the Swat Valley (Fig. 24).

Sixty nine samples from the MFZ were analysed for major, trace and rare earth elements. Most of the samples (64) are from the Indus Valley and five are from the Swat Valley (Table 5).

Sample localities are given in Figure 38. The analytical procedure for all these samples is the same as described for the samples of the Kamila Amphibolites.

3-4.1 Major oxides distribution

The rock assemblages of Main Facies Zone (MFZ) from the Indus Valley (IV) and from Swat Valley (SV) have essentially similar compositional ranges and geochemical trends (Table 5; Fig. 39). The rocks from these areas are mainly characterized by relatively low silica (45 -60 wt %), high abundances of Al_2O_3 (15 - 20 wt %) and CaO (6 - 10 wt %) and low abundances of K_2O (< 1 wt %) and MgO (4 - 7 wt %). However, granite and quartz-diorite rocks from the Chilas area have elevated silica contents, SiO_2 > 60 wt %, and MgO < 4 wt %. Samples from Swat Valley have higher MgO, ranging from 6 to 8 wt % at similar SiO_2 contents. The range of Al_2O_3 concentrations is on the average slightly higher in the Indus Valley than in the rocks of Swat Valley, in the overlap range of 54 wt % SiO_2. In the rocks of the Main Facies Zone exposed in the Indus Valley, Al_2O_3 decreases more or less systematically with silica, indicating plagioclase crystallization effects.

CaO in the rocks of MFZ from the Chilas Igneous Complex decreases from 12 wt % in the mafic samples towartds 7 wt % in the diorite, in general accordance with crystallization of plagioclase and pyroxene observed as in the thin-section study. In the quartz-diorite, CaO contents are < 6 wt %.

On Harker diagrams (Fig. 39) all the rock assemblages from both the valleys show relatively well-defined trends with increasing SiO_2. Of the major elements, FeO^T, MgO, CaO and to a lesser extent Al_2O_3, show compatible behaviour (bulk partition coefficient, $D^{xst/liq}$ >1), with concentrations falling in more evolved melts. These trends appear to reflect the crystallization of plagioclase and mafic phases, such as pyroxene from the melts. In contrast K_2O and Na_2O behave incompatiably ($D^{xst/liq}$ >1) and increase in concentration in more evolved magmas. Particularly diorites appear richer in K_2O due probably to biotite and some due to alteration. P_2O_5 and TiO_2 show rather more subtle behaviour and a great deal more scatter than do the other major elements (Figs. 39H,G).

Table 5. Major, trace and rare earth element analytical data from the Chilas Igneous Complex (Main Facies Zone). Major elements are recalculated to 100% without LOI.
(Données analytiques pour les terres rares et les éléments majeurs et en trace du Complexe Igné de Chilas (Zone du Faciès Principal).

S.No.	SW-22	SW-08	SW-19	SW-23A	SW-12	SW-14	9303	9308B	CH-40	CH-41	CH-20	CH-69	CH-73	CH-80	CH-90	CH-99	CH-92	CH-100	CH-27	CH-88	CH-101	CH-102	CH-72	CH-38
rock name	dolerite	gab-norite	gab-norite	gab-norite	hb-diorite	hb-diorite	gab-norite	gab-norite	gab-norite	gab-norite	gab-norite	gab-norite	gab-norite	gab-norite	gab-norite	granodiorite	gabbronorite	gab-norite	gab-norite	gab-norite	gab-norite	gabbro	gabbro (deform)	gabbro
Locality	Swat	Swat	Swat	Swat	Swat	Swat	KKH	KKH	ThurliGah-KKH	ThurliGah-KKH	ThakGah	Darel River	KhanbariGah	KhanbariGah	KinnerGah	KinnerGah	KinnerGah	KinnerGah	Thak Gah	KinnerGah	Thor Gah	Thor Gah	Bunar Gah	KhanbariGah
Group	MFZ	MFZ	MFZ	MFZ	MFZ	MFZ	MFZ	MFZ	MFZ	MFZ	MFZ	MFZ	MFZ	MFZ	MFZ	MFZ	MFZ	MFZ	MFZ	MFZ	MFZ	MFZ	MFZ	MFZ
major element (wt.%)																								
SiO2	51.82	53.08	52.54	53.38	54.30	54.57	53.23	51.85	50.06	50.62	51.70	52.56	45.53	52.53	41.34	58.28	51.59	51.97	49.72	50.31	49.20	51.12	52.01	50.14
TiO2	0.63	0.45	0.67	0.83	0.71	0.92	0.89	0.44	1.47	1.01	0.40	0.87	1.08	0.95	1.17	0.93	0.48	0.84	0.70	0.97	0.98	0.99	0.84	0.88
Al2O3	18.80	15.04	18.74	17.39	17.08	16.13	17.08	20.31	17.08	18.37	20.38	17.34	16.12	18.67	20.09	16.32	19.68	19.63	15.41	16.30	16.36	19.10	19.47	20.94
Fe2O3	9.71	9.99	8.91	9.38	9.03	9.17	9.05	7.00	11.52	10.11	7.61	9.37	14.80	9.04	13.90	7.74	8.56	8.92	9.08	8.19	11.71	9.38	8.81	9.46
MnO	0.15	0.17	0.14	0.15	0.14	0.15	0.12	0.11	0.17	0.16	0.12	0.16	0.20	0.14	0.18	0.12	0.14	0.14	0.15	0.14	0.18	0.14	0.14	0.19
MgO	6.91	8.09	6.12	6.31	6.00	7.03	7.04	7.60	6.10	5.83	5.92	6.24	9.36	5.59	6.28	4.34	6.29	4.81	9.66	6.42	8.28	5.03	4.95	4.61
CaO	9.37	10.61	9.85	9.53	9.56	8.43	8.41	9.89	10.11	10.49	10.63	9.56	11.27	9.35	15.43	7.31	10.03	9.87	12.22	13.80	11.08	10.20	9.67	10.02
Na2O	2.31	2.43	2.72	2.51	2.66	2.33	3.83	2.39	2.98	2.96	3.05	3.25	1.56	3.25	0.95	3.33	2.88	3.41	2.34	3.56	1.94	3.57	3.59	3.38
K2O	0.27	0.13	0.30	0.45	0.49	1.11	0.25	0.36	0.36	0.30	0.18	0.50	0.07	0.33	0.09	1.43	0.32	0.28	0.58	0.19	0.18	0.30	0.37	0.18
P2O5	0.03	0.01	0.02	0.07	0.03	0.17	0.11	0.05	0.15	0.15	0.01	0.15	0.01	0.15	0.58	0.20	0.02	0.12	0.15	0.12	0.08	0.17	0.15	0.21
Total	100.00	100.00	100.00	100.00	100.00	100.00	100.00	100.00	100.00	100.00	100.00	100.00	100.00	100.00	100.00	100.00	100.00	100.00	100.00	100.00	100.00	100.00	100.00	100.00
LOI			0.10	0.22	0.19	0.85	2.48	0.01																
Trace element (ppm)																								
Ba	82.6	67	85	123	128.5	177	60	100	99	156	43.20	140	40	140	43	331	60	150	71	28	73	141	173	62
Rb	2.89	0.61	3.29	11.75	5.64	41.1	3	4	4	4	0.58	4	2	4	3	34	4	3	12	5	4	4	3	4
Sr	404.5	375	453	447	408	365	290	340	380	374	391.18	364	310	350	881	372	384	320	249	253	284	470	480	554
Ta	0.14	0.03	0.05	0.16	0.15	0.62	0.35	0.3			0.01			1.25				0.74						
Th	0.11	0.02	0.21	1.07	0.27	2.97	0.75	0.68			0.01			0.65				0.56						
Zr	21	23	30	50	59	110	72	9	53	34	16	50	17	47	59	163	19	27	44	73	28	41	41	36
Nb	0.69	0.5	0.78	2.06	2.71	6.18	2	2	3	2	0.13	3	0.85	3	3	5		1	4	3	2	2	2	2
Y	7.04	12.23	9.14	13.53	15.17	22.68	18	10	20	17	5.52	22	6	16	28	23	8	10	22	20	16	17	11	9
Hf	0.58	0.64	0.83	1.39	1.63	3.05	4	2			0.23			1.25				1.05						
V	167	149	179	224	202	215	252	143	341	228	82	195	475	243	400	171	188	184	218	204	325	207	250	212
Cr	166	262	179	213	183	373	156	150	122	126	194	218	129	97	39	157	115	92	533	289	126	71	85	79
Ni	75	83	62	70	66	120	54	13	53	46	143	73	64	57	11	38	39	28	78	112	53	23	31	19
Co	38.73	43	37	36.01	35	36	26	3	38	38	3	36	30	37	44	26	37	33	48	45	47	33	35	31
U											0.01													
Sc									32	32	29	27		27	34	24	25	28	45	31	47	25	25	29
Cu	20	9	23	41	120	33			210	42	6	46	165	38	187	91	5	60	47	65	202	16	125	16
Zn	76	70	69	73	67	80			87	75	53	79	116	85	76	64	61	73	70	59	91	75	84	102
Pb	1.31	0.95	1.2	1.79	2.32	4.82					1.27													
Cs	0.15	0.01	0.12	0.5	0.24	2.37					0.06													
REE (ppm)																								
La	3.04	2.29	2.92	4.68	5.55	13.59	4.00	2.00			1.23		0.56	4.00				3.00						
Ce	6.19	5.41	6.49	10.58	12.50	29.94	13.00	9.00			2.64		3.00	12.00				8.00						
Pr	0.79	0.81	0.90	1.45	1.71	3.83	1.60	0.90			0.37		0.40	1.50				1.00						
Nd	3.53	3.97	4.26	6.88	7.49	15.77	8.00	5.00			1.82		3.00	7.00				5.00						
Sm	0.90	1.18	1.20	1.91	1.93	3.64	2.10	1.30			0.57		0.90	1.80				1.60						
Eu	0.65	0.55	0.74	0.91	0.72	1.02	0.70	0.60			0.42		0.50	0.80				0.80						
Gd	1.09	1.55	1.45	2.22	2.20	3.70	1.80	1.30			0.75		0.90	2.00				1.40						
Tb	0.18	0.28	0.25	0.36	0.39	0.61	0.30	0.20			0.13		0.20	0.30				0.20						
Dy	1.19	1.89	1.58	2.19	2.50	3.77	2.30	1.30			0.88		0.90	2.30				1.80						
Ho	0.27	0.42	0.34	0.47	0.54	0.81	0.60	0.40			0.19		0.30	0.50				0.40						
Er	0.77	1.19	0.96	1.32	1.55	2.29	1.40	0.70			0.58		0.50	1.20				1.00						
Tm	0.11	0.17	0.14	0.20	0.22	0.31	0.20	0.10			0.00		0.10	0.20				0.20						
Yb	0.85	1.19	0.98	1.31	1.51	2.20	1.60	0.90			0.57		0.70	1.20				1.10						
Lu	0.14	0.18	0.15	0.21	0.24	0.33	0.20	0.20			0.09		0.10	0.10				0.10						
K/Rb	776	1769	757	318	721	222	664	747	747	623	2576	1038	291	664	249	349	664	775	394	315	374	623	1024	374
Sr/Rb	140	615	138	38	72	9	97	85	95	94	674	91	155	88	294	11	96	107	21	51	71	118	160	139
K/Ba	27	16	29	30	32	52	33	25	25	39	74	35	20	35	14	10	15	50	6	6	18	35	58	16
Ba/Rb	29	110	26	10	23	4	20	25	25	39	74	35	20	35	14	10	15	50	6	6	18	35	58	16

Table 5. (continued)

S.No.	CH-32	CH-94	CH-63	CH-65	CH-68	CH-43	CH-85	KO-51	9301B	CH-01	9302A	CH-26	CH-114	CH-52	CH-91	CH-52B	CH-53	CH-93	CH-78	CH-110	CH-59	CH-84	CH-61	CH-62	CH-89
rock name	gabbro	gabbro	gabbro	gabbro (deformed)	gabbro	qtz-gabbro	qtz-gabbro	diorite	diorite	diorite	diorite	diorite	diorite	diorite	diorite	diorite	diorite	diorite	diorite	diorite(deformed)	diorite	diorite	diorite	diorite	diorite
Locality	ThakGah	KinnerGah	ThorGah	Darel River	Darel River	ThurliGah-KKH	KhanbariGah	Chillas	KKH	KKH	KKH	ThakGah	ThurliGah	KKH	KinnerGah	KKH	ThurliGah-KKH	KinnerGah	KhanbariGah	Hoeder Gah	ThorGah	KhanbariGah	ThorGah	ThorGah	KinnerGah
Group	MFZ	MFZ	MFZ	MFZ	MFZ	MFZ	MFZ	MFZ	MFZ	MFZ	MFZ	MFZ	MFZ	MFZ	MFZ	MFZ	MFZ	MFZ	MFZ	MFZ	MFZ	MFZ	MFZ	MFZ	MFZ
major element (wt.%)																									
SiO2	47.18	52.39	51.41	50.15	51.25	53.51	52.94	56.85	54.35	55.03	55.05	55.88	54.43	55.85	54.07	55.16	55.53	55.99	54.38	54.90	54.78	54.07	55.45	55.35	56.68
TiO2	1.15	0.87	0.82	0.92	1.21	0.37	0.87	0.88	0.92	0.75	1.17	1.39	0.97	1.03	0.86	0.93	0.96	0.86	0.99	0.99	0.84	0.70	0.95	0.95	1.09
Al2O3	19.36	18.80	18.84	20.61	17.88	18.98	18.85	17.48	17.54	18.05	17.74	15.93	17.47	16.95	18.65	16.66	16.74	17.37	18.23	17.76	17.80	19.57	16.88	16.91	17.05
Fe2O3	12.12	10.36	9.69	10.00	10.23	7.38	10.29	8.37	8.14	8.44	9.19	9.59	8.88	8.74	8.97	8.90	8.48	8.94	8.40	9.28	8.95	7.57	8.40	8.43	8.34
MnO	0.18	0.17	0.16	0.15	0.17	0.12	0.19	0.14	0.13	0.14	0.15	0.15	0.14	0.14	0.14	0.14	0.14	0.15	0.13	0.14	0.16	0.13	0.13	0.13	0.13
MgO	5.49	4.66	5.46	5.24	5.38	6.33	4.10	4.07	5.82	4.68	3.98	4.78	4.98	5.12	4.36	5.22	4.96	4.39	4.55	4.18	4.60	4.25	5.24	5.23	4.33
CaO	11.18	9.01	9.91	9.67	10.25	9.41	8.52	7.72	8.65	8.88	7.65	7.13	8.69	8.39	8.59	8.60	8.27	8.18	8.78	8.45	9.39	8.80	8.63	8.63	7.82
Na2O	2.93	3.12	3.25	2.96	3.03	3.33	3.54	2.98	3.49	3.48	4.08	3.04	3.50	3.53	3.55	3.32	3.52	3.09	3.67	3.01	3.04	3.99	3.18	3.21	3.70
K2O	0.18	0.42	0.36	0.11	0.37	0.53	0.51	1.35	0.77	0.42	0.78	1.82	0.72	0.02	0.62	0.87	1.19	0.87	0.67	1.16	0.31	0.78	0.94	0.95	0.62
P2O5	0.22	0.19	0.10	0.19	0.24	0.04	0.19	0.16	0.20	0.13	0.22	0.30	0.22	0.23	0.18	0.20	0.20	0.16	0.19	0.13	0.14	0.15	0.19	0.19	0.23
Total	100.00	100.00	100.00	100.00	100.00	100.00	100.00	100.00	100.00	100.00	100.00	100.00	100.00	100.00	100.00	100.00	100.00	100.00	100.00	100.00	100.00	100.00	100.00	100.00	100.00
LOI								1.56	0.45		0.70														
Trace element (ppm)																									
Ba	41	168	89.51	258	140	120	122	205	180	127	220	306	180	318	180	226	315	202	204	126	162	337	120	198	140
Rb	4	5	1.86	4	4	7	6	49.07	16	5	5	53	6	11	6	13	30	15	9	33	4	10	16	20	7
Sr	440	418	365	523	410	411	397	352	360	369	310	278	340	375	350	348	341	346	420	353	389	461	411	329	369
Ta			0.06					0.4	0.35		0.45		0.54		1.1						1.32		1.25		1.05
Th			0.11					7.24	1		0.85		0.75		1						0.75		3		1
Zr	27	47	27	28	101	33	54	120	75	77	81	194	102	99	48	132	114	103	64	72	48	58	72	97	192
Nb	1	3	0.83	2	5	1	2	5.08	4	2	6	9	2	4	2	4	5	4	4	4	4	4	4	4	6
Y	11	19	13.55	6	26	9	24	25	16	16	22	38	18	24	16	23	25	24	20	22	17	19	20	24	24
Hf			0.57					3.32		1.65	8		1.03		1.35						1.42		1.4		6
V	356	217	159	258	308	117	180	244	256	189	290	253	186	183	249	250	169	192	225	284	176	159	162	260	213
Cr	36	71	84	90	118	159	80	122	86	108	24	159	136	124	71	170	137	106	90	83	81	85	84	169	184
Ni	22	15	9	42	55	83	3	35	20	28	8	49	39	52	25	53	45	20	35	15	12	27	9	58	43
Co	42	21	17	36	35	37	30	24.94	29	31	29	28	30	29	32	32	29	27	31	28	30	30	17	32	28
U			0.03						0.6		0.4		0.4		0.2								1.2		0.2
Sc	33	21	23	12	24	19	27	28		29		29	21	22	25	26	23	25	25	33	30	25	16	30	28
Cu	22	47	82	62	58	19	35	26		53		50	70	95	84	80	76	78	37	126	7	30	149	72	67
Zn	101	86	75	113	100	56	87	78		73		103	73	70	71	81	68	73	80	88	76	66	100	77	85
Pb			2.71					5.66																	
Cs			0.12					3.49																	
REE (ppm)																									
La			3.68					12.58	8.00	28.00	8.00		7.00		7.00						5.00		9.00		12.00
Ce			8.10					28.64	20.00	41.00	22.00		20.00		15.00						13.00		21.00		29.00
Pr			1.14					3.73	2.50	4.60	2.50		2.40		1.90						1.60		2.40		3.60
Nd			5.35					16.11	11.00	18.00	11.00		11.00		8.00						8.00		11.00		16.00
Sm			1.58					3.90	2.80	3.60	2.90		2.60		2.20						1.90		2.50		3.90
Eu			0.88					1.15	0.90	1.10	1.30		0.90		1.00						1.10		1.00		0.90
Gd			1.93					4.61	2.50	3.60	2.70		2.30		2.00						1.70		2.50		3.40
Tb			0.33					0.69	0.40	0.60	0.50		0.40		0.40						0.30		0.50		0.60
Dy			2.17					4.16	2.70	4.40	3.10		2.70		2.60						2.30		2.70		3.80
Ho			0.47					0.87	0.60	1.10	0.80		0.60		0.50						0.60		0.70		0.80
Er			1.37					2.44	1.40	2.30	1.50		1.30		1.30						1.10		1.90		1.90
Tm			0.00					0.38	0.20	0.40	0.30		0.30		0.20						0.20		0.30		0.30
Yb			1.31					2.34	1.30	2.40	1.70		1.30		1.50						1.60		2.10		2.10
Lu			0.20					0.36	0.20	0.30	0.20		0.20		0.20						0.20		0.30		0.30
K/Rb	374	697	1607	228	747	629	706	225	400	697	1278	282	996	15	858	556	329	481	618	292	643	648	483	394	735
Sr/Rb	110	84	196	131	103	59	66	7	23	74	62	5	57	34	58	27	11	23	47	11	97	46	26	16	53
K/Ba	36	21	33	4	21	37	35	54	36	27	29	49	33	0.5	29	32	31	36	27	76	16	19	64	40	37
Ba/Rb	10	34	48	65	35	17	20	4	11	25	44	6	30	29	30	17	11	13	23	4	41	34	8	10	20

Table 5. (continued)

S.No.	CH-112	CH-115	CH-33	CH-35	CH-60	CH-81	CH-82	CH-83	CH-103	CH-86	CH-87	CH-104	CH-107	CH-108	CH-22	CH-111	CH-109	CH-39
rock name	diorite	diorite	diorite (deformed)	diorite (deformed)	qtz-diorite	qtz-diorite	qtz-diorite	qtz-diorite	qtz-diorite	qtz-diorite	qtz-diorite	qtz-diorite	qtz-diorite	granite	tonalite	tonalite(deformed)	trondhjemite	trondhjemite
Locality	Hoedar Gah	KKH	Khanberri Gah	Khanberri Gah	ThorGah	KhanbariGah	KhanbariGah	KhanbariGah	Thor Gah	KhanbariGah	KhanbariGah	Thor Gah	Hoedar Gah	Hoeder Gah	ThakGah	Hoeder Gah	Hoeder Gah	KhanbariGah
Group	MFZ	MFZ	MFZ	MFZ	MFZ	MFZ	MFZ	MFZ	MFZ	MFZ	MFZ	MFZ	MFZ	MFZ	MFZ	MFZ	MFZ	MFZ
major element (wt.%)																		
SiO2	55.71	54.03	55.52	56.35	58.93	59.93	58.10	56.15	57.11	56.08	55.05	55.91	57.01	78.72	71.08	61.47	76.72	69.07
TiO2	0.64	0.91	1.05	1.00	0.93	0.58	0.68	0.76	0.90	0.86	0.88	0.98	1.16	0.53	0.13	0.54	0.41	0.66
Al2O3	16.49	17.38	16.72	16.90	16.00	18.39	18.29	18.58	17.64	17.69	17.31	17.67	16.69	9.27	15.84	17.49	10.80	14.42
Fe2O3	8.76	8.90	8.76	8.23	7.25	6.25	7.37	8.10	7.83	8.07	8.82	8.10	8.34	3.94	2.49	6.21	3.87	5.76
MnO	0.14	0.14	0.14	0.13	0.11	0.12	0.13	0.15	0.13	0.14	0.14	0.13	0.14	0.06	0.08	0.14	0.06	0.08
MgO	5.07	5.40	4.95	4.55	4.33	2.59	3.13	3.47	4.14	4.66	4.86	4.31	4.09	1.39	1.02	2.29	1.52	2.23
CaO	9.95	8.87	8.24	7.96	6.90	7.42	7.91	8.37	8.04	8.07	8.51	8.21	7.59	4.56	3.80	5.64	4.13	4.87
Na2O	2.69	3.36	3.13	3.31	3.48	4.02	3.71	3.60	3.60	3.46	3.23	3.66	3.41	1.03	4.62	4.42	1.13	0.88
K2O	0.48	0.84	1.31	1.36	1.89	0.53	0.50	0.63	0.39	0.81	1.06	0.80	1.29	0.38	0.90	1.59	1.27	1.89
P2O5	0.07	0.17	0.18	0.21	0.18	0.17	0.17	0.19	0.22	0.16	0.14	0.22	0.28	0.10	0.04	0.20	0.09	0.14
Total	100.00	100.00	100.00	100.00	100.00	100.00	100.00	100.00	100.00	100.00	100.00	100.00	100.00	100.00	100.00	100.00	100.00	100.00
LOI																		
Trace element (ppm)																		
Ba	139	218	218	233	300	194	293	235	199	248	263	256	262	140	43.20	250	124	103
Rb	5	12	38	45	70	7	4	6	4	13	22	10	28	10	0.58	51	57	85
Sr	229	429	317	327	292	491	496	480	419	405	337	369	310	178	391.18	418	189	200
Ta														1.04	0.01	0.75		
Th														7	0.01	2		11
Zr	60	75	109	108	127	98	121	107	38	79	95	117	165	321	29	54	150	186
Nb	2	2	5	6	6	3	3	4	3	4	4	4	7	8	0.13	4	7	12
Y	14	19	24	23	26	20	27	27	17	20	21	25	33	18	5.52	44	23	29
Hf														8	0.23	2		
V	270	194	265	241	206	111	132	168	159	181	171	176	193	84	28	124	83	103
Cr	166	134	132	126	159	143	89	126	98	142	105	92	129	264	62	83	202	245
Ni	22	45	48	44	59	12	8	11	25	33	42	31	38	34	8	7	33	48
Co	31	33	33	29	28	19	21	23	26	29	30	29	28	6	9	16	9	13
U														0.8	0.01	1		
Sc	34	23	33	25	21	16	23	25	21	30	19	20	29	15		30	16	12
Cu	64	60	93	75	116	21	45	27	25	82	78	144	36	16	12	44	23	19
Zn	62	70	82	77	63	69	63	77	63	82	69	64	85	47	44	83	52	85
Pb															1.27			
Cs															0.06			
REE (ppm)																		
La														21.00	9.00	10.00		
Ce														40.00	17.00	30.00		
Pr														4.10	1.70	3.70		
Nd														17.00	6.00	19.00		
Sm														3.30	0.80	4.90		
Eu														0.90	0.70	0.90		
Gd														2.30	1.00	4.60		
Tb														0.40	0.10	0.80		
Dy														2.10	0.40	5.70		
Ho														0.50	0.10	1.50		
Er														1.20	0.20	3.20		
Tm														0.20	0.06	0.60		
Yb														1.30	0.20	4.00		
Lu														0.20	0.07	0.70		
K/Rb	797	581	286	249	223	629	1038	872	809	517	400	664	379	315	12739	257	184	184
Sr/Rb	46	36	8	7	4	70	124	80	105	31	15	37	11	18	674	8	3	2
K/Ba	29	32	50	48	52	23	14	22	16	27	33	26	41	23	171	52	84	152
Ba/Rb	28	18	6	5	4	28	73	39	50	19	12	26	9	14	74	5	2	1

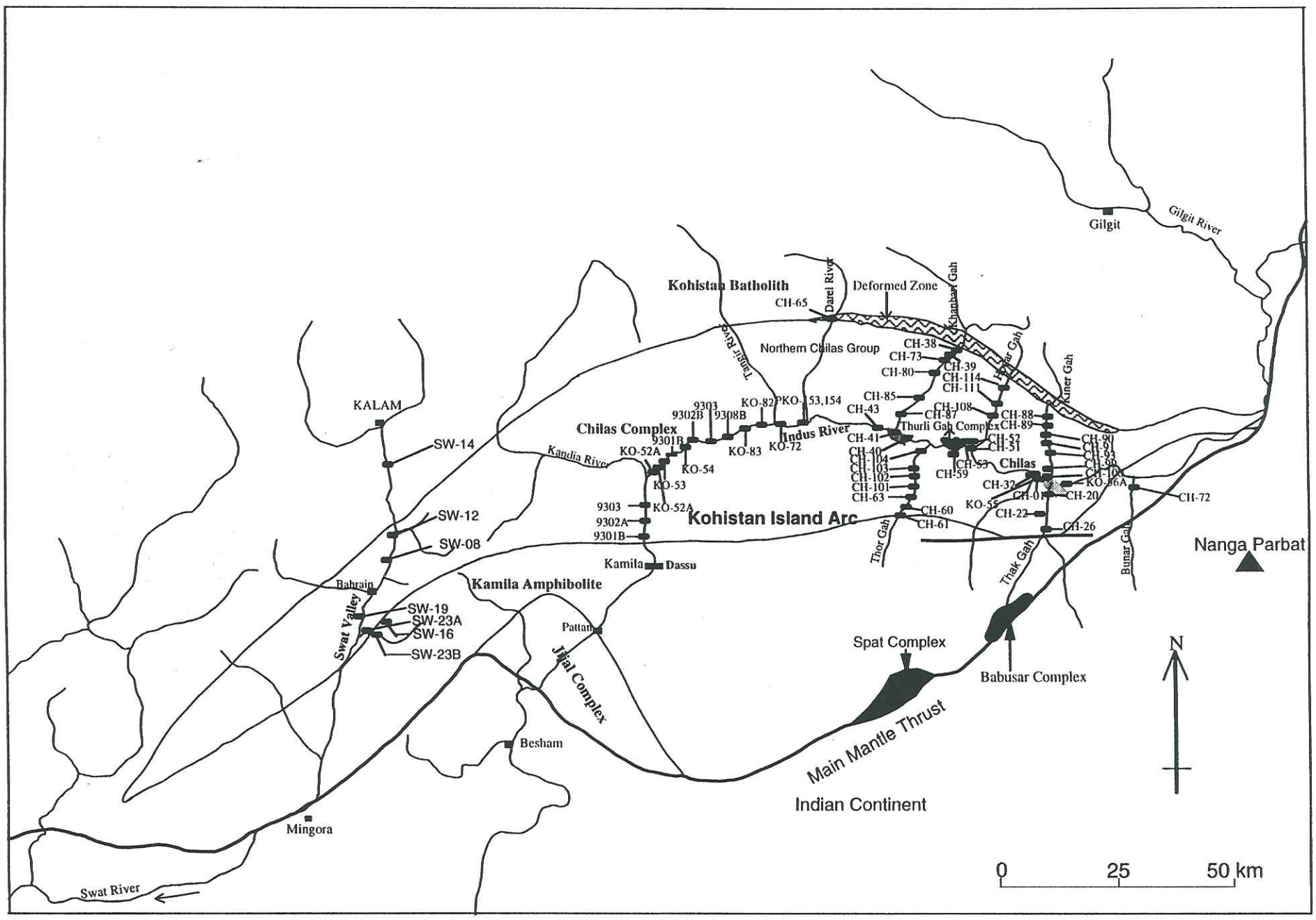

Figure 38. Sample location map of the Kamila Amphibolites and Chilas Igneous Complex, Kohistan arc, northern Pakistan.

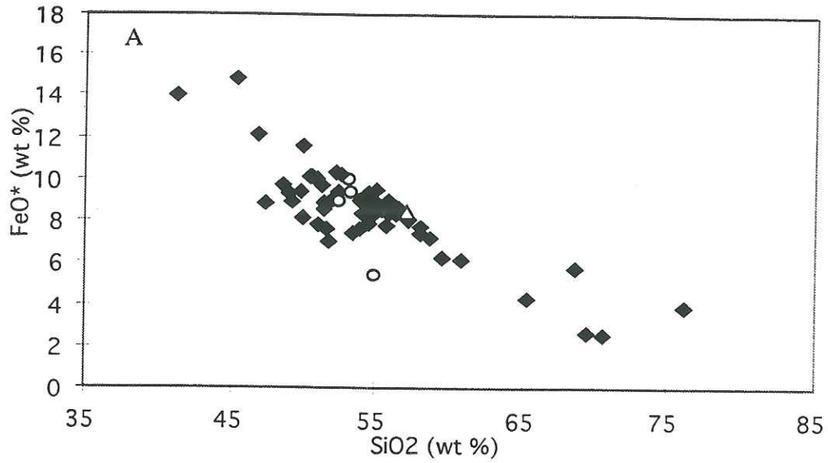

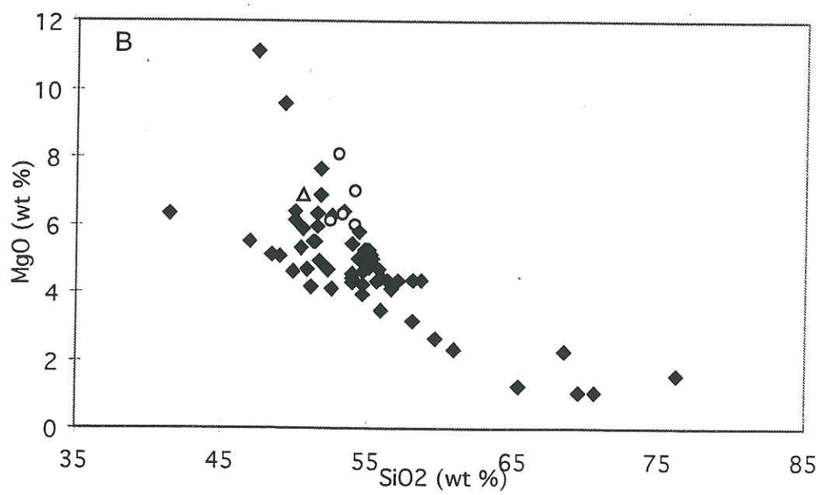

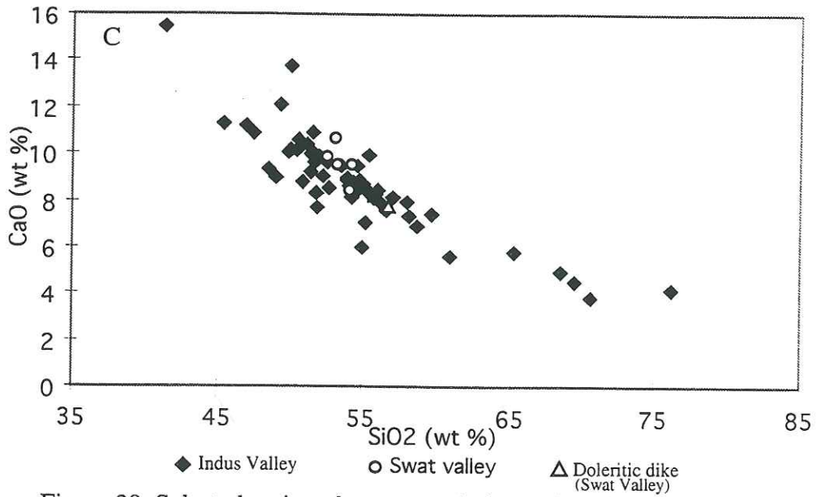

Figure 39. Selected major elements variations, plotted against SiO2, for the Chilas Igneous Complex (Main Facies Zone).

Variations des éléments majeurs sélectionnés en fonction de la teneur en SiO_2, dans le Complexe Igné de Chilas (zone du faciès principal).

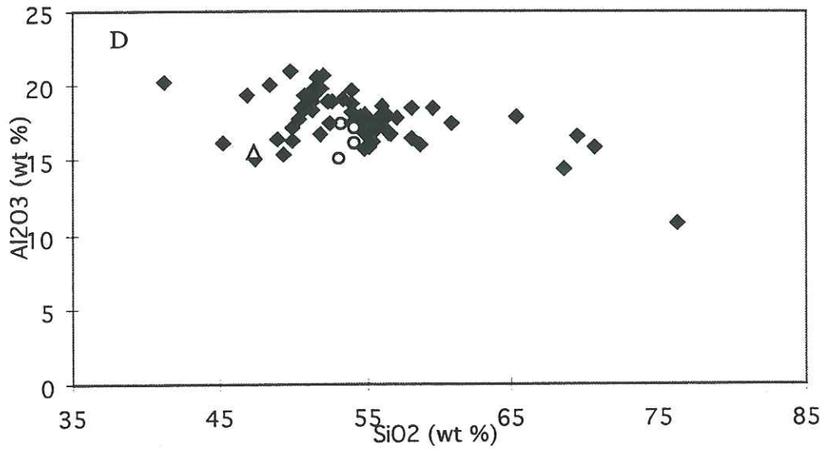

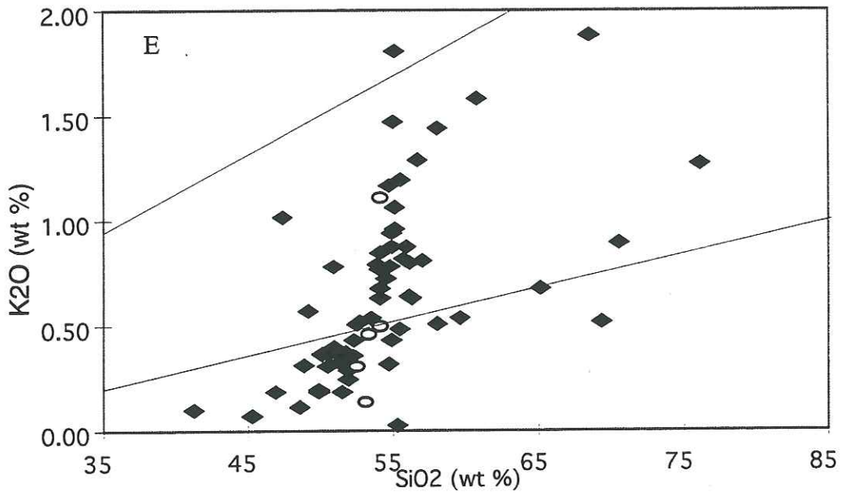

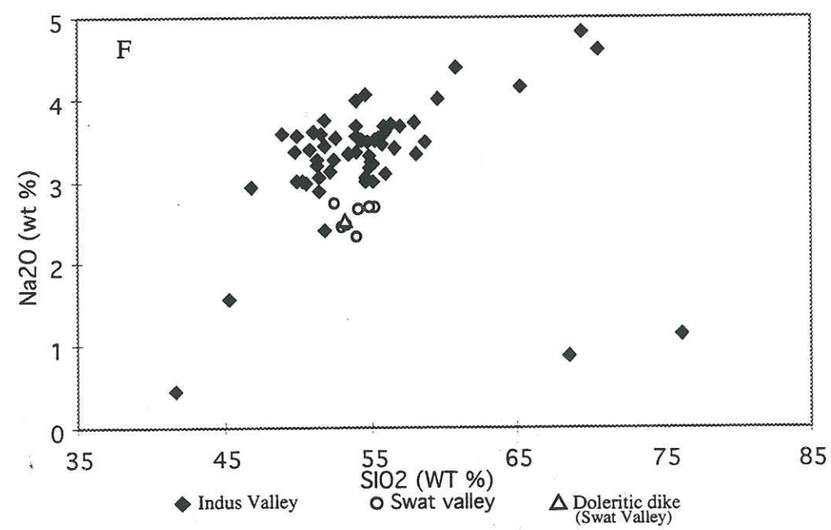

Figure 39. Selected major elements variations, plotted against SiO2, for the Chilas Igneous Complex (Main facies Zone).

Variations des éléments majeurs sélectionnés en fonction de la teneur en SiO_2, dans le Complexe Igné de Chilas (zone du faciès principal).

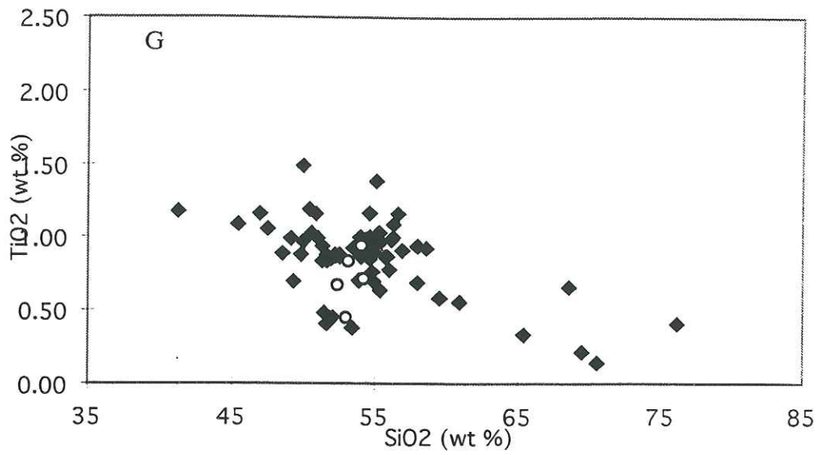

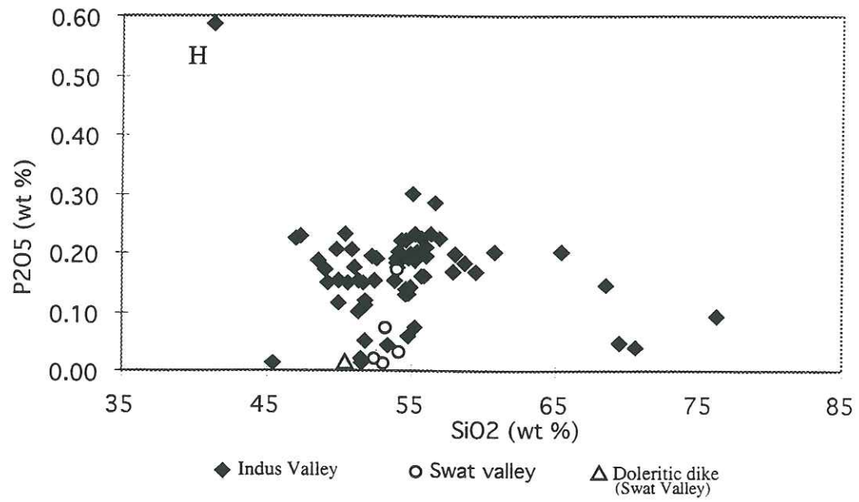

Figure 39. Selected major elements variations, plotted against SiO2, for the Chilas Igneous Complex (Main Facies Zone).
Variations des éléments majeurs sélectionnés en fonction de la teneur en SiO2, dans le Complexe Igné de Chilas (zone du faciès principal).

TiO_2 concentrations in the Chilas Igneous Comples range from 0.5 to 1 wt % in the whole compositional range. Although, some samples from the Thurli Gah (Indus Valley) have noticeably higher TiO_2, between 1 and 1.50 wt % (Table 5; Fig. 39G). It is generally assumed that the TiO_2 content of plutonic rocks remains relatively uneffected over a wide range of.

All the samples from the Main Facies Zone of the Indus Valley are characterized by relatively low Mg-numbers (30 - 35) but, samples from the Swat Valley have slightly higher Mg-numbers (40 - 42) and display limited SiO_2 enrichment. The low Mg-numbers suggest that none of the samples considered in this study represent primary mantle-derived melts.

The trondhjemite, intrusive in the pegmatoidal pyroxenite in the Thak Gah (MFZ), is characterized by relatively high abundances of Al_2O_3 (16 wt %) and Na_2O (5 wt %) and low abundances of K_2O (0.89 wt %), TiO_2 (0.13 wt %) and P_2O_5 (0.04 wt %) and generally high silica contents (> 70 wt %) with Mg-number 29.

3-4.2 Trace and rare earth elements distributions

Trace elements abundances in the Main Facies Zone of the Chilas Igneous Complex are reported in Table 5. The large ion lithophile elements (LILE) show relatively well-defined trends in gabbro, gabbronorite, diorite and quartz-diorite with increasing SiO_2, as demonstrated by increase in Rb, Ba but no visible trend with Sr (Fig. 40). Most LILE (especially Rb and Sr) abundances in the samples from the deformed rocks in the Chilas Igneous Complex vary considerably from the relatively fresh plutonic rocks at a similar SiO_2 range (Figs. 40A & C). But these elements behave similarly to related major elements in these different rock types.

The Rb contents in gabbro and gabbronorite having silica less than 54 wt % are less than 15 ppm with the majority containing between 4 and 10 ppm. Rb concentration is highly dependent on the behaviour of K_2O, and thus displays as K_2O an important variation in diorites and in more felsic rocks. Figure 41 illustrates the good correlation between Rb and K_2O content due to possible crystallization of K-rich phases (K-feldspar and biotite). For example sample CH-39 is from Khanberri Gah and represents the highly foliated zone and has primary as well as secondary biotite phase marking the foliation. Its silica content is also high (68 wt %). It has 1.88 wt % of K_2O and, as a result, its Rb content is relatively on the higher side (85 ppm).

Ba contents are characterized between 50 and 350 ppm in gabbro, gabbronorite and diorite with lower values in samples having SiO_2 value less than 50 wt %, whereas in the more evolved rocks (SiO_2 > 60 wt %), the trend is almost flat (Fig. 40B). As a result, a strong positive correlation exists between SiO_2 wt % and Ba ppm as a result of differentiation (Fig. 40B). The rock assemblages of the MFZ from the Indus Valley have similar Ba

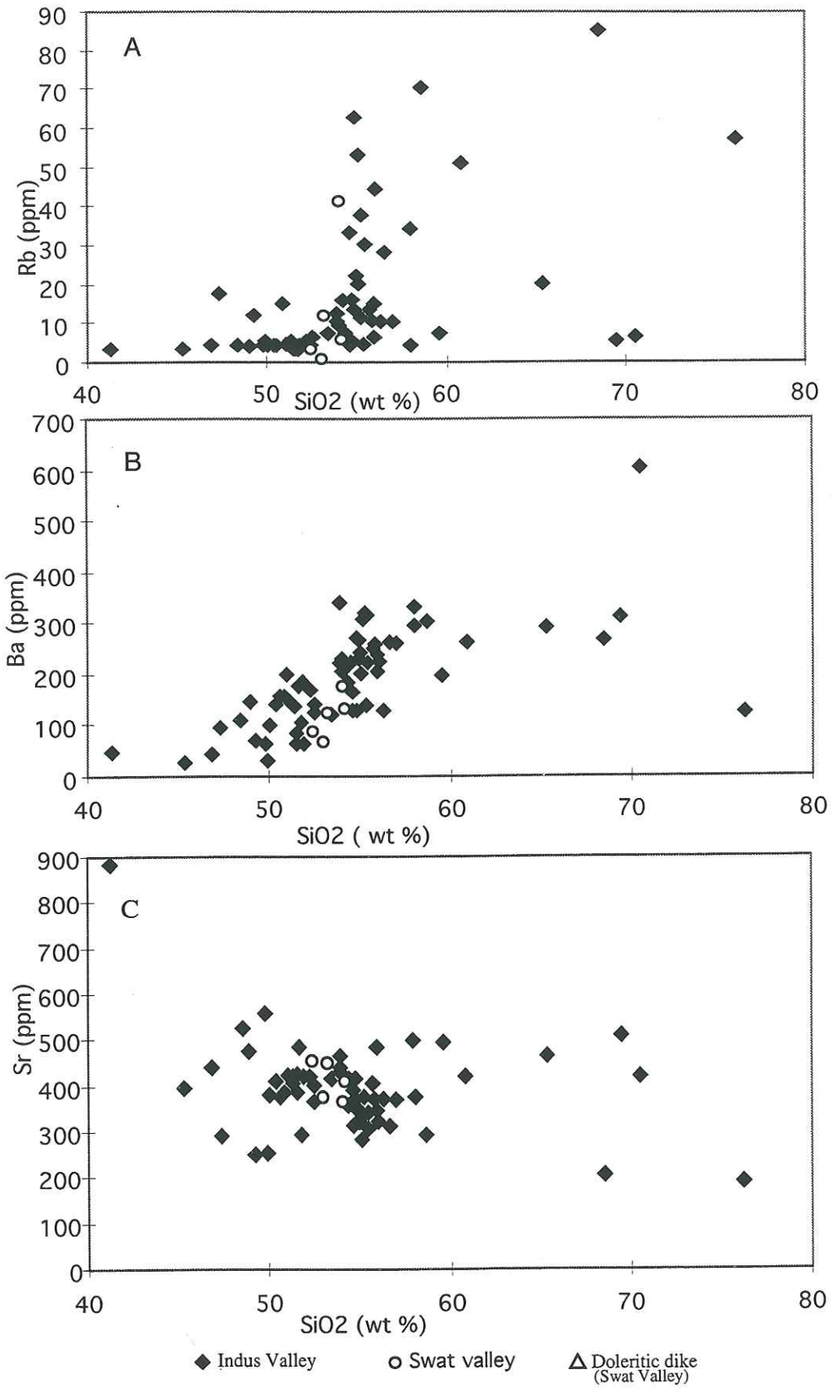

Figure 40. Selected trace elements variations, plotted against SiO2, for the Chilas igneous complex.

Variations des éléments majeurs sélectionnés en fonction de la teneur en SiO_2, pour la Zone du Faciès Principal du Complexe Igné de Chilas.

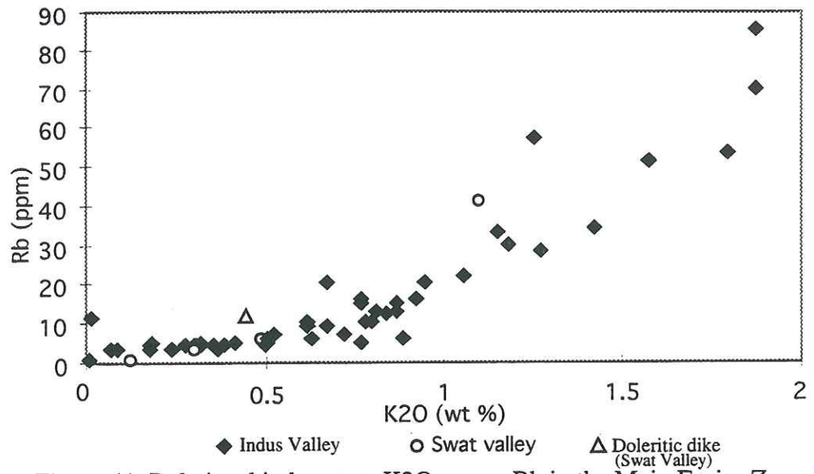

Figure 41. Relationship between K2O versus Rb in the Main Facies Zone (MFZ) of the Chilas Igneous Complex.

Corrélation K_2O-Rb dans la Zone du Faciès Principal (MFZ) du Complexe Igné de Chilas.

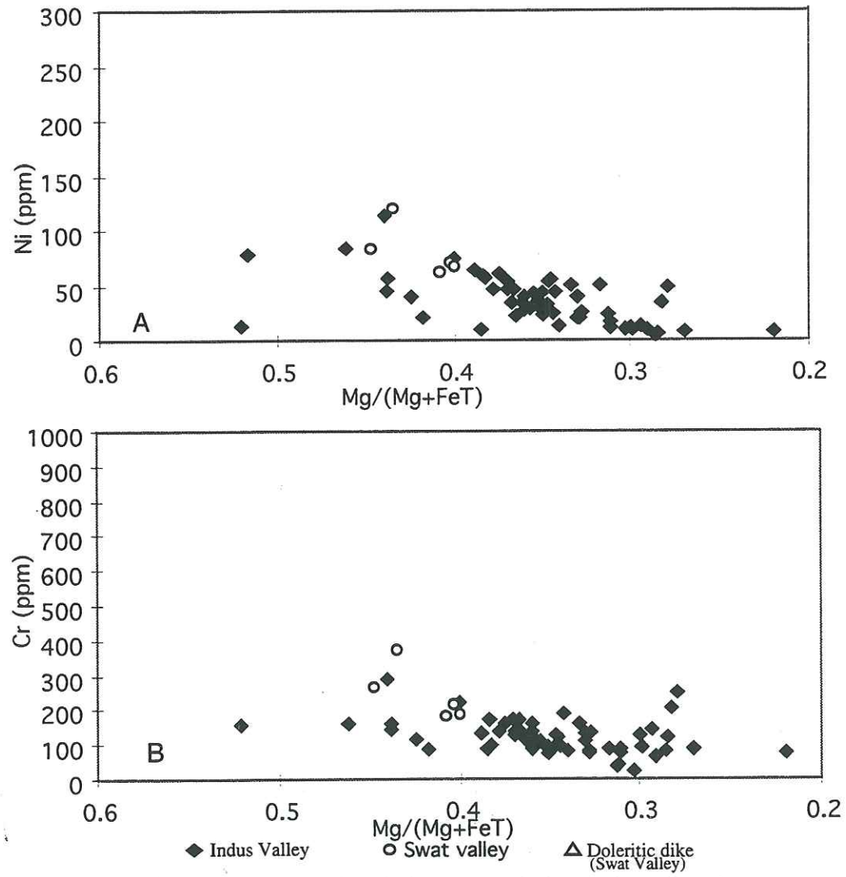

Figure 42. Selected transitional element variations, plotted against Mg-numbers, for the rocks of the Chilas Igneous Complex (MFZ).

Variations des éléments incompatibles sélectionnés en fonction de la teneur en Mg-numbers, pour les roches de la Zone du Faciès Principal, Complexe Igné de Chilas.

contents at constant SiO_2 while the rocks from the Swat Valley have relatively lower Ba contents (67 - 128 ppm).

Sr abundances range from 200 to 600 ppm with important variations for same SiO_2 contents between 250 and 460 ppm and bulk mean Sr content of the complex is 360 ppm.

The rocks from the Main Facies Zone of the Chilas Igneous Complex, exhibit a rather wide range in, and generally low values of Mg-number, Cr, Ni and Co (Table 5; Fig. 42). This, together with the general decrease in Cr might have been caused by precipitation of clinopyroxene. Likewise Cr, V and Sc also decrease with differentiation. The decrease of abundances of Cr and V with SiO_2 (Fig. 43) indicates that clinopyroxene has been an important fractionating phase as the two are expected to partition in clinopyroxene (Frey et al., 1974).

The content of Zr ranges from 20 to 110 ppm in Swat valley samples with SiO_2 content of 53 to 55 wt. %. (Fig. 43B). In the Indus Valley samples, Zr ranges from 10 to 190 ppm; and despite considerable scatter it tends to increase with SiO_2.

The REE chondrite-normalized patterns are presented in Figures 44, 45, & 46. All these rock-types from the Swat- as well as from the Indus-Valleys, having similar mineral abundances and major chemical compositions, display remarkably similar REE patterns. All are near flat in the heavier REE with typically 8 - 20 times chondritic levels, and have a moderate enrichment in the light REE. The significant feature of the data in the MFZ, is that (1) the REE fractionation varies systematically from mafic to more evolved rocks, and (2) there is similar fractionation for HREE and LREE, leading to a regular decrease from La to Lu on a chondrite-normalized diagram. The $(La/Yb)_N$ ratio varies from 1.30 to 4.18 in rock assemblages of Swat Valley and 3.86 to 7.87 in rocks of the Indus Valley. The fractionation of LREE and HREE is similar for most of the samples, and the major difference between the samples is their bulk REE content (Table 5). Sample 92CH-22 (Fig. 47B) of trondhjemite from Thak Gah is also distinct in the abundance and fractionation in the LREE. It shows strong enrichment in LREE and strong depletion in mid to heavy REE patterns ($La_N/Yb_N = 30.37$).

3-5 Discussion and Conclusion

3-5.1 Petrogenesis

It is difficult to determine in detail the crystallization processes of different rock types of the Chilas Igneous Complex, limiting insight into the possible source rocks. The field relations show that small masses of layered pyroxene gabbros and layered hornblende gabbros, exposed in the Indus Valley, cannot be treated as a single magmatic suite with other major rock

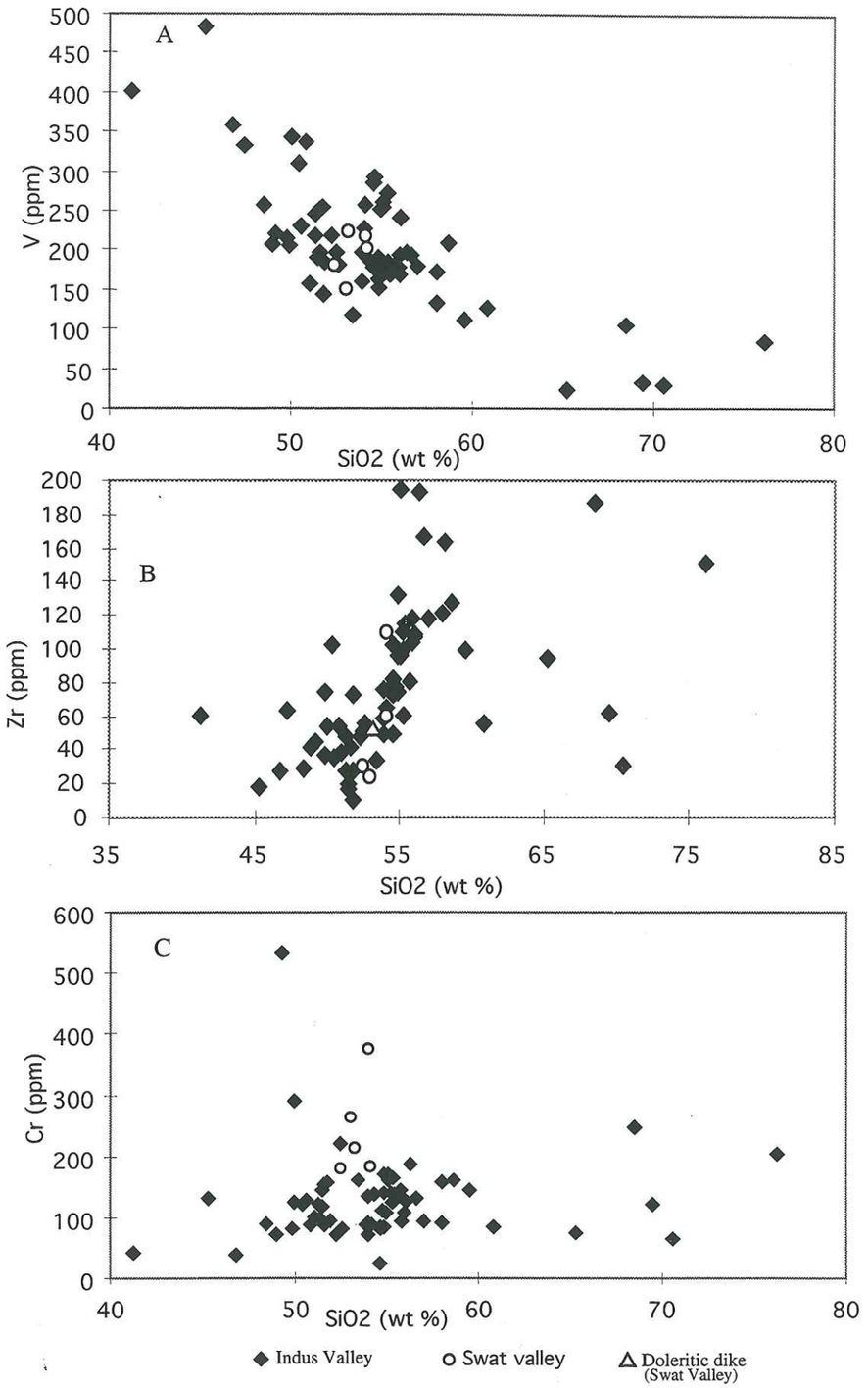

Figure 43. Incompatible and transitional trace element abundances plotted against SiO2 abundances for the rocks of the Chilas igneous complex.
Teneur en en éléments trace incompatibles en fonction de la richesse en SiO_2 pour les roches de la Zone du Faciès Principal, Complexe Igné de Chilas.

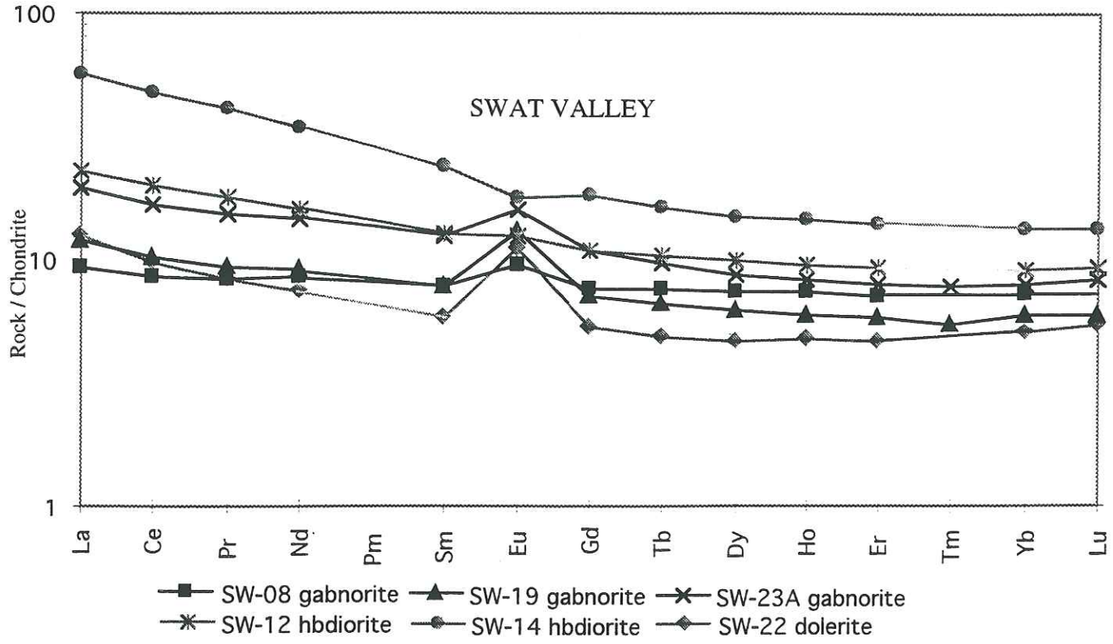

Figure 44. Chondrite-normalized REE data for the rocks of Swat Valley, Chilas Igneous Complex. Normalization values are from Nakamura (1974).

Données de terres rares normalisées aux chondrites pour les roches de la Zone du Faciès Principal de la vallée de Swat, Complexe Igné de Chilas. Valeurs de normalisation par Nakamura (1974).

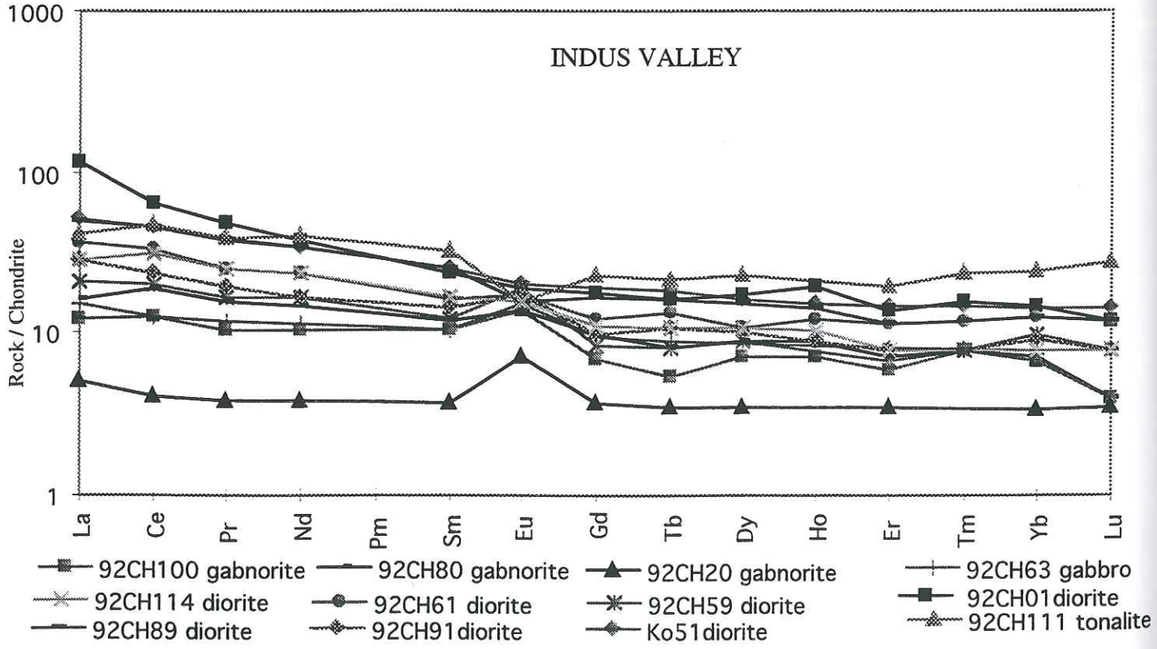

Figure 45. Chondrite-normalized REE data for the rocks of Indus Valley, Main Facies Zone, Chilas Igneous Complex. Normalization values are from Nakamura (1974).

Valeurs de terres rares normalisées aux chondrites pour les roches de la Zone du Faciès Principal dans la vallée de l'Indus, Complexe Igné de Chilas. Valeurs de normalisations de Nakamura (1974).

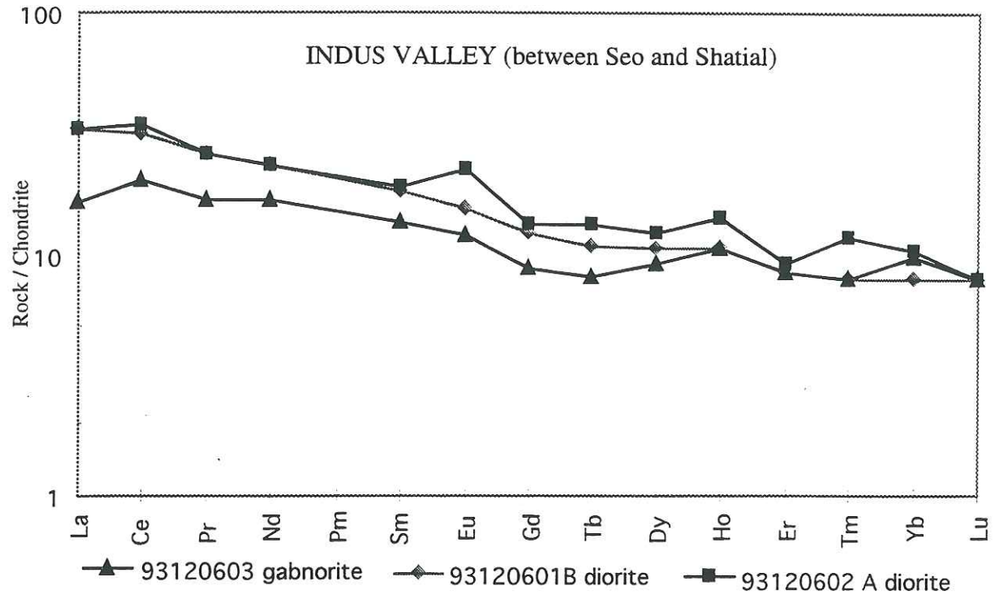

Figure 46. Chondrite-normalized REE data for the rocks of Main Facies Zone between Seo and Shatial, Chilas Igneous Complex. Normalization values are from Nakamura (1974).

Données de terres rares normalisées aux chondrites pour les roches de la Zone du Faciès Principal entre Seo et Shatial, Complexe Igné de Chilas. Valeurs de normalisation par Nakamura (1974).

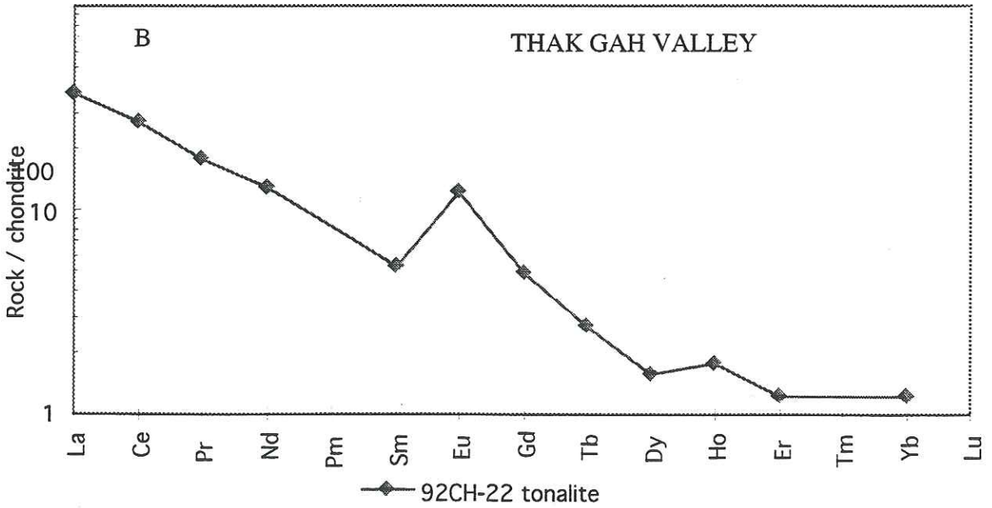

Figure 47. Chondrite-normalized REE data for tonalite (Thak Gah) of Indus Valley, Main Facies Zone, Chilas Igneous Complex. Normalization values are from Nakamura (1974).

Données de terres rares normalisées aux chondrites pour une tonalite (Thak Gah) de la vallée de l'Indus, Zone du Faciès Principal, Complexe Igné de Chilas.Valeurs de normalisation par Nakamura (1974).

assemblages of the MFZ. The rocks of ultramafic-mafic association (UMA) show relatively abundant cumulus phenomenon and are not suitable to decipher the magmatic processes, and are, hence, used only to underline the differences between the rocks, their possible relationships and to help constraint the source rocks.

The MFZ includes a range of rock-types from gabbro, pyroxene- and quartz-diorites to silicic rocks. The field, petrographic and geochemical data suggest that all these various rock types are comagmatic. Sharp contacts between the various rock types indicate that most of the petrologic diversity was generated below the level of emplacement.

In contrast to the suggestion of Khan et al. (1989), that the Chilas Complex consists up to 85 percent by volume of generally uniform gabbronorites, our data suggests the Main Facies Zone of the Chilas Igneous Complex includes a wide range of rock types, from gabbronorite to trondhjemite, with the main lithologies typically being gabbros and diorites. The field, petrographic and geochemical data suggest that the various rock types are linked through fractional crystallization and that the Chilas Complex represents a differentiating sub-arc magma chamber that fed a volcanic arc. Evidence for common parentage includes a close spatial and temporal association, systematic variations in mode and mineralogy, and a progression through time towards more evolved compositions.

Basic rock assemblages from the MFZ are Al-rich and on average Ti (< 1.20 wt %) and K_2O (<1 wt %; at SiO_2 < 54 wt %) poor. The intermediate composition rocks are slightly SiO_2-saturated (particularly in Indus Valley) and enriched in Na2O (3 wt % < Na2O < 4 wt %; Table 5). Generally, the rocks from the two regions (Swat and Indus Valleys) are enriched in Sr, Ba and Rb contents relative to commonly found in island arc tholeiites (Michard et al., 1985). The Sr-enrichment may reflect accumulation of relatively An-rich (An 40-60 mol %) plagioclase that is also obvious in the positive Eu anomalies in Figures 44 &45. Rb/Sr ratios are slightly higher but K/Ba ratios (16-40 at 53 wt %) are in the range, found in arc tholeiites (Gill, 1989). Similarly, the Ba/Rb ratios (16-50 at 53 wt %) are in the range commonly found in island-arc tholeiites (Gill, 1989; Pearce, 1983), with the exception of some rock assemblages that display high Ba and very low Rb contents (Table 5). The rock assemblages from the MFZ have high Ba/Nb and Ba/La ratios relative to chondrite and oceanic island basalts as typical of arc lavas. The exception being the more deformed rocks from the Indus Valley of MFZ which display high Ba, Rb and K. Similarly, Ti/V and Ti/Zr ratios (Table 5) are similar to those previously reported for lavas with island arc tholeiite through to calc-alkaline character (Pearce, 1983; Gill, 1989).

In the rock assemblges of the Chilas Igneous Complex there is a rather wider range, and generally low values of Mg-number (100*Mg/Mg+Fe), Cr and Ni content (Table 5). This, together with the rapid decrease in Ni and Cr with decreasing Mg-number (Fig. 42) and the increasing Zr abundance, implies that much of the chemical variation in these rocks may be attributed to crystal fractionation processes. Furthermore, to exhibit the fractional crystallization

in the Chilas Complex, we have used the variation in Al_2O_3/TiO_2 and CaO/TiO_2 against TiO_2 (Figs. 48 A & B). Such linear trends can only be caused by a mechanism of fractional crystallization where a very calcic plagioclase and Ca-bearing phase (clinopyroxene) are substracted from the successive melts. Particularly noteworthy is the inability to distinguish between the different rocks assemblage of the MFZ in these diagrammes.

The result of this study suggest that many of the basic assemblages from the MFZ may be the products of cumulus enrichment processes and the crux of the argument relies on REE data for a large body of samples from the Chilas Igneous Complex. In common with many island arc suites (White and Duprè, 1986; Davidson, 1986), magmas from the Chilas Igneous Complex have variable Eu anomalies both in the Swat and Indus Valleys (Figs. 44 & 45). The positive to negative Eu anomalies in the REE profiles for the basic to more evolved rocks indicate that fractionation has taken place during magma evolution. If we are to assume that plagioclase enrichment is the major control on the development of Eu anomalies, then evolved magmas with more than approximately 53 wt % SiO_2 have negative anomalies which indicates that plagioclase fractionation has taken place during their evolution. More basic magmas, with less than approximately 53 wt %, have positive anomalies indicative of accumulation of more plagioclase than is lost due to crystal settling. This suggestion is further strengthen by a positive correlation between modal plagioclase content and Al_2O_3 and a negative correlation between modal plagioclase content and SiO2. The flat profile, as shown by some samples (SW-12, 92CH-01; Figs. 44 & 45), from the Swat and Indus Valleys suggests that Eu loss by plagioclase fractionation was compensated by Eu gained by plagioclase settling into it. Crystallization and removal of a gabbroic assemblage, as seen above, could then produce more evolved magmas (53 - 65 SiO_2wt %), while simultaneous cumulous enrichment processes produce apparently less evolved magmas (48 - 53 SiO_2 wt %; Haris, 1983). Similarly, the study of Hawkesworth et al. (1977) of the Scotia arc (South Sandwich Island) shows similar REE distributions, with positive Eu anomalies in basic samples and negative anomalies in more evolved samples (Fig. 49). This is similar to the trend as observed in the Chilas Complex magmas, thus cumulus enrichment in plagioclase appears to be a common feature of many island arc basalts.

3-5.2 Magmatic signatures and tectonic setting

Most of the rock assemblages from the Chilas Igneous Complex display typical iron enrichment relative to silica and plot in the tholeiitic field on an FeO^T/MgO versus SiO_2 diagram (Fig. 50) and are classified as low- to medium-K tholeiites.

With respect to the variation of SiO_2 with $Na_2O + K_2O$ (Fig. 51), the data from the two regions fall in the field of subalkaline and to a lesser extent in the alkaline field of Miyashiro

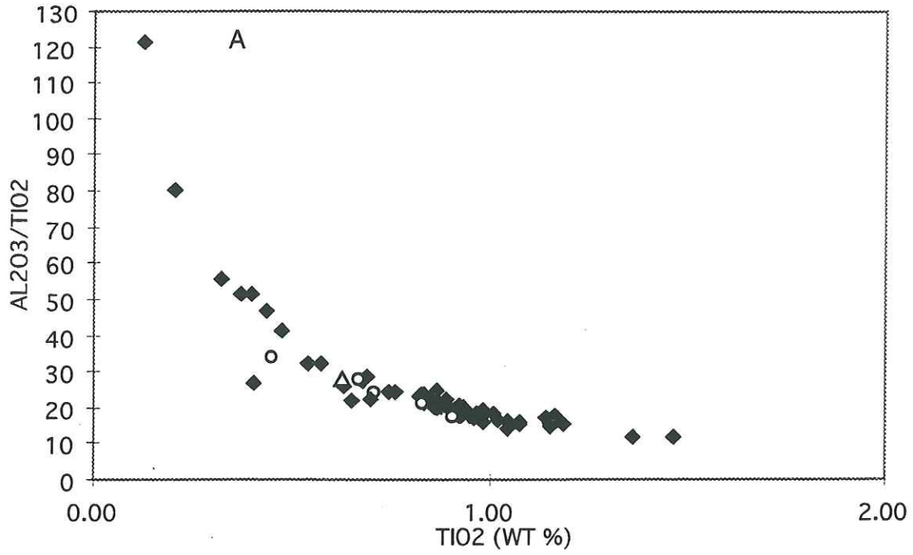

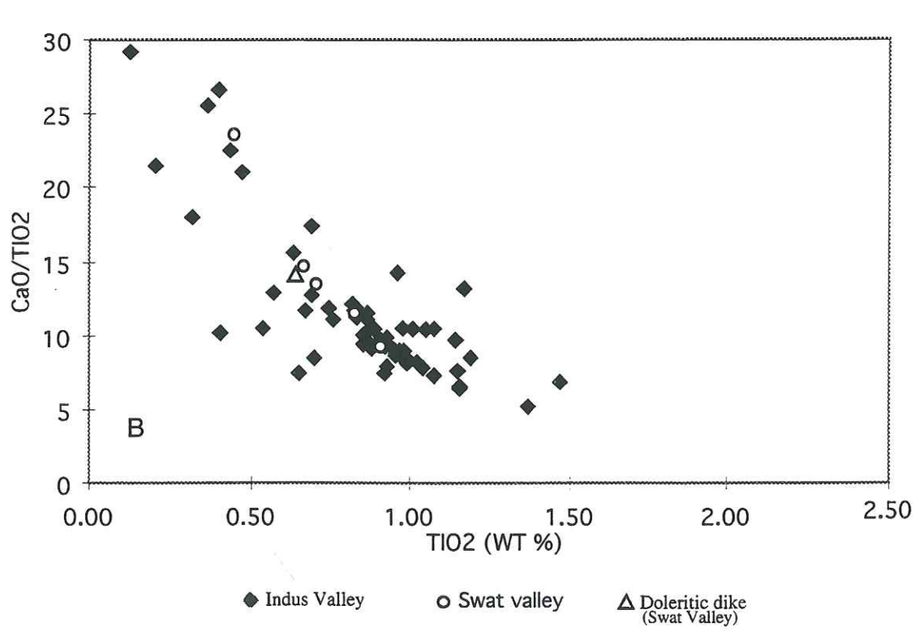

Figure 48. Plot of Al2O3/TiO2 and CaO/TiO2 against TiO2 for the rocks of the Chilas Igneous Complex (MFZ).

Diagramme de variation de Al_2O_3/TiO_2 et CaO/TiO_2 en fonction de TiO_2 pour les roches du Complexe Igné de Chilas.

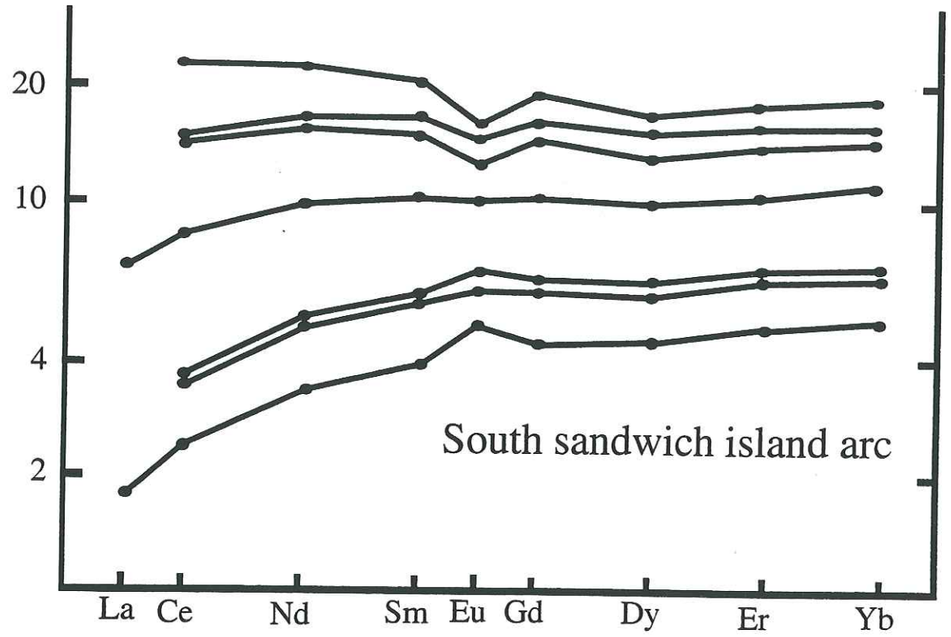

Figure 49. REE data for the Scotia arc (Hawkesworth et al., 1977) showing progressive development of negative Eu anomalies in more evolved samples and positive anomalies in basic samples.

Données de terres rares de l'arc de Scotia (Hawkesworth et al., 1977) illustrant le développement progressif d'anomalies négatives en Eu dans les roches évoluées et d'anomalies positives dans les roches primitives.

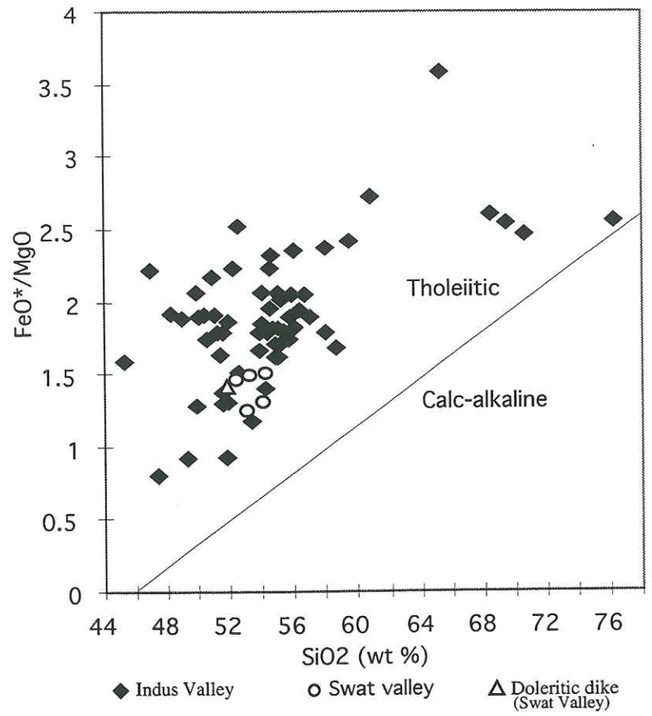

Figure 50. FeO/MgO versus SiO2 illustrating the compositions of the Chilas Igneous Complex (Main Facies Zone). All samples are tholeiitic following the definition of Miyashiro (1974).

Diagramme FeO/MgO en fonction de SiO2 montrant les compositions rencontrées dans le Complexe Igné de Chilas (Zone du Faciès Principal). Tous les échantillons sont des tholéiites, selon la définition de Miyashiro (1974).

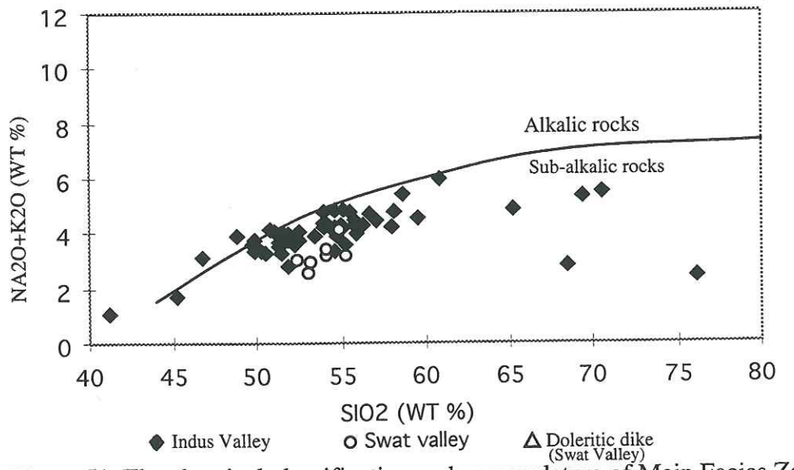

Figure 51. The chemical classification and nomenclature of Main Facies Zone rocks using the total alkalis versus silica (TAS) diagramme of Cox et al. (1979). The curved solid line subdivides the alkalic from subalkalic rocks.

Classification chimique des roches de la Zone du Faciès Principal basée sur la quantité totale d'alcalins en fonction de la silice. La courbe en trait continu sépare les roches alcalines et subalcalines.

(1978), although scatter can be attributed to metamorphic processes. Some samples from these areas, particularly from the Indus Valley, have anomalous values of SiO_2 and alkali contents and this can be related to the postmagmatic alteration. Such a finding may restrict the application of alkali-based classification diagrams. Therefore, all analyses are also plotted on the Zr/TiO_2 versus Nb/Y classification diagram of Winchester and Floyd (1977), which involves only relatively immobile elements (Fig. 52). On this diagram all gabbros and diorites from the MFZ fall in the subalkaline basalt to basaltic-andesite field while the more felsic rocks are located in the subalkaline andesitic field. Samples from the Swat Valley also fall in the sub-alkaline basalt to basaltic-andesite field.

Trace element abundances in the rock assemblages from the Main Facies Zone are plotted in different discrimination diagrams with the object of determining the likely tectonic affinity of the suit. Relationships between TiO_2-MnO-P_2O_5, and comparison with fields for oceanic-island tholeiites, MORB, island-arc calc-alkaline basalt and island-arc tholeiite, are illustrated in Figure 53. In this diagram, the samples from the Main Facies Zone of the Chilas Complex plot mostly in the field of island-arc tholeiites but also do record the calc-alkaline development of these plutonic rocks.

Figure 54 is a triangular diagram based upon Y/15-La/10-Nb/8 concentrations which discriminates between volcanic-arc basalts, continental basalts and oceanic basalts (Cabanis and Lecolle, 1989). Elemental concentrations from the Swat and Indus Valleys plot in tholeiitic and calc-alkaline fields in this discrimination diagram and show evolutionary trend from gabbros, gabbronorites to diorites. Using discrimination diagram (Fig. 55) of Pearce (1983) by plotting Th/Yb vs Ta/Yb, gabbros and gabbronorites from the Indus and Swat Valleys are found to plot in an oceanic arc tholeiites and diorites to calc-alkaline fields. This diagram also illustrates that all these rocks are derived from the depleted mantle source and contribution from crustal sources during magma genesis is not so significant in the case of gabbros and gabbronorites but with evolution, subduction-related components were involved.

Figures 56, 57 & 58 illustrate the MORB-normalized trace element variation for the different rock types from the Swat and Indus Valleys of the MFZ. Patterns of different rock types do not differ significantly and elements plotted from Th to Lu vary systematically between the basic and intermediate rock assemblages of the MFZ. The samples (SW-08, SW-19) representing more basic compositions in the Swat Valley, are more depleted with respect to Ta, Nb, Th, and K to those of equivalent rocks exposed in the Indus Valley. As a whole, the MORB-normalized curves slope from left to right indicating their enrichment in the more incompatible elements. Over-abundance of LILE relative to REE and HFSE is regarded as one distinct criterion for magmas generated in subduction-related settings. It is generally explained by metasomatic enrichment of these elements in the overlying mantle wedge (e.g. Hawkesworth et al., 1977; Saunders and Tarney, 1979; Pearce, 1983).

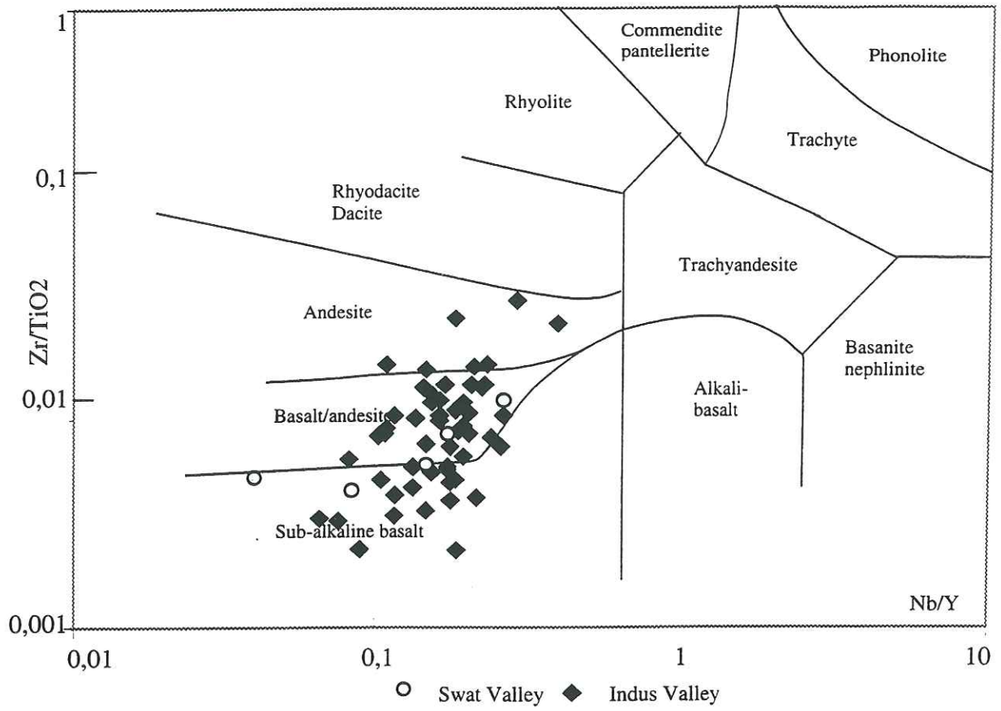

Figure 52. Zr/TiO2 versus Nb/Y plot (Winchester & Floyd, 1977) for Main Facies Zone of the Chilas Igneous Complex.
Diagramme du Zr/TiO2 en fonction de Nb/Y pour la Zone du Faciès Principal du Complexe Igné de Chilas.

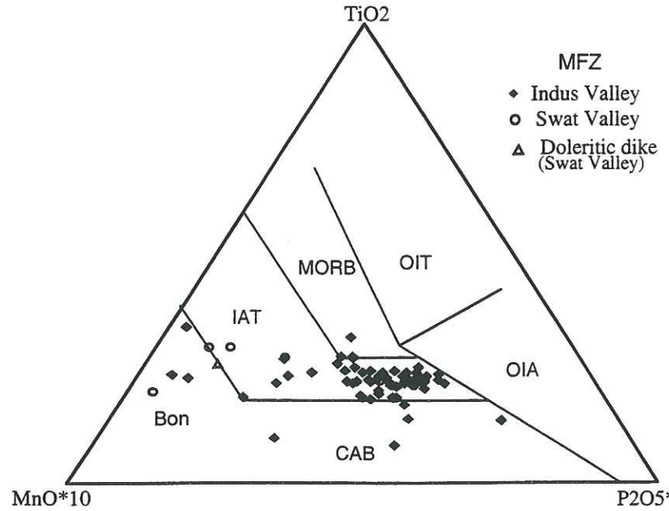

Figure 53. MnO-TiO2-P2O5 discrimination diagram for Main facies Zone of the Chilas Igneous Complex (after Mullen, 1983). The samples from the Swat Valley and Indus Valley occupy the island-arc field but some samples also fall in the calc-alkaline field. The fields are MORB; OIT- ocean-island tholeiite; OIA-ocean-island alkali basalt; CAB-calc-alkaline basalt; IAT-island-arc tholeiite.
Diagramme MnO-TiO2-P2O5 de discrimination pour la Zone du Faciès Principal du Complexe Igné de Chilas (d'après Mullen, 1983). Les échantillons des vallées de la Swat et de l'Indus sont contenus dans le champ des arcs insulaires, mais quelques uns tmobe aussi dans le domaine calco-alcalin.

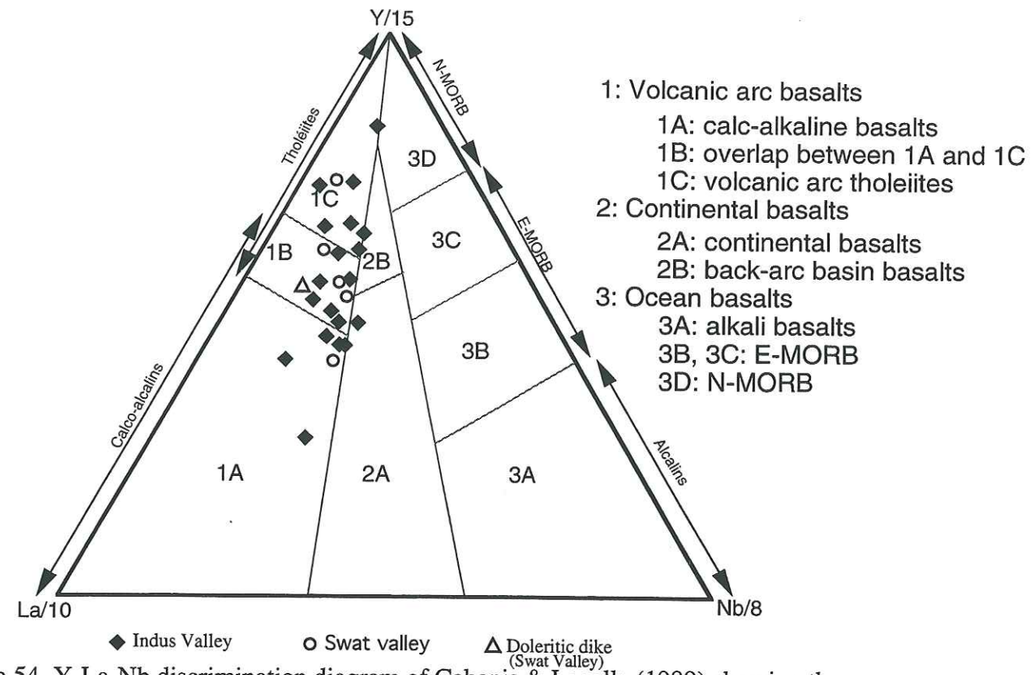

Figure 54. Y-La-Nb discrimination diagram of Cabanis & Lecolle (1989) showing the separation of volcanic-arc basalts, continental basalts and oceanic basalts. Samples from the Main facies Zone plot in the tholeiitic to calc-alkaline island-arc fields.
Diagramme Y-La-Nb de discrimination de Cabanis & Lecolle (1989) avec la délimitation des champs des basaltes d'arc, des basaltes continentaux et des basaltes océaniques. Les échantillons de la Zone du Faciès Principal tombent dans les champs des arcs insulaires tholéiitiques à calco-alcalins.

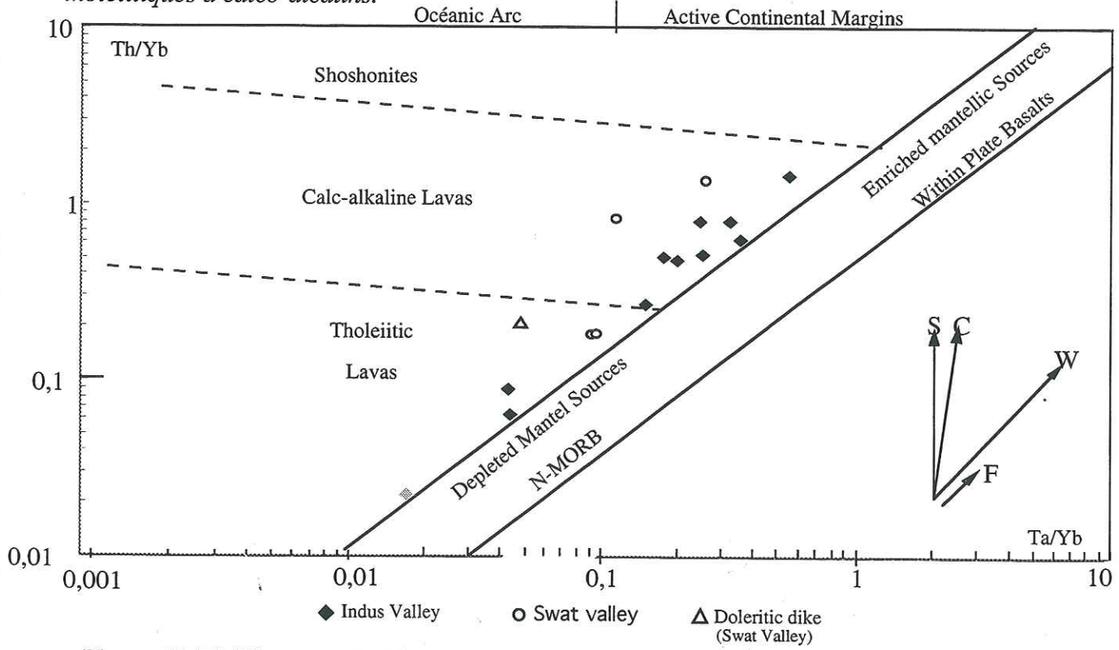

Figure 55. Th/Yb versus Ta/Yb diagram (Pearce, 1983) indicates that the involvement of crustal rocks in the magma genesis of Chilas Complex is not significant. Vectors indicate contribution of: S-subduction; C-crustal contamination; W-within-plate component; F-fractional crystallization.
Le diagramme Th/Yb en fonction de Ta/Yb (Pearce, 1983) indique que la participation crustale n'est pas significative dans la genèse des magmas du Complexe Igné de Chilas.

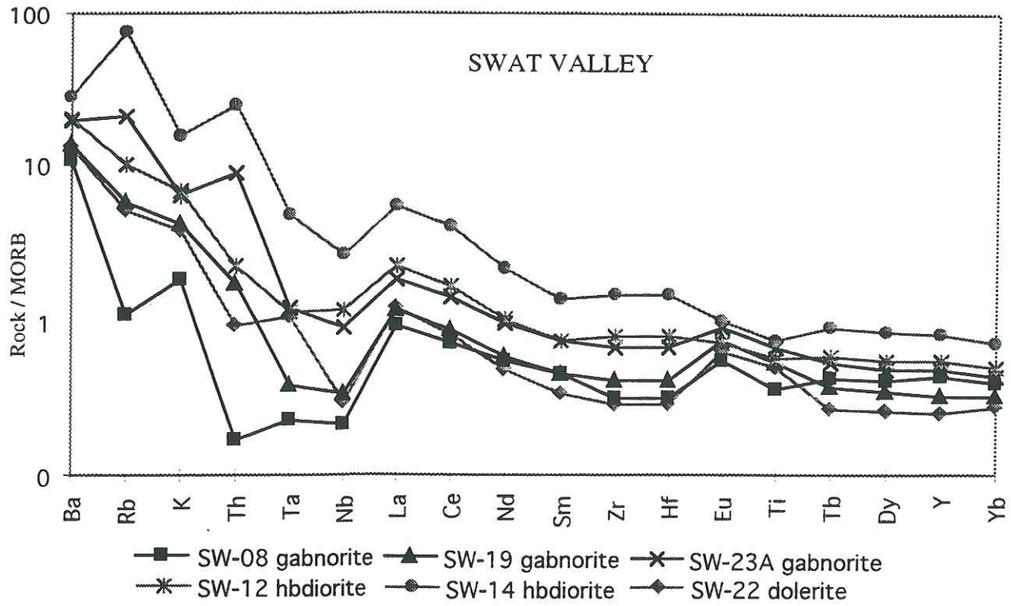

Figure 56. MORB-normalized incompatible trace elemnt diagram illustrating geochemical characteristics of the Main Facies Zone, Chilas Igneous Complex in Swat Valley. Normalization values are from Sun and McDonough (1989).

Spectre d'éléments trace incompatibles normalisés aux MORB illustrant les caractéristiques géochimiques de la Zone du Faciès Principal, Complexe Igné de Chilas dans la vallée de la Swat. Valeurs de normalisation par Sun and McDonough (1989).

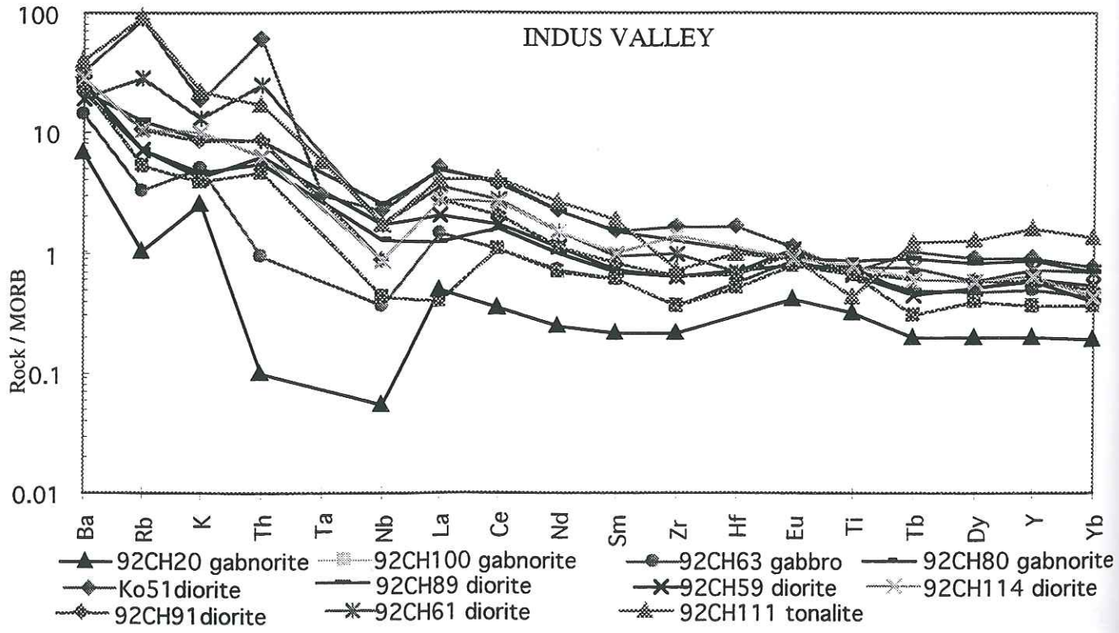

Figure 57. MORB-normalized incompatible trace elemnt diagram illustrating geochemical characteristics of the Main Facies Zone in Indus Valley. Normalization values are from Sun and McDonough (1989).

Spectre d'éléments trace incompatibles normalisés aux MORB illustrant les caractéristiques géochimiques de la Zone du Faciès Principal, Complexe Igné de Chilas dans la Vallée de l'Indus. Valeurs de normalisation par Sun and McDonough (1989).

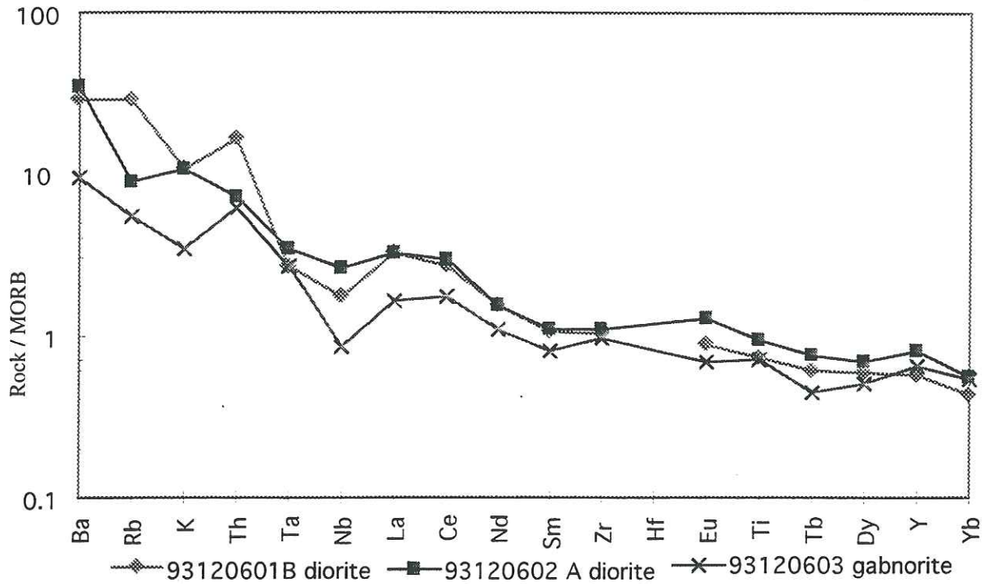

Figure 58. MORB-normalized incompatible trace elemnt diagram illustrating geochemical characteristics of the Chilas Igneous Complex . Normalization values are from Sun and McDonough (1989).

Spectre d'éléments trace incompatibles normalisés aux MORB illustrant les caractéristiques géochimiques de la Zone du Faciès Principal, Complexe Igné de Chilas dans la Vallée de l'Indus , entre Shatial and SeO. Normalisations par Sun and McDonough (1989).

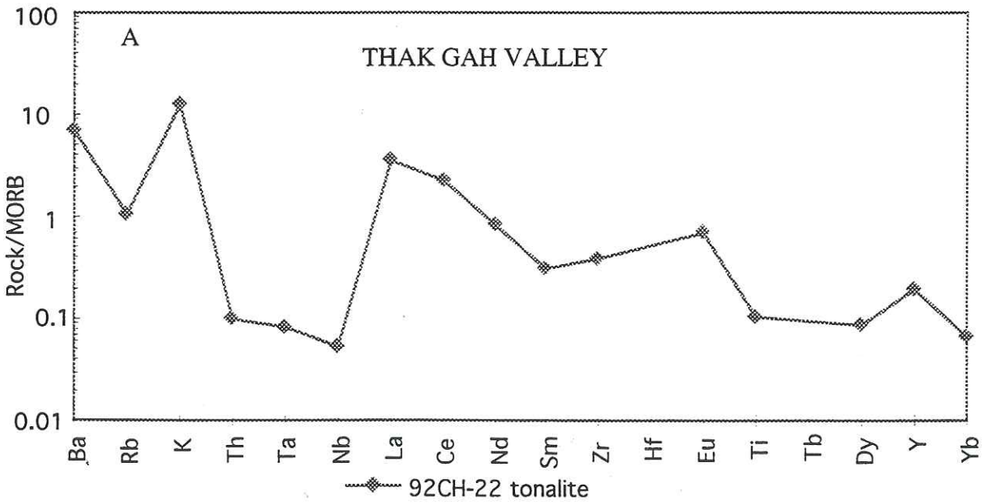

Figure 47. MORB-normalized incompatible trace element diagram illustrating geochemical characteristics of tonalite (Thak Gah) in Main Facies Zone, Chilas Igneous Complex. Normalization values are from Sun and McDonough (1989).

The compositional range and behaviour of Ta and Nb in all the rocks of the Chilas Igneous Complex is the same and show negative anomalies in the comparatively more mafic rocks, i.e. stronger depletion than other HFSE relative to MORB, a phenomenon which is well known from other subduction-related magmas (Briqeu et al., 1984; Ellam and Hawkesworth, 1988). However, depletion of Ta and Nb relative to other HFSE is less pronounced in the more evolved rocks (SW-12 in SV, 92CH-89 in IV) in each group and not evident in the more fractionated rocks (between Dassu and Shatial; Fig. 38; Table 5) of the Indus Valley.

The trace-element patterns for more evolved rocks (diorites and quartz-diorites) are marginally more enriched in their abundances of the incompatible elements and REE curves also discriminate these samples from the more basic rocks. MORB-normalized patterns for the MFZ (Chilas Igneous Complex) are notable in that they remain roughly parallel and smooth, without significant crossovers and which is more consistent with the more evolved mineralogies. All the mafic samples have positive Eu anomalies (Figs. 56 and 57) which show crystallization of An-plagioclase but more evolved samples have modest negative Eu anomalies and have higher concentrations of trace elements. Parallel patterns and higher total trace element in more differentiated samples, no significant crossovers and from positive Eu anomalies (e.g. mafic rocks) to modest negative Eu anomalies (e.g. more evolved rocks) are consistent with the fractionation of more-mafic magmas to silicic magmas which would be dominant by removal of An-rich plagioclase. The trace and REE patterns from the Indus Valley of MFZ show minor positive to negative Ce anomalies, widely described as typical of arc volcanic rocks. Negative Ce anomalies have been explained by; 1) the presence of small amounts of subducted sediments such as in Mariana arc lavas (Hole et al., 1984); 2), by fractionation by fluids originating from dehydration of the subducted slabs (White & Patchett, 1984); 3), and by hydrothermal alteration (Brouxel et al., 1987).

Ryerson and Watson (1987) have used the Ce/Nb ratio to characterize the magma produced in an island-arc environment. Basic rocks in the MFZ have a Ce/Nb ratio ($3.25 < Ce/Nb < 11$) which is comparable to those of island-arc tholeiites. The erratic behaviour of the elements Ba to Th may be a result of the subduction-related magmas, differences in source character (Sun et al., 1979; Tarney et al., 1980), from differences in the degree of melting (Langmuir et al., 1977), or may reflect metamorphic redistribution in the amphibolitized samples.

The two main conclusions that can be reached from the study of these MORB- and chondrite-normalized patterns are, 1) that there is a clear island-arc affinity among the rock assemblages of the Chilas Igneous Complex, and, 2) that they show evidence of perfect fractional crystallization. The flat profiles shown by CH-01 and SW-12 suggest that Eu lost by plagioclase fractionation was accompanied by Eu gained by plagioclase settling into it.

In contrast to Jan (1980), Jan and Kempe (1973) and Khan et al. (1989) whose interpretation that the Chilas Complex has more calc-alkaline affinity, our geochemical data show that mafic to more evolved rock of the Chilas Igneous Complex form a chemically

continuous, and possibly genetically related rock series and displays tholeiitic to slightly calc-alkaline affinities. Thus, it seems reasonable to believe that the complex has evolved from a nascent to a mature stage of the Late Mesozoic intra-oceanic island arc, with plutonic rocks crystallized in a relatively shallow magma chamber.

CHAPTER-3

PETROLOGY AND MINERAL CHEMISTRY OF THE JIJAL ULTRAMAFIC-MAFIC COMPLEX: implications on magmatic processes

CHAPTER-3

3.1- INTRODUCTION

The Kohistan arc, northern Pakistan, is an intriguing place to study a record of deeper to shallower level magmatic processes involved in the formation of crust. Due to collision of Asian-Kohistan block with Indian continent at about 50 Ma (Patriat & Achache, 1984; Searle et al., 1987), several deeper crustal level ultramafic and mafic blocks, considered to be the root zone of Kohistan arc, are exposed through uplift/erosion and emplaced along the Main Mantle Thrust (MMT). The study of these ultramafic-mafic complexes will provide an insight into rocks that once marked the lower crustal cumulates as well as possibly the metamorphic equivalents of these cumulates and their differentiates.

The Jijal ultramafic-mafic complex is one of these several uplifted blocks and is composed of ultramafic and garnet-bearing granulite rocks. Several hypotheses have been proposed as to their significance. According to Jan and Howie (1981) ultramafic rocks are composed of dunite, diopsidite, harzburgite and websterite and these are alpine-type in nature. Garnet granulite represents the differentiated tholeiitic magma of oceanic affinity or crystallized from a calc-alkaline magma of island arc or continental margin affinity. Further, garnet granulite has been intruded by the ultramafic rocks as plastic crystalline material and then both had been independently metamorphosed before the entire complex was tectonically uplifted into its present position. Pressure-temperature conditions for the garnet granulite have been estimated to be 670-790°C at 11-15 kbar (Jan & Howie, 1981) and 697-949°C at 11-17 kbar (Yamamoto, 1993). Jan and Windley, 1990, proposed that the ultramafic cumulates derived from an arc-related high-Mg tholeiitic magma and ultramafic and garnet granulite are either continuous sequence of arc cumulates or the two are produced from different source magmas.

A second school of thought believes that this complex represents either the basal part of an arc, discrete from the rest of Kohistan, or the deep level metamorphic equivalent of the Chilas Complex (Bard, 1987). South of Jijal Complex, along the MMT, between the Indus and the Swat Rivers, there is a suture zone about 12 km wide containing high pressure, low temperature metamaorphic assemblages like glaucophane schists and piedmontite schists (Shams, 1980; Coward et al., 1982). As a result of this tectonic setting, much controversy exists in the literature regarding the origin of the Jijal Complex.

The isotopic ages of the deep-seated rocks of the Kohistan rocks are mainly from the Upper Cretaceous to the lower Paleogene. Treloar et al. (1989) described ^{40}Ar-^{39}Ar dating on

the Jijal Complex using hornblendes in garnet gabbro with the lack of stable plateaus and huge amount of excess argon released in low-temperature fractionations from the sample with K-Ar ages of 130 to 340 Ma. Yamamoto and Nakamura (1996) have reported a Sm-Nd mineral isochron age of 118 ± 13 Ma on a pyroxene granulite of the Jijal Complex. Recently, Sano et al. (1996) have described a Sm-Nd whole-rock age of 114 ± 39 Ma which does not contradict the result of Yamamoto and Nakamura (1996), although the whole-rock age makes poor constraints to the history because of a large error.

Since these rocks have been frequently mentioned in the literature (e.g. Jan & Howie, 1981; Jan & Jabeen, 1991; Khan & Coward, 1991; Yamamoto, 1993; Yamamoto & Nakamura, 1996), a detailed geochemical study is needed to define their characteristics and provide clues to their origin.

The over-all approach in this paper is to supplement, and to some extent revise, the petrographic and chemical data of Jan and Howie (1981), incorporating a study of more recently collected material; then to examine the integrated field, petrology, mineral phase chemistry and REE data of the basal cumulate ultramafic-mafic rocks of the Jijal Complex. One of our main conclusion demonstrated here is that these rocks crystallized from a basaltic magma at high pressures (> 10 kbar) near the crust-mantle boundary beneath an island arc.

3.2- GEOLOGY OF THE JIJAL COMPLEX

The Jijal Complex (Fig. 59) extends for more than 35 km E-W and is some 15 km wide in its central part. To the north, the Jijal Complex is separated from the Kamila Amphibolites by the Pattan fault. On the western side, a serpentinite body separates the Jijal Complex from the Kamila Amphibolites.

The rock assemblage of the Jijal Complex is composed of two distinct ultramafic and mafic sections. The lower ultramafic section consists basically of dunite and pyroxenite which grades into upper garnet gabbro section (garnet granulite of Jan and Howie, 1981).

In the ultramafic section, pyroxenite displays large variations in mineralogy and subdivided into several mappable units; olivine clinopyroxenite, websterite and garnet websterite. In the Duber Valley (Fig. 59), olivine clinopyroxenite forms two units (U1 and U3) intercalated by thin horizons of dunite. These are separated by a massive dunite unit (U2) and grade to websterite (U4) and garnet websterite (U5). Along the KKH, unit 3 is missing, while

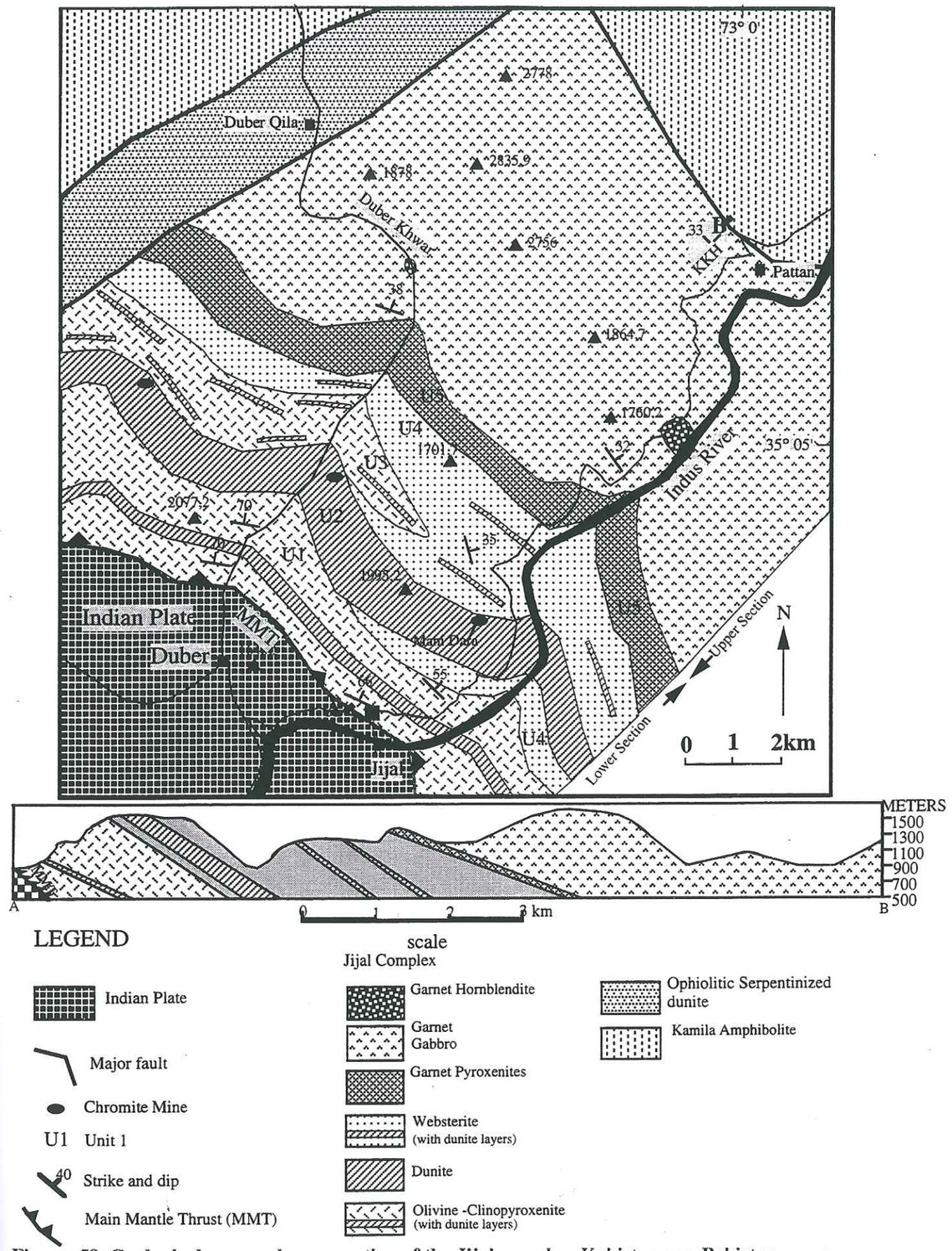

Figure 59. Geological map and cross-section of the Jijal complex, Kohistan arc, Pakistan (modified after Miller et al., 1991).
Carte géologique et coupe du Complexe de Jijal, Arc du Kohistan, (modifié d'après Miller *al.*, 1991).

unit 4 becomes thicker and intercalated by unit 2. In Duber Valley, the lower level websterite (below U2) is missing. The contacts between these units are always very sharp and marked by sudden variations in mineral compositions. These structural relations and mineralogical changes suggest that U2 dunite probably intrudes the other units.

Bands of dunites are frequent in unit 1 where they are continuous and thicker (2-10 meters, exceptionnally 20 meters) along strike length, while they are less common, discontinuous and thinner (10 cm to 1 meter thick) in unit 3 (Fig. 60). Similarly, small bands of clinopyroxenite occur in dunitic U2 as compositional layers 20-50 cm thick (Fig. 61). Alternating lenses of clinopyroxenite and dunite of varying thickness also occur in the upper section of the websterite. Chromite-rich layers are also common as stringers (2-4 mm thick) and lenses in dunite. In U2, some range in thickness from 2 to 3 metres and 50 metres strike length forming chromitic ore-bodies as Mani-Dara mine (Fig. 59).

Garnet websterite is the upper unit (U5) of the Jijal Ultramafic Cumulates. Websterite unit (U4) grades progressively into the garnet websterite. In the middle of the websterite, the amount of garnet increases with the decrease of the orthopyroxene-clinopyroxene ratio. In the beginning, garnet is fine-grained and gradually starts increasing in its size and volume and becomes medium- to coarse-grained to the north (Fig. 62). To the top, the pyroxenite is dominated by garnet and clinopyroxene with amphibole, forming a garnet clinopyroxenite level (too thin to map).

The contact of the garnet websterite with the overlying garnet gabbro is not really sharp but marked with sudden appearance of plagioclase. This quick progressive contact indicates that the mafic and ultramafic rocks are genetically related.

Garnet gabbro is 40-45 vol.% of the Jijal Complex and displays a layered and banded fabric formed by late magmatic flow and recrystallization. All the section of garnet gabbro displays compositional banding of mafic and felsic layers which generally strike N 40° to 60°W and dipping 30 to 35°NE. These are generally conformable to the layering in garnet websterite. Olivine is absent in this unit. The garnet gabbro is locally crosscut by small bodies of garnet hornblendites. Finally, it is separated from the Kamila Amphibolites in the north by the high-angle Tertiary Pattan fault (Fig. 59).

3.3 PETROGRAPHY AND MINERAL CHEMISTRY.

3.3.1 Petrographic characteristics

The ultramafic rocks of the Jijal Complex are made up almost entirely of olivine, clinopyroxene, orthopyroxene and garnet. Cr-spinel, Al-spinel, amphibole, titano-magnetite and magnetite are the important minor constituents. Garnet gabbro is made up of

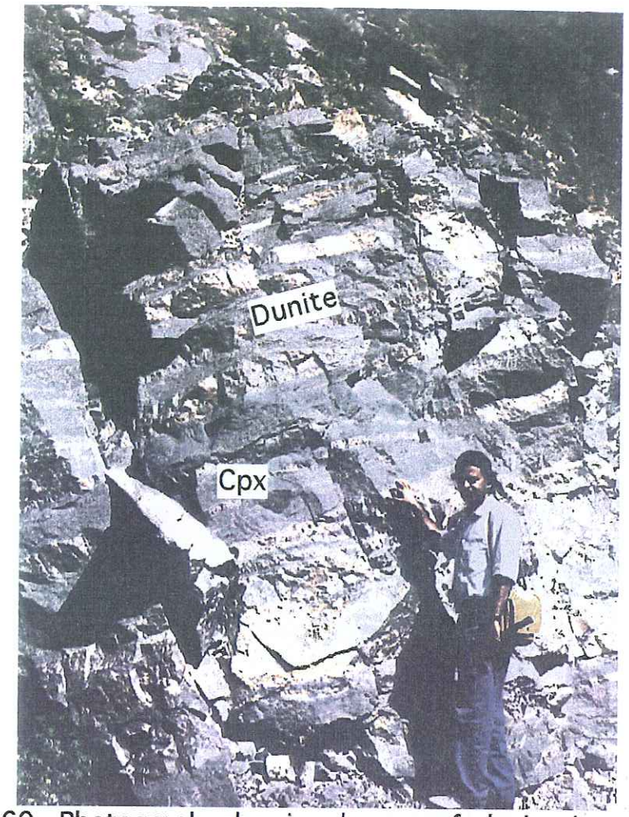

Figure 60. Photograph showing lenses of dunite intercalated with clinopyroxene in Duber Valley, Jijal Complex
Photographie montrant des lentilles de dunite en intercalation avec des clinopyroxènes dans la vallée du Duber, Complexe de Jijal .

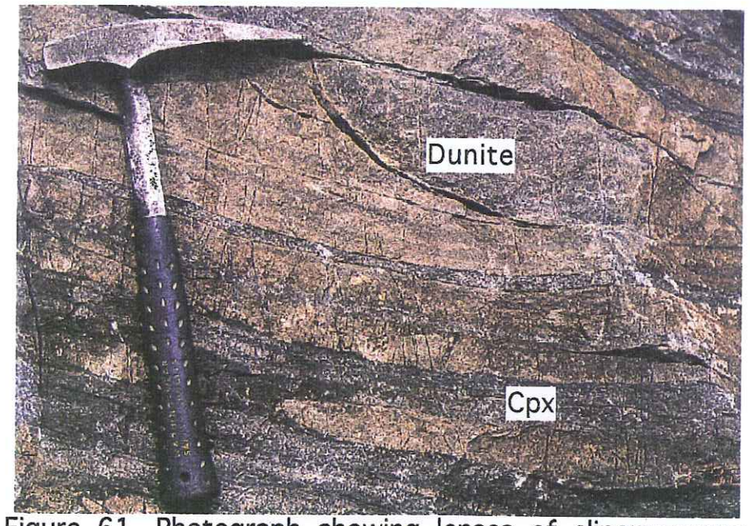

Figure 61. Photograph showing lenses of clinopyroxene intercalated with dunite in Duber Valley, Jijal Complex
Photographie montrant des clinopyroxènes lités en intercalation avec de la dunite dans la vallée du Duber, Complexe de Jijal .

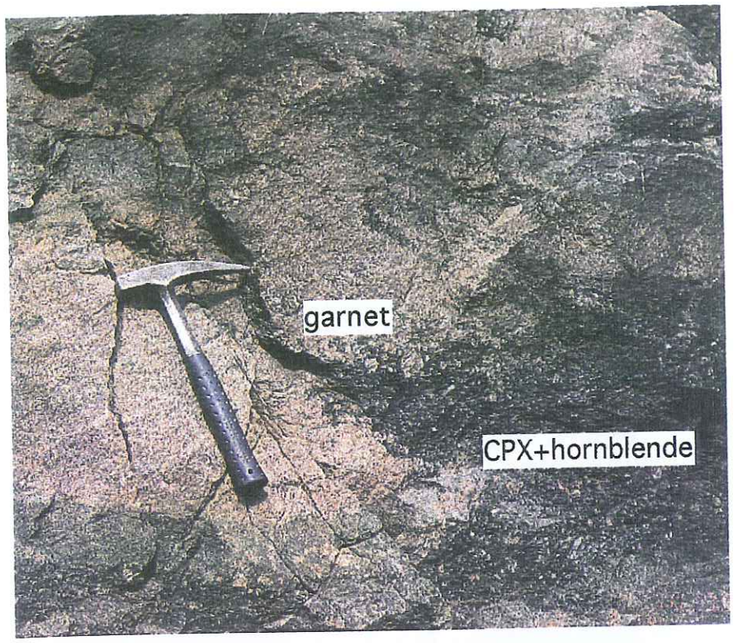

(A) Garnet concentration in garnet clinopyroxenite unit

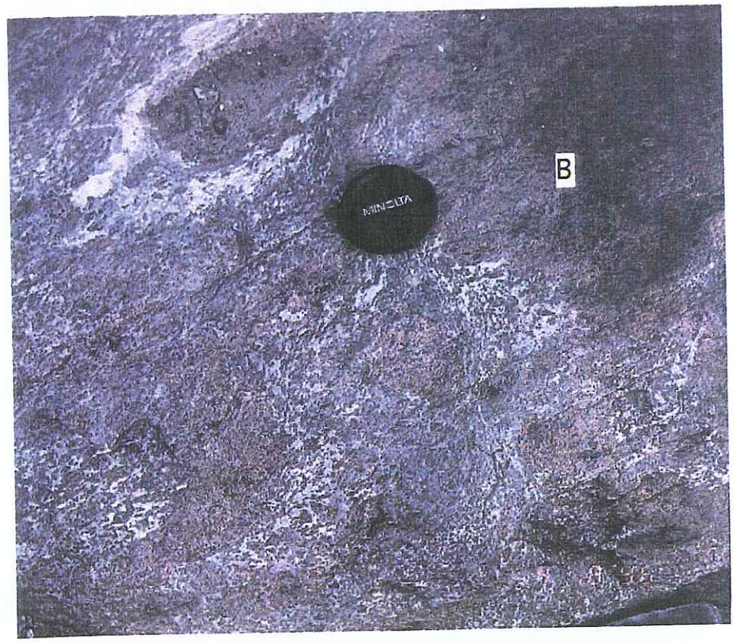

Figure 62. Photographs showing the concentrations of garnet in garnet clinopyroxenite (A) and layered gabbro (B), Jijal Complex.
Photographie montrant des accumulations de grenat dans une clinopyroxènite à grenats, le long de la coupe de la KKH à travers le Complexe de Jijal .

clinopyroxene, garnet, plagioclase, amphibole, scapolite, quartz, ilmenite, rutile and magnetite. Petrographic summary of the Jijal Complex is summarized in Table 6.

Dunite is dominantly olivine-rich (95 vol.%) and minor amounts of clinopyroxene (1-4 vol.%), Cr-spinel (1-2 vol.%) and magnetite (average 0.5 vol.%) are also present. No orthopyroxene is found in the dunites. Textures vary from tabular to granoblastic. Olivine in the dunite varies in grain size and shape and has irregular and interlocking grain boundaries. Coarse grains (2 to 5 mm) present undulatory extinction and kink bands. Their elongation is approximately parallel to the layering. The coarse grain olivine recrystallized into smaller grains (< 0.5 mm; Fig. 63). These crystals are clearly distinguished from the coarse deformed olivine on account of equigranular and polygonal shape of grain, rare occurrence of kink bands and lack of elongation and stretching. A marked difference in occurrence of the polygonal olivines is that they are more frequently found in the lower level of the dunite as compared to the upper level. Clinopyroxene is present in some dunite as cumulate phase; however, most clinopyroxene is present as an intercumulus phase. Clinopyroxene is subhedral, sometimes kinked and often encloses olivine. Cr-spinel is present as disseminated grains as well as in layers in these dunites but becomes more abundant in unit 2. The layers are few milimeters in thickness. Disseminated spinel generally forms rounded crystals (2 to 4 mm), suggesting interaction with liquid or olivine crystals. Olivine and Cr-spinel apparently crystallized as cumulus phases, followed by a stage of post-cumulus growth of clinopyroxene and magnetite.

Kink banded porphyroblastic olivine surrounded by polygonal grains suggests both high temperature plastic deformation and static recrystallization as observed in many alpine-type peridotites e.g., Twin Sisters dunite (Ragan, 1963), Piedmont Alps lherzolite (Nicolas et al., 1971), Vulcan Peak peridotite (Himmerberg and Lonely, 1973). The experimental study by AvéLallemant and Carter (1970) shows that such polygonal olivines were produced near the grain boundaries of the host grains at 1100°C and 13 kbar.

Pyroxenites in Jijal ultramafic complex display large variations in mineralogy and four rock types are petrographically distinct (Fig. 59):

Olivine clinopyroxenite is composed of medium- to coarse-grained clinopyroxene (65-70 vol.%), orthopyroxene (8-12 vol.%) and olivine (20-25 vol.%), with minor Cr spinel and magnetite. Textures are generally adcumulate, with both pyroxene present as cumulate phases. Clinopyroxene (4-6 mm) commonly contains growth twins and, less commonly, narrow exsolution lamellae of orthopyroxene. Clinopyroxene presents kink bands and has been subsequently broken and surrounded by smaller, unstrained polycrystalline aggregates suggesting high-temperature recrystallization. Similar deformation textures in clinopyroxenites exposed at Duke Island, Alaska, are presumed to be due to tectonism of cumulus material in the presence of intercumulus liquid (Irvine, 1974).

Table 6. Modal and textural summary of petrography of the Jijal Ultramafic-Mafic Complex.
(Synthèse structurake et composition modale des roches Complexe de Jijal)

Rock name	Relative abundance	Mineral assemblage	Mg #	Remarks
Garnet-gabbro	40 - 45 %	Cpx 25-30% Plg 20-25% Gt 45-50% Hb 8-12% Scp+Qtz+Ep+Mag +Rt as accessory phases	Hb = 70	Poikilitic. Large pophyroblast of Gt poikilitically enclosing Cpx, Plg, and opaque. Scp mostly replacing plg. Opx is missing.
Garnet-hornblendite	< 0,5 %	Hb 55-65% Gt 40-45% cpx 2-3% Rt+Ilm 1-2%	Hb = 71	Holocrystalline, coarse-grained, adcumulate texture, massive and no preferred mineral orientation visible.
Garnet-websterite	10 -15 %	Ol 3-5% Cpx 30-40% Opx 15-20% Gt 50-60% Hb 1-2% Sp+TiMag+Mag accessory phases	Ol = 79-78 Cpx = 87-83 Opx = 80-76 Sp = 59-49 Hb = 83	Poikilitically enclosed the grains of Sp in Gt. Gt subhedral to anhedral. Sp slightly greenish. Exsolution lamellae of Opx in Cpx. Gt exsolved along the cleavage of Cpx. Opx subhedral. Garnetiferous pods up to 2,4 m in length are encountered.
Websterite	16 - 20 %	Ol 20-25% Cpx 65-70% Opx 8-12% Sp+Mag 3-5%	Ol = 93-79 Cpx = 92-86 Opx = 84-81 Sp = 34-29	Hypidiomorphic granular and relict texture indicate adcumulate texture. Large porphyroclasts of Cpx often surrounded by smaller neoblastic Cpx. Exsolution lamellae of Opx seen in Cpx.
Olivine-clinopyroxenite	25 - 30 %	Ol 20-25% Cpx 65-70% Opx 8-12% Sp+Mag 3-5%	Ol = 90 Cpx = 93 Sp = 13	Xenomorphic to hypidiomorphic with large porphyroclasts of Cpx surrounded by smaller neoblastic Cpx. Complex interlocking of Ol and Cpx frequent. Tripple junctions also common. Opx is subhedral and shows pink pleochroism. Relict igneous textures show adcumulus growth.
Dunite	4 - 6 %	Cr-sp 2-4% Ol 93-95% Cpx 2-4% Mag <1%	Sp = 29-39 Ol = 94-90 Cpx = 95	Porphyroclastic Ol affected by plastic deformation with many kink bands of the slip system. Elongation of the grains formed translation gliding and varies from none to medium. Complex interlocking of Ol grains common. Px is hypidiomorphic. Ol poikilitically encloses Sp. Cr-spinel is brownish black.

Abbreviations: Cr-sp = chromian spinel; Ol = olivine; Cpx = clinopyroxene; Opx = orthopyroxene; Gt = garnet; Sp = spinel; Hb = hornblende; TiMag = titanomagnetite; Qtz = quartz; Scp = scapolite; Rt = rutile; Ep = epidote; Mag = magnetite; Plag = plagioclase; Chl = chalcopyrite; Pyt = pyrrhotite.; Ilm = ilmenite

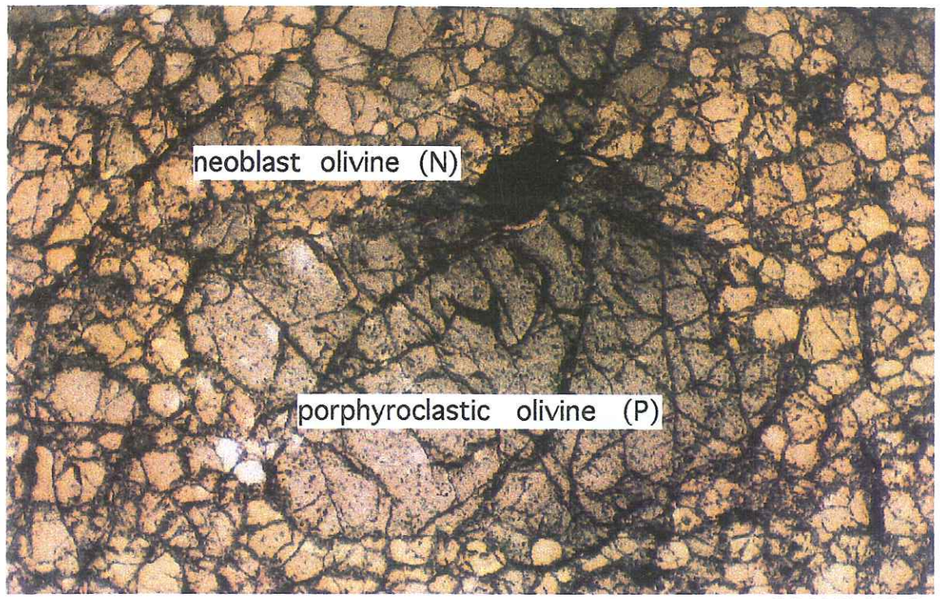

SCALE=X6,3

Figure 63. Photomicrograph showing strongly strained and recrystallized olivine and relationships between porphyroclastic olivine (P) and neoblastS(N).
Microphotographie montrant une olivine fortement étirée et recristallisée et les relations entre les porphyroclastes (P) et les néoblastes (N) d'olivine.

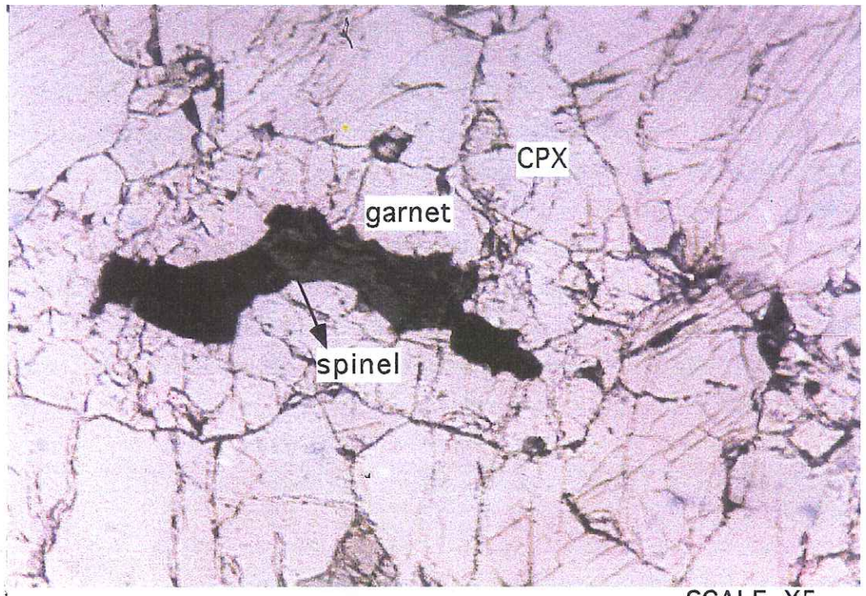

SCALE=X5

Figure 64. Photomicrograph showing exsolution of green spinel, surrounded by exsolved garnet in CPX grain in garnet websterite from KKH, Jijal Complex.
Microphotographie montrant une exsolution de spinelle vert, entourée de grenat exsolvé dans un grain de pyroxène d'une websterite à grenat de la vallée du Duber, Complexe de Jijal .

Websterite (U4) are characterized by medium- to coarse- grained (2-5mm) texture, and composed dominantly of 70-75 vol.% clinopyroxene, 20-25 vol.% orthopyroxene, 5-10 vol.% olivine. Cr-spinel, titano-magnetite and magnetite are the accessory phases. The texture is generally adcumulate, with both pyroxenes present as cumulate phases. Spinel is present as discrete grains as well as exsolution lamellae in the clinopyroxene. It is brownish in the lower part of the unit and is green in the higher levels. In the Duber valley, websterite typically contains some PGE enriched horizons with disseminated pyrrhotite and pentlandite and veinlets of chalcopyrite.

Garnet websterite (U5) is characterized by variable amounts of garnet (30 to 60%), clinopyroxene (30-40%), orthopyroxene (15-20%) and olivine. Garnet increases when both olivine and orthopyroxene decrease towards north. Garnetiferous rich pods up to 2-3 m in length are also seen and give heterogeneous appearance to the unit (Fig. 62). Pargasite hornblende starts appearing in this unit and is about 10-15 %. Green-spinel (hercynite), titano-magnetite and magnetite are the accessory phases. Orthopyroxene grains are pleochroic and rounded subidioblastic. Clinopyroxene grains are colourless to light green and subidioblastic to xenomorphic. These grains have exsolution blebs of garnet, green spinel, rutile and orthopyroxene. Garnets are light pink, normally rounded to subidioblastic and also contain inclusions of green-spinel. Some garnet grains also show interstitial texture. Sometimes, green-spinel is bounded by magnetite bands. Titanomagnetite is present and forms exsolution lamellae of titanium within magnetite.

Garnet clinopyroxenite is medium- to coarse-grained and characterized by clinopyroxene (45-55 vol.%), garnet (25-30 vol.%) and amphibole (15-20 vol.%) with minor amount of green-spinel (1-2 vol.%), titanomagnetite (1 vol.%) and magnetite (1 vol.%). Texture ranges from cumulate to prophyroblastic, where igneous clinopyroxene grains are surrounded by smaller recrystallized, unstrained grains. Garnet is not evenly distributed and sometimes its concentration exceeds 70 vol.%. Amphibole is present as intercumulus phase. Exsolution of garnet, green spinel, rutile and orthopyroxene in clinopyroxene is frequent (Fig. 64).

Garnet gabbro consists of a heterogeneous mineral assemblage dominated by medium- to coarse-grained variable proportions of plagioclase, garnet, amphibole and clinopyroxene. Quartz, epidote, and magnetite are the accessory phases. Orthopyroxene and olivine are altogether absent in these rocks. Pophyroblasts of garnet, up to 9 cm across and in some cases surrounded by thick mafic and /or felsic envelopes, are common (Jan & Howie, 1981). Cumulus clinopyroxene and intercumulus plagioclase are enclosed in subhedral garnet, suggesting that garnet formed as a subsolidus phase. At some places, garnet gabbro is cut by felsic veins and studded by small to large garnet porphyroblasts, up to 10 cm across.

3.3.2 Mineral Chemistry

Compositions of coexisting minerals from 15 rocks of Jijal Ultramafic and Mafic Complex along KKH (Fig. 65) were determined by quantitative electronprobe microanalysis in Clermont Ferrand University, France. Analyzed minerals include olivines, clinopyroxenes, orthopyroxenes, spinels, garnets and amphiboles. Cation proportions were calculated from the analyses and form the basis for much of the discussion in this part. As far as possible, samples showing phase heterogenity were avoided. All iron was assumed to be present as Fe^{2+} in the olivines and pyroxenes. For spinels, the cation sum was normalized to 24.00 per formula unit and the proportions of Fe_2O_3 and FeO were obtained accordingly. Most analyzed phases are of uniform composition in each rock. In few cases in which systematic mineral zoning was detected, volumes near the grain margins were analyzed.

3.3.2.1 Olivine

Olivine is the most dominant among the minerals. It constitutes more than 95 % of dunites and 10-15 % of pyroxenites (clinopyroxenites and websterites) but is absent in garnet gabbros. Textures in the ultramafic rocks are characterized by coexisting phases of porphyroclastic-primary olivine, kink-banded olivine and recrystallized polygonal olivine.

The chemical composition and the structural formula of the olivines are presented in Table 7. However cation totals, based on four oxygens, range from 2.969 to 3.036, in reasonable agreement with the theoretical value of 3.

Olivine compositions vary with lithology (Table 7). The forsterite content is greater and ranges from 95 to 90 in dunite, 90 in olivine clinopyroxenite, 93 to 80 in websterite. Jan and Windley (1990), however, have reported comparatively closer ranges in the composition of the olivines (Fo 92-89) from the Jijal Complex. Olivine from the chromitites of Jijal Complex (sample KO-29) has forsterite content of 95. Himmerberg and Lonely (1973) found that in the Vulcan Peak peridotite, Oregon, chromitites contain the most magnesian olivine. CaO contents are negligible (0.08 wt %); Mn contents range from 0.05 to 0.43 wt % but show no systematic trend with differentiation. NiO contents (0.05-0.84 wt %) in olivines from dunites also overlap those from olivine-clinopyroxenites; websterites and garnet-websterite (0.03-0.23 wt %). Figure 66 shows the plot of NiO vs FeO/MgO in olivine. Ni contents in the cumulus olivine show a general decrease with decreasing Mg number. Depletion of Ni with increasing Fe content, but locally variable, is observed in dunite and peridotite layers in stratiform intrusions and ophiolitic complexes (Jaques, 1981).

There is no compositional difference in the ratio 100Mg/(Mg+Fe) between the large porphyroclastic-primary olivine and polygonal-recrystalized olivine and Mg number correlates positively with Fo content of olivine in coexisting pyroxene and with Cr number in coexisting spinel (Table 7). Furthermore, no signs of compositional zoning are observed in large

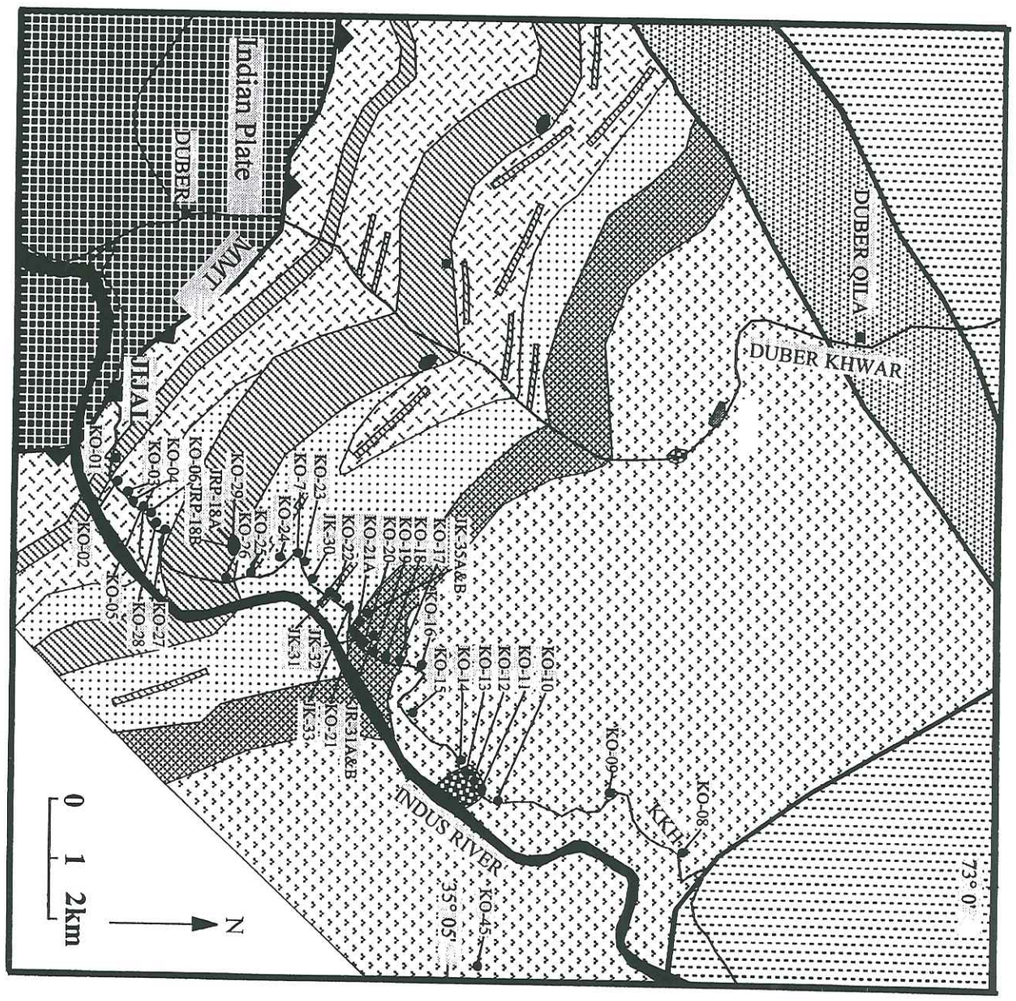

Figure 65. Locations of analyzed samples in the Jijal Complex, Kohistan Arc, Pakistan
Localisation des échantillons analysés dans le Complexe de Jijal , Arc du Kohistan, Pakistan.

Table 7. Representative mineral chemistry data for olivine in Jijal Complex.
Composition chimique représentative pour les minérauxd'olivine du Complexe de Jijal .

s.no.	JD-02			KO-26			KO-29	KO-35	KO-02	KO-23		JK-30	KO-21A	JR-31B		JK-35
rock name	dunite (UI)			dunite (U2)			dunite (U2)	web.(U4)	ol-clinop.(U1)	websterite (U4)		web. (U4)	ga-web. (U5)	ga-web. (U5)		ga-web. (U5)
no of probe	2			3			2	1	1	1	1	2	1	1	1	2
locality	megacryst(C)	megacryst(R)	polygonal	megacryst(C)	megacryst(R)	polygonal				core	rim			core	rim	
	Duber			KKH			ManiDara	Duber	KKH	KKH		KKH	KKH	KKH		KKH
SiO2	41.23	41.14	41.03	41.41	42.37	41.72	40.89	40.1	39.28	39.06	39.27	41.56	39.87	39.48	39.38	40.89
Al2O3		0.26	0.02	0.04			0.02			0.01	0.03		0.01	0.03		0.02
TiO2	0.1	0.32	0.02		0.07	0.06	0.01			0.05	0.01	0.02				0.01
Cr2O3	0	0.06	0.04	0.12	0.15		0	0.01	0.06		0.06	0.09	0.04	0.06	0.06	
FeO	8.97	8.94	8.84	6.76	5.4	6.22	4.69	9.43	9.98	17.87	18.34	6.36	19.2	19.96	19.8	4.69
MgO	48.94	48.75	48.79	51.01	52.01	51.63	53.27	50.2	50.87	42.4	42.14	50.94	41.48	41.24	41.48	53.27
MnO	0.24	0.19	0.19		0.1	0.18	0.05	0.19	0.15	0.34	0.43	0.13	0.32	0.18	0.31	0.05
CaO	0.03	0.05	0.05		0.02	0.04	0.03		0.02	0.08	0.04	0.03		0.01		0.03
Na2O			0.02		0.02		0.01			0.02	0.02			0.04		0.01
K2O			0.02		0.01		0.01	0.01					0.01		0.03	
NiO	0.3	0.84	0.26	0.18		0.23	0.22	0.19	0.17	0.14	0.1	0.15	0.05	0.03	0.15	0.22
Total	99.71	100.56	99.28	99.52	100.15	100.09	99.19	100	100.53	100.52	100.43	99.28	100.99	101.04	101.21	99.18
Cations																
Si	1.009	1.001	1.008	1.003	1.014	1.005	0.989	0.98	0.963	1.003	0.998	1.009	1.009	1.003	0.999	0.989
Aliv		0.007	0.001	0.001							0.001			0.001		
Alvi																
Ti		0.006			0.001	0.001				0.001			0.001			
Cr		0.001	0.002	0.002	0.003		0.001		0.001	0	0.001	0.002		0.001	0.001	
Fe*	0.184	0.182	0.182	0.131	0.108	0.125	0.095	0.19	0.205	0.379	0.39	0.129	0.406	0.424	0.42	0.095
Mg	1.786	1.768	1.787	1.856	1.855	1.853	1.92	1.83	1.861	1.6	1.597	1.844	1.565	1.561	1.569	1.92
Mn	0.005	0.004	0.004		0.002	0.004	0.001		0.003	0.007	0.009	0.001	0.007	0.004	0.007	0.001
Ca	0.001	0.001	0.001		0.001	0.001	0.001			0.002	0.001	0.001				0.001
Na			0.001		0.001		0.001			0.001	0.001					0.001
K			0.001												0.001	
Ni	0.006	0.016	0.005	0.004		0.005	0.004		0.003	0.003	0.002	0.003	0.001	0.001	0.003	0.004
Total	2.99	2.99	2.992	2.995	2.985	2.994	3.011	3.01	3.036	2.996	3	2.989	2.989	2.995	3	3.011
Fo(%)	92	90	91	93	94	93	94	90	90	80	80	93	79	78	78	95
Fa(%)	8	10	9	7	6	7	6	10	10	20	20	7	21	22	22	5
Mg# (%)	90.66	90.67	90.76	93.41	94.5	94	95.29	90.5	90.08	80.85	80.37	93.46	79.4	78.64	78.88	95.29
FeO/MgO	0.18	0.18	0.18	0.13	0.1	0.12	0.09	0.19	0.2	0.42	0.44	0.12	0.46	0.48	0.48	0.09

Mg # (%) = 100Mg / (Mg+Fe); (C) = core; (R) = rim; polygonal = recrystallized neoblast of olivine megacryst , web.= websterite, U1= unit 1, ga-web. garnet websterite, ol-clinop. = olivine-clinopyroxenite, n = number of probe.

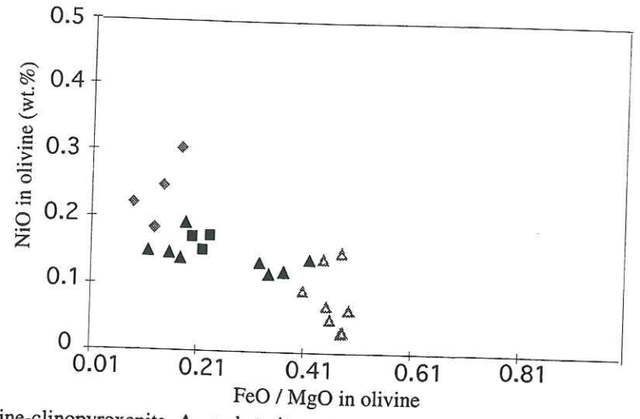

Figure 66. Trend of decreasing NiO in Jijal olivines with differentiation (FeO/MgO ratio).
Tendance à la décroissance du NiO dans le Complexe de Jijal avec la différenciation (FeO/MgO ratio).

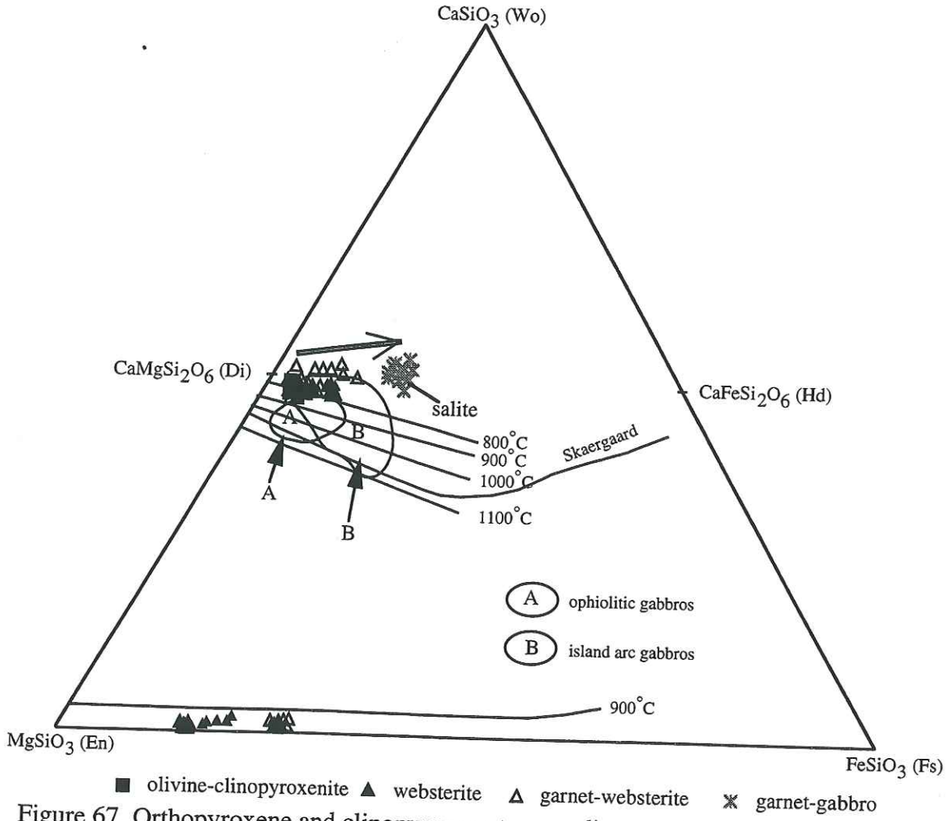

Figure 67. Orthopyroxene and clinopyroxene ternary diagram showing trend of Jijal pyroxenes. Pyroxenes in ultramafic and garnet gabbro clearly define a distinctly salitic trend with differentiation.
Compositional fields of island-arc gabbros (Arculus & Wills, 1980; Meijer & Reagan, 1981) and ophiolitic gabbros (Coleman, 1977) are also indicated.
Temperature estimates from Ross and Huebner (1975).
Diagramme ternaire à orthopyroxène et clinopyroxène montrant l'évolution des pyroxènes de Jijal. Les pyroxènes dans les gabbros ultramafiques et à grenat forment clairement une suite salitique avec la différenciation.

porphyroclasts of primary peridot and are homogeneous within individual samples. A wide range of forsterite contents is also displayed by the magmatic series of dunite-wehrlite-clinopyroxenite (Lonely et al., 1971; Jackson and Thayer., 1972). Arculus & Wills (1980) have reported the presence of Fo_{90} cumulate peridot in the xenoliths from the Lesser Antilles. Compositionally similar peridot is typically found in cumulate xenoliths in island arcs, e.g. Japan (Akoi,1971), New Guinea (Gust and Johnson, 1981), the Marianas (Stern, 1978) and the Lesser Antilles (Lewis, 1973).

2-3.2 Clinopyroxene

Clinopyroxene occurs in almost all types of the Jijal ultramafic and mafic rocks, but in the dunites it occurs only sporadically. The chemical compositions and structural formulae of representative clinopyroxenes are presented in the Table 8. Within a single thin-section, compositions of clinopyroxene grains in the Jijal area are identical within analytical uncertainity. Oxide totals range from 98.78 to 100.96 wt %. Based on six oxygens, cation sums range from 3.95 to 4.055 and average precisely 4.005 - the ideal stoichiometric value. In all cases, sufficient Al is present which, along with silicon, allows complete filling of the four-fold structural sites.

Trend of compositional variation within cumulus clinopyroxene is displayed in the pyroxene quadrilateral (Fig. 67). This indicates that clinopyroxene is diopsidic in composition and moderate Fe enrichment with differentiation. The salitic trend is marked by moderate enrichment in CaO and TiO_2, and greatly increased Al_2O_3 (Fig. 67). The salitic clinopyroxene trend in the suite of ultramafic and hornblende gabbro xenoliths from Mt. Moffett is interpreted as reflecting crystallization of successive assemblages from progressively more hydrous melts. This was suggested by Murray (1972) as the primary reason for the occurrence of salitic clinopyroxene in Alaskan type ultramafic complexes. Progressive enrichment of H_2O in the Jijal parent melt is seen lithologically; increasing modal percent amphibole occurs as differentiation proceeds from ultramafic to garnet gabbros.

A gradual increase in the Fe and Ca content with decrease in the Mg content is observed in dunite, olivine clinopyroxenite, websterite and garnet websterite. A plot of Cr_2O_3 vs FeO/MgO in clinopyroxene (Fig. 68) also shows a general decrease with increasing FeO/MgO ratio, suggesting that all types of clinopyroxene are related by fractional crystallization from melts of initially similar Fe, Mg and Cr contents.

Figure 69 shows the relationship between SiO_2 and Al_2O_3 in clinopyroxene of Jijal Complex. The clinopyroxene from the ultramafic rocks is higher in SiO_2 and lower in Al_2O_3, whereas that from the garnet-gabbroic rocks is higher in Al_2O_3 and lower in SiO_2. The likeliest reason for lowering of silica activity in melts which are capable of crystallizing clinopyroxene- and hornblende-bearing gabbros is high water content (Depaolo, 1979).

Table 8. Representative mineral chemistry data for clinopyroxene in Jijal Complex.
Composition chimique représentative pour les minéraux de clinopyroxène du Complexe de Jijal .

s.no.	KO-26	KO-02	KO-06	KO-28	KO-23	JK-30	KO-22	JK-32	KO-21A	JK-35B	JR-31B	JK-35A	JR-31A	KO-15	KO-09
rock name	dunite(U2)	ol-clinop.(U1)	web.(U4)	web.(U4)	web.(U4)	web.(U4)	web.(U4)	ga-web.(U5)	ga-web.(U5)	ga-web.(U5)	ga-web.(U5)	ga-web.(U5)	ga-web.(U5)	ga-gabbro	ga-gabbro
no of probe	2	4	2	2	2	2	3	3	2	1	2	2	2	3	2
locality	KKH	KKH	KKH	KKH	KKH	KKH	KKH	KKH	KKH	KKH	KKH	KKH	KKH	KKH	KKH
SiO_2	55.03	54.77	53.56	56.78	53.16	54.19	51.82	53.41	51.94	51.27	52.45	51.4	50.52	48.7	48.72
Al_2O_3	0.44	0.46	1.25	0.94	1.74	1.99	3.79	1.95	3.3	2.73	2.71	3.62	5.43	8.78	9.03
TiO_2	0.01	0.06	0.07	0.05	0.1	0.15	0.29	0.12	0.29	0.19	0.29	0.31	0.55	0.76	0.69
Cr_2O_3	1.01	0.24	0.46	0.44	0.23	0.27	0.11	0.28	0.11	0.073	0.12	0.05	0.17	0.06	0.15
FeO	1.62	2.04	2.76	2.59	3.45	3.82	5.13	4.15	4.42	4.84	4.21	4.34	4.96	9.32	7.78
MgO	17.69	17.49	16.82	17.26	16.48	16.36	14.92	16.22	15.83	14.66	15.64	15.68	13.73	9.93	10.3
MnO	0.1	0.04	0.09	0.19	0.31	0.18	0.16	0.2	0.11	0.02	0.12	0.09	0.04	0.08	0.07
CaO	24	24.94	24.17	21.95	23.84	23.69	23.49	23.26	23.21	26.83	23.78	24.04	24.81	20.68	20.54
Na_2O	0.35	0.15	0.19	0.19	0.21	0.13	0.11	0.17	0.19	0.34	0.15	0.31	0.23	1.95	1.93
K_2O			0.07		0.04		0.01		0.01	0.01		0.01	0.01		0.01
NiO	0.03	0.02	0.07	0.07		0.03	0.04				0.02	0.03	0.02		0.04
Total	100.3	100.21	99.52	100.46	99.56	100.81	99.87	99.76	99.41	100.96	99.49	99.88	100.48	100.26	99.26
Cations															
Si	1.99	1.986	1.964	2.033	1.954	1.962	1.909	1.958	1.921	1.98	1.932	1.894	1.858	1.817	1.822
Al^{iv}	0.01	0.014	0.036		0.046	0.038	0.091	0.042	0.079	0.11	0.068	0.106	0.142	0.183	0.178
Al^{vi}	0.009	0.005	0.018	0.041	0.03	0.047	0.076	0.042	0.065	0.007	0.051	0.051	0.094	0.205	0.22
Ti		0.001	0.002	0.001	0.003	0.004	0.008	0.003	0.039	0.005	0.008	0.008	0.015	0.021	0.019
Cr	0.029	0.006	0.013	0.013	0.007	0.008	0.003	0.008	0.003	0.002	0.003	0.002	0.005	0.002	0.004
Fe*	0.049	0.061	0.085	0.078	0.106	0.116	0.158	0.127	0.137	0.149	0.13	0.134	0.153	0.291	0.243
Mg	0.954	0.945	0.919	0.921	0.902	0.883	0.819	0.886	0.858	0.806	0.859	0.861	0.753	0.552	0.574
Mn	0.003	0.001	0.003	0.006	0.01	0.006	0.005	0.006	0.004	0.001	0.018	0.003	0.001	0.002	0.002
Ca	0.93	0.969	0.95	0.842	0.938	0.92	0.927	0.914	0.919	1.06	0.939	0.949	0.977	0.826	0.823
Na	0.025	0.01	0.014	0.013	0.014	0.009	0.008	0.012	0.014	0.025	0.011	0.021	0.016	0.141	0.141
K			0.003		0.001				0.001				0.001		
Ni	0.001		0.002	0.002		0.001	0.001				0.001	0.001	0.001	0.001	0.001
Total	4	3.998	4.009	3.95	4.011	3.994	4.005	3.998	4.003	4.055	4.02	4.022	4.016	4.039	4.027
Mg#(%)	95.11	93.84	92	92.19	89.47	88.39	83.83	87.46	86.23	84.4	86.86	86.53	83.11	65.48	70.25
FeO/MgO	0.09	0.12	0.09	0.15	0.21	0.23	0.34	0.26	0.28	0.33	0.27	0.28	0.36	0.94	0.76
WO	48	49	49	46	48	48	48	47	49	53	48	49	52	49	50
EN	49	48	47	50	46	46	43	46	44	40	45	44	40	33	35
FS	3	3	4	4	6	6	9	7	7	7	7	7	8	17	15

Mg # (%) = 100Mg / (Mg+Fe); WO = Diopside; EN = Enstatite; FS = Ferrosilite, ol-clinop. = olivine-clinopyroxene, web. = websterite, ga-web. = garnet-websterite, n = 2, number of probe.

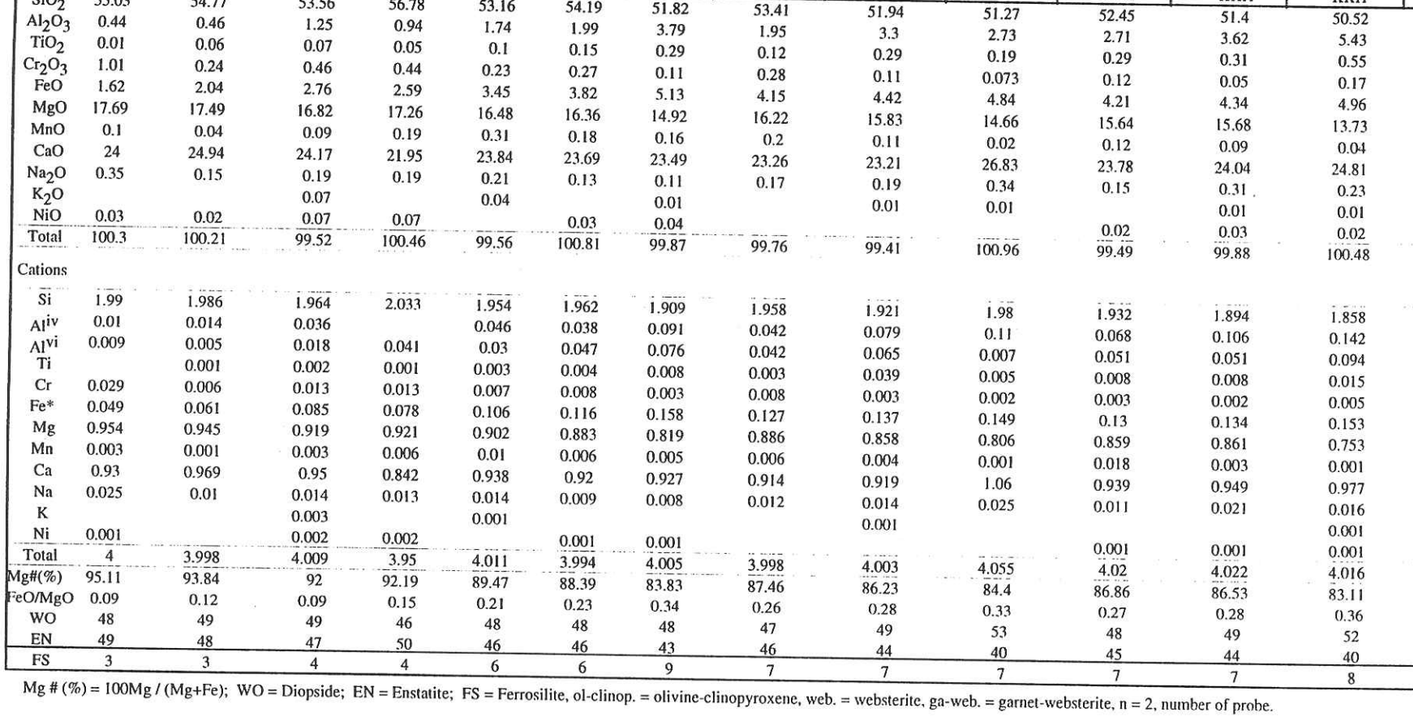

◆ Dunite ■ Ol-clinopyroxenite ▲ Websterite ▲ Ga-websterite ✱ Ga-gabbro

Figure 68. Trend of decreasing Cr2O3 in Jijal clinopyroxenes with differentiation (increasing FeO/MgO ratio).
Le Cr_2O_3 a tendance à décroître avec la différenciation dans le clinopyroxène du Jijal (croissance du rapport FeO/MgO).

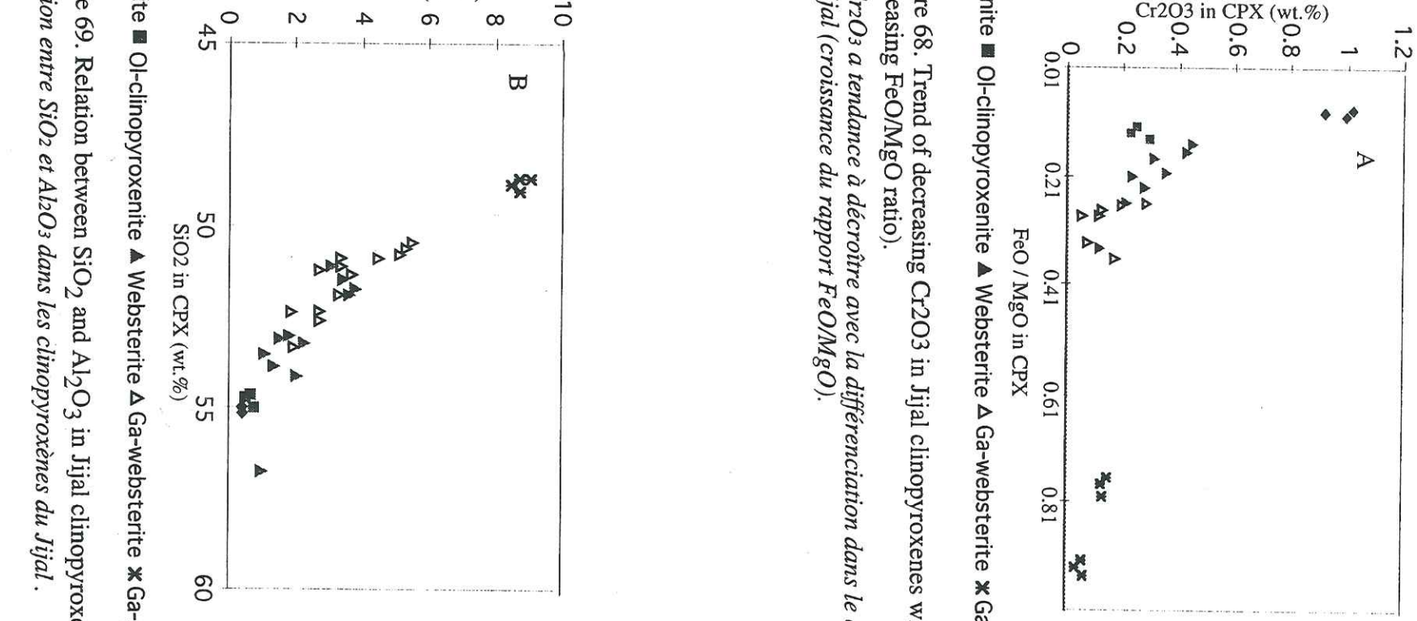

◆ Dunite ■ Ol-clinopyroxenite ▲ Websterite ▲ Ga-websterite ✱ Ga-gabbro

Figure 69. Relation between SiO_2 and Al_2O_3 in Jijal clinopyroxenes.
Relation entre SiO_2 et Al_2O_3 dans les clinopyroxènes du Jijal .

The Al-enrichment trend in clinopyroxene of Jijal Complex is marked by moderate enrichment to greatly increased, with Al_2O_3 contents reaching values from 0.44 wt % in dunite to as high as 9.03 wt % in garnet-gabbro. The trend of this enrichment is perpendicular to the trend observed in typical low-pressure igneous intrusions (Fig. 70; e.g., Skaergaard and Samail ophiolite). But this is parallel to the trend observed in Aleutian lower crustal xenoliths (Conrad and Kay, 1984; Debari et al., 1987) as well as the trend defined by Debari and Coleman (1989) for Tonsina ultramafic and mafic assemblages, Alaska and by Medaris (1972) for high-pressure peridotites from southwestern Oregon. Presnall et al. (1978) have shown that the primary phase volume of clinopyroxene expands with increasing pressure in the diopside-fosterite-anorthite system until, at > 7 kbar, plagioclase is no longer stable in the presence of olivine. Yoder and Tilley (1962) have also shown that at high pressure, the crystallization of plagioclase is suppressed. Thus all the available Ca and Al in the magma went into the pyroxene structure. Consequently all these factors account for increasingly Al-rich pyroxenes at high pressures in the Jijal rocks. Furthermore, a plot of tetrahedrally versus octahedrally Al in the Jijal pyroxenes, a discriminating factor for high-pressure crystallization (Green and Ringwood, 1967; Aoki and Kushiro, 1968), falls within the field defined for granulites and mantle inclusions in basaltic rocks (Fig. 71).

High Mg numbers in the clinopyroxene (Table 8) also support the hypothesis that the Jijal ultramafic rocks did not crystallize in a shallow magma chamber. In Figure 72A, the Mg numbers of olivines and clinopyroxenes from Jijal ultramafic-mafic rocks, from mantle peridotites, from oceanic gabbros and from 1-atm experimental results are shown. The field of mineral analyses from cumulate ultramafic rocks of Jijal area overlaps with the field of analyses from mantle peridotites and extends towards lower Mg numbers, where the oceanic gabbro data plot. Note that the 1-atm experimental data are characterized by comparatively low Mg numbers. The low Mg numbers is a consequence of the observation that many of the samples in this study have undergone variable amounts of subsolidus reequilibration, as evidenced by recrystallization textures and fabric resulting from high-temperature ductile deformation. It is also likely, nonetheless, that the Mg numbers of the mafic minerals in the ultramafic rocks have not been significantly changed by this reequilibration and that Fe-Mg cation exchange between these minerals will produce only minor changes in the mineral Mg numbers.

3.3.2.3 Orthopyroxene

Orthopyroxenes constitute about 5% of the olivine-clinopyroxenite and 10-20 % of the websterite and garnet-websterite. No orthopyroxene was found in thin-sections so far studied from dunites and garnet gabbro and is restricted to pyroxenite. Generally, the porphyroclastic grains are anhedral to subhedral and 2-6 mm in size.

Chemical compositions and structural formulae for representative orthopyroxenes from Jijal ultramafic rocks are presented in Table 9. Almost all analyzed grains in the same thin-

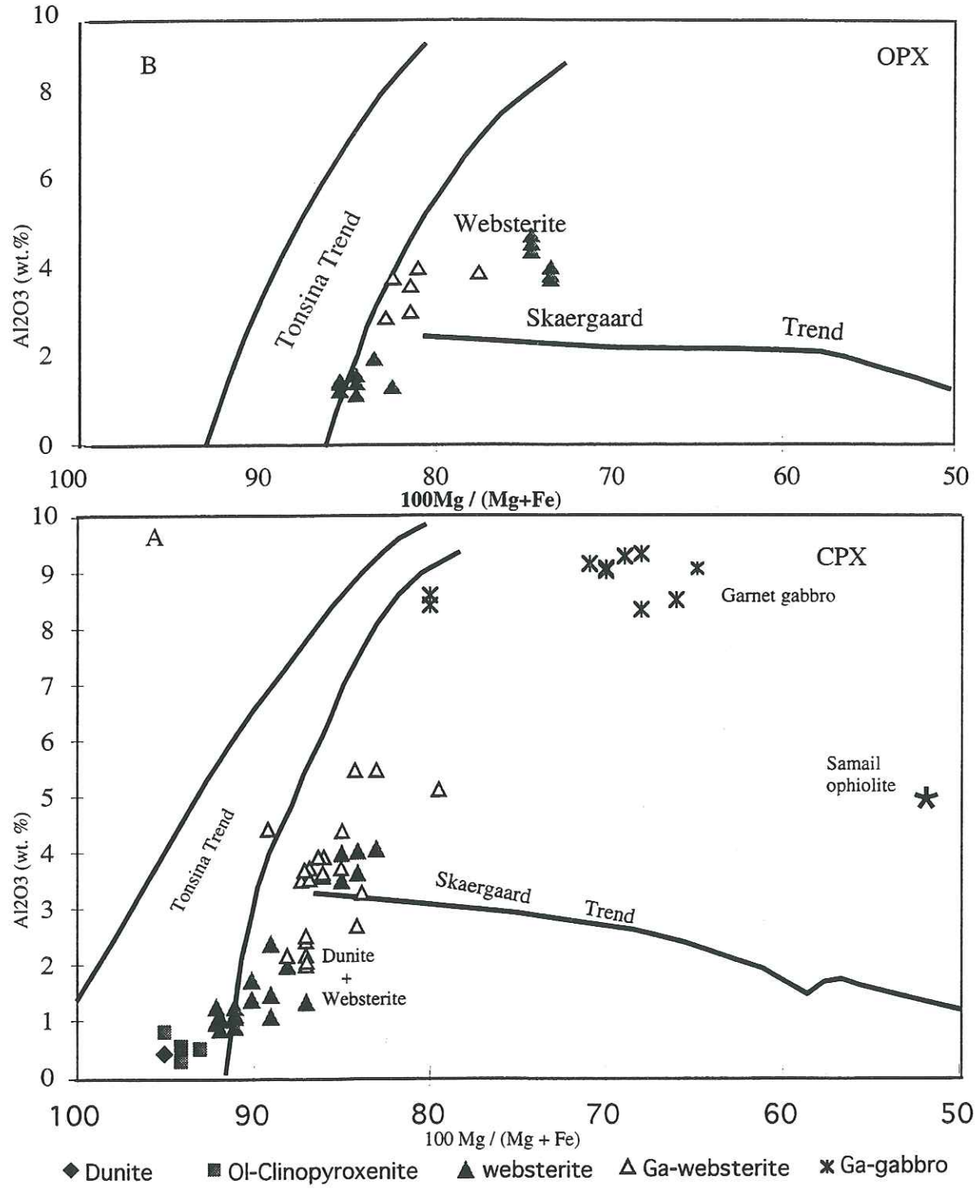

Figure 70 A& B. Plots of Al2O3 vs. 100Mg / (Mg+Fe) ratio showing trend in Al content of the Jijal clinopyroxene and orthopyroxene with fractional crystallization. Solid lines enclose a field for all assemblages from Tonisa cumulates. Note field for high-pressure Tonisa assemblages and proximity of Jijal complex (after Debari & Coleman, 1989). The low-pressure cumulates from Skaergaard and Samail ophiolite have opposite trend with differentiation.

Courbes de Al_2O_3 en fonction du rapport 100Mg/(Mg+Fe) montrant que la teneur en Al a tendance à décroître dans les clinopyroxènes (A) et les orthopyroxènes (B) du Jijal pendant la cristallisation fractionnée. La tendance est inverse dans les cumulats du Skaergaard et dans les ophiolites du Semail.

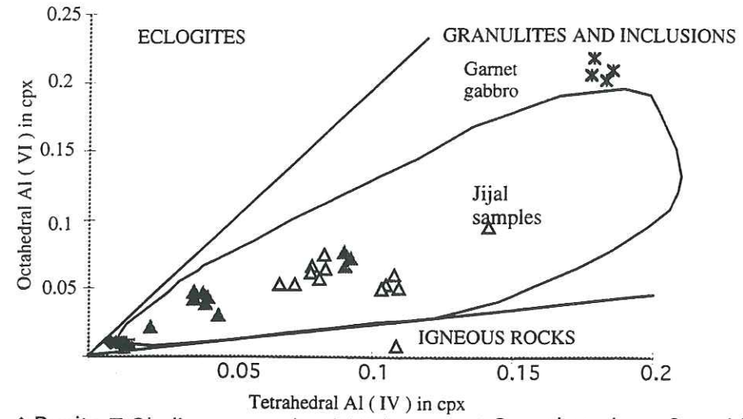

◆ Dunite ■ Ol-clinopyroxenite ▲ Websterite △ Ga-websterite ✱ Ga-gabbro

Figure 71. Plote of Al in octahedral vs. Al in tetrahedral coordination in clinopyroxene of Jijal complex. Outlined fields from Aoki and Kushiro (1968) are for eclogites, granulites and inclusions and ingneous rocks. The samples from Jijal complex occupy the compositional field for granulite indicating high-pressure of formation for these rocks.

Diagramme de l'Al en site octahèdrique fonction de l'Al en site tétraèdriquedans les clinopyroxènes du Complexe de Jijal. Les échantillons du Jijal occupent le champ des granulites.

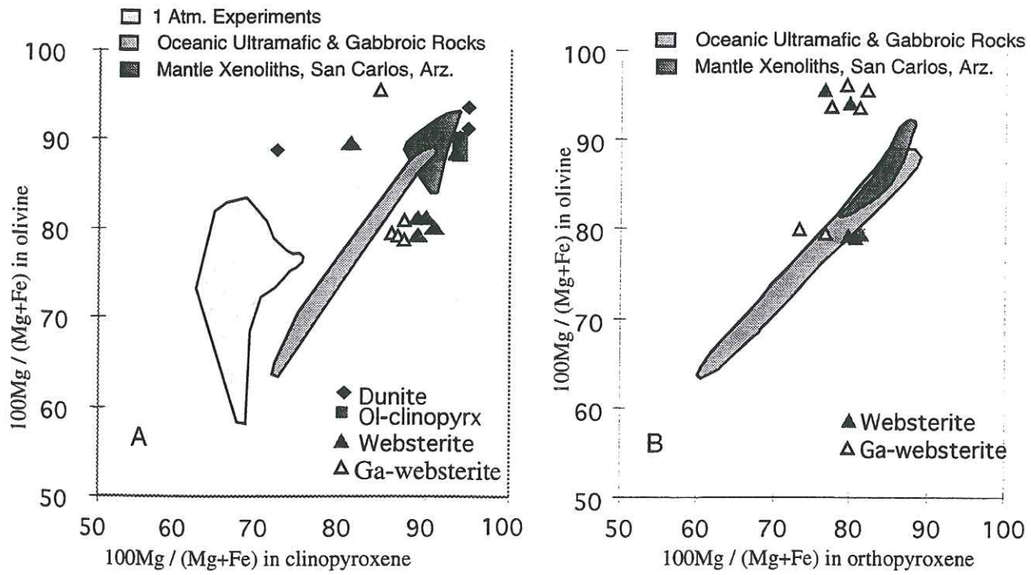

Fig. 72A&B. The Mg number (100 Mg / (Mg+Fe) of coexisting olivine vs. clinopyroxene and orthopyroxene of Jijal complex is plotted. The compositional fields for 1 atm. experiments; oceanic ultramafic and gabbro rocks (Tiezzi & Scott, 1980; Hodges & Papike, 1978); San Carlos mantle xenoliths (Frey & Prinz, 1978) are referred for comparison. Note field for high-pressure mantle xenoliths and proximity of Jijal samples.

Mg-number (100Mg / (Mg+Fe) de l'olivine fonction de celui du clinopyroxène et de l'orthopyroxène du Complexe de Jijal. Les xénolithes mantelliques de San Carlos sont reportés pour comparaison.

Table 9. Mineral chemistry of orthopyroxene from Jijal Complex.
Composition chimique des orthopyroxenes du Complexe de Jijal.

s.no.	KO-06	KO-28	JK-30	KO-22	KO-21A	JK-35B	JK-35A
rock-name	web.(U4)	web.(U4)	web.(U4)	web.(U4)	ga-web.(U5)	ga-web.(U5)	ga-web.(U5)
no of probe	2	2	2	1	1	1	1
locality	KKH	KKH	KKH	KKH	KKH	KKH	KKH
SiO2	56.24	57.29	55.23	52.88	54.05	54.09	55.46
Al2O3	1.4	1.33	1.83	4.13	3.41	4.04	3.86
TiO2	0.04	0.05	0.04	0.11	0.1	0.07	0.02
Cr2O3	0.33	0.33	0.07	0.12	0.08	0.05	0.04
FeO	9.9	9.85	12.09	16.51	12.27	14.27	11.47
MgO	31.45	31.17	29.45	28.85	29.21	26.29	29.4
MnO	0.2	0.37	0.34	0.4	0.29	0.23	0.31
CaO	0.46	0.34	0.28	0.44	0.2	0.32	2.25
Na2O	0.02			0.03			0.02
K2O	0.01					0.01	
NiO	0.03		0.01	0.01	0.06	0.02	0.01
Total	100.08	100.73	99.34	100.48	99.67	99.44	99.12
Cations							
Si	1.97	1.99	1.967	1.905	1.927	1.942	1.95
Aliv	0.03	0.01	0.033	0.095	0.077	0.058	0.05
Alvi	0.028	0.04	0.044	0.08	0.066	0.113	0.028
Ti	0.001	0.001	0.001	0.003	0.007	0,002	0.001
Cr	0.009	0.009	0.002	0.003	0.002	0.001	0.001
Fe*	0.29	0.361	0.36	0.497	0.365	0.428	0.337
Mg	1.642	1.614	1.564	1.388	1.549	1.406	1.548
Mn	0.006	0.011	0.01	0.012	0.009	0.007	0.009
Ca	0.017	0.012	0.011	0.017	0.007	0.012	0.085
Na	0.001			0.002			0.001
K							
Ni	0.001				0.002	0.001	
Total	3.995	4.048	3.992	3.984	4.011	3.97	4.01
Wo	1	1	1	1	0	0	0
En	84	81	80	73	81	76	82
Fs	15	18	19	26	19	24	18
#Mg	84.99	81.72	81.29	73.63	80.93	76.66	82.12

web. = websterite, ga-web. = garnet websterite, #Mg = 100Mg / (Mg+Fe), U1 = unit 1

Fe* = total iron

section are homogeneous. Analyses all sum to between 99.12 and 100.73 total oxide wt %, suggesting reasonable accuracies of determinations. Perhaps more importantly, based on six oxygens, cation sums range between 3.97 and 4.08 and average 4.001, in excellent agreement with the ideal value of 4.00. Because of the presence of significant amounts of Al in the analyses, some of which is formally assigned to four-fold coordinated sites, all contain the stoichiometric 2.00 tetrahedrally coordinated cations.

The data of Table 9 indicate that very small, eratic amounts of Na and K are present in the analyzed orthopyroxenes. Minor quantities of manganese are also present in all the analyzed samples. Based on six oxygens, the number of Mn atoms ranges from 0.006 to 0.012 but manganese does not display concentration contrasts as a function of occurrence. On pyroxene quadrilateral (Fig. 67), orthopyroxene are hypersthene in composition. The CaO content of the Jijal orthopyroxenes ranges from 0.2 wt % to 2.25 wt % and no pronounced zoning is visible in the orthopyroxene grains in the same thin-section.

The Fe-enrichment in orthopyroxenes with differentiation is extreme, with FeO contents reaching values as high as 16.51 wt.% and increases with decrease of MgO (Table 9). Further, Orthopyroxene in the websterite reaches highly Cr-rich compositions (Cr_2O_3 to 0.33 wt.%; Table 4), similar to the clinopyroxene in olivine clinopyroxenite and websterite (Table 8). Like clinopyroxene, orthopyroxene of Jijal cumulate ultramafic have higher Mg numbers ranging from 84.99 to 73.63. The orthopyroxene from websterite sample KO-22 has relatively smaller Mg number (e.g. 73.63), reflecting the lower mol. ratio Mg/ (Mg+Fe) compared to other cumulate ultramafics in Jijal area. The Mg numbers of the orthopyroxenes from Jijal ultramafics are also similar to those of Tonsina Ultramafic, Alaska (Fig. 70B) but the Cr contents are slightly lower than the ultramafics of Tonsina (e.g. Cr_2O_3= 0.58 wt.%, Table 5; Debari and Coleman, 1989). This is a consequence of the .observation that cocrystalizing olivines, clinopyroxenes and orthopyroxenes have approximately similar Mg numbers (e.g. Jan and Howie, 1981) and that Fe-Mg cation exchange between these minerals will produce only minor changes in the mineral Mg numbers (Fig. 72).

The Al_2O_3 content of the Jijal orthopyroxenes ranges from 1.4 wt % to 4.13 wt % and it increases with increasing Fe contents. The same trend of Al enrichment in clinopyroxenes is also observed in orthopyroxenes but Al_2O_3 contents in orthopyroxenes are slightly on higher side than in coexisting clinopyroxenes (Fig. 70B). Discussions on pressure and temperature dependence of solubility of Al_2O_3 in orthopyroxene have been made by many workers (Boyd and England, 1964; MacGregor, 1974; Onuma and Arima, 1975). Petrological data obtained in the present study indicate that the magma becomes rich in Al with high pressure, so that the pyroxenes crystallized from this liquid will be enriched in Al. Hence it is suggested that the Al_2O_3 content of the orthopyroxene is affected by pressure and temperature, rather than chemical composition of the magma from which the orthopyroxene crystallized out.

3.3.2.4 Spinel

Electron microprobe data for Cr spinels and Al spinels are listed in Table 10. Oxide totals closely approximate 100 wt %. Based on twenty four oxygens, cation totals range from 24.00 to 24.025 and average 24.013, in excellent agreement with the ideal value of stoichiometry.

Small amounts of silicon seem to be present in few of the samples. Based on twenty four oxygens, the average Si concentration is 0.004; although such values are included in the cation totals, it is not clear whether they represent Si occupancy of the tetrahedral structural site in spinel, or are a measure of the excitation of adjacent silicate grains by the electron beam during analysis.

The oxides CaO, Na_2O and K_2O appear to be absent or are present in negligible amounts. The Al_2O_3 content from Jijal spinels shows increasing chemical trends from dunites to pyroxenites (e.g. 7.79 wt % and 11.87 wt. %,(U2) in dunites and 63.11 wt % in pyroxenites). Spinels in the basal part of the Jijal ultramafic section is more Cr and Fe rich (Cr / (Cr+Al) 0.58 to 0.83; Table 10), those in the upper part of the section, pyroxenites are Al-rich (Cr / (Cr+Al) from 0.01 to 0.06; Table 10). On Fe^{+2} / ($Mg+Fe^{+2}$) vs Cr / (Cr+Al) such as the ones used by Debari et al. (1987), the Jijal spinels follow the same trend as spinels from cumulate xenoliths, Adak Island and Tonsina dunites and harzburgites and fall in the field of stratiform complexes (Fig. 73). Spinels in Aleutian lower crustal xenoliths record similar behaviour (Debari et al., 1987); increasing wt % Al_2O_3 and Fe^{+3} / Fe^{+2} ratio with differentiation. According to Dick and Bullen (1984), spinels with Cr number (Cr / (Cr+Al) greater than 0.6 are generally found in volcanics, stratiform complexes, zoned Alaskan complexes and oceanic plateau basalts. Spinels from lower portion of the Jijal ultramafic sequence have Cr number higher than 0.6 (Fig. 73; Table 10) and thus suggest that the complex is associated with the arc environment. Green spinels from the upper ultramafic sequence are characteristically rich in Al and Mg (Table 10), indicate that the upper section of the ultramafic sequence (garnet websterite and garnet clinopyroxenite) were crystallized out at the latter stage of fractional crystallization and at relatively elevated pressure.

As already discussed in clinopyroxene composition, crystallization of plagioclase is suppressed with increasing pressure and with further lack of crystallization of Al-phases causes enrichment of Al in the fractionating magma. The spinel crystallizing from this fractionating magma will document higher Al values by decreasing the Cr / Al ratio (Sigurdsson and Schilling, 1976; Sigurdsson, 1977). This is exactly what happened at Jijal spinels and also at

Tonsina and in Aleutian xenoliths. So pressure can play an indirect role on Al content of spinel (Debari and Coleman, 1989).

Jan and Howie (1981) presented analyses of two spinels from the basal part of Jijal ultramafic along KKH and one spinel from harzburgite in the upper of the cumulate ultramafic

Table 10. Mineral chemistry data for spinel in Jijal Complex.
Composition chimique des spinelles du Complexe de Jijal

s. no.	JD-02	KO-02	KO-06	KO-26	KO-35	KO-22	KO-21A	JR-31B	JR-31A
rock name	dunite(U1)	ol-clinop. (U1)	web.(U4)	dunite(U2)	dunite(U4)	web.(U4)	ga-web.(U5)	ga-web.(U5)	ga-web.(U5)
no. of probe	2	2	2	3	3	2	2	2	1
locality	Duber	KKH	KKH	KKH	Duber	KKH	KKH	KKH	KKH
SiO2	0.03		0.02		0.05			0.02	0.01
Al2O3	17.38	9.6	17.68	7.79	11.87	58.08	63.11	59.17	54.02
TiO2	0.42	0.58	0.75	0.15	0.28	0.07	0.03	0.05	0.12
Cr2O3	44.08	43.36	36.13	55.46	52.78	2.09	0.72	3.24	5.43
FeO*	22.32	29.29	25.41	21.22	28.85	28.68	18.64	19.57	21.48
Fe2O3	7.52	14.34	11.94	7.41		2.73	2.6	3.69	4.56
MgO	8.14	2.43	5.95	7.61	6.67	8.19	15.28	14.15	11.5
MnO	0.39	1.12	0.24	0.53	0.51		0.17	0.19	0.7
CaO	0.04		0.26	0.01	0.01	0.12	0.05	0.03	0.04
Na2O			0.01		0.01				0.04
K2O	0.02	0.01		0.02			0.05		0.09
NiO	0.32	0.01	0.1		0.04	0.08	0.21	0.16	0.18
Total	100.66	100.74	98.49	100.21	101.07	100.04	100.85	100.27	98.37
Cations									
Si	0.007		0.005		0.01			0.004	0.001
Aliv	5.301	3.16	5.584	2.497	2.957	15.134	15.44	14.824	14.202
Alvi									
Ti	0.081	0.122	0.15	0.031	0.044	0.012	0.005	0.008	0.02
Cr	9.024	9.577	7.652	11.92	8.839	0.366	0.118	0.546	0.958
Fe*	4.832	6.843	5.694	4.825	5.101	5.304	3.235	3.48	4.046
Fe+3	1.466	3.015	2.407	1.516		0.454	0.406	0.591	0.765
Mg	3.14	1.013	2.374	3.082	2.102	2.698	4.726	4.483	3.825
Mn	0.085	0.264	0.054	0.122	0.092		0.029	0.034	0.132
Ca	0.011		0.075	0.004	0.002	0.027	0.012	0.007	0.01
Na	0.001		0.01		0.004				0.019
K	0.004	0.004		0.004			0.012		0.025
Ni	0.067	0.003	0.021		0.008	0.014	0.035	0.028	0.033
Total	24.019	24	24.03	24.001	19.159	24	24.018	24.005	24.036
#Mg	0.39	0.13	0.29	0.39	0.29	0.34	0.59	0.56	0.49
#Cr	0.63	0.75	0.58	0.83	0.75	0.02	0.01	0.04	0.06
#Fe *	0.61	0.87	0.71	0.61		0.66	0.41	0.44	0.51
#Fe+3	0.09	0.19	0.15	0.1		0.03	0.03	0.04	0.05

#Mg = Mg / (Mg+Fe) #Cr = (Cr+Al) #Fe^{+2} = Fe* / (Fe*+Mg) #Fe^{+3} = (Cr+Al+Fe^{+3})
ol-clinop. = olivine clinopyroxenite web. = websterite ga-web. = garnet websterite

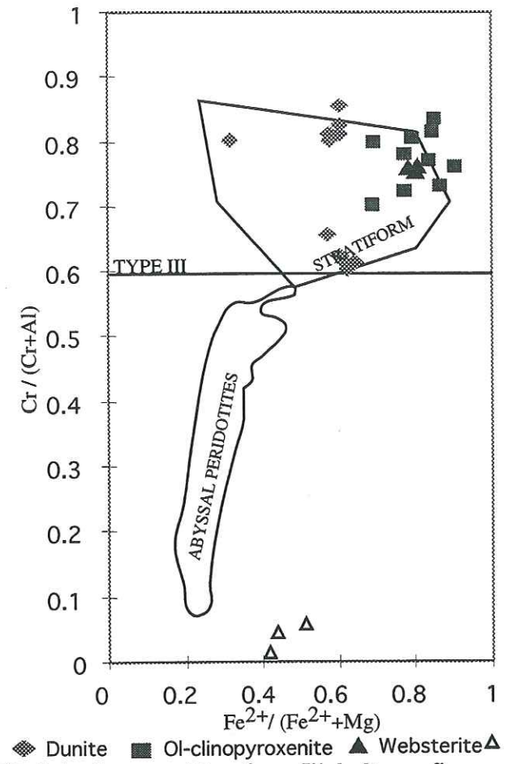

Figure 73. Spinel composition from Jijal ultramafic cumulate rocks. Also plotted are Type III spinel field, including spinels of arc, oceanic, plateaus, stratiform complexes, from Dick & Bullen (1984). Stratiform field from Irvine (1967). Abyssal peridotite field from Dick & Bullen (1984).
Composition des spinelles des cumulats ultramafiques-mafiques du Jijal. Le champ des spinelles de type III est représenté, incluant les spinelles d'arc, de plateau océanique, de complexe stratiforme.

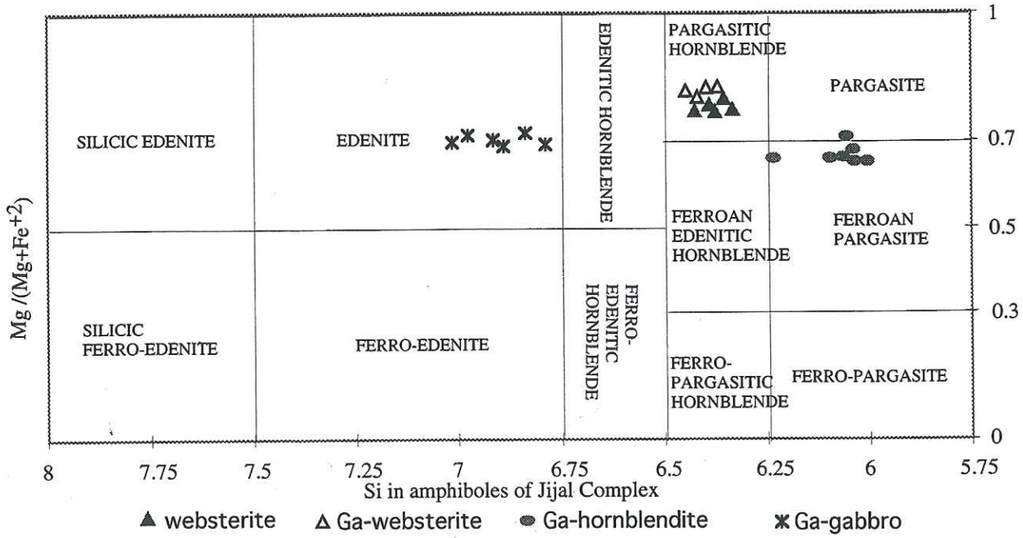

Figure 74 . Si vs Mg /(Mg+Fe+2) plots of amphiboles in Jijal Complex.
Courbes du Si en fonction de Mg /(Mg+Fe+2) des amphiboles dans le Complexe de Jijal

in Duber River. The spinel from KKH exhibit no Cr and less extreme Fe and more Al (e.g. 63.19 wt %) as compared to our new data in Table 10.

3.3.2.5 Garnet

Chemical analyses of representative garnets from garnet-websterite, garnet-hornblendite and garnet-gabbro along with their formulae are presented in the Table 11.

Based on twenty four oxygens, cation totals range from 15.959 to 16.121 with the average value 16.02, in good agreement with the ideal value. More remarkable is the relatively high chromium content in garnet-pyoxenites, which ranges from 0.027 to 0.594 based on 24 oxygens as compared with garnet-gabbros, where it ranges from 0.001 to 0.011. The high chromium value of garnets in garnet-pyroxenites is rather influenced by their host rocks. The sum of $Al^{vi} + Ti + Cr + Fe^{+3}$ ranges from 3.86 to 4.00, close to the ideal value of 4.00 based on twenty four ogygens. Likewise, the sum of Fe + Mg + Mn + Ca + (Na+K) ranges from 6.00 to 6.04, close to the ideal value of 6.00. As seen from the Table 11, the concentrations of the major elements are quite uniform. The garnets are composed essentially of the components almandine (43.24 to 37.03), pyrope (33.34 to 22.21), grossular (34.15 to 19.33) and andradite (2.55 to 1.45). Samples JK-32 and 35B from garnet-websterite have almandine 16 and 39 and pyrope 69 and 40 respectively. The chemical composition across a garnet porphyroblast in garnet-gabbro (KO-15) is from core Alm_{43} Pyp_{33} Grs_{19} Adt_3 Sps_1 to rim Alm_{42} Pyp_{33} Grs_{22} Adt_3 Sps_1 and in garnet-hornblendite (KO-13) is from core Alm_{39} Pyp_{24} Grs_{32} Adt_2 Sps_2 to rim Alm_{39} Pyp_{22} Grs_{34} Adt_2 Sps_2. The grossular content increase by 2 mol %. But in garnet-hornblendite the pyrope component increases by 2 mol % and grossular content remains constant. This slight increase in grossular content towards the rim indicates either a pressure increase, or cooling for the assemblage garnet-clinopyroxene-plagioclase-quartz (Newton and Perkins, 1982). The accommodation of grossular relative to almandine in Fe^{+2}-Mg garnets is also suggested due to increase in pressure in garnets of glaucophane schists, eclogites (Coleman et al., 1965; Dobretsov et al., 1972), granulites (Jan and Howie, 1981) and by experimental work (Green and Ringwood, 1967; Akella and Kennedy, 1971; Hensen, 1976).

3.3.2.6 Amphibole

The chemical compositions and structural formulae from amphiboles are given in the Table 12. The amphibole from olivine-pyroxenite (KO-21A) is pargasitic hornblende and from garnet-hornblendite and garnet-gabbro is ferroan-pargasite and edenite respectively (Leake, 1978; Table 12; Fig.74).

The amphibole in the garnet websterite (KO-21A) has relatively low TiO_2 , but is notable for its higher Cr contents, 0.15 wt % Cr_2O_3 (Table 12). Because the amphibole in this assemblage is in reaction with clinopyroxene, breakdown of clinopyroxene is one possible

Table 11. Mineral chemistry data for garnet in Jijal Complex.
Composition chimique des grenats du Complexe de Jijal

s. no.	JK-32	JK-35B	JR-31A	KO-15		KO-09	KO-13	
rock name	ga-websterite	ga-websterite	ga-websterite	ga-gabbro		ga-gabbro	ga-hornblendite	
no of probe	2	3	4	3		2	2	
				core	rim		core	rim
locality	KKH	KKH	KKH	KKH		KKH	KKH	
SiO_2	40.5	41.2	39.71	39.93	40.16	39.65	40.01	40.17
Al_2O_3	19.49	20.81	22.06	21.96	22.17	22.25	22.16	22.95
TiO_2	0.12	0.87	0.05	0.1	0.19	0.03	0.19	0.17
Cr2O3	5.16	0.23	0.23	0.09	0.05	0.01	0.06	0.03
FeO*	7.58	18.22	17.71	20.6	20.22	18.93	18.84	18.45
Fe_2O_3			0.48	0.84	0.44	0.42	0.69	0.17
MgO	20.08	11.56	8	8.94	8.66	9.08	6.46	5.87
MnO	0.6	0.79	0.77	0.55	0.55	0.45	1.01	0.96
CaO	5.63	7.87	11.78	8.28	8.8	9.48	13.18	13.51
Na_2O	0.07	0.01		0.02	0.02	0.03	0.03	
K2O		0.01		0.02	0.03		0.05	0.01
NiO	0.07			0.13		0.11		
Total	99.22	101.57	100.79	101.47	101.22	100.43	102.68	101.83
Cations								
Si	5.905	6.136	5.981	5.991	6.021	5.978	5.973	6.036
Al^{iv}	0.095		0.019	0.009		0.022	0.027	
Al^{vi}	3.254	3.651	3.897	3.875	3.918	3.931	3.873	3.887
Ti	0.013	0.011	0.006	0.012	0.021	0.003	0.021	0.019
Cr	0.594	0.027	0.027	0.011	0.005	0.001	0.007	0.004
Fe*	0.925	2.27	2.231	2.586	2.535	2.387	2.352	2.319
Fe^{+3}	0		0.055	0.095	0.05	0.048	0.078	0.08
Mg	4.362	2.567	1.797	2	1.936	2.041	1.437	1.315
Mn	0.074	0.1	0.098	0.07	0.064	0.057	0.128	0.122
Ca	0.879	1.256	1.901	1.331	1.413	1.531	2.108	2.176
Na	0.02	0.002		0.006	0.007	0.008	0.01	
K	0	0.001		0.003	0.005		0.01	0.001
Ni	0			0.016		0.013		
Total	16.121	16.021	16.012	16.005	15.975	16.02	16.024	15.959
Alm	16	39	37.03	43.24	42.71	39.69	39.12	39.17
Pyrp	69	40	29.84	33.44	32.61	33.93	23.9	22.21
Spl	1	2	1.63	1.18	1.08	0.96	2.13	2.07
Grs	14	19	29.38	19.33	21.88	24.15	32.43	34.15
And	1		1.45	2.55	2.55	1.24	2.26	2.3
Uvt			0.68	0.27	0.27	0.04	0.16	0.1

Alm = almandine Pyrp = pyrope Spt = spessartine Grs = grossular, ga-websterite = garnet websterite,
And = andradite Uvt = uvarovite.

Table 12 . Mineral chemistry data for amphibole in Jijal Complex.
Composition chimique des amphiboles du Complexe de Jijal

sample no	KO-22	KO-21A	KO-13	KO-09
rock name	websterite	ga-websterite	ga-hornblendite	ga-gabbro
locality	KKH	KKH	KKH	KKH
SiO_2	44.06	44.7	41.26	47.47
Al_2O_3	15.65	13.44	16.16	9.32
TiO_2	0.6	0.56	0.89	0.8
Cr_2O_3	0.34	0.15	0.06	0.04
FeO	7.95	6.44	11.74	7.92
MgO	14.58	17.14	12.47	10.18
MnO	0.16	0.17	0.02	
CaO	0.6	12.11	11.99	20.43
Na_2O	1.9	2.42	3.01	1.73
K_2O		0.18	0.35	0.04
NiO	0.05	0.02	0.06	0.03
OH	2.09	2.09	2.05	2.06
Total	99.17	99.42	100.06	100.02
Cations				
Si	6.328	6.397	6.047	6.908
Al^{iv}	1.672	1.603	1.953	1.092
Al^{vi}	0.977	0.665	0.839	0.505
Ti	0.065	0.061	0.098	0.087
Cr	0.038	0.017	0.006	0.004
Fe*	0.955	0.771	1.439	0.964
Mg	3.122	3.657	2.724	2.207
Mn	0.019	0.02	0.003	
Ca	1.816	1.857	1.883	3.184
Na	0.529	0.672	0.855	0.488
K		0.032	0.065	0.008
Ni	0.006	0.002	0.006	0.003
OH	1	1	1	1
Total	16.527	16.752	16.922	16.45
Mg#	0.77	0.83	0.71	0.7

Mg# = Mg / (Mg+Fe)

source for Cr in the amphibole. Hence, it is suggested that the Cr-rich amphibole in assemblage KO-21A must have crystallized as a near-liquidous phase, following clinopyroxene, before substantial clinopyroxene fractionation could deplete the melt in Cr. Cr-rich pargasite is also reported in ultramafic xenoliths from at least three other localities: (a) in a cumulate Mt. Moffett xenoliths from adak island, Aleutian arc (Conrad and Kay, 1984), (b) in a cumulate assemblage of Grenada xenolith (Arculus, 1978), and (c) in lherzolite and websterite xenoliths of upper mantle origin from Itinoma-gata, Japan (Aoki and Kanisawa, 1979).

Amphibole in the garnet-hornblendite and garnet-gabbro assemblages contains higher TiO_2 (0.89 wt % & 0.8 respectively), FeO (KO-09; 7.92 wt %) and lower Cr_2O_3 contents (0.06 & 0.04 wt % respectively) than cumulus amphibole in garnet websterite (Table 12). However, components of Na_2O and K_2O are approximately similar in amphiboles in all these rocks. Amphibole in the garnet-gabbro appears to be a separate crystallizing phase and the grains occur mainly as intercumulus material, representing the late-stage crystallization of the residual liquid. Mg numbers in these amphiboles are generally equivalent to coexisting clinopyroxenes (Table 8) in garnet websterite and garnet gabbro, suggesting that amphibole crystallization is correlative with both the Mg and H_2O evolution of parent magma which is in contrast to the origin suggested by Jan and Howie (1981) that these amphiboles are of primary metamorphic origin and formed under elevated P_{H2O} , the necessary water being provided internally during the formation of granulite.

In the Jijal pyroxenites, pargasite generally occurs as minor replacement rims on clinopyroxene. Experimental results of Jenkins (1983) indicate that pargasite is stable at greater temperatures than other amphiboles and its maximum temperature stability occurs at 1050°C between 8 and 16 kbar (Jenkins, 1983).

3.3.3 DISCUSSION: IMPLICATION OF MINERAL CHEMISTRY ON MAGMATIC EVOLUTION

3.3.3.1 Pressure-Temperature Conditions

Samples were collected from different lithological units of Jijal ultramafic and mafic units for probing the different mineral assemblages and to find the temperature and pressure of their crystallization. In this section, new data on temperature and pressure of Jijal Complex are presented. According to the stable mineral assemblages observed in the different units, different thermobarometers are used to constrain the P-T evolution of the Jijal Complex. Pressure and temperature uncertainties, quoted at 2σ, take into account only the microprobe uncertainties.

In the dunitic rocks (sample KO-26), the olivine-spinel thermometer of Li et al. (1995) gives a good temperature estimate of 840 ± 60°C. The co-stability of the orthopyroxene and the clinopyroxene in the websterite KO-22 and KO-6 and in the garnet websterite K0-21, allow the temperature to be estimated at 880 ± 90°C and 935 ± 60°C respectively with the calibrations of Wells (1977), Wood and Banno (1973) and Bertrand and Mercier (1985). Moreover, temperature of equilibrium between coexisting garnet and orthopyroxene in the garnet websterite JK-35b is estimated at 880 ± 80°C and 8 ± 2 kbar with the calibration of Harley (1984a & b) and 11 ± 3 kbar with the barometer of Nickel and Green (1985). In the garnet clinopyroxenite (JR-31A), the temperature is evaluated at 770 ± 40°C by the Ellis and Green (1979) thermometer whereas the garnet-amphibole thermometer of Graham and Powell (1984) on the sample KO-13 gives a higher temperature of 850 ± 60°C. Finally, the P-T conditions in the garnet gabbro (KO-9 and KO-15) is evaluated at 13 ± 2 kbar and 930 ± 100°C by the Newton and Perkins barometer and Ellis and Green (1979) thermometer respectively. The garnet-amphibole thermometer allows the high temperature retrogression to be evaluated at 780 ± 50°C.

By the occurrence of garnet in the upper part of the Jijal Complex, Jan and Howie, (1981) and Yamamoto (1993) suggested that it suffered higher metamorphic conditions (12-17 kbar - 700-950°C) than the Lower Jijal Complex and are magmatically unrelated. According to our P-T estimations and uncertainties we show that the P-T data partly overlap from the base to the top. This suggests that the complete Jijal Complex recorded a similar final P-T evolution of about 860 ± 90°C and 11 ± 3 kbar. The occurrence of garnet in the upper part of the Jijal Complex does not necessarily imply a pressure increase as suggested by Yamamoto (1993) but more probably a cooling as suggested by the occurrence of exsolution of garnet and orthopyroxene from clinopyroxene (in the garnet websterite (sample JR-31A). Irvine (1974) and Morten and Obata (1983) reached a similar conclusion that these changes could take place in an initial high-temperature pyroxene(s)-spinel(-olivine) assemblages (e.g. 1050-1100°C; 13-17Kbar) as it cooled approximately isobarically during its ascension to enter the clinopyroxene+garnet+spinel. Lovering and White (1969) also reached a similar conclusion from consideration of Kushiro and Yoder's (1966) experimentally determined phase relationships in the system CaO-MgO-Al_2O_3-SiO_2. Moreover, the presence of spinel along with garnet and absence of plagioclase in the rocks of Jijal Complex constrains the pressure of origin to within the spinel lherzolite facies (e.g. within the pressure interval of 10 to 25 kbar; Kushiro & Yoder, 1965; Presnall et al., 1978, 1979; Elthon & Scarfe, 1982). The deduced range of pressures suggests an origin in the uppermost part of the Earth's mantle at depths of approximately 40 ± 10 km. This is in excellent agreement with the work of Jan and Howie (1981) and Miller and Christensen (1994) who have generated the synthetic seismic profile of the rocks of Kohistan sequence and placed the base of the lowermost intrusions (Jijal ultramafic cumulates) crystallized at a depth of about 45 km.

Display of sectoral plastic strain, kink bands, neoblastic-recrystallized olivine in olivine and similar features in clinopyroxene indicate high temperature mantle deformation shortly after their crystallization. This suggests that these rocks were formed in an extremely dynamic environment. AvéLallemant and Carter (1970) determined through their experimental study that polygonal olivines were produced near the grain boundaries of the host grains at 1100°C and 13 kbar. Deformation and recrystallization of olivine and pyroxene may be related to the earliest movement when suturing of Kohistan arc occurred with the Asian plate. Petterson & Windley (1985) have dated this collision between Kohistan and Asia between 102 and 85 Ma. This shows that the crystallization of Jijal Complex is predated or is coeval with the Kohistan-Asia collision (e.g. Yamamoto, 1993).

3.3.3.2 The magmatic evolution

Several oceanic and ophiolitic basalts have been experimentally studied and their phase relationships have been determined (e.g. Bender et al., 1978; Green et al., 1979; Walker et al., 1979; Dungan et al., 1978; Fisk et al., 1980; Elthon, 1981). Their experimental results indicate that in oceanic setting, plagioclase starts crystallizing early, directly after olivine and spinel (e.g. Basaltic Volcanism Study Project 1981), clinopyroxene crystallizes after plagioclase while ultramafic cumulate sequence is relatively thin (Bonatti and Hamlyn, 1981). The Jijal ultramafic-mafic rocks have important characteristics which distinguish them from the rocks crystallizing in the oceanic settings; like virtual absence of plagioclase in these ultramafic rocks that contain both clinopyroxene and orthopyroxene, early crystallization of clinopyroxene than plagioclase, absence or near absence of olivine and orthopyroxene in the late mafic rocks, thick ultramafic unit and spinels with Cr-number (Cr/(Cr+Al) greater than 0.6. All these characteristics of the rocks in the Jijal Complex presents a striking case for island-arc and not oceanic origin.

The compositional variation observed in the Jijal ultramafic sequence is in accordance with the lithological change in the sequence. The characteristics of chemical composition of the olivine and pyroxene indicate that their Mg numbers decrease from dunite to olivine clinopyroxenite to websterite to garnet websterite (Fig. 75). The maximum Fo content of olivine is found in the dunitic layers, and decrease upward into the garnet websterite zone. Similarly, the enstatite content of clinopyroxene is consistent with the Fo content of the coexisting olivine as well as with the Mg number of orthopyroxene (Fig. 75). This is an important feature that Fe content of these minerals gradually increases from bottom to the top of the section.

The Cr content of the spinel tends to decrease from base to top. The Cr-rich spinel is present in the dunite (Cr-number=0.75), olivine clinopyroxene (Cr-number=0.75) and websterite (Cr-number=0.58) while Al-rich spinel occurs in the upper level, garnet websterite

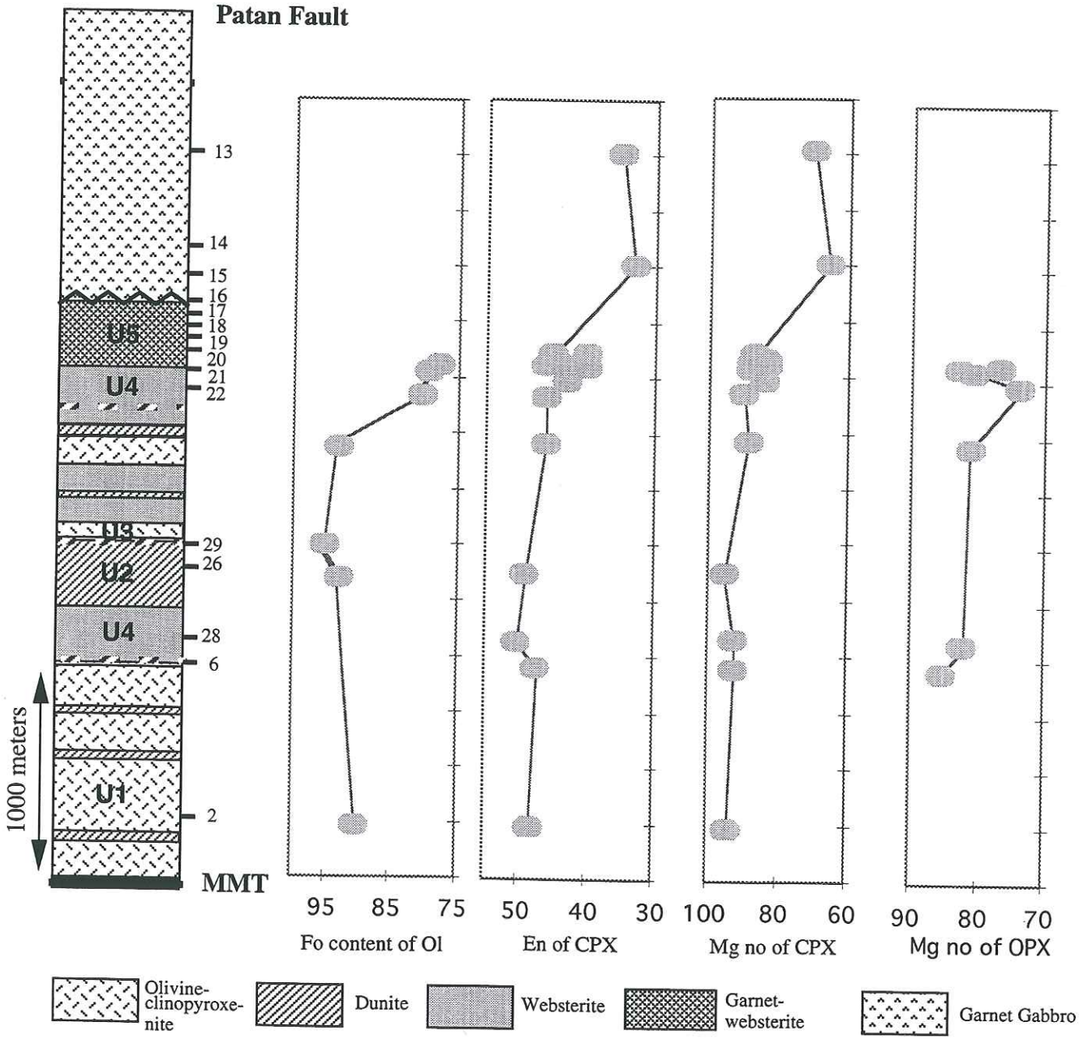

Figure 75. Compositional variation in Fo content of olivine, En content and Mg no. of clinopyroxene, and Mg no. of orthopyroxene in the columnar section along the KKH section of Jijal Complex.

Variations de la composition en Fo de l'olivine, en En et $Mg^{\#}$ du clinopyroxène, et en $Mg^{\#}$ de l'orthopyroxène dans la colonne composite établie le long de la KKH à travers le Complexe de Jijal

(Cr-number=0.06-0.01). Most Al-rich clinopyroxene is present in the upper garnet websterite and garnet gabbro.

The texture of dunite shows that Cr-spinel and olivine crystallized at the early stage of crystallization. The Mg content of olivine (Fo 94) gradually decrease with successive crystallization, and iron-rich olivine (Fo 78) crystallized at the final stage. The clinopyroxene also crystallized at the early stage. The clinopyroxene crystallized at the early stage, is rich in Mg (Mg#=94). The orthopyroxene probably crystallized slightly later with Mg number 85 in the earlier stage of crystallization and gradually decreasing to Mg number 77 in the latter stage. The mineralogy shows wide systematic ranges in chemical compositions and as might be expected, fractional crystallization produces diverse lithologies and wide variations in chemical composition of silicate minerals (Fig. 76). Absence of primary hydrous minerals, such as hornblende, in early crystallizing units indicates that the activity of H_2O was low during this upper mantle or lower crust stage of crystallization. Later, fractional evolution of primary magma shows enrichment of water and is evidenced by incease in amphibole content with differentiation. So the genesis of the Jijal Complex can be explained by a successive fractional crystallization of a basaltic melt that produced a series of rocks from dunite to garnet gabbro.

From the facts mentioned above it is considered that the main order of crystallization for the Jijal Complex resulted in the following sequence:

ol + (Cr, Al) sp	dunite
ol + cpx + opx + (Cr, Al) sp	olivine clinopyroxenite
ol + cpx + opx + (Cr, Al) sp	websterite
ol+(Mg,Al)sp+cpx+opx+grt+amp	garnet websterite
cpx+grt+amp+plg	garnet gabbro

It is anticipated, in the light of above discussion, that the types of cumulate rocks formed in Jijal Complex were not crystallized at temperatures and pressures typical of a shallow igneous intrusions. The cumulate rocks formed by the low-pressure crystallization of basaltic magma would be dominated by dunites, troctolites and olivine gabbros (e.g. Bender et al., 1978; Green et al., 1979; Walker et al., 1979; Elthon, 1981). So the petrologically significant features that need to be addressed for the origin of these cumulate ultramafic rocks from Jijal Complex are the absence of plagioclase and the high Mg numbers of the mafic phases. Presnall et al. (1978) experimental data in the diopside-fosterite-anorthite system shows that with increase of pressure clinopyroxene is more abundant and at >7 kbar, plagioclase is no longer stable in the presence of olivine (Fig. 77). Similarly, in the CaO-MgO-Al_2O_3-SiO_2 system, the primary phase volume of clinopyroxene expands with increasing pressure and continues up to 9.3 kbar and at greater pressure, plagioclase is no longer stable in the presence of olivine

	Dunite (U1)	Ol-clinop. (U1)	Websterite (U4)	Dunite (U2)	Websterite (U4)	Ga-websterite (U5)	Ga-gabbro	Ga-hornblendite
Olivine	Fo 92	Fo 92		Fo 94	Fo 93-80	Fo 78		
Clinopyro-xene		Mg# 94	Mg# 92	Mg# 95	Mg# 89-83	Mg# 87-83	Mg# 70-65	
Orthopyro-xene			Mg# 84		Mg# 81-73	Mg# 82-76		
Cr-spinel	Cr# 63	Cr# 75	Cr# 58	Cr# 83	Cr# 75			
Al-spinel						Cr# 6-4		
Garnet						$Alm_{16-37}Pyr_{69-29}Grs_{14-29}$	$Alm_{40-43}Pyr_{33}Grs_{24-21}$	$Alm_{39}Pyr_{22}Grs_{33}$
Amphibole					Ti=0.6 wt%	Ti=0.56 wt%	Ti=0.8 wt%	Ti=0.89 wt%

Figure 76. Compositional variation in mineral chemistry with crystallization sequence in the Jijal Complex along the KKH section. *(Variation de la composition chimique minérale selon la suite de cristallisation dans le Complexe de Jijal le long de la coupe de la KKH)*

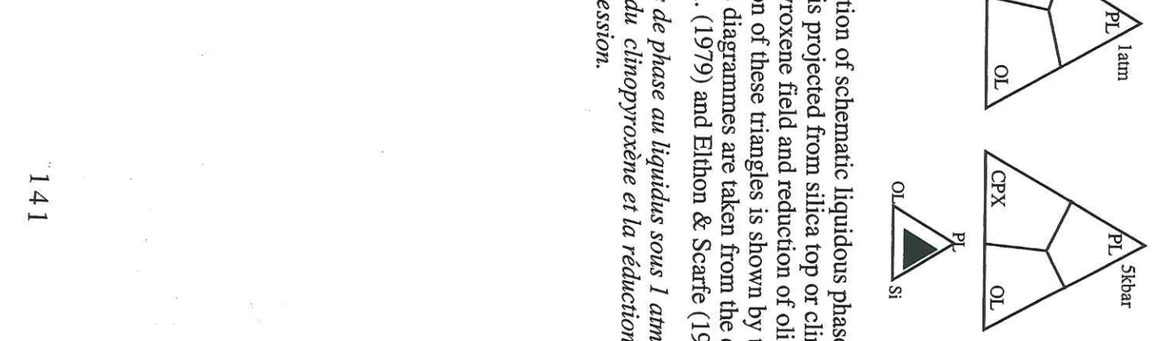

Figure. 77. Composition of schematic liquidous phase boundaries at1 atmosphere, 5 kbar and 10 kbar. It is projected from silica top or clinopyroxene bottom. Note expansion of clinopyroxene field and reduction of olivine field with increasing pressure. The location of these triangles is shown by the inset in olivine-plagioclase-silica triangle. These diagrammes are taken from the experimental data of Walker et al. (1979), Presnall et al. (1979) and Elthon & Scarfe (1982).

Evolution des limites de phase au liquidus sous 1 atmosphère, 5 kbar et 10 kbar. Noter l'inflation du champ du clinopyroxène et la réduction du champ de l'olivine avec l'augmentation de pression.

(Presnall et al., 1979). With increasing pressure, primary phase field of olivine is reduced prior to clinopyroxene crystallization and, consequently, the Mg numbers of cocrystallizing olivine and clinopyroxene are higher (Walker et al., 1979; Presnall et al., 1979; Elthon and Scarfe, 1982). Therefore, the absence of plagioclase and presence of highly magnesian olivine and pyroxene (Mg number = 85-92) suggest high-pressure (approximately 10 kbar) crystallization of basaltic melts (e.g; Green and Ringwood, 1967; Elthon et al., 1982) and this is schematically shown in Figure 77. In the ultramafic cumulate rocks of Jijal Complex, the Mg numbers of olivine and pyroxene range from 80-94, but most of the values are above 85, in agreement with Elthon et al. (1982) predicted values. It is also important to note that pyroxene is unzoned and shows consistent diopsidic composition in the Jijal Complex. This feature is unlikely at shallow level typical of oceanic crust or convergence zones but such environment would be quite likely at the base of an island arc where these rocks cooled very slowly and latter re-equilibrated under subsolidus conditions.

Similarly, preferential partitioning of Al into octahedral versus tetrahedral sites in clinopyroxene is an indication of moderate to high pressure (Green & Ringwood, 1967; Aoki & Kushiro, 1968). The clinopyroxene in Jijal Complex displays $Al^{(vi)}$ / $Al^{(iv)}$ values of 0.36 to 1.24. Aoki and Kushiro (1968) have described that $Al^{(vi)}$ / $Al^{(iv)}$ values greater than roughly 0.25 were generally present in granulites and in mantle inclusions in basaltic rocks. They concluded that the higher ratios were probably due to greater pressure and possibly lower temperature reequilibration than is common in shallow crustal igneous rocks. Thus mineral chemistry as well as phase relationships in the Jijal ultramafic cumulates suggest that these rocks were crystallized at high pressures and temperatures near the crust-mantle boundary.

3-4 Geochemistry

3-4.1 Sample selection and analytical procedure

Selection of samples for the whole rock geochemistry of Jijal Complex were made on the basis of field and petrography study to select unaltered samples, as well as lithological coverage of this complex. The procedure of analyses for major, trace and REE have already been described under 'Sample selection and analytical procedure' in Chapter-1, Kamila Amphibolites. The geochemical analyses are presented in Tables 13 and 14.

3-4.2 Major and transitional elements distribution

The major and trace element chemistry of the cumulate of Jijal Complex has been examined. All of the rocks have clear tholeiitic affinities.

The lower dunite unit has low concentrations of SiO_2 (35 to 39 wt %) and Al_2O_3 (0.45 to 0.65 wt %) and an enrichment of CaO (0.9 to 2.8 wt %) and FeO^T (10 to 11 wt %) as

Table 13. Major, trace and platinum-group element analytical data from the KKH-section, Jijal Complex. Major elements are recalculated to 100% without LOI.
Données analytiques sur les éléments majeurs et en traces de la coupe de la KKH. Complexe de Jijal.

S. No.	KO-1A	KO-2	KO-3	KO-4	KO-5	KO-6	KO-28	KO-27	KO-26	KO-25	KO-29	JRP-18A	JRP-18B	KO-24	KO-23	KO-7	JK-31	KO-22	JK-33
Rock-type	dunite	ol-clinopyr.	ol-clinopyr.	ol-clinopyr.	ol-clinopyr.	ol-clinopyr.	webst.	webst.	dunite	dunite	dunite	dunite	dunite	webst.	webst.	webst.	dunite	webst.	webst.
Mineralization		tr sulf+chr		tr sulf		tr sulf	tr sulf	chr	chr dis	Chromitite	Chromitite	Chromitite	Chromitite	tr sulf	tr sulf	sulf Cp		tr sulf	
Position	m.	62	250	437	625	812	969	1063	1156	1375	1469	1520	1520	1562	2156	2163	2200	2236	2250
Major Elements(wt%)																			
SiO2		39.10	44.82	53.34	52.72	52.99	54.08	53.83	52.66	39.85	40.04	N.D.	N.D.	53.35	47.06	43.08	39.69	49.86	43.44
TiO2		0.04	0.05	0.12	0.17	0.15	0.09	0.10	0.16	0.03	0.03			0.08	0.12	0.08	0.15	0.28	0.16
Al2O3		0.83	0.62	2.09	2.85	2.64	1.54	1.73	2.68	0.78	0.44			1.49	1.84	1.24	3.84	4.91	2.11
Fe2O3		14.28	10.34	7.53	9.54	8.35	6.05	5.10	9.73	9.60	10.72			7.03	11.32	16.19	15.42	10.95	16.23
MnO		0.16	0.06	0.16	0.19	0.18	0.13	0.10	0.19	0.00	0.09			0.16	0.16	0.17	0.00	0.21	0.25
MgO		45.32	41.29	19.91	20.55	19.83	21.60	19.20	21.73	49.47	48.33			21.35	27.60	32.11	34.85	18.26	27.39
CaO		0.26	2.82	16.83	13.98	15.86	16.51	19.93	12.84	0.27	0.36			16.55	11.90	7.13	6.06	15.53	10.43
Na2O																			
K2O																			
P2O5		0.02																	
Total		100.00	100.00	100.00	100.00	100.00	100.00	100.00	100.00	100.00	100.00			100.00	100.00	100.00	100.00	100.00	100.00
LOI		1.29	11.48	1.92	2.49	1.88	0.76	1.06	1.68	0.29	2.58			4.39	2.09	0.02			
Trace elements (ppm)																			
Zn		58	15	32	44	37	23	12	46	41	42			22	36	53	87	33	52
Ni		1490	807	193	180	241	207	362	188	1971	1560	1952		197	438	967	963	158	188
Cr		4202	922	1779	1587	1812	1705	1645	1546	29500	3857	95000		1624	2571	1481	5654	921	679
V		154	65	257	348	312	197	158	367	164	62	558		256	371	234	250	692	258
Cu		9	9	9	10	82	322	528	5	4	9	10		9	16	2043	15	253	4.00
Sc		BDL	11	89	89	93	64	51	88	BDL	BDL	BDL		96	66	27		156	BDL
Ga		BDL	BDL	BDL	BDL	BDL	BDL	BDL	BDL	BDL	BDL	BDL		BDL	BDL	BDL	BDL	BDL	BDL
U		BDL	BDL	BDL	BDL	BDL	BDL	BDL	BDL	BDL	BDL	BDL		BDL	BDL	BDL	BDL	BDL	BDL
Ce		BDL	BDL	BDL	BDL	BDL	BDL	BDL	BDL	BDL	130	128		67	115	145	135	73	98
Co		115	106	61	60	78	63	19	61	128	0.14	BDL		BDL	BDL	BDL	BDL	BDL	BDL
Rb		BDL	BDL	BDL	BDL	BDL	BDL	BDL	BDL	BDL	0.98	BDL		10	10	BDL	8.00	10	BDL
Sr		BDL	13	13	10	11	14	14	11	BDL	0.06	BDL		BDL	BDL	BDL	6.00	10	7.00
Y		BDL	BDL	BDL	BDL	BDL	BDL	BDL	BDL	BDL	0.18	BDL		BDL	BDL	BDL	BDL	BDL	BDL
Zr		BDL	BDL	BDL	BDL	BDL	BDL	BDL	BDL	BDL	0.59	BDL		BDL	BDL	BDL	BDL	BDL	BDL
Nb		BDL	BDL	BDL	BDL	BDL	BDL	BDL	BDL	BDL	0.01	BDL		BDL	BDL	BDL	BDL	BDL	BDL
Cs		BDL	BDL	BDL	BDL	BDL	BDL	BDL	BDL	BDL	4.41	BDL		BDL	BDL	BDL	BDL	BDL	BDL
Ba		BDL	BDL	BDL	BDL	BDL	10	BDL	BDL	BDL									

Abbreviations: ol-clinopy. = olivine clinopyroxenite, webst. = websterite, gt-pyrox. = garnet pyroxenite, Tr Sulf. = trace sulphides
Chr dis = disseminated chromite, Cp = chalcopyrite, py = pyrite, BDL = below detection limit (1ppm for Nb,Zr,Y,Sr,Cu; 7ppm for Sc,Ga,U; 24 ppm for Ba; 30 ppm for Nd,Ce; 0.002 wt % for Na,K and P2O5.

Table 13. (Continued)

S..No.	KO-21	KO-21A	KO-20	KO-19	KO-18	KO-17	KO-16	KO-15	KO-14	KO-12	KO-11	KO-45	KO-13	KO-10	KO-9A	KO-8A
Rock-type	webst.	webst.	webst.	gt-pyrox.	gt gabbro	gt gabbro	gt gabbro	gt gabbro	gt gabbro	gt hornbl.	gt hornbl.	gt gab.	gt hornbl.	gt gabbro	gt gabbro	gt gabbro
Mineralization	sulf	sulf										Py-Cp	tr sulf			
Position	2312	2315	2375	2438	2500	2563	2625	2750	2875	3063	3156	3219	3313	3406	3594	3906
Major Elements (wt%)																
SiO2	44.08	49.19	49.91	44.80	42.25	47.32	44.25	52.26	45.04	42.08	41.28	48.17	38.86	51.41	52.85	52.65
TiO2	1.21	0.30	0.39	1.34	0.60	0.90	0.82	0.85	1.38	1.82	1.86	0.75	1.40	0.67	0.70	0.88
Al2O3	14.73	5.05	5.61	11.44	15.74	8.40	19.54	18.08	17.50	14.13	15.56	15.08	17.04	18.85	17.96	17.57
Fe2O3	11.22	10.40	9.55	11.87	16.36	9.92	14.71	11.67	16.21	16.29	14.17	10.60	19.03	10.76	10.72	10.75
MnO	0.11	0.19	0.17	0.12	0.37	0.12	0.22	0.20	0.23	0.14	0.10	0.08	0.31	0.18	0.19	0.16
MgO	14.84	18.15	16.41	11.98	11.20	11.64	7.02	4.73	7.19	12.06	12.91	6.71	9.87	5.30	5.19	5.60
CaO	11.62	16.72	17.92	16.94	13.35	21.48	12.59	9.92	11.42	11.68	11.91	17.44	12.08	10.48	10.08	10.17
Na2O	2.03	0.00	0.04	1.45	0.14	0.22	0.72	2.05	0.87	1.65	2.00	1.12	1.28	2.19	2.03	1.88
K2O	0.17						0.10	0.12		0.15	0.21		0.14	0.09	0.23	0.26
P2O5							0.02	0.13	0.16	0.00	0.00	0.06	0.00	0.08	0.05	0.09
Total	100.00	100.00	100.00	100.00	100.00	100.00	100.00	100.00	100.00	100.00	100.00	100.00	100.00	100.00	100.00	100.00
LOI	1.42	0.11	0.79	0.39	0.14	0.20	1.21	0.37	0.12	0.86	0.62	1.99	0.30	0.77	0.64	0.16
Trace elements(ppm)																
Zn	39	32	31	62	55	43	97	93	106	93	72	67	81	83	80	76
Ni	229	147	201	85	38	72	22	13	43	35	60	80	27	19	21	11
Cr	682	1012	1116	431	581	1072	182	225	1558	83	77	126	267	327	331	57
V	941	451	446	727	582	512	544	266	518	1021	874	422	867	306	289	247
Cu	105	69	43	35	5	8	24	123	145	158	111	1648	32	152	37	48
Sc	114	BDL	128	101	165	BDL	72	46	63	110	98		92	50	42	BDL
Ga	11	BDL	BDL	16	10	11	18	21	19	16	16	17	16	20	18	15
U	BDL	BDL	BDL	BDL	BDL	BDL	BDL	BDL	BDL	BDL	BDL	BDL	BDL	BDL	BDL	BDL
Ce	BDL	BDL	BDL	BDL	BDL	BDL	BDL	BDL	BDL	BDL	BDL	BDL	BDL	BDL	BDL	BDL
Co	84	66	78	73	62	39	53	31	47	80	83	105	65	34	30	70
Rb	BDL	BDL	BDL	BDL	BDL	BDL	BDL	BDL	BDL	BDL	BDL	BDL	BDL	BDL	BDL	BDL
Sr	142	10	19	92	36	37	196	273	186	106	199	307	130	256	254	305
Y	10	9	10	10	31	8	12	18	18	11	10	13	25	15	17	13
Zr	BDL	BDL	BDL	BDL	BDL	BDL	BDL	16	BDL	BDL	BDL	17	BDL	11	25	35
Nb	BDL	BDL	BDL	BDL	BDL	BDL	BDL	BDL	BDL	BDL	BDL	BDL	BDL	BDL	BDL	BDL
Cs	BDL	BDL	BDL	BDL	BDL	BDL	BDL	BDL	BDL	BDL	BDL	BDL	BDL	BDL	BDL	BDL
Ba	BDL	BDL	BDL	15	BDL	BDL	BDL	64	10	BDL	BDL	15	28	78	98	236

Table 14. Rare earth elements (ppm) composition of Jijal Copmplex.
Données analytiques sur les éléments en traces de la coupe de la KKH, Complexe de Jijal

sample no	KO-1A	KO-25	KO-3	KO- 6	KO-27	KO-22	KO-23	KO-24	KO-21A	KO-17	KO-16	KO-9A	KO-11.
rock name	dunite	dunite	ol-clinopyroxenite	websterite	websterite	websterite	websterite	websterite	Ga-websterite	gt gabbro	gt gabbro	gt gabbro	gt hornblendite
locality	KKH	KKH	KKH	KKH	KKH	KKH	KKH	KKH	KKH	KKH	KKH	KKH	KKH
La	0.02	0.02	0.18	0.18	0.16	0.09	0.02	0.10	0.10	0.47	1.14	3.25	0.45
Ce	0.05	0.02	0.35	0.26	0.60	0.43	0.08	0.06	0.47	2.29	2.88	7.62	1.88
Pr	0.01	0.01	0.11	0.08	0.12	0.10	0.02	0.04	0.10	0.52	0.51	1.11	0.49
Nd	0.02	0.02	0.54	0.29	0.65	0.74	0.18	0.13	0.66	3.29	2.62	5.67	3.43
Sm	0.01	0.01	0.28	0.14	0.25	0.40	0.10	0.1	0.32	1.13	1.02	1.82	1.40
Eu	0.002	0.004	0.1	0.05	0.10	0.19	0.05	0.05	0.15	0.46	0.55	0.79	0.55
Gd	0.01	0.01	0.28	0.14	0.41	0.75	0.19	0.12	0.60	1.32	1.35	2.35	1.04
Tb	0.001	0.002	0.08	0.04	0.08	0.17	0.04	0.04	0.14	0.21	0.25	0.40	0.24
Dy	0.01	0.01	0.6	0.29	0.62	1.29	0.30	0.29	1.12	1.24	1.77	2.62	1.46
Ho	0.003	0.003	0.14	0.07	0.15	0.31	0.07	0.07	0.27	0.24	0.39	0.59	0.29
Er	0.01	0.01	0.42	0.2	0.42	0.89	0.18	0.2	0.79	0.60	1.23	1.68	0.80
Tm	0.002	0.002	0.07	0.03		0.13		0.03	0.13	0.10	0.21	0.28	0.12
Yb	0.01	0.01	0.36	0.17	0.40	0.78	0.15	0.17	0.66	0.45	1.21	1.74	0.58
Lu	0.002	0.002	0.06	0.03	0.06	0.11	0.02	0.03	0.09	0.06	0.19	0.28	0.08
(La/Sm)n	2.20	2.10	0.40	0.81	0.41	0.13	0.1	0.63	0.20	0.26	0.70	1.13	0.20
(La/Yb)n	1.09	1.35	0.34	0.71	0.27	0.07	0.07	0.40	0.10	0.70	0.64	1.26	0.52

compared to the upper unit of dunite (U2, Table 13). The presence of high FeO in dunite of unit 2 can be explained in terms of the relatively ferriferous composition of the olivine and the presence of disseminated as well as layered ferrochromite. There is no change in the concentrations of other major elements.

The lower cyclic unit, Olivine clinopyroxenite exhibits a gradual decrease from U1 to U3 in MgO (25 to 19 wt %), CaO (17 to 13 wt %), Cr (0.24 to 0.17 wt %) and Ni (0.05 to 0.03 wt %) and up section these elements fluctuate markedly (Table 13). This change is also followed in the upper cumulate sequence from websterite (U4) to garnet websterite (U5) but with some degree of overlap (MgO=22 to 8 wt%; CaO=18 to 7 wt.%; Cr=0.25 to 0.01 wt%; Ni = 0.06 to 0.03 wt %). Similar patterns of gradual decrease in contents of MgO, CaO, Ni and Cr is clearly evident in garnet gabbro, the uppermost unit of Jijal Complex (Table 13). Increasing contents of SiO_2, Al_2O_3 and FeO^T from dunite, olivine clinopyroxenite, websterite, garnet websterite to garnet gabbro is inversely related to MgO and CaO (Table 13). The level of TiO_2 increases upwards gradually from dunite to garnet websterite (on average 0.03 wt % in dunite and 0.05 wt.% in olivine clinopyroxenite, 0.47 to 0.64 wt % in garnet websterite), but again declines in garnet gabbro (TiO_2= 0.04 to 0.21 wt.%). Low Cr concentrations reflect the content of chromite. Generally, P_2O_5, Na_2O and K_2O are not present (below detection limit) in these ultramafic-mafic rocks of Jijal Complex except in one sample of garnet gabbro (Na_2O- 0.11 wt %) and one in garnet websterite (KO-37, Na_2O- 1.27 wt % and K_2O- 0.13 wt %).The onset of the crystallization of plagioclase as a separate cumulate phase in the garnet gabbro is reflected in increased Al_2O_3 and CaO. Chemical changes in the garnet gabbro (SiO_2 with average 42 wt %, Al_2O_3 = 21 to 26 wt %, CaO = 13 to 16 wt %, MgO = 9 to 12 wt %, MnO = 0.08 to 0.14 wt % and the remainder) are similar to variations established in the garnet websterite, the upper unit of Jijal ultramafic cumulate. It appears that the major elements distribution variations of the garnet gabbroic rocks are extensions of changes established in the garnet websterite unit (except for more increase in the Al_2O_3 and concomitant fall in MgO brought on by the plagioclase crystallization).

The different units of pyroxenites and garnet gabbro in Jijal Complex have higher Mg# values (100*Mg/Mg+Fe) ranging from 92 to 71. By means of this ratio, the Jijal Complex can also be divided into two major units, depending on whether Mg# increases or decreases with height. The lower portion, with an overall increase of Mg#, can be equated with the ultramafic cumulate unit, while the upper unit, characterized by a general decrease (Mg# = 79 to 71), is part of the garnet gabbro. Garnet gabbro are strongly depleted in TiO_2, P_2O_5, Na_2O, K_2O, Th and enriched in CaO (Table 13). Evolutionary trend of these rocks is also evident in Figure 78, where Cr and Ni indicate negative correlation with decrease of Mg# whereas Zr correlate positively with decrease of Mg# (Table 13).

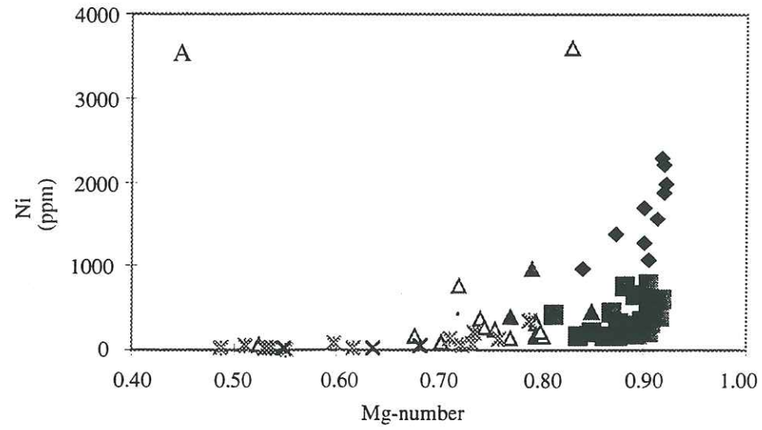

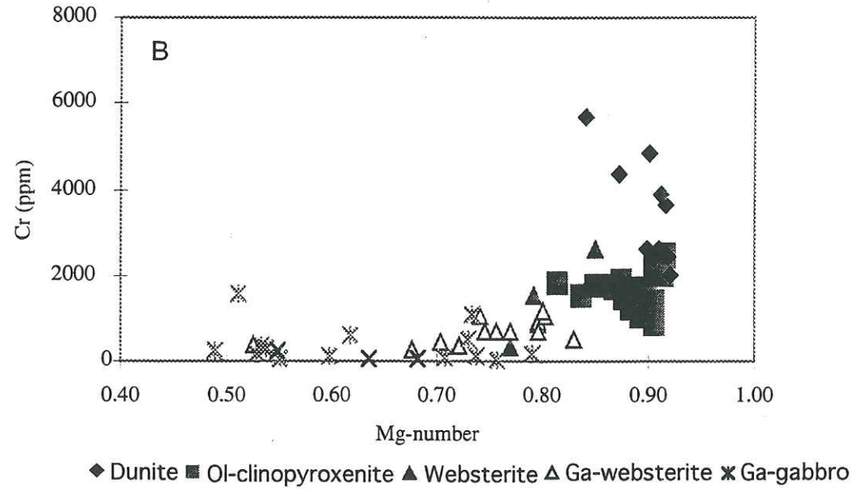

Figure 78. Relationship between Ni (A) and Cr (B) and Mg-number in the rocks of the Jijal Complex.
Relations entre le Ni (A) et le Cr (B) et le Mg-number dans les roches du Complexe de Jijal.

3.4.2 REE in Jijal Complex

Thirteen whole rock samples; two dunites rocks, two olivine-clinopyroxenites, four websterites, two garnet-websterites and three garnet-gabbros; have been selected along KKH (Table 14, Fig. 65). This allowed REE variations among the different lithological types to be identified and provided some insight into the processes that gave rise to the petrological diversity. It is emphasized that sampling for these purposes was generally restricted to major intrusive units. Six mineral phases including olivine, clinopyroxene, garnet and hornblende in dunite, olivine clinopyroxenite, websterite, garnet websterite and garnet gabbros have been analysed for trace and rare earth elements after mineral separation by dense liquors by ICPMS in Grenoble (see data on Table. 14A). Chondrite-normalized REE distribution patterns of dunite, olivine-clinopyroxenite, websterite, garnet-websterite, garnet hornblendite and garnet-gabbro and from separated minerals are presented in Figures 79A & B.

- REE in ultramafic rocks.

The chondrite REE patterns of the analyzed **websterite and garnet websterite** appear very similar. They are characterized by low REE contents (0.1 to 2 times chondrite), a strong LREE depletion ($0.1 < (La/Sm)_N < 0.41$; $0.07 < (La/Yb)_N < 0.4$) and flat HREE patterns. Their patterns are very similar to those obtained for Cpx (Fig. 76B), though they are a little more depleded due to presence of garnets (these latter exhibiting a very stong LREE depletion, and HREE enrichment). Such garnet are comparable to those of magmatic origin. If the garnet websterite initially formed as garnet-free pyroxenite cumulate, the garnet in these rocks formed by either subsolidous reaction or exsolution from clinopyroxenes. A cumulate origin for the garnet-websterite is consistent with their trace element contents. Relative to basalts, sample KO-21A have high abundances of elements Sc (66 ppm) and Cr (1012 ppm), that are compatible in clinopyroxene and garnet, and this sample has low abundances of incompatible elements, such as REE. Formation of garnet during high pressure crystallization in magmatic chamber by exsolution from Cpx is consistent with the relatively low HREE contents of these garnet websterite (Fig. 79) because relatively higher HREE abundances are expected in cumulates with primary garnet. In addition, the convex-upward shape of the chondrite-normalized REE pattern (Fig. 79A) is typical of pyroxenites interpreted to be cumulates (Frey & Prinz, 1977).

In olivine clinopyroxenite, REE contents are also very low (0.3 to 2 times chondrite), but their LREE depletion is less ($0.4 < (La/Sm)_N < 0.8$; $0.3 < (La/Yb)_N < 0.7$) and they have similar flat HREE patterns. These differences are probably due to absence of garnet, while LREE contents of olivine and CPX are relatively similar. Olivines are, however, more enriched with HREE

In dunite, REE contents are the lowest (0.03 to 0.1 time chondrite), but their LREE and HREE patterns are different with a slight LREE enrichment, $(La/Sm)_N = 2.1\text{-}2.2$ and $(La/Yb)_N = 1.1\text{-}1.4$. This normally could be explained by olivine accumulation, but is not in accordance

Table n°14A: Trace and Rare earth element in separated mineral phases from the Jijal Complex in the different types of lithologies. Analyses by ICP-MS in Grenoble (1998) after mineral liquor dense separation.

Eléments majeurs et en traces de phases minérales séparées du Complexe de Jijal pour differents types de lithologies. Analyses par ICP-MS à Grenoble (1998), séparationpar liquides denses

Field number		KO-21B	KO-21B	KO-21B	KO-22	KO-06	KO-26
Laboratory number		:1022	:1023	:1024	:1025	:1027	:1028
Lithology		Gt Websterit	Gt Websterit	Gt Websterit	Websterite	Ol Clinopyr	Dunite ?
Mineral		Amph-Cpx	Amph	Garnet	Cpx	Olivine	Cpx
Ba	ppm	<,05	23.32	<,05	<,05	<,05	<,05
Rb	ppm	0.04	0.72	0.18	<,05	<,05	<,05
Sr	ppm	35.69	138.79	5.76	14.19	25.10	14.39
Ta	ppm	0.00	0.01	0.01	<,05	0.01	0.04
Th	ppm	0.00	0.00	0.00	<,05	0.00	<,005
Zr	ppm	3.19	3.41	1.72	0.84	7.17	0.17
Nb	ppm	0.01	0.11	0.01	<,05	0.02	<,05
Y	ppm	2.22	6.14	47.48	2.92	39.56	1.99
Hf	ppm	0.24	0.24	0.08	0.06	0.17	0.02
Ni	ppm	82.68	223.00	8.71	92.07	6.19	132.58
Co	ppm	41.39	80.24	63.30	36.66	70.53	27.66
U	ppm	0.01	0.01	0.01	0.00	0.01	0.01
Cu	ppm	875.15	57.36	78.08	21.34	54.52	75.47
Zn	ppm	28.71	68.95	24.94	12.49	128.34	5.39
Pb	ppm	0.18	0.30	0.11	0.07	0.29	0.70
Rare earth Elements							
La	ppm	0.15	0.27	0.01	0.11	0.19	0.05
Ce	ppm	0.68	1.42	0.03	0.46	0.55	0.18
Pr	ppm	0.17	0.37	0.01	0.10	0.14	0.04
Nd	ppm	1.21	2.79	0.13	0.71	1.54	0.27
Sm	ppm	0.61	1.46	0.32	0.34	1.89	0.14
Eu	ppm	0.30	0.76	0.34	0.17	1.13	0.06
Gd	ppm	0.74	2.00	1.61	0.47	3.88	0.23
Tb	ppm	0.12	0.31	0.57	0.09	0.83	0.04
Dy	ppm	0.57	1.59	5.73	0.59	5.97	0.35
Ho	ppm	0.09	0.25	1.71	0.12	1.34	0.08
Er	ppm	0.20	0.48	6.05	0.33	4.00	0.21
Tm	ppm	2.77	2.30	3.63	2.37	2.92	2.36
Yb	ppm	0.13	0.25	7.40	0.27	4.01	0.19
Lu	ppm	0.02	0.03	1.27	0.04	0.65	0.03
(La/Sm)n		0.12	0.08	0.01	0.16	0.04	0.20
(La/Yb)n		0.77	0.73	0.00	0.28	0.03	0.18

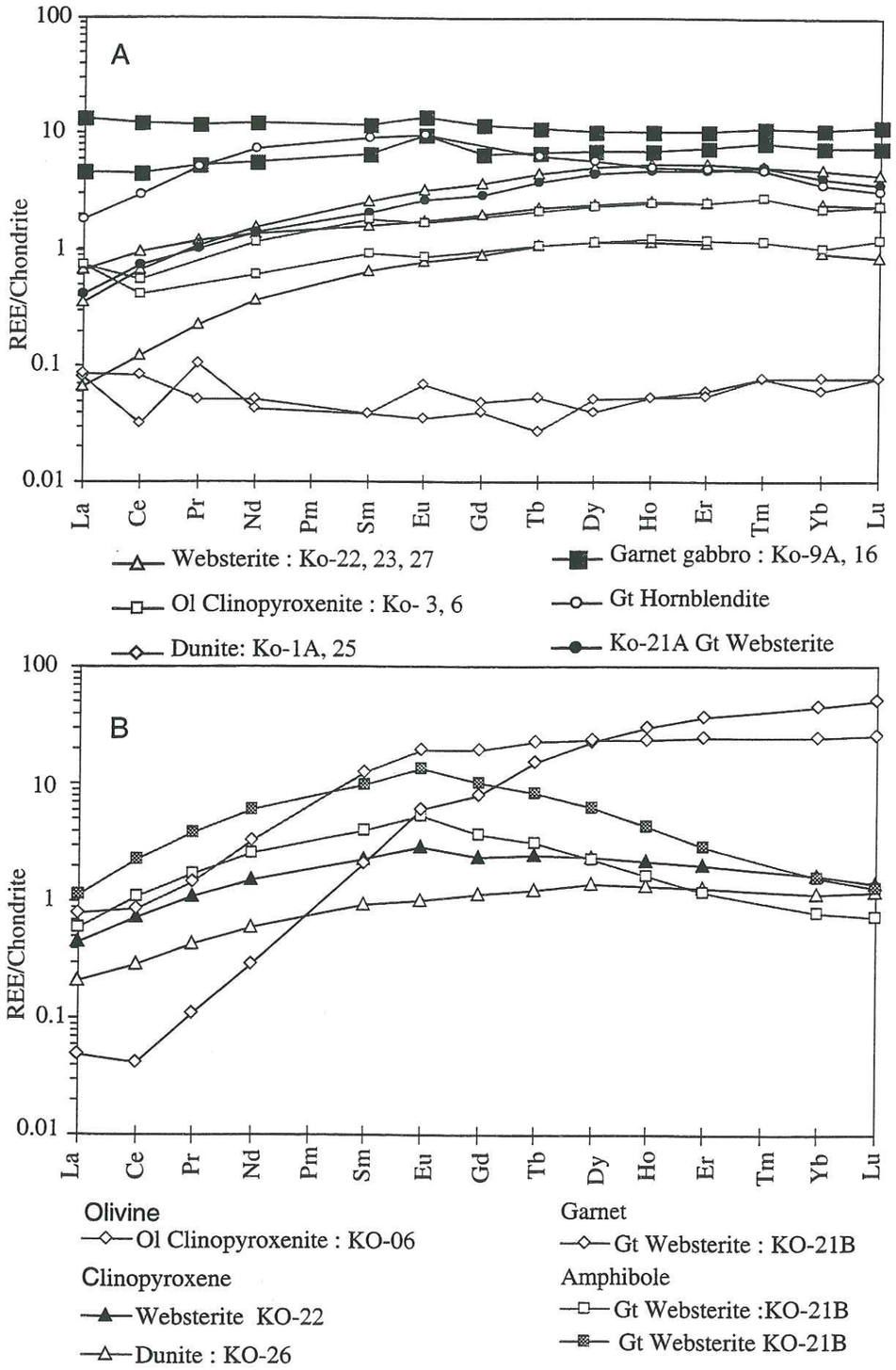

Figure 79 : Chondrite-normalized REE patterns from the Jijal Complex : A) for whole rocks; B) for separated minerals phases in the main lithologies. Normalization values are from Nakamura (1974).

with the observed olivine composition in olivine clinopyroxenite whiche are more REE enriched. Howeve olivine in dunite has not been analysed, due to intense serpentinization.

Finally, Garnet hornblendites are more REE enriched (2 to 8 times chondrite) with convex patterns marked by both depleted LREE and HREE patterns, $(La/Sm)_N = 0.2$; $(Sm/Yb)_N = 2.58$. Such patterns clearly reflect abondance of the hornblende crystals which exhibit similar patterns (Fig. 79B), with, however, higher HREE contents due to enrichments by garnets.

Textural observations and chemistry, thus, indicate that the major phases appearing early in the crystallization sequences of the cumulate ultramafic rocks are spinel, olivine, clinopyroxene, orthopyroxene, and garnet. Olivine and clinopyroxene are significant phases in dunites, olivine-clinopyroxenites, websterites and garnet websterite and may have participated in the crystallization differentiation of the magma of these rocks. The common presence of these minerals as phenocrysts in volcanic rocks, and the occurrence of these minerals as liquidous or near liquidous phases in experimental studies conducted in the range of crustal pressure (e.g., Eggler & Burnham, 1973; Allen & Boettcher, 1978; Nichollas & Harris, 1980) support the textural observations.

REE behaviour during crystallization is principally controlled by mineral / melt partitioning. REE partitioning between melt and spinel, olivine, clinopyroxene, orthopyroxene and garnet have been measured by many workers in a wide variety of peridotites, volcanics and in experimental studies. These studies have yielded consistent mineral / melt REE pattern shapes for the trivalent REE, which are taken as close approximations to equilibration fractionation shapes. These shapes are controlled by crystal chemical considerations (e.g. Onume et al., 1968; Fred & Frey, 1969; Matsui et al., 1977; Gromet, 1979; Nicholls & Harris, 1980), and are primarily sensitive to changes in the configuration of the sites in which the REE reside. For example, the M1 and M2 enstatite cation sites are much smaller than REE ions and with the increase of ionic size from Lu to La, there will be increasing discrimination against the REE and pattern will be much more steeper. Similarly in the high Al-diopside structure the M2 site is larger than the M1 site and this M2 site ideally corresponds to an ionic size which occurs in the middle of the lanthanide series (Fred & Frey, 1969). Thus REE ions larger than the M2 site may be increasingly discriminated against and pattern will be steeper beyond some MREE (e.g. Tb or Gd). For olivine, the LREE are not relatively discriminated against as in the pyroxenes and this type of distribution is also observed by Masuda's redetermination of the REE in the olivine phase of the Brenham meteorite (Masuda, 1968).

- REE in upper mafic rocks.

REE abundances of **garnet-gabbros** are relatively high (around 10 times chondrites) which is very equivalent to most of the tholeiitic primitive liquids. Despite a marked positive europium anomaly because of the abundance of plagioclase, these rocks exhibit whole rock compositions (major, trace and rare earth elements) similar to basaltic liquids. So even these

rocks present cumulative effects (for instance with plagioclase). We can consider with some cautions their chemical signature as relatiely good indicator of the chemical composition of parental magmas. Their chondrite-normalized REE patterns are almost flat with slight LREE over HREE enrichments having $(la/Sm)_N$ = 0.7-1.13 and $(La/Yb)_N$ = 0.71 - 1.37. The fractionation of light and heavy REE is similar for all these samples, and the major difference between the samples is their bulk REE content. So flat REE distribution patterns may be considered to be typical for mantle derived rocks from a MORB like source (Johnson et al., 1990) at relatively high degrees of melting without major crustal contamination. Garnet was not a residual phase because the HREE are not depleted. The REE patterns of garnet-gabbro are typical for mafic cumulates where the patterns are dominated by the crystallization of plagioclase and ferromagnesian and their mineral/melt distribution coefficients (McKay, 1989).

Figure 80 shows the MORB normalized trace element distribution for garnet-gabbro. The general pattern with a moderate enrichment in Rb, Ba and K relative to the other incompatible elements and with strong negative Ta and Nb anomalies, is a feature characteristic of arc-related rocks (Pearce, 1983) and is similar to that of primitive island-arc tholeiites. Position of the representative points for these gabbros in the Arc basalt tholeiitic field in the ternary diagramme of Cabanis and Lecolle (1989), corroborates this point. Hence the similarity between the Jijal garnet gabbro and island-arc tholeiites is reasonable.

3.4.3 Discussion

The Jijal Complex has suffered a complex petrogenetic history, marked by a subsolidous recrystallization following early emplacement. The distribution of the trace elements in minerals was partially modified during recrystallization; for instance, the HREE, Cr and Sc were preferentially incorporated in the secondary garnet, at the expense of pyroxenes. This process has not significantly modified the whole-rock composition which may be affected by a slight metasomatic enrichment near the margins of the layers.

Chondrite-normalized REE patterns from the Jijal ultramafic section have geochemical features typical of segregates. A process involved in the mineral-liquid separation, at high pressure-temperaure fractionation, in ascending primary magmas through spinel lherzolite 'en route' to the surface, a mechanism described in detail by Irving (1980). Contrary to the pyroxenite xenoliths which are usually assumed to be derived from alkali basaltic magma (Frey and Prinz, 1978; Menzies, 1983; Frey, 1984), the studied pyroxenites are depleted in the most incompatible elements particularly LREE, Ti, K, P, Zr and Hf and are consistent with the tholeiitic character of the parental magma of these ultramafic rocks. In particular, it suggests that pyroxenitic segregation can account at least partially for the LREE enrichment in the ascending magmas.

Based on these field and mineral phase chemistry evidence, a crystallization model is proposed whereby the Jijal ultramafic cumulate rocks may reside at the upper mantle and lower

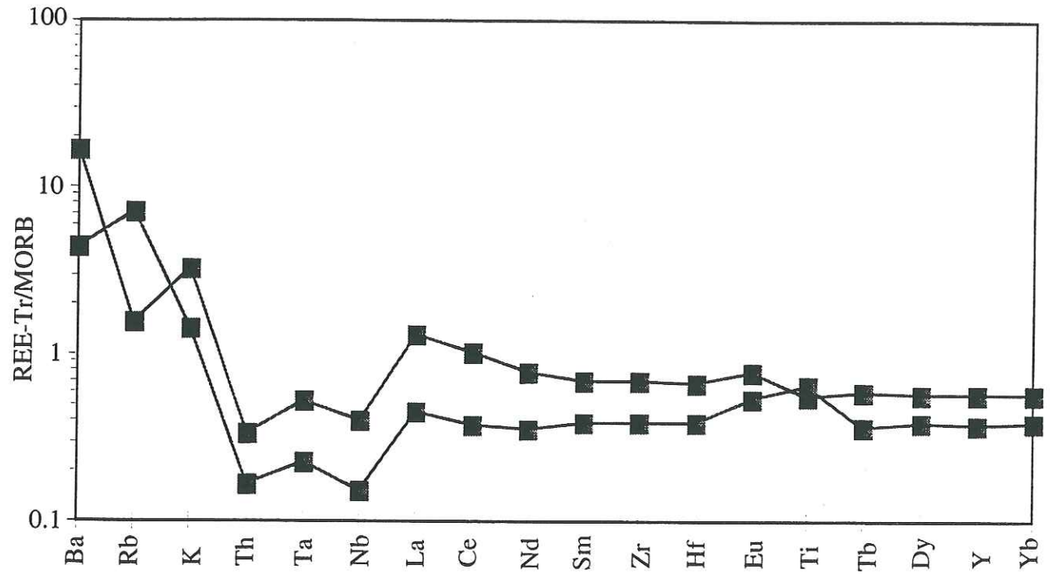

Figure 80 : Incompatible element abundances, normalized to N MORB values in Garnet Gabbro, Jijal complex. Normalization values are from Sun & McDonough (1989).

Spectre des éléments incompatibles normalisés aux MORB, dans un gabbro à grenats du Complexe de Jijal. Valeurs de normalisation par Sun & McDonough (1989).

crust beneath the arc and garnet gabbro represents a contemporaneous intrusion at shallower level in the same arc.

3.5 CONCLUSION

The main conclusion about Jijal Complex is as follows:

Field relationships suggest that the Jijal Ultramafic-Mafic Complex is clearly not compatible with the models proposed for oceanic crust, either at a mid-ocean ridge or rocks genetically related with convergenence zones and crystallized at shallow levels (e.g. lacking of the igneous stratigraphy typical of oceanic crust). From stratigraphy in the field as well as chemical composition of the primary minerals, the genesis of this complex indicates that the ultramafic-mafic rcks of the Jijal Complex formed from the same process or similar process and that these rocks were part of the Early Cretaceous time.

The main sequence can be defined in the following series: dunite, olivine-clinopyroxenite, websterite, garnet-websterite and garnet-gabbro. Olivine and clinopyroxene in the Jijal Complex display approximately complete variation trends for Ni, Cr and Fe/Mgo ratio which supports the hypothesis that both the olivine and clinopyroxene are related by similar parent melts. Primary crystallization is followed by deformation and recrystallization where primary minerals were strongly strained and deformed with many kink-bands. As a result, large amount of olivine and clinopyroxene neoblasts were formed by inter- and intracrystalline recrystallization of primary grains. These deformation textures are interpreted as indicative of high-temperature flow related to recycling of ultramafic cumulates back into the mantle (Pope, et al., 1981; Kay & Kay, 1985a; Debari et al., 1987). But such deformation textures in Jijal ultramafic cumulates may be related to the suturing of the Kohistan arc with Asian plate, while these rocks were still hot enough to deform plastically.

Petrology as well as mineralogy in Jijal Complex indicate that these rocks represent the high-temperature and pressure crystallization fractionation events at the upper mantle or at the lower crust. The temperatures calculated for coexisting garnet-clinopyroxene range from 930° to 1130°C and these are similar to those anticipated during the high-pressure fractionation of basalts if the experimental work of Elthon & Scarfe (1982) is used for reference. Evidence for moderate to high pressure includes (1) the absence of plagioclase as early fractionating phase and appearance of clinopyroxene and orthopyroxene having high Mg numbers (93-65; 85-74 respectively) coprecipitating with forsteritic olivine (95-79)(Green and Ringwood, 1967; Elthon et al., 1982), (2) the preferential partitioning of Al into octahedral rather than tetrahedral sites of clinopyroxene is an indication of moderate to high pressure (Green and Ringwood, 1967; Aoki and Kushiro, 1968), (3) trend of increasing alumina in clinopyroxene of pyroxenites and garnet gabbro parallel to trends observed in several high-pressure igneous intrusions such as in

southwestern Oregon (Medaris, 1972), and (4) REE typical of cumulates derived by high-temperature and pressure crystal segregation. Evidence of high temperatures during crystallization is suggested by the presence of pargasite hornblende as postcumulus phase, which has upper temperature stability limit of 1050°C (Jenkins, 1983).

The experimentally produced garnets and clinopyroxenes at 14.4 and 16.2 kbar, 1100°C from garnet pyroxenite xenoliths in the Delegate basaltic breccia pipes (Irving, 1974; Table 7) are quite similar in texture and composition to the garnets and clinopyroxenes of the garnet pyroxenites of Jijal ultramafic rocks.

The effects of high-pressure and high-temperature crystal fractionation have, thus, been documented, and in the absence of specific criteria to reject them, these effects should not be ignored in models for the generation and evolution of deep-seated cumulate rocks in arc setting environments. Because, characterization of these deep-level cumulate assemblages are extremely important to our understanding of the nature of island arc crust.

The Jijal Complex is not an isolated example of lower level island arc magmatism. Cumulate ultramafic-mafic sequences, similar to the Jijal Complex, have been described from the Border Ranges Ultramafic and Mafic Complex (BRUMC) and Tonsina Ultramafic-Mafic Assemblages, Alaska, and these have been interpreted to be high-pressure cumulates. The striking resemblance of petrological and mineral phase chemistry data suggest that the processes of formation of these complexes are similar. The BRUMC (Burns, 1985) and Tonsina Ultramafic-Mafic Assemblages (DeBari & Coleman, 1989) have been interpreted as blocks of the lower crust and upper mantle of a mature Jurassic island arc. Similar comparison of Jijal Complex can be made to the ultramafic and mafic inclusions (Conard & Kay, 1984) from Adak Island, Aleutian arc, Canyon Mountain arc (Gerlach et al., 1981) and Guanajuato magmatic sequence, Alisitos-Teloloapan intra-oceanic island arc, Mexico (Lapierre et al., 1992).

CHAPTER-4

CONCLUSION

PETROLOGICAL AND GEODYNAMICAL EVOLUTION OF SOUTHERN KOHISTAN

CHAPTER-4

CONCLUSION

Petrological and Geodynamical Evolution of Southern Kohistan

The intra-oceanic immature arc crust in the southern Kohistan is represented by the Kamila Amphibolite Belt, the Chilas Igneous Complex and the Jijal Ultramafic-Mafic Complex. Results of petrographic, mineralogical and geochemical studies of rock assemblages representing the southern Kohistan arc can be summarized as follows:

Texturally and geochemically, the **Kamila Amphibolites** contain two distinct facies: 1) a fine-grained facies (metavolcanic), which are intruded by plutonic rocks, have volcanic protolith, except some fine-grained rocks that represent sheared and recrystallized plutonic protolith and 2) a coarse-grained facies representing plutonic rocks mainly metagabbros and metadiorites. The main conclusion that can be reached on the basis of geochemical studies is that there is a bimodality of compositions in the rocks from the Kamila Amphibolites. The differences between the metavolcanic rocks and metaplutonic rocks are well-defined by comparing their major and trace element characteristics. The metavolcanic rocks have notably higher MgO, FeO, CaO and TiO_2 , lower SiO_2, P_2O_5, Al_2O_3 and Na_2O contents. Their REE and trace patterns have relative enrichment in HFSE, particularly in Ti, Ta and Nb, low and variable concentrations of most large ion lithophile elements (Ba, Rb and Sr). They have low $(La/Sm)_N$ and $(La/Yb)_N$ = 0.27 to 0.54 ratios and exhibit no negative anomalies in Ta and Nb. The differences in rare earth and trace element contents support the conclusion that the metavolcanic rocks are not the deformed/recrystallized protolith of other plutonic rocks from the Kamila Amphibolites. As such the metavolcanic rocks appear to represent basalt with N-type MORB affinity.

In contrast, the metaplutonic rocks show subduction related affinities such as a depletion in Nb and Ta content. These results are confirmed by La/Ta ratios which show ocean floor characteristics (La/Ta ratios 5-14) for the metavolcanic rocks and island arc affinity (La/Ta ratio >30) for the metaplutonic rocks.

We ,therefore, suggest that metavolcanic amphibolites may represent fragments of ancient oceanic crust as originally suggested by Tahirkheli et al. (1979) and Treloar et al. (1996), intruded by the metaplutonic rocks, having subduction related affinity.

The Main Facies Zone of the Chilas Igneous Complex has a wide range of rock types, ranging from gabbronorite, gabbro, diorite, granodiorite to trondhjemite, with the main

lithologies typically being gabbronorite, gabbro and diorite. Several lines of evidence from the Main Facies Zone support a transitional character from tholeiitic to calc-alkaline arc affinity. Major and trace element geochemistry, and MORB- and chondrite-normalized patterns from the Swat- and Indus-Valleys do not differ significantly. The samples are characterized by enrichment of LILE and negative Ta and Nb anomalies, which are similar to modern arc related basaltic to andesitic rocks. Differences between the samples, from the two valleys, occur mainly in the overall REE abundances and not in the shape of the patterns.

Low values in Mg#, Cr and Ni contents, together with rapid decrease in Ni and Cr with decreasing Mg# and increasing Zr abundance, implies that much of the chemical variation in these rocks may be attributed to crystallization processes. Positive to negative Eu anomalies in the REE profiles for the basic to more evolved rocks indicate that fractionation has taken place during magma evolution.

Thus, the main conclusion includes; 1) that there is a clear island-arc affinity among the rock assemblages of the Main Facies Zone of the Chilas Igneous Complex, and 2) they show evidence of perfect fractional crystallization.

Consequently, it seems reasonable to believe that the Chilas Igneous Complex has evolved from nascent to a mature stage of arc growth.

The Jijal Complex is a layered body which contains a continuous sequence of ultramafic through mafic plutonic rocks. The ultramafic rocks generally consist of layered dunite, olivine clinopyroxenite and websterite which evolves to garnet websterite and garnet clinopyroxenite on the top of the sequence. Whole rock geochemistry and mineral chemistry indicates that the rock assemblages within the Jijal Compex are linked by fractional crystallization from a high-Mg tholeiitic melt in an island arc environment.

The Mg# of olivine and clinopyroxene decrease systematically through the rock series dunite through olivine clinopyroxenite, websterite, garnet websterite to garnet gabbro. The most aluminous clinopyroxenes occur in the most differentiated, olivine- and orthopyroxene-poor garnet gabbro.

Petrologically and mineralogically the Jijal Complex indicates that these rocks represent high-temperature and pressure crystallization fractionation events at the upper mantle or the lower crust. The temperatures and pressures calculated, for coexisting olivine-spinel in dunite, orthopyroxene-clinopyroxene in websterite and garnet-clinopyroxene in garnet-websterite partly overlap from the base to the top of this complex, suggesting that the complete Jijal Complex recorded a similar final P-T evolution of about 860°C ± 90°C and 11 ± 3 kbar. The occurrence of garnet in the upper part of the Jijal Complex does not necessarily imply a pressure increase

but more probably a cooling as suggested by the occurrence of exsolution of garnet, spinel and orthopyroxene from clinopyroxene in the garnet websterite unit.

Evidence for relatively high crystallization pressures for the complex includes: 1) the absence of plagioclase as an early fractionating phase and appearance of clinopyroxene and orthopyroxene having high Mg numbers; 2) the preferential partitioning of Al into octahedral rather than tetrahedral sites in clinopyroxene; 3) trend of increasing alumina in clinopyroxenes parallel to trends observed in several high-pressure igneous intrusions such as in southwestern Oregon and, 4) REE typical of cumulates derived by high-pressure and temperature crystal segregation.

Comparison of the rock assemblages of the Jijal Complex with Aleutian lower crustal xenoliths as well as other exposures of arc-related lower crustal magma chambers in Japan and western North America indicates that this process is a common mechanism for island arc magma evolution at depth.

The rock assemblages of the **Thak Gah Association** were crystallized from a melt at a temperature of 800° to 950°C, deduced from two pyroxene geothermometry. Mineralogy and textural relationships differ significantly from the lower Jijal cumulates. Pyroxene and spinel in Thak Gah cumulates are more Fe-rich. As a result, chemical trends in minerals do not indicate the same high-pressure origin as Jijal cumulates. Based on phase relationships in the cumulus assemblages, pressure of formation for this complex can be constrained within 5 to 6 kbar. Hence the high level Thak Gah Association probably represents a contemporary, shallow magma chamber in the same Kohistan arc, with crystallization from a primitive magma at relatively shallower levels in the crust.

Geodynamic evolution

Field, petrographic, geochemical and mineralogic data suggest that mafic-ultramafic complexes (Thak Gah and Jijal) formed from the same or similar processes and these rocks were part of the southern Kohistan terrane by Early-Cretaceous time. The oldest unit within the sequence is represented by the fine-grained (metavolcanics) Kamila Amphibolites. We can consider that the metavolcanic rocks geochemically reflect N-type MORB affinities and may represent part of the ancient oceanic crust that formed entirely within an intra-oceanic setting. The fact that no oceanic crust is discernable in the Kohistan arc suggests that some part of the oceanic crust has either been incorporated into the latter plutonic rocks or was partially melted or digested in subduction. In the first stages of island arc development, basaltic magmas intruded near the crust-mantle boundary as represented by the basic plutons of the Kamila Amphibolites. These metaplutonic amphibolites are genetically tholeiitic in nature and have Nb contents < 3 ppm. The transitional tholeiitic to calc-alkaline composition of the Chilas Igneous

Complex indicates the next stage of magmatism. These magmas exhibit subduction component, as reflected by negative Nb and Ta anomalies and trace elements, similar to the plutonic rocks of the Kamila Amphibolites. Further, the presence of igneous textures, magnesio-hornblende and the chemical evolution suggests that these rocks crystallized in the oceanic crust, at pressures between 5 and 6 kbar. The ultramafic-mafic cumulates of the Thak Gah Association (UMA of Khan et al., 1989) represents a stratigraphically lower unit in the Kohistan arc magma chamber, which was probably located in the plutonic middle crust. The Jijal Ultramafic-Mafic assemblage represents a piece of the lower crust and upper mantle of a mature island arc. Lack of significant late-stage intrusions, suggest that the Jijal cumulates represent the last magmatic phase in a series of intrusions emplaced at the crust/mantle boundary. Our study indicates that the arc crust was very thick and the active magma chamber was present at a depth such that the pressure was between 10 to 12 kbar. The exposed thickness of the Jijal Complex is approximately 5 km which indicates that significant amounts of igneous material was underplatted through crystallization. If the crust is already thickened, this underplating will take the form of high-pressure cumulate assemblages such as seen at Jijal Complex.

Thus, the southern Kohistan terrane represents the crustal section of the nascent to mature stage of Early-Cretaceous intra-oceanic arc. Early arc magmatism was followed by Late-Cretaceous accretion of the Kohistan island arc to the Karakoram plate in the north. This marks the cessation of intra-oceanic arc magmatism in southern Kohistan.

PART-II

PLATINUM-GROUP ELEMENTS (PGE's) AND PLATINUM-GROUP MINERALS (PGM's) DISTRIBUTIONS IN THE SOUTHERN KOHISTAN:

with special emphasis on the Jijal Complex, N. Pakistan.

INTRODUCTION

The platinum-group elements (PGE) and Au together form a coherent group of siderophile and chalcophile elements that could be used to reveal some aspects of the history of the earth, or the evolution of a magma. Because of the difficulty in analyzing PGE at the levels that they occur in non-sulphide bearing rocks the data set has previously been limited to Pd, Pt and Ir concentrations in mafic rocks. Developments in the analytical field now allow the analysis of the entire group at the levels at which these elements occur in common crustal rocks (for example, analysis by ICP-MS)

As a result, over the past several years, many quantitative data on the distribution of platinum-group elements in ultramafic to mafic stratiform complexes (Gijbels et al. 1976; Naldret, 1981; Keays et al., 1981), ultramafic nodules (Mitchell and Keays, 1981), oceanic basalts (Crocket and Teruta, 1977) and ophiolitic complex have been published. These studies, in general, indicate that the highest absolute abundances of platinum-group element (PGE) concentrations are generally associated with nickel sulphide and chromitite occurrences in ultramafic-mafic rocks within large layered intrusions (Stillwater, Bushveld, Noril'sk), or in greenstone belts of komatiitic affinity (Kambalda, Katniq deposit).

The PGE abundance patterns of basalts are quite different from those of mantle peridotites. Information on the abundance and distribution of PGE in the upper mantle is, therefore, relevant to theories of basalt petrogenesis and the origin of economic deposits of magmatic PGE-rich sulphide ores. But the abundance and distribution of PGE in these rocks is not well constrained. It is difficult to establish the primitive nature of these rocks due to many successive stages of liquid extraction that may have occurred. As a result, there are wide variations in abundance between the original mantle source, the initial liquids and the melt products. Furthermore, behaviour of the PGE + Au during magma generation (e.g. Campbell and Barnes, 1984; Brugmann et al., 1987) and evolution (e.g. Crocket and Chyi, 1972; Hertogen et al., 1980; Crocket, 1981; Keays 1982; Hamlyn et al., 1985) is poorly understood, thus complicating interpretation of basaltic PGE data in terms of magma generation at convergence zones. The only consistent picture to emerge from these studies is that PGE distributions appear to be principally controlled by partial melting, which determines the PGE concentrations in the magma and subsequent fractional crystallization (Hertogen et el., 1980) of poorly soluble PGE (Os, Ir, Ru) and more soluble PGE (Rh, Pt, Pd) in basaltic melts (Amossé et al., 1987). Consequently Ir, Os, and Ru tend to be concentrated early in the most refractory cumulates (chromite and olivine); whereas Rh, Pt and Pd behave apparently as incompatible elements and get progressively concentrated in the liquid. However, apart from this general feature, the restricted nature of the database has prevented any detailed modelling of the geochemical behaviour of the PGE in these rocks. This partly reflects the difficulty of accurately determining background PGE concentrations (Greenough and Owen, 1992), a

situation that is changing as new analytical techniques and instrumentation are developed (Jackson et al., 1990).

Surprisingly few ultramafic-mafic rocks or their extrusive equivalents (e.g. tholeiitic basalts) related to arc magmatism have been analyzed for their PGE concentrations. So little is known about the geochemical behaviour of PGE in arc systems, despite their likely application to fundamental geological problems such as formation of magmatic sulphide deposits, mantle evolution and its differentiation. However, in southern Kohistan arc, Mesozoic plutonic rocks in which PGE's concentrations have been reported by Miller et al. (1991), a number of layered mafic-ultramafic complexes may contain or have the potential for PGE mineralization.

In this part, we report on whole rock abundance data on PGE's+Au concentrations in Thak Gah Ultramafic-Mafic, Chilas; Spat Ultramafic-Mafic, and Jijal Ultramafic-Mafic Complex, aiming to add to the data set by presenting results for PGE and Au for convergence zone ultramafic-mafic rocks.

We also want to improve our understanding of factors controlling PGE distribution in these mafic-ultramafic rocks; to locate platinum-group minerals (PGM) and to determine their chemical compositions; and to examine their petrogenetic and economic implications.

CHAPTER-1
GENERALITIES OF PLATINUM-GROUP ELEMENTS AND ANALYTICAL METHODS

CHAPTER-1

1-PLATINUM-GROUP ELEMENTS: DEFINITION AND CHARACTERISTICS

1-1 - General Characteristics of PGE's:

The platinum-group elements include osmium (Os), iridium (Ir), ruthenium (Ru), rhodium (Rd), platinum (Pt) and palladium (Pd). These elements are said to be 'noble', because in the metallic state they are relatively inert to corrosion, and are not easily oxidized. Gold (Au), stricktly speaking, is not a platinum-group element but it is a noble metal and will be included with the PGE's. In recent years, the latter are receiving world-wide attention as an attractive exploration target because they offer the dual attraction of rare, high value precious metals as well as major industrial uses. Because of their physico-chemical nature, the PGE's have multiple applications (Table 15). While the catalytic properties of PGE's are widely utilized within the chemical industry, palladium has a fairly widespread use in telephone exchanges. Pt has a vital role in vehicle emission control, where it performs the dual function of reducing nitrous oxide to nitrogen and oxygen, while hydrocarbons are oxidized to carbon dioxide and water. Because of their resistance to corrosion, they have multiple uses in medical, chemical as well as in dentistry and jewellery.

The PGE's generally occur in the earth's crust and upper mantle at part-per-billion levels, though Os and Ir may be as low as part-per-trillion levels in basalts and granites, and all the PGE's + Au may reach part-per-million levels in ore deposits (Crocket et al., 1967; Crocket, 1979; Hertogen et al., 1980).

The most obvious characteristics displayed by the PGE's are their siderophile nature and their affinity for sulphides in mafic and ultramafic rocks (Arculus and Delano, 1981). Rhenium (Re) is considered to be a PGE by some cosmochemists (e.g. Chou, 1978); however, Re differs from the PGE's in forming stable oxyanions (e.g. ReO_4^-, ReO_4; Cotton and Wilkinson, 1972) at relatively low oxygen activities, and Re shows little coherrence with the noble metals in terrestrial environments.

In the past, there are relatively few studies of PGE's in typical crustal and mantle rocks (Crocket, 1979). Most studies of PGE's geochemistry have been restricted to ore deposits. and, therefore, the PGE's remain one of the least understood geochemical groups. The understanding of PGE's geochemistry has been constrained until relatively recently by the inability to analyse these elements at levels in which they typically occur in unmineralized rocks. Recent developments in the analytical field, particularly with the aid of radiochemical, instrumental neutron activation analysis (INAA) and ICP-MS, and improved knowledge of the equilibrium partitioning of PGE's between sulphide liquid and silicate melt, offer the potential for significant new insight into processes that influence PGE's concentration in the crust and in

Table 15. Technical applications and industrial uses of platinum-group elements.
Applications techniques et industrielles des éléments du groupe du platine.

	Applications and Industrial uses
Os	catalyst, incandence lamps, micrography, stylograph points, metallization, coatings.
Ir	catalyst, filamants of incandence lamps, electronic industry, thermocouples for measurement of high temperatures.
Ru	catalysts, incandence lamps, electrical industry, stylograph points, compas pointer, electrodes, coating against corrosion, photographic emulsions and thick-film integrated circuits.
Rh	catalysts, Pt-Rh thermocouples for measurement of high temperatures, electronic industry, electrodes, jewellery, alloy with Pt to produce nitrous oxide, resistance to chemical and mechanical resistance, use in dentistry, crucibles.
Pt	Catalysts, metrology, Pt-Rh thermocouples for measurement of high temperatures, thick-film integrated circuits onto ceramic substrates, electro-mechanical switch for telephone exchanges, fuel cells, vehicle emission control, jewellery, dentistry, chemical industry for nitrous oxide, crucibles.
Pd	electronic industry for thick-film integrated circuites onto ceramic substrates, hydrogenization, jewellery (alloy of Au+Pd), fabrication of dental crowns and bridges, photographic films with emulsion, protection from oxidation.
Au	jewellery, dentistry, electrical industry.

the ore deposits. The most comprehensive survey of PGE geochemistry has been presented in books by Cabri (1981) and Buchanan (1988).

1-2 Geochemical Properties

Although in some respects the PGE's resemble one another, but their chemical behaviour differs markedly from that of their cogeners in Group 8b, Fe, Co and Ni. Some of their physical properties are shown in Table 16. Their metallic properties are such that they may be grouped in pairs. These pairs are : (1) Ru & Os, (2) Rh & Ir, (3) Pd & Pt. Group (1) metals crystallize in an hexagonal c-packed lattice. These elements are thus hard, least malleable, and have the highest moduli of elasticity, rigidity and bulk compressibility. In contrast, Pd and Pt have a face-centered cubic crystal lattice and are relatively soft and malleable. Alloys of these metals with Rh and especially Ir become very strong. Despite crystallographic differences, there is a clear relationship expressed in the chemistries of the PGE's: they tend to be mutually soluble in one another and can frequently substitute for one another in compounds with other elements.

These noble metals are fourth and fifth row transition elements of group V111 in the periodic table, so the outer electrons of their ions are d electrons. Some PGE's (Pd, Rh and Pt) form metal-rich chalcogenides (e.g. S, Se, and Te) with short metal-metal bonds; these compounds are probably characterized by metallic bonding, and it is doubtful that meaningful oxidation states can be assigned to the PGE's in metal-rich chalcogenides.

1-3. Geochemical Behaviour

several attempts have been made to predict the geochemical behaviour of the PGE's on the basis of crystal chemical and thermodynamic arguments (Crocket, 1969; Keays and Crocket, 1970; Arculus and Delano, 1981; Amossé et al., 1990). At present, there is no consensus in the literature as to what factors control PGE's geochemistry.

In particular, Gottfried and Greenland (1972) suggested that differences in source mineralogy, depth and percentage of melting, extent of previous melt extraction, and variations in source region PGE's concentrations may be responsible for, or contribute to, apparent concentration variations of the PGE's in basaltic rocks. Moreover, the investigations of Barnes et al. (1985, 1988), Peach et al. (1990), Fleet et al. (1991) and Stone et al. (1990) have led notably to a better understanding of PGE's behaviour by taking account of their partition coefficients with the different liquids or solid phases. PGE's behaviour is also controlled by major element composition of the magma (Haughton et al. , 1974) which act on the variations

Table 16. Physical properties of the platinum-group elements.
Propriétés physiques des éléments du groupe du platine.

	Os	Ir	Ru	Rh	Pt	Pd	Au
Atomic Number	76	77	44	45	78	46	79
Atomic Weight	190.2	193.1	101.7	102.91	195.23	106.7	197.2
Atomic Radius, (A°)	1.33	1.35	1.34	1.34	1.38	1.37	1.37
Valence state	3, 4, 6, 8	1, 3, 4	2, 3, 4, 6, 8	1, 3	2, 4	2, 4	1
Lattice Type	h. c. p	f. c. c	h. c. p	f. c. c	f. c. c	f. c. c	f. c. c
Lattice constants, a,c, A°, c / a ratio	a = 2.714 c = 4.316	a = 3.84	a = 2.68 c = 4.261	a = 3.82	a = 3.93	a = 3.888	a = 4.078
Density (g/cm^3) at 20°C	22.7	22.65	12.3	12.42	21.45	12.03	19.32
Melting Point, °C	2700	2454	2400	1966	1774	1555	1064
Boiling Point, °C	5000	4400	4150	3727	4050	3600	2966
Magnetic Susceptibility, (cm^3/gx10^6)	+ 10	+ 25	+ 43	+ 102	+ 189	+ 558	-

h. c. p. = hexagonal close-packed f. c. c. = face-centred cubic

Westland (1981); Legendre (1982); Fischer (1988)

The preferences of the PGE's for different co-ordinations and oxidation states may be a fundamental cause of noble metal fractionation during partial melting. The elements Os, Ru and Ir show the strongest preference for octahedral co-ordination; Pt and Rh show a lesser preference for octahedral co-ordination; and Pd and Au strong preference for distorted, or unusual site geometries. Octahedral sites are abundant in the solid silicates, oxides and sulphides which might contain noble metals in solid solution in the mantle {e.g. olivine, spinel, and perovskite monosulphide solid solution (MSS)}, but the distorted or unusual site geometries are probably much more abundant in partial melts. Hence, partial melting may provide a fractionation of the PGE's such that the elements preferring distorted sites (Pd, Pt, Rh and Au) are enriched in the melts over the elements preferring octahedral co-ordination (Saint Jours, 1988).

1-4. Geochemical classification of PGE's

On the basis of similarities in geochemistry, the PGE's are frequently separated into two groups, based on systematics from a growing database of geochemical analyses from igneous systems, recently reviewed by Barnes et al. (1985).

(1) **The *iridium*-PGE's (IPGE's)** are Os, Ir and Ru, and these elements are considered compatible in igneous systems. They are often associated with chromite in the form of alloys or sulphides in dunitic cumulates.

(2) **The *palladium*-PGE's (PPGE's)**, Rh, Pt and Pd comprise the second group, and they are thought to be incompatible in igneous processes. These elements are easily associated with sulphides of Fe, Ni and Cu (Barnes et al., 1985), often occurring in norites, gabbros, and sometimes in dunites.

The differentiation of the PGE's into two sub-groups, related either to an oxidized phase (chromite) or a sulphide phase (pentlandite, chalcopyrite), suggest some control based on oxygen or sulphur fugacity during the fractionation processes. This has already been demonstrated by Amossé et al. (1987, 1990).

2 - DISTRIBUTION OF PGE's

Available data on PGE's in rocks are listed in Table 17, and is illustrated in Figs. 81, 82, & 83. There are three major factors which should be evaluated in regard to PGE distribution in layered mafic-ultramafic complexes, namely (1) PGE's abundances in the magma source; (2) transport mechanisms of the PGE's, and (3) PGE's concentration mechanisms (magmatic and non-magmatic) in the magma chamber. Several favourable conditions have been proposed including (1) anomalous enrichment of PGE and Au in the mantle source, (2) specific rock types (e.g. boninite, komatiite and lamprophyre) as parent

Table 17. PGE, Au, Cu, Ti and Y abundances in various mantle-derived mafic-ultramafic rocks.
Abondance des EGP, Au, Ti and Y dans diférentes roches mafiques et ultramafiques dérivées du manteau.

	MgO %	Pd (ppb)	Ir (ppb)	Pt (ppb)	Au (ppb)	Cu (ppm)	Ti (ppm)	Y (ppm)	References
Fertile mantle	38	4	4	7	1	28	1300	4.6	(1,3,4,6,9)
Komatiites									
Abitibi, Canada	24	10	1.2	10	3	50	2400	9	(5,12,13)
Eastern Goldfields	25	9	1.5	-	4.5	6.5	2300	10	(2,5,11)
Belingwe	18	13	0.5	12	1.8	73	2520	9	(5)
Gorgona Island	18	12	1.7	-	5	120	3800	14	(12)
Kambalda	10	16	0.35	-	5	94	3660	18	(11)
Picrites									
Disko Island	17.1	11	1.1	-	4	-	7380	-	(5)
King Island	-	20	0.6	-	3	18	1600	-	(5,8)
SHMB = siliceous high magnesian basalts									
Munni Munni	12	18	-	14	3	85	4000	11	(15)
Cooya Pooya	14	12	0.4	12	3	60	3000	12	(15)
Bushveld B4	12	12	0.35	17	3	56	2160	13	(10)
Low-Ti-Tholeiites									
Woodward Dolerite	9	14	0.08	16	5	80	3300	14	(15)
Tasmanian Dolerite	6.7	-	0.1	-	-	-	3900	20	(14)
Boninite									
average	12	15	-	-	2	20	1200	6	(8)

References:

(1) Jagoutz et al. (1979);
(2) Ross and Keays (1979);
(3) Morgan et al. (1981);
(4) Mitchell and Keays (1981);
(5) Keays (1982a,b);
(6) Sun (1982);
(7) Ford (1983);
(8) Hamlyn et al. (1985);
(9) Barnes et al. (1985);
(10) Davies and Tredoux (1985);
(11) Redman and Keays (1985);
(12) Brugmann et al. (1987);
(13) Barnes and Naldrett (1985);
(14) Hergt (1987);
(15) Sun et al. (1991);

- = not determined

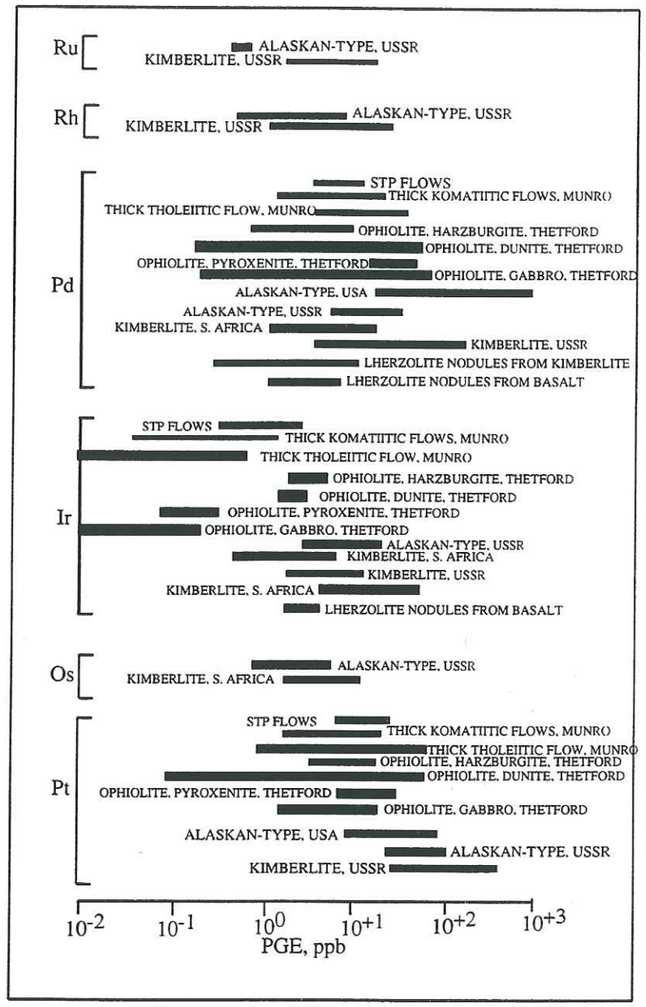

Figure 81. Range and average values for PGE in various types of ultramafic rocks (Crocket, 1981).
Valeur moyenne et intervalle possible pour chacun des éléments du groupe des platinoïdes (EGP) dans différents types de roches ultramafiques (Crocket, 1981).

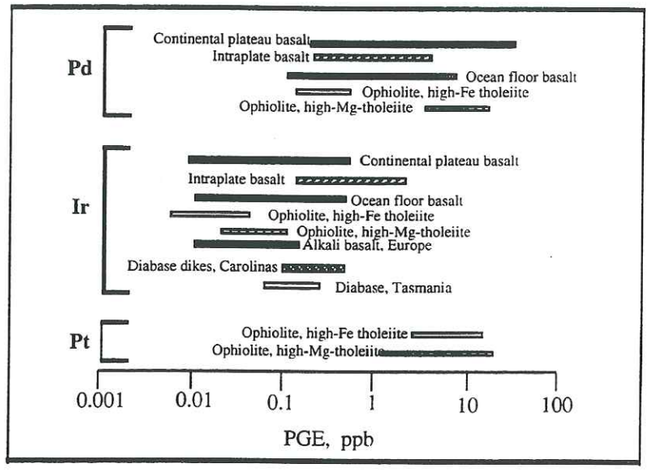

Figure 82. Range and average values for PGE's in various types of mafic rocks (Crocket, 1981).
Valeur moyenne et intervalle possible pour chacun des EGP dans différents types de roches ultramafiques (Crocket, 1981).

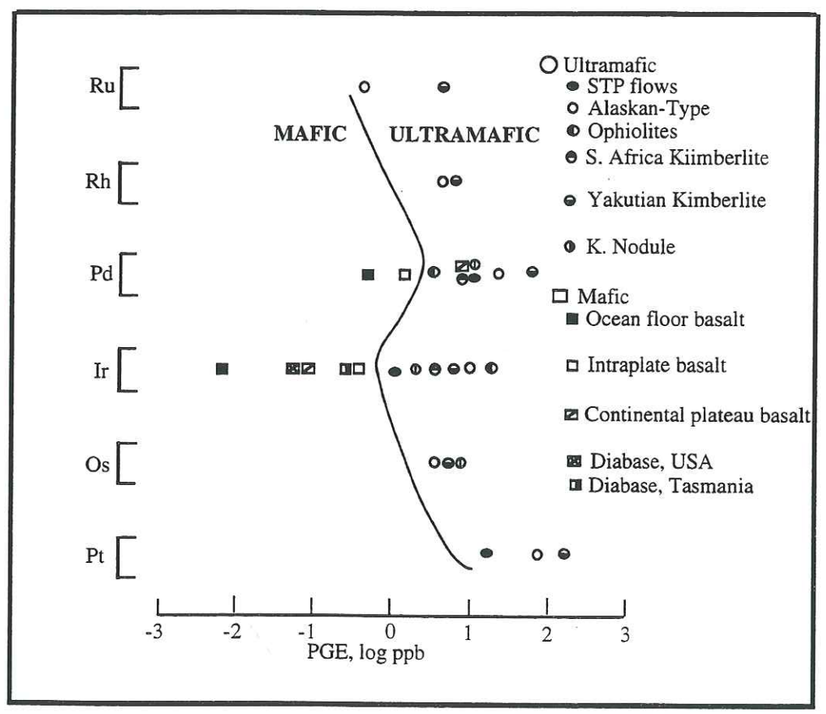

Figure 83. Comparison of average PGE contents of ultramafic and mafic rocks, showing the generally lower concentrations in mafic rocks (Crocket, 1981).
Comparaison des teneurs moyennes en EGP de roches mafiques et ultramafiques. Les roches mafiques ont en général des concentrations plus faibles (Crocket, 1981).

magmas (Hamlyn et al., 1985; Rock and Groves, 1988; Rock et al., 1988), and (3) very efficient concentration of PGE and Au into small amounts of sulphide droplets from large quantities of silicate melt (high R factor, which is the mass ratio of silicate liquid to sulphide liquid) through convective mixing (Campbell et al., 1983).

2-1. PGE's in Mantle

PGE are concentrated much more in the mantle and core of the earth than in the crust. However, it is clear that the phases hosting the PGE's in mantle source rocks are poorly understood. The possible existence of magma source regions in the mantle anomalously enriched in PGE's can be evaluated in terms of a global survey of PGE contents in a variety of mantle-derived rocks, including ultramafic-mantle xenoliths, and alpine peridotites (Table 17; Fig. 81).

Mantle xenoliths are not necessarily a true representation of the mantle, due to their unique mode of emplacement and their size (usually < 15 cm); possibly more representative samples are those obtained from the larger ophiolitic tectonites and alpine complexes. Ultramafic rocks carry high PGE's contents, and they host economic mineral deposits of the PGE. Mineralogical and geochemical investigations of these mantle materials provide clues as to the cause of low Pd/Ir ratios in alkali basalts and komatiites but high ratios in tholeiites (especially MORB). Relatively undepleted spinel lherzolite xenoliths from alkali basalts and kimberlites show flat chondrite-normalized patterns (Jagoutz et al., 1979; Mitchell and Keays, 1981; Morgan et al., 1981), and in the same range as mantle xenoliths, thus indicating that primitive mantle material may have unfractionated PGE's patterns. The PGE's predominantly reside in intergranular sulphide globules apparently trapped between grains during episodes of partial melting (Mitchell and Keays, 1981). Highly depleted residual mantle materials such as harzburgites and dunites show chondrite-normalized patterns substantially enriched in the high-melting IPGE's relative to low-melting PPGE's (Page and Talkington, 1984; Barnes et al., 1985). The IPGE's are hosted in a wide variety of minor phases (Page and Talkington, 1984; Barnes et al., 1985), which can be summarily referred to as Os-, Ir-, and Ru-based alloys. Modal proportions of these alloy phases apparently increase as sulphide percentages decrease, and it has been suggested (Frey, 1983; cited in Barnes et al., 1985) that they form when the sulphides melt incongruently. However, there are relatively few data on the solid solution of PGE's in silicates and oxides in the mantle.

Sun et al. (1991) have suggested that the average values for suites of fertile mantle samples from different areas are very similar (within 30% ?), and corresponding to about 1% of the PGE's abundances in C1 chondrites (Chou et al., 1983). Studies of Re-Os isotope systematics of mantle derived ultramafic rocks and basalts with ages ranging from Archaean to the present also support a mantle evolution history with close to chondritic Re/Os ratios (Allègre and Luck, 1980; Luck et al., 1988; Walker et al., 1988). Obvious exceptions to this

generalization are garnet lherzolite xenoliths in kimberlites from Lesotho and South Africa, as reported by Paul et al. (1979). They show very high average contents of Ir (18 ppb) and Au (6.9 ppb), but lower Pd content (3.7 ppb), similar to samples from other areas (Barnes et al., 1985).

2-2. PGE's in Komatiites

Ultramafic lavas of komatiitic affinity are considered by many to have been generated by large-percentage partial melting of rising mantle diapirs. Table 17 and Fig. 81 show data on komatiites from various parts of the world ranging in age from 2.7 Ga to about 50 Ma (Ross and Keays, 1979; Keays, 1982a, b; Brugmann et al., 1987; Barnes and Naldrett, 1985). They have fairly constant Ti/Pd ratios ($3x10^5$), similar to those of fertile mantle xenoliths and estimated primitive mantle (e.g. Sun, 1982; brugmann et al., 1987). Even the pillow lavas and spinifex-textured komatiite of the 3.5 Ga James town greenstone belt of south Africa appear to have quite normal PGE, and Au abundances in contrary to the suggestion made by de Wit and Tredoux (1988) that they were derived from a mantle source highly enriched in PGE. The homogeneous distribution of chalcophile elements, Cu, PGE's and Au with respect to the lithophile elements in the convecting mantle since the Archean can be explained by effective convective mixing during the early history of the Earth (Sun, 1982).

Komatiites frequently contain nickel sulphide deposits and magmatic origin for these deposits is widely accepted. This leads to the problem that the absolute abundances of PGE's in the sample depend on the percentage of sulphide present. It might be expected that similarity of PGE's ratios in ores and host rocks would be strong if the ore-forming process involves scavenging of PGE's by an immiscible sulphur-rich phase. Pd/Ir ratios in nickel-copper ores of komatiitic host rocks and spinifex-textured peridotites (STP) flows vary between 5.9 and 8.8 which suggest that, on the average, the proportions of Pd and Ir in nickel-copper sulphide ores and STP flows are essentially identical.

2-3. PGE's in Lamprophyres

The suggestion that some magmas such as lamprophyres were derived from the core-mantle boundary and consequently are anomalously enriched in PGE and Au (Rock and Groves, 1988) can be evaluated by examining PGE's and Au abundances in komatiites and Icelandic and Hawaiian tholeiites. These are the best candidates of magmas derived from mantle plumes believed by many geoscientists to have originated at the core-mantle boundary. Available data on PGE and Au abundances in komatiites, as discussed above indicate that they were not derived from PGE and Au enriched mantle sources (Sun et al., 1991). This conclusion also applies to the tholeiites of Iceland and the Hawaiian islands (Crocket and Kabir, 1988). Furthermore lamprophyres commonly show strong Nb depletion relative to La; this

suggests a connection to subduction zone related processes in the shallow parts of the upper mantle (Johnson et al., 1978; Wyman and Kerrich, 1989).

2-4. PGE's in Layered Intrusions

Economic deposits of PGE's are associated with layered mafic-ultramafic complexes (Naldrett, 1989), as in the cases of the Merensky Reef in the Bushveld Complex and the Johns-Manville prospect in the Stillwater Complex. Therefore, an examination of these two complexes could help in explaining the origin of PGE's distribution in layered intrusions.

The Bushveld and Stillwater Complexes exhibit considerable morphological, lithological, mineralogical and chemical similarities. The Bushveld Complex hosts the world's largest PGE's reserves in the Merensky Reef, the Upper Group Chromitite layer or UG-2 Reef and in cross-cutting dunitic pipes. Gijbels et al. (1974) have originally elucidated the PGE's geochemistry of Bushveld Complex which followed by recent works by many researchers (Campbell et al., 1983). The proposed parent liquids for the Bushveld Complex have (Pd/Ir) ratios of approximate 30 (Sharpe, 1982), much lower than either than continental tholeiites or ocean-floor material. The Pd content is similar to that of continental tholeiites but the Ir content is three times higher. In the ore-bearing horizons UG-2 (Upper Group 2) and Merensky Reef the Pd/Ir ratios are 14 and 20, respectively. This drop in Pd/Ir ratio is achieved by increase in Ir by a factor of 450 over the initial liquid while Pd only increased by a factor 170. Similarly, in the Merensky Reef, Ir increased 211 times over the second-cycle initial liquids while Pd increased by a factor of 153. Since both of these reefs contain chromite it could be argued that the Ir was concentrated by the chromite. Cousins and Vermaak (1976) and Vermaak and Hendriks (1976), however, discount this on the ground that there is no relation between the PGE's and Cr. Although the precise genetic relationship between PGE's and chromite may be a source of disagreement, it should not obscure the widespread association of PGE's and chromite applicable in many different geological settings. The overall shape of the PGE's patterns for both the horizons is similar, a steady increase from Ir to Pd.

Page (1971) and Page et al. (1972; 1976) have provided an extensive data base on the variation and distribution of PGE in the Stillwater Complex. Their studies identify a number of environments in which PGE's enrichment occurs. During normal fractional crystallization, ratios of Pt and Pd to total PGE's increase while ratios of Rh, Ru and Ir to total PGE decrease. These trends are similar to those applicable to PGE's in many other geological environment and closely resemble non-sulphide-bearing continental tholeiites, except for the low-level Pt anomaly. However, Pd is enriched by a factor of 5 and Ir by a factor of 2.5 over continental tholeiites. The chromite seams of the lower portion of the Stillwater Complex exhibit an overall enrichment over the initial liquid but unlike the patterns of chromitite from the ophiolitic complexes. However, the (Pd/Ir) ratio of the Stillwater chromitites is much lower (14) than that of the initial liquid (220), indicating that the chromite may have concentrated Ir.

2-5. PGE's in Magmatic Liquids

The PGE's abundance patterns of basalts are quite different from those of mantle peridotites. This point is illustrated in Figure 84, in which chondrite-normalized noble metal abundances of basalts and peridotites have been plotted versus the noble metals arranged in order of decreasing metal melting temperatures. The noble metal abundance patterns of basalts show fractionation of the IPGE's from the PPGE's. This fractionation has either taken place during partial melting or during a subsequent process such as fractional crystallization (Hertogen et al., 1980).

3 - PGE's and PGM's in Ore Bodies

The aim of this section is to provide a general genetic framework in which to consider the several types of deposits of the PGE's (Os, Ir, Ru, Rh, Pt, Pd). As can be seen from Figure 83, the average Pt content of unmineralized mafic and ultramafic rocks is approximately 10 ppb, with a range from 0.1 to 500 ppb, the concentration of this element in PGE deposits are 1000 to 10,000 ppb. This suggests that the geologic processes which are responsible for formation of a PGE deposit involve enrichment factors of approximately 100 to 1000; e.g. partial melting, crystal fractionation and possible remobilization with hydrothermal solutions. Although the sulphide content of igneous rocks hosting magmatic PGE's deposits can be highly variable, the precious metals display a ubiquitous association with chromites or sulphides, which has led most researchers to suggest that formation of an economically significant deposit is dependent upon the segregation of chromite or immiscible sulphides, into which the PGE's preferentially partition (Naldrett and Duke, 1980). The ultimate source of the PGE's is the mantle. In order to obtain a magma rich in PGE's, sufficient partial melting (more than 20%) of the mantle must occur for the sulphides in the mantle to dissolve into the silicate magma and release the PGE's from the mantle into the magma. For sulphide to become a discrete phase within a mafic/ultramafic magma, the solubility of sulphur in the magma must be exceeded. The precipitation of an immiscible sulphide phase, which is critical step in the formation of a PGE's deposit, may result by: (1) assimilation of sulphur from an external source, (2) rapid cooling of the magma, (3) assimilation of silica, (4) blending of two or more disparate magmas (Irvine, 1975, 1977; Todd et al., 1982) and (5) Fe activity.

The study of the PGM mineralogy is an invaluable aid in understanding the mechanism of concentration and possibly the origin of PGE's. Much work has been done to identify the many and chemically complex minerals such as 'CIM Special Volume 23' (Cabri, 1981).

In general, PGM-bearing minerals occur as opaque inclusions in other minerals, with maximum dimensions of about 200 um. In polished-sections, PGM-bearing minerals are usually characterized by high reflectivities. Due to the minute grain size and lack of suitable single crystals, highly refined X-ray crystallographic data are difficult to obtain. X-ray powder

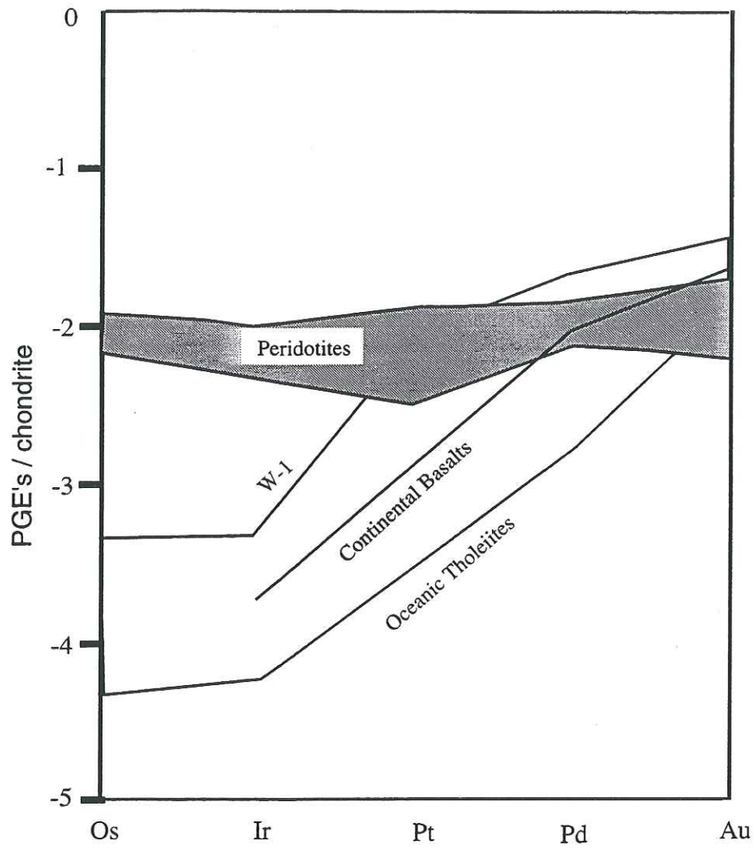

Figure 84. A comparison of the abundances of PGE's in basalts and mantle peridotites. The range for peridotites is derived from the average of analyses of the Mt. Albert alpine peridotite by Crocket and Chyi (1972), the lherzolite nodule averages of Mitchell and Keays (1980) and Morgan et al. (1980), and the range of Pt values reported for the USGS standard PCC-1 (Ahmad et al., 1977). The continental basalt average is from Paul et al. (1979) and Hertogen et al. (1980). The values for W-1, a diabase, are from Ahmad et al. (1977). All abundances are normalized to the C1-chondrite averages of Crocket et al. (1967).

Teneurs moyennes en EGP dans des basaltes et des péridotites mantelliques. Les concentrations sont normalisées aux valeurs moyennes des chondrites C1 de Crocket et al. (1967).

diffraction data, electron microprobe analyses and ore microscopy descriptions are generally combined for positive identification of a mineral.

The studied PGM deposits depict the diversity of platinum-group mineralogy and their modes of occurrence which are linked to the various environments of formation and to the original chemistry of these particular environments. A classification of PGE's deposit types is given in Table 18, based upon the inferred process by which the PGE's were concentrated, and where the PGE's are the primary product, a co-product or a by-product.

In the crust of the earth, platinum-group minerals (PGM) are concentrated in basic and ultrabasic rocks in quantities ranging from rare micrometer-sized bleb-like inclusions to ore bodies with abundant Ni-Cu sulphides (Naldrett and Cabri, 1976; Cabri and Laflamme, 1976). To have economic deposits of PGM's concentrated in the crust, a transfer of mantle material to the crust is presumed to occur. This transfer of material may take place in two principal ways according to Naldrett (1981):

3-1. Orthomagmatic Deposits

Melting of portions of the mantle under different tectonic environments produces ultramfic to mafic magmas which rises into the crust. The rising magma is not necessarily initially rich in PGE's, but in certain cases, such as those forming magmatic sulphide deposits, sulphide droplets may form in the magma, and these droplets would tend to concentrate the chalcophile PGE's within sulphides liquids. The droplets are much denser than the surrounding magma and settle to the bottom of the magma chamber. Such sulphide concentrations are usually of economic interest for Cu, Ni and possibly PGM's. These type of deposits are referred as '**sulphide-rich deposits**'. Examples are: Sudbury deposit in Ontario; Noril'sk deposit in Siberia; Kambalda, Australia.

Cu-Ni deposits of the Sudbury area, Canada, from which Cabri and Laflamme (1976) identified 13 PGM's. These minerals are froodite, insizwaite, kotulskite, merenskyite, michenerite, moncheite, niggliite, sperrylite, sudburyite, unnamed Pd(Te,Sb,Bi), unnamed PdSb and unnamed AgPdTe.

In the disseminated sulphide ores (Cu-Ni sulphide ores) of the Noril'sk, USSR, isoferroplatinum and cooperite are the main platinum-group minerals (Genkin and Evstigneeva, 1986). The textural features indicate that PGM's formed at a late stage of crystallization of the ores.

Those PGE's deposits whose formation is attributed to mixing of more than one magma are called as '**reef-type deposits**'. The Merensky-Reef (sulphide), UG2 reef (chromitite) and platreef in the Bushveld Complex, South Africa, together with the J-M Reef (sulphide) in the Stillwater Complex, Montanna, USA, and the Great Dyke of Zimbabwe (sulphide).

Table 18. A classification of PGE Deposits
Une classification des modes de gisements des EGP.

Deposit Class	Examples
1. ORTHOMAGMATIC	
1a) Magma Mixing	UG2, Merensky Reef, Platreef, Bushveld Igneous Complex, J-M Reef, Stillwater Igneous Complex, Great Dyke, Zimbabwe,
2b) Magma Contamination	Noril'sk, USSR Sudbury, Canada Kambalda, Australia Thompson, Canada
2. PLACER	Witwatersrand, South Africa
3. HYDROTHERMAL	New Rambler, USA Rathbun, Canada Allard Stock, USA Kupferschiefer, Poland Coronation Hill, Australia

Vermaak and Hendriks (1976) found that the major discrete platinoid minerals are braggite, cooperite and laurite, with minor amounts of sperrylite in the Merensky Reef, Bushveld Complex, Republic of South Africa.

In the chromite seams of the Stillwater Complex, Talkington and Lipin (1986) determined that laurite occurs as inclusions in chromite, and that the occurrence of sperrylite and isoferroplatinum is confined to the interstices of chromite.

Concentrations of PGE's also occur in conjunction with chromite concentrations in '**ophiolitic complexes**', but these contain high Ru, Ir and Os concentrations and very low Pt and Pd concentrations, and are not viable economically. Exceptions are the deposits of the Unst (Shetland) ophiolite (Prichard et al., 1986), particularly the Cliff deposits, which are extremely rich in Pt and Pd. The other example are Thetford Mines in Canada and Krasta in Albania.

3-2. Placer Deposits

Large slabs of mantle material are thrust into the crust along zones of weakness such as convergence zones. Where overlying rocks of a mantle slab are eroded, especially in climates suitable to rapid chemical and mechanical weathering, very dense PGE's in the slab may then be concentrated in gravels or river beds and streams that drain the area, giving rise to placer deposits (e.g. Ural Mountains of the Russia; Choco, Colombia).

Placer deposits of the PGE's are spatially associated with mafic/ultramafic complexes, most commonly of 'Alaskan-' or 'Alpine-type' of mafic/ultramafic intrusions. The only known paleoplacer PGE's deposit of economic significance, the Witwatersrand, may have resulted from greenstone belt erosion, although arguments still rage as to the origin of other constituents, such as gold (Skinner and Merewether, 1986).

3-3. Hydrothermal Deposits

Hydrothermal PGE's deposits form from epigenetic fluids, whose compositions are, as yet, not well constrained, in a wide variety of geological environments; including: (1) associated with shear zones cutting mafic/ultramafic host rocks; (2) associated with alkaline porphyry copper-precious metal deposits; (3) in late diagenetic flow of metal-bearing brines in carbonaceous sediments. This deposit type is generally rich in palladium (± Pt), with respect to the other PGE's (Naldrett, 1981).

The New Rambler copper-iron deposit, Medicine Bow Mountains, Wyoming, has been interpreted as representing a nonmagmatic accumulation of PGE's and other metals that have been concentrated by processes of hydrothermal leaching of ordinary gabbroic rocks and redeposition of the leached metals along shear zones as Pd- and Pt-rich copper sulphide ore (McCallum and Orback, 1968).

Ten platinoid minerals have been encountered in New Rambler ores and these are native Pt, sperrylite, and eight tellurides and bismuthotellurides of Pd and Pt. Hydrothermal PGE's deposits have yet to contribute significantly to global PGE production, although this may be a function of lack of exploration for this deposit type.

3-4. Conclusion

The relationship between sulphides and PGM's is still not clearly understood. Some researchers have shown that sulphides act as collectors (Genkin and Evstigneeva, 1986; Naldrett, 1981). However, other researchers discredit this information (Hiemstra, 1979, 1986). Some believe that chromite is the collector in some cases (Hiemstra, 1986). This hypothesis is also debatable (Crocket et al., 1976). Mineralogical studies may be the key to understanding the mechanisms of concentration and possibly the origin of PGMs. Therefore, research shall have to increase in order to understand more thoroughly the concentration processes of PGM's as well as the geologic environments in which they may be found

4- PGE's Analytical Procedure

4-1 PGE's Analyses

The analytical chemistry of the PGE's may be said to reflect their occurrence in nature as rare, discrete, inhomogeneously distributed, mineral species, and their very high financial values. These factors have resulted in the need for an analytical method offering complete dissolution of a representative sample allied with an accurate measurement technique.

In general, the classical lead assay provides pre-concentration for Pt, Pd and Rh (Au), although their efficient collection on a silver cupellation bead is critically dependent on 'flux' composition and assay conditions. The neo-classical fire assay procedure with nickel sulphide collection (Robert et al., 1971) is gaining popularity. However, the difficulty of obtaining nickel sulphide entirely free of PGE's remains a drawback in this method (Amossé, 1997). More recently, Stone and Crocket (1993) have developed a radiochemical NAA technique - using Te as a carrier - which enables the determination of Pd, Pt, Ir, Au, Ag, Se, As and Sb. For all that, radiochemical techniques that include the manipulation of irradiated samples can be dangerous for the analyst and necessitate complex facilities with strict radioprotection controls (Amossé, 1997). The advent of ICP-MS, with its multi-element capability and high sensitivity for heavy elements, offers a valuable alternative approach for the determination of the PGE's.

Amossé et al. (1986) have described an analytical technique which involves dissolution of samples by fusing with sodium peroxide in a zirconium crucible, and a wet chemical reduction and extraction of the PGE's from solution using stannous chloride in the presence of Se and Te carriers by 'electrothermal atomic absorption spectrometry (ETAAS)'. The extraction yield obtained for Pt, Pd, Rh was satisfactory but for Ir and Ru, the results were not up to the

standard. But satisfactorily extraction yield between 95 and 100 % is achieved in the presence of a catalyst (KI; (Amossé, 1998).

4-2. Used Analytical Procedure

The PGE's and Au were determined at Grenoble Laboratory by ICP-MS, after extraction by hydrolysis / reduction using $SnCl_2$ and collection onto Se-Te (Amossé, 1997). The outlines of the precedure are as follows:

(1) Five grams of sample are carefully mixed with 20 grams of Na_2O_2, 3-4 g of $NaKaCO_3$ and 3 g of KOH.

(2) The mixture is placed in a zirconium crucible and fused until homogenization of the mass is completed.

(3) After cooling, the fused product is dissolved in hot water (250-300 ml), and the solution is acidified by HCL 10M (50 ml) in order to dissolve the oxides. 1 ml of H_2O_2 (30%) is added to bring about reduction of $Cr^{(VI)}$ to $Cr^{(III)}$.

(4) 10 ml of a solution is added containing 5 mg Se and 5 mg Te (in the form of their oxides) as well as 10 ml of a solution containg $500g.1^{-1}$ KI (5g). Then, the final solution (200 ml) is made up to 4N HCL, by adding 100 ml of HCL 10M.

(5) The solution is brought to boiling and then dropwise additions are made of $SnCl_2$ ($20g.1^{-1}$ Sn freshly prepared) while observing the successive reduction of SeO_2, then TeO_2 and finally Fe^{+3}. The solution is left to boil for 10 minutes.

(6) After cooling for 5 min, the solution is filtered under vacuum on a 0.22 mm Millipore cellulose acetate filter. The filtrate is then washed on the filter with HCL 2M.

(7) The filter is transferred to a small beaker (30ml), where the precipitate is dissolved using 2 ml HNO_3 and 3 ml HCL 10M at a temperature of about 50°C. The filter is then rinsed off with distilled water and the solution is evaporated in sand bath at 40°C.

(8) The dry residue is dissolved in 3 ml of aqua regia (2 ml HNO_3 7M and 1 ml HCL 10M), and evaporated to 0.5 ml approximately and the solution is finally made up to produce analyte volumes of 5 ml for ICP-MS.

(9) The measurements were made using a Fisons Instruments VG Elemental ICP-MS instrument (type PQ2turbo+).

5. Methodology for PGE's+Au Studies

The contents of PGE's and Au are extremely, inhomogeneously distributed in the mantle as well as within the mafic-ultramafic intrusions. However, the distribution of PGE's in these rocks is thought to be controlled by sulphide, chromite, olivine and platinum-group minerals. But there persists a paucity of information relating to the distribution of these metals

in these rocks and to distinguish the effects of partial melting, sulphide segregation, chromite and olivine crystallization.

One way to present and compare the total PGE's distribution within the intrusions of different tectonic environments, is the approach of Naldrett et al. (1979). They showed that if the PGE's analyses of sulphides are chondrite-normalized, and plotted in order of descending melting point (Os, Ir, Ru, Rh, Pt, Pd, Au), smooth curves, much like REE patterns, are obtained (various PGE's contents given by different researchers for chondrite C1 are shown in Table 19). But the REE's are lithophile and the order of fractionation of the REE's is related to their ability to substitute for major elements in common minerals, which is controlled by their position in the periodic table. In contrast, the order of fractionation of the PGE's (Os < Ir <Ru < Rh < Pt < Pd) is not the order in which they occur in the periodic table.

Later, Barnes et al. (1985) extended this approach to silicate rocks and demonstrated that it is possible to differentiate between PGE's patterns from silicate rocks, representing the upper mantle (flat PGE's patterns), komatiites (slightly Pd-enriched PGE's patterns) and podiform chromitites (Os-, Ir- and Ru-enriched patterns). However, the chondrite-normalized PGE's patterns from layered intrusions, ocean-floor basalts, continental-flood basalts, alkaline rocks and the non-tectonized portions of the ophiolites cannot be easily distinguished from each other (Barnes et al., 1988).

Naldrett and Barnes (1986) added Cu and Ni next to Au on the chondrite-normalized PGE's patterns. Barnes et al. (1988) suggested that Ni is compatible ($D^{solid/liquid} > 1$) with early crystallizing phases like olivine and pyroxene, therefore, it is logical that Ni should be placed to the left side of Os. Cu, on the other hand, is relatively incompatible ($D^{solid/liquid} < 1$) in the mafic rocks, and hence the position of Cu should be on the right side of Au.

By placing Ni to the left of Os and Cu to the right of Au, even then the chondrite-normalized curve for mantle lherzolites is not smooth (Fig. 85A) because the ratio of Ni and Cu in the mantle to C1 chondrites is approximately 0.13 and 0.17 respectively, and the ratio of Ir and Pd in the mantle to Ir and Pd in C1 chondrites is about 0.00815 (4.4/540). Therefore, the Ni chondrite values will tend to be 16 times (0.13/0.00815) the Ir values and Cu values will tend to be 21 times the Pd values, this gives rise to the trough-shaped PGE's pattern in Figure 85A.

A second approach to presenting PGE's, Ni and Cu is given by Barnes et al. (1988) and their suggested mantle values are given in Table 20. They argue that as most terrestrial rocks are derived from the mantle, it would be more realistic to normalize the PGE's values to average mantle values and adding Ni and Cu to either end of the PGE's pattern. These patterns are called 'mantle-normalized metal patterns'. The average PGE's content of all the mantle material that has been analyzed is close to 0.00815*C1 chondrite (Barnes S-J, et al., 1988). This value is similar to, but slightly higher than, the values obtained by Morgan (1986) for his estimate of the Os, Ir, Pd and Au contents of the upper mantle based on spinel lherzolite but is very close to Chou et al. (1983) estimate that the mantle has experienced an addition of 0.74 % chondrite

Table 19. Published chondrite C1 values for PGE's + Au in the literature (all values are in ppb).
Valeurs publiées pour les EGP et Au des chondrites CI .

Element/Reference	Os	Ir	Ru	Rh	Pt	Pd	Au
McBryde (1972)	700	500	1000	200	1500	1200	-
Nadkarini& Morisson (1974)	970	830	840	-	1020	1560	-
Wasson (1977)	720	800	1900	300	1200	1300	-
Janssens et al. (1977)	757	771	-	-	-	617	-
Naldrett&Duke (1988)	514	540	690	200	1020	545	152
McDonough&Sun (1995)	490	455	710	130	1010	550	140

Table 20. Mantle-normalization values for Ni+PGE's+Au+Cu as proposed by Barnes et al. (1988).
Valeurs de normalisation au manteau pour Ni+EGP's+Au+Cu proposées par Barnes et al. (1988).

Ni	Os	Ir	Ru	Rh	Pt	Pd	Au	Cu
2000	4.2	4.4	5.6	1.6	8.3	4.4	1.2	28

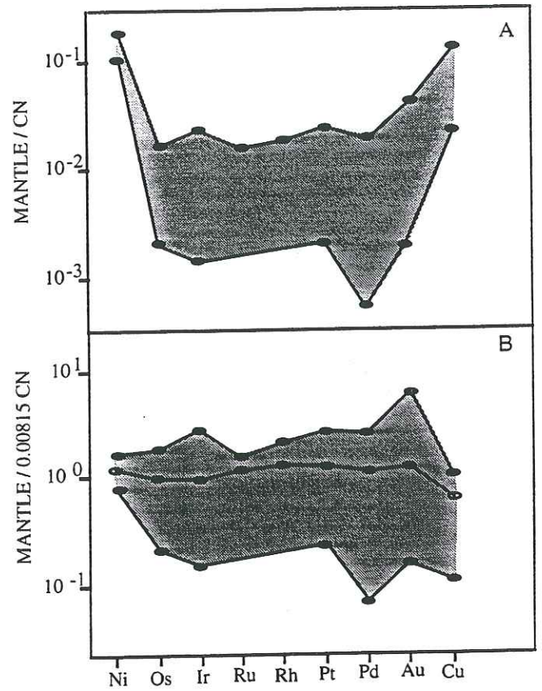

Figure 85. (A) Chondrite-normalized metal patterns showing the range of rocks representing mantle with Ni to the left of Os and Cu to the right of Au. Note the peaks at Ni and Cu which reflect the fact that there is 10-20 times more Ni and Cu chondrite-normalized in the mantle than there are noble metals. If metal diagrammes from ultramafic and mafic rocks are chondrite-normalized they too will have peaks at Ni and Cu because they are mantle derived.
(B) Revised metal pattern for the range of rocks representing mantle-normalized to 2000 ppm for Ni, 28 ppm for Cu, and 0.00815*chondrites for the noble metals (Barnes S-J et al., 1988). Note that the metal patterns are now flat (øpen circle indicat the average value from the data base).

material by bombardment from meteorites after formation of the core. The mantle abundances for Ni and Cu given by Sun (1982) were used for these elements. The main argument against mantle normalization is the heterogeneous nature of the mantle with respect to PGE's distribution contents. Therefore, any value chosen to represent the mantle will be somewhat arbitrary. Moreover, Pattou et al. (1996) reported high-precision analyses of PGE's from fertile upper-mantle lherzolites, suggesting that the upper mantle is heterogeneous in its PGE's content on scales of approximately 100 km. Thus, much of the debate against mantle normalization is still there regarding the relability of the estimate of mantle abundances for PGE's. Despite these drawbacks, the advantages from mantle normalization are significant. The result of this mantle-normalized patterns can be seen by comparing Figures 85 (A) and (B). Figure 85(A) shows the chondrite-normalized PGE's pattern but with Ni next to Os. Note the enrichment of Ni and Cu relative to the PGE's. Figure 85(B) shows the same pattern but normalized to mantle and now it is smooth and almost flat.

To avoid the apparent contradiction with respect to reliability of mantle abundance of the PGE's and, moreover, the presence of sulphides in a rock presents the dilemma of whether to recalculate the data to 100% sulphides or not, Barnes et al. (1988) suggested another approach to present PGE's, Ni and Cu by using the metal ratio diagrammes Pd/Ir versus Ni/Cu, Ni/Pd versus Cu/Ir and Cu/Pd versus Pd. Not only the effects of partial melting, crystal fractionation and sulphide saturation on the PGE's patterns can be seen on these diagrammes, but it is easier to separate rocks representing mantle, komatiites, high-MgO basalts, flood basalts, Pt-reef, ophiolite chromitites and Cu-rich sulphide veins (Fig. 86).

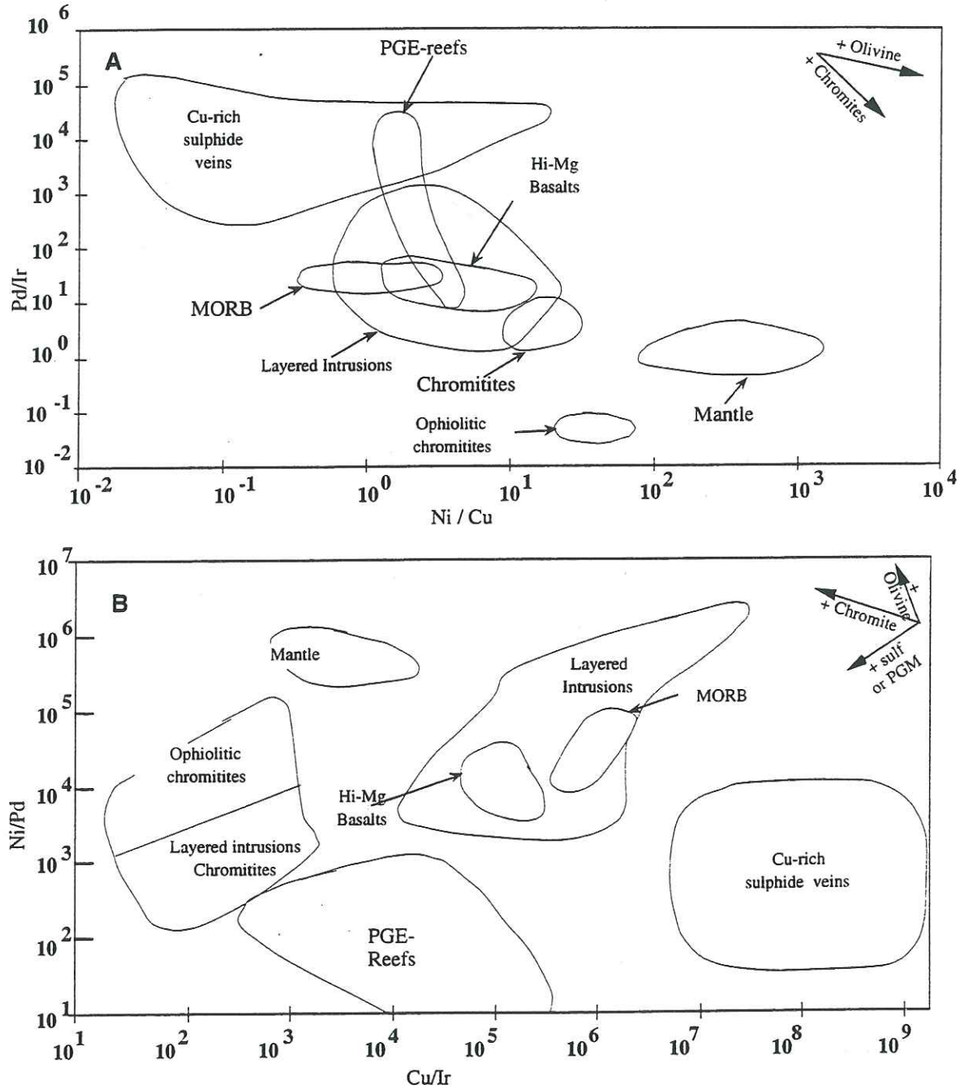

Figure 86. A. Pd/Ir versus Ni/Cu and B. Ni/Pd versus Cu/Ir; for various mafic and ultramafic rock types , Cu-rich sulphide veins and PGE reefs. Vectors indicate the change in metal ratios for olivine, chromite, sulphide and PGM enrichment. Sources for the fields are listed in Barnes et al. (1986, 1988).

CHAPTER-2

PGE'S AND PGM'S IN JIJAL ULTRAMAFIC-MAFIC COMPLEX

CHAPTER-2

1- PGE'S AND PGM'S IN JIJAL ULTRAMAFIC-MAFIC COMPLEX

1-1 PGE's+Ni+Cr+Cu Distribution

Two complete stratigraphic sections were measured and described in order to establish lithological, chemical and PGE's variations through ultramafic to mafic series of the Jijal Complex (see petrographic characteristics in PART-I under Chapter-3). These sections are located; 1) along the Duber River; and 2) along the Karakoram Highway (KKH) (Fig. 87). Forty three samples along the Duber River and thirty two samples along KKH-section from different lithologies, were collected for PGE's determinations and the location of these samples is shown in Figure 87.

The whole-rock PGE's data for the rocks of chromitite, dunite, olivine clinopyroxenite, websterite, garnet websterite, garnet hornblendite and garnet gabbro of the Jijal Complex is listed and grouped according to the section-wise and rock-type in Tables 21A & B.

PGE's distribution with respect to the stratigraphy, is shown in Figures 88 and 89. Total concentrations of PGE's in whole rocks vary from 13 ppb in garnet gabbro to 1417 ppb in garnet websterite along Duber section while along KKH section it is between 7 ppb and 412 ppb. The important variations in PGE's in all these lithologies are reflecting the enrichment of chromitites or sulphides. PGE's concentration appears abundant mainly in the ultramafic lithologies and particularly in the pyroxenites where we find the highest values. More in details, we observe 11 peaks of PGE's enrichment through the whole sequence and these are successively marked as 1 to 6 (according to the unit) and further subdivided in each unit with letters a, b, c and d, particularly along the Duber section which was studied in more detail. Although the pyroxenites have the higher contents of PGE's, the statistical results show that, in the case of garnet websterite, the variance is high and this is because the modal content of sulphide is higher in these rocks (total concentration = 1417 ppb; Duber Valley) than in the other rock types. KKH- and Duber-sections (Figs. 88 & 89) show an enrichment of Cr in the ultramafic zone, with the maximum concentrations occurring in the dunite unit. But the garnet gabbros are depleted with respect to Cr content. The distribution pattern of Ni is normally similar to that of MgO (Fig. 75) with marked peaks within the dunite units representing the abundances of olivine while Ni enrichments are due to sulphides in pyroxenites and gabbros. Anyhow, the distribution of the PGE's-Ni-Cu appears to be independent of the variation in silicate phases along the KKH and Duber sections.

The whole-rock concentrations of PGE's+Ni+Cu in the different rock-types of the Jijal Complex are as follows:

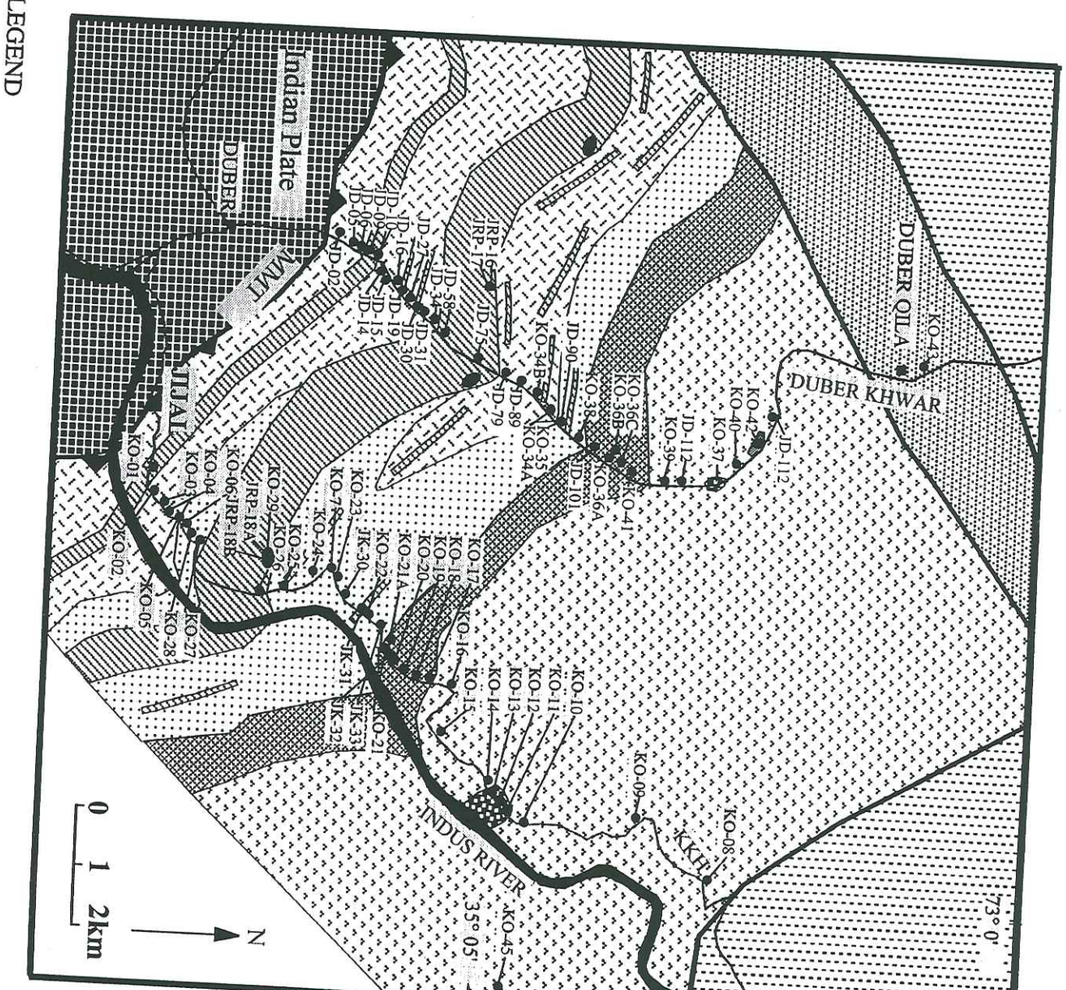

LEGEND

Jijal Complex

- Garnet Hornblendite
- Garnet Gabbro
- Garnet Pyroxenites
- Websterite (with dunite layers)
- Dunite
- Olivine -Clinopyroxenite (with dunite layers)
- Kamila Amphibolite
- Ophiolitic Serpentinized dunite
- Indian Plate
- Major fault
- Chromite Mine
- Main Mantle Thrust (MMT)
- KO-02 Sample No.

Figure 87. Locations of analyzed samples in the Jijal Complex, Kohistan Arc, Pakistan
Localisation des sites de prélèvement dans le Complexe de Jijal , Arc du Kohistan, Pakistan.

Table 21A. Major, trace and platinum-group element analytical data from the KKH-section, Jijal Complex. Major elements are recalculated to 100% without LOI.
Données analytiques sur les éléments majeurs, en traces, et les EGP des échantillons de la coupe de la KKH, Complexe de Jijal.

S..No.		KO-1A	KO-2	KO-3	KO-4	KO-5	KO-6	KO-28	KO-27	KO-26	KO-25	KO-29	JRP-18A	JRP-18B	KO-24	KO-23	KO-7	JK-31	KO-22	JK-33
Rock-type		dunite	ol-clinopyr.	ol-clinopyr.	ol-clinopyr.	ol-clinopyr.	ol-clinopyr.	webst.	webst.	dunite	dunite	dunite	dunite	dunite	webst.	webst.	webst.	dunite	webst.	webst.
Mineralization			tr sulf+chr		tr sulf		tr sulf	tr sulf		chr	chr dis	Chromitite	Chromitite	Chromitite	tr sulf	tr sulf	sulf Cp		tr sulf	
Position	m.	62	250	437	625	812	969	1063	1156	1375	1469	1520	1520	1520	1562	2156	2163	2200	2236	2250
Major Elements(wt%)																				
SiO2		39.10	44.82	53.34	52.72	52.99	54.08	53.83	52.66	39.85	40.04	N.D.	N.D.	N.D.	53.35	47.06	43.08	39.69	49.86	43.44
TiO2		0.04	0.05	0.12	0.17	0.15	0.09	0.10	0.16	0.03	0.03				0.08	0.12	0.08	0.15	0.28	0.16
Al2O3		0.83	0.62	2.09	2.85	2.64	1.54	1.73	2.68	0.78	0.44				1.49	1.84	1.24	3.84	4.91	2.11
Fe2O3		14.28	10.34	7.53	9.54	8.35	6.05	5.10	9.73	9.60	10.72				7.03	11.32	16.19	15.42	10.95	16.23
MnO		0.16	0.06	0.16	0.19	0.18	0.13	0.10	0.19	0.00	0.09				0.16	0.16	0.17	0.00	0.21	0.25
MgO		45.32	41.29	19.91	20.55	19.83	21.60	19.20	21.73	49.47	48.33				21.35	27.60	32.11	34.85	18.26	27.39
CaO		0.26	2.82	16.83	13.98	15.86	16.51	19.93	12.84	0.27	0.36				16.55	11.90	7.13	6.06	15.53	10.43
Na2O		0.00	0.00	0.00	0.00	0.00	0.00	0.00	0.00	0.00	0.00				0.00	0.00	0.00	0.00	0.00	0.00
K2O		0.00	0.00	0.00	0.00	0.00	0.00	0.00	0.00	0.00	0.00				0.00	0.00	0.00	0.00	0.00	0.00
P2O5		0.02	0.00	0.00	0.00	0.00	0.00	0.00	0.00	0.00	0.00				0.00	0.00	0.00	0.00	0.00	0.00
Total		100.00	100.00	100.00	100.00	100.00	100.00	100.00	100.00	100.00	100.00				100.00	100.00	100.00	100.00	100.00	100.00
LOI		1.29	11.48	1.92	2.49	1.88	0.76	1.06	1.68	0.29	2.58					4.39	2.09	0.02		
Trace elements (ppm)																				
Zn		58	15	32	44	37	23	12	46	41	42				22	36	53	87.00	33	52.00
Ni		1490	807	193	180	241	207	362	188	1971	1560	1952			197	438	967	963.00	158	188.00
Cr		4202	922	1779	1587	1812	1705	1645	1546	29500	3857	95000			1624	2571	1481	5654.00	921	679.00
V		154	65	257	348	312	197	158	367	164	62	558			256	371	234	250.00	692	258.00
Cu		9	9	9	10	82	322	528	5	4	9	10			9	16	2043	15.00	253	4.00
Sc		BDL	11	89	89	93	64	51	88	BDL	BDL	BDL			96	66	27		156	BDL
Ga		BDL	BDL	BDL	BDL	BDL	BDL	BDL	BDL	BDL	BDL	BDL			BDL	BDL	BDL	BDL	BDL	BDL
U		BDL	BDL	BDL	BDL	BDL	BDL	BDL	BDL	BDL	BDL	BDL			BDL	BDL	BDL	BDL	BDL	BDL
Ce		BDL	BDL	BDL	BDL	BDL	BDL	BDL	BDL	BDL	BDL	BDL			BDL	BDL	BDL	BDL	BDL	BDL
Co		115	106	61	60	78	63	19	61	128	130.000	128			67	115	145	135.00	73	98.00
Rb		BDL	BDL	BDL	BDL	BDL	BDL	BDL	BDL	BDL	0.140	BDL			BDL	BDL	BDL	BDL	BDL	BDL
Sr		BDL	13	13	10	11	14	14	11	BDL	0.980	BDL			10	10	BDL	8.00	10	BDL
Y		BDL	BDL	BDL	BDL	BDL	BDL	BDL	BDL	BDL	0.060	BDL			BDL	BDL	BDL	6.00	10	7.00
Zr		BDL	BDL	BDL	BDL	BDL	BDL	BDL	BDL	BDL	0.180	BDL			BDL	BDL	BDL	BDL	BDL	BDL
Nb		BDL	BDL	BDL	BDL	BDL	BDL	BDL	BDL	BDL	0.590	BDL			BDL	BDL	BDL	BDL	BDL	BDL
Cs		BDL	BDL	BDL	BDL	BDL	BDL	BDL	BDL	BDL	0.005	BDL			BDL	BDL	BDL	BDL	BDL	BDL
Ba		BDL	BDL	BDL	BDL	BDL	10	BDL	BDL	BDL	4.410	BDL			BDL	BDL	BDL	BDL	BDL	BDL
PGE(ppb)																				
Ir		2.10	0.26	0.16	0.29	0.38	1.17	0.69	0.24	1.83	0.96	3.35	7.04	11.72	0.16	0.65	0.57	1.61	0.22	0.23
Ru		1.88	0.30	0.46	0.38	1.47	1.77	0.81	0.66	3.69	1.24	8.36	10.72	10.31	0.38	0.44	0.49	2.53	0.33	1.18
Rh		2.83	0.50	3.90	1.13	2.14	3.11	1.99	1.33	2.13	6.20	6.03	7.12	8.09	1.33	2.61	1.32	2.78	0.47	0.78
Pt		12.80	2.15	29.65	5.40	10.45	14.20	10.70	16.16	2.75	41.70	5.04	3.65	1.49	8.00	15.65	182.50	42.11	9.80	2.79
Pd		7.35	0.09	3.79	1.17	5.35	14.00	5.05	13.09	3.20	0.74	3.94	0.99	2.04	1.08	6.75	144.00	40.69	9.05	1.61
Au		3.17	5.75	2.48	35.25	7.35	3.85	5.25	7.23	7.05	2.93	21.81	1.90	1.19	2.24	2.94	15.85	3.02	1.11	1.13
∑PGE		30.13	9.04	40.43	43.6	27.13	38.09	24.49	38.71	20.65	53.75	48.518	31.42	34.84	13.18	29.04	344.72	92.74	20.97	7.72
Pd/Ir		3.5	0.35	23.69	4.09	14.27	11.97	7.32	54.54	1.75	0.77	1.18	0.14	0.17	6.97	10.47	252.63	25.27	41.14	7

Abbreviations: ol-clinopy. = olivine clinopyroxenite, webst. = websterite, gt-pyrox. = garnet pyroxenite, Tr Sulf. = trace sulphides
Chr dis = disseminated chromite, Cp = chalcopyrite, py = pyrite, BDL = below detection limit (1ppm for Nb,Zr,Y,Sr,Cu; 7ppm for Sc,Ga,U; 24 ppm for Ba; 30 ppm for Nd,Ce; 0.002 wt % for Na,K and P2O5.

Table 21A. (Continued)

S..No.	KO-21	KO-21A	KO-20	KO-19	KO-18	KO-17	KO-16	KO-15	KO-14	KO-12	KO-11	KO-45	KO-13	KO-10	KO-9A	KO-8A
Rock-type	ga-webst.	ga-webst.	ga-webst.	gt-webst.	gt clinopyrox.	gt gabbro	gt gabbro	gt gabbro	gt gabbro	gt hornbl.	gt hornbl.	gt gab.	gt hornbl.	gt gabbro	gt gabbro	gt gabbro
Mineralization	sulf	sulf										Py-Cp	tr sulf			
Position	2312	2315	2375	2438	2500	2563	2625	2750	2875	3063	3156	3219	3313	3406	3594	3906
Major Elements(wt %)																
SiO2	44.08	49.19	49.91	44.80	42.25	47.32	44.25	52.26	45.04	42.08	41.28	48.17	38.86	51.41	52.85	52.65
TiO2	1.21	0.30	0.39	1.34	0.60	0.90	0.82	0.85	1.38	1.82	1.86	0.75	1.40	0.67	0.70	0.88
Al2O3	14.73	5.05	5.61	11.44	15.74	8.40	19.54	18.08	17.50	14.13	15.56	15.08	17.04	18.85	17.96	17.57
Fe2O3	11.22	10.40	9.55	11.87	16.36	9.92	14.71	11.67	16.21	16.29	14.17	10.60	19.03	10.76	10.72	10.75
MnO	0.11	0.19	0.17	0.12	0.37	0.12	0.22	0.20	0.23	0.14	0.10	0.08	0.31	0.18	0.19	0.16
MgO	14.84	18.15	16.41	11.98	11.20	11.64	7.02	4.73	7.19	12.06	12.91	6.71	9.87	5.30	5.19	5.60
CaO	11.62	16.72	17.92	16.94	13.35	21.48	12.59	9.92	11.42	11.68	11.91	17.44	12.08	10.48	10.08	10.17
Na2O	2.03	0.00	0.04	1.45	0.14	0.22	0.72	2.05	0.87	1.65	2.00	1.12	1.28	2.19	2.03	1.88
K2O	0.17	0.00	0.00	0.06	0.00	0.00	0.10	0.12	0.00	0.15	0.21	0.00	0.14	0.09	0.23	0.26
P2O5	0.00	0.00	0.00	0.00	0.00	0.00	0.02	0.13	0.16	0.00	0.00	0.06	0.00	0.08	0.05	0.09
Total	100.00	100.00	100.00	100.00	100.00	100.00	100.00	100.00	100.00	100.00	100.00	100.00	100.00	100.00	100.00	100.00
LOI	1.42	0.11	0.79	0.39	0.14	0.20	1.21	0.37	0.12	0.86	0.62	1.99	0.30	0.77	0.64	0.16
Trace elements (ppm)																
Zn	39	32	31	62	55	43	97	93	106	93	72	67	81	83	80	76
Ni	229	147	201	85	38	72	22	13	43	35	60	80	27	19	21	11
Cr	682	1012	1116	431	581	1072	182	225	1558	83	77	126	267	327	331	57
V	941	451	446	727	582	512	544	266	518	1021	874	422	867	306	289	247
Cu	105	69	43	35	5	8	24	123	145	158	111	1648	32	152	37	48
Sc	114	BDL	128	101	165	BDL	72	46	63	110	98		92	50	42	BDL
Ga	11	BDL	BDL	16	10	11	18	21	19	16	16	17	16	20	18	15
U	BDL	BDL	BDL	BDL	BDL	BDL	BDL	BDL	BDL	BDL	BDL	BDL	BDL	BDL	BDL	BDL
Ce	BDL	BDL	BDL	BDL	BDL	BDL	BDL	BDL	BDL	BDL	BDL	BDL	BDL	BDL	BDL	BDL
Co	84	66	78	73	62	39	53	31	47	80	83	105	65	34	30	70
Rb	BDL	BDL	BDL	BDL	BDL	BDL	BDL	BDL	BDL	BDL	BDL	BDL	BDL	BDL	BDL	BDL
Sr	142	10	19	92	36	37	196	273	186	106	199	307	130	256	254	305
Y	10	9	10	10	31	8	12	18	18	11	10	13	25	15	17	13
Zr	BDL	BDL	BDL	BDL	BDL	BDL	BDL	16	BDL	BDL	BDL	17	BDL	11	25	35
Nb	BDL	BDL	BDL	BDL	BDL	BDL	BDL	BDL	BDL	BDL	BDL	BDL	BDL	BDL	BDL	BDL
Cs	BDL	BDL	BDL	BDL	BDL	BDL	BDL	BDL	BDL	BDL	BDL	BDL	BDL	BDL	BDL	BDL
Ba	BDL	BDL	BDL	15	BDL	BDL	BDL	64	10	BDL	BDL	15	28	78	98	236
PGE(ppb)																
Ir	0.20	0.25	0.41	0.16	0.27	0.20	0.16	0.15	0.23	0.27	0.37	2.41	0.16	0.92	0.17	0.10
Ru	0.29	0.86	1.12	0.97	1.20	3.83	1.46	0.64	1.28	1.09	1.10	1.83	0.74	0.77	0.71	0.45
Rh	0.90	0.38	0.51	0.05	0.31	0.65	0.59	0.12	0.53	0.39	0.05	1.09	0.30	0.04	2.63	0.36
Pt	15.45	39.03	2.88	5.20	13.45	8.30	5.45	3.95	5.40	6.55	8.40	118.85	4.79	2.71	22.00	5.90
Pd	17.10	20.22	1.58	1.55	0.73	2.39	5.30	4.32	0.57	6.70	5.70	17.01	3.56	3.30	1.09	1.00
Au	6.80	7.25	5.25	1.57	2.70	7.19	1.25	3.85	3.11	1.50	2.92	55.20	3.64	3.99	0.66	1.19
ΣPGE	40.74	67.99	11.75	9.49	18.65	22.56	14.20	13.02	11.11	16.49	18.54	196.39	13.185	11.72	27.24	8.99
Pd/Ir	85.5	80.88	3.85	10	2.75	11.95	34.19	28.8	2.53	24.81	15.41	7.05	22.25	3.58	6.58	10.53

Table 21B. Major, trace and platinum-group element analytical data for samples from the Duber Valley, Jijal Complex. Major elements are recalculated to 100% without LOI.
Données analytiques sur les éléments majeurs, en traces, et les EGP des échantillons de la vallée de la Duber, Complexe de Jijal.

S..No.		JD-5	JD-6	JD-9	JD-10	JD-14	JD-15	JD-16	JD-19	JD-27	JD-30	JD-31	JD-34	JD-58	JRP-16	JRP-17	JD-75	KO-35	JD-79	JD-89	KO-34A	KO-34B
Rock-type		ol-cpx.	ol-cpx.	dunite	dunite	ol-cpx.	ol-cpx.	ol-cpx.	dunite	ol-cpx.	dunite	ol-cpx.	ol-cpx.	dunite	dunite	dunite	dunite	websterite	websterite	ol-cpx.	ol-cpx.	ol-cpx.
Mineralization															chromitite	chromitite		chr + tr sulf			Py-Po-Cp	Py-Po-Cp
Position	m.	35	240	300	435	630	735	1095	1320	1470	1560	1620	1800	1920	1920	1920	1935	2040	2100	2280	2400	2400
SiO2 (wt%)		50.46	51.68	41.40	39.14	51.82	49.99	52.07	38.80	48.37	40.60	51.95	47.35	44.67	N.D.	N.D.	43.47	50.04	52.67	51.73	44.95	51.33
TiO2		0.05	0.05	0.03	0.03	0.07	0.07	0.08	0.04	0.07	0.03	0.08	0.15	0.02			0.03	0.06	0.08	0.06	0.05	0.06
Al2O3		1.07	1.17	0.47	0.72	1.33	1.36	1.73	1.01	1.84	0.51	1.37	2.51	0.67			0.69	1.33	1.66	1.28	0.89	1.23
Fe2O3		5.95	5.29	10.84	12.03	5.91	7.40	5.44	15.11	8.57	11.76	5.46	9.48	9.03			9.27	5.95	4.74	5.56	10.74	6.62
MnO		0.09	0.09	0.14	0.00	0.12	0.14	0.11	0.10	0.13	0.14	0.09	0.16	0.11			0.10	0.08	0.08	0.10	0.14	0.11
MgO		26.56	24.36	44.20	47.12	20.56	25.29	19.69	44.45	25.48	45.54	22.15	26.29	45.39			45.64	26.09	22.07	22.31	33.93	22.92
CaO		15.81	17.35	2.93	0.96	20.18	15.76	20.87	0.49	15.54	1.41	18.90	14.05	0.11			0.80	16.46	18.69	18.95	9.29	17.73
Na2O		BDL	BDL	BDL	BDL	BDL	BDL	BDL	BDL	BDL	BDL	BDL	BDL	BDL			BDL	BDL	BDL	BDL	BDL	BDL
K2O		BDL	BDL	BDL	BDL	BDL	BDL	BDL	BDL	BDL	BDL	BDL	BDL	BDL			BDL	BDL	BDL	BDL	BDL	BDL
P2O5		BDL	BDL	BDL	BDL	BDL	BDL	BDL	BDL	BDL	BDL	BDL	BDL	BDL			BDL	BDL	BDL	BDL	BDL	BDL
Total		100.00	100.00	100.00	100.00	100.00	100.00	100.00	100.00	100.00	100.00	100.00	100.00	100.00			100.00	100.00	100.00	100.00	100.00	100.00
LOI		4.72	3.77	4.65	9.38	2.20	4.30	1.83	0.98	1.95	0.78	2.88	4.17	7.58			3.79	1.67	2.57	1.13	0.00	1.81
Trace elements (ppm)																						
Zn		17	17	38	53	21	27	29	65	28	43	16	32	31			42	13	17	42	34	16
Ni		462	424	1067	1686	194	301	234	1359	342	1269	556	456	1852			2192	543	610	234	769	665
Cr		2062	2495	2392	4801	1556	1753	1403	4316	1529	2558	2306	1746	2007			2412	2572	2522	1448	1289	1105
V		40	49	BDL	BDL	118	78	119	27	112	BDL	115	141	BDL			BDL	88	BDL	BDL	185	216
Cu		5	4	12	9	524	20	4	5	27	4	485	142	4			5	31	450	33	248	726
Sc		BDL	BDL	BDL	BDL	BDL	BDL	BDL	BDL	BDL	BDL	BDL	BDL	BDL			BDL	BDL	BDL	BDL	33	57
Ga		BDL	BDL	BDL	BDL	BDL	BDL	BDL	BDL	BDL	BDL	BDL	BDL	BDL			BDL	BDL	BDL	BDL	BDL	BDL
U		BDL	BDL	BDL	BDL	BDL	BDL	BDL	BDL	BDL	BDL	BDL	BDL	BDL			BDL	BDL	BDL	BDL	BDL	BDL
Ce		BDL	BDL	BDL	BDL	BDL	BDL	BDL	BDL	BDL	BDL	BDL	BDL	BDL			BDL	BDL	BDL	BDL	BDL	BDL
Co		100	94	152	161	90	121	97	148	118	151	88	111	46			BDL	BDL	BDL	BDL	BDL	BDL
Rb		BDL	BDL	BDL	BDL	BDL	BDL	BDL	BDL	BDL	BDL	BDL	BDL	BDL			BDL	6	10	18	BDL	10
Sr		7	9	10	18	11	12	6	BDL	5	BDL	11	10	BDL			7	6	6	8	BDL	BDL
Y		6	6	6	6	6	6	6	6	6	6	6	7	6			BDL	BDL	BDL	BDL	BDL	BDL
Zr		BDL	BDL	BDL	BDL	BDL	BDL	BDL	BDL	BDL	BDL	BDL	BDL	BDL			BDL	BDL	BDL	BDL	BDL	BDL
Nb		BDL	BDL	BDL	BDL	BDL	BDL	BDL	BDL	BDL	BDL	BDL	BDL	BDL			BDL	BDL	BDL	BDL	BDL	BDL
Cs		BDL	BDL	BDL	BDL	BDL	BDL	BDL	BDL	BDL	BDL	BDL	BDL	BDL			BDL	BDL	BDL	BDL	BDL	BDL
Ba		BDL	BDL	BDL	BDL	BDL	BDL	BDL	BDL	BDL	BDL	BDL	24	BDL			BDL	BDL	BDL	BDL	BDL	BDL
PGE(ppb)																						
Ir		0.88	0.78	0.53	2.82	0.12	0.26	0.32	2.96	0.37	1.86	0.26	0.32	3.58	45.00	1.40	4.21	0.41	1.36	0.33	0.26	0.15
Ru		0.51	0.48	0.65	6.21	0.93	0.55	0.57	6.14	0.84	1.74	0.86	0.69	7.06	120.00		8.05	0.97	1.82	1.31	1.07	0.40
Rh		1.89	2.04	1.35	2.62	0.72	4.13	0.71	1.97	0.81	3.68	0.42	0.53	2.01	10.00	2.20	2.10	1.00	1.59	0.72	0.96	5.85
Pt		6.78	18.68	12.52	13.08	20.51	88.78	20.46	15.24	22.73	15.99	9.32	42.09	16.38		71.00	12.61	7.05	125.82	33.41	10.05	58.00
Pd		3.71	12.21	7.19	9.12	40.96	52.41	7.11	6.79	33.71	9.55	13.65	45.52	16.22	16.00	81.00	11.90	5.10	123.11	40.96	11.90	3.10
Au		2.97	2.39	3.37	30.34	11.01	4.01	2.30	1.12	2.89	3.34	9.14	14.17	0.76	5.30	10.00	2.20	3.41	18.02	6.99	8.45	19.30
ΣPGE		16.74	36.58	25.61	64.19	74.25	150.14	31.47	34.22	61.35	36.16	33.65	103.32	46.01	196.3	165.6	41.07	17.93	271.72	83.72	32.684	86.785
Pd/Ir		4.22	15.65	13.57	3.23	341.33	201.58	22.22	2.29	91.11	5.13	52.5	142.25	4.53	0.12	7.14	2.83	12.59	90.52	124.12	45.77	21.34

Abbreviation: ol-cpx. = olivine clinopyroxenite, ga-pyroxe. = garnet pyroxenite, ga-gabbro = garnet gabbro, all Fe as Fe2O3, BDL = below detection limit, N.D. = not determined, Po = pyrrhotite, Pn = pentlandite, Cp = chalcopyrite, Serp. = ophiolitic serpentinite, Tr sulf = trace sulphides, Webst. = websterite, Ga-hornbl. = garnet hornblendite; 0.002 wt% for Na, K & P2O5; 1 ppm for Nb,Zr,Y,Sr,&Cu; 7 ppm for Sc,Ga & U; 24 ppm for Ba; 30 ppm for Nd & Ce.

Table 21B. (continued)

S..No.	JD-90	JD-101	KO-36A	KO-36B	KO-36C	KO-37	KO-41	KO-42	KO-38	KO-39	KO-40	JD-115	JD-112	KO-43
Rock-type	websterite	gt webst.	gt webst.	gt webst.	gt webst.	gt hornbl.	gt pyrox	gt pyrox	websterite	gt gabbro	gt gabbro	gt gabbro	gt gabbro	dunite
Mineralization				Cp+Po+Py	Cp+Po+Py	Tr sulf				bornite				serp
Position	2460	2760	2975	3000	3010	3040	3750	4875	3090	3300	3540	4260	4335	5250
SiO2	50.19	48.43	43.90	42.61	45.81	45.95	42.64	40.77	42.83	42.93	40.53	43.17	43.01	40.80
TiO2	0.37	0.63	0.64	0.59	0.47	0.98	1.31	1.75	0.26	0.21	0.07	0.16	0.04	0.04
Al2O3	5.47	8.30	12.54	8.98	11.91	12.14	16.90	16.10	8.48	20.83	13.02	24.32	26.30	0.85
Fe2O3	9.89	8.77	11.51	16.35	11.15	9.45	13.54	18.24	16.65	10.29	15.14	7.71	6.65	10.00
MnO	0.16	0.12	0.12	0.11	0.17	0.10	0.09	0.31	0.27	0.14	0.14	0.09	0.08	0.10
MgO	18.25	12.62	12.67	12.38	13.67	15.86	12.10	8.59	23.90	12.30	24.70	8.69	8.93	48.02
CaO	15.67	21.13	18.61	18.98	16.81	15.51	13.43	14.22	7.60	13.30	6.41	15.86	14.99	0.18
Na2O	BDL	BDL	BDL	BDL	BDL	BDL	BDL	BDL	BDL	BDL	BDL	BDL	BDL	BDL
K2O	BDL	BDL	BDL	BDL	BDL	BDL	BDL	BDL	BDL	BDL	BDL	BDL	BDL	BDL
P2O5	BDL	BDL	BDL	BDL	BDL	BDL	BDL	BDL	BDL	BDL	BDL	BDL	BDL	BDL
Total	100.00	100.00	100.00	100.00	100.00	100.00	100.00	100.00	100.00	100.00	100.00	100.00	100.00	100.00
LOI	0.75	0.35	0.72	2.85	0.29	1.38	0.77	0.63	2.70	0.83	5.44	1.32	1.33	5.23
Trace elements (ppm)														
Zn	17	41	94	BDL	31	32	68	84	90	32	59	34	30	68
Ni	429	141	756	3577	349	310	157	44	378	168	340	82	124	2267
Cr	1877	651	369	500	1005	839	259	335	304	126	97	387	14	3592
V	BDL	BDL	640	BDL	513	532	571	608	343	176	8	BDL	BDL	82
Cu	252	13	1305	3307	266	85	932	218	37	180	12	25	10	4
Sc	BDL	BDL	61	BDL	125	BDL	BDL	83	45	34	BDL	BDL	BDL	BDL
Ga	BDL	9	17	BDL	BDL	8	14	12	BDL	BDL	BDL	11	10	BDL
U	BDL	BDL	BDL	BDL	BDL	BDL	BDL	BDL	BDL	BDL	BDL	BDL	BDL	BDL
Ce	BDL	BDL	BDL	BDL	BDL	BDL	BDL	BDL	BDL	BDL	BDL	BDL	BDL	BDL
Co	109	50	127	BDL	68	73	77	67	103	128	114	63	108	126
Rb	BDL	BDL	BDL	BDL	BDL	BDL	BDL	BDL	BDL	BDL	BDL	BDL	BDL	BDL
Sr	5	30	26	BDL	20	99	175	47	59	171	64	280	326	BDL
Y	6	8	BDL	BDL	9	9	8	33	BDL	BDL	6	6	6	BDL
Zr	BDL	BDL	BDL	BDL	BDL	BDL	5	BDL	BDL	BDL	BDL	5	6	BDL
Nb	BDL	BDL	BDL	BDL	BDL	BDL	BDL	BDL	BDL	BDL	BDL	BDL	BDL	BDL
Cs	BDL	BDL	BDL	BDL	BDL	BDL	BDL	BDL	BDL	BDL	BDL	BDL	BDL	BDL
Ba	BDL	BDL	BDL	BDL	BDL	BDL	BDL	BDL	BDL	13	BDL	BDL	BDL	BDL
PGE(ppb)														
Ir	0.16	0.23	0.16	13.43	0.27	0.27	0.03	0.29	0.26	0.11	0.29	0.17	0.11	3.89
Ru	1.05	1.14	0.47	16.90	0.51	0.58	1.48	1.19	0.68	0.79	1.40	1.11	0.90	8.37
Rh	0.27	0.59	1.05	26.00	0.58	0.71	0.15	1.15	0.33	0.53	0.81	0.46	0.20	1.44
Pt	10.17	12.18	14.45	751.00	22.50	25.25	3.92	5.40	5.00	5.74	8.45	4.07	1.31	3.40
Pd	5.27	4.43	8.95	506.00	24.35	14.80	7.70	3.30	3.93	6.15	0.40	7.25	1.65	4.46
Au	1.18	2.04	79.00	104.00	56.50	4.86	19.35	14.42	4.12	27.30	1.99	2.50	0.82	7.07
ΣPGE	18.1	20.61	104.075	1417.33	104.705	46.455	32.629	25.75	14.305	40.62	13.33	15.56	4.99	28.63
Pd/Ir	32.94	19.26	57.74	37.68	91.89	55.85	226.47	11.38	15.41	55.91	1.38	42.65	15	1.15

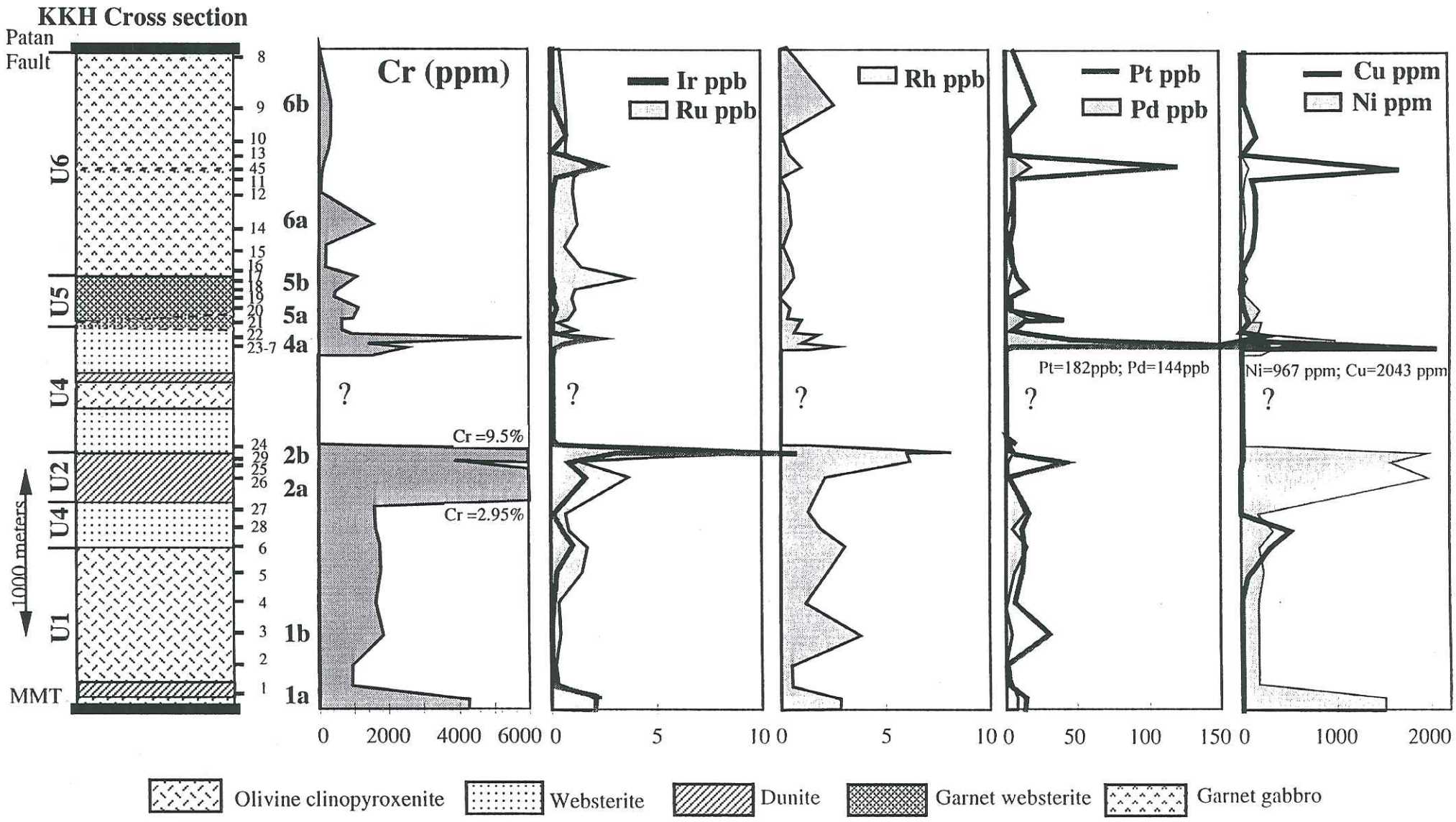

Figure 88. Distribution of transitional and platinum-group elements along the Karakoram (KKH) section, of the Jijal Complex. U1 to U6 are the successive units mentionned in the text? 1a to 6b represent the successive PGE's enriched observed horizons.
Distribution des éléments transitionnels et de ceux du groupe du platine. Prélèvements le long de la KKH, Complexe de Jijal.

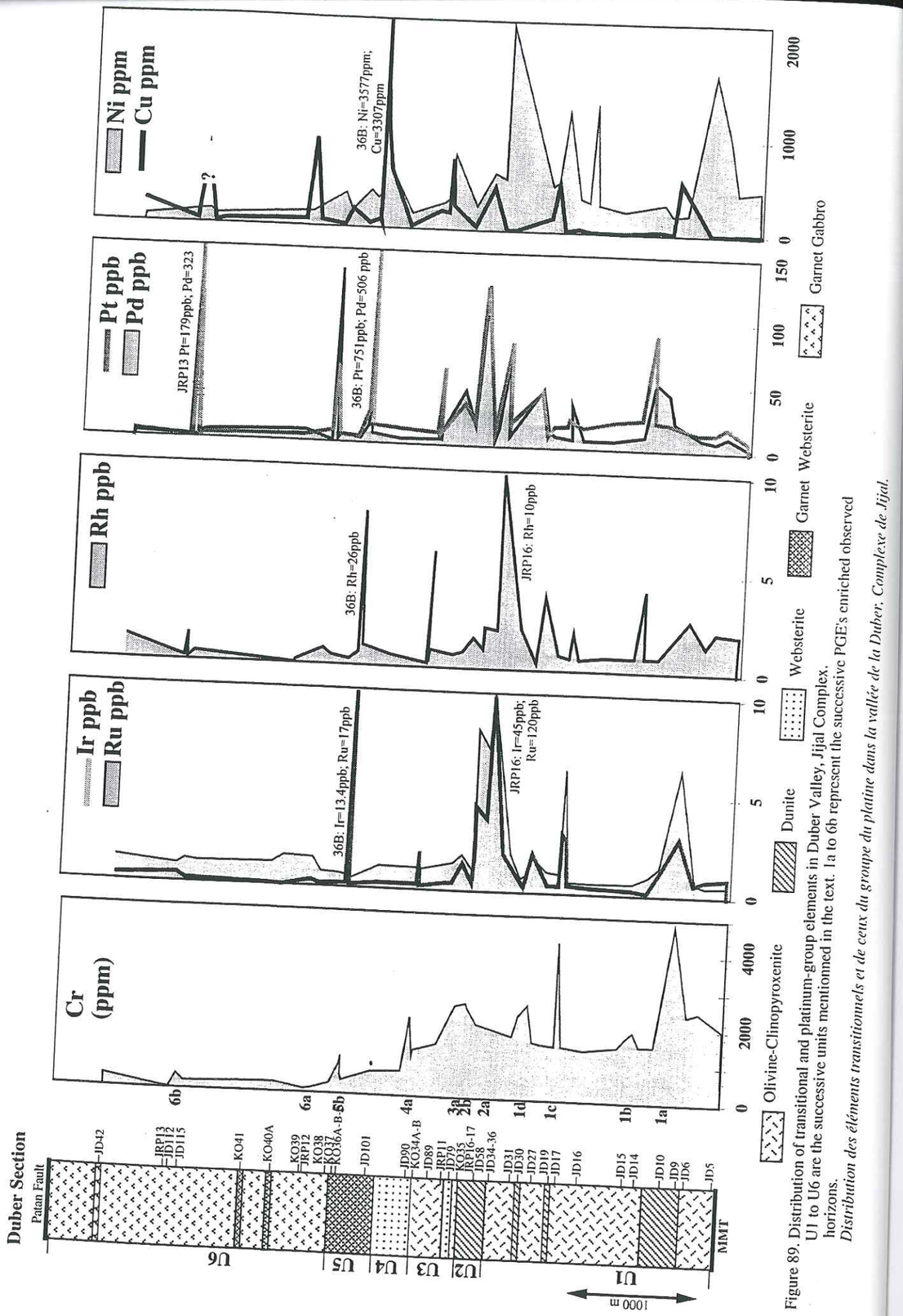

Figure 89. Distribution of transitional and platinum-group elements in Duber Valley, Jijal Complex. U1 to U6 are the successive units mentionned in the text. 1a to 6b represent the successive PGE's enriched observed horizons.
Distribution des éléments transitionnels et de ceux du groupe du platine dans la vallée de Duber, Complexe de Jijal.

1-1.1 Dunites (U1-U2)

PGE's concentrations in dunites from Duber- and KKH- sections are given in Tables 21A&B and shown in Figures 88 and 89. Most of the dunites from Duber-section contain total PGE's + Au concentrations between 26 and 64 ppb (Pd/Ir ratio=1.2 to 13.6) and from KKH, the total concentrations vary from 20.7 to 93 ppb (Pd/Ir ratio=0.8 to 3.5). Along Duber section, sample JD-10 shows higher value of Au (30 ppb; Table 21B) as compared to other samples and this can be due to secondary processes like serpentinization (loss on ignition is higher than other samples) and is also supported by petrographic study.

All dunitic levels are enriched in IPGE's (Ir, Ru, Rh) in the Duber-section (Fig. 93). These different enrichment zones are named as 1a, 1c, 1d, 2a and 2b (Figs. 88 & 89). Along KKH section, only 1a, 2a and 2b dunitic levels have been sampled for PGE's+Au analyses and they also reflect IPGE's enrichment (Fig. 88; total values vary between 30 and 49 ppb). Comparatively, PPGE's are low in the dunites except in 2b (U2) where Pt enrichment is observed along KKH (Fig. 88; Pt=42 ppb) and Pt and Pd in the Duber Valley (Fig. 89; Pt=71 ppb and Pd=81 ppb. All these enrichment zones are positively correlated with peaks of Cr and Ni (Cr=3857 ppm, Ni=1560 ppm in KKH section and Cr and Ni not analyzed in Duber section) whereas Cu values are very low (Cu=9 ppm in KKH section). Correspondance of IPGE's enrichment with the Ni, reflects the compatible behaviour of Ni with olivine and incompatible behaviour of Cu.

In **unit-2** three samples (KO-29, JRP-18A and JRP-18B) representing the **chromitites of Mani Dara mine** (Fig. 87) near the KKH, were analyzed (Table 21A). The total platinum-group element concentrations are 48.5 ppb, 31.4 ppb and 34.8 ppb respectively while Cr2O3 varies from 3857 ppm in dunite to 95000 ppm in chromitite. All the three samples are relatively enriched in Ir, Ru and Rh than to Pt and Pd and have moderate to low Pd/Ir ratios (1.2 to 0.1). The extremely low Ir (3.4 ppb, 7 ppb, 11.7 ppb) and Ru (8.4 ppb, 10 ppb, 72 ppb, 10 ppb) contents in chromitites are surprizing and reflect the absence of PGM in these chromitites, although we search them through Scan Electron Microscopy (SEM).

JRP-16 from another chromitite lense in the middle dunite (U2) of Duber section (Fig. 89; 2a) which also gives relatively high concentrations of Ir (45 ppb) and Ru (120 ppb).

1-1.2 Olivine clinopyroxenite (U1)

Along KKH-section, the distribution of Cr-Ni-Cu-PGE's in olivine clinopyroxenites is generally low (Cr=912 to 2500 ppm; Ni=194 to 800 ppm; PGE's=9 to 44 ppb) with Pd/Ir ratio = 0.3 to 4. Just a very small Pt enrichment is observed at the base of the sequence corresponding to 1b level (Fig. 88). Similarly, in Duber section, we observe one enriched zone (1b on Fig. 89; sample JD-15), having Pt and Pd values 89 ppb and Pd 52 ppb respectively. To

the top of the unit, another small anomaly is seen (sample JD-34) where Pt contents are 42 ppb and Pd 46 ppb.

1-1.3 Websterite (U4)

Whole-rock PGE's concentration in websterite along KKH and Duber sections is presented in Figures 88 & 89, and listed in Tables 21A & B. In the Duber Valley, the total PGE's contents are from 18 ppb to 271 ppb (samples JD-79, JD-90 and KO-35). The gold content in sample JD-79 of this unit is comparatively higher (18 ppb). The Pd/Ir ratio varies from 13 to 90. Along this section, 2 PGE's enrichment zones (noted 3a and 4a on Fig. 89) are observed and are characterized mainly by PPGE's enrichment (JD-79 where Pt=126 ppb and Pd=123 ppb and Pt=10 ppb in JD-90). Along KKH section (KO-23 and KO-7), there is one enrichment zone of PGE's (total PGE's=335 ppb with Pt=182 ppb and Pd=144 ppb in sample KO-7) corresponding to 4a enrichment level along Duber-section. Relatively high Pd and Pt contents in these websterite are consistent with their much higher Cu contents (e.g. 2043 ppm in KO-07; 450 ppm in JD-79; Tables 21A&B). Microscopic observations also reveal presence of base metal sulphides (chalcopyrite and pentlandite) in these PGE-rich websterites leading to suggest a PGE concentration in a sulphide phase.

1-1.4 Garnet websterite (U5)

In garnet websterite, background of PGE's contents is between 8 and 10 ppb. However, they contain important anomalies in PGE's, Au, Cu and Ni which are distributed in thin horizons (less than 1 metre thick). Mainly two enriched horizons have been detected in this unit (U5); one along the KKH-section where it is present at the base of U5 (noted 5a on Fig. 88); and second along the Duber-section and here it is present in the upper part of the U5 (noted 5b in Fig. 89). The lower horizon along KKH-section is characterized by medium concentration of Pt (15 ppb). The horizon 5b in Duber-section is more enriched and displays a strong concentration in Ni, Cu; Ir, Rh, Ru, Pd, Pt (values on Fig. 89). Disseminated sulphides, PGM's and anomalous PGE's contents are mostly concentrated in this zone. Whole-rock PGE contents are up to 1417 ppb. The gold values are also very high ranging from 56 to 104 ppb ppb in these samples. The relatively high Pd and Pt contents in these horizons are consistent with their much higher whole-rock Cu and Ni contents (e.g. total Pt+Pd=1257 ppb with Au=104 ppb; Cu and Ni values are 3307 ppm and 3577 ppm respectively in KO-36B; Table 23B). Pd/Ir ratio shows a wider range from 11 to 226 in Duber Valley and 9 to 68 along KKH-section.

1-1.5 Garnet gabbro and garnet hornblendite (U6)

Whole-rock platinum-group element data for garnet gabbro from Jijal Complex is listed in Tables 21A & B. Total PGE abundances are low and vary from 5 ppb to 40 ppb in the Duber section and 9 ppb to 196 ppb along the KKH section and are commonly in the range of 20 to 8 ppb.

Two positive anomalies are observed in both KKH and Duber sections (noted 6a and 6b on Figs. 88 & 89). The first anomaly (6a, noted on Fig. 88) along KKH section is marked by enrichment in Ru (4 ppb; sample KO-17) and second anomaly (6b, noted on Fig. 88) is marked by enrichment in Ir (up to 2.4 ppb), Pt (up to 118 ppb). The gold contents also show higher values (55 ppb; Table 21A). This corresponds to the presence of minor amounts of chalcopyrite as indicated by the positive correlation between Cu concentration (1641 ppm). Simillarly, two anomalies (6a and 6b noted on Fig. 89) are evident along Duber section. The first anomaly (6a; sample JRP-12) is marked by enrichment in Pt (60 ppb) and Pd (137 ppb) and the second anomaly (6b) is marked by slight enrichment in Rh (1.4 ppb), Pt (179 ppb) and Pd (323 ppb). The most common enrichment trend displayed by these anomalies involve Pt > Pd.

Garnet hornblendite has generally the same distribution of total PGE contents as garnet gabbro (Table 21A) and Pd/Ir ratio is commonly in the range of 11-22.

1-2 Mineralization

The different PGE's enriched horizons correspond to three different main types of PGE's distribution and mineralogical associations. The first type is marked by association of olivine and chromite in the dunites (horizons 1a, 1c, 1d, 2a and 2b). The second is a IPGE's and PPGE's enriched-type, marked by presence of Ni and Cu rich sulphides and PGM's in websterites and garnet websterites (horizons 3a, 4a, 5a and 5b). The third is a Pt-Pd enriched-type which is associated with disseminated Cu-rich sulphides (in thin horizons) within the garnet gabbros (6a and 6b).

1-2.1 Chromititic-type mineralization

The occurrence of chromite deposits in the Jijal Complex was first reported by Ashraf and Hussain (1982). Chromitite and chromium-rich spinel is the most common accessory phase which are known to occur as low-grade disseminations as well as on mm scale layers in all levels dunite and in some olivine clinopyroxenite, websterite and garnet websterite. However, massive chromitites appear to be restricted to upper level of the thick dunitic unit (U2) in the middle of the ultramafic section (Fig. 87). The massive chromite occurs in lenses and pods. These bodies taper at their ends and may peter out into a sparse dissemination of chromite

grains. Sometimes they reach 2 to 3 meter thickness and 50 meter strike length (e.g. Miller et al., 1991) and generally too small for economic exploitation. The chromitite samples from Mani Dara chromite mine (Fig. 87) consist of 92-95 volume % chromite; the remainder is largely olivine.

The chromite-rich ores display a banding on macro level and consist of subhedral to rounded chromite grains in an olivine gangue. The most common feature in these orebodies is massive to disseminated chromite cemented by primary olivine. Chromite displays mainly euhedral to rounded forms. The individual chromite grains are generally 2-5 mm in diameter and are relatively uniform in composition. Microscopic studies and microprobe analyses show that three different chromitic compositions can be distinguished in the ultramafic layers with different degrees of differentiation.

The massive chromitite lense in dunite has a Cr_2O_3 content averaging 54 wt. % (in Mani Dara mine) and Al_2O_3 is around 9,50 wt. % and grades towards chromian-aluminous spinel in olivine clinopyroxenite and websterite with a Cr_2O_3 content ranging from 43.36 to 36.13 wt.% and Al_2O_3 content from 9.6 to 17.68 wt. % respectively in the disseminated form.

The most differentiated, upper unit, garnet websterite contains aluminous-spinel with Cr_2O_3content varies from 0.72 to 5.43 wt.% and Al_2O_3 ranging from 63.11 to 54.02 wt.%. The IPGE's are generally associated with chromite and will be discussed latter in this section. **However, no PGM's have been found in these chromitite-rich ore bodies.**

These data and the behaviour of other major and minor elements of chromite reflect the chemical evolution of the silicate cumulates of the Jijal Complex (see PART-I, Chapter-3)..

1-2.2 Sulphide Occurrences

Two main types of mineralizations have been observed, 1) pentlandite, pyrrhotite and chalcopyrite mineralization in websterites and garnet websterites (4a, 5a ans 5b), and 2) disseminated chalcopyrite in garnet gabbros-type mineralization.

1-2.2.1 Mineralization in websterite and garnet websterite

The pyroxenites that contain Ni-Cu sulphide occurrences are generally small in surface area (<10 m^2) and consist principally of websterite and garnet-websterite and are mainly exposed in Duber valley (Fig. 87). Generally, sulphides occur disseminated throughout the upper part of garnet websterite and in zones of local enrichment, particularly in association with pyrrhotite, as cross-cutting veins and as a major component of sulphide stringers. It is dominated by the typical magmatic assemblage pentlandite (Pn), pyrrhotite (Po), chalcopyrite (Cp), and minor pyrite.

In the garnet websterite, the sulphide phase is Cp-rich with variable but low Pn and Po contents, particularly in the horizons 3a, 4a, 5a and 5b (Fig. 89). In Jijal Complex, Pn, Po, and Cp are seemed to be primary because they are normally enclosed in the pyroxene minerals (Figs. 91,93 & 94). Typically, Pn is associated with the Po (Figs. 90 & 91) and this textural feature, together with its Co-rich character (Table 22) suggest that Pn is contemporaneous with Po, and therefore, primary (e.g. Ewers & Hudson, 1972). Some of the sulphides occur as stringers, fracture fillings in narrow veinlets and a few millimeters wide in clinopyroxene grain.

Modal proportions of sulphide phases vary widely between aggregates due to non-uniform phase distribution. A study of samples representing the mineralized rocks revealed that they occur either as interstitial to grains of silicates (Figs. 91 & 93), or as inclusions in pyroxenes (Figs. 90 & 92) and are thought to have segregated as an immiscible liquid at the high temperature magmatic stage. Chalcopyrite, remobilized along fissures and cracks, is also frequent. It forms relatively large accumulations (1-4 mm) together with pyrrhotite. In association with pyrrhotite and pentlandite in silicates, chalcopyrite is anhedral and often surrounds the previously formed crystals of pyrrhotite and pentlandite (Figs. 90 & 91). Exsolution intergrowths of Cp in Pn are also frequent. Pyrite is rarer than chalcopyrite, pyrrhotite and pentlandite in the Jijal Complex. It occurs as isolated subhedral to anhedral crystals and sometimes appears to form intergrowth with the other sulphides. Pyrite of garnet websterite has Ni (0.95 wt. %) but is Co free. At some places the composition of the sulphides has been extensively modified by solid state mass-induced transfer and hydrothermal remobilization to the extent that the origin of the sulphides cannot be deduced with any certainty. The inclusions of sulphide are more common in clinopyroxene. Commonly, isolated sulphide occurs as elongated inclusions in pyroxenes. Interstitial sulphides are anhedral and display curvilinear margins moulded around silicates, reflecting solidification of immiscible sulphide liquids (Garuti et al., 1984; Lorand, 1987). The oxidized type consists mainly of limonite with local enrichment of malachite and azurite. Relics of primary sulphides are rare.

The chemical composition of some sulphides are given in the Table 22. Pn and Po exhibit a wide range of compositions with respect to Ni/Fe and base metal/sulphur ratio, but have Cu concentrations of less than 0.1 wt.% (Table 22). Cp is slightly Cu-deficient with respect to stoichiometric CuFeS2, in agreement with its presence in Py and Pn-bearing sulphide assemblages. The total-metal/sulphur ratio of the Po ranges from 0.84 to 0.91 and Ni rarely exceeds 0.7 wt.%. After chalcopyrite and pyrrhotite the most abundant sulphide is pentlandite. Pentlandite was the first phase to crystallize among the sulphide minerals of the pyroxenite in Jijal Complex. It also occurs as primary pseudo-eutectic intergrowths with, and as exsolution lamellae in, pyrrhotite (Fig. 94). The Pn has always less than 33 wt.% Ni.

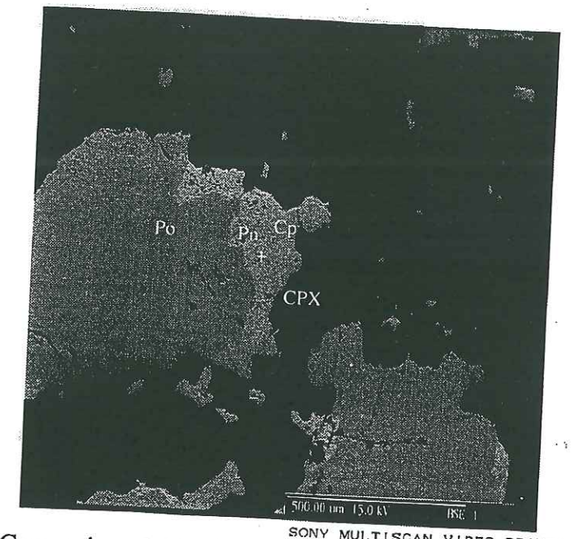

SONY MULTISCAN VIDEO PRINTE

Figure 90. Composite sulphide inclusion in clinopyroxene (dark). The main mass of the inclusion consists of pyrrhotite (Po) mantled by pentlandite (Pn) and chalcopyrite (Cp) (sample KO-36C; U5).

Inclusion composite de sulfures dans un clinopyroxène (en sombre). L'essentiel de la masse de l'inclusion est en pyrrhotite (Po), entourée de pentlandite (Pn) et de chalcopyrite (Cp).

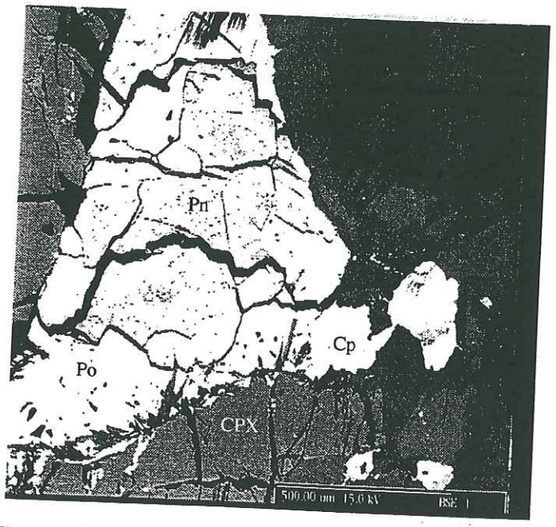

Figure 91. Composite sulphide include at the contact between two clinopyroxenes. The main mass of the inclusion consists of pentlandite (Pn) exsolved into pyrrhotite (Po) and chalcopyrite (Cp). All of the sulpde mass is in optical continuity indicating that they are remanants of a larger pentlandite grain (sample KO-36C; U5).

Sulfure composite inclus entre deux clinopyroxènes. L'essentiel de l'inclusion est constitué de pentlandite (Pn) exsolvée en pyrrhotite (Po) et chalcopyrite (Cp). Tout l'amas de sulfures est en continuité optique, indiquant qu'ils proviennent d'un ancien grain de pentlandite plus vaste.

Figure 92. Sulphide inclusion in clinopyroxene crystal containing pentlandite (Pn) in the core and grading out into pyrrhotite (Po) (sample KO-36; U5).

Inclusion de sulfures dans un clinopyroxène constituée de pentlandite (Pn) au coeur passant à de la pyrrhotite (Po) à la périphérie.

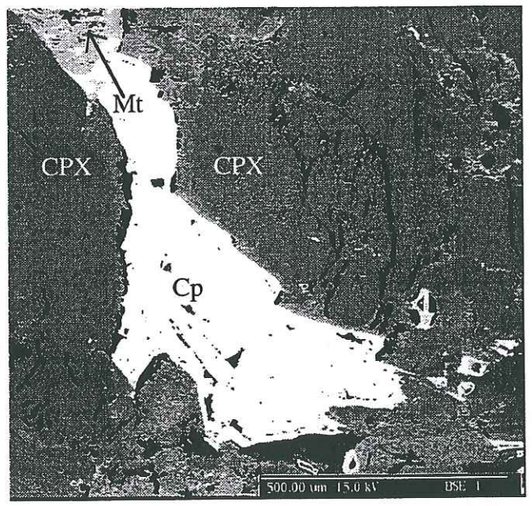

Figure 93. Sulphide-rich veinlet between clinopyroxene crystals. Magnetite (Mt) is seen to replace homogeneous chalcopyrite (Cp) (sampleKO-36; U5).

Veinule riche en sulfures entre deux cristaux de clinopyroxène. La chalcopyrite (Cp) est remplacée de manière homogène par la magnétite (Mt).

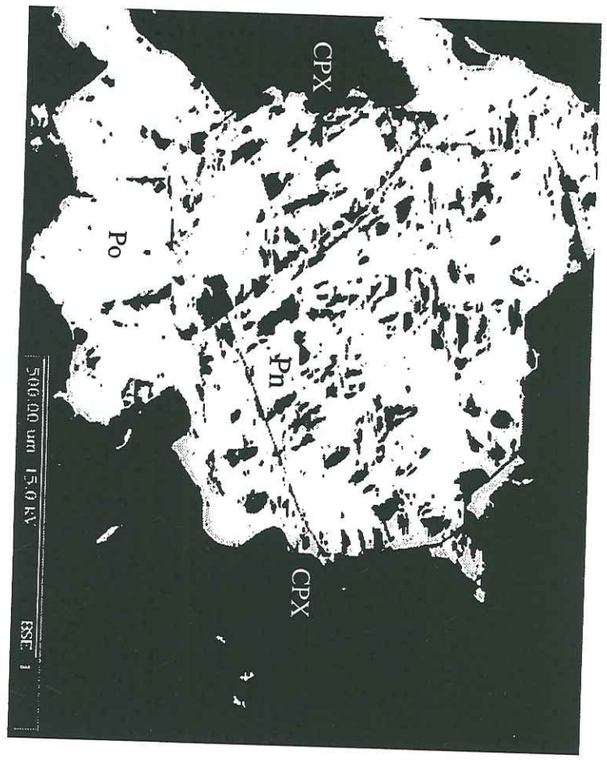

Figure 94. Composite sulphide inclusion within clinopyroxene crystal. The main mass of the sulphide consists of pentlandite (Pn), alongwith exsolved Pn blebs (dark). This mass as a whole is mantled by pyrrhotite (Po) (sample KO-127A; U5).

Inclusion composite de sulfures dans un clinopyroxène, essentiellement constituée de pentlandite (Pn) maculée d'exsolutions de pentlandite. Elle est entièrement recouverte de pyrrhotite (Po).

Table 22. Representative electron microprobe analyses of individual sulphides included in silicates.
Analyses représentative à la microsonde électronique des sulfures inclus dans des silicates, Complexe de Jijal.

	KO-127A					KO-36B			
Minerals	Pn	Po	Cp	Py	Minerals	Pn	Po	Cp	Py
Cation					Cation				
Fe	29.45	60.22	30.09	41.83	Fe	24.15	46.36	24.98	30.78
Ni	33.22	0.61	0.06	1.83	Ni	25.91	0.45	0.05	1.28
Co	2.29				Co	1.78			
Cu	0.07	0.001	33.42	0.01	Cu	0.05	0.001	24.38	0.01
S	33.54	39.64	34.9	52.92	S	47.9	53.16	50.45	67.85
Te			0.03	0.02	Te			0.01	0.01
Au					Au				
As	0.02	0.051	0.01	0.04	As	0.01	0.03	0.01	0.02
Hg	0.8		0.55	0.12	Hg	0.18		0.13	0.03
Zn	0.01			0.06	Zn	0.01			0.04
Total	99.4	100.52	99.06	96.82	Total	100	100	100	100
Atomic ratio					Atomic ratio				
Fe/Ni	0.88	98.72	501.5	22.86	Fe/Ni	0.93	103.02	499.6	24.04
Cu/Fe	0.002		1.11		Cu/Fe	0.002		0.98	
Fe/S	0.88	1.52	0.86	0.79	Fe/S	0.5	0.87	0.5	0.45

Abbreviations: Pn = pentlandite, Po = pyrrhotite, Cp = chalcopyrite, Py = pyrite.
Analytical conditions: acceleration voltage : 15 kV, counting time : 6s:peak, 6s:background,
specimen current : 10 nA. Pure metal standards except for Fe and S (natural pyrite), below detection (0.05 wt%).

1.2.2.2 Mineralization associated to garnet gabbro

Concentration of sulphides in garnet gabbro is very sparse and we can only see scarcely distributed chalcopyrite at some places (horizons 6a and 6b on Figs. 88 & 89) but less than 0.1 vol. %. At some places the composition of the chalcopyrite is extensively modified by hydrothermal remobilization to the extent that the origin of the sulphides cannot be deduced with any certainty. Encrustation of azurite and malachite is very common along the joints and fractures.

1-2.3. Platinum Group Minerals

In the present study four PGM have been identified in the sulphide and silicate phases which are all confined to the basal part of the garnet websterite in the Duber Valley (horizons 4a & 4b on Fig. 89). These PGM are temagamite, merenskyite, moncheite, and sperrylite. Temagamite, moncheite and merenskyite seem to be by far the most prevalent species in the Jijal Complex. PGM's are present as multiphase aggregates and as single grain ranging in size from 2 to 16 mm. Small grain sizes generally do not permit quantitative analyses of PGM grains, but semi-quantitative analyses were obtained of all PGM grains by Scan Electron Microscopy (SEM). These analyses are not sufficient to decide in many cases whether PGM represent members of a solid solution series or whether they represent separate minerals. So, all PGM are listed by their major components and the findings on the compositions of PGM are summarized in Table 23. Most of the PGM contain small amount of Fe, Ni and Co which are thought to substitute for the PGE in these minerals or matrix effect of host pentlandite or pyrrhotite.

SEM images of PGM and PGM-bearing phases in sulphides and silicates from garnet websterite are shown in Figures 95 to 99. Three distinct modes of occurrence are recognized: 1) as inclusions in the sulphides (Figs. 95 & 96A); 2) at the boundaries between the sulphides and silicate mineral (Figs. 97A & C); 3) in the silicate minerals (Fig. 98B). The distribution of PGM is related to the well-defined topology of the sulphide-silicate assemblage.

Figure 95 shows the presence of temagamite (Pd3 Hg Te3) in zone 1, merenskyite (Pd Te2) in zone 2, Au-Ag alliage (Hessite) in zone 3, Ni arseniure in zone 4 and complex alloy of As, Pd, S, Ni, Fe and Co represents zone 5. All these assemblages are again surrounded by pyrrhotite (zone-6) whose composition is Fe 53 wt.% and S 46 wt.%, with Ni about 0.95 wt.%. This whole phase is located as inclusion in the clinopyroxene.

Figure 96A shows a cavity, measuring approximately 20 mm in length and 3 to 4 mm in width and is located between pyrrhotite and pentlandite. A complex assemblage of **Au-Ag-Pd-Sb-Te alloy** (grain A-1 on Fig. 96A and its energy spectra 'a') was found associated with

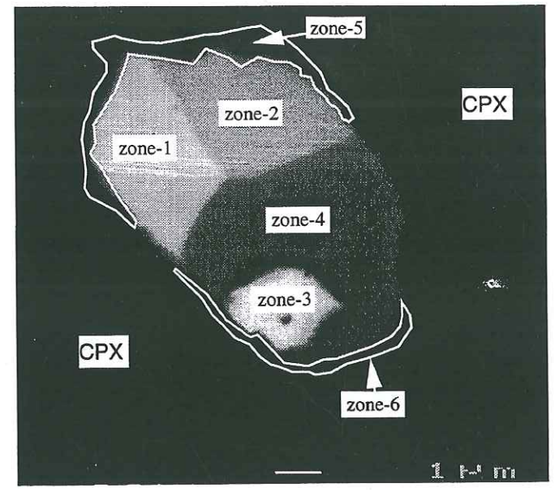

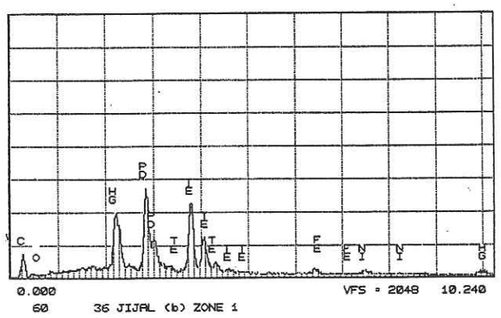

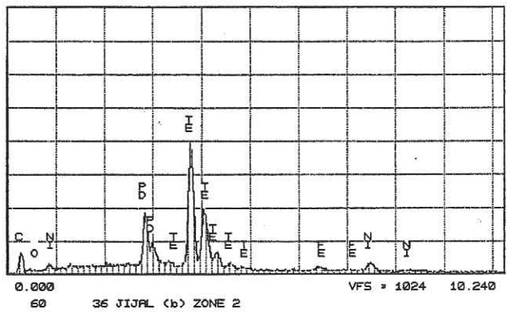

Figure 95. SEM photomicrographs showing composite PGM in pyrrhotite which is included in clinopyroxene. Zone-1 represents temagamite; zone-2 consists of merenskyite attached to temagamite; zone-3 shows Au-Ag-electrum (hessite?); Ni-arseniere in zone-4; and complex alloy of Ni-Fe-As-Pd-Co-Te represents zone-5. This whole composite is included in pyrrhotite which is present as inclusion in clinopyroxene (sample KO-36B).

Microphotographies au MEB d'un agglomérat de PGM dans de la pyrrhotite inclue dans un clinopyroxène. Zone-1: temagamite; zone-2: merenskyite et temagamite; zone-3: amalgame Au-Ag (hessite?); arséniure de Ni in zone-4; alliage complexe en Ni-Fe-As-Pd-Co-Te dans la zone-5. Le grain entier est lui même inclus dans une pyrrhotite, elle-même incluse dans un clinopyroxène.

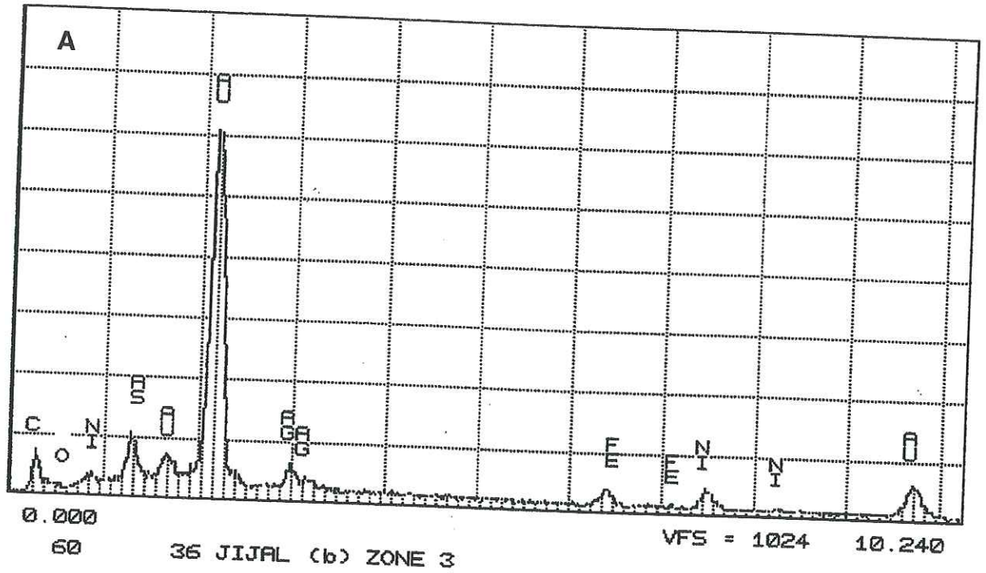

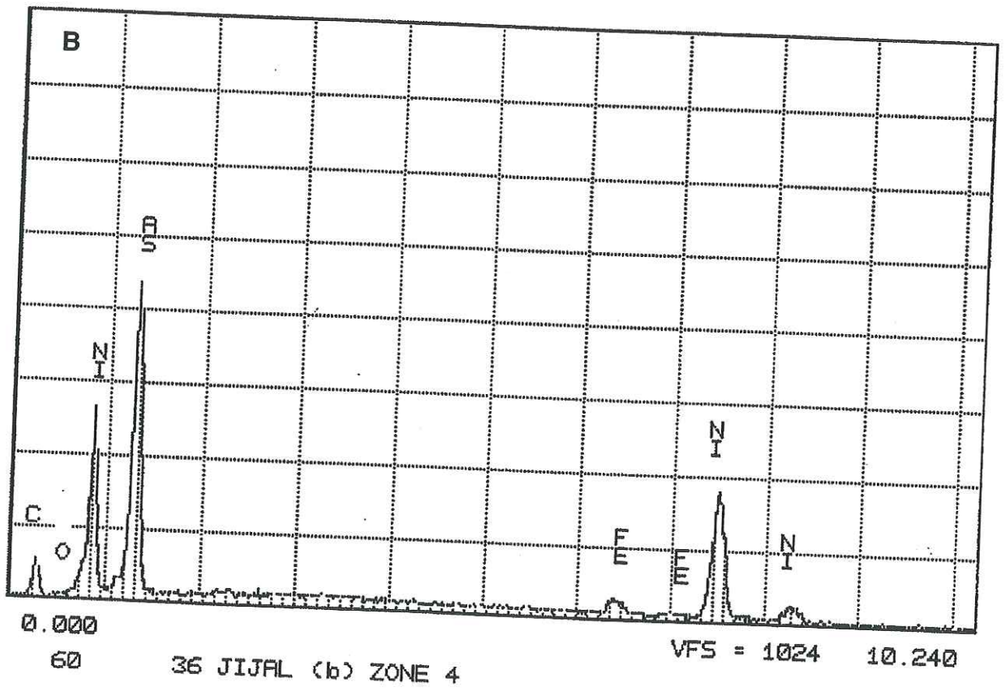

Figure 95. (A) shows the energy spectrum of zone-3 and (B) shows the energy spectrum of zone-4 .

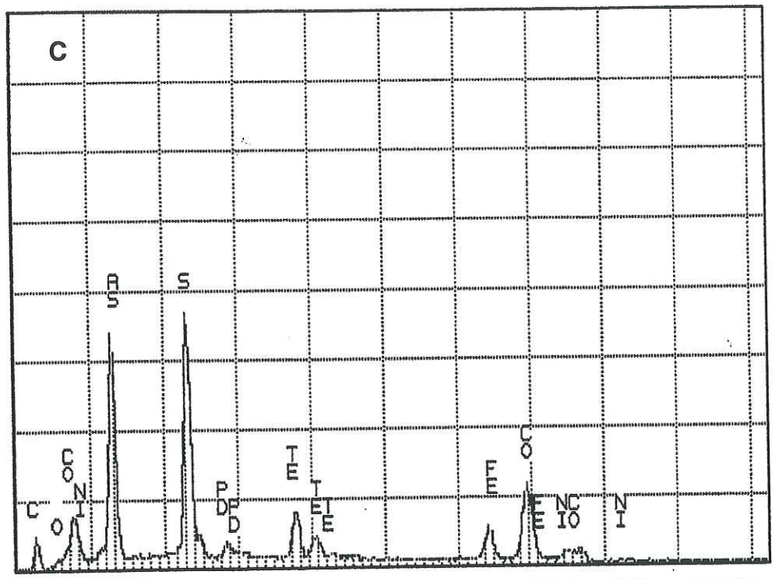

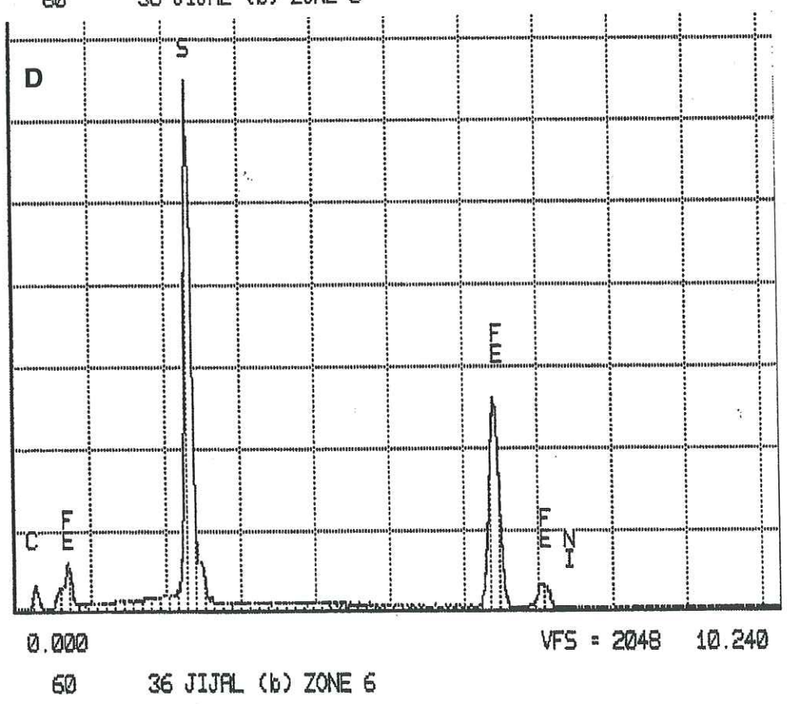

Figure 95. (C) shows energy spectrum of zone-5 and (D) shows energy spectrum of zone-6.

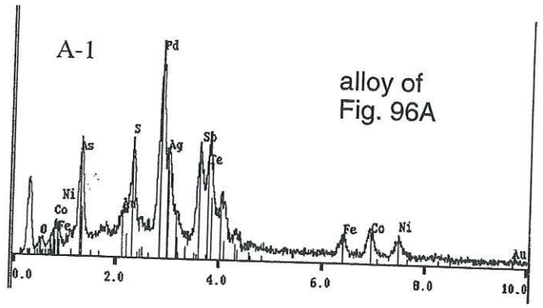

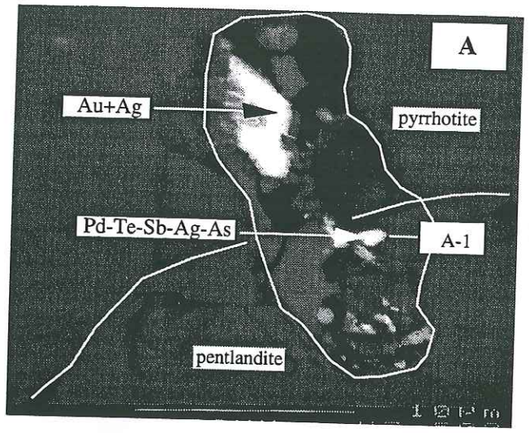

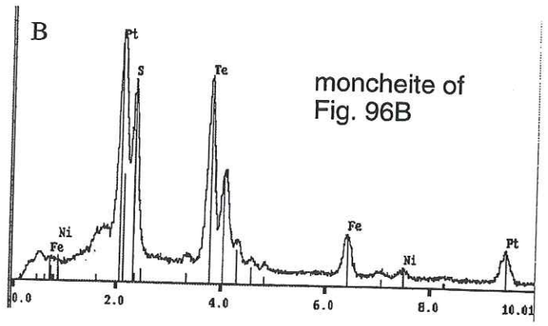

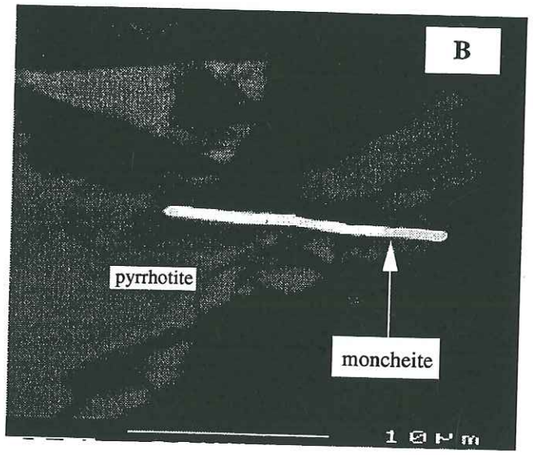

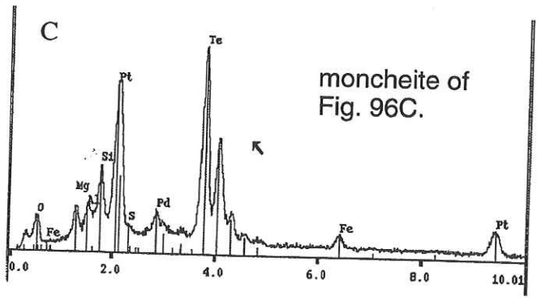

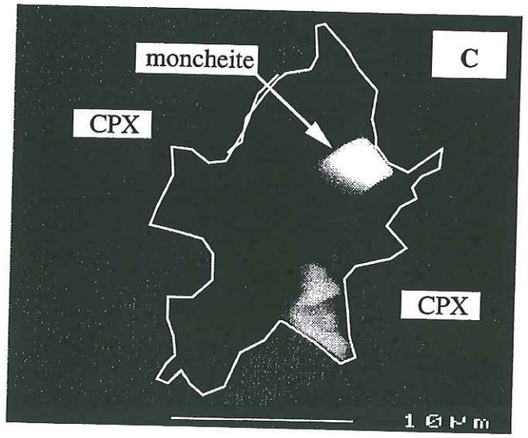

Figure 96. SEM photomicrographs along with energy spectrum showing complex assemblages of electrum and alloy both in pyrrhotite and pentlandite (A). (B) shows snail-like SEM photomicrograph of moncheite in pyrrhotite. (C) cubic moncheite as inclusion in a clinopyroxene grain (sample KO-127A; U5).

Photographie au MEB et spectre d'énergie, montrant un assemblage complexe d'amalgames et d'alliages à la fois dans de la pyrrhotite et de la pentlandite (A). (B) Photographie au MEB de moncheite dans de la pyrrhotite. (C) moncheite cubique en inclusion dans un grain de clinopyroxène.

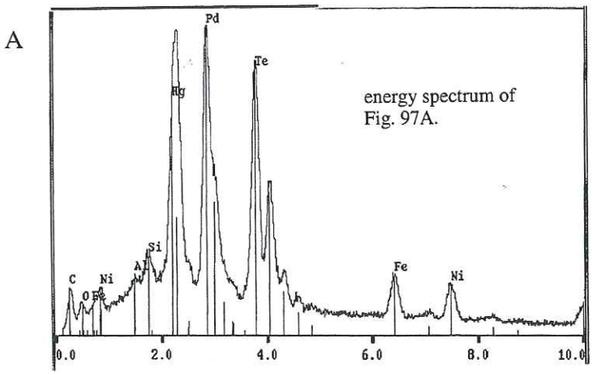

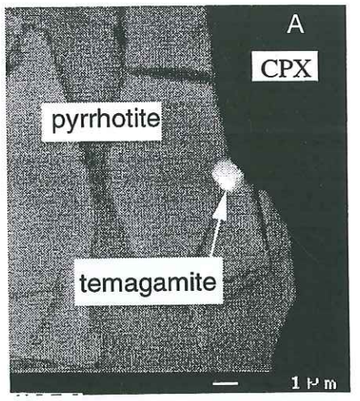

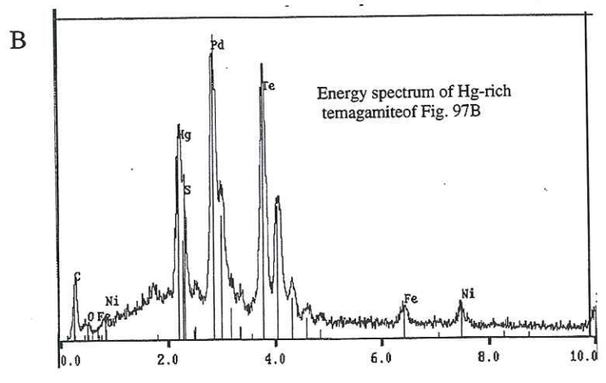

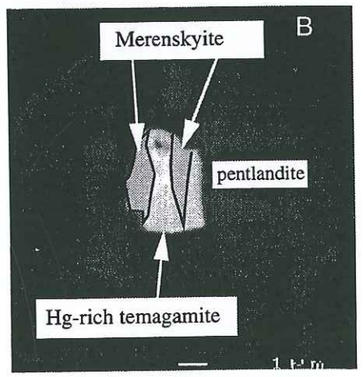

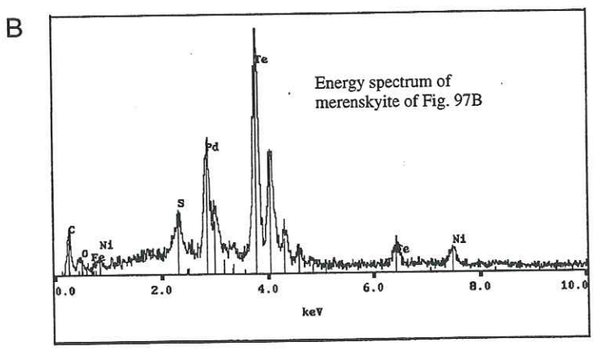

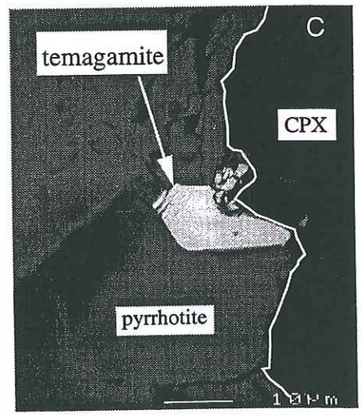

Figure 97. SEM photomicrographs showing temagamite inclusion both at the contact of pyrrhotite and clinopyroxene (A); exsolution feature in temagamite, merenskyite (grey) and Hg-rich temagamite (white) in pentlandite phase (B); and figure (C) shows temagamite in contact with pyrrhotite and clinopyroxene (sample KO-36; U5).

Microphotographies au MEB montrant une inclusion de temagamite au contact d'une pyrrhotite et d'un clinopyroxène (A); figure d'exsolution dans la temagamite, merenskyite (gris) et temagamite riche en Hg (blanc) dans la pentlandite (B); figure (C): temagamite en contact avec une pyrrhotite et un clinopyroxène.

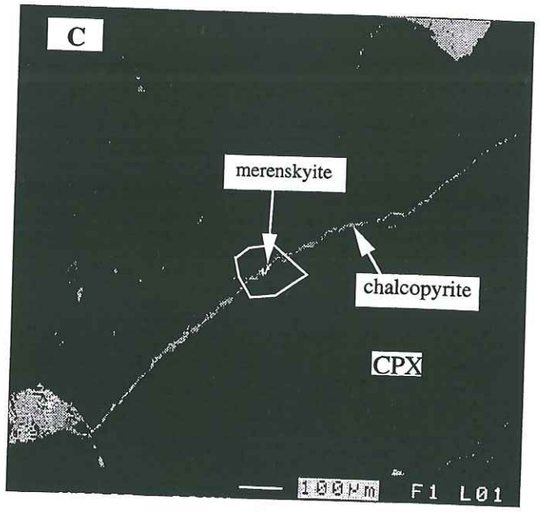

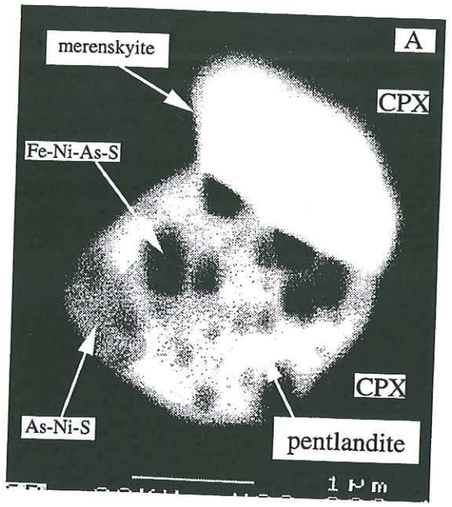

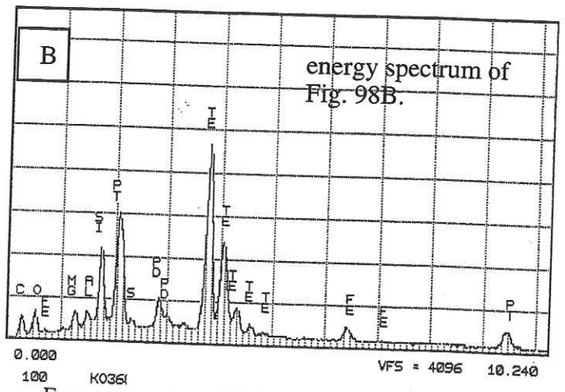

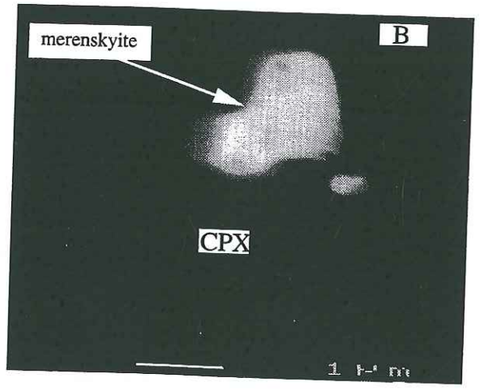

Energy spectrum of SEM photomicrograph of PGM (B)

Figure 98. SEM photomicrograph of merenskyite inclusion in clinopyroxene together with pentlandite (A); (B) shows merenskyite inclusion in clinopyroxene; (C) merenskyite associated with chalcopyrite which is filling a fracture in clinopyroxene (sample KO-36C).

Microphotographie au MEB d'une inclusion de merenskyite dans un clinopyroxène et dans une pentlandite (A); en (B): inclusion de merenskyite dans un clinopyroxène; C: merenskyite associée à de la chalcopyrite en remplissage d'une fracture dans un clinopyroxène.

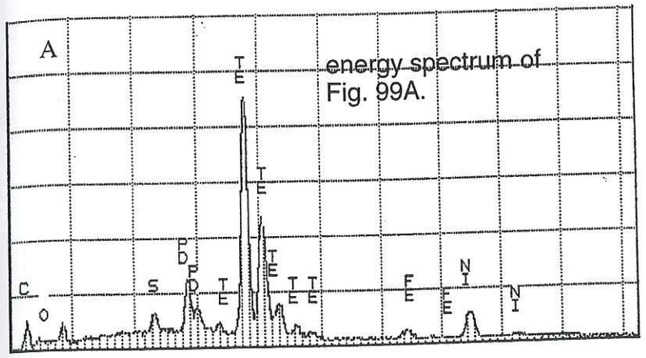

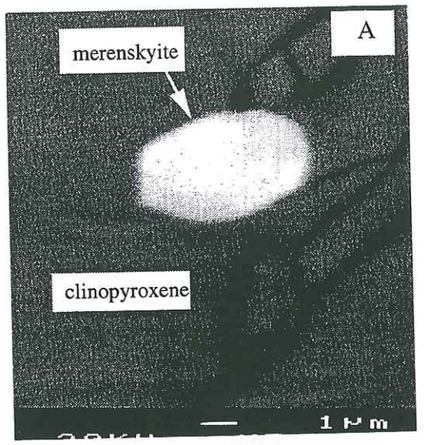

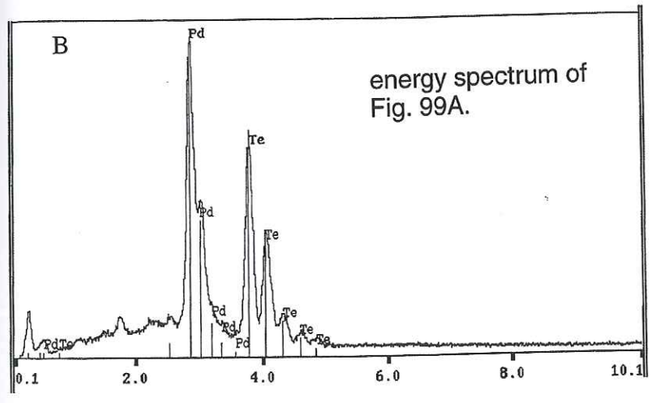

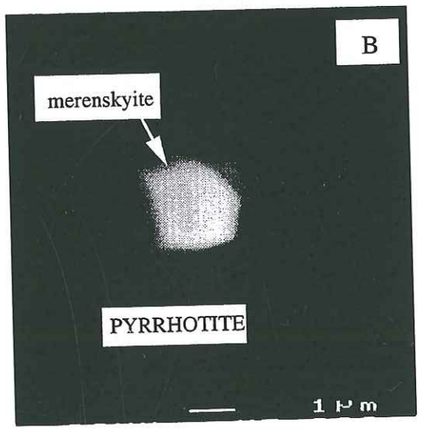

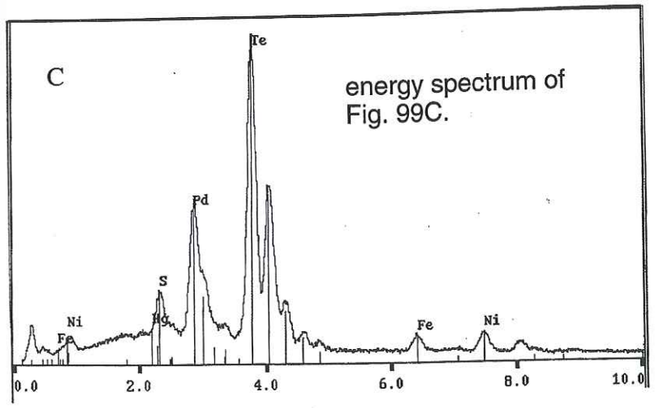

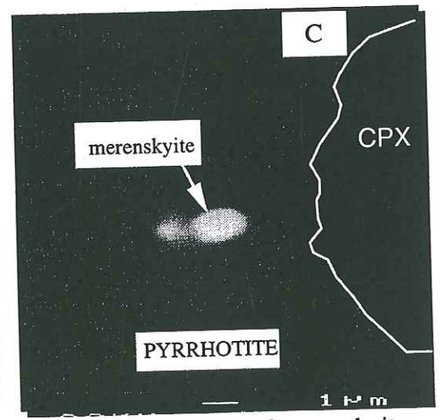

Figure 99. SEM photomicrographs (along with energy spectrum) showing inclusion of merenskyites in pyrrhotites (B & C) and in clinopyroxene (A) (sample KO-36).

Microphotographie au MEB et spectre d'énergie montrant une inclusion de merenskyites dans des pyrrhotites (B&C) and et dans un clinopyroxène (A).

Table 23. Semi-quantitative chemical composition of platinum-group minerals recognized and determined by SEM.
Composition chimique semi-quantitative des mineraaux du groupe du platine reconnus et caractérisés au MEB.

S.No.	KO-36	KO-36	KO-36	KO-36	KO-36C	KO-127	KO-127	KO-127
PGM	temagamite(z-1) temagamite(G-f merenskyite (G- temagamite(G-10) moncheite(G-10)				moncheite	merenskyite (G-1)	merenskyite (G-	moncheite(G-4)
Elements (wt%)	white band	grey band						
Pt					49.65	39.09	3.98	38.01
Pd	10.59	26.85	26.21	14.45	0.42	1.69	13.82	3.46
Te	77.89	42.11	48.1	78.03	49.93	59.22	76.71	56.43
Hg		27.2	25.69					
As	11.52			6.07			4.91	
Ni								
Atomic %								
Pt					39.17	29.46	2.41	27.55
Pd	10.98	30.13	32.79	15.48	0.6	2.34	15.37	4.6
Te	67.36	39.39	50.18	69.75	60.23	68.21	71.1	62.54
Hg		16.19	17.05					
As	21.66			11.78			9.9	
Ni								

S.No.	KO-36	KO-36	KO-36	KO-36	KO-36	KO-36
PGM	temagamite(z-1) temagamite(G-f merenskyite (G- merenskyite (G temagamite(G-; merenskyite (G temagamite(C merenskyite (G-4)					
Elements (wt%)	white band	grey band				
Pt	27.38	24.04	16.89	15.09	24.02	32.3
Pd	40.53	53.16	82.7	83.86	54.24	50.83
Te	29.53	22.92		0.78	21.02	15.96
Hg						
As						
Ni						
Atomic %						
Pt	33.61	32.17	22.48	20.23	32.3	42.8
Pd	41.49	49.59	76.72	78.37	50.83	57.19
Te	19.23	17.35		0.59	15.96	
Hg						
As						
Ni						

S.No.	KO-36	KO-36	KO-36	KO-36	KO-36	KO-36
PGM	temagamite(z-1) temagamite(G-f merenskyite (G- merenskyite (G temagamite(G-; merenskyite (G temagamite(C merenskyite (G-4)					
Elements (wt%)	white band	grey band				
Pt	34.04	19.42				
Pd	54.23					
Te	50.31					
Hg						
As						
Ni	14.61					
Atomic %						
Pt	34.23					
Pd	50.31					
Te	14.61					
Hg						
As						
Ni						

Abbreviations: G-1= grain-1; Z-1 = zone-1.
Analytical conditions: 20 kev acceleration voltage, 10nA current.

the pyrrhotite in this cavity while **electrum of Au-Ag** along with alloy of **As-Ni-Fe** is also present, enclosed by pentlandite.

Moncheite (ideal formula, $PtTe_2$) varies from 1 to 10 um in grain size and is the main PGM in the samples studied. It occurs mostly as roundish to oval-shaped inclusions in sulphide phases and clinopyroxene (Figs. 96B & C; sample KO-127A). It is found as euhedral crystals enclosed by clinopyroxene (Fig. 96C) and rod-shaped in pyrrhotite (Fig. 96B). Semi-quantitative analyses show that small amount of Pd was detected in most analyses (see energy spectra on Fig. 96C). However, we have not found the merenskyite-moncheite solid solution series in the rocks of Jijal Complex.

Temagamite (ideal formula=Pd_3HgTe_3) ranging in grain size from 2 to 15 um. It has variable composition and is widespread within the Fe-Ni-Cu sulphide of Jijal Complex (Fig. 97). Most temagamite grains studied are located as inclusion in pentlandite (Fig. 97B), but they also occur at the margins of clinopyroxene and pyrrhotite (Figs. 97A&C). Temagamite shows a wide range of composition with Pd ranges from 14 to 27 wt.%, and Te from 41 to 78 wt.% (energy spectra of Fig. 97A). Figure 97A shows small orthorhombic grain of temagamite with values of Te 54 wt.%, Pd 24 wt.%, and Hg 21 wt.%. This grain is located at the boundary of clinopyroxene and pyrrhotite. The analytical data of Figure 97B reveals two types of PGM: 1) temagamite (white colour) and, 2) merenskyite (grey colour) and both phases are present in pentlandite. Further, this sulphide phase is present as inclusions in clinpyroxene.

Merenskyite has ideal formula of $PdTe_2$. Its grain size varies between 3 and 10 um. In Figures 98 and 99, the merenskyite grains are observed in three different modes of occurrence: as aggregate with other PGM or as single mineral grain and included in pyrrhotite (Fig. 95, zone-2; Fig. 99B & C); as inclusion in clinopyroxene (Figs. 98B & 99A) and in mm-scale veinlets of chalcopyrite. They show different Te- and Pd-bearing mineral assemblages and representative semi-quantitative compositions are listed in Table 23. A small and isolated hexagonal grain of merenskyite with composition Te 78 wt. % and Pd 11 wt.% was encountered as inclusion in clinopyroxene (Fig. 99A; energy spectra in Fig; 99A). Many small grains of merenskyite (1-3 mm) were found associated with clinopyroxene and sulphide phases together with temagamite. In addition to the isolated grains, merenskyite was also observed as intergrowth with temagamite (Fig. 95; zone-2).

The occurrence of **sperrylite** is very rare and only one tiny, isolated grain (<1 μm) was encountered in pyrite. This is the only PGM so far found in pyrite.

Electrum (gold and silver assemblages) is also not widespread in these rocks. Only two grains of electrum were found and their grain size is <2 μm. In Figure 95 (zone-4) it is enclosed in the complex alloy of Ni-As, while in Figure 96A (A-1) it is enclosed in pentlandite.

1-2.4. Discussion

As mentioned earlier, three main types of mineralization have been observed in the Jijal Complex. In chromitite-type mineralization, no PGM's have been found, despite some IPGE's concentrations. This type seems typically a orthomagmatic-type mineralization due to early crystallization of chromites in dunites under probably high oxygen fugacity. In this type IPGE's form probably solid solution in oxides or alloys. Ni is mainly concentrated in olivine.

The sulphides (second-type mineralization) in the ultramafic section of the Jijal Complex are all enriched in Pd-group elements (Rh, Pd, Pt). They represent typical platinum-group element-rich base metal sulphide deposits. The major platinum-group minerals in the Jijal Complex are sperrylite, temagamite, merenskyite and moncheite. Thus, these mineralizations can be classified as a Merenskyite reef-type of sulphide association according to Cabri and Naldrett (1984).

As suggested by the mineralogical observations, the sulphur content of the Jijal Complex increases from dunite through olivine clinopyroxenite to garnet websterite and shows a positive correlation with the pyroxene. So, the residual magmatic liquid representing websterite was able to concentrate the available dissolved sulphur in the system, eventually leading to the crystallization of a sulphide phase enriched in PGM and PGE.

In all studied samples, the sulphides occur as disseminated and their mineralogy is dominated by the typical magmatic assemblage pyrrhotite-chalcopyrite, pentlandite and minor pyrite. Primary sulphides occur as disseminated chalcopyrite-pyrrhotite-pentlandite as a dissemination of droplets and nodular patches interstitial to silicates, or along the the cleavage planes of pyroxenes and are thought to have segregated as an immiscible liquid at the high temperature magmatic stage. Chalcopyrite is usually associated with pyrrhotite and pentlandite in silicates. Most of these sulphides are considered primary minerals exsolved subsequently during subsolidous cooling and during degassing.

At this stage a question which needs to be addressed is whether all the PGM's and PGE's are still related to typical magmatic events or subsequent postmagmatic, subsolidous recrystallization or intercumulous remobilization of Cu or precious metals could modify a primary profile. There is abundant evidence in the garnet pyroxenite sulphides for millimetre-scale mobility of sulphide components, in the form intergrowth of sulphides with late stage alteration assemblages and penetration of sulphides along pyroxene cleavage or cracks. These are typical features of disseminated magmatic sulphides (Barnes and Campbell, 1988; Prendergast, 1990). The scale of postcumulus mobility of sulphide components is unlikely to be greater than tens of centimetres.

The relation between the total-metal / sulphur of the Po and total Ni content of Pn is generally similar to that previously found in experimental as well as in natural Fe-Ni-S ores (Graterol and Naldrett, 1971; Misra and Fleet, 1973). In upper mantle rocks as well as in crustal basic and ultrabasic rocks, the Pn-Po-Cp assemblage is considered to be an unmixing product of high-temperature monosulphide solid solutions (MSS) (Kullerud et al., 1969; Craig and Kullerud, 1969) and they are considered to be primary. According to Lorand and Conquéré (1983) the crystallization temperature of an MSS containing 38.5 wt.% sulphur and Ni/(Ni+Fe) ratio of 0.39, would be at about 1070°C from the sulphide liquid. Ryzhenko and Kennedy (1973) reached the same conclusion and reported that the temperature of the first crystallization of the MSS is expected to increase up to 1150°C for 15 kbar pressure and this is in conformity with the mineral chemistry data already discussed in PART-1, Chapter-3. Further, lack of primary magnetite with sulphide suggests that there was pure sulphide phase. The likely reason for lack of oxygen is pressure which greately reduces the solubility of oxygen in sulphide melt (Wendlandt, 1982).

Similar zone of sulphide enrichment in garnet websterite is also found in the Kolai stream on the left bank of the Indus River. This has a thickness of 20-30 meters and extension of several meters (Khan et al., 1996). Covellite is often observed along the periphary of chalcopyrite grain.

This is in agreement with the previous studies of Naldrett et al. (1979), Naldrett and Barnes (1986) and Naldrett (1989), who found that the formation and behaviour of immiscible sulphide-bearing liquid phases have an important effect on the precipitation of PGE relative to associated silicate rocks. Partition coefficients between sulphide liquids and silicate melts are believed to be high (10^4 to 10^5) for all the PGE's (Campbell et al., 1983; Campbell and Barnes, 1984; Peach et al., 1989), but there is some evidence, particularly from the Great Dyke, that they vary for the different PGE's. Anyhow, the enrichment of PPGE's in sulphide-bearing rocks of the Jijal Complex shows that the process of entrapment of PGEs operated in sulphide-forming events.

Sulphide-bearing rocks from garnet-websterite, Duber Valley have approximately 0.36 percent Ni and 0.33 percent Cu, with 610 ppb Pt and Pd and they are depleted in IPGE (Table 21B). They have extremely fractionated PGE patterns with Pd/Ir ratios of 55 to 90 or more. The most distinctive features of the garnet websterites are their low IPGE contents and high Cu contents. Sulphides rich in Cu and depleted in IPGE are found in association with many igneous massive sulphide bodies (Barnes, S-J. et al., 1993).

In Jijal ultramafic section, during the crystallization of silicate minerals, the sulphur fugacity in equilibrium with the residual melt increases until an Fe-Ni-Cu-S liquid with the scavenging of associated PGE's is separated. PGE in monosulphide solid solution might

normally exsolve to form platinum-group minerals (PGM) or might crystallize directly from the Fe-Ni-Cu-S liquid at lower temperature (Makovicky et al., 1986; Naldrett, 1989). This is regarded as the key to the origin of PGE mineralization in the sulphide phases and other platinum-group minerals such as the tellurides and mercurides.

1-3. PGE's Behaviour

1-3.1. Patterns Signatures

Plots of mantle-normalized abundances of Ni-PGE-Au-Cu provide a useful means of examining the variations in PGE's abundances in different lithological rocks of various tectonic settings and then allow the effects of partial melting, sulphide segregation, chromite and olivine crystallization to be clearly recognized. Because Ni, Cu, and PGE's have different partition coefficients into sulphides, olivine, chromite and PGM, the relative timing of sulphide saturation, sulphide removal and crystal fractionation may be deduced from the metal patterns (Barnes et al., 1988). In the following section, we will present the distributions metal patterns of chromite-rich, chromite-poor rocks, sulphide-rich rocks and from different unmineralized facies from the Jijal-Complex.

The mantle-normalized diagrams (Figs. 100 & 101) illustrate that there are important differences in the PGE's patterns in **chromitite ore and Cr-enriched dunite** samples. Plots for the chromitites display negatively sloping (depleted in PPGE; Pd/Ir=0.14 to 1.18; Table 21A), which reflects their relatively enrichment in Ni and IPGE's (the iridium group of the PGE's; Barnes et al., 1985). In contrast, samples from Cr-enriched dunites show flat to rather slight positively patterns (Fig. 100 & 101; Pd/Ir=0.77 to 3.5; Table 21A), which indicates a relative enrichment in PPGE's. The curves show a tendency towards enrichment in Ni and IPGE's and depletion in Au and Cu relative to the PPGE's in samples from Cr-enrich dunite. In contrast, Cr-poor dunite samples display positively sloped patterns (Figs. 100; Pd/Ir=5.13 to 13.57; Table 21B) but have relative lower Ni and Ir abundances than Cr-riched dunites, a reflection of their slightly evolved composition. Mantle-normalized patterns for dunites along the KKH. show some dispersion with respect to Pt and Pd and Sample KO-26 (Cr-rich dunite; Cr=29500 ppm; Table 21A) shows depletion in Pt and Pd (Pd/Ir ratio of 1.75). Similarly Sample KO-25 has important Pd depletion anomaly but shows positive anomaly of Rh and Pt (Pd/Ir ratio=0.77).

Chromite crystallization has an effect similar to, but more intense than, olivine crystallization. The difference can be seen by examining the relative positions of chromitites and Cr-enriched and Cr-poor dunites within the Jijal Complex. The dunite shows a large change in Ni/Cu ratio from the initial melt but a relatively small change in Pd/Ir ratio, the chromitite shows a large change in Pd/Ir and a small change in Ni/Cu ratio. Most of the variation in Pd/Ir and

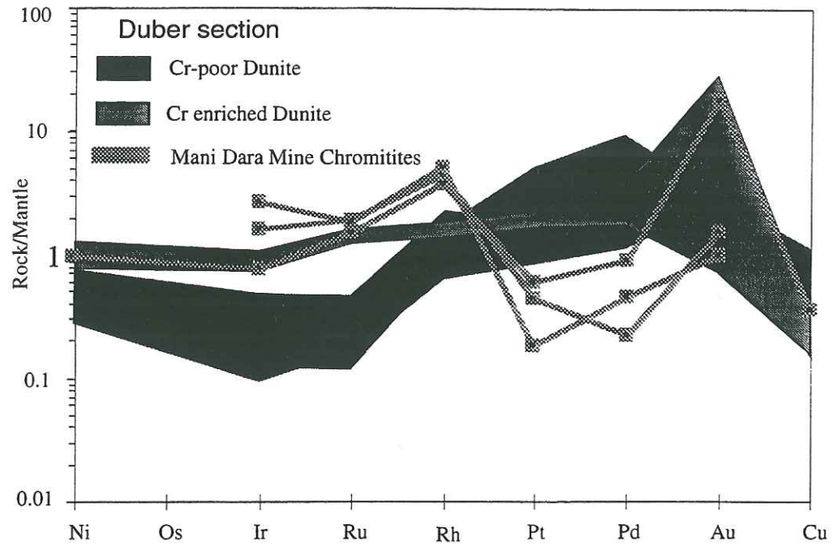

Figure 100. Mantle-normalized diagram showing Ni-PGE-Au-Cu patterns for the dunites of the Jijal Complex and average mantle-normalizing values from Barnes et al. (1988).

Spectre d'EGP des dunites riches en Cr de la coupe de la Duber, Complexe de Jijal , Arc du Kohistan.

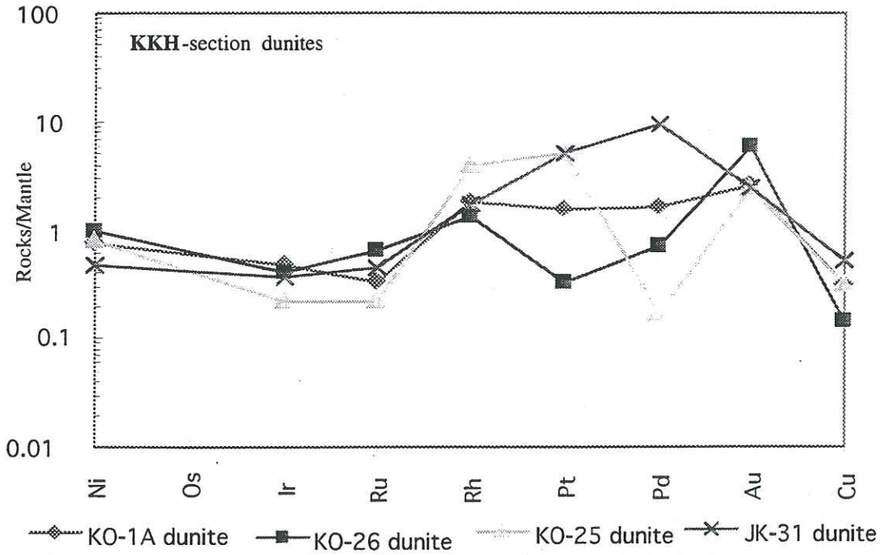

Figure 101. Mantle-normalized metal abundances for the dunitic rock exposed along the KKH-section, Jijal Complex, Kohistan Arc and average mantle-values are from Barnes et al. (1988).

Spectre normalisé au manteau des éléments Ni-EGP-Au-Cu des dunites de la coupe de la KKH, Complexe de Jijal.

Ni/Cu ratios for the layered intrusions and other lithologies of different tectonic settings may be accounted for by in olivine or chromite crystallization and variation in conditions of partial melting.

Figures 102 & 103 show mantle-normalized Ni-PGE-Au-Cu element abundances in **olivine-clinopyroxenites** and **websterites** along KKH and Duber sections. Such plots in both the sections reveal that all the lithologies display positively sloping patterns from Ir to Pd (Pd/Ir ratio=0.35 to 23.69 for ol-clinopyroxenite and 7 for websterite along KKH; 4.22 to 341 for ol-clinopyroxenite and 12 to 91 for websterite along Duber section; Tables 21A&B), which highlights their relatively enrichment in PPGE's (the palladium group of the PGE's).

Figures 104 & 105 show the profiles of mantle-normalized Ni-PGE's-Au-Cu values for **sulphide-enriched garnet websterite** and the patterns are from the Duber and KKH sections of the Jijal Complex. All the patterns show consistent shapes and features: Ni, Ir and Ru portion of the profile is fairly flat but pronounced positive slopes and a strong enrichment in Pd, Pt and Au and relatively enriched in Cu (3307 ppm) and Ni (500 ppm). But the pattern of the more sulphide-rich rock (KO-36B) shows more pronounced enrichment in PGE (1417 ppb). The sulphide-enriched pyroxenites display distribution patterns similar to those of sulphide-poor lithologies of the Jijal Complex, but are enriched in PGE's by a factor of 10 to 100 in Duber and 8 to 50 in KKH-section, as expected from their very high sulphide silicate partition. The depletion of Ir and Ru relative to Cu, Au and Pd is remarkably similar in sulphide-poor cumulates and sulphide-rich cumulates and indicates the cogenetic character of sulphides and cumulates.

Several anomalous patterns can be identified on the abundance plots. For example negative Pd anomalies for some pyroxenites of the KKH-section (Fig. 102A). In contrast, pyroxenite samples from the Duber-section do not display such Pd negative anomalies (except sample JD-79 in sulphide-enriched pyroxenite). Similarly, sample KO-11 from garnet hornblendite shows negative anomaly with respect to Rh. The significance of these features will be considered in a latter section.

Garnet gabbro and garnet hornblendite samples also display similar patterns (Figs. 106&107) to those of the dunites and pyroxenites, but have relative lower Ni and Ir abundances, probably a reflection of their more evolved composition, typical of mafic magmas in general (Barnes et al., 1988). These patterns indicate that the PPGE's, Au and Cu were preferentially incorporated into residual liquid, and the IPGE's and Ni were strongly partitioned into the most primitive ultramafic cumulates during the formation of the Jijal Complex. The overall shape of the mantle-normalized patterns for these rocks is similar to MORB-patterns.

The Au values, not far from Clarke values in ultramafic rocks, indicate that the role of hydrothermal fluid was not dominant in the concentration of this metal. In the mantle-normalized patterns of sulphide-enriched zone, Cu peak corresponds exactly to the

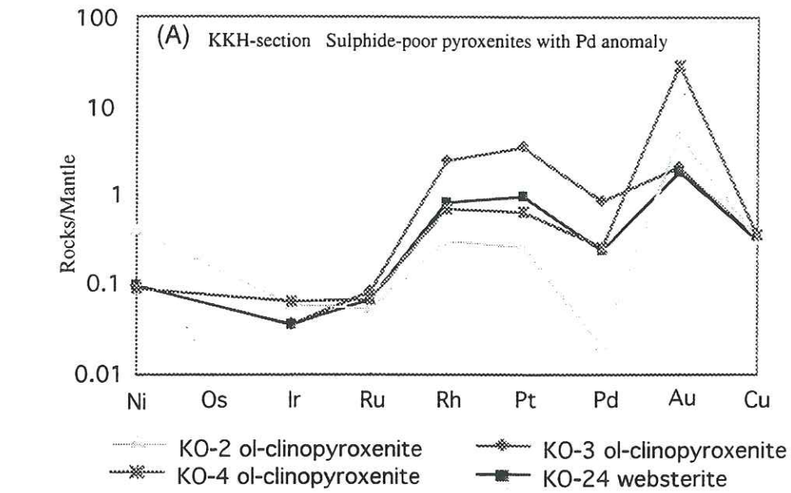

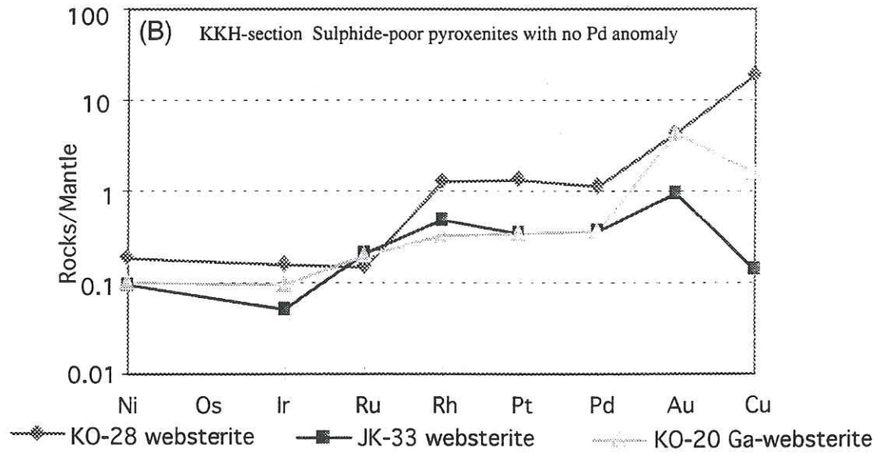

Figure 102. Mantle-normalized metal abundances for the pyroxenitic rock exposed along the KKH-section, Jijal Complex, Kohistan Arc. Average mantle-values are from Barnes et al. (1988). (A) with negative Pd anomaly; (B) with no negative Pd anomaly.
Concentrations métalliques dans les pyroxénites de la coupe de la KKH, Complexe de Jijal , Arc du Kohistan. (A) avec anomalie negative en Pd; (B) sans anomalie négative

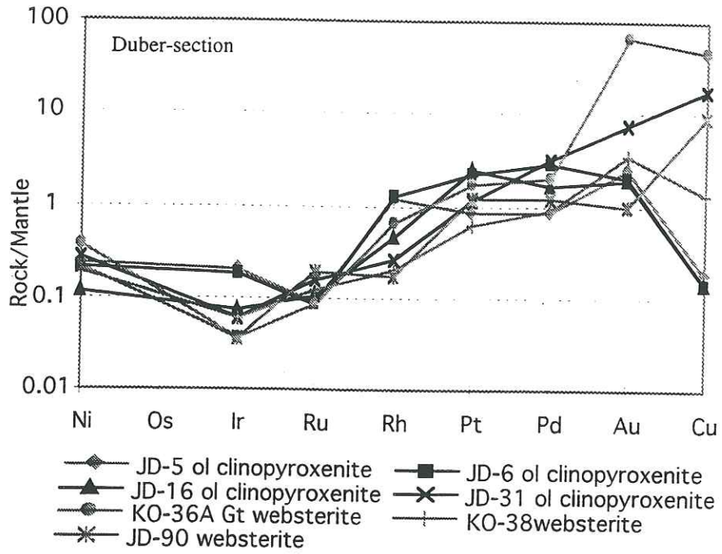

Figure 103. Mantle-normalized distribution of Ni-PGE-Au-Cu in ol-CPX and websterite pyroxenites of the Duber section, Jijal Complex, Kohistan Arc. Average Mantle-normalized values are from Barnes et al. (1988).

Concentrations normalisées au manteau de Ni-EGP-Au-Cu des ol-CPX & websterite de la coupe dela Duber, Complexe de Jijal , Arc du Kohistan.

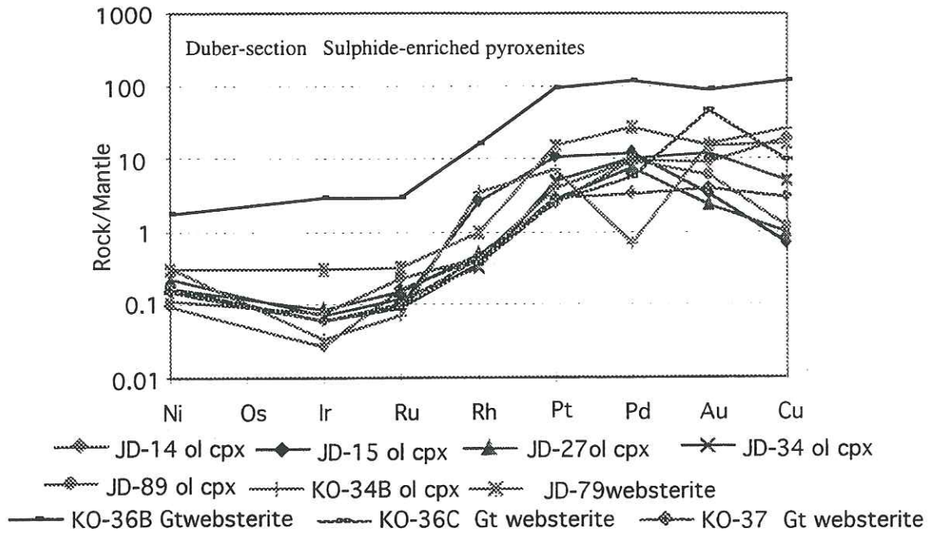

Figure 104. Mantle-normalized diagrams showing Ni-PGE-Au-Cu patterns for the pyroxenite rocks of theJijal Complex and average mantle-normalizing values from Barnes et al. (1988).

Concentrations normalisées au manteau de Ni-EGP-Au-Cu dans les pyroxènites enrichies en sulfures de la coupe de la Duber, Complexe de Jijal , arc du Kohistan.

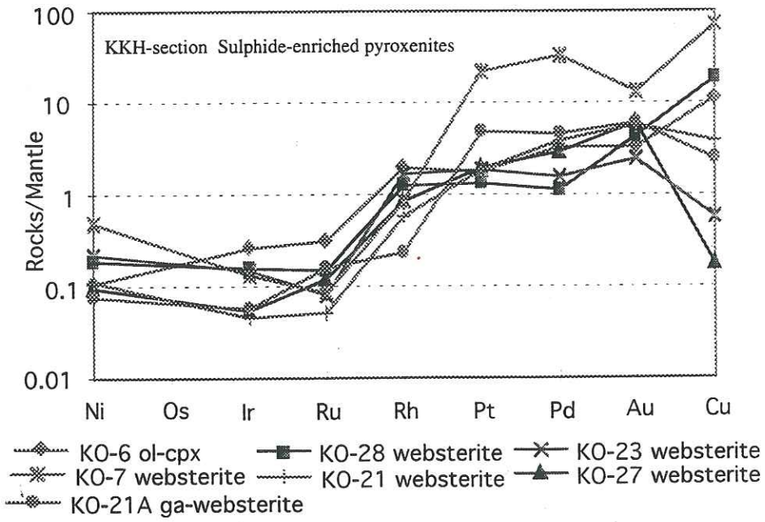

Figure 105. Mantle-normalized metal abundances for the slightly sulphide-enriched pyroxenitic rock exposed along the KKH-section, Jijal Complex, Kohistan Arc and average mantle-values are from Barnes et al. (1988).

Spectres normalisés au manteau de Ni-EGP-Au-Cu des gabbros à grenat enrichis en sulfures du Complexe de Jijal le long de la KKH

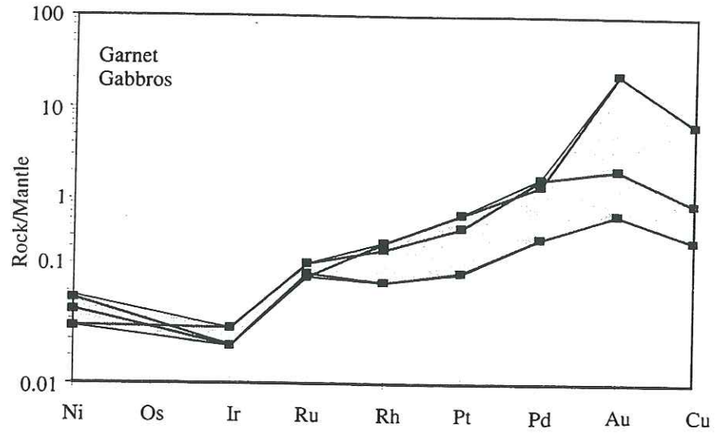

Figure 106. Mantle-normalized diagram showing Ni-PGE-Au-Cu patterns for the garnet gabbro of theJijal Complex and average mantle-normalizing values from Barnes et al. (1988).
Spectre normalisé au manteau de Ni-EGP-Au-Cu des gabbros à grenat du Complexe de Jijal.

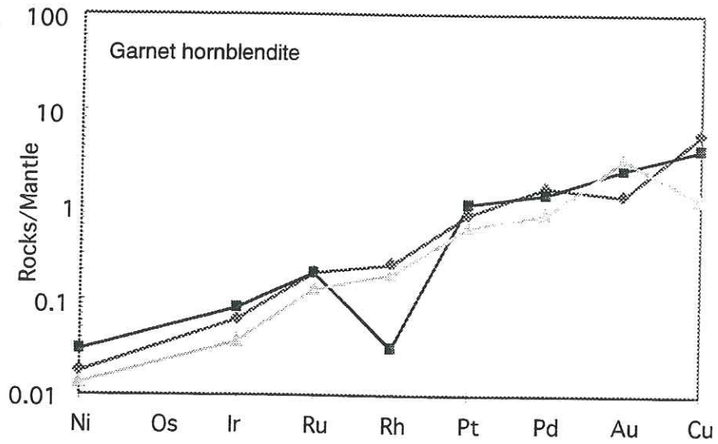

Figure 107. Mantle-normalized diagram showing Ni-PGE-Au-Cu patterns for the garnet hornblendite of theJijal Complex and average mantle-normalizing values from Barnes et al. (1988).

Valeurs normalisées au manteau de Ni-EGP-Au-Cu des hornblendites à grenat du Complexe de Jijal.

corresponding peaks of Au, Pd and Pt (Fig. 104). This feature is so consistently developed that it is unlikely to be secondary consequence of postmagmatic remobilization. Hydrothermal or deuteric remobilization of initially homogeneous sulphides would be expected to disperse the more mobile elements (Au,Cu &Pd) in an irregular fashion. This feature is well documented in the case of sulphides in garnet gabbro (Fig. 106). Here, the alteration has strongly disturbed the positive correlation between the Cu and Au and PPGE's. It is the most unlikely that such remobilization would move PGE's consistently downward below the original level, or would effect Ir, Ru and Rh more than Pt and Pd, and all the PGE's more than Au. The highly persistent shape of sulphide-bearing metals patterns and lack of decoupling of Au, Cu, Ni and S, all argue against any significant postcumulus effects. It is, therefore, justifiable to assume that the observed sulphide and PGE's distribution reflects primary cumulus processes.

1.3.2 Ni/Cu vs Pd/Ir and Cu/Ir vs Ni/Pd diagrammes.

Figures 108 a & b showing Pd/Ir versus Ni/Cu and Ni/Pd versus Cu/Ir ratio respectively, first proposed by Barnes et al. (1985), provide another discriminant of the tectonic association of different rock types; as well, it allows recognition of evolutionary trends for cogenetic igneous suites.

In these diagrams (Fig. 108a-b), dunites samples both from the KKH and Duber sections, plot within the mantle field which highlight the primitive nature of the complex and corroborate previous findings that ultramafic rocks from the Jijal complex crystallized near the crust-mantle boundary. The majority of the remaining samples fall in or adjacent to the field for layered intrusions, in accordance that this complex represents remnants of a deep magmatic chamber. The Ni/Cu and Pd/Ir ratios of the sulphide samples from the Jijal Complex also show a broader range but on the ratio diagrams (Fig. 108) they also cover the layered intrusions field, corroborating their magmatic origin.

Due to bulk partition coefficients of Ni, Cu, Pd and Ir with olivine, sulphide and chromite, the important variations of the metal ratios Ni/Cu (Fig. 108A) indicate that the more evolved lithologic units can mainly be related to the more primitive rocks through extensive fractional crystallization of olivine. Variations of the Cu/Ir (low Cu/Ir ratio) and more evolved rocks, while the different representative points are also scattered parallel to the vector for sulfide precipitation (important Ni/Pd and Cu/Ir variations).

In this way, the entire sequence of crystallization upwards from the base of the ultramafic cumulate is accompanied by the precipitation of chromitites and sulphides.

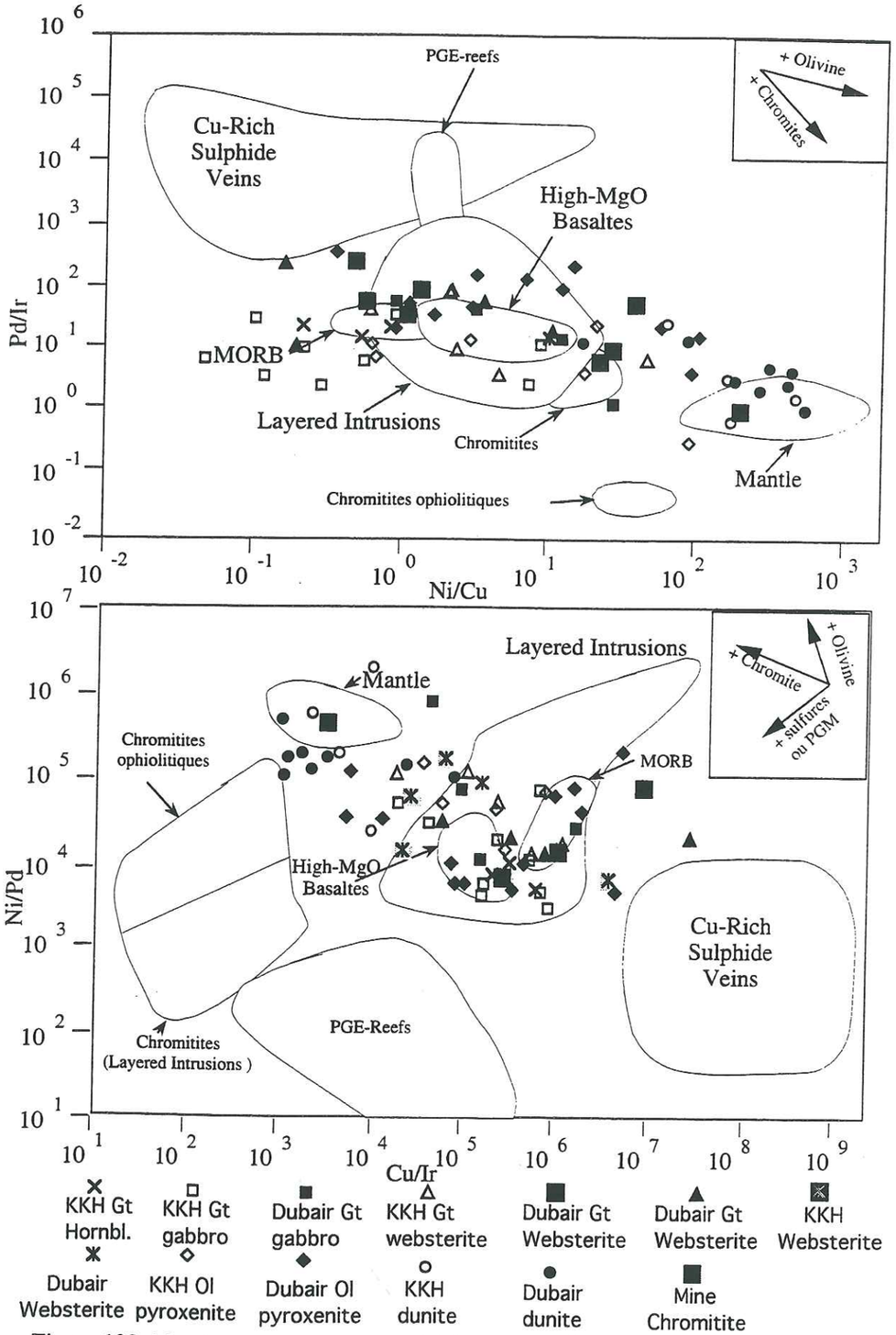

Figure 108. Metal ratio diagrammes of Pd/Ir versus Ni/Cu and Ni/Pd versus Cu/Ir for the Jijal Complex. Fields boundaries for mantle, high-MgO basalt, layered intrusions, PGE-reef, Cu-rich sulphides, chromitite ophiolites, MORB, and mineral-control vectors, are taken from Barnes et al. (1988); Barnes (1990).

Diagrammes Pd/Ir en fonction de Ni/Cu, et Ni/Pd en fonction de Cu/Ir pour le Complexe de Jijal. Limites des champs du manteau, des intrusions litées de basalte riche en MgO, des EGP-reef, des sulfures riches en Cu, des ophiolites à chromite, et des MORB

1.3.3 Thermodynamic constraints for PGE's distributions

Ir and its geochemical analogues Os and Ru form high-temperature alloys and behave as compatible elements, being retained in refractory mantle residues (Lorand, 1989) or precipitate early, and are usually associated with the chromite precipitation which occurs during an increase of the oxygen fugacity in equilibrium in the silicate melt. The Pd-group PGE's are postulated to be incompatible elements partitioned into the silicate melts, but they are also strongly partitioned into sulphides relative to silicate minerals and melts (Naldrett and Duke, 1980). The investigations of Barnes et al. (1985, 1988), Peach et al. (1990), Fleet et al. (1981) and Stone et al. (1990) have led notably to a better understanding of PGE's behaviour by taking account of their partition coefficients with different liquid or solid phases. These observations suggest that in a silicate magma the differentiation and precipitation of PGE's are basically controlled by the oxygen fugacity and sulphur fugacity in equilibrium in the silicate melt.

The most comprehensive thermochemical experimental data on the behaviour of PGE's in the silicate melts has been published by Amossé et al. (1990), Amossé and Allibert (1993) and Amossé et al. (1996), from which the following summary is presented.

IPGE's (Os, Ir, Ru) precipitate at an early stage, when the oxygen fugacity in equilibrium with the silicate melt is of the order of 10^{-5} bar. This is similar to oxygen fugacity occurring during the precipitation of chromite (Hill and Roeder, 1974). It was also suggested that the Ir-bearing minerals may nucleate in association with chromite.

In the presence of a sulphide liquid, the PGE's behave as chalcophile elements and the most important phase controlling the PGE's in all of these processes is sulphide liquid. Around oxygen fugacity of 10^{-7} bar, the solubility of PPGE's (Rh, Pt, Pd) increases sharply when the sulphur fugacity reaches a value of the order of 2.10^{-2} bars, then the formation of a sulphidic complex liquid (e.g. Monosulphide Solid Solution) soluble in the silicate melt is formed. Monosulphide solid solution (MSS) then crystallizes from this liquid at relatively lower temperature. PGE's in MSS might normally exsolve to form PGM's or might crystallize directly from the Ni-Cu-Fe-S liquid (Makovicky et al., 1986; Naldrett, 1989). The value of the sulphur capacity in the silicate melt is then very important for the continuity of this process. Such processes act as promoters for the PPGE's sulphides and other PGM's such as the arsenides and tellurides. The precipitation of PPGE's sulphide phases is thus a function of the degree of saturation of sulphur in the melt. This can be linked to the 'sulphide capacity', Cs, of the magma in the following equation:

$$Cs = \frac{S\% \times (fo_2)^{1/2}}{(fS_2)^{1/2}}$$

Effectively, the decrease of the sulphide capacity, due to a modification of the silicate melt composition, induces a concomittant increase of the sulphur fugacity in equilibrium with this

melt. If saturation occurrs, an Fe-Ni-Cu-S liquid (with PGE) may be separated. These thermochemical data will be useful to explain the PGE's behaviour during differentiation processes of the Jijal Complex silicate melt.

In the **Duber- and KKH-sections** (Figs. 88 & 89), as well as the precipitation of ferrochromite, are the consequence of an increase in oxygen fugacity (Hill, 1984; Hill and Roeder, 1974) in equilibrium with a magmatic liquid after the precipitation of minerals containing ferrous iron (Merkle and VonGruenewaldt, 1986; VonGruenewaldt et al., 1989). Of the above, the ability of chromite to remove the IPGE's appears well established (Barnes et al., 1988).

Five enrichment zones of IPGE's in Duber Valley (Fig. 89; horizons 1a, 1d, 1c, 2a and 2b) and, similarly, two enrichment zones of IPGE's along KKH (Fig. 88; horizons 1a, 2a and 2b) can be interpretted in terms of the above considerations. In the light of experimental results of Amossé et al. (1990) Ir solubility decreases with increasing oxygen fugacity similar to those occurring during the precipitation of chromite. As confirmed by mineralogical observations, the IPGE's are normally associated with chromite. However, we do not find any IPGM's in chromites. Keays (1982) suggested that olivine also plays an important role in concentrating the IPGE's, although this idea failed to receive general acceptance and will be dealt in detail in the following section. Anyhow, in the profiles of Duber and KKH; Ir, Ru, and Rh correlate strongly with one another and peak at the same position as Cr . Enrichment of Cr is related to spinel and chromite and Ni is compatible with olivine (no sulphide is found in dunites). These Cr, Ni and IPGE's represent the first-type of mineralization.

Second-type of enrichment anomaly of both Ni-Cu-PPGE's and IPGE's with small Cr enrichment, is associated with Ni and Cu sulphides (horizons 4a, 5a and 5b; Figs. 88&89). These enrichment zones are located in the websterites and garnet websterites. The enrichment zone 4a in websterite along Duber Valley and KKH presents a very weak Cr, Ni and Cu enrichment that corresponds to precipitation of disseminated sulphides, chalcopyrite and pentlandite. The enrichment zone 4a and 5a along KKH, is comparatively more enriched in Cr, base metal sulphides and PPGE's than the same levels in Duber Valley. The enrichment horizon 5b in Duber valley is more enriched than the KKH. This stage of sulphide precipitation appears to have followed the crystallization of ferrochromites in dunites. Following the main precipitation of chromite in dunites, high Cr contents suggest again relatively high oxygen fugacity, while sulphides reveal increasing sulphur fugacity in equilibrium with the liquid. Palladium, palatinum and rhodium are complexed by the sulphur, being maintained in solution and then precipitated with the base metal sulphides (Ni, Cu and Fe).

The most important enrichment zone involving Ni, Cu, Ir, Ru, Pt, Pd and Au in Duber valley (Fig. 89) corresponds in the garnet websterite (U5) to prominent peaks of Ni-Cu

sulphide abundance while Cr contents are low. Ir, Ru and Rh correlate strongly with one another and show similar patterns to those of Pt and Pd. This precipitation of Fe-Ni and sulphides is linked to the relative increase of Fe and S activities in the remaining silicate melt.

These PGE's data confirm that the Jijal PGM chemistry, mainly dominated by Pd and Pt minerals and by the relative scarcity of Ir and Ru minerals. The formation and behaviour of immiscible sulphide-bearing liquid phases without any ambiguity have an important effect on the precipitation of PGE from magma. But presence of mercurides, arsenides and tellurides in some PGM complicates the mode for distribution of PGE's, suggesting the possible involvement of magmatic fluid phases, in part, for PGE formation and distribution.

Finally, the **garnet gabbro** in Duber as well as in KKH sections shows small enrichment horizons (6a and 6b, Figs. 88&89) involving Pd, Pt and Cu in the former. This corresponds to the third type of PGE's enrichment. Such PPGE's enrichment in gabbros could also suggest Merensky Reef type mineralization, and Pt and Pd enrichment may suggest probably magmatic origin. But high Cu and low Ni contents suggest a possible mobilization of these elements by fluids.

1.3.4 IPGE's Behaviour

The observed fractionation of IPGE's from the PPGE's during the crystallization of the Jijal Complex is a well-documented feature of ultramafic silicate melt. While the compatible behaviour of Ir, Os and Ru during the fractionation of mafic magmas is generally accepted, the reason for this, and the mineral which accommodates these elements, are subject to debate. Although the most straightforward interpretation is that the IPGE's are compatible with olivine (the main fractionating phase), this idea has failed to receive general acceptance, for two main reasons. Firstly, it is not obvious that IPGE's should be accommodated in the olivine lattice, and until recently, no experimental data were available to suggest otherwise. Second, attempts to measure directly the PGE's contents of olivine have yielded contradictory results. Olivine orthocumulates are reported to have higher Ir contents than mafic and ultramafic volcanics (Crocket and Chyi, 1972; Crocket, 1981; Oshin and Crocket, 1982). Olivine separated from the cumulate zone of a komatiite flow in the Kambalda area of Western Australian was found by Ross and Keays (1979) to contain 5.7 ppb of Ir. On the other hand, olivines from spinel and garnet lherzolites have variable but much lower Ir contents between 0.07 and 0.5 ppb (Mitchell and Keays, 1981). This result led to speculation that Ir is incompatible with olivine. However, ultramafic nodules often contain sulphide phases, which may indicate that they equilibrated with a sulphide liquid during their complex history (Keays et al., 1981), and their Ir contents need not necessarily be comparable to those of olivines that crystallized from sulphide-free liquids.

A number of studies indicate that chromite is a major concentrator of IPGE's (Gijbels et al., 1974; Agiorgitis and Wolf, 1978; Oshin and Crocket, 1982; Page and Talkington , 1984;

Stockman and Hlava, 1984). Chromite mineral separates from Heazlewood River Complex, Tasmania, contribute 3-71 % of the total Ir in the sample which corresponds to an enrichment factor of 4-180 for the chromite fraction relative to the silicate minerals (Peck and Keays, 1990). This result suggests that IPGE's are compatible with chromite, and might be taken to indicate that crystallization of chromite, an important accessory phase in ultramafic rocks of Jijal Complex, may have caused the depletion of Ir-group in low-MgO samples (such as garnet gabbro).

The good positive correlation between Mg-number, Ni and chromite composition and whole-rock Ir abundance (Figs. 109A, B & C) clearly demonstrates that the IPGE's are partitioned into the most primitive cumulates. The fact that IPGE's-enrichment is only observed in the most primitive sequence of cumulates (dunites) is evidence for a fractional crystallization-temperature control and oxygen fugacity. A similar conclusion was reached by Tredoux et al. (1986) from their study of the PGE geochemistry of mafic and ultramafic rocks from the Kaapvaal Craton, South Africa. It, therefore, seems likely that chromite along with olivine can be an effective concentrator of IPGE's in the silicate melt. Furthermore, coprecipitation of PGE-bearing phases with early crystallizing silicate minerals, as proposed by Keays (1982), is a process that may cause irregular distribution of Ir and Ru throughout the magma body, in a way similar to that caused by crystallization of chromite (and moreover sulphides).

1.3.5 Negative Pd anomalies

The distribution of Rh, Pt, Pd and Au in the Jijal Complex are more easily understood as these elements are mainly controlled by sulphides precipatation. Both Pt/Ir and Pd/Ir increase from the most primitive cumulates (dunite) to more evolved rocks. The most chalcophile precious metals (Pt, Pd, Au) should experience a steady increase during fractional crystallization. Therefore, evolved silicate melts represent an extremely fertile magma for the formation of PPGE's + Au mineralization.

However, the more incompatible behaviour of Pd than Pt in the parent silicate melts for the Jijal Complex may explain the negative Pd anomaly in some olivine-clinopyroxenites of the KKH-section. In the case of Jijal Complex, some part of the chamber did not reach the S-saturation through fractional crystallization or contamination, and hence their great potential for generating PPGE's deposits remained untrapped.

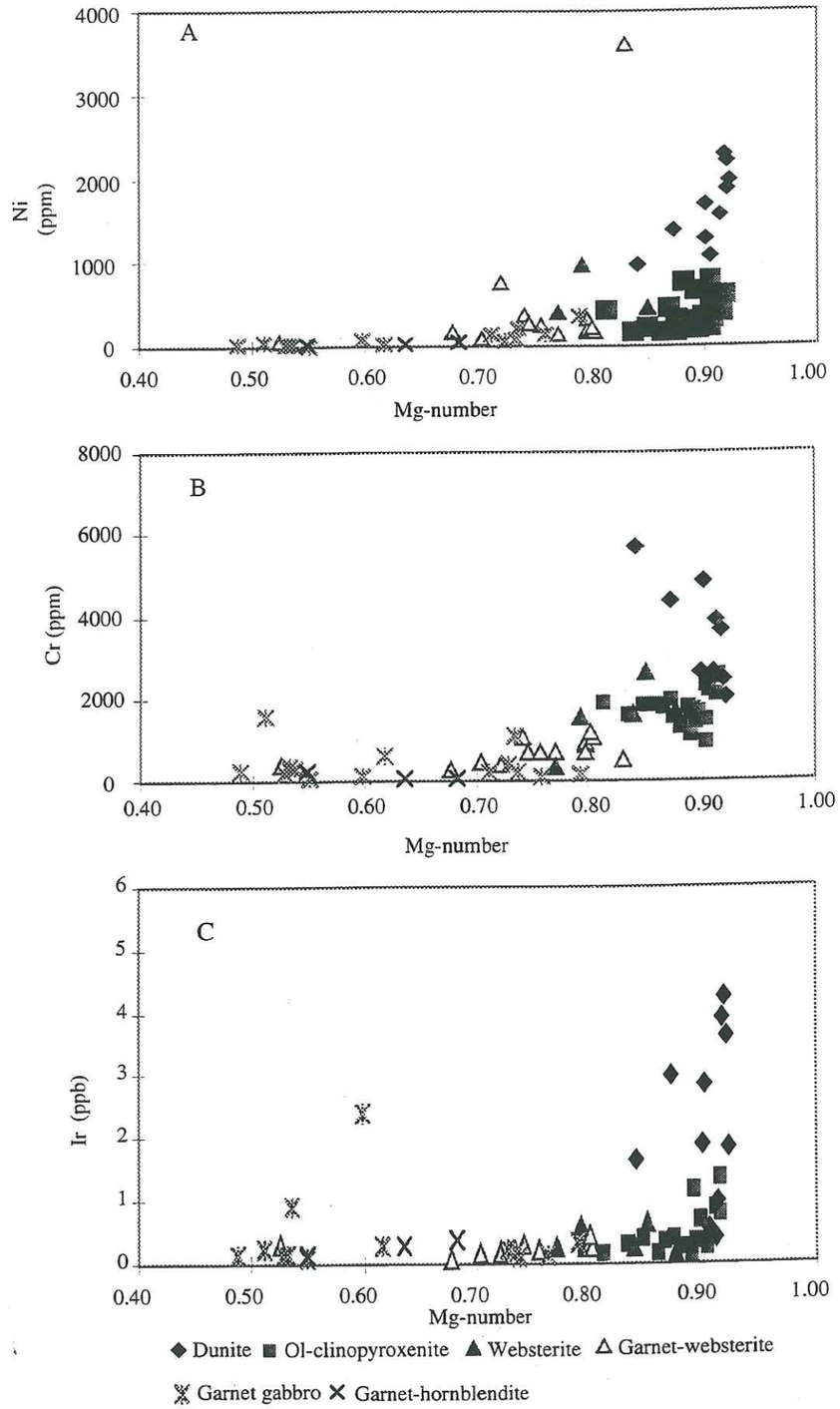

Figure 109. Selected variation diagrams based on values of abundances of Ni, Cr and Ir versus whole-rock Mg-number for the rocks of the Jijal Complex.
Diagrammes des teneurs en Ni, Cr et Ir en fonction de l'indice de Mg sur roche totale pour les roches du Complexe de Jijal .

CONCLUSION

Spat and Chilas Complexes

In Spat and Chilas complexes, PGE's contents are lower than in Jijal Complex, and no significative anomalies have been observed.

In Spat Complex, total concentrations of PGE's in dunites are variable from 13.7 ppb to 122 ppb. Olivine clinopyroxenite has relatively more total PGE's concentration ranging from 49 ppb to 58 ppb and the most evolved rock gabbro has total PGE's concentration of 13 ppb.

In the Chilas complex, dunites from the **Thak Gah Ultramafic Association**, have total PGE's concentrations between 14 ppb and 34 ppb, except for some Cr-enriched dunite which has 1002 ppb abundances. Pyroxenites have total PGE's concentration from 13 ppb to 19 ppb and total concentration of PGE's in gabbro range between 6 ppb and 20 ppb. In **Main Facies Zone**, gabbronorite shows total PGE's concentration between 8 ppb to 17 ppb.

So Spat and Chilas Complexes are not likely prospect for stratiform-sulphide mineralization owing to the failure of these liquids to reach S-saturation.

Metal patterns of mantle-normalized abundances for both the complexes reveal that dunite display slightly negative to almost flat (Pd/Ir=0.4 to 1.3; Spat Complex) to slightly positively sloping (Pd/Ir=4 to 7; Thak Gah Complex), which exhibits their relative enrichment in Ni and IPGE's. In contrast, samples from the pyroxenite display more pronounced positively sloping metal patterns from Ir to Pt, which indicates their relative enrichment in PPGE's (Pd/Ir=4 to 30; Thak Gah Complex). The gabbro and gabbronorite from Thak Gah Ultramafic-Mafic Complex have similar fractionated pattern from Ir to Pt and show negative Pd anomaly similar to olivine-clinopyroxenite of Jijal Complex. In contrast, gabbronorite from the Main Facies Zone shows almost flat pattern from Rh to Pd.

These metal patterns indicate that the PPGE's and Cu were preferentially incorporated into more evolved rocks implies relatively incompatible behaviour for these elements. Such incompatible behaviour of Pt, Pd and Au in both the complexes is attested by their increasing abundances in more evolved rocks. An exception to this general trend involves the Pt-enrichment for the dunite sample from the Thak Gah Complex. The observed enrichment particularly in Pt in dunite sequence (KO-57B) may be related to the precipitation of isoferroplatinum alloy. The factors responsible for the anomalous high Pt abundances in this sample (KO-57B) are however poorly understood.

The IPGE's and Ni were strongly partitioned into the most primitive rock (dunite) during the formation of these complexes, which reflects the compatible behaviour of these elements. The good positive correlation between IPGE's and Ni and Cr clearly indicates that olivine fractionation in combination with early chromite removal can explain the decrease in Ir and Ni

values between primitive and more evolved rocks from the Thak Gah and Spat Complexes. It also accounts for the substantial negative IPGE's anomalies on the mantle-normalized diagrammes of both the complexes.

To summarize, the results indicate that IPGE's behaved as compatible and partitioned into the early crystallizing cumulates, and Pt, Pd and Au remained in residual melts during the crystallization of these complexes.

Jijal Complex

Three main types of magmatic concentration of PGE's are present in the Jijal Complex in chromitite and in sulphide deposits.

1- IPGE's concentrations related to the crystallization of chromite in the different dunite units (1a to 2b; total PGE's concentration=196 ppb).

2- IPGE's and PPGE's concentrations related to the crystallization of Ni-Cu sulphides as thin horizons in the websterite and garnet websterite units (4a and 5a-b; total PGE's concentration=1417 ppb).

3- mainly PPGE's concentrations related to the crystallization of Cu sulphides in the garnet gabbro units (6a and b; total PGE's concentration=196 ppb).

These three types of mineralization correspond to three stages of magmatic evolution.

During the first stage, IPGE's were partitioned into early-formed cumulates (chromitite and dunite) while Rh, Pt, Pd and Au remained in residual silicate melts. IPGE's distribution is mainly controlled by high oxygen fugacity of the magma which favoured chromite, spinel and probably IPGM's crystallization (though not observed in thin sections). The precipitation of chromite and iron have brought abrupt thermodynamic change and induced increasing of sulphur fugacity in upper residual magmas. Olivine fractionation in combination with early chromite removal can explain the decrease in Ni and IPGE's values respectively between primitive and evolved cumulates. It also accounts for the substantial negative IPGE's anomalies on the mantle-normalized diagrams.

During the second stage, clinopyroxene and orthopyroxene precipitated at high temperature and pressure (900° to 1100°C, 10 to 12 kbar) under higher sulphur fugacities favouring formation of an immiscible sulphide liquid which segregated in websterite and garnet websterite. This latter collected almost all PGE's, leaving a depleted silicate liquid. In the corresponding enriched horizons, base metal sulphides are pentlandite, pyrrhotite, chalcopyrite and pyrite. These are present in the form of inclusions in or on the edges of the silicate

assemblages. Platinum-group minerals (temagamite, moncheite, merenskyite and sperrylite) and platinum-group element (PGE's) bearing phases occur as inclusions within sulphides and silicates, and as interstitial grains between silicate and sulphide grains. These PGM are believed to form two generations, the first having been trapped during sulphide and clinopyroxene segregation, the second having been formed during subsolidous recrystallization.

During the last stage, garnet gabbros crystallized under lower temperature (800 to 900°C) and pressure (9 to 10 kbar). Residual PGE's have been concentrated in the late magmatic fluids, then collected by chalcopyrite and precipitated as disseminated phases (horizons 6a-b).

The experimental work of Stone et al. (1990) indicates that all PGE's have very high partition coefficient between sulphide and silicate liquid. In the PGE's enrichment horizon 4a, 5a and b (type-2) where there is little olivine and chromite fractionation, the IPGE's metals distribution is similar to that of PPGE's, indicating that sulphide segregation alone controlled the PGE's in these enrichment horizons. From this, it can be concluded that the high concentrations of PGE's within these horizons could be explained by the segregation of magmatic immiscible sulphide liquids.

The precious metals display the following affinity for primitive cumulates, in order of increasing compatibility Au<Pd<Pt<Rh<Ru<Ir. This sequence illustrates the influence of melting point on the solubility of the PGE's and Au in primitive magmas (Tredoux et al., 1986). The positively sloping mantle-normalized metal patterns of olivine clinopyroxenite, websterite, garnet websterite, garnet hornblendite and garnet gabbro from the Jijal Complex are a consequence of the range of compatibility displayed by the PGE's during fractional crystallization. Negative Pd anomaly in some pyroxenite samples is a consequence of the extremely incompatible behaviour of this element in relatively S-poor silicate melts.

So the high concentrations of all PGE's, the relatively strong positive mantle-normalized patterns and low to medium values of Pt/(Pt+Pd) ratios support a magmatic origin for these ores.

However, PGM's are mainly tellurides with less or more mercury suggest fluid participation in sub-solidous crystallization processes. The silicate mineral associations, indicate anhydrous conditions of crystallization in ultramafic sequences, while fluids phase played a relatively important role in upper sequences (garnet clinopyroxenites to garnet gabbros). Such fluid could be an heritage from metasomatized mantle in the subduction coin.

Such types of PGE's concentration observed in the ultramafic cumulate of the Jijal Complex (and other mafic-ultramafic complexes like Spat, Thak Gah and Chilas) present important differences with layered intrusions like Bushveld or Stillwater-types. Deep in the

ultramafic zone, where mixing of new inputs of primitive magma with resident magma may has occurred before sulphide saturation, chromitites (U2) that are not enriched in sulphide and thus are poor in Pt and Pd, have formed. These may be the equivalents of the chromitites of the Bushveld Lower Zone and most of the Stillwater Complex.

Our results provide a satisfactory explanation of the observed PGE distribution whilst no evidence implying the influence of the magma mixing at the origin of the sulphide-riched horizons was found, as it has been suggested in other layered intrusions. The onset of sulphide saturation due to simple crystallization without magma mixing can give rise to deposits such as we see in the garnet websterite (U5) of the Jijal Complex. In the Merensky Reef, there is evidence to suggest that magma mixing in a turbulent plume assisted the sulphides to scavenge PGE's from the magma. In Jijal, such types of sulphide concentrations can occur at any level in an intrusion, depending on how close the magma was to sulphide saturation initially. These sulphide zones are not likely to be associated with the bases of cyclic units such as the Merensky Reef. Finally, field as well as petrographic study indicates that the highly fractionated PGE's proportions of the garnet websterite of Jijal Complex are unlikely to be the consequence of direct hydrothermal deposition of the PGM's.

Our results are in agreement with derivation of high Mg-melts from partial melting of a refractory mantle source characteristic of an arc environment. **So, the Jijal Complex and its PGE's enriched ores might be considered as a PGE-arc type mineralization.** Pyroxenitic cumulates could be good indicators of local PGE's concentration in this type of ore-body.

GENERAL CONCLUSION

GENERAL CONCLUSION

The Kohistan-Ladakh tectonic province of northern Pakistan, linking the Indian plate to the south and Asian plate to the north, is an intriguing place which provides a window to a system, having a continuous sequence of an initial immature to short-lived mature intra-oceanic island arc and from then on to an Andean-type magmatism. During the Himalayan collision, this arc was partially subducted under the Asian plate and then obducted onto the Indian plate. Deep dissection, through uplift and deep erosion, exposes a virtually complete section from its ultramafic underpinnings at the crust/mantle boundary to surface volcanic rocks through the crust of an oceanic island arc. The resulting terrane, then allows to study the deep, early magmatic processes to the higher-emplaced differentiates of lower crustal magma chambers. The intra-oceanic nascent arc crust in the southern Kohistan, is represented by the Jijal Complex along with Spat Complex, the Kamila Amphibolites and the Chilas Igneous Complex.

Petrologic and tectonic evolution of the southern Kohistan

The main petrological and geochemical features of the igneous rocks representing the southern Kohistan have been discussed and compared in PART-1 of this thesis.

The **Jijal Ultramafic-Mafic Complex**, exposed along the northern fringe of the Main Mantle Thrust (MMT), is interpreted to be the root zone of the Kohistan arc that crystallized at the base of an immature intra-oceanic island arc. The Jijal Complex is a layered sequence that contains two distinct sections. The basal section is composed of ultramafic rocks consisting basically of layered dunites, olivine-clinopyroxenite and websterite which evolves to garnet-websterite and garnet-clinopyroxenite to the top. The upper section is mainly composed of layered garnet gabbros. Whole rock geochemistry and mineral chemistry indicate that the Jijal Complex formed by fractional crystallization from a high-Mg tholeiitic melt in an island arc environment. The ferromagnesian minerals show large chemical variations in accordance with the lithological change in the series from dunite to garnet gabbro. Mg content of olivine regularly decreases from Fo_{94} to Fo_{78}. Clinopyroxene also evolves from $Ca_{48}Mg_{49}Fe_3$ in dunite to $Ca_{49}Mg_{33}Fe_{18}$ in garnet gabbro, while Al and Ti contents increase with decrease of Mg-number. Orthopyroxene probably crystallized late with Mg-number 85 in the earlier stage to 76 in the latter stage. Garnet, which clearly exhibits exsolution from clinopyroxene as well as subsolidous recrystallization, characterized by $Al_{37}Py_{30}Gr_{29}Sp_2Ad_2$ in garnet websterite to $Al_{43}Py_{33}Gr_{21}Sp_1Ad_2$ in garnet gabbro.

The rocks from the Jijal Complex were crystallized from a melt at pressures between 10 and 12 kbar (35 to 40 km depth) and equilibrated at temperatures of 800° to 1100°C based on the phase relationships in the cumulus assemblages, clinopyroxene-orthopyroxene, garnet-orthopyroxene and garnet-amphibole thermobarometry and olivine-spinel thermometry. Mineral

chemistry, appearance of clinopyroxene and orthopyroxene having high Mg-number (92-85), coprecipitating with forsteritic olivine (Fo $_{94-85}$) and absence of plagioclase as an early fractionating phase, also point to a high-pressure crystallization history.

In the '**Thak Gah Association**, Chilas Complex, mineralogy and textural relationships are quite different from the Jijal cumulates. Pyroxene and spinel are more Fe-rich. As a result, chemical trends in minerals do not indicate the same high-pressure origin as Jijal cumulates. Based on phase relationships in the cumulus assemblages, pressure of formation for this complex can be constrained within 5 to 6 kbar. They were crystallized from a melt at a temperature of 800° to 950°C, as deduced from geothermometery based on two pyroxene pairs. This lower pressure implies that Thak Gah Complex probably represents a contemporary, shallower magma chamber in the same Kohistan arc. Their mafic bulk composition (Mg/(Mg+Fe)= 69 in dunite, 67 in wehrlite to 45 in isotropic gabbro and FeO/MgO= 0.45 to 1.24) probably represent crystallization of a primitive magma at relatively shallower levels in the crust.

The coarse-grained plutonic Kamila Amphibolites and the Chilas Igneous Complex formed from similar processes during Early - Cretaceous time. Field, petrographic and geochemical data indicate similarities in petrogenetic and tectonic setting between these different rock assemblages of the southern Kohistan arc. These are further evidenced by the striking similarity and uniformity in their MORB- and chondrite-normalized pattern shapes and Eu anomalies. The general pattern with a LILE enrichment and a negative Nb and Ta anomalies is similar to modern arc related basaltic to andesitic rocks. The rocks from the garnet gabbro of the Jijal Complex and the coarse-grained Kamila Amphibolites show the insular arc tholeiitic character while rocks from the Main Facies Zone of the Chilas Complex exhibit the progression from tholeiitic to calc-alkaline arc affinity. Nb contents, which are abnormally high for arc tholeiites, are in the range of N-MORB, suggesting emplacement in the nascent stage of the arc development. Thus, it seems reasonable to believe that the southern Kohistan terrane has evolved from a nascent to a mature stage of the Early-Cretaceous intra-oceanic arc, with plutonic rocks from the Kamila Amphibolites and Main Facies Zone of the Chilas Complex crystallized in a relatively shallow magma chamber. The final collision of the Kohistan arc with the Asian plate to the north (Late-Cretaceous) ceased the intraoceanic stage of magmatism in southern Kohistan.

Within the Kamila Amphibolites, some **blocks of fine-grained amphibolites representation of metavolcanics** are more depleted in K-group element, having low Rb/Sr ratio relative to island arc associations, relatively enriched in some high-field strength (Ti, Ta and Nb) and heavy rare-earth elements. Their chemistry is more akin to the N-type MORB, suggesting that the complex-metavolcanic amphibolite association of the Kamila Amphibolites, and similar units occurring elsewhere in the Kamila Amphibolites may represent the fragments

of pre-existing oceanic crust that formed entirely within an intra-oceanic setting. The fact that relict of oceanic crust is discernible in the Kohistan arc may suggest that some part of oceanic basement has either been incorporated into the latter plutonic rocks or was partially melted or digested in subduction.

In the first stages of island arc development, basaltic magmas cumulated near the crust-mantle boundary and are represented by the basic plutons of the Kamila Amphibolites which are arc tholeiitic in nature. The transitional arc tholeiitic to calc-alkaline composition of the Chilas Igneous Complex indicates the next stage of magmatism and shows subduction component, as reflected by negative Nb and Ta anomalies and trace elements. Further, the presence of igneous texture, magnesio-hornblende and the chemical evolution, suggest that these rocks crystallized in the upper plutonic unit of the oceanic crust. The Thak Gah Complex represents a stratigraphically lower unit in the Kohistan arc magma chamber, which was probably located in the plutonic middle crust. The Jijal Complex represents a piece of the lower crust and just up the mantle/crust boundary of a mature island arc. Lack of significant late-stage intrusions, suggest that the Jijal cumulates represent the last magmatic phase in a series of intrusions, emplaced at the crust/mantle boundary before suturing to the Asian plate in the north. Our study indicate that the arc crust was very thick and the magma chamber was present at a depth such that the pressure was between 10 to 12 kbar. The exposed thickness of the Jijal Complex is approximately 5 km which indicates that significant amounts of igneous material was underplated through crystallization. If the crust is already thickened, this underplating will take the form of high-pressure cumulate assemblages such as seen at Jijal Complex.

Thus, the southern Kohistan terrane represents the crustal section of the nascent to mature stage of Early-Cretaceous intra-oceanic arc. During the Early Cretaceous this arc was collided with the Asian plate in the north and latter obducted over the Indian plate during Miocene, exposing the full section.

PGE's and PGM's distribution in mafic-ultramafic complexes

Distribution of precious metals in mafic-ultramafic complexes from the southern Kohistan reflects several basic geochemical properties of the platinum-group elements (PGE's) and Au in arc environment.

The melts of **Chilas-, Thak Gah- and Spat-Complexes** remained S-undersaturated throughout the crystallization history. These complexes have low PGE's concentrations that correlate with indicators of magma evolution (Mg/(Mg+Fe). The PPGE's (Rh-Pt-Pd) and Cu behaved incompatibly as magma evolved, indicating that sulphide fractionation did not occur and they hold little economic prospects. However, the observed enrichment of Ir and Ru in chromite-rich dunite of both the complexes may be related to the early crystallization of Cr-spinel and olivine.

In the Jijal Complex, base metal sulphides (BMS), platinum-group minerals (PGM) and platinum-group element (PGE's) bearing phases are present in the form of inclusions in or on the edges of the silicate assemblages. The sulphide phases, characterized by pentlandite, pyrrhotite, chalcopyrite and pyrite, occur associated with the websterite and garnet websterite and interpreted to have segregated as an immiscible liquid at the high temperature magmatic stage. They occur as sulphide inclusions within silicates, and as interstitial grains between silicate grains. The PGE content of the BMS is dominated by Pt, Pd and Rh. The PGM and BMS, which are described here, are modally much less abundant and generally small in size (< 45 mm BMS; and < 20 mm PGM). The main PGM detected are temagamite, moncheite, merenskyite and sperrylite. Two generations of PGM are believed to be present, the first having been trapped during sulphide and clinopyroxene segregation, the second having been formed during subsolidous recrystallization. The silicate mineral associations indicate anhydrous conditions of crystallization in most ultramafic sequences, while fluid phase has played a more and more important role in the upper sequences (garnet clinopyroxenite to garnet gabbro). Such fluid could be an heritage from metasomatized mantle in the subduction environment.

Three main types of PGE's abundances in the Jijal Complex are:

1) **IPGE's concentrations corresponding to the crystallization of chromite in different levels of dunites.** This can be linked to the high oxygen fugacity of the magma which favours chromite, spinel and possible IPGM's crystallization. The chromite precipitation along with iron has induced increasing of sulphur fugacity in evolved magmas. As such, olivine fractionation in combination with early chromite crystallization can explain the decrease in Ni and IPGE's contents respectively between primitive and evolved cumulates. The IPGE's abundances in dunites are indicative of the compatible behaviour of these elements and good positive correlation between Ir, Ru and Ni and Cr demonstrates that both Ir and Ru are partitioned into the most primitive cumulate chromitite and Cr-rich dunites and can be clearly corroborated to early ferrochromite crystallization.

2) **IPGE's and PPGE's concentrations associated with Ni-Cu sulphides present as thin horizons in websterite and garnet websterite.** This can be linked to clinopyroxene and orthopyroxene crystallization at high temperature and pressure (900 to 1100°C and 10 to 12 kbar) under high sulphur fugacity. Such conditions favour formation of an immiscible sulphide liquid which segregated in websterite and garnet websterite. Various distinctive positive anomalies of IPGE's (Ir-Ru) and PPGE's (Rh-Pt-Pd) in Duber as well as along KKH sections of Jijal Complex are corresponding to prominent peaks of sulphide abundance reflected in Ni and Cu concentration. This is interpreted to suggest that Ir, Ru, Rh, Pt and Pd were controlled by sulphide segregation. Precipitation of sulphides have brought about the almost total removal of PGE's, whose concentrations in the residual melt

then became very low. As a result, the sulphide-bearing reef is overlain by a PGE-poor cumulate containing abundant plagioclase (garnet gabbro).

3) **PPGE's concentrations related to the crystallization of Cu-sulphides in garnet gabbro**. During this last stage, garnet gabbro crystallized under relatively low temperature (800 to 900°C) and pressure (9 to 10 kbar). Residual PGE's have been concentrated in the late magmatic fluids, then collected by chalcopyrite and precipitated as dessiminated phases.

The types of PGE's concentrations observed in the Jijal Complex present important differences with others layered intrusions like Bushveld or Stillwater-types. In the ultramafic zone, where mixing of new pulses of primitive magma with resident magma may have occurred and resulted in the increase of oxygen fugacity which precipitated chromite and ferrochromite. These chromitites (U2) are sulphide poor as they precipitated before sulphide saturation, and thus are poor in Pt and Pd. These may be the equivalents of the chromitites of the Bushveld Lower Zone and most of the Stillwater Complex.

In the Merensky Reef, there is evidence to suggest that magma mixing in a turbulent plume assisted the sulphides to scavenge PGE's from the magma. But in Jijal Complex, no evidence implying the influence of the magma mixing at the origin of the sulphide-riched horizons was found. Sulphide concentrations which are present in the Jijal Complex, can occur at any level in an intrusion, depending on how close the magma was with the bases of cyclic units such as the Merensky Reef. The onset of sulphide saturation due to simple crystallization without magma mixing can give rise to deposits such as we see in the garnet websterite (U5) of the Jijal Complex. Finally, field as well as petrographic study indicates that the highly fractionated PGE's proportions of the garnet websterite of the Jijal Complex are unlikely to be the consequence of direct hydrothermal deposition of the PGM's.

Our results are in agreement with derivation of Mg-rich tholeiitic melts from partial melting of a refractory mantle source and that the Jijal Complex **represents** a layered intrusions characteristic of an arc environment. **So, the Jijal Complex and its PGE's enriched ores might be considered as a PGE-arc type mineralization**. Pyroxenitic cumulates could be good indicators of local PGE's concentration in this type of ore-body.

REFERENCES

REFERENCES

Ahmed, Z. & Chaudhary, M. N. 1976. Geology of Babusar area, Diamir District, Gilgit, Pakistan. *Geol. Bull. Punjab University*, 12, 67 - 78.

Agiorgitis, G., Becker, R. & Wolf, R. 1977. Aspects of platinum elements distribution in some ultramafic and related rocks. *In*: Ahrens, A.H. (ed.) *Origin and distribution of the Elements*. Pergamon Press, Oxford, United Kingdom, 233 - 238.

Akella, J. & Kennedy, G. C. 1971. Studies on anorthite+diopside-hedenbergite at high pressures and temperatures. *Am. J. Sci.*, 270, 155 - 165.

Allégre, J. C. & Luck, J. M. 1980. Osmium isotopes as petrogenetic and geological traces. *Earth Planet. Sci. Lett.*, 48, 148 - 154.

Allen, J. C. & Boettcher, A. 1978. Amphiboles in andesite and basalt II. Stability as a function of P-T-fH_2O-fO_2. *Am. Mineral.*, 63, 1074 - 1087.

Amossé, J. & Allibert, M. 1993. Partitioning of iridium and platinum between metals and silicate melts: evidence for pervassivation of the metals depending on ¶o_2. *Geochim. Cosmochim., Acta*, 57, 2395 - 2398.

Amossé, J., Allibert, M., Fischer, W. & Piboule, M. 1990. Experimental study of the solubility of platinum and iridium in basic silicate melts- Implications for the differentiation of platinum-group elements during magmatic processes. *Chem. Geology*, 81, 45 - 53.

Amossé, J., Allibert, M., Fischer, W. & Piboule, M. 1987. Etude de l'influence des fugacités d'oxygène et de soufre sur la différenciation des platinoides dans les magmas ultramafiques-Résultats préliminaires. *Académie des Sciences Comptes Rendus*, 304, 1183 - 1185.

Amossé, J., Fischer, W., Allibert, M. & Piboule, M. 1986. Méthode de dosage d'ultra-trace de platine, palladium, rhodium et or dans les roches silicatées par spectrophotométrie d'absorption atomique électrothermique. *Analusis*, 14, 26 - 31.

Aoki, K. 1971. Petrology of mafic inclusions from Itinome-gata, Japan. *Contrib. Mineral. Petrol.*, 30, 314 - 331.

Aoki, K. & Kanisawa, S. 1979. Fluorine contents of some hydrous minerals derived from the upper mantle and lower crust. *Lithos*, 12, 167 - 171.

Aoki, K. & Kushiro, I. 1968. Some clinopyroxenes from ultramafic inclusions in Dreiser Weiher, Eifel. *Contrib. Mineral. Petrol.*, 21, 743 - 749.

Arbaret, A., Burg, J. P., Chaudhary, N. Dawood, H., Hussain, S. & Zeilinger, G. 1998. Different sets of anastomosing shear zones in the Kamila Belt, Kohistan. *Univ. Peshawar Geol. Bull.*, Special Issue, 31, 15 - 17.

Arculus, R. J. 1978. Mineralogy and petrology of Grenada, Lesser Antilles island arc. *Contrib. Mineral. Petrol.*, 65, 413 - 424.

Arculus, R. J. & Delano, J. W. 1981. Siderophile element abundances in the upper mantle: evidence for a sulphide signature and equilibrium with the core. *Geochem. Cosmochim., Acta*, 45, 1331 - 1343.

Arculus, R. J. & Power, R. 1986. Source component mixing in the regions of arc magma generation. *J. Geophys. Res.*, 91, 5913 - 5926.

Arculus, R. J. & Wills, K. J. A. 1980. The petrology of plutonic blocks and inclusions from the Lesser Antilles island arc. *J. Petrology*, 65, 743 - 799.

Ashraf, M. & Hussain, S. S. 1982. Chromite occurrences in Indus Suture ophiolites of Jijal, Kohistan, Pakistan. In: Sinha, A.K. (ed.) *Contemporary geoscientific researchs in Himalaya/ Dera Dun, India*, Blshen Singh Mahendra Pal Singh Co., 2, 129 - 132.

AvéLallemant, H. G. & Carter, N. L. 1970. Syntectonic recrystallization of olivine and mode of flow in the upper mantle. *Geol. Soc. Amer. Bull.*, 81, 2203 - 2220.

Banno, S. 1970. Classification of eclogites in terms of physical conditions of their origin. *Phy. Earth Plannet. Interiors*, 3, 405-421.

Banno, S. & Matsui, Y. 1965. Eclogite types and partition of Mg, Fe, and Mn between clinopyroxene and garnet. *Proc. Japan Acad.*, 41, 716-721.

Bard, J. P. 1983. Metamorphism of an obducted island arc; Example of the Kohistan sequence (Pakistan) in the Himalayan collided range. *Earth Planet. Sci. Lett.* , 65, 113 - 144.

Bard, J. P., Maluski, H., Matte, P. H. & Proust, F. 1980. The Kohistan sequence: crust and mantle of an obducted island arc. *Univ. Peshawar, Geol. Bull.*, Special Issue, 13, 87-93.

Barnes S-J. & Barnes S-J. 1990. A new interpretation of the Kantiniq nickel deposit. *Econ. Geol.* 85, 1269 - 1272.

Barnes S-J., Boyd, R., Korneliussen, A., Nilsson L-P., Often, M., Pedersen R-B. & Robins, B. 1988. The use of mantle normalization and metal ratios in discriminating between the effects of partial melting, crystal fractionation and sulphide segregation on platinum-group elements, gold, nickel, and copper: examples from Norway. *In*:: Prichard, H.M. , Potts, P.J., Bowles, J.F.W. & Cribb, S.J. (eds.) *Geo-platinum 87* , 113 - 143.

Barnes S-J., Couture, J. F., Sawyer, E. W. & Bouchaib, C. 1993. Nickel-copper occurrences in the Belleterre-Anglier Belt of the Pontiac Subprovince and the use of Cu-Pd ratios in interpreting platinum-group elemnt distributions. *Econ. Geol.*, 88, 1402 - 1418.

Barnes, S-J. & Campbell, I. H. 1988. Role of late magmatic fluids in Merensky-type platinum deposits: A discussion. *Geology*, 16, 488 - 491.

Barnes S-J. & Naldrett, A. J. 1985. Geochemistry of the J-M reef of the Stillwater Complex, Minneapolis Adit Area. 1 Sulphide chemistry and sulphide-olivine equilibrium. *Econ. Geol.*, 80, 165 - 183.

Barnes S-J., Naldrett, A. J. & Gorton, M. P. 1985. The origin of the fractionation of platinum-group elements in terrestrial magmas. *Chem. Geology*, 53, 303 - 323.

Barrat, J. A., Keller, F. & Amossé, J. 1996. Determination of rare earth elements in sixteen silicate reference samples by ICP-MS after Tm addition and ion exchange separation. *Geostandards Newsletter*, 20, 133 - 139.

Bartels, K. S., Kinzler, R. J. & Grove, T. L. 1991. High pressure phase relations of primitive high-alumina basalts from Medicine Lake volcano, northern California. *Contrib. Mineral. Petrol.*, 108, 253 - 270.

Beard, J. S. & Lofgren, G. E. 1991. Dehydration melting and water saturated melting of basaltic and andesitic greenstones and amphibolites at 1.3 and 6.9 kbar. *J. Petrol.*, 32, 365 - 401.

Bender, J. F., Hodges, F. N. & Bence, A. E. 1978. Petrogenesis of basalts from the project FAMOUS area; experimental study from 0 to 15 kbar. *Earth Planet. Sci. Lett.*, 41, 277 - 302.

Bertrand, P. & Mercier, J.-C. C. 1985. The mutual solubility of coexisting ortho- and clinopyroxene: towards an absolute geothermometer for the natural system. *Earth Planet. Sci. Lett.*, 76, 109 - 122.

Boyd, F. R. & England, J. L. 1964. The system enstatite-pyrope. Carnegie Inst. Wash. Year Book, 63, 157-161.

Bonatti, E. & Hamlyn, P. R. 1981. Oceanic ultramafic rocks. *In*:: Emiliani, C. (ed.) *The Sea; the oceanic lithosphere*. John Wiley & Sons, New York, NY, 7, 241 - 283.

Briqueu, L., Bougault, H. & Joron, J. L. 1984. Quantification of Nb, Ta, Ti and V anomalies in magmas associated with subduction zones: petrogenetic implications. *Earth Planet. Sci. Lett.*, 68, 297 - 308.

Brouxel, M., Lapierre, H., Michard, A. & Albarède, F. 1987. The deep layers of a Paleozoic arc: Geochemistry of the Copley-Balaklala Series, northern California. *Earth Planet. Sci. Lett.*, 85, 386 - 400.

Brugmann, G. E., Arndt, N. T., Hoffmann, A. W. & Tobschall, H. J. 1987. Noble metal abundances in komatiite suites from Alexo, Ontario and Gorgona Island, Colombia. *Geochim. Cosmochim. Acta*, 51, 2159 - 2169.

Buchanan, D. L. 1988. Platinum-group element exploration. *In*: Buchanan, D.L. (ed.) development in economic geology, 26.

Burns, L. E. 1985. The Border ranges ultramafic-mafic complex, south-central Alaska: cumulate fractionates of island-arc volcanics. *Can. J. Earth Sci.*, 22, 1020 - 1038.

Burns, R. G. & Fyfe, W. S. 1966. Distribution of elements in geological processes. *Chem. Geol.*, 1, 49 - 56.

Cabanis, B. & Lecolle, M. 1989. Le diagramme La/10-Y/15-Nb/8: un outil pour la discrimination des series volcaniques et la mise en evidence des processus de melange et/ou de contamination crustale. *C. R. Acad. Sci. Ser.*, II, 309, 2023 - 2029.

Cabri, L. J. 1981. The platinum-group minerals. *In*:: Cabri, L.J. (ed.) *Platinum-Group Elements: Mineralogy, Geology, Recovery*, CIM Special Volume 23, Chapter 7.

Cabri, L. J. & Laflamme, J. H. G. 1976. The mineralogy of the platinum-group elements from some copper-nickel deposits of the Sudbury Area, Ontario. *Econ. Geol.*, 71, 1159 - 1195.

Campbell, I. H. & Barnes S-J. 1984. A model for the geochemistry of the platinum-group elements in magmatic sulphide deposits. *Can. Mineral.*, 22, 151 - 160.

Campbell, I. H., Naldrett, A. J. & Barnes S-J. 1983. A model for the origin of the platinum-rich sulphide horizons in the Bushveld and Stillwater Complexes. *J. Petrol.*, 24, 133 - 165.

Capobianco, C. J. & Drake, M. J. 1990. Experimental investigation of the partitioning of noble siderophile elements among basaltic liquidus phases. *V.M. Goldschmidt Conf. Prog.*, abstract, 35.

Chou, C. L. 1978. Fractionation of siderophile elements in the earth's upper mantle. *Proc. Lunar Planet. Sci.*, 9th, 219 - 230.

Chou, C. L., Shaw, D. M. & Crocket, J. H. 1983. Siderophile trace elements in the earth's oceanic crust and upper mantle. *J. Geophys. Res.*, 88, A507 - 518.

Craig, J. R. & Kullerud, G. 1969. Phase relations in the Cu-Fe-Ni-S system and their application to magmatic ore deposits. *In*: Wilson, H.D.B. (ed), *Magmatic ore deposits, Econ. Geol.*, Monograph 4, 344 - 358.

Crawford, A. J., Falloon, T. J. & Eggins, S. 1987. The origin of island arc high-alumina basalts. *Contrib. Mineral. Petrol.*, 97, 417-430.

Crocket, J. H. 1969. Platinum metals. *In*: Wedepohl, K.H. (ed.), *Handbook of Geochemistry 11/5*. Springer-Verlag, Berlin.

Crocket, J. H. 1979. Platinum-group elements in mafic and ultramafic rocks - a survey. *Can. Mineral.*, 17, 391 - 402.

Crocket, J. H. 1981. Geochemistry of the platinum-group elements. *Can. Inst. Min. Metall.*, Special Issue, 23, 47 - 64.

Crocket, J. H. & Chyi, L. L. 1972. Abundances of Pd, Ir, Os and Au in an Alpine ultramafic pluton. *24th Inter. Geol. Cong.*, Section 10, 202 - 209.

Crocket, J. H. & Kabir, A. 1988. PGE in Hawaiian basalt: implications of hydrothermal alteration on PGE mobility in volcanic fluids. *In*: Prichard, H.M., Potts, P.J., Bowles, J.F.W. & Cribb, S.J. (eds.) *Geo-platinum 87*. Elsevier Applied Science, London & New York, 259.

Crocket, J. H., Keays, R. R. & Hsieh, S. 1967. Precious metal abundances in some carbonaceous and enstatite chondrites. *Geochem. Cosmochim, Acta*, 31, 1615 - 1623.

Crocket, J. H. & Teruta, Y. 1977. Palladium, irridium and gold contents of mafic and ultramafic rocks drilled from the Mid-Atlantic Ridge, leg 37, Deep Sea Drilling Project. *Can. J. Earth Sci.*, 14, 777 - 784.

Crocket, J. H., Teruta, Y. & Garth, J. 1976. The relative importance of sulfides, spinels and platinoid minerals as carriers of Pt, Pd, Ir and Au in the Merensky Reef at Western Platinum Limited, Near Marikana, South Africa. *Econ. Geol.*, 71, 1308 - 1323.

Coleman, R. G. 1977. Ophiolites. Berlin, Springer-Verlag, 229.

Coleman, R. G., Lee, D. E., Beaty, L. B. & Brannock, W. W. 1965. Eclogites and eclogites: their differences and similarities. *Geol. Soci. Amer. Bull.*, 76, 483-508.

Conrad, W. K. & Kay, R. W. 1984. Ultramafic and mafic inclusions from Adak Island: Crystallization history, and implications for the nature of primary magmas and crustal evolution in the Aeutian arc. *J. Petrology*, 25, 88-125.

Cousins, C. A. & Vermaak, C. F. 1976. The contribution of Southern African ore deposits to the geochemistry of the platinum group metals. *Econ. Geol.*, 71, 287 - 305.

Coward, M. P., Butler, R. W. H., Khan, M. A. & Knipe, R. J. 1987. The tectonic history of Kohistan and its implications for Himalayan structure. *Jour. Geol. Soci.*, London, 144, 377-391.

Coward, M. P., Jan, M. Q., Rex, D., Tarney, J., Thirwall, M. & Windley, B. F. 1982. Geotectonic framework of the Himalaya of N. Pakistan. *Jour. Geol. Soci.*, London, 139, 299-308.

Coward, M. P., Windley, B. F., Broughton, R. D., Luff, I. W., Petterson, M. G., Pudsey, C. J. & Khan, M. A. 1986. Collision tectonics in the NW Himalaya, *In*: Coward, M.P. & Ries, A.C. (eds.) *Collision Tectonics*. Geological Society, London, Special Publications, 19, 203-219.

Cox, K. G., Bell, J. D. & Pankhurst, R. J. 1979. The interpretation of igneous rocks. George, Allen & Unwin, London.

Davidson, J. P. 1986. Isotope and trace element constraints on petrogenesis of subduction related lavas from Martinique, Lesser Antilles. *J. Geophys. Res.*, 91, 5943 - 5962.

Davis, B. T. & Boyd, F. R., JR. 1966. The join Mg2Si2O6-CaMgSi2O6 at 30 kilobars pressure and its application to pyroxenes from kimberlites. *J. Geophys. Res.*, 71, 3367 - 3376.

DeBari, S. M. & Coleman, R. G. 1989. Examination of the deep levels of an island arc: evidence from the Tonsina, Alaska. *J. Geophys. Res.*, 94, no. B4, 4373-4391.

DeBari, S. M., Kay, S. M. & Kay, R. W. 1987. Ultramafic xenoliths from Adagdak Volcano, Adak, Aleutian Islands, Alaska: Deformed igneous cumulates from the Moho of an island arc. *J. Geology*, 95, 329-341.

Debon, F., LeFort, P., Dautel, D., Sonet, J. & Zimmermann, J. L. 1987. Granites of western Karakoram and northern Kohistan (Pakistan): a composite Mid-Cretaceous to Upper Cenozoic magmatism. *Lithos*, 20, 19 - 40.

DePaolo, D. J. 1979. Estimation of the depth of origin of basic magmas: a modified thermodynamic approach and comparison with experimental studies. *Contr. Mineral. Petrol.*, 69, 265 - 278.

Dietrich, V. J., Frank, W. & Honegger, K. 1983. Jurassic-Cretaceous island arc in the Ladakh-Himalayas. *J. Vol. Geothermal Res.*, 18, 405 - 433.

Dobretsov, L. N., Khlestov, V. V., Reverdatto, V. V., Sobolev. N. V. & Sobolev, V. S. 1972. The facies of metamorphism. (transl. by Brown, D.A.). Canberra: Australian National University.

Dungan, M. A., Long, P. E. & Rhodes, J. M. 1978. The petrology, mineral chemistry, and one-atmosphere phase relations of basalts from site 395. *Initial Rep. Deep Sea Drill. ProJ.*, 45, 461 - 472.

Eggler, D. H. & Burnham, C. W. 1973. Crystallization and fractionation trends in the system andesite-H_2O-CO_2-O_2 at pressures to 10 kilobars. *Geol. Soc. Am. Bull.*, 84, 2517-2532.

Ellam, R. M. & Hawkesworth, C. J. 1988. Elemental and isotopic variations in subduction related basalts: evidence for a three component model. *Contrib. Mineral. Petrol.*, 98, 72 - 80.

Ellis, D. J. & Green, D. H. 1979. An experimental study of the effect of Ca upon garnet-pyroxene Fe-Mg exchange equilibria. *Contr. Mineral. Petrol.*, 71, 13 - 22.

Elthon, D. 1981. 1 atm phase equilibria of basalts from the Tortuga ophiolite complex, with implications for magma chamber processes. Paper presented at the Chapman Conference on the Generation of the Oceanic Lithosphere, AGU, Warrenton, Va.

Elthon, D., Casey, J. F. & Komor, S. 1982. Mineral chemistry of ultramafic cumulates from the North Arm Mountain Massif of the Bay of Islands Ophiolite: Evidence for high-pressure crystal fractionation of oceanic basalts. *J. Geophys. Res.*, 87, 8717-8734.

Ewers, W. E. & Hudson, D. R. 1972. An interpretive study of a nickel-iron sulphide ore intersection, Lunnon Shoot, Kambalda, Western Australia. *Econ. Geol.*, 67, 1075 - 1092.

Fischer, W. 1988. Approche experimentale du fractionnement magmatique et exemples de redistributions hydrothermales des éléments du groupe du platine (PGE). Thése de l'Université Joseph Fourier, grenoble, 160.

Fisk, M. R., Schilling, J. G. & Sigurdsoon, H. 1980. An experimental investigation of Iceland and Reykjanes Ridge tholeiites, I, Phase relations. *Contrib. Mineral. Petrol.*, 74, 361 - 374.

Fleet, M. E., Macrae, N. D. & Osborne, M. D. 1981. Crystal fractionation and partial melting in the petrogenesis of a proterozoic high-MgO volcanic suite, Ungava, Quebec. *Cont. Mineral. Petrol.*, 78, 27 - 36.

Fleet, M. E., Stone, W. E. & Crocket, J. H. 1991. Partitioning of palladium, iridium and platinum between sulphide liquid and basalt melt: effects of melt composition, concentration and oxygen activity. *Geochim. Cosmochim. Acta*, 55, 2545 - 2554.

Floyd, P. A. & Winchester, J. A. 1975. Magma type and tectonic setting discrimination using immobile elements. *Earth Planet. Sci. Lett.*, 27, 211 - 218.

Frey, F. A. 1969. Rare earth abundances in a high-temperature peridotite intrusion. *Geochem. Cosmochim. Acta*, 33, 381-387.

Frey, F. A., 1984. Rare earth abundances in upper mantle rocks; *In*: Henderson, P. (ed.) *Rare Earth Element Geochemistry*, Elsevier, Amsterdam, 153 - 203.

Frey, F. A., Bryan, W. B. & Thompson, G. 1974. Atlantic Ocean floor: geochemistry and petrology of basalts from Legs 2 and 3 of the Deep-Sea Drilling Project. *J. Geophys. Res.*, 79, 5507 - 5527.

Frey, F. A. & Prinz, M. 1978. Ultramafic inclusions from San Carlos, Arizona: Petrologic and geochemical data bearing on their petrogenesis. *Earth Planet. Sci. Lett.*, 38, 129-176.

Garuti, G., Gorgoni, C. & Sighinolfi, G. P. 1984. Sulphide mineralogy and chalcophile element abundances in the Ivrea-Verbano mantle peridotites (western Italian Alps). *Earth Planet. Sci. Lett.*, 70, 69 - 87.

Genkin, A. D. & Evstigneeva, T. L. 1986. Associations of platinum-group minerals of the Norilsk Copper-Nickel sulphide ores. *Econ. Geol.*, 81, 1203 - 1212.

Gijbels, R., Henderson, P. & Zels, J. 1976. Geochemistry of some trace elements in mineral separates from Rhum, Inner Hebrides, with special emphasis on irridium. *Econ. Geol.* 71, 1364 - 1370.

Gijbels, R., Millard, H. T., Desborough, G. A. & Bartel, A. J. 1974. Osmium, ruthenium, iridium and chromite from the eastern Bushveld Complex, South Africa. *Geochim. Cosmochim., Acta*, 38, 319 - 337.

Gill, J. B. 1981. Orogenic andesites and plate tectonics. Berlin, Springer-Verlag, 358.

Gottfried, D. & Greenland, L. P. 1972. Variation of iridium and gold in oceanic and continental basalts. *Proc. 24th Intern. Geol. Congress*, Montréal, Que., Section 10, 135 - 144.

Graham, C. M. & Powell, R. 1984. A garnet-hornblende geothermometer: calibration, testing and application to the Pelona Schist, Southern California. *J. Metamorphic Petrol.*, 2, 13 -21.

Graterol, M. & Naldrett, A. J. 1971. Mineralogy of the Marbridge No. 3 and No. 4 nickel-iron sulphide deposits. *Econ. Geol.*, 66, 886 - 900.

Green, D. H., Hibberson, W. O. & Jaques, A. L. 1979. Petrogenesis of mid-ocean ridge basalts. *In*: McElhinney, M.W. (ed.) The Earth: *Its Origin, Structure, and Evolution*, Academic, New York, 265 - 299.

Green, D. H. & Ringwood, A. E. 1967. The stability fields of aluminous pyroxene peridotite and garnet peridotite and their relavance in upper mantle structure. *Earth Planet. Sci. Lett.*, 3, 151-160.

Greenough, J. D. & Owen, J. V. 1992. Platinum-group elements geochemistry of continenetal tholeiites: Analysis of the Long Range dyke swarm, Newfoundland, Canada. *Chem. Geol.*, 98, 203 - 219.

Gromet, L. P. 1979. Rare earth abundances and fractionations and their implications for batholithic petrogenesis in the Peninsular Ranges batholith, California, USA, and Baja California, Mexico. PhD thesis, California Institute of Technology, 337.

Gust, D. A. & Johnson, R. W. 1981. Amphibole-bearing inclusions from Boisa Island, Papua New Guinea: evaluation of the role of fractional crystallization in an andesitic volcano. *Jour. geology*, 89, 219-232.

Hamlyn, P. R., Keays, R. R., Cameron, W. E., Warrington, E., Crawford, A. J. & Waldon, H. M. 1985. Precious metals in magnesian low-Ti-lavas: Implications for metallogenesis and sulfur saturation in primary magmas. *Geochim. Cosmochim. Acta*, 49, 1797 - 1811.

Hanson, G. N. 1980. Rare earth elements in petrogenetic studies of igneous systems. *Annual Review of Earth and Planetary Sciences*, 8, 371 - 406.

Haris, C. 1983. The petrology of lavas and associated plutonic inclusions of Ascension Island. *J. Petrol.*, 24, 424 - 470.

Harley, S. L. 1984a. An experimental study of the partitioning of Fe and Mg between garnet and orthopyroxene. *Contr. Miner. Petrol.*, 86, 359 - 373.

Harley, S. L. 1984b. The solubility of alumina in orthopyroxene coexisting with garnet in FeO-MgO-Al_2O_3-SiO_2. *J. Petrol.*, 25, 665 - 696.

Haughton, D. R., Roeder, P. L., & Skinner, B. J. 1974. Solubility of sulfur in mafic magmas. *Econ. Geol.,* 69, 451 - 467.

Hawkesworth, C. J., O'Nions, R. K., Pankhurst, R. J., Hamilton, P. J. & Evenson, N. M. 1977. A geochemical study of island arc and back-arc tholeiites from the Scotia Sea. *Earth Planet. Sci. Lett.*, 36, 253 - 262.

Hellman, P. L. & Henderson, P. 1977. Are the rare earth elements mobile during spilitization? *Nature*, 267, 38 - 40.

Hensen, B. J. 1976. The stability of pyrope-grossular garnet with excess silica. *Contri. Miner. Petrol.*, 55, 279-292.

Hertogen, J., Janssen, M. J. & Palme, H. 1980. Trace elements in ocean ridge basalt glasses: implications for fractionation during mantle evolution and petrogenesis. *Geochim. Cosmochim.* Acta, 44, 2125 - 2143.

Herzberg, C. T., 1972. Stability fields of plagioclase- and spinel-lherzolite. *In*: *Porgress in Experimental Petrology*, Natural Environment Research Council Publications, London, 145 - 148.

Hiemstra, S. A. 1979. The role of collectors in the formation of platinum deposits in the Bushveld Complex. *Cand. Mineral.*, 17, 469 - 482.

Hiemstra, S. A. 1986. The distribution of chalcophile and platinum-group elements in the UG-2 chromite layer of the Bushveld Complex. *Econ. Geol.*, 81, 1080 - 1086.

Hill, R. E. T. 1984. Experimental study of phase relations at 600°C in a portion of the Fe-Ni-Cu-S system and its application to natural assemblages. *In*: *Sulphide deposits in mafic and ultramafic rocks*: London, Institute of Mining and Metallurgy, 14 - 21.

Hill, R. & Roeder, P. 1974. The crystallization of spinel from basaltic liquid as a function of oxygen fugacity. *J. Geology*, 82, 709 - 729.

Himmelberg, G. R. & Loney, R. A. 1973. Petrology of the Vulcan Peak Alpine-type peridotite, southwestern Oregon. *Geol. Soc. Amer. Bull.* 84, 1585-1600.

Hole, M.J., Saunders, A. D., Marriner, G. F. & Tarney, J. 1984. Subduction of pelagic sediments: implications for the origin of Ce-anomalous basalts from the Mariana islands. *J. Geol. Soc.* London, 141, 453 - 472.

Honegger, K., Dietrich, V., Frank, W., Gansser, A., Thoni, M. & Trommsdorff, V. 1982. Magmatism and metamorphism in the Ladakh Himalaya. *Earth Planet. Sci. Lett.*, 60, 253 - 292.

Irvine, T. N. 1974. The Duke Island ultramafic complex, southern Alaska. *Geol. Soc. Amer.*, memoir 138, 1 - 240.

Irvine, T. N., 1975. Crystallization sequences in the Muskox intrusion and other layered intrusions-11. Origin of chromitite layers and similar deposits of magmatic ores. *Geochim. Cosmochim. Acta*, 39, 991 - 1020.

Irvine, T. N. 1977. Origin of chromitite layers in the Muskox intrusion: A new interpretation. *Geology*, 5, 273 - 277.

Irving, A. J. 1969. Experimental duplication of mineral assemblages in xenoliths of the Delegate breccia pipes (abstr.). Abstracts, *International Symposium on Phase Transformations and the Earth's Interior*, Canberra, 90-92.

Irving, A. J. 1974. Geochemical and high pressure experimental studies of garnet pyroxenite and pyroxene xenoliths from the Delegate basaltic pipes, Australia. *J. Petrology*, 15, 1-40.

Irving, A. J. 1978. A review of experimental studies of crystal/liquid trace element partitioning. *Geochim. Cosmochim. Acta*, 42, 743 - 770.

Ivanac, J. F., Traves, D. M., & King, D. 1956. The geology of the north-west portion of the Gilgit Agency: *Geol. Surv. Pakistan*, Records, 8, 6 - 13.

Jackson, S. E., Fryer, B. J., Gosse, W., Healey, D. C., Longerich, H. P. & Strong, D. F. 1990. Determination of the precious metals in geological materials by inductively coupled plasma -mass spectrometry (ICP-MS), with nickel sulphide fire-assay collection and tellurium coprecipitation. *Chem. Geol.*, 83, 119 - 132.

Jackson, E. D. & Thayer, T. P. 1972. Some criteria for distinguishing between stratiform, concentric and Alpine peridotite-gabbro complexes. *24th Inter. Geol. Cong. Montreal*, Sect. 2, 289-296.

Jagoutz, E., Palme, H., Baddenhausen, H., Blum, K., Cendales, M., Gerlind, D., Spettel, B., Lorenz, V. & Wanke, H. 1979. The abundances of major, minor and trace elements in the earth's mantle as derived from primitive ultramafic nodules. *Proc. 10th Lunar Planet. Sci. Conf.* 2031 - 2050.

Jakes, P. & Gill, J. B. 1970. Rare earth elements and the island arc tholeiitic series. *Earth Planet. Sci. Lett.*, 9, 17 - 28.

Jan, M. Q. 1979. Petrography of pyroxene granulites from northern Swat and Kohistan, N.W. Pakistan. *Univ. Peshawar Geol. Bull.*, Special Issue, 11, 65 - 87.

Jan, M. Q. 1980. Petrology of the obducted mafic and ultramafic metamorphites from the southern part of the Kohistan island arc sequence. *Univ. Peshawar Geol. Bull.*, Special Issue, 11, 65 - 87.

Jan, M. Q. 1988. Geology of amphibolites from the southern part of the Kohistan arc, N. Pakistan. *Mineral. Magaz.*, 52, 147-159.

Jan, M. Q. & Howie, R. A. 1980. Ortho- and clinopyroxene from pyroxene granulites of Swat, Kohistan, northern Pakistan. *Mineral. Mag.*, 110, 285 - 300.

Jan, M. Q. & Jabeen, N. 1990. A review of mafic-ultramafic plutonic complexes in the Indus Suture Zone of Pakistan. *Phys. Chemis. Earth*, 17, 93 - 113.

Jan, M.Q. & Kempe, D. R. C. 1973. The petrology of the basic and intermediate rocks of Upper Swat, Pakistan. *Geol. Mag.*, 110, 285-300.

Jan, M. Q., Khan, M. A. & Qazi, M. S. 1993. The Sapat mafic-ultramafic complex, Kohistan arc, North Pakistan. *In*: Treloar, P.J. & Searle, M.P. (eds.) *Himalayan Tectonics*, Geological Society, London. Special Publications, 74, 113 - 121.

Jan, M. Q., Khattak, M. U. K., Parvez, M. K. & Windley, B. F. 1984. The Chilas stratiform complex; Field and mineralogical aspects. *Univ. Peshawar Geol. Bull.*, 17, 163 - 169.

Jan, M. Q. & Windley, B. F. 1981. The mineralogy and geochemistry of the metamorphosed basic and ultrabasic rocks of the Jijal complex, Kohistan, NW Pakistan. *J. Petrol.*, 22, 85-126.

Jan, M. Q. & Windley, B. F. 1990. Chromian spinel chemistry in ultramafic rocks of the Jijal Complex northwestern Pakistan. *J. Petrol.*, 22, 667-715.

Jaques, A. L. 1981. Petrology and petrogenesis of cumulate peridotites and gabbro from the maru9m ophiolite complex, northern Papua, New Guinea. *J. Petrol.*, 21, 743 - 799.

Jellinek, F. 1972. Sulphides, selenides, and tellurides of the transition elements. In: Sharp, D.W.A. (ed.) *Inorganic Chemistry*, Series 1, MTP, International Reviews of Science, Butterworths, Oxford, 5, 339 - 396.

Jensen, L. S., 1976. A new cation plot for classifying subalkalic volcanic rocks. Ontario Division of Mines MP66, 22.

Jenkins, D. M. 1983. Stability and composition relations of calcic amphiboles in ultramafic rocks. *Contrib. Mineral. Petrol.*, 83, 375-384.

Johannes, A. D. 1978. Melting of plagioclase in the system Ab-An-H_2O at PH_2O= 5 kbars, an equilibrium problem. *Contrib. Mineral. Petrol.*, 66, 295 - 303.

Johnson, R. W., Mackenzie, D. E., & Smith, I. E. M., 1978. delayed partial melting of subduction-modified mantle in papua New Guinea. Tectonophysics, 46, 197 - 216.

Johnson, K. T., Dick, H. J. B. & Shimizu, N. 1990. Melting in the oceanic upper mantle: An ion microprobe study of diopsides in abyssal peridotites. *J. Geophys. Res.*, 95, 2661-2678.

Kay, S. M. & Kay. R. W. 1985b. Aleutian tholeiitic and calc-alkaline magma series. I: The mafic phenocrysts. *Contrib. Mineral. Petrol.*, 90, 276-296.

Keays, R. R. 1982. Palladium and irridium in kokatiites and associated rocks: implication to petrogenetic problems. *In*: Arndt, N.T. & Nisbet, E.G. (eds.) *Komatiites*. Allen, London, 435 - 457.

Keays, R. R. & Crocket, J. H. 1970. A study of precious metals in the Sudbury nickel irruptive ores. *Econ. Geol.*, 65, 438 - 450.

Keays, R. R., Ross, J. R. & Woolrich, P. 1981. Precious metals in volcanic peridotite-associated nickel sulphide deposits in western Australia 11: distribution within the ores and host rocks at Kambalda. *Econ. Geol.*, 76, 1645 - 1674.

Kellerud, G., Yund, R. A. & Moh, G. H. 1969. Phase relations in the Cu-Fe-S, Cu-Ni-S and Fe-Ni-S systems. *In*: Wilson, H.D.B. (ed.) *Magmatic ore deposits, Econ. Geol.*, Monograph 4, 323 - 343.

Khan, I. H., Khan, R. H. & Nakagawa, M. 1995. Occurrence of platinum-group mineral in sulphide ore from Jijal complex, northern Pakistan. *Proc. Geosc. Colloq., Geosci. Lab.*, GSP, 12, 5 - 12.

Khan, M. A., Habib, M. & Jan, M. Q. 1985. Ultramafic and mafic rocks of Thurly gah and their relationship to the Chilas complex, N. Pakistan. *Univ. Peshawar Geol. Bull.*, 18, 83 - 102.

Khan, M. A., Jan, M. Q. & Weaver, B. L. 1993. Evolution of the lower arc crust in Kohistan, N. Pakistan: temporal arc magmatism through early, mature, and intra-arc rift stages. In: Treloar, P.J. & Searle, M.P. (eds.) *Himalayan Tectonics*, Geological Society, London. Special Publications, 74, 123 - 138.

Khan, M. A., Jan, M. Q., Windley, B. F., Tarney, J . & Thirlwall, M. F. 1989. The Chilas mafic-ultramafic igneous complex; the root of the Kohistan Island Arc in the Himalaya of northern Pakistan. *In*: Malinconico, L.L. & Lillie, R.J. (eds.) *Tectonics of the Western Himalayas*. Geological Society of America, Special Paper, 232, 75-93.

Khan, M. A., Stern, R. J., Gribble, R. F. & Windley, B. F. 1997. Geochemical and isotopic constraints on subduction polarity, magma sources, and palaeogeography of the Kohistan intra-oceanic arc, northern pakistan Himalaya. *J. Geol. Soc. Lond.*, 154, 935 - 946.

Khan, M. A. & Thirwall, M. F. 1988. Babusar amphibolites: arc tholeiites from the southern Kohistan arc, N. Pakistan. *Univ. Peshawar Geol. Bull.*, 21, 147 - 158.

Klootwijk, C., Sharma, M. L., Gergan, J., Tirkey, B., Shah, S. K. & Agarwal, U. 1979. The extent great India II, Paleomagnetic data from the Ladakh intrusives at Kargil, northwestern Himalaya. *Earth Planet. Sci. Lett.*, 44, 47-64.

Kushiro, I. & Yoder, H. S. 1978. Anorthite-forsterite and anorthite-enstatite reactions and their bearing on the basalt-eclogite transformation. *J. Petrol.*, 7, 337 - 362.

Kushiro, I. & Yoder, Jr. 1965. The reactions between forsterite and anorthite at high pressures. Year Book Carnegie Inst., Washington, 64, 89 - 94.

Langmuir, C. H., Bender, J. B., Bence, A. E., Hanson, G. N. & Taylor, S. R. 1977. Petrogenesis of basalts from the FAMOUS are; Mid-Atlantic Ridge. *Earth Planet. Sci. Lett.*, 36, 133 - 156.

Lapierre, H., Ortiz, L. E., Abouchami, W., Monod, O., Coulon, C. & Zimmermann, J. L. 1992. A crustal section of an intra-oceanic island arc: The Late Jurassic-Early Cretaceous Guanajuato magmatic sequence, central Mexico. *Earth Planet. Sci. Lett.*, 108, 61-77.

Lappin, M. A. 1967. Structural and petrofabric studies of the dunites of Almklovkalen, Nordfjord, Norway. *In*: Wyllie, P.J. (ed.) *Ultramafic and related rocks*: Wiley, New York, 403-416.

Leake, B. 1978. Nomenclature of amphiboles. *Am. Mineral.*, 63, 1023-1052.

Legendre, O. 1982. Minéralogie et géochimie des platinoïdes dans les chromitites ophiolitiques. Comparaison avec d'autres types de concentrations en platinoïdes. Thèse Doct. 3° cycle, Université Sciences, Paris VII, 157.

Lewis, J. F. 1973. Petrology of the ejected plutonic blocks of the Soufrière volcano, St. Vincet, West Indies. *J. Petrol.*, 14, 81-112.

Lonely, R. A., Himmelberg, G. R. & Coleman, R. G. 1971. Structure and petrology of the Alpine-type peridotite at Burro Mountain, California, U.S.A. *J. Petrol.*, 12, 245-309.

Lorand, J. P. 1987. Caractéré minéralogiques et chimiques généraux des microphases du systéme Cu-Fe-Ni-S dans les roches du manteau supérieur: examples d'hétérog énéités en domaine sub-continental. *Bull. Soc. Géol. Fr.* (8) 11, 4, 643 - 657.

Lorand, J. P. 1989. Abundance and distribution of Cu-Fe-Ni sulphides, sulfur, copper and platinum-group elements in orogenic-type spinel lherzolite massifs of ariège (northeastern Pyrenees, france). *Earth Planet. Sci. Lett.*, 93, 50 - 64.

Lorand, J. P. & Conquéré, F. 1983. Contribution à l'étude des sulfures dans les enclaves de lherzolite à spinelle des basaltes alcalins (Massif Central et Languedoc, France). *Bull. Minéral.*, 106, 585 - 606.

Loucks, R. R., Miller, D. J., Ashraf, M., Awan, M. A. & Khan, M. S. 1990. The Jijal Complex: layered mafic-ultramafic arc cumulates from the crust-mantle boundary, Pakistani Himalayas. *EOS*, 71, 664.

Lovering, J. F., & White, A. J. R., 1969. Granulitic and eclogitic inclusions from basic pipes at Delegate, Australia. *Contrib. Mineral. Petrol.*, 21, 9-52.

Luck, J. M., Pegram, W. J. & Allegre, C. J. 1988. Osmium isotopes in orogenic lherzolites and ultramafic samples. *Chem. Geol.*, 70, 54.

MacGregor, I. D. 1970. The effect of CaO, Cr_2O_3, Fe_2O_3, and Al_2O_3 on the stability of spinel and garnet peridotites. *Phys. Earth Planet. Inter.*, 3, 327-377.

MacGregor, I. D. 1974. The system MgO-Al2O3-SiO2: solubility of Al2O3 in enstatite for spinel and garnet peridotite composition. *Amer. Min.*, 59, 110 - 119.

Makovicky, M., Makovicky, R. & Rose-Hansen, J. 1986. Experimental studies on the solubility and distribution of platinum group elements in base-metal sulphides in platinum deposits. In: Gallagher, M.J. Mixer, R.A. Neary, C.R. & Prichard, H.M. (eds.)

Metallogeny of basic and ultrabasic rocks, The Institution of Mining and Metallurgy, Londres, 415 - 425.

Masuda, A. 1968. Lanthanide concentrations in the olivine phase of the Brenham pallasite. *Earth Planet. Sci. Lett.*, 5, 59-62.

Matsui, Y., Onuma, N., Nagasawa, H., Higuchi, H. & Banno, S. 1977. Crystal structure control in trace element partitioning among crystals and magma. *Bull. Soc. Fr. Miner. Cristallogor*, 100, 315-324.

McCallum, I. S., Raedeke, L. D. & Mathez, E. A. 1980. Investigations of the Stillwater complex: part I. Stratigraphy and structure of the Banded zone. *Am. J. Sci.* 280-A, 59 - 87.

McKay, G. A. 1989. Partitioning of rare earth elements between major silicate minerals and basaltic melts. In: Ribbe, P.H. (ed.) *Geochemistry and Mineralogy of Rare Earth Elements. Rev. Mineral.*, 21, 45-74.

Medaris, L. G. 1972. High-pressure peridotites in south-western Oregon. *Geol. Soc. Am. Bull.*, 83, 41-58.

Meijer, A. & Reagan, M. 1981. Petrology and geochemistry of the island of Sarigan in the Mariana Arc; calc-alkaline volcanism in an oceanic setting. *Contrib. Mineral. Petrol.*, 77, 337 - 354.

Menzies, M. 1983. Mantle ultramafic xenoliths in alkaline magmas: evidence for mantle heterogeneity modified by magmatic activity. *In*: Hawkesworth, C.J. & Norry, M.J. (eds.) *Continental Basalts and Mantle Xenoliths*, Shiva Publishing, Cheshire, U.K. 92 - 110.

Merkle, R. K. W. & Von Gruenewaldt, G. 1986. Compositional variation of Co-rich pentlandite: Relation to the evolution of the upper zone of the western Bushveld Complex, South Africa. *Can. Mineral.*, 24, 529 - 546.

Meschede, M. 1986. A method of discriminating between different types of mid-ocean ridge basalts and continental tholeiites with the Nb-Zr-Y diagram. *Chem. Geol.*, 56, 207 - 218.

Michard, P., Gurriet, P., Soudant, M. & Albarède, F. 1985. Nd isotopes in French Phanerozoic shales: External vs internal aspects of crustal evolution. *Geochim. Cosmochim., Acta*, 49, 601 - 610.

Miller, D. J. & Christensen, N. I. 1994. *J. Geophys. Res.*, 99, (B6), 11643 - 11662.

Miller, D. J., Loucks, R. R. & Ashraf, M. 1991. Platinum-group element mineralization in the Jijal Layered Ultramafic-Mafic Complex, Pakistani Himalayas. *Econ. Geol.*, 86, 1093 - 1102.

Mikoshiba, M. U., Takahashi, Y., Kubo, K., Kausar, A. B., Khan, T., Takahashi, Yuh. & Shirahase, T. 1998. Petrochemical characteristics of the eastern part of the Chilas igneous complex, Kohistan, northern Pakistan. *Univ. Peshawar Geol. Bull.*, Special Issue, 31, 129 - 131.

Misch, P. 1949. Metasomatic granitization of batholithic dimensions. *Amer. Jour. Sci.*, 247, 209 - 245.

Misra, K. C. & Fleet, M. E. 1973. The chemical composition of synthetic and natural pentlandite assemblages. *Econ. Geol.*, 68, 518 - 539.

Mitchell, R. H. & Keays, R. R. 1981. Abundance and distribution of gold, palladium and irridium in some spinel and garnet lherzolite, Implications for the nature and origin of precious metal-rich intergranular components in the upper mantle. *Geochim. Cosmochim., Acta*, 45, 2425 - 2442.

Miyashiro, A., 1978. Nature of alkalic volcanic rock series. *Contrib. Mineral. Petrol.*, 66, 91 - 104.

Morgan, J. W. 1986. Ultramafic xenoliths: Clues to earth's late accretionary history. *J. Geophys. Res.*, 91, (B12), 12375 - 12387.

Morgan, J. W., Wandless, G. A., Petrie, R. K. & Irving, A. J. 1981. Composition of the earth's upper mantle, 1. Siderophile trace elements in ultramafic nodules. *Tectonophysics*, 75, 47 - 67.

Morten, L. & Obata, M. 1983. Possible high-temperature origin of pyroxenite lenses within garnet peridotite, northern Italy. *Bull. Mineral.*, 106, 775 - 780.

Mullen, E. D. 1983. MnO/TiO2/P2O5: a minor element discriminant for basaltic rocks of oceanic environments and its implications for petrogenesis. Earth Planet. Sci. Lett., 62, 53 - 62.

Murray, C. G. 1972. Zoned ultramafic complexes of the Alaskan type: Feeder pipes of andesitic volcanoes, studies in Earth and Space Sciences. *Mem. Geol. Soc. Am.*, Hess Volume, 132, 313-335.

Naldret, A. 1981. Platinum-group element deposits. *Can. Inst. Min. Metall.*, Special Issue, 23, 197 - 232.

Naldret, A. 1989. Magmatic Sulphide deposits: Clarendon Press. Oxford University Press. 186.

Naldrett, A. J. & Barnes S-J. 1986. The fractionation of the platinum-group elements with special reference to the composition of sulphide ores. *Fortsch. Mineral. Petrol.*, 64, 113 - 133.

Nicolas, A., Bouchez, J. L., Boudier, F. & Mercier, J. C. 1971. Textures, structures and fabrics due to solid state flow in some European lherzolite. *Tectonophysics*, 12, 55-86.

Naldret, A. J. & Cabri, L. J. 1976. Ultramafic and related mafic rocks: Their classification and genesis with special reference to the concentration of nickel sulphides and platinum-group elements. *Econ. Geol.*, 71, 1131 - 1158.

Naldrett, A. J. & Duke, J. M. 1980. Pt metals in magmatic sulphide ores; the occurrence of these metals is discussed in relation to the formation and importance of these ores. *Science*, 208, 1417 - 1484.

Naldrett, A. J., Hoffman, E. L., Green, A. H., Chou, C. L. & Naldrett, S. R. 1979. The composition of Ni-sulphide ores, with particular reference to their content of PGE and Au. *Can. Mineral.*, 17, 403 - 415.

Newton, R. C. & Perkins, D. 1982. Thermodynamic caliberation of geobarometers based on the assemblages garnet-plagioclase-orthopyroxene (clinopyroxene)-quartz. *Amer. Mineral.*, 67, 203-222.

Nicholls, I. A. & Harris, K. L. 1980. Experimental rare earth element partition coefficients for garnet, clinopyroxene and amphibole coexisting with andesitic and basaltic liquids. *Ibid.*, 44, 287-308.

Nickel, K. G. & Green, D. H. 1985. Empirical geothermobarometry for garnet peridotites and implications for the nature of the lithosphere, kimberlites and diamonds. *Earth Planet. sci. Lett.*, 73, 203 - 222.

Niida, K. 1984. Petrology of the Horman ultramafic rocks in the Hidaka metamorphic belt, Hokkaido, Japan. *Jour. Fac. Sci., Hokkaido Uni. Ser. IV*, no.2, vol. 21, 197-250.

Noddack, I. & Noddack, W. 1931. die geochemie des Rheniums. *Z. Physikal Chem.*, 154, 207 - 244.

Onuma, K. & Arima, M. 1975. The join MgSiO3-MgAl2SiO6 and the solubility of Al2O3 in enstatite at atmospheric pressure. *J. Japan Assoc. Min. Pet. Econ. Geol.*, 7, 53-60.

Onuma, N., Higuchi, N., Wakita, H. & Nagasawa, H. 1968. Trace element partitioning between pyroxenes and the host lava. *Earth Planet. Sci. Lett.* 5, 47-51.

Oshin, I. O. & Crocket, J. H. 1982. Noble metals in Thetford Mines ophiolites, Quebec, Canada. Part 1: distribution of gold, iridium, platinum and palladium in the ultramafic and gabbroic rocks. *Econ. Geol.*, 77, 1556 - 1570.

Page, N. J. 1971. Sulphide minerals in the G and H chromitite zone of the Stillwater complex, Montana. *U. S. Geol. Surv., Prof. Paper*, 694.

Page, N. J., Rowe, J. J. & Haffty, J. 1972. Platinum metals lateral variations of platinum, palladium and rhodium in the Stillwater Complex, Montana. *Econ. Geol.*, 67, 915 - 923.

Page, N. J., Rowe, J. J. & Haffty, J. 1972. Platinum metals in the Stillwater Complex, Montana. *Econ. Geol.*, 71, 1352 - 1363.

Page, N. J. & Talkington, R. W. 1984. Palladium, platinum, rhodium, ruthenium and iridium in peridotites from ophiolite complexes in Newfoundland. *Can. mineral.*, 22, 137 - 149.

Patriat, P. & Achache, J. 1984. India-Eurasia collision chronology and its implications for crustal shortening and driving mechanisms of plates. *Nature*, 311, 615-621.

Pattou, L., Lorand, J. P. & Gros, M. 1996. Non-chondritic platinum-group element ratios in the earth's mantle. *Nature*, 379, 712 - 715.

Paul, D., Crocket, J. H. & Nixon, P. H. 1979. Abundances of palladium, iridium and gold in kimberlites and associated nodules. *Proc. 2nd Int. Kimberlite Conf., 1, Am. Geophys. Union*, Washington, DC, 272 - 279.

Peach, C. L., Mathez, E. A. & Keays, R. R. 1990. Sulphide melt- silicate melt distribution coefficients for the noble metals as deduced from MORBs. *Geochim. Cosmochim., Acta*, 54, 3379 - 3389.

Pearce, J. A. 1982. Trace element characteristics of lavas from destructive plate boundaries. In: Thorpe, R.S. (ed.) *Andesites*, Wiley, Chichester, 525 - 548.

Pearce, J. A. 1983. Role of subcontinental lithosphere in magma genesis at active continental margins. *In*: Hawkesworth, C.J. & Norry, M.J. (eds.) *Continental Basalts and Mantle Xenoliths*, Nantwich, UK, Shiva, 230 - 249.

Pearce, J. A. & Cann, J. R. 1973. Tectonic setting of basic volcanic rocks determined using trace element analyses. *Earth Planet. Sci. Lett.*, 19, 290 - 300.

Peck, D. C. & Keays, R. R. 1990. Insight into the behaviour of precious metals in primitive, s-undersaturated magmas: evidence from the Heazlewood River Complex, Tasmania. *Can. Mineral.*, 28, 553 - 577.

Perfit, M. R. 1977. The geochemistry of igneous rocks from the Cayman Trench and the Captains Bay pluton, Unalaska Island: Their relation to tectonic process at plate margins. PhD, thesis, 237.

Petterson, M. G. & Windley, B. F. 1985. Rb-Sr dating of the Kohistan arc-batholith in the Trans-Himalaya of N. Pakistan and tectonic implications. *Earth Planet. Sci. Lett.*, 74, 54-75.

Picard, C., Amossé. J., & Piboule, M. 1985. Physical and chemical constraints on platinum-group element behaviour during crystallization of a basaltic komatiite liquid: Example of the Proterozoic Delta Sill, New Quebec. *Canada. Econ. Geol.*, 90, 2287 - 2302.

Pitcher, W. S. 1978. The anatomy of a batholith. *J. Geol. Soc. Lond.*, 135, 157 - 182.

Pope, R. R., Kay, S. M. & Kay, R. W. 1981. Ultramafic xenoliths from Kanaga Island: insight into mantle composition and dynamics below the island arc (abstract). *EOS Trans. Am. Geophys. Un.*, 62, 1092.

Prendergast, M. D. 1990. Platinum-group minerals and hydrosilicate " alteration " in Wedza-Mimosa platinum deposit, Great Dyke, Zimbabwe-Genetic and metallurgical implications. *Trans. Inst. Mining Metall. Sect.*, 99, B91 - B105.

Presnall, D. C., Dixon, S. A., Dixon, J. R., O'Donnel, T. H., Brenner, N. L., Schrock, R. L. & Dycus, D. W. 1978. Liquidus phase relations on the join diopside-forsterite-anorthite from 1 atm. to 20 Kbar: Their bearing on the generation and crystallization of basaltic magma. *Contrib. Mineral. Petrol.* , 66, 203-220.

Presnall, D. C., Dixon, J. R., O'Donnel, T. H. & Dixon, S. A. 1979. Generation of Mid-Ocean Ridge Tholeiites. *J. Petrol.*, 20, 3 - 35.

Pricard, H. M., Neary, C. R. & Potts, P. J. 1986. Platinum group minerals in the Shetland Ophiolite. In: Gallagher, M.J., Ixer, R.A. Neary, C.R. & Prichard, H.M. (eds) *Metallogeny of Basic and Ultrabasic rocks, London*. Special Publication of Inst. Min.Metall.

Pudsey, C. J. 1986. The Northern Suture, Pakistan: margin of a Cretaceous island-arc. *Geol. Magaz.*, 123, 405-423.

Ragan, D. M. 1963. Emplacement of the Twin Sisters dunite, Washington. *Amer. Jour. Sci.*, 261, 549-565.

Rai, A. & Pande, I. C. 1983. Study of norite from the Kargil igneous complex, Indus suture zone, Ladakh, India. In: Sinha, A.K. (ed.) *Contemporary Geoscientific Researches in Himalaya*, 2, 41 - 47.

Rickwood, P. C. 1989. Boundary lines within petrologic diagrams which use oxides of major and minor elements. *Lithos*, 22, 247 - 263.

Robert, R. V. D. , Vanwyk, E. & Palmer, R. 1971. Concentration of the noble metals by a fire-assay technique using nickel sulphide as the collector. *Nation. Inst. Metallurgy Repot 1371*, Johannesburg.

Rock, N. M. S. & Groves, D. I. 1988. Can lamprophyes resolve the genetic controversy over mesothermal gold deposits? *Geology*, 16, 538 - 541.

Rock, N. M. S., Hallberg, J. A., Groves, D. I. & Mather, P. J. 1988. Archaean lamprophyres in the Goldfields of the Yilgarn Block, Western Australia: new indications of their widespread distribution and significance. *Univ. Western Australia Geol. Dept. Extension Publ.*, 12, 245 - 275.

Ross, J. R. & Keays, R. R. 1979. Precious metals in volcanic-type nickel sulphide deposits in Western Australia, 1. Relationship with the composition of the ores and their host rocks. *Can. Mineral.*, 17, 417 - 435.

Ryerson, F. J. & Watson, E. B. 1987. Rutile saturation in magmas: implications for Ti-Nb-Ta depletion in island arc basalts. *Earth Planet. Sci. Lett.*, 86, 225 - 239.

Ryzenkho, B. & Kennedy, G. 1973. The effect of pressure on the eutectic in the Fe-FeS system. *Am. J. Sci.*, 273, 800 - 810.

Saint-Jours, C. 1988. Thermodynamique des mélanges polyanioniques liquides à base d'oxydes: Modélisation thermodynamique et mesures de capacités en soufre. PhD thesis, Grenoble, France, Institut National Polytechnique, 169.

Sano, S., Nakajima, T. & Khan, S. R. 1996. Geology and isotope geochemistry of the Jijal Complex, Northern pakistan. *Proc. Geosci. Colloquium*, Special Issue 15, 127 - 136.

Saunders, A. D. & Tarney, J. 1979. The geochemistry of basalts from a back-arc spreading centre in the East Scotia Sea. *Geochim. Cosmochim. Acta.*, 43, 555 - 572.

Saunders, A. D., Tarney, J. & Weavers, S. D. 1980. Transverse geochemical variations across the Antarctic Peninsula: implications for the genesis of calc-alkaline magmas. *Earth Planet. Sci. Lett.*, 46, 344 - 360.

Saunders, A. D., Norry, M. J. & Tarney, J. 1991. Fluif influence on the trace element composition of subduction zone magmas. *Phil. Tran. R. Soci.*, London, A335, 377 - 392.

Searl, M. P., Windley, B. F., Coward, M. P., Cooper, D. J. W., Rex, A. J., Rex, D., Tingdong, L., Xuchang, X., Jan, M. Q., Thakur, V. C. & Kumar, S. 1987. The closing of the Tethys and the tectonics of the Himalaya. *Geol. Soc. Amer. Bull.*, 98, 678 - 701.

Shams, F. A. 1975. The petrology of the Thak valley igneous complex, Gilgit Agency, northern Pakistan. *Acad. Nazionale Dei Lincei*, series 8, 59, 453 - 464.

Shams, F. A. 1980. Origin of the Shangla blueschists, Swat Himalaya, Pakistan. *Univ. Peshawar Geol. Bull.*, Special Issue, 13, 67 - 70.

Sharpe, M. 1982. Noble metals in the margin rocks of the Bushveld Complex. *Econ. Geol.*, 77, 1286 - 1295.

Shervais, J. W. 1982. T/V plots and the petrogenesis of modern and ophiolitic lavas. *Earth Planet. Sci. Lett.*, 59, 101 - 118.

Sigurdsson, H. & Schilling, J. G. 1976. Spinels in mid-Atlantic Ridge basalts: Chemistry and occurrence. *Earth Planet. Sci. Lett.*, 29, 7-20.

Sigurdsson, H. 1977. Spinels in Leg 37 basalts and peridotites: Phase chemistry and zoning. *Initial Rep. Deep Sea Drill. Proj.*, 37, 883-892.

Skinner, B. J. & Merewether, P. 1986. Genesis of Witwatersrand ores: evidence vs. prejudice. *Geocongress'86, Extended Abstracts*, Johannesburg, July, 7 - 11.

Stern, R. J. 1978. Agrigan: an introduction to the geology of an active volcano in the northern Mariana Island arc. *Bull. Volcan.* 41, 42-55.

Stockman, H. W., & Hlava, P. F., 1984. Platinum-group minerals in Alpine chromitites from south-western Oregon. Econ. Geol., 79, 491 - 508.

Stone, W. E., Crocket, J. H. & Fleet, M. E. 1990. Partitioning of palladium, iridium, platinum and gold between sulphide liquid and basalt melt at 1200°C. *Geochim. Cosmochim. Acta*, 54, 2341 - 2344.

Sun S-S. 1982. Chemical composition and origin of the Earth's primitive mantle. *Geochim. Cosmochim. Acta*, 46, 179 - 192.

Sun, S. S. & McDonough, W. F. 1989. Chemical and isotopic systematics of oceanic basalts: implications for mantle composition and processes. In: Saunders, A.D. & Norry, M.J. (eds.) *Magmatism in the Ocean Basins*. Geological Society of London Special Publication 42, 313 - 315.

Sun S-S., Nesbitt, R. W. & Sharaskin, A. Ya. 1979. Geochemical characteristics of mid-ocean ridge basalts. *Earth Planet. Sci. Lett.*, 44, 119 - 138.

Sun S-S., Wallace, D. A., Hoatson, D. M., Glikson, A. Y. & Keays, R. R. 1991. Use of geochemistry as a guide to platinum-group element potential of mafic-ultramafic rocks: Examples from the west Pilbara block and halls creek Mobile Zone, Western Australia. *Precamb. Res.* 50, 1 - 35.

Tahirkheli, R. A. K. 1979. Geology of Kohistan, and adjoining Eurasian and Indo-Pakistan continents, Pakistan. *Uni. Peshawar Geol. Bull.*, 11, 1-30.

Tahirkheli, R. A. K. & Jan, M. Q. 1979. Geology of Kohistan, Karakoram Himalaya, Northern Pakistan. *Uni. Peshawar Geol. Bull.*, Special Issue, 75-121.

Tahirkheli, R. A. K., Mattauer, M., Proust, F. & Tapponnier, P. 1979. The India-Eurasia suture zone in northern Pakistan; synthesis and interpretation of data on plane scale. In: Farah, A. & DeJong, K. (eds.) *Geodynamics of Pakistan: Geological Survey of Pakistan, Phil. Trans. R. Soc.* Lond., A297, 179 - 202.

Takahashi, H., Jassens, M.-J., Morgan, J. W. & Anders, E. 1978. Further studies of trace elements in C3 chondrites. *Geochim. Cosmochim. Acta*, 42, 97 - 106.

Takahashi, Y., Takahashi, Y., Kausar, A. B. & Mikoshiba, M. 1996. Geology and geochemistry of Eastern part of the Chilas Complex, Northern Pakistan- Implication for the tectonic development of the Kohistan island arc. *Proc. Geoscience Colloq.*, Special Issue, 15, 183 - 206.

Talkington, R. W. & Lipin, B. 1986. Platinum-group minerals in chromite seams of the Stillwater Complex, Montana. *Econ. Geol.*, 81, 1179 - 1186.

Tarney, J., Saunders, A. D., Mattey, D. P., Wood, D. A., & Marsh, N. G., 1981. Geochemical aspects of back-arc spreading in the Scotia Sea and western Pacific. *Phil. Trans. R. Soc. Lond.* A300, 263 - 285.

Tarney, J., Wood, D. A., Saunders, A. D., Cann, J. R. & Varet, J. 1980. Nature of mantle heterogeneity in the North Atlantic: evidence from deep sea drilling. *Phil. Trans. R. Soc. Lond.*, 297A, 179 - 202.

Thompson, R. S., Morrison, M. A., Hendry, G. L. & Parry, S. J. 1984. An assessment of the relative roles of a crust and mantle in magma genesis: an elemental approach. *Phil. Trans. R. Soc. Lond.*, A310, 549 - 590.

Todd, S. G., Keith, D. W., LeRoy, L. W., Schissel, D. J., Mann, E. L. & Irvine, T. N. 1982. The J-M platinum-palladium reef of the Stillwater Complex, Montana I-Stratigraphy and petrology. *Econ. Geol.*, 77, 1454 - 1480.

Treloar, P. J., Brodie, K. H., Coward, M. P., Jan, M. Q., Khan, M. A., Knipe, R. J., Rex, D. C. & Williams, P. M. 1990. Evolution of the Kamila Shear-Zone, Kohistan, Pakistan. *In*: Salisbury, M.H. & Fountain, D.M. (eds.) *Exposed cross-sections of the continental crust*. Kluwer Academic Publishers, 175 - 214.

Treloar, P. J., Petterson, M. G., Jan, M. Q. & Sullivan, M. A. 1996. A re-evaluation of the stratigraphy and evolution of the Kohistan arc sequence, Pakistan Himalaya: implications for magmatic and tectonic arc-building processes. *J. Geol. Soc. Lond.*, 153, 681-693.

Treloar, P. J., Rex, D. C., Coward, M. P., Petterson, M. G., Windley, B. F., Jan, M. Q. & Luff, I. W. 1989. K-Ar and Ar-Ar geochronology of the Himalayan collision in NW Pakistan: Constraints on the timeing of suturing, deformation, metamorphism and uplift. *Tectonics*, 8, 881-909.

Treudoux, M., Davies, G., Lindsay, N. M. & Sellschop, J. P. F. 1986. The influence of temperature on the geochemistry of the platinum-group elements and gold. *In*: *Geocongress 86*, Johannesburg, South Africa, 625 - 628.

Vermaak, C. F. & Hendriks, L. P. 1976. A review of the mineralogy of the Merensky reef with specific reference to new data on precious metal mineralogy. *Econ. Geol.*, 71, 1244 - 1269.

Von Gruenewaldt, G., Hulbert, L. J. & Naldrett, A. J. 1989. Contrasting platinum-group element concentration patterns in cumulates of the Bushveld complex. *Mineralium Deposita*, 24, 219 - 229.

Walcott, R. I. 1968. Geology of the Red Hill complex, Nelson, New Zealand. *Trans. R. Soc. N.Z., Earth Science*, 7, 57-88.

Walker, D., Shibata, T. & DeLong, S. E. 1979. Abyssal tholeiites from the oceanographer Fracture Zone, II, Phase equilibria and mixing. *Contrib. Mineral. Petrol.*, 70 , 111 - 126.

Walker, R. J., Shireyp, S. B. & Stecher, O. 1988. Comparative Re-Os, Sm-Nd and Rb-Sr isotope and trace element systematics for Archaean komatiite flows from Munro Township, Abitibi Belt, Ontario. *Earth Planet. Sci. Lett.*, 87, 1 - 12.

Weaver, B. L. & Tarney, J. 1981. Chemical changes during dyke metamorphism in high-grade basement terrains. *Nature*, 289, 47 - 49.

Wells, P. R. A. 1977. Pyroxene thermometry in simple and complex systems. *Contrib. Miner. Petrol.*, 62, 129 - 139.

Wendlandt, R. F. 1982. Sulfide saturation of basalt and andesite melts at high preesure and temperature. *Am. Mineral.*, 67, 877 - 885.

Westland, A. D. 1981. Inorganic chemistry of the platinum-group elements. *In*:: Cabri, L.J. (ed.) *Platinum-Group Elements: Mineralogy, Geology, Recovery*, CIM Special Volume 23, Chapter 7.

Winchester, J. A. & Floyd, P. A. 1977. Geochemical discrimination of different magma series and their differentiation products using immobile elements. *Chem. Geol.*, 20, 325 - 343.

White, W. M. & Dupré, B. 1986. Sediment subduction and magma genesis in the Lesser Antilles: isotopic and trace element constraints. *J. Geophys. Res.*, 91, 5927 - 5941.

White, W. M. & Patchett, J. 1984. Hf-Nd-Sr isotopes and incompatible element abundances in island arcs: implications for magma origin and crust mantle evolution. *Earth Planet. Sci. Lett.*, 67, 167 - 185.

Wilson, M. 1989. Igneous Petrogenesis. Unwin Hyman, London.

Wood, B. J. & Banno, S. 1973. Garnet-orthopyroxene and orthopyroxene-clinopyroxene relationships in simple and complex systems. *Contrib. Mineral. Petrol.*, 42, 109 - 124.

Wood, D. A., Mattey, D. P., Jordan, J. L., Marsh, N. G., Tarney, J. & Trueuil, M. 1981. A geochemical study of 17 samples from basement cores recovered at sites 447, 448, 449, and 451, Deep Sea Drilling Project Leg 59. *In*: Orlofsky, S. (ed.) *Init. Rep. Deep Sea drill. Proj.*, 59, 743 - 752.

Wood, D. A., Tarney, J., Varet, A. D., Saunders, H., Bougault, J. L., Treuil, M. & Cann, J. R. 1979. Geochemistry of basalts drilled in the north Atlantic by IPOD LEG 49: implications for mantle heterogeneity. *Earth Planet. Sci. Lett.*, 42, 77.

Wyman, D. & Kerrich, R. 1989. Archaean shoshonite lamprphyres associated with Superior province deposits: distribution, tectonic setting, noble metal abundances, and significance for gold mineralization. The Geology of Gold Deposits. The Perspective, 1988. *Econ. Geol.*, Monograph, 6, 651 - 667.

Yoder, H. S. & Tilley, C. E. 1962. Origin of basaltic magmas: an experimental study of natural and synthetic rock systems. *J. Petrol.*, 3, 342-532.

Yamamoto, H. 1993. Contrasting metamorphic P-T time paths of the Kohistan granulites and tectonics of the western Himalayas. *J. Geol. Soc. Lond.*, 150, 843-856.

Yamamoto, H. & Nakamura, E. 1996. Sm-Nd dating of garnet granulites from the Kohistan complex, northern Pakistan. *J. Geol. Soc. Lond.*, 153, 965-969.

ANNEXE
PLATINUM-GROUP ELEMENT DISTRIBUTION IN OTHER ULTRAMAFIC-MAFIC ROCKS: SPAT AND CHILAS COMPLEXES

1 - SPAT ULTRAMAFIC-MAFIC COMPLEX

1-1. General Features

Spat Complex is situated east of Jijal Complex and on the northern margin of the Main Mantle Thrust (MMT; Fig. 38). Lithologically, it is subdivided into a lower ultramafic sequence and overlying gabbroic sequence. NE-SW striking fault separates gabroic rocks from the lower ultramafic sequence. The geology and mineral chemistry of the Spat complex has been described by Jan et al. (1993).

The ultramafic rocks of Spat Complex comprise two units, dunite at the base and olivine clinopyroxenite with interspersed dunite layers in the upper unit. The lower part of the dunite is strongly sheared and serpentinized and this phenomenon is also frequent in upper part of this unit. Near the zone between dunite and olivine clinopyroxenite, very thin layers (mm to cm scale) of clinopyroxenite are present in the dunite. Very thin layers of anorthosite crop out in the upper portion of the dunite.

Dunite consists of 90 to 95 vol. % olivine, 2 to 3 vol. % clinopyroxene and approximately 1 to 2 vol. % chromian spinel. Serpentinization of dunite is intense near the suture.

Olivine-clinopyroxenite is mostly intercalated with thin layers of dunite and websterites. The main constituents are clinopyroxene (60-70 vol.%) and olivine (15-20 vol; %). Orthopyroxene is less than 10 vol. % and with some accessory of spinel and magnetite.

The gabbroic rocks are well-layered to homogeneous and mainly composed of plagioclase, clinopyroxene, orthopyroxene and hornblende.

During this study, one section was measured from dunite at the base to gabbro top, and samples were collected for PGE and PGM determination in these rocks (Fig. 110).

1-2. Rock Chemistry of the Spat Complex

The major and trace element chemistry of the Spat Complex has been examined and presented in Table 24. Sample locations are shown in Figure 110. The geochemistry of the different lithological units suggests that they are probably progressively differentiated batches of a tholeiitic melt like the Jijal Complex, and with a certain degree of overlap.

The range of SiO_2 concentrations in the different dunitic units of the ultramafic section is limited from 40 to 43 wt %. But they exhibit gradual increase in MgO concentrations from 41 wt % in the lower unit (SPT-23; Fig. 110) to 48 wt % in the upper dunite unit (SPT-15; Table 24). Similarly, total Fe (expressed as Fe_2O_3) contents increase from 8.32 at the base to 11.42 wt % in the upper dunite (SPT-11). The presence of high Fe_2O_3 in the dunite units can be explained in terms of the presence of disseminated as well as layered ferrochromite. In contrast, CaO is decreasing with increasing stratigraphic height, from the lowermost dunite to the uppermost

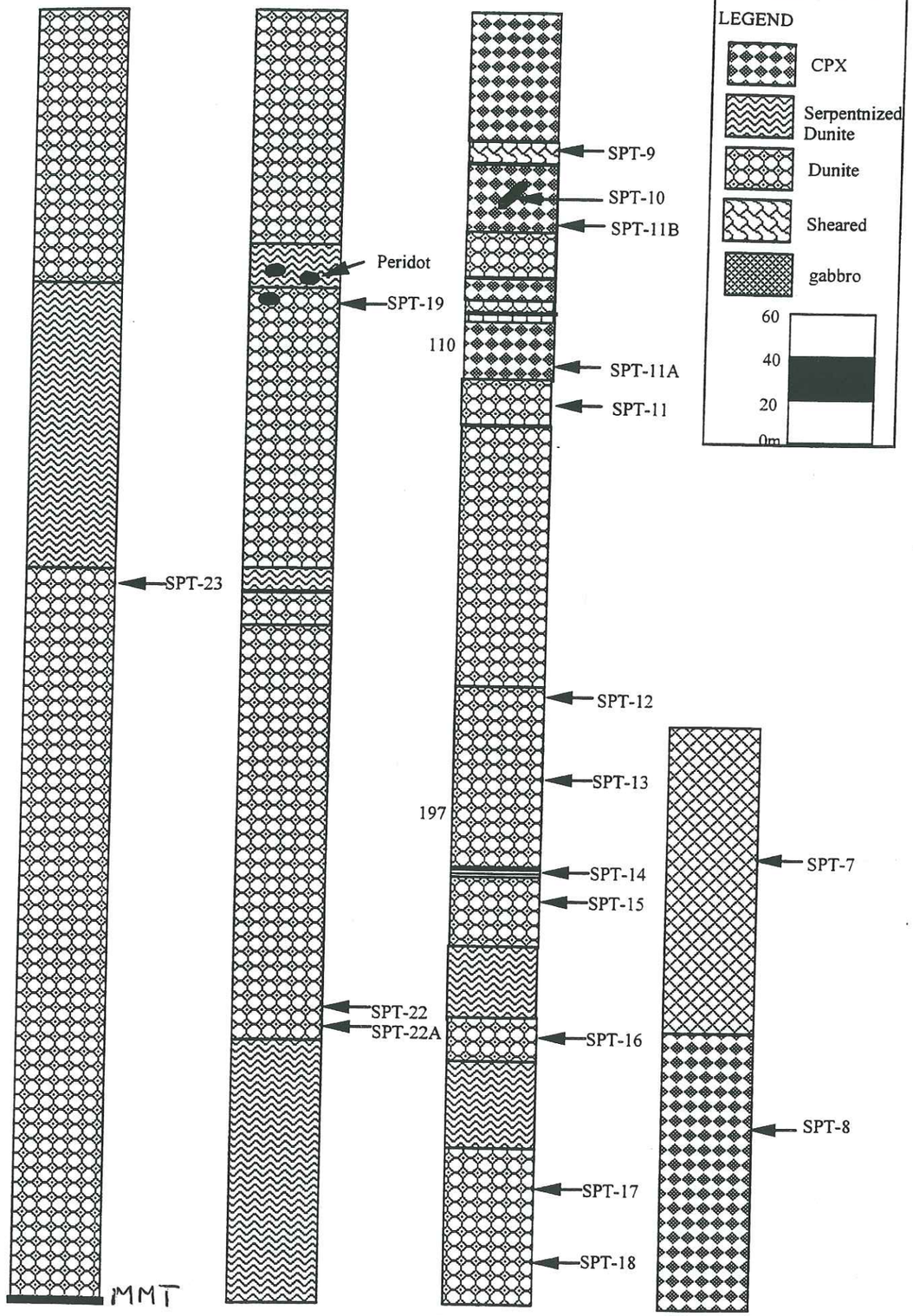

Figure 110. Stratigraphic column of rocks intersected in Spat Complex, along with sample location.
Colonne stratigraphique des roches recoupées dans le Complexe Mafique-Ultramafique de Spat avec localisation des sites d'échantillonnage.

Table 24. Major, trace and platinum-group element analytical data for samples from the Spat Complex. Major elements are recalculated to 100% without LOI.
Données analytiques sur les éléments majeurs, en traces, et les EGP des échantillons du complexe de Spat .

S. No.	SPT-2	SPT-4	SPT-5	SPT-6	SPT-7	SPT-8	SPT-11	SPT-23
Facies	dunite	dunite	dunite	gabbro	gabbro	ol-clinopy.	dunite	dunite
Major elements (wt %)								
SiO2	43.97	40.99	43.66	47.89	47.73	50.99	40.50	
TiO2	0.03	0.02	0.02	0.21	0.21	0.10	0.03	
Al2O3	1.48	0.43	0.80	16.87	16.00	2.66	0.73	
Fe2O3	9.46	9.24	8.98	10.09	9.27	6.09	11.53	
MnO	0.11	0.11	0.10	0.18	0.18	0.09	0.13	
MgO	43.65	49.07	45.36	11.29	10.47	20.71	46.94	
CaO	1.29	0.14	1.09	13.47	16.12	19.35	0.13	
Na2O								
K2O								
P2O5								
Total	100.00	100.00	100.00	100.00	100.00	100.00	100.00	
LOI	9.50	0.60	4.40	3.31	2.23	2.07	1.00	
Trace elements (ppm)								
Ba	9	BDL	BDL	BDL	BDL	BDL	BDL	
Rb	BDL	BDL	BDL	BDL	BDL	BDL	BDL	
Sr	BDL	BDL	BDL	43	48	5	BDL	
Ta	BDL	BDL	BDL	BDL	BDL	BDL	BDL	
Th	BDL	BDL	BDL	BDL	BDL	BDL	BDL	
Zr	BDL	BDL	BDL	BDL	BDL	BDL	BDL	
Nb	BDL	BDL	BDL	BDL	BDL	BDL	BDL	
Y	6	6	6	7	7	7	6	
V	18	BDL	7	181	254	172	BDL	
Cr	2196	2206	2106	95	264	2162	2798	
Ni	1851	2459	2258	77	77	327	1712	
Co	141	159	147	61	55	100	151	
Cu	20	24	11	103	58	165	12	
Zn	39	42	36	66	54	16	48	
PGE (ppb)								
Ir	N.D.	N.D.	N.D.	N.D.	0.08	0.2	0.74	
Ru					0.91	1.02	3.16	
Rh					0.1	0.59	1.96	
Pt					0.88	27.85	83.33	
Pd					0.81	23.55	28.22	
Au					9.88	4.66	4.73	
∑PGE					12.66	57.87	122.14	
Pd/Ir					10.13	117.75	38.14	
Mg-no.	0.92	0.93	0.92	0.72	0.73	0.89	0.91	

S. No.	SPT-15	SPT-17	SPT-19	SPT-23	SPT-23
Facies	dunite	dunite	dunite	dunite	dunite
Major elements (wt %)					
SiO2	40.33	43.32	43.35	44.82	44.52
TiO2	0.03	0.02	0.02	0.02	0.02
Al2O3	0.84	0.76	0.64	0.88	0.84
Fe2O3	9.34	9.10	8.92	9.05	8.82
MnO	0.09	0.10	0.11	0.11	0.10
MgO	48.89	46.17	46.35	44.28	44.10
CaO	0.47	0.53	0.62	0.84	1.61
Na2O					
K2O					
P2O5					
Total	100.00	100.00	100.00	100.00	100.00
LOI	0.01	2.02	4.78	2.50	5.62
Trace elements (ppm)					
Ba	33	BDL	BDL	BDL	BDL
Rb	BDL	BDL	BDL	BDL	BDL
Sr	BDL	BDL	BDL	BDL	BDL
Ta	BDL	BDL	BDL	BDL	BDL
Th	BDL	BDL	BDL	BDL	BDL
Zr	BDL	BDL	BDL	BDL	BDL
Nb	BDL	BDL	BDL	BDL	BDL
Y	6	6	6	6	6
V	BDL	BDL	BDL	5	14
Cr	3015	2417	2023	2216	2132
Ni	2000	2335	2265	2126	2149
Co	169	147	148	138	149
Cu	BDL	BDL	BDL	9	7
Zn	35	39	36	29	40
PGE (ppb)					
Ir	1.93	2.11	4.06	N.D.	1.02
Ru	8.29	4.12	8.19		8.53
Rh	0.72	0.63	1.59		1.45
Pt	3.14	4.52	9.53		6.78
Pd	1.71	0.75	5.3		12.24
Au	2.66	1.59	2.35		2.16
∑PGE	18.45	13.72	31.02		32.18
Pd/Ir	BDL	BDL	BDL	1.31	12
Mg-no.	0.89	0.92	0.92	0.92	0.92

Abbreviations: ol-clinopy. = olivine clinopyroxenite, BDL = below detection limit, N.D. = not determined.

dunite (1.52 wt % in SPT-23 and 0.47 wt % in SPT-15; Table 24). Concentrations of TiO_2 and MnO are low and virtually remain unchanged. Concentrations of NaO_2, K_2O and P_2O_5 are negligible and below detection limit. Mg-number of dunite in all level is 92 and does not show any change with stratigraphic height.

In the dunit units, Cr contents show a gradual increase from 2132 ppm in the lower unit (SPT-23; Table 24) to 3015 (SPT-15) in the upper unit. In contrast, Ni concentrations increase from 2149 to 2335 ppm and then decrease to 1712 ppm in sample SPT-11.

In the olivine-clinopyroxenite, there is slight increase in MgO concentrations from 19.36 to 20.10 wt %. Likewise, Al_2O_3 and Fe_2O_3 both show increase from 2.51 to 2.58 wt % and from 5.35 to 5.91 wt % respectively (Table 24). The concentrations of CaO decrease from 20.37 to 18.78 wt %. The contents of TiO2 and MnO are low (< 0.11 and 0.13 wt % respectively) and remained unchanged.

In the olivine-clinopyroxenites, the Cr concentration range is from 1925 to 2162 ppm and that of Ni from 244 to 327 ppm, both exhibit general increase with stratigraphic height. Similarly, Co also shows increase from 79 ppm in the lower unit to 100 ppm in the upper unit.

The layered gabbro exhibits SiO_2 concentrations of 46 wt % with MgO 10 wt %, Al_2O_3 15 wt %, Fe_2O_3 9 wt % and CaO 15 wt % (Table 24).

1-3. PGE's Distribution

Total PGE contents of Spat Ultramafic-Mafic Complex are shown in Table 24. Dunite shows a strong Ir (1.93, 2.11 and 4.06 ppb), Ru (8.29, 4.12 and 8.19 ppb) enrichment, and show slight impoverishment in Rh, Pd and Pt (except in SPT-19 where Pt=9.53 ppb), resulting in flat to slightly negative Pd/Ir ratio (1.31 to 0.36). Au contents are low in dunite (<2.66 ppb) but increase towards clinopyroxenite and gabbro. Clinopyroxenite shows more concentration of PGE's (48.95 to 57.9 ppb), and exhibits extremely steep patterns (Pd/Ir=112 to 147). Pt, Pd and Au are the least depleted PGE contents in this pyroxenite. Ir contents drop from dunite to clinopyroxenite, and Pt and Pd contents increase from dunite to clinopyroxenite, but again drop in gabbro (Table 24). Dunite, interlayered with pyroxenite cumulate, has maximum total PGE contents (122 ppb) and relatively less fractionated as compared to pyroxenite (Pd/Ir=38.14).

2 - THAK GAH ULTRAMAFIC-MAFIC COMPLEX

2-1. PGE's Distribution

The whole-rock PGE data for twelve analyzed rock samples are listed in Table 25 and grouped according to rock types. Ultramafic-mafic rocks from Thak Gah display a restricted range of total PGE contents (8-34 ppb) and exhibit positive slope (Pd/Ir = 3.95 to 50.33 ratio),

Table 25. Major (wt%), trace (ppm) and platinum-group elements (ppb) analytical data for the Thak Gah Complex and Main Zone of Chilas Igneous Complex.
Données analytiques sur les éléments majeurs (pds%) en traces (ppm), et les EGP (ppb) du Complexe de la Thak Gah et de la Zone du Faciès Principal du Complexe Igné de Chilas .

S.No.	KO-56B	KO-56C	KO-63B	KO-57B	KO-61A	KO-62	KO-57A	KO-58	KO-59A	KO-82	KO-52B
rock name	dunite	dunite	dunite	dunite Chr	dunite Chr	pyroxenite	pyroxenite	gab troct	gab troct	opx-diorite	gab-nor
mineralization	sp		sulf		+/- chr-sp	+/- chr-sulf				sulf	
Major elements (wt%)	UMA	UMA	UMA	UMA	UMA	UMA	UMA	UMA	UMA	UMA	UMA
SiO2	40.32	38.82	39.27	N. D.	38.22	47.38	50.76	44.89	43.41	43.80	41.93
TiO2	0.12	0.07	0.09		0.04	0.30	0.15	0.18	0.04	1.38	3.35
Al2O3	1.83	1.45	1.91		0.63	4.39	1.96	2.64	22.14	18.17	17.96
Fe2O3	17.68	18.05	17.82		18.58	10.99	12.00	11.87	7.74	14.53	13.31
MnO	0.22	0.20	0.20		0.21	0.15	0.28	0.16	0.10	0.16	0.18
MgO	36.73	39.99	38.33		41.77	22.91	22.85	29.57	14.11	5.31	5.31
CaO	3.11	1.43	2.38		0.34	13.64	7.71	10.48	12.24	11.56	11.65
Na2O	0.00	0.00	0.00		0.00	0.00	0.00	0.00	0.07	0.76	1.76
K2O	0.00	0.00	0.00		0.00	0.00	0.00	0.00	0.00	0.57	0.47
P2O5	0.00	0.00	0.00		0.00	0.00	0.00	0.00	0.00	0.07	1.54
Total	100	100	100		100	100	100	100	100	100	100
LOI											
Trace elements(ppm)											
Nb	BDL	BDL	N. D.	BDL	BDL	BDL	BDL	BDL	BDL	BDL	BDL
Zr	BDL	BDL		BDL	BDL	BDL	BDL	BDL	BDL	BDL	BDL
Y	BDL	BDL		BDL	BDL	10.00	BDL	BDL	BDL	BDL	BDL
Sr	21	13		BDL	BDL	25	13	19	401	448	449
Rb	BDL	BDL		BDL	BDL	BDL	BDL	BDL	BDL	BDL	BDL
Zn	101	108		BDL	107	57	110	61	41	88	77
Ni	950	1211		722	1312	469	403	700	361	44	39
Cr	1873	3774		96000	3218	1815	1986	2133	140	120	42
V	170	200		BDL	102	358	297	260	12	BDL	452
Ba	82	BDL		BDL	BDL	BDL	BDL	BDL	BDL	BDL	166
Cu	BDL	21		41	BDL	BDL	BDL	BDL	BDL	195	277
Co	161	124		BDL	123	92	59	109	99	61	46
Sc	11	BDL		BDL	BDL	96	66	66	10	46	27
PGE (ppb)											
Ir	0.91	1.03	0.81	28.40	0.78	0.70	0.15	0.40	0.51		
Ru	1.06	0.97	1.15	23.90	1.89	0.73	0.73	1.51	1.22		
Rh	1.03	1.20	1.08	35.30	0.95	0.57	0.29	0.55	0.42		
Pt	4.81	10.30	6.50	792.00	14.88	5.15	10.90	1.93	1.17		
Pd	3.59	7.20	3.38	55.00	13.75	3.04	4.51	2.04	0.49		
Au	1.73	1.25	1.03	67.00	1.30	2.93	2.23	1.28	2.64		
ΣPGE	13.13	21.94	13.94	1001.60	33.54	13.10	18.80	7.71	6.44		
Pd/Ir	3.95	6.99	4.17	1.94	17.74	4.37	30.03	5.16	0.97		

Abbreviations: gab-troc = gabbro-troctolite, gab-nor = gabbro-norite, opx-diorite = orthopyroxene-diorite, sulf = sulphide, chr = chromite, sp = spinel, UMA = ThakGah Complex, BDL = below detection limit, N.D. = not determined, MFZ = Main Facies Zone.

S.No.	KO-60	KO-83	KO-53	KO-54	KO-55	KO-56A	KO-72	KO-52A	KO-82	KO-52B
rock name	gab-nor	gabbro	gab-nor	gab-nor	gab-nor	gab-nor	gab-nor	opx-diorite	opx-diorite	gab-nor
mineralization		sulf		sulf	sulf				sulf	
Major elements (wt%)	UMA	MFZ	MFZ	MFZ	MFZ	contact UMA	MFZ	MFZ	MFZ	MFZ
SiO2	52.53	47.03	51.48	49.60	56.29	50.82	52.25	54.00	43.80	41.93
TiO2	0.50	1.04	0.97	1.11	0.73	0.20	0.36	0.68	1.38	3.35
Al2O3	17.86	19.89	18.35	18.23	17.78	20.97	19.44	15.46	18.17	17.96
Fe2O3	9.13	10.20	9.87	10.54	8.17	6.06	8.35	9.46	14.53	13.31
MnO	0.15	0.11	0.15	0.16	0.13	0.11	0.14	0.14	0.16	0.18
MgO	7.47	4.19	6.20	5.19	4.39	6.55	6.48	6.93	7.10	5.31
CaO	9.90	13.26	10.00	10.49	8.31	11.96	10.64	8.48	13.56	11.65
Na2O	2.30	2.10	2.72	2.19	2.68	1.77	2.26	2.38	0.76	1.76
K2O	0.13	0.04	0.10	0.12	0.68	0.07	0.10	0.04	0.00	0.47
P2O5	0.04	0.02	0.16	0.29	0.11	0.01	0.00	0.07	0.57	1.54
Total	100	100	100	100	99	100	100	100	100	100
LOI		2.11		2.09	0.17	1.48	0.00	2.34		2.55
Trace elements(ppm)										
Nb	BDL	BDL	BDL	BDL	BDL	16.00	BDL	BDL	BDL	BDL
Zr	15.00	29.00	42.00	48.00	64.00	16.00	13.00	37.00	20.00	61.00
Y	10.00	BDL	16.00	18.00	18.00	BDL	BDL	15.00	12.00	27.00
Sr	361	470	475	421	337	449	380	341	448	449
Rb	BDL	BDL	BDL	BDL	18	BDL	BDL	BDL	BDL	BDL
Zn	68	66	78	94	73	47	55	80	88	77
Ni	83	30	50	47	30	50	50	118	44	39
Cr	317	85	183	113	136	176	191	333	120	42
V	144	420	190	331	199	94	129	325	318	452
Ba	62	30	67	74	130	30	56	BDL	BDL	166
Cu	33	105	66	101	27	10	17	28	195	277
Co	41	45	40	39	29	46	43	37	61	46
Sc	27	34	29	35	32	37	38	41	46	27
PGE (ppb)										
Ir	0.24	0.12	0.16	0.14	0.21	0.22	0.16	0.18	0.20	0.62
Ru	1.53	0.83	1.27	1.35	1.31	0.51	1.15	1.16	0.87	0.84
Rh	0.30	0.56	0.64	1.56	0.30	0.87	1.61	0.12	0.07	0.07
Pt	8.20	5.65	3.61	13.70	4.20	7.55	10.45	5.10	2.14	0.68
Pd	5.65	0.82	0.68	0.80	1.55	4.54	3.63	1.40	1.39	0.62
Au	4.54	0.24	1.24	2.38	1.49	2.06	0.56	1.66	2.48	8.85
ΣPGE	20.45	8.21	7.58	19.91	9.04	15.74	17.55	9.61	7.13	11.66
Pd/Ir	23.54	7.13	4.35	5.68	7.36	21.09	22.69	8.00	7.10	1.00

except one sample from layered gabbro (KO-59A), which has a nearly unfractionetd ratio (Pd/Ir = 0.96).

Dunites within this complex have medium Pt (4.81 to 14.88 ppb) and Pd (3.4 to 13.8 ppb) but there is no change in Au value (average 1.3 ppb). Two samples (56B and 56C) are from the same dunite but other two samples (61 and 63B) come from two different bodies interlayered with clinopyroxenite (Fig. 25).

Pyroxenite layers (KO-57A and KO-62), with Pt (10.9-5.2 ppb respectively), and Pd (4.5-3 ppb respectively), and Au (0.7 ppb), have total PGE contents close to dunites (Table 25).

Layered gabbro (sample KO-56A) is the more fractionated part of dunite (KO-56B&C) and represents more fractionated Pd/Ir ratio (20.6).

Similarly **gabbro norite** with 6.99 and 7.5 wt. % MgO, has high Pt (8.1 and 8.2 ppb), Pd (7.6 and 5.7 ppb) and Au 1.5 to 0.9 ppb, and comparatively high Pd/Ir ratio (23.54-50.33). Gabbronorite (KO-55) which surrounds this whole ultramafic-mafic body has low abundances of Pt (4.2 ppb) and Pd (1.6 ppb) and less fractionated (Pd/Ir=7.4) as compared to gabbro norite present in the complex. These data suggest that magmas feeding the complex were carrying appreciable levels of PGE.

2-2. MINERALIZATION

2-2.1 Occurrence of sulphides

During our field surveys we did not find any sulphide phase in the rocks of Spat and Thak Gah Complexes.

2-2.2. Occurrence of Chromite

2-2.2.1-Thak Gah and Spat Complexes

No chromite assemblages of large concentrations are known in the ultramafic and mafic rocks of Thak Gah (Chilas Complex) and Spat Complexes. However, chrome-spinel occurs disseminated throughout the pyroxenite, and in the dunite, where it is an intercumulus phase forming about 1 to 2 vol. % of the rock in Spat Complex but < 1 vol. % in dunite of Thak Gah Complex. Small concentrations of chromite occur in the form of thin layers (<5 mm thick layer in Thak Gah and <1 cm thick in Spat) or streaks in the dunites and may disappear laterally within a few meters, but very rare in the pyroxenite. Although black and shiny megascopically, in thin-section it is dark red and partially translucent. Some grains in dunite of Spat area possess opaque rims of magnetite presumably concentrated during serpentinization. At the base of dunite near the suture zone, chromite has been altered completely to ferrochromite and

concentrated along the cracks of serpentinized portion. These chromites are thought to be cumulate in origin.

Chromite analyses from Spat are characterized by high Cr No. (100Cr/Cr+Al) from 75 to 67 and is akin to Jijal chromite-spinel (Jan et al., 1993). Chromian-spinel from Thak Gah Complex are characterized by 31.59 wt.% Cr_2O_3 in dunite but pyroxenite has less Cr_2O_3 (19 to 5 wt. %; Khan et al., 1989).

2-3. PGE's Distribution Patterns

2-3.1. Thak Gah Complex

The result of the mantle-normalized patterns from the various rock types of the Thak Gah Complex can be seen in Figure 88. The Cr-enriched dunite has quite an irregular shape (Fig. 111). The relatively low Ru, Pd and Cu and high Ir, Pt and Au contents give a sawtooth appearance, yet slightly positive slope to the curve, for this sample. Ni tends to be depleted relative to Ir, and Cu is depleted relative to Pd and Au. According to the PGE data for Alaskan-type complexes from the Soviet Union and Alaska as reported by Crocket (1981), similar high absolute abundances for Pt and Ir and lower values for Ru are common for chromite-rich and chromite-bearing ultramafic rocks. All other dunite samples do not exhibit greatly differing PGE's signatures which have gentle positive slopes. The curves show a tendency towards depletion in Ni relative to PGE's. Overall, the PGE's appear to indicate a common signature, with the principal variable the absolute concentration of the metals.

Figure 112 shows the profiles of mantle-normalized Ni-PGE's-Au-Cu values of mafic rocks of Main Facies Zone (MFZ) of Chilas Igneous Complex and all the curves follow a positive slope from Ni to Cu, disturbed only by a strong negative Pd anomaly (Fig. 89) in some gabbro and gabbro-norite samples. Similarly, Opx-diorite samples (MFZ) show strong negative Rh and slight Pd anomalies. The overall depletion in IPGE's and enrichment in PPGE's, is a pattern typical of fractionation.

Clear similarities in PGE's signatures exist between the different lithological units and this offers support to hypotheses that similar geochemical processes may have operated on or around these lithologies.

2-3.2. Spat Complex

The data from dunites of the Spat Complex are presented mantle normalized (Fig. 113) as described by Barnes et al. (1988). The metal patterns display relatively flat mantle-normalized PGE's patterns with slight PPGE's enrichments. The individual patterns show consistent shapes and features; Ir depletions and positive Rh anomalies, accompanied by slight to pronounced Pt enrichment (except sample SPT-11, having positive Pt anomaly). $(Pd/Ir)_N$

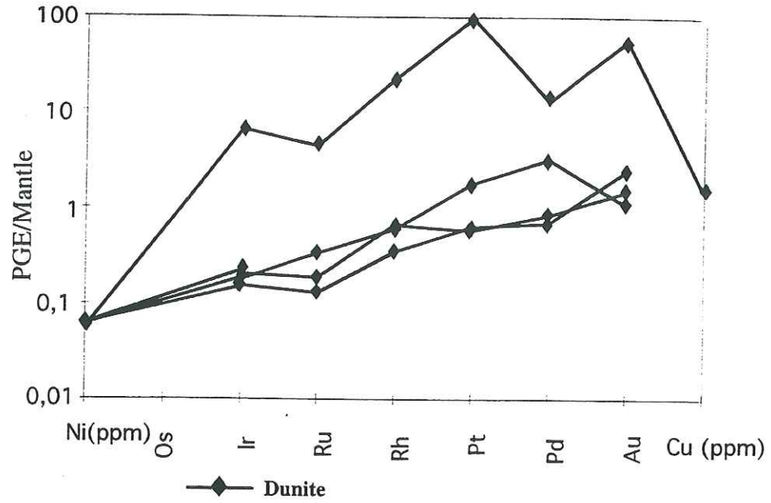

Figure111. Mantle-normalized diagram showing Ni-PGE-Au-Cu patterns for dunite/wehrlite of Thak Gah Complex, Chilas Igneous Complex, Kohistan Arc. Mantle-normalization values are from Barnes et al. (1988).

Spectres normalisés au manteau de Ni-EGP-Au-Cu pour la dunite/wehrlite du Complexe de Thak Gah, Complexe Igné de Chilas, Arc du Kohistan.

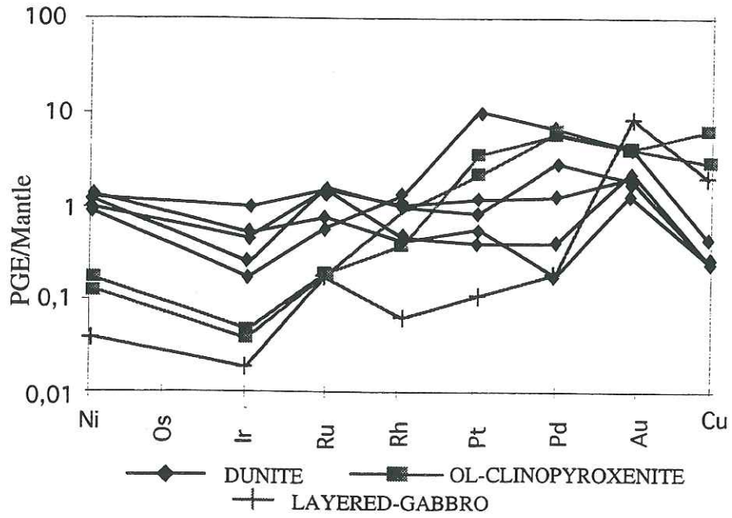

Figure 113. Mantle-normalized diagram showing Ni-PGE-Au-Cu patterns for the rocks of Spat Complex, Kohistan Arc and average mantle-normalizd values from Barnes et al. (1988).

Spectres normalisés au manteau de Ni-EGP-Au-Cu pour les roches du Complexe de Spat.

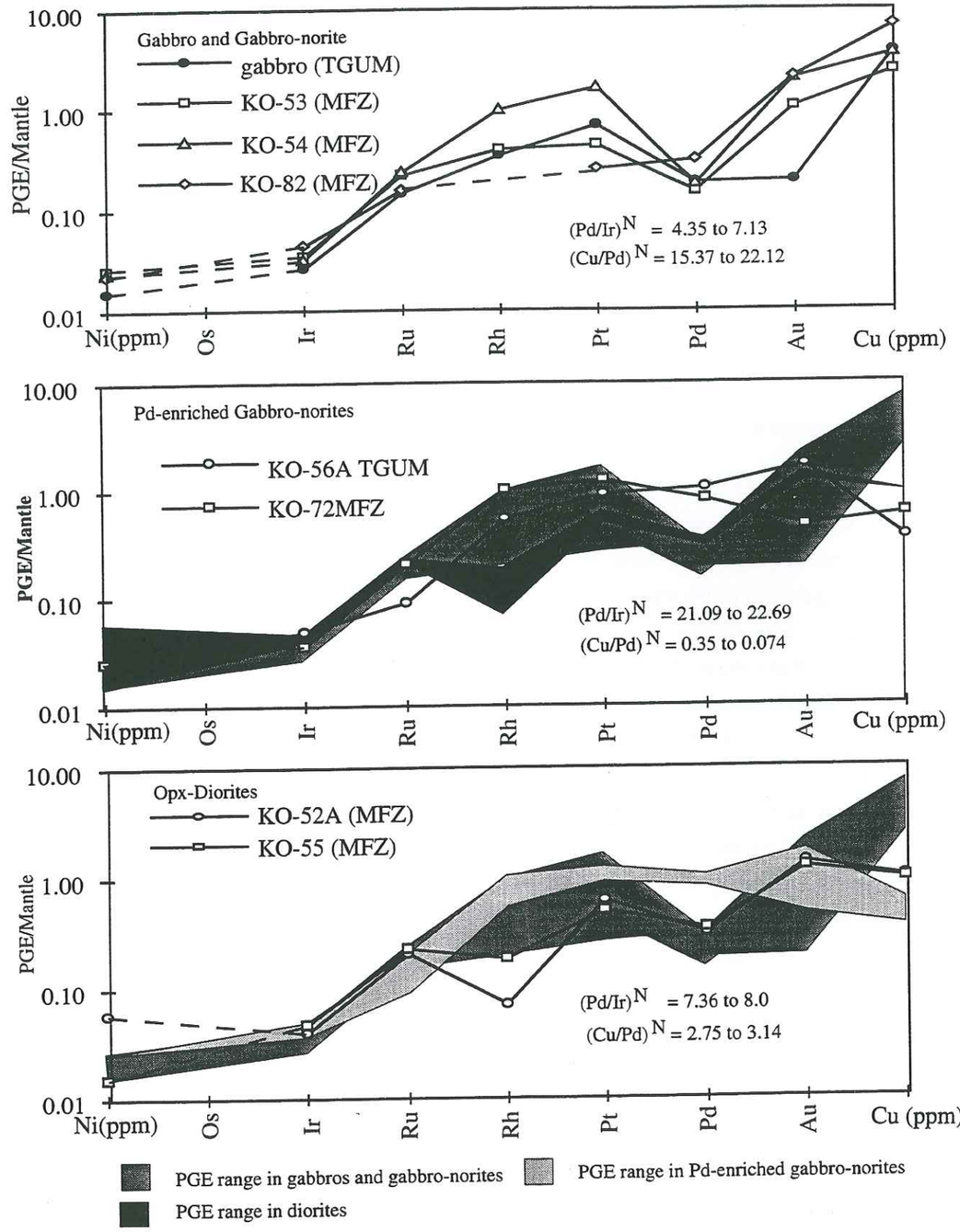

Figure 112. Mantle-normalized diagrams showing Ni-PGE-Au-Cu patterns for the rocks of the Chilas Igneous Complex and average mantle-normalizing values from Barnes et al. (1988).

Spectres normalisés au manteau de Ni-EGP-Au-Cu pour les roches du Complexe Igné de Chilas (MFZ).

ratios, a measure of the overall pattern slope, range from 0.35 to 12.08. But sample SPT-11 intercalated with olivine-clinopyroxenite is comparatively more fractionated (37.70). Ni contents tend to be enriched relative to Ir and Cu is depleted relative to Au. In contrast, Figure 90 exhibits that olivine-clinopyroxenites show PGE's patterns and ratios which have pronounced positive slopes and strong enrichment in Pt, Pd, Au and Cu. Ni tends to be enriched relative to Ir. Gabbro also show fractionated pattern from Ir to Cu, disturbed only by a strong positive Ru and Au anomalies (Fig. 113) but with low concentrations of PGE's as compared to pyroxenites and dunites.

2-4 Discussion

In the Main Facies Zone of Chilas Igneous Complex, the absolute abundances of the PGE's and Au are low (except KO-57B which is Cr-enrich dunite). (Tables 21). Total PGE's abundances are higher in dunite (122.14 ppb) and olivine-clinopyroxenite (57.87 ppb) and lowest in gabbro (12.66 ppb) in Spat Complex. Of the Thak Gah Complex, Cr-rich dunite (sample KO-57B) shows the maximum concentrations of total PGE's (1001.60 ppb) and lowest in orthopyroxene-diorite (7.13 and 9.61 ppb). Table 21 shows that Ir and Ru from the rocks of Spat Complex are often strongly correlated with Ni and do not show good correlation with Cr. The opposite holds for Thak Gah Complex, where all IPGE's are strongly correlated with Cr (Table 25). Consequently, both the pyroxenites from the Thak Gah and Spat Complexes show strongly fractionated patterns, with lower concentrations of IPGE's and elevated PPGE's concentrations (Figs. 111&113). Clear similarities in PGE's signatures exist between the two complexes and this supports to hypotheses that similar geochemical processes may have operated on or around both the complexes.

RÉSUMÉ : La croûte intra-océanique du sud-Kohistan comprend les complexes de Spat et Jijal, les amphibolites de Kamila et le complexe de Chilas.

Le complexe de Jijal est une intrusion litée constituée de dunite, clinopyroxénite à olivine, websterite, webstérite à grenat et de gabbro à grenat. Mis en place à l'interface manteau croûte, il résulte de la cristallisation fractionnée sous haute pression et haute température (10-12 Kbars; 800-1100°C) d'un liquide tholéiitique d'arc intra-océanique hautement magnésien. Les roches de Thak Gah (complexe de Chilas) ont cristallisé sous plus faible pression et température (5 - 6 kbars, 800 à 950°C) dans un réservoir magmatique plus superficiel. Les métaplutonites de Chilas et Kamila présentent également des signatures géochimiques analogues à des tholéiites d'arc insulaire. Au contraire, les amphibolites à grains fins du Groupe de Kamila apparaissent comme des métavolcanites de type N-MORB, elles représentent des reliques de croûte océanique et le substratum de l'arc du Kohistan.

Plusieurs horizons enrichis en PGE caractérisent le complexe de Jijal. Des enrichissements en Ir, Ru, Ni corrélés au Cr dans les dunites, indiquent que l'irridium et le ruthénium précipitent précocément avec la chromite sous haute fugacité d'oxygène. Des enrichissements en Ir et Ru du même type caractérisent les dunites chromifères des complexes de Thak Gah et de Spat. Dans les webstérites à grenat de Jijal, des sulfures disséminés (chalcopyrite, pentlandite, pyrrhotite± pyrite) et des minéraux du Groupe du platine (témagamite, monchéite, mérenskyite et sperrylite) correspondent à des enrichissments en Ir, Ru, Pt, Pd, Au, Ni et Cu. Ils résultent de la formation d'un liquide sulfuré consécutif à la baisse de fO_2. Dans les gabbros à grenats, des enrichissements en Pt, Pd et Cu traduisent l'action de fluides hydrothermaux tardi-magmatiques. Ces minéralisations diffèrent de celles du Bushveld. La saturation en soufre induite par les processus de cristallisation sous haute pression apparaît le moteur essentiel des dépôts observés dans les webstérites à grenats. De telles minéralisations représentent un exemple type de dépôts de PGE associés aux arcs insulaires.

Platinum Group Elements (PGE) and Platinum Group Minerals (PGM) Distribution and Petrological Evolution of Southern Kohistan Arc, Northern Pakistan.

ABSTRACT : The intra-oceanic arc crust in the southern Kohistan is represented by the Jijal-Spat- Complexes, Kamila Amphibolite and Chilas Complex.

The Jijal Complex is a layered intrusion having dunite, olivine-clinopyroxenite, websterite, garnet websterite and garnet gabbro. Geochemistry indicates that this formed by fractional crystallization from a high-Mg tholeiitic melt in an arc environment with pressures between 10 and 12 kbar, equilibrated at temperatures of 800° to 1100°C. The rocks of Thak Gah (Chilas complex) crystallized under lower pressure (5 to 6 kbar) and equilibrated at temperature between 800° and 950°C. They represent a shallow magma chamber in the same arc. Plutonic rocks from Kamila and Chilas-are also geochemically similar to modern intra-oceanic arc. However, fine-grained Kamila metavolcanics, are more akin to the N-type MORB, suggesting fragments of pre-existing oceanic crust.

In the Jijal Complex, BMS, PGM and PGE bearing phases are present in the form of inclusion in or on the edges of the silicate assemblages. The main PGM's are temagamite, moncheite, merenskyite and sperrylite. In dunites, Ir, Ru, Ni and Cr enrichments indicate that both Ir and Ru are partitioned with chromites and can be clearly correlated to high fO_2. Ir and Ru enrichments in chromite-rich dunite of Thak Gah and Spat Complexes have the same origin. In Jijal Garnet-websterite, Ir, Ru, Pt, Pd and Au correspond to a prominent peak of Ni and Cu which is due to the precipitation of sulphide under lower fO_2. In upper garnet gabbro, Pt-Pd-Cu enrichments correspond to late removal of PPGE by magmatic fluids.Such mineralizations present important variations with Bushveld-type. They indicates that sulphide saturation due to simple crystallization can give rise to deposits such as can be seen in the Ga-websterite. Such mineralization characterizes arc related PGE's deposits.

DISCIPLINE : SCIENCES DE LA TERRE

MOTS CLÉS: Kohistan, Pakistan, Jijal, Kamila, Chilas, Géochimie, Minéralogie, Evolution géodynamique, Eléments du Groupe du Platine; Minéraux du Groupe du platine, chromites, sulfures.

INTITULÉ ET ADRESSE DE L'UFR OU DU LABORATOIRE :
Laboratoire Géodynamique des Chaînes Alpines (LGCA-ESA 5025) - UFR Géologie